U.S. DEPARTMENT OF COMMERCE
National Technical Information Service

PB-295 228

Symposium on the Transfer and Utilization of Particlate Control Technology: Volume 3 Scrubbers, Advanced Technology, and HTP Applications

Denver Research Inst., CO

Prepared for

Industrial Environmental Research Lab., Research Triangle Park, NC

Feb 79

TECHNICAL REPORT DATA
(Please read Instructions on the reverse before completing)

1. REPORT NO. EPA-600/7-79-044c

2\.

3. RECIPIENT'S ACCESSION NO. PB295228

4. TITLE AND SUBTITLE Symposium on the Transfer and Utilization of Particulate Control Technology: Vol. 3. Scrubbers, Advanced Technology, and HTP Applications

5. REPORT DATE February 1979

6. PERFORMING ORGANIZATION CODE

7. AUTHOR(S) F.P. Venditti, J.A. Armstrong, and Michael Durham

8. PERFORMING ORGANIZATION REPORT NO.

9. PERFORMING ORGANIZATION NAME AND ADDRESS
Denver Research Institute
P.O. Box 10127
Denver, Colorado 80208

10. PROGRAM ELEMENT NO. EHE624

11. CONTRACT/GRANT NO. Grant R805725

12. SPONSORING AGENCY NAME AND ADDRESS
EPA, Office of Research and Development
Industrial Environmental Research Laboratory
Research Triangle Park, NC 27711

13. TYPE OF REPORT AND PERIOD COVERED Proceedings: 10/77-10/78

14. SPONSORING AGENCY CODE EPA/600/13

15. SUPPLEMENTARY NOTES IERL-RTP project officer is Dennis C. Drehmel, Mail Drop 61, 919/541-2925.

during the Symposium

16. ABSTRACT

Papers in the proceedings were presented at the Symposium on the Transfer and Utilization of Particulate Control Technology, in Denver, Colorado, July 24 through 28, 1978. The symposium was sponsored by the Particulate Technology Branch of EPA's Industrial Environmental Research Laboratory--Research Triangle Park, and was hosted by the University of Denver's Denver Research Institute. The symposium brought together researchers, manufacturers, users, government agencies, educators, and students to discuss new technology and to provide an effective means for the transfer of this technology out of the laboratories and into the hands of the users. The three major categories of control technologies--electrostatic precipitators, scrubbers, and fabric filters--were of major concern. These technologies were discussed from the perspectives of economics; new technical advances in science and engineering; and applications. Several papers dealt with combinations of devices and technologies, leading to a concept of using a systems approach to particulate control, rather than device control. → This volume covers scrubbers, advanced technology, and high temperature high pressure applications. ←

17. KEY WORDS AND DOCUMENT ANALYSIS

a. DESCRIPTORS		b. IDENTIFIERS/OPEN ENDED TERMS	c. COSATI Field/Group	
Pollution	Fabrics	Pollution Control	13B	11E
Dust	Economics	Stationary Sources	11G	05C
Aerosols	Sampling	Particulate	07D	14B
Electrostatic Precipitators		Fabric Filters	13I	
Scrubbers		Fugitive Dust	07A	
Filtration				

18. DISTRIBUTION STATEMENT Unlimited

19. SECURITY CLASS (This Report) Unclassified

20. SECURITY CLASS (This page) Unclassified

21. NO. OF PAGES 500

22. PRICE A21 - A01

EPA Form 2220-1 (9-73)

☆U.S. GOVERNMENT PRINTING OFFICE: 1979-640-013 4206 REGION NO. 4

PB 295228

United States
Environmental Protection
Agency

Industrial Environmental Research
Laboratory
Research Triangle Park NC 27711

EPA-600/7-79-044c
February 1979

EPA

Symposium on the Transfer and Utilization of Particulate Control Technology:
Volume 3. Scrubbers, Advanced Technology, and HTP Applications

Interagency Energy/Environment R&D Program Report

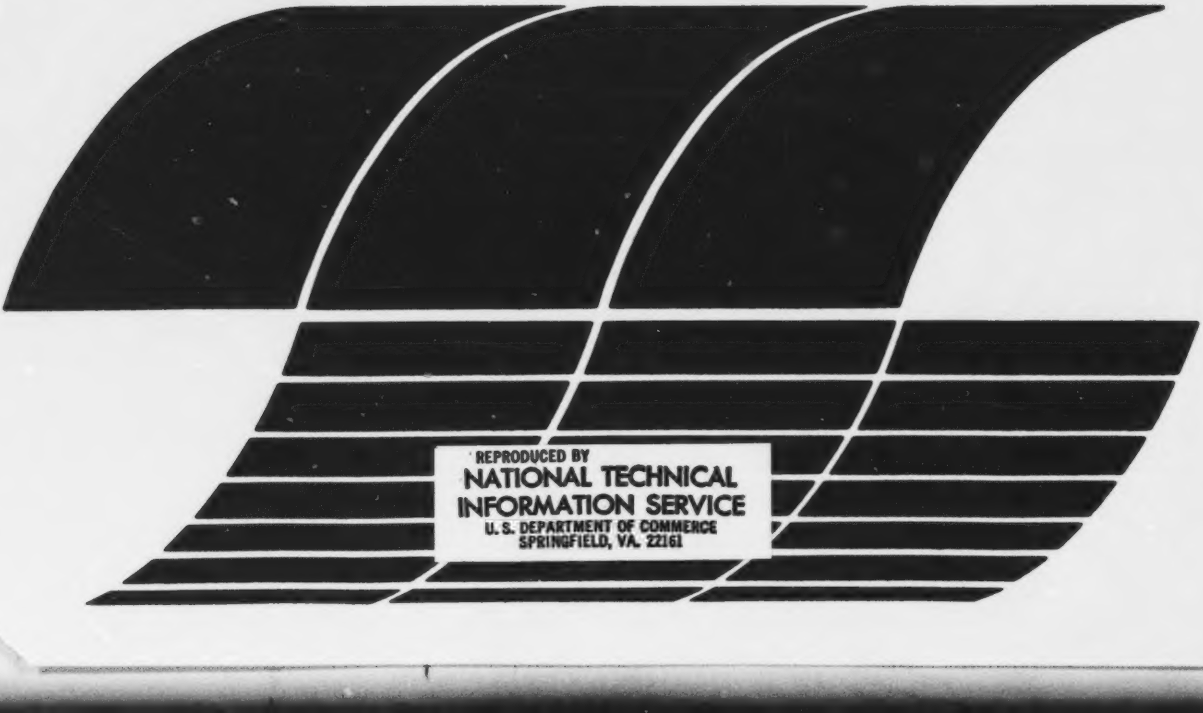

REPRODUCED BY
NATIONAL TECHNICAL
INFORMATION SERVICE
U. S. DEPARTMENT OF COMMERCE
SPRINGFIELD, VA. 22161

RESEARCH REPORTING SERIES

Research reports of the Office of Research and Development, U.S. Environmental Protection Agency, have been grouped into nine series. These nine broad categories were established to facilitate further development and application of environmental technology. Elimination of traditional grouping was consciously planned to foster technology transfer and a maximum interface in related fields. The nine series are:

1. Environmental Health Effects Research
2. Environmental Protection Technology
3. Ecological Research
4. Environmental Monitoring
5. Socioeconomic Environmental Studies
6. Scientific and Technical Assessment Reports (STAR)
7. Interagency Energy-Environment Research and Development
8. "Special" Reports
9. Miscellaneous Reports

This report has been assigned to the INTERAGENCY ENERGY-ENVIRONMENT RESEARCH AND DEVELOPMENT series. Reports in this series result from the effort funded under the 17-agency Federal Energy/Environment Research and Development Program. These studies relate to EPA's mission to protect the public health and welfare from adverse effects of pollutants associated with energy systems. The goal of the Program is to assure the rapid development of domestic energy supplies in an environmentally-compatible manner by providing the necessary environmental data and control technology. Investigations include analyses of the transport of energy-related pollutants and their health and ecological effects; assessments of, and development of, control technologies for energy systems; and integrated assessments of a wide range of energy-related environmental issues.

EPA REVIEW NOTICE

This report has been reviewed by the participating Federal Agencies, and approved for publication. Approval does not signify that the contents necessarily reflect the views and policies of the Government, nor does mention of trade names or commercial products constitute endorsement or recommendation for use.

This document is available to the public through the National Technical Information Service, Springfield, Virginia 22161.

EPA-600/7-79-044c

February 1979

Symposium on the Transfer and Utilization of Particulate Control Technology:

Volume 3. Scrubbers, Advanced Technology, and HTP Applications

by

F.P. Venditti, J.A. Armstrong, and Michael Durham

Denver Research Institute
P.O. Box 10127
Denver, Colorado 80208

Grant No. R805725
Program Element No. EHE624

EPA Project Officer: Dennis C. Drehmel

Industrial Environmental Research Laboratory
Office of Energy, Minerals, and Industry
Research Triangle Park, NC 27711

Prepared for

U.S. ENVIRONMENTAL PROTECTION AGENCY
Office of Research and Development
Washington, DC 20460

i.a

ABSTRACT

The papers in these four volumes of Proceedings were presented at the Symposium on the Transfer and Utilization of Particulate Control Technology, held in Denver, Colorado during 24 July through 28 July 1978 sponsored by the Particulate Technology Branch of the Industrial Environmental Research Laboratory of the Environmental Protection Agency and hosted by the Denver Research Institute of the University of Denver.

The purpose of the symposium was to bring together researchers, manufacturers, users, government agencies, educators and students to discuss new technology and to provide an effective means for the transfer of this technology out of the laboratories and into the hands of the users.

The three major categories of control technologies, electrostatic precipitators, scrubbers, and fabric filters were the major concern of the symposium. These technologies were discussed from the perspectives of economics; new technical advancements in science and engineering; and applications. Several papers dealt with combinations of devices and technologies, leading to a concept of using a systems approach to particulate control rather than device control.

These proceedings are divided into four volumes, each volume containing a set of related session topics to provide easy access to a unified technology area.

TABLE OF CONTENTS

Volumes 1 through 4

VOLUME I

ELECTROSTATIC PRECIPITATORS

Section A - ESP's for Coal Fired Boilers

Page

ELECTROSTATIC PRECIPITATOR PERFORMANCE
J. P. Gooch 1

SPECIFICATIONS OF A RELIABLE PRECIPITATOR
R. L. Williams 19

EXPERIENCE WITH COLD SIDE PRECIPITATORS ON LOW SULFUR COALS
S. Maartmann 25

A PERFORMANCE ANALYSIS OF A HOT-SIDE ELECTROSTATIC PRECIPITATOR
G. H. Marchant, J. P. Gooch, L. E. Sparks 39

AIR FLOW MODEL STUDIES FOR ELECTROSTATIC PRECIPITATORS
H. L. Engelbrecht 57

Section B - Flue Gas Conditioning for ESP'S

CHEMICAL CONDITIONING OF FLY ASH FOR HOT-SIDE PRECIPITATION
P. B. Lederman, P. B. Bibbo, J. Bush 79

CONDITIONING OF DUST WITH WATER-SOLUBLE ALKALI COMPOUNDS
H. H. Petersen 99

CHEMICAL ENHANCEMENT OF ELECTROSTATIC PRECIPITATOR EFFICIENCY
R. P. Bennett, A. E. Kober 113

METHOD AND COST ANALYSIS OF ALTERNATIVE COLLECTORS FOR LOW SULFUR COAL FLY ASH
E. W. Breisch 121

Page

BENCH-SCALE EVALUATION OF DRY ALKALIS FOR REMOVING SO_2 FROM BOILER FLUE GASES
N. D. Shah, D. P. Teixeira and L. J. Muzio 131

ANALYSIS OF THERMAL DECOMPOSITION PRODUCTS OF FLUE GAS CONDITIONING AGENTS
H. K. Dillon and E. B. Dismukes 155

FLUE GAS CONDITIONING EFFECTS ON ELECTROSTATIC PRECIPITATORS
R. Patterson, R. Riersgard, R. Parker and L. E. Sparks 169

FLUE GAS CONDITIONING AT ARIZONA PUBLIC SERVICE COMPANY FOUR CORNERS UNIT NO. 4
R. E. Pressey, D. Osborn and E. Cole 179

SODIUM CONDITIONING TEST WITH EPA MOBILE ESP
S. P. Schliesser 205

Section C - Novel Electrostatic Precipitators

NOVEL ELECTRODE CONSTRUCTION FOR PULSE CHARGING
S. Masuda 241

PULSED ENERGIZATION FOR ENHANCED ELECTROSTATIC PRECIPITATION IN HIGH-RESISTIVITY APPLICATIONS
P. L. Feldman and H. I. Milde 253

A NEW PRECHARGER FOR TWO-STAGE ELECTROSTATIC PRECIPITATION OF HIGH RESISTIVITY DUST
D. H. Pontius, P. V. Bush and L. E. Sparks 275

ELECTRON BEAM IONIZATION FOR COAL FLY ASH PRECIPITATORS
R. H. Davis and W. C. Finney 287

WIDE SPACING E.P. IS AVAILABLE IN CLEANING EXHAUST GASES FROM INDUSTRIAL SOURCES
R. Ito and K. Takimoto 297

Section D - Fundamentals--Electrical and Particle Characteristics

Page

DESCRIPTION OF A MATHEMATICAL MODEL OF ELECTROSTATIC PRECIPITATION
J. R. McDonald and L. E. Sparks 307

BACK DISCHARGE PHENOMENA IN ELECTROSTATIC PRECIPITATION
S. Masuda 321

MEASUREMENT OF EFFECTIVE ION MOBILITIES IN A CORONA DISCHARGE IN INDUSTRIAL FLUE GASES
J. R. McDonald, S. M. Banks and L. E. Sparks 335

PILOT SCALE ELECTROSTATIC PRECIPITATORS AND THE ELECTRICAL PERFORMANCE DIAGRAM
K. J. McLean and R. B. Kahane 349

THEORETICAL STUDY OF PARTICLE CHARGING BY UNIPOLAR IONS
D. H. Pontius, W. B. Smith and J. H. Abbott 361

AGING CAUSED INCREASE OF RESISTIVITY OF A BARRIER FILM AROUND GLASSY FLY ASH PARTICLES
W. J. Culbertson 373

ELECTROSTATIC PRECIPITATORS: THE RELATIONSHIP OF ASH RESISTIVITY AND PRECIPITATOR ELECTRICAL OPERATING PARAMETERS
H. W. Spencer, III 381

A TECHNIQUE FOR PREDICTING FLY ASH RESISTIVITY
R. E. Bickelhaupt 395

ELECTRICAL PROPERTIES OF THE DEPOSITED DUST LAYER WHICH ARISE BECAUSE OF ITS PARTICULATE STRUCTURE
K. J. McLean 409

VOLTAGE AND CURRENT RELATIONSHIPS IN HOT SIDE ELECTROSTATIC PRECIPITATORS
D. E. Rugg and W. Patten 421

PRECIPITATOR EFFICIENCY FOR LOG-NORMAL DISTRIBUTIONS
P. Cooperman and G. D. Cooperman 433

Section E - Industrial Applications of ESP's

Page

ELECTROSTATIC PRECIPITATION USING IONIC WIND FOR VERY LOW RESISTIVITY DUSTS FROM HIGH TEMPERATURE FLUE GAS OF PETROLEUM-COKES CALCINING KILN
F. Isahaya 453

THE USE OF ELECTROSTATIC PRECIPITATORS FOR COLLECTION OF PARTICULATE MATTER FROM BARK AND WASTE WOOD FIRED BOILERS IN THE PAPER INDUSTRY
R. L. Bump 467

ROOF-MOUNTED ELECTROSTATIC PRECIPITATOR
S. Ito, S. Noso, M. Sakai and K. Sakai 485

POM EMISSIONS FROM COKE OVEN DOOR LEAKAGE AND THEIR CONTROL BY A WET ELECTROSTATIC PRECIPITATOR
R. E. Barrett, P. R. Webb, C. E. Riley and A. R. Trenholm 497

VOLUME II

FABRIC FILTERS AND CURRENT TRENDS IN CONTROL EQUIPMENT

Section A - Fabric Filters

Page

FABRIC FILTER USAGE IN JAPAN
K. Iinoya 1

PERFORMANCE OF A PULSE-JET FILTER AT HIGH FILTRATION VELOCITIES
D. Leith, M. W. First, M. Ellenbecker and D. D. Gibson 11

ELECTROSTATIC EFFECTS IN FABRIC FILTRATION
E. R. Frederick 27

EPA IN-HOUSE FABRIC FILTRATION R&D
J. H. Turner 45

ENVIRONMENTAL PROTECTION AGENCY MOBILE FABRIC FILTER PROGRAM - A COMPARISON STUDY OF UTILITY BOILERS FIRING EASTERN AND WESTERN COAL
B. Lipscomb 53

EVALUATION OF FELTED GLASS FILTER MEDIA UNDER SIMULATED PULSE JET OPERATING CONDITIONS
L. R. Lefkowitz 75

INFLUENCE OF FIBER DIAMETER ON PRESSURE DROP AND FILTRATION EFFICIENCY OF GLASS FIBER MATS
J. Goldfield and K. D. Gandhi 89

FUNDAMENTAL EXPERIMENTS OF FABRIC FILTERS
K. Iinoya and Y. Mori 99

A DUAL PURPOSE BAGHOUSE FOR PARTICLE CONTROL AND FLUE GAS DESULFURIZATION
S. J. Lutz 111

SIMULTANEOUS ACID GAS AND PARTICULATE RECOVERY
A. J Teller 119

Page

TECHNOLOGY OF FIBER GLASS FILTER FABRIC DESIGN
C. E. Knox, J. Murray and V. Schoeck 133

VERIFICATION OF PROJECTED FILTER SYSTEM DESIGN AND OPERATION
R. Dennis and H. A. Klemm 143

PRECIPITATORS? SCRUBBERS? OR BAGHOUSES? FOR SHAWNEE (WHY TVA IS INSTALLING BAGHOUSES)
J. A. Hudson 161

HIGH RATIO FABRIC FILTERS FOR UTILITY BOILERS
B. L. Arnold and B. Melville 183

RETRO-FITTING BAGHOUSES ON COAL-FIRED BOILERS - A CASE STUDY
J. M. Osborne and L. R. Cramer 197

MATCHING A BAGHOUSE TO A FOSSIL FUEL FIRED BOILER
D. W. Rolschau 211

START-UP, OPERATION AND PERFORMANCE TESTING OF FABRIC FILTER SYSTEM-HARRINGTON STATION, UNIT #2
G. Faulkner and K. L. Ladd 219

APPLYING HIGH VELOCITY FABRIC FILTERS TO COAL FIRED INDUSTRIAL BOILERS
J. D. McKenna, G. P. Greiner and K. D. Brandt 233

FABRIC FILTER RESEARCH AND DEVELOPMENT FOR PC BOILERS USING WESTERN COAL
D. A. Furlong, R. L. Ostop and P. Gelfand 247

A PILOT PLANT STUDY OF VARIOUS FILTER MEDIA APPLIED TO A PULVERIZED COAL-FIRED BOILER
J. C. Mycock 263

APPLICATION OF SLIP-STREAMED AIR POLLUTION CONTROL DEVICES ON WASTE-AS-FUEL PROCESSES
J. M. Bruck, C. J. Sawyer, F. D. Hall and T. W. Devitt 287

Section B - Current Trends in Control Equipment

ASSESSMENT OF THE COST AND PERFORMANCE OF PARTICULATE CONTROL DEVICES ON LOW-SULFUR WESTERN COALS
R. A. Chapman, T. F. Edgar and L. E. Sparks 297

ELECTROSTATIC PRECIPITATION IN JAPANESE STEEL INDUSTRIES
S. Masuda 309

INSTALLED COST PROJECTIONS OF AIR POLLUTION CONTROL EQUIPMENT IN THE U. S.
R. W. McIlvaine 319

DUST EMISSION CONTROL FOR STATIONARY SOURCES IN THE FEDERAL REPUBLIC OF GERMANY: STANDARDS OR PERFORMANCE, BEST AVAILABLE CONTROL TECHNOLOGY AND ADVANCED APPLICATIONS
G. Guthner 333

ENGINEERING MANAGEMENT TRENDS IN THE DESIGN OF PRECIPITATORS AND BAGHOUSES
S. Negrea 361

CONTROL OF PARTICULATES FROM COMBUSTION
J. H. Abbott and D. C. Drehmel 383

VOLUME III

SCRUBBERS, ADVANCED TECHNOLOGY, AND HTHP APPLICATIONS

Section A - Scrubbers

Page

ENTRAINMENT SEPARATORS FOR SLURRY SCRUBBERS
S. Calvert, H. F. Barbarika and L. E. Sparks 1

SCRUBBER DEMISTER TECHNOLOGY FOR CONTROL OF SOLIDS EMISSIONS FROM SO_2 ABSORBERS
W. Ellison 13

IMPROVED MIST ELIMINATOR PERFORMANCE THROUGH ADVANCED DESIGN CONCEPTS
R. P. Tennyson, S. F. Roe, and R. H. Lace 35

FINE PARTICLE COLLECTION IN A MOBILE BED SCRUBBER
S. Yung, R. Chmielewski, S. Calvert and D. Harmon 47

CONTROL OF PARTICULATE EMISSIONS WITH U.W. ELECTROSTATIC SPRAY SCRUBBER
M. J. Pilat and G. A. Raemhild 61

UNION CARBIDE'S HIGH INTENSITY IONIZER APPLIED TO ENHANCE A VENTURI SCRUBBER SYSTEM
M. T. Kearns and C. M. Chang 73

PERFORMANCE TESTS OF THE MONTANA POWER COMPANY COLSTRIP STATION FLUE GAS CLEANING SYSTEM
J. D. McCain 85

RESULTS OF THE TEST PROGRAM OF THE WEIR HORIZONTAL SCRUBBER AT FOUR CORNERS STEAM ELECTRIC STATION UNIT NO. FIVE
G. Bratzler, G. T. Gutierrez and C. F. Turton 99

MATERIALS PERFORMANCE PROBLEMS ASSOCIATED WITH THE SCRUBBING OF COKE OVEN WASTE HEAT FLUE GAS
M. P. Bianchi and L. A. Rosales 113

VENTURI SCRUBBER DESIGN MODEL
S. C. Yung, H. Barbarika, S. Calvert and L. E. Sparks 149

EXPERIMENTAL STUDY OF PARTICLE COLLECTION BY A VENTURI SCRUBBER DOWNSTREAM FROM AN ELECTROSTATIC PRECIPITATOR
G. H. Ramsey, L. E. Sparks and B. E. Daniels 161

Page

EFFECTS OF SURFACE TENSION ON PARTICLE REMOVAL
G. J. Woffinden, G. R. Markowski and D. S. Ensor 179

CONCLUSIONS FROM EPA SCRUBBER R&D
D. L. Harmon and L. E. Sparks 193

Section B - Advanced Technology

FINE PARTICLE EMISSION CONTROL BY HIGH GRADIENT MAGNETIC SEPARATION
C. H. Gooding and D. C. Drehmel 219

THE USE OF ACOUSTIC AGGLOMERATORS FOR PARTICULATE CONTROL
J. Wegrzyn, D. T. Shaw and G. Rudinger 233

ANALYTICAL AND EXPERIMENTAL STUDIES ON GRANULAR BED FILTRATION
C. Gutfinger, G. I. Tardos and N. Abuaf 243

THE EFFECTS OF ELECTRIC AND ACOUSTIC FIELDS ON THE COLLISION RATES OF SUBMICRON SIZED DOP AEROSOL PARTICLES
P. D. Scholz, L. W. Byrd and P. H. Paul 279

ELECTROSTATIC SEPARATION IN CYCLONES
W. B. Giles 291

EVALUATION OF THE ELECTRIFIED BED PROTOTYPE COLLECTOR ON AN ASPHALT ROOFING PLANT
R. M. Bradway, W. Piispanen, and V. Shortell 303

EVALUATION OF AN APITRON ELECTROSTATICALLY AUGMENTED FABRIC FILTER
J. D. McCain, P. R. Cavenaugh, L. G. Felix and R. L. Merritt 311

CORONA ELECTRODE FAILURE ANALYSIS
R. E. Bickelhaupt and W. V. Piulle 323

HIGH TEMPERATURE AND HIGH VELOCITY POROUS METAL GAS FILTRATION MEDIA
L. J. Ortino and R. M. Bethea 341

DRY DUST COLLECTION OF BLAST FURNACE EXHAUST GAS BY MOVING GRANULAR BED FILTER
H. Kohama, K. Sasaki, S. Watanabe and K. Sato 351

Page

CERAMIC FILTER, SCRUBBER AND ESP
R. A. Clyde 361

Section C - High Temperature High Pressure Applications

FUNDAMENTAL PARTICLE COLLECTION AT HIGH TEMPERATURE AND PRESSURE
R. Parker, S. Calvert and D. Drehmel 367

PARTICULATE CONTROL FOR FLUIDIZED BED COMBUSTION
D. F. Becker and M. G. Klett 379

HIGH TEMPERATURE GLASS ENTRAINMENT OF FLY ASH
W. Fedarko, A. Gatti and L. R. McCreight 395

A.P.T. DRY SCRUBBER FOR PARTICLE COLLECTION AT HIGH TEMPERATURE AND PRESSURE
R. Patterson, S. Calvert, S. Yung and D. Drehmel 405

ELECTROSTATIC PRECIPITATION AT HIGH TEMPERATURE AND PRESSURE: CAPABILITIES, CURIOUSITIES AND QUESTIONS
M. Robinson 415

HIGH TEMPERATURE, HIGH PRESSURE ELECTROSTATIC PRECIPITATION
J. R. Bush, P. L. Feldman and M. Robinson 417

BARRIER FILTRATION FOR HTHP PARTICULATE CONTROL
M. A. Shackleton and D. C. Drehmel 441

AEROSOL FILTRATION BY GRANULAR BEDS
S. L. Goren 459

PERFORMANCE CHARACTERISTICS OF MOVING-BED GRANULAR FILTERS
J. Geffken, J. L. Guillory and K. E. Phillips 471

VOLUME IV

FUGITIVE DUSTS AND SAMPLING, ANALYSIS AND CHARACTERIZATION OF AEROSOLS

Section A - Fugitive Dusts

Page

FUGITIVE SULFUR IN COAL-FIRED POWERPLANT PLUMES
R. F. Pueschel 1

RESEARCH IN WIND-GENERATED FUGITIVE DUST
D. A. Gillette and E. M. Patterson 11

DEVELOPING CONTROL STRATEGIES FOR FUGITIVE DUST SOURCES
G. Richard and D. Safriet 25

STATE OF CONTROL TECHNOLOGY FOR INDUSTRIAL FUGITIVE PROCESS PARTICULATE EMISSIONS
D. C. Drehmel, D. P. Daugherty and C. H. Gooding 47

FUGITIVE DUST EMISSIONS AND CONTROL
B. H. Carpenter and G. E. Weant 63

SETTING PRIORITIES FOR THE CONTROL OF PARTICULATE EMISSIONS FROM OPEN SOURCES
J. S. Evans, D. W. Cooper, M. Quinn and M. Schneider 85

USE OF ELECTROSTATICALLY CHARGED FOG FOR CONTROL OF FUGITIVE DUST, SMOKE AND FUME
S. A. Hoenig 105

COLLECTION AND CONTROL OF MOISTURE LADEN FUGITIVE DUST
C. D. Turley 131

Section B - Sampling, Analysis, and Characterization of Aerosols

THE VISIBILITY IMPACT OF SMOKE PLUMES
D. S. Ensor 141

MUTAGENICITY OF COAL FLY ASH
C. E. Chrisp 153

Page

BIO-ASSESSMENT OF CHRONIC MANGANESE INGESTION IN RATS
G. L. Rehnberg, D. F. Cahill, J. A. Elder, E. Gray and J. W. Laskey 159

THE USE OF SHORT TERM BIOASSAY SYSTEMS IN THE EVALUATION OF ENVIRONMENTAL PARTICULATES
N. E. Garrett, J. A. Campbell, J. L. Huisingh and M. D. Waters 175

A KINETIC AEROSOL MODEL FOR THE FORMATION AND GROWTH OF SECONDARY SULFURIC ACID PARTICLES
P. Middleton and C. S. Kiang 187

PARTICLE GROWTH BY CONDENSATION AND BY COAGULATION--BASIC RESEARCH OF ITS APPLICATION TO DUST COLLECTION
T. Yoshida, Y. Kousaka, K. Okuyama and K. Sumi 195

TRANSIENT CHEMISORPTION OF A SOLID PARTICLE IN A REACTIVE ATMOSPHERE OF RECEDING GAS CONCENTRATION
R. Wang 213

STABILITY OF FINE WATER DROPLET CLOUDS
Y. Kousaka, K. Okuyama, K. Sumi and T. Yoshida 231

PARTICLE SIZE ANALYSIS OF AEROSOLS INCLUDING DROPLET CLOUDS BY SEDIMENTATION METHOD
Y. Kousaka, K. Okuyama and T. Yoshida 249

PARTICLE MASS DISTRIBUTION AND VISIBILITY CONSIDERATIONS FOR LARGE POWER PLANTS
T. L. Montgomery and J. C. Burdick III 261

AN OPTICAL INSTRUMENT FOR DILUTE PARTICLE FIELD MEASUREMENTS
W. D. Bachalo 275

IMPACT OF SULFURIC ACID EMISSIONS ON PLUME OPACITY
J. S. Nader and W. D. Conner 289

PARTICLE CHARGE EFFECTS ON CASCADE IMPACTOR MEASUREMENTS
R. Patterson, P. Riersgard and D. Harmon 307

A HIGH-TEMPERATURE HIGH-PRESSURE, ISOKINETIC-ISOTHERMAL SAMPLING SYSTEM FOR FOSSIL FUEL COMBUSTION APPLICATIONS
J. C. F. Wang, R. R. Boericke and R. A. Fuller 319

Page

A PROTOTYPE OPTICAL SCATTERING INSTRUMENT FOR PARTICULATE SIZING IN STACKS
A. L. Wertheimer, W. H. Hart and M. N. Trainer 337

UTILIZATION OF THE OMEGA-1 LIDAR IN EPA ENFORCEMENT ACTIVITIES
A. W. Dybdahl and M. J. Cunningham 347

THE MONITORING OF PARTICULATES USING A BALLOON-BORNE SAMPLER
J. A. Armstrong and P. A. Russell 357

A STUDY OF PHILADELPHIA PARTICULATES USING MODELING AND MEASUREMENT TECHNIQUES
F. A. Record, R. M. Bradway and W. E. Belanger 377

DECISION-TREE ANALYSIS OF THE RELATIONSHIP BETWEEN TSP CONCENTRATION AND METEOROLOGY
J. Trijonis and Y. Horie 391

DESIGNING A SYSTEMATIC REGIONAL PARTICULATE ANALYSIS
J. A. Throgmorton, K. Axetell and T. G. Pace 403

IMPORTANCE OF PARTICLE SIZE DISTRIBUTION
L. E. Sparks 417

THE MORPHOGENESIS OF COAL FLY ASH
G. L. Fisher 433

THE EFFECT OF TEMPERATURE, PARTICLE SIZE AND TIME EXPOSURE ON COAL-ASH AGGLOMERATION
K. C. Tsao, J. F. Bradley and K. T. Yung 441

TEST PROGRAM TO UPDATE EQUIPMENT SPECIFICATIONS AND DESIGN CRITERIA FOR STOKER FIRED BOILERS
S. C. Schaeffer 457

TRACE ELEMENT EMISSIONS FROM COPPER SMELTERS
R. L. Meek and G. B. Nichols 465

AUTHOR NAME	PAGE
Abbott, James H.	I-361, II-383
Abuaf, Nesim	III-243
Armstrong, James A.	IV-357
Arnold, B. L.	II-183
Axetell, Kenneth W.	IV-403
Bachalo, William D.	IV-275
Banks, Sherman M.	I-335
Barbarika, Harry F.	III-1, III-149
Barrett, Richard E.	I-497
Becker, David F.	III-379
Belanger, William E.	IV-377
Bennett, Robert P.	I-113
Bethea, Robert M.	III-341
Bianchi, M. P.	III-113
Bibbo, P. B.	I-79
Bickelhaupt, Roy E.	I-395, III-323
Boericke, Ralph R.	IV-319
Bradley, Jeffrey F.	IV-441
Bradway, Robert M.	III-303, IV-377
Brandt, Kathryn D.	II-233
Bratzler, Gene E.	III-99
Breisch, Edgar W.	I-121
Bruck, John M.	II-287

AUTHOR NAME	PAGE
Bump, Robert L.	I-467
Burdick, J. Clement	IV-261
Bush, John R.	I-79, III-417
Bush, P. V.	I-275
Byrd, Larry W.	III-279
Cahill, D. F.	IV-159
Calvert, Seymour	III-1, III-47, III-149 III-367 III-405
Campbell, James A.	IV-175
Carpenter, B. H.	IV-63
Cavenaugh, Paul R.	III-311
Chang, C. M.	III-73
Chapman, Richard A.	II-297
Chmielewski, Richard D.	III-47
Chrisp, Clarence E.	IV-153
Clyde, Robert A.	III-361
Cole, Edward A.	I-179
Conner, William D.	IV-289
Cooper, Douglas W.	IV-85
Cooperman, Gene D.	I-433
Cooperman, Phillip	I-433
Cramer, Larry R.	II-197
Culbertson, William J.	I-373
Cunningham, Michael J.	IV-347

AUTHOR NAME	PAGE
Daniels, B. E.	III-161
Daugherty, David P.	IV-47
Davis, Robert H.	I-287
Dennis, Richard	II-143
Devitt, Timothy W.	II-287
Dillon, H. Kenneth	I-155
Dismukes, Edward B.	I-155
Drehmel, Dennis C.	II-383, III-219, III-367 III-405, III-441, IV-47
Dybdahl, Arthur W.	IV-347
Edgar, Thomas F.	II-297
Elder, J. A.	IV-159
Ellenbecker, Michael	II-11
Engelbrecht, Heinz L.	I-57
Ensor, David S.	III-179, IV-141
Evans, John S.	IV-85
Faulkner, George	II-219
Fedarko, William	III-395
Feldman, Paul L.	I-253, III-417
Felix, Larry G.	III-311
Finney, Wright C.	I-287
First, Melvin W.	II-11
Fisher, Gerald L.	IV-433
Frederick, Edward R.	II-27

AUTHOR NAME	PAGE
Fuller, R. A.	IV-319
Furlong, Dale A	II-247
Gandhi, Kumud	II-89
Garrett, Neil E.	IV-175
Gatti, Arno	III-395
Geffken, John	III-471
Gelfand, Peter	II-247
Gibson, Dwight D.	II-11
Giles, Walter B.	III-291
Gillette, Dale A.	IV-11
Goldfield, Joseph	II-89
Gooch, John P.	I-1, I-39
Gooding, Charles H.	III-219, IV-47
Goren, Simon L.	III-459
Gray, E.	IV-159
Greiner, Gary P.	II-233
Guthner, Gerhard O.	II-333
Guillory, J. L.	III-471
Gutfinger, Chaim	III-243
Gutierrez, Gilbert T.	III-99
Hall, Fred D.	II-287
Harmon, D. L.	III-47, III-193, IV-307
Hart, W. H.	IV-337

AUTHOR NAME	PAGE
Hoenig, Stuart A.	IV-105
Horie, Yuji	IV-391
Hudson, J. A.	II-161
Huisingh, Joellen L.	IV-175
Iinoya, Koichi	II-1, II-99
Isahaya, Fumio	I-453
Ito, Shijo	I-485
Ito, Ryozo	I-297
Kahane, Ronald B.	I-349
Kearns, Michael T.	III-73
Kiang, C. S.	IV-187
Klemm, Hans A.	II-143
Klett, Michael G.	III-379
Knox, Charles	II-133
Kober, Alfred E.	I-113
Kohama, Hiroyuki	III-351
Kousaka, Yasuo	IV-195, IV-231, IV-249
Lace, Robert H.	III-35
Ladd, Kenneth L.	II-219
Laskey, J. W.	IV-159
Lederman, Peter B.	I-79
Lefkowitz, Leonard R.	II-75
Leith, David	II-11

AUTHOR NAME	PAGE
Liscomb, Bill	II-53
Lutz, Stephen J.	II-111
Maartmann, Sten	I-25
Marchant, G. H.	I-39
Markowski, Gregory R.	III-179
Masuda, Senichi	I-241, I-321, II-309
McCain, Joseph D.	III-85, III-311
McCreight, Louis R.	III-395
McDonald, Jack R.	I-307, I-335
McIlvanine, Robert W.	II-319
McKenna, John D.	II-233
McLean, Kenneth J.	I-349, I-409
Meek, Richard L.	IV-465
Melville, B.	II-183
Merritt, Randy L.	III-311
Middleton, Paulette	IV-187
Milde, Helmut I.	I-253
Montgomery, Thomas L.	IV-261
Mori, Yasushige	II-99
Murray, Joel	II-133
Muzio, L. J.	I-131
Mycock, John C.	II-263
Nader, John S.	IV-289

AUTHOR NAME	PAGE
Negrea, Stefan	II-361
Nichols, Grady B.	IV-465
Noso, Shigeyuki	I-485
Okuyama, K.	IV-195, IV-231, IV-249
Ortino, Leonard J.	III-341
Osborn, D. A.	I-179
Osborne, J. Michael	II-197
Ostop, Ronald L.	II-247
Pace, Thompson G.	IV-403
Parker, Richard D.	I-169, III-367
Patten, Whitney	I-421
Patterson, Edward M.	IV-11
Patterson, Ronald G.	I-169, III-405, IV-307
Paul, Phillip H.	III-279
Petersen, Hoegh H.	I-99
Phillips, K. E.	III-471
Piispanen, William	III-303
Pilat, Michael J.	III-61
Piulle, Walter V.	III-323
Pontius, D. H.	I-275, I-361
Pressey, Robert E.	I-179
Pueschel, Rudolf F.	IV-1
Quinn, Margaret	IV-85

AUTHOR NAME	PAGE
Raemhild, Gary A.	III-61
Ramsey, Geddes H.	III-161
Record, Frank A.	IV-377
Rehnberg, Georgia L.	IV-159
Richard, George	IV-25
Riersgard, Phillip	I-169, IV-307
Riley, Clyde E.	I-497
Robinson, Myron	III-415, III-417
Roe, Sheldon F.	III-35
Rolschau, David W.	II-211
Rosales, L. A.	III-113
Rudinger, G.	III-233
Rugg, Don	I-421
Russell, Phillip A.	IV-357
Safriet, Dallas W.	IV-25
Sakai, Kiyoshi	I-485
Sakai, Masakazy	I-485
Sasaki, K.	III-351
Sato, K.	III-351
Sawyer, Charles J.	II-287
Schaeffer, Stratton C.	IV-457
Schliesser, Steven P.	I-205
Schneider, Maria	IV-85

AUTHOR NAME	PAGE
Schoeck, Vincent	II-133
Scholz, Paul D.	III-279
Shackleton, Michael A.	III-441
Shah, N. D.	I-131
Shaw, David T.	III-233
Shortell, Verne	III-303
Smith, Wallace B.	I-361
Sparks, Leslie E.	I-39, I-169, I-275 I-307, I-335 II-297 III-1, III-149, III-162 III-193, IV-417
Spencer, Herbert W.	I-381
Sumi, K.	IV-195, IV-231
Takimoto, Ken	I-297
Tardos, Gabriel I.	III-243
Teixeira, D. P.	I-131
Teller, Aaron J.	II-119
Tennyson, Richard P.	III-35
Throgmorton, James A.	IV-403
Trainer, M. N.	IV-337
Trenholm, Andrew R.	I-497
Trijonis, John C.	IV-391
Turner, James H.	II-45
Tsao, Keh C.	IV-441
Turley, C. David	IV-131

AUTHOR NAME	PAGE
Turton, C. F.	III-99
Wang, James	IV-319
Wang, Roa-Ling	IV-213
Watanabe, S.	III-351
Waters, Michael D.	IV-175
Weant, George E.	IV-63
Webb, Paul R.	I-497
Wegrzyn, J.	III-233
Wertheimer, Alan L.	IV-337
Williams, Roger L.	I-19
Woffinden, George J.	III-179
Yoshida, T.	IV-195, IV-231, IV-249
Yung, Kuang T.	IV-441
Yung, Shui-Chow	III-47, III-149, III-405

ENTRAINMENT SEPARATORS FOR SLURRY SCRUBBERS

S. Calvert and H. F. Barbarika
Air Pollution Technology, Inc.
San Diego, California

and

L. E. Sparks
Industrial Environmental Research Laboratory
U. S. Environmental Protection Agency
Research Triangle Park, North Carolina

INTRODUCTION

Gas scrubbers create mist while collecting particles. This mist is entrained by the gas to an extent depending on the type of scrubber and the operating conditions. The entrained drops carry dissolved and suspended solids which will constitute a particulate emission if they are carried out of the stack. It is always important, sometimes overwhelmingly so, to separate this entrainment from the gas before it is emitted to the atmosphere.

Air Pollution Technology, Inc. (A.P.T.) has performed research and development on entrainment separators under several Environmental Protection Agency (E.P.A.) contracts. The work has been reported in the "Scrubber Handbook" and other reports and papers by Calvert et al.[1,2,3,4,5,6].

This paper deals with further work on entrainment separators applicable to scrubbers which use liquid containing suspended solids. An entrainment separator design which would be least affected by solids deposits and would be easiest to wash was chosen for study. The basic design selected was the discontinuous zigzag baffle; it was tested in several configurations in order to develop an optimum design.

A major purpose of the work was to determine the amount and drop size distribution of entrainment from scrubbers. To do this, a pilot-scale scrubber/entrainment separator system was built. The scrubber section was replaceable so that the mobile bed, sieve plate, and spray scrubbers could be tested.

Another objective was to determine the performance characteristics of the entrainment separator (E.S.) when used on entrainment from actual scrubbers. This was accomplished by measuring the drop size distributions and total liquid loading upstream and downstream of the E.S. during the pilot-scale scrubber/E.S. system operation. Results of these measurements have recently been presented[7].

Finally, the performance of the E.S. during slurry scrubber operation was determined and the optimum washing system developed. This phase of the work has recently been completed and is the primary subject of this paper.

PILOT PLANT

The pilot plant was a scaled-down representation of an industrial scrubber/E.S. system. The design gas flow rate was a minimum of 1.42 m^3/s (3,000 cfm) and was 50 percent higher when the system pressure drop was low enough. Windows and special sampling conveniences were included in the system. The system is shown schematically in Figure 1.

Location of the E.S. in a horizontal duct was an important design feature. Previous work[5] had demonstrated that a configuration with the gas flowing horizontally and the drainage surfaces in vertical planes was least subject to reentrainment. The E.S. designed for horizontal gas flow was therefore able to handle the highest entrainment loading and gas velocity for its size.

The scrubber/E.S. system was designed with enough vertical height between the scrubber and the E.S. so that complete disengagement of the large drops could occur. The loading on the E.S. is consequently greatly decreased without using any energy.

Finally, because of the system design a preseparator was easily incorporated in the form of the turning vanes in the elbow transition between the vertical scrubber and the horizontal E.S. duct. The turning vanes collect a considerable amount of the large size entrainment which would either settle on the horizontal duct or overload the E.S.

The purpose of designing the system to have a disengagement space, a turning vane preseparator, and a short horizontal run was to minimize the loading on the E.S. If the loading is too great, the E.S. begins reentraining and its performance is seriously degraded. Detailed information on the effects of and conditions for reentrainment has been provided[3].

E.S. Design

The E.S. was a discontinuous zigzag baffle type, containing up to six rows in two configurations. One configuration was vertical and the other was forward sloping (30° from the vertical). The baffles were type 304 stainless steel in row modules so that any number of rows from one to six could be used. Figure 2 is a plan view of the baffles. The duct containing the E.S. was 61 cm (24 in.) high and 51 cm (20 in.) wide. The lower front edge of the first row was located 2.35 m horizontally downstream from the transition section.

Scrubber Operating Conditions

Two types of scrubbers were used to generate slurry entrainment: sieve plate and spray. A single sieve plate was operated at two conditions, as shown in Table 1; the spray scrubber was operated with two types of nozzles, as shown in Table 2.

Slurry

The slurry consisted of commercially available fine limestone ($CaCO_3$) powder, nominally 325 mesh size. When sized with a Coulter counter the mass median particle diameter was found to be 12 μm. The particle density of $CaCO_3$ is 2.7 g/cm^3.

SOLIDS DEPOSITION

The character of the solids deposition on the zigzag baffle surfaces was determined by operating the pilot system in a normal manner with slurry. For each condition the scrubber was operated approximately 7 hours per day for at least 7 days. The slurry was well stirred before starting each day and it was sampled twice a day for concentration.

Experimental Results

At the end of a run set the entrainment separator (E.S.) baffles were removed, inspected, and photographed. The deposits were nonuniform in most cases, but average thickness could be estimated. These average deposit thicknesses were used to determine a rate of deposition, or a thickness buildup rate for each run set. Figures 3 and 4 present the average thickness rates for spray scrubber and sieve plate scrubber operation, respectively. The thickness rate has been normalized for a 10 percent slurry for comparison purposes. Curves have been drawn for the average of each row that had a measurable deposit.

The first three rows of the E.S. during spray scrubber operation had no deposit except for 1 or 2 cm at the top leading edge. There was no measurable deposit on the rear surfaces of the baffles of any row. Based on the thickness rates shown in Figures 3 and 4, it would take at least 100 hours of operation before the deposits became thick enough to affect the pressure drop.

Table 1. SIEVE PLATE SCRUBBER
OPERATING CONDITIONS

Single plate
Located 1.47 m below horizontal section

1. Low ΔP Operation

   Gas flow rate = 0.71 m^3/s (1,500 cfm)
   Water flow rate = 8-9.5 ℓ/s (125-150 gpm)
   Pressure drop ≈ 11 cm W.C.

2. High ΔP Operation

   Gas flow rate = 1.04 m^3/s (2,200 cfm)
   Water flow rate = 8-9.5 ℓ/s (125-150 gpm)
   Pressure drop ≈ 23 cm W.C.

Table 2. SPRAY SCRUBBER
OPERATING CONDITIONS

Cocurrent operation, nozzles located 2.13 m below horizontal section
Scrubber cross sectional area = 0.581 m^2 (6.25 ft^2)
Gas flow rate = 1.42 m^3/s (3,000 cfm)

Nozzle Type:	Spraying Sys. Whirljet	Bete Spiral
Model No.	1/2-B-50	3/4-ST-24-FCN
Pressure:	207 kPa (30 psig)	69 kPa (10 psig)
Flow Rate:	5 ea - 2.68 ℓ/s, total	4 ea - 2.82 ℓ/s, total

Solids deposition was significant in only one other location in the pilot system: the horizontal section upstream of the E.S. had to be flushed periodically to clear solids built-up on its floor. Because no significant deposit occurred on the turning vanes, they were not flushed.

Comparison with Solids Deposition Model

Using a laboratory scale apparatus, Calvert et al.[3] derived an empirical equation for the solids deposition rate. We have modified the model slightly to account for slurry particle size and to account for the deposition occurring while the dry baffle surface is being wetted. The equation for deposition rate is,

$$R_s = W \Phi \exp [-k(\delta - d_{pg})] \qquad (1)$$

where $k = 0.13 + 0.53\Phi$, μm^{-1} (2)

R_s = solid deposition rate on a vertical flat surface, mg/cm^2-s

W = weight fraction of solid in slurry

Φ = slurry flux, mg/cm^2-s

δ = laminar liquid film thickness, μm

d_{pg} = slurry particle mass median diameter, μm

The laminar film thickness is,

$$\delta = \left(\frac{3 \mu_L h \Phi}{1{,}000 \rho_L{}^2 g} \right)^{1/3} \times 10^4 \qquad (3)$$

Equation (1) applies when $\delta \geq d_{pg}$, but when $\delta < d_{pg}$:

$$R_s = W \Phi \qquad (4)$$

The thickness rate is related to the deposition rate by

$$\tau = \frac{36 R_s}{\rho_s} \qquad (5)$$

where τ = thickness rate, mm/hour

ρ_s = solid deposit density, g/cm^3

At the start of each daily run the deposit on the baffle surface is dry. Before any slurry will run off the surface it must be wetted. To account for the solids deposition occurring during this initial wetting of the surface, the following equation has been derived:

$$\tau' = \tau(1 + f_\tau)^m \tag{6}$$

where τ' = corrected thickness rate, mm/hour

m = number of times the dry surface is wetted

and

$$f_\tau = \frac{\varepsilon f_v}{1 - f_v - \varepsilon} \tag{7}$$

with ε = porosity of surface deposit, fraction

f_v = volume fraction of slurry particles in the slurry, fraction

The slurry flux, Φ, was not measured directly. It was calculated based on the entrainment loading and size distribution, and the penetration through the various rows of the E.S. The penetration model was essentially that derived by Calvert et al.[2,3]. The calculated slurry flux for the operating conditions of the spray and sieve plate scrubbers are given in Table 3.

The model is compared with the data in Figures 5 and 6 for the 5-nozzle spray scrubber and the sieve plate scrubber, respectively. The agreement is fairly good for row 6 of the spray scrubber run and row 3 of the sieve scrubber run where the deposit was the most uniform. A significant underestimate is evident for row 5 of the spray scrubber operation and row 2 of the sieve plate operation. It appears that "end effects" or the effects of the ceiling and the end construction of the baffles have caused a downward shift of the location of heaviest deposit. Another real effect causing this shift is gravity which reduces the entrainment loading somewhat on the top few centimeters of the baffles. Also, the higher than predicted deposit thickness could be caused by periods of unsaturated operation.

Should the water drops be evaporating within or upstream of the E.S., the liquid film thickness on the baffle would decrease below that predicted by equation (3). A thinner liquid film would cause a higher deposition rate. The humidity was monitored closely and on days with low ambient humidity an extra fog nozzle was used upstream of the scrubber to keep the air as nearly saturated as possible.

Conclusions

Because of the nonideal flow pattern at the top of the E.S., the nonuniform concentration of drops due to gravity, and some periods of

Table 3. CALCULATED SLURRY FLUX ON ROWS 1 THROUGH 6

Scrubber	u_G in E.S.	Total Loading	d_{dg}	σ_g	Φ_1	Φ_2	Φ_3	Φ_4	Φ_5	Φ_6
	m/s	ml/m^3	μmA		mg/cm^2-s					
Spray-5	4.6	9.0	160	1.6	2.4	1.3	0.31	0.097	0.037	0.016
Spray-4	4.6	3.2	130	1.5	0.71	0.49	0.14	0.049	0.019	0.0086
Sieve-High	3.4	0.14	100	1.5	0.017	0.016	0.0066	0.0031	0.0015	0.0008

Table 4. TOTAL WASHING RATES FOR TYPICAL E.S. FOR 10 MINUTE OPERATION

	To Wash Row:					
	1	2	3	4	5	6
Wash Spray Flux						
ℓ/m^2-s	0.0074	0.039	0.26	0.95	2.49	5.36
gpm/ft^2	0.0109	0.057	0.39	1.40	3.67	7.89
Wash Spray L/G						
ℓ/m^3	0.0016	0.0084	0.057	0.207	0.54	1.16
gal./1,000 ft^3	0.0120	0.0626	0.430	1.55	4.05	8.71

unsaturated operation, the model underpredicted the solids deposition rate. It was accurate to within an order of magnitude and indicated correctly the rows of the E.S. which should have significant solids deposition. The model is thought to be adequate for design purposes.

WASHING SYSTEM

There is a strong possibility that an E.S. design will be unable to avoid solids deposition. Either the entrainment loading will be below that which is self-washing or it will be above the loading which causes an insignificant deposition. Thus, a washing system must be used.

An adequate washing system must not interfere with E.S. operation and should use a minimum amount of liquid, preferrably recycled slurry. We designed a system using several small spray nozzles in a manifold about 23 cm upstream of the E.S. The nozzles were operated at 210-350 kPa (30-50 psi) using slurry and produced drops with mass median diameters of 400 and 360 μm, respectively.

Experimental Results

The washing system was tested at the end of solids deposition runs and using artificially coated baffles. An intermittent mode was found to be satisfactory with the wash system being run for only 10 minutes during the cycle. The results of the wash system tests are shown in Figures 7 and 8, where the washing flux on each row of baffles is plotted against the percent of the surface cleaned. Since the "percent cleaned" may be somewhat subjective due to the nonuniformity of the deposit, these figures should be primarily used to determine the washing flux required for total cleaning. The washing flux was calculated from the liquid flow rate, the spray drop size distribution, the gas velocity, and the E.S. geometry, as described previously.

Comparison with Predictions

The slurry flux required for washing should be predictable using the solids deposition model. The minimum washing flux should correspond to a limiting negligible deposition rate or thickness rate.

From analysis of the solids deposition rate data for the spray scrubber operation, the minimum washing flux appeared to be about 0.1 mg/cm^2-s. This value applied for continuous washing and a superficial gas velocity of 4.6 m/s. Using the deposition model this slurry flux will cause a deposit thickness rate of 0.027 mm/hour at 5 cm from the top and 0.002 mm/hour at 20 cm for a slurry concentration of 10 percent.

For the 10 minute washing periods the minimum washing fluxes appeared to be 0.6 mg/cm^2-s for a superficial gas velocity of 3.4 m/s and 0.9 mg/cm^2-s for 2.3 m/s. The difference due to velocity is probably the result of more reentrainment from upstream rows at the higher velocity. The flux, Φ, calculation is conservative: it assumes no reentrainment. A slurry flux of 0.6 mg/cm^2-s corresponds to a thickness rate of 9.9×10^{-7} mm/hour at 5 cm and 1.0×10^{-11} mm/hour at 20 cm from the top. The rates are even lower at 0.9 mg/cm^2-s. These predicted thickness rates are truly negligible, but are based on continuous operation.

Design Criteria

The variable that determines the washing effectiveness is the washing flux on the baffles. It is a function of the total wash spray flux into the E.S. and the penetration of the spray drops through the preceding rows of baffles. Since the penetration is a function of the E.S. geometry, gas velocity, and the wash spray drop size distribution, the calculation of the flux is complicated.

In order to estimate the amount of washing required in a typical E.S. installation, we will assume the following typical conditions:

E.S. geometry - as we used (figure 2)

E.S. superficial gas velocity = 4.6 m/s (15 ft/s)

Spray drop size distribution

$d_{dg} = 400\ \mu m$

$\sigma_g = 2.2$

Washing duration = 10 minutes

Required washing flux, $\Phi_{wash} = 0.6\ mg/cm^2$-s

Table 4 presents the calculated total washing rates required upstream of the first row of baffles in order to provide washing of the specified row for the above conditions. Rows 4, 5 and 6 would probably require less washing than shown since there would be considerable reentrainment from preceding rows at these high liquid loadings. The amount of washing could be reduced by decreasing the gas velocity or lowering the spray drop size at the cost of E.S. efficiency or increased spray nozzle pressure, respectively. Washing rates may also be reduced by separating a 6-row E.S. into two 3-row modules, again at the cost of E.S. efficiency.

ACKNOWLEDGEMENT

The work described in this publication was performed under Contract No. 68-02-2184 with the U.S. Environmental Protection Agency.

REFERENCES

1. Calvert, S., J. Goldshmid, D. Leith, and D. Mehta. Scrubber Handbook. EPA-R2-72-118a. NTIS No. PB 213-016. August 1972.

2. Calvert, S., I. L. Jashnani, S. Yung, and S. Stahlberg. Entrainment Separators for Scrubbers -- Initial Report. EPA-650/2-74-119a. NTIS No. PB 241-189. October 1974.

3. Calvert, S., S. Yung, and J. Leung. Entrainment Separators for Scrubbers -- Final Report. EPA-650/2-74-119b. NTIS No. PB 248-050. August 1975.

4. Calvert, S., I. L. Jashnani, and S. Yung. Entrainment Separators for Scrubbers. J. Air Pollution Control Association. 24: 971, 1974.

5. Calvert, S., S. Yung, H. F. Barbarika, and L. E. Sparks. Entrainment Separators for Scrubbers. In: Second EPA Fine Particle Scrubber Symposium, EPA-600/2-77-193. NTIS No. PB 273-828. September 1977. pp. 75-95.

6. Calvert, S. Guidelines for Selecting Mist Eliminators. Chemical Engineering. February 27, 1978, pp. 109-112.

7. Calvert, S., H. F. Barbarika, and L. E. Sparks. Entrainment Separator Development. Paper No. 78-17.5 (Presented at 71st Annual Meeting of A.P.C.A. Houston, Texas. June 25-30, 1978.)

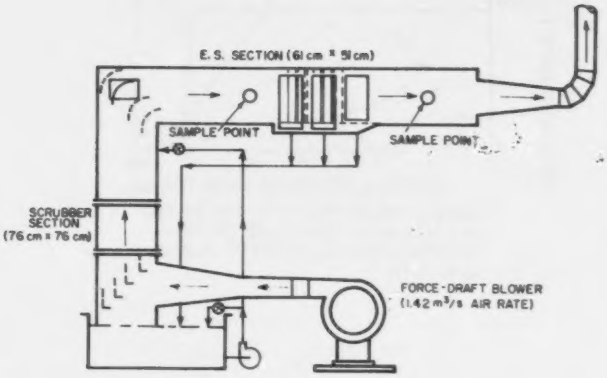
E. S. SECTION (61 cm × 51 cm)
SAMPLE POINT
SAMPLE POINT
SCRUBBER SECTION (76 cm × 76 cm)
FORCE-DRAFT BLOWER (1.42 m³/s AIR RATE)

FIGURE 1. SCHEMATIC DIAGRAM OF SCRUBBER/ENTRAINMENT SEPARATOR SYSTEM

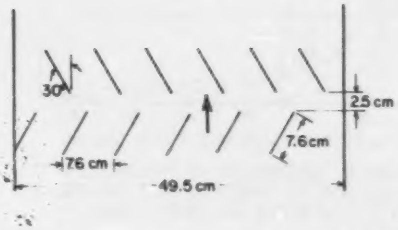
30°
2.5 cm
7.6 cm
7.6 cm
49.5 cm

FIGURE 2. TOP VIEW OF ZIGZAG BAFFLE ARRANGEMENT

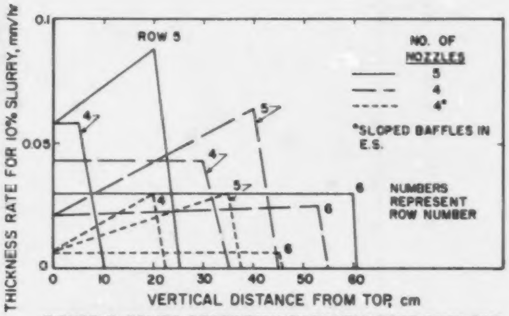

FIGURE 3. SOLIDS DEPOSITION THICKNESS RATE DATA FOR SPRAY SCRUBBER OPERATION.

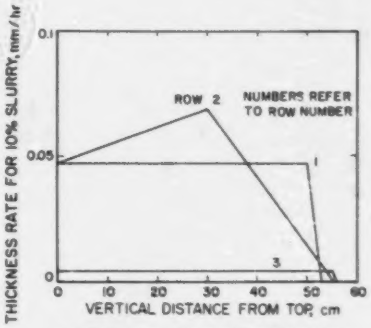

FIGURE 4. SOLIDS DEPOSITION THICKNESS RATE DATA FOR SIEVE PLATE SCRUBBER OPERATION.

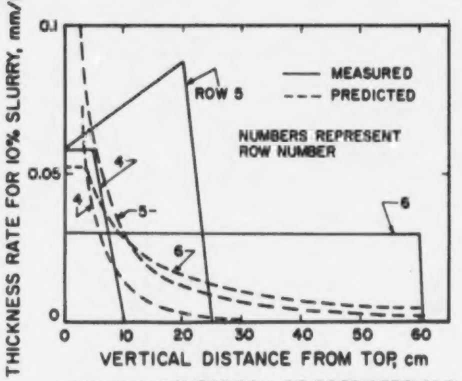

FIGURE 5. COMPARISON OF PREDICTED AND MEASURED SOLID DEPOSITION THICKNESS RATE FOR SPRAY SCRUBBER USING 5 NOZZLES.

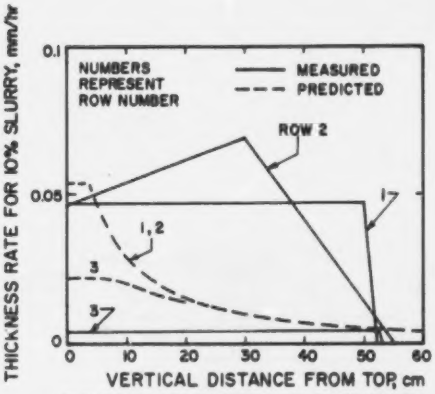

FIGURE 6. COMPARISON OF PREDICTED AND MEASURED SOLID DEPOSITION THICKNESS RATE FOR SIEVE PLATE SCRUBBER.

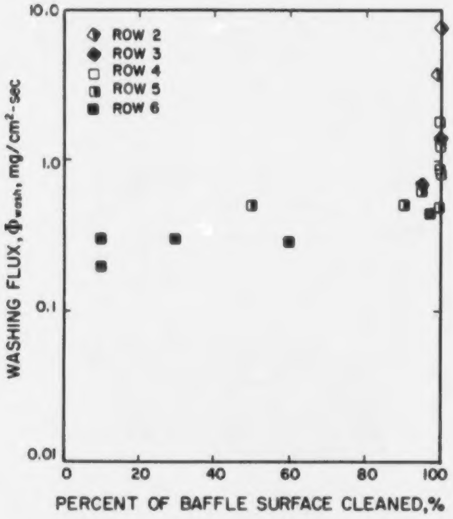

FIGURE 7. WASHING FLUX VS PERCENT OF BAFFLE SURFACE CLEANED AFTER 10 MINUTES FOR u_g = 2.3 m/s.

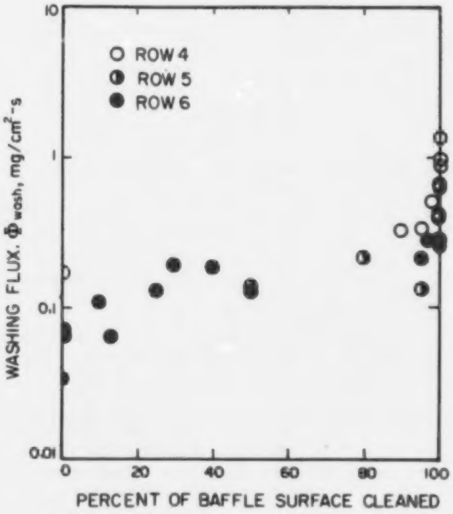

FIGURE 8. WASHING FLUX VS PERCENT OF BAFFLE SURFACE CLEANED AFTER 10 MINUTES FOR u_g = 3.4 m/s.

SCRUBBER DEMISTER TECHNOLOGY FOR CONTROL OF SOLIDS EMISSIONS FROM SO_2 ABSORBERS

William Ellison
Environmental Safeguards Division
NUS Corporation
4 Research Place
Rockville, Maryland 20850

ABSTRACT

This paper provides an assessment of the utility FGD demister problem and includes an analysis of related studies and reports on FGD state-of-the-art by EPA, EPRI and major workers in the field. Applicable technologies, related commercial experience, and principal system development activities are evaluated to identify current advancements in demister design practices for improved reliability and performance in control of carryover solids emissions. A detailed discussion of effective washing and scale control techniques is included as well as a review of latest commercial advancements in demister design and application along with the level of actual or anticipated emission control performance.

INTRODUCTION

Wet scrubbing type gas-desulfurization systems utilize mist eliminators to separate and remove scrubbing-liquid mist droplets entrained in the flue gas. Baffles or demister elements provide means by which air flow is redirected and the mist droplets are removed by inertial forces. Mist elimination is required to avoid incrustation and corrosion of downstream system components, as well as to control carryover to the stack of suspended solids, dissolved salts and liquid. Results of operation of flue gas desulfurization systems in utility plants indicate that demister facilities may be a major operational and maintenance problem detracting from gas cleaning system reliability. This paper reviews commercial design practices in selection and application of demister equipment and technology and assesses critical system engineering considerations in achieving desired levels of performance.

BACKGROUND OF UTILITY DEMISTER PROBLEM

General Arrangement of Demisters

There are two principal mist-eliminator configurations: horizontal gas flow and vertical gas flow types. The vertical-flow arrangement has been regularly used in utility service in this country. The horizontal-flow mist eliminator design, which is more common in Japan and Germany, has only recently been introduced in utility applications in the United States. It lends itself to use of higher design gas velocity and higher inlet liquid loading with increased droplet-removal efficiency since it provides better drainage and removal of collected liquid with reduced reentrainment. It also permits ready segregation of the demister liquid-catch from the recirculating slurry stream of the scrubber, which is of significance in connection with demister washing system design discussed later.

Vertical flow eliminators generally use the chevron type design which incorporates continuous zig zag baffling comprising 2 to 6 passes. (See Figure 1.) An improvement in this design through slanting of baffles, thereby providing a vertical directional component for liquid flow along the length of the baffle to give better means of drainage of wash water and collected mist is described by Moen et al[1] (installed downstream of a bulk entrainment separator of horizontal orientation designed to collect most of the inlet mist). (See Figure 2.) Calvert[2] presents data indicating that inclining of mist eliminator baffles in this manner at 30 degrees from the horizontal increases inlet liquid loading capability free of significant reentrainment by at least 100% at superficial vertical gas velocity in the critical high-velocity range of 5 to 7 meters/second, (16 to 22 ft/sec.).

Baffles in the horizontal-flow eliminators are oriented in a generally vertical position. Tennyson[3] illustrates J-shaped phase separation chambers or disengaging columns extending from the surface of the baffles counter to the gas flow direction in a high gas-velocity design mode, affording drainage paths external to the gas-flow regime for removal of liquid and thereby avoiding reentrainment by the high-velocity gas stream. (Figure 3).

Specific Design Practices

A general review by EPA[4] of commercial FGD design in the utility industry reports the following U. S. practices in demister application:

1. Principal use of mist eliminators of chevron multi-pass (continuous-vane) construction in a vertical-gas flow configuration is favored from strength and cost considerations. Baffle-type units which substitute noncontinuous-slat construction are also commonly used and, like the chevron design, offer comparatively simple, open geometry with low gas pressure drop.

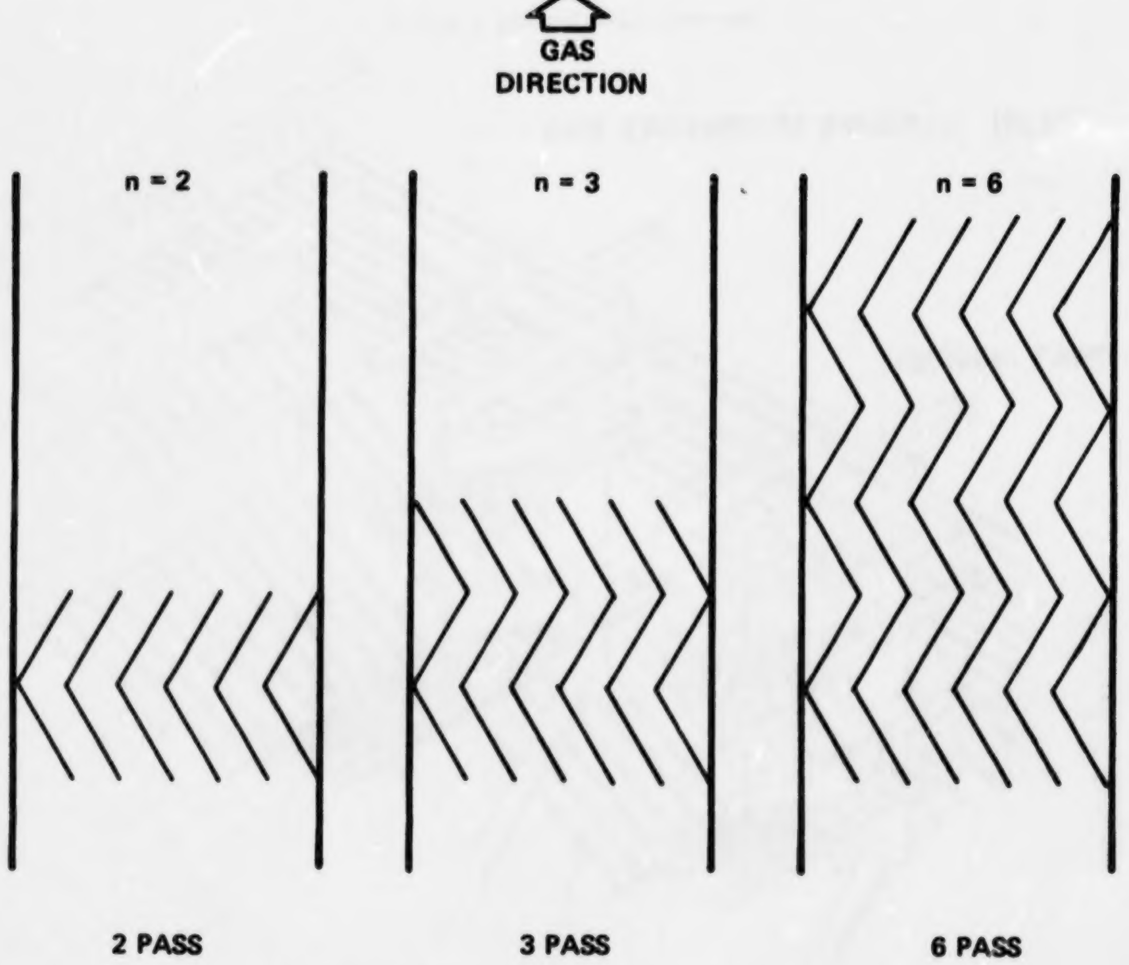
GAS
DIRECTION
n = 2
n = 3
n = 6
2 PASS
3 PASS
6 PASS

Figure 1 Multi-pass chevron mist eliminators

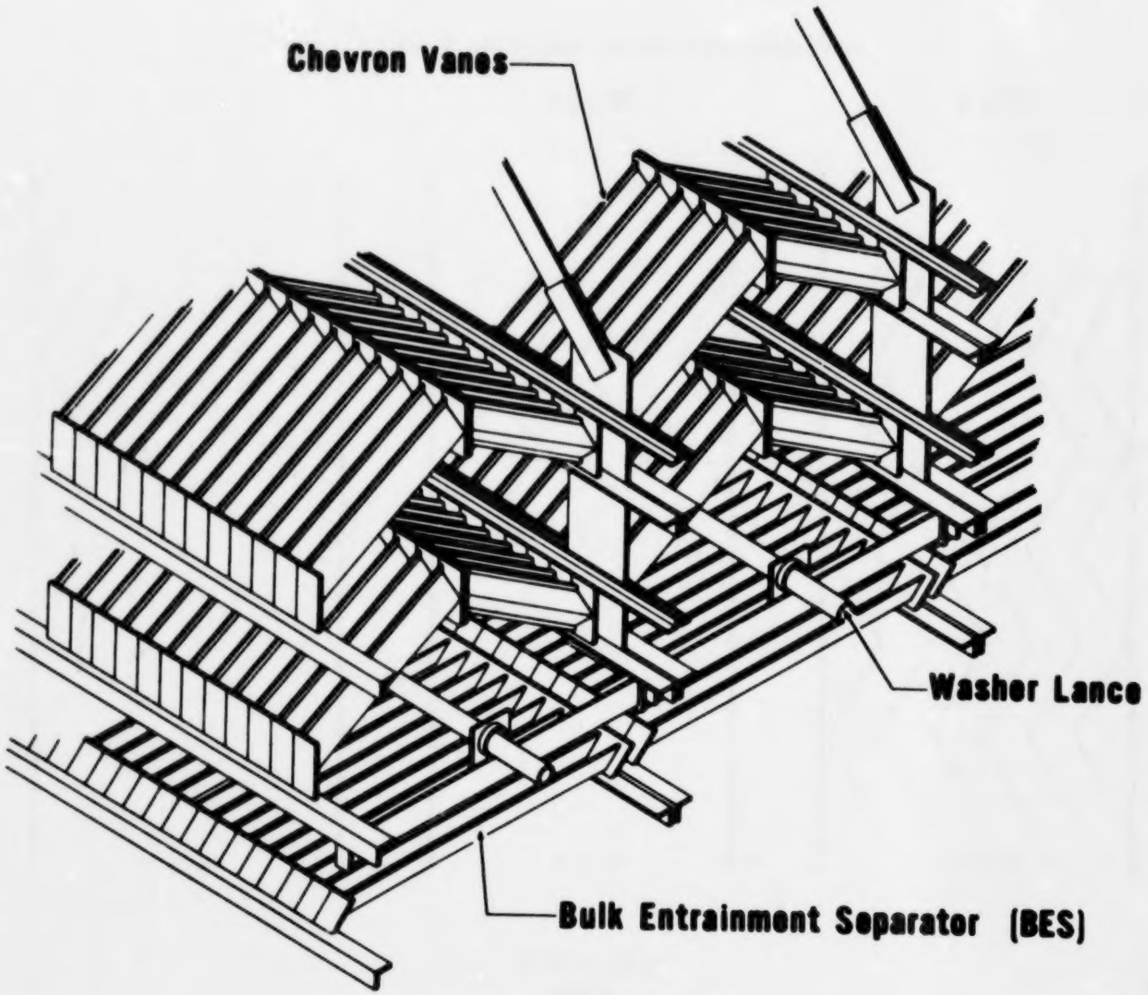
Chevron Vanes
Washer Lance
Bulk Entrainment Separator (BES)

Figure 2 Slanted-baffle demister

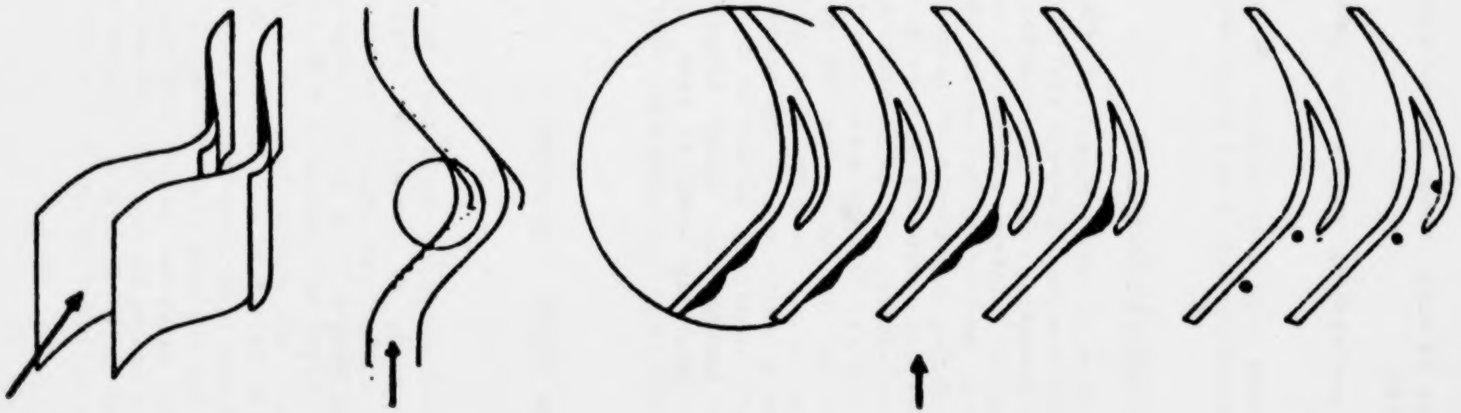

Figure 3 Function of phase separation chamber at elevated gas velocity

2. Vane spacing is normally 1½ to 3 inches except in the second stage of two-stage designs which generally use 7/8 to 1 inch spacing.

3. Plastic construction is most common due to reduced weight, cost and corrosion tendencies.

4. Precollection and pre-washing stages are commonly used to improve demister operation.

5. Demister wash systems typically operate intermittently and use a mixture of clear scrubbing liquid and fresh water makeup.

Overview of Utility FGD Demister Experience

The April, 1978 issue of the Journal of Electric Power Research Institute[5] contains a status report giving a statistical review of utility company experience with commercial FGD installations up to and including 1977. In an evaluation of thirteen operational utility lime/limestone scrubber systems that came on-line in the period 1972-1977, representing evolving design and operating experience of seven FGD system suppliers, plugging/scaling, erosion and corrosion of mist eliminators, inefficient performance of mist eliminators, and deterioration of stack liners are listed among the most critical factors detracting from high operability. (Operability is defined as the hours the FGD system is available to operate, whether operated or not, compared with boiler operating hours in the period, expressed as a percentage.) The primary trend noted by EPRI over the above five-year reporting period is the introduction of mist eliminator and reheater designs that reduce plugging and scaling. They further note that this generally seems to have reduced aerosol removal efficiency, thus contributing to increased stack liner failure and rainout.

EXPERIENCE WITH DEMISTER CONTROL PERFORMANCE

EPA Evaluation

In a recent detailed study of field test data to identify the most efficient of a large group of commercial utility FGD systems EPA[6] determined that total outlet particulate emissions from the selected systems (measured by EPA Method 5) is in the range of 0.02 to 0.07 lb/10^6 Btu, less than the 0.1 lb/10^6 Btu Federal New Source Performance Standard that has been in effect, and within range of a lower pending standard expected to call for 0.03 lb/10^6 Btu. (Included in this grouping are FGD systems installed by Nevada Power Company, Montana Power Company, Arizona Public Service Company and Duquesne Light Company.) In an extensive series of measurements of outlet carryover-solids loadings in flue gas discharges from 10-20 MW coal-fired demonstration FGD systems with vertical-flow mist eliminators (tested with mist eliminator surfaces in clean condition and gas flow distribution believed to be nearly uniform) demister outlet concentration of these scrubbing-liquor solids was consistently lower than 0.01 lb/10^6 Btu. EPA reviewers conclude that well designed mist eliminator systems are capable of limiting scrubber-liquor particulate entrainment from FGD systems to a level less than 0.01 lb/10^6 Btu if mist eliminator surfaces are clean. Assessment of this test data evaluation also points to the major significance to demister performance of uniform gas flow distribution among the deentrainment elements. Moen et al[1] call for complete three-dimensional gas flow modeling for individual FGD scrubber designs, reporting that local vertical gas-flow velocities entering the first level of spray banks of a spray tower ranged from approximately 120 to 20% of average velocity with addition of internal gas distribution vaning as compared to a range of 250% to negative 20% without. (Figure 4.)

Demister Fouling

Available data on commercial systems strongly suggest that many instances of poor emission control performance by FGD demisters are the direct result of fouling of baffles causing upset of design gas flow conditions. The EPA study further indicates that:

1. Measures such as installation of wash sprays upstream and downstream of the mist eliminator are employed to correct plugging problems.

2. If the problem stems from deposition of soft solids on the mist eliminator surfaces, sprays will usually correct the problem.

3. Often the deposition problem is a combination of soft solids deposition accompanied by the formation of hard scale from precipitation of solids from a $CaSO_4$-supersaturated liquid.

4. Techniques employed to correct this combined problem in addition to spray washing involve pH control and the use of unsaturated mist eliminator wash liquid.

Demister Scale Control

Thus control of internal fouling due to chemical scaling by gypsum deposits ($CaSO_4 \cdot 2H_2O$) is a highly critical factor in maintaining operation of mist eliminators at their design efficiency. Gypsum scale control in commercial FGD systems is generally provided by either of two alternative wet-process chemical design techniques applied in U.S.A.:

1. Supersaturated-$CaSO_4$ mode: Scrubbing-liquid to gas flow-ratio is maintained sufficiently high in open-geometry type spray-tower absorbers to prevent the dissolved calcium sulfate concentration from reaching an excessively supersaturated level, thus preventing or adequately limiting the rate of formation of gypsum scale. (Calcium sulfite and calcium sulfate are precipitated as separate and distinct compounds on addition of lime or limestone to the scrubber outlet

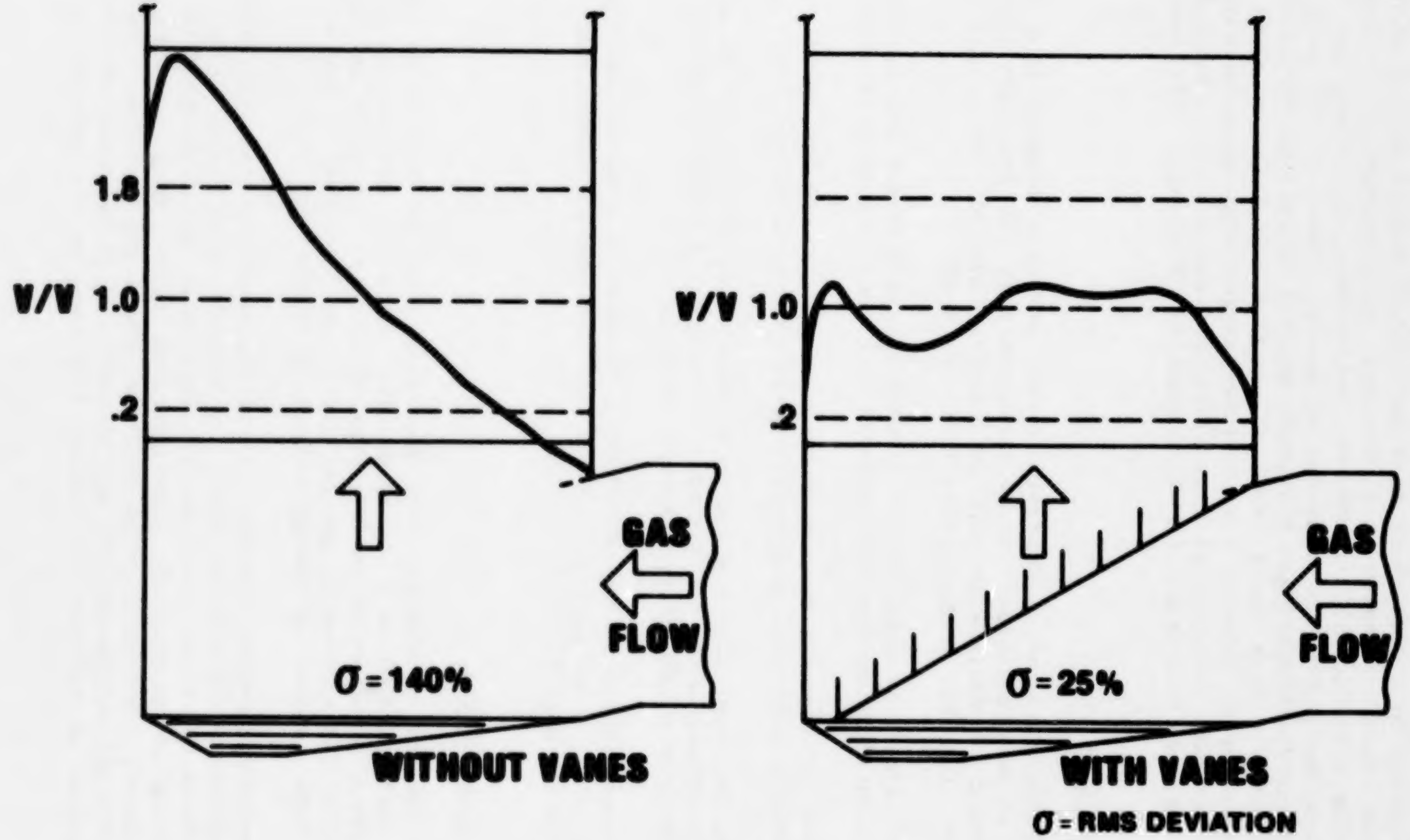

Figure 4 Effect of vaning on gas distribution in spray tower

liquid.) Techniques for forced oxidation of the recirculating scrubbing liquor now being introduced for use in slurry scrubbing type FGD systems in the United States are reported to improve the effectiveness of chemical scale control technology applicable to systems operating in the supersaturated mode.

2. Unsaturated-$CaSO_4$ mode: A high concentration of dissolved magnesium sulfite, (in magnesia buffered lime/limestone slurry scrubbing systems), or dissolved sodium sulfite, (in concentrated-active-alkali type double alkali systems), is maintained in the scrubbing liquid so as to depress the dissolved calcium concentration to approximately 200 ppm or less, thereby holding the combined the steady state concentration of dissolved calcium and sulfate below the $CaSO_4$ saturation level. Precipitation of sulfate for disposal as a solid waste is achieved solely by joint precipitation of calcium sulfate with calcium sulfite as a combined crystal having a sulfate to sulfite mole ratio no higher than approximately 0.3. Utilization of unsaturated mode FGD operation is therefore feasible only on emission sources such as medium-to-high sulfur fossil-fueled utility boilers which have limited liquor oxidizing tendencies due to moderate O_2/SO_2 concentration ratios in the boiler flue gas. (Unsaturated mode FGD systems lend themselves more readily than supersaturated systems to operation in a closed scrubbing-liquid loop -- zero blowdown of scrubbing liquid -- with process purge thereby limited to the occluded liquid in the waste sludge or filter cake.)

Clearly, the mist eliminator is the most likely component of the scrubbing system to be fouled since carryover liquid collected on and wetting its extensive internal surface absorbs residual SO_2 and O_2 from the scrubbed gas. Moreover, above described provisions for chemical scale control designed into the recirculating slurry circuit of the scrubber can only be expected to achieve their intended purpose in the absorber section where dispersal of liquid at high flow-rates throughout this zone provides adequately for continuous irrigation of internal absorber surfaces. Thus the surfaces of demister elements must be effectively washed during system operation to prevent solids deposition from sulfite/sulfate-solids laden droplets and of gypsum scale originating from dissolved calcium sulfate and suspended lime/limestone in the scrubbing liquid. Although proper washing can be best accomplished with fresh water, customary material-balance constraints for FGD systems operating in a closed-recirculating-scrubbing-liquid loop require the close limiting of total fresh water input. For this reason recycled scrubber liquids must be used in many existing scrubber systems of the vertical-gas-flow type to achieve required demister wash-spraying intensity and duration.

Demister Washing

Vertical-Flow Chevron Demisters-

Following an exhaustive program of pilot testing in coal-fired service at Colbert Steam Plant since 1971, TVA[7] reports recent success in establishing a workable technique for washing vertical-flow chevron demisters operating at 13 ft/sec. gas velocity under closed loop FGD conditions. Continuous mist eliminator operation for over 1,000 hours without pressure drop buildup was achieved in the limestone-mode by washing the bottom of the mist eliminator intermittently with all the available clarified scrubbing liquor followed by an allocated amount of the allowable FGD-system makeup water. The top of the mist eliminator was washed intermittently with the remaining amount of allowable makeup water. A similar washing technique that excluded the clarified liquor step achieved similar success in lime-mode pilot plant testing.

In the 360 MW lime/fly-ash SO_2 scrubbing system design at Montana Power Company's Colstrip Station, which recirculates scrubbing slurry with suspended solids in excess of 10%, a bubble-cap type water-wash tray is utilized ahead of a conventional chevron demister to trap and permit recirculation of demister wash water and to dilute the entrainment from the absorber.[8] Suspended solids in this recirculating wash water system is minimized by circulating trapped wash water through a settling pond. (Figure 5). Test results from prior pilot plant runs indicated that the concentration of suspended solids in the liquid entrained at the demister inlet is thereby reduced to less than 1% with approximately a 10/1 reduction in comparative mist-eliminator fouling rates as indicated by gas pressure drop measurements.

Willett[9] of Peabody Process Systems emphasizes that chemical process design for preventing liquid-phase precipitation in the demister is more critical in fulfilling demister performance requirements than is hardware selection and design. A commercial design achieving non-scaling demister characteristics is described in which a sieve-type water-wash tray is fed a continuous scrubber-slurry stream which has been processed in a liquid cyclone separator to preferentially remove suspended limestone particles. TVA's extensive pilot test activity also emphasizes the adverse effect in fouling of demisters of increasing concentrations of suspended limestone solids with rising limestone stoichiometric ratio in FGD systems.[10] EPA similarly reports reduced mist eliminator fouling at high alkali utilization.[11] Following from this, unsaturated-$CaSO_4$ clear-liquor double alkali FGD process systems coming into extensive commercial use in utility service in 1979 may be expected to provide major advancement in mist eliminator reliability and performance.

Horizontal-Flow Chevron Demisters-

Balakrishnan[12] of Environeering reviews the trial performance of a commercial coal-fired slurry-type FGD system at Central Illinois Light Company's Duck Creek Station which incorporates a two-stage horizontal-flow chevron demister (13 ft/sec.) equipped with recirculating wash sprays at the inlet of each stage fed by FGD system makeup water. (Figure 6.) Inspections after a trial run indicate minimum evidence of solids build-up in the mist eliminator section, and measured stack solids loading is consistently less than half that at the absorber inlet at measured inlet loadings from 0.005 to 0.20 grains/SCF, (0.01 to 0.40 lb/10^6 Btu).[13]

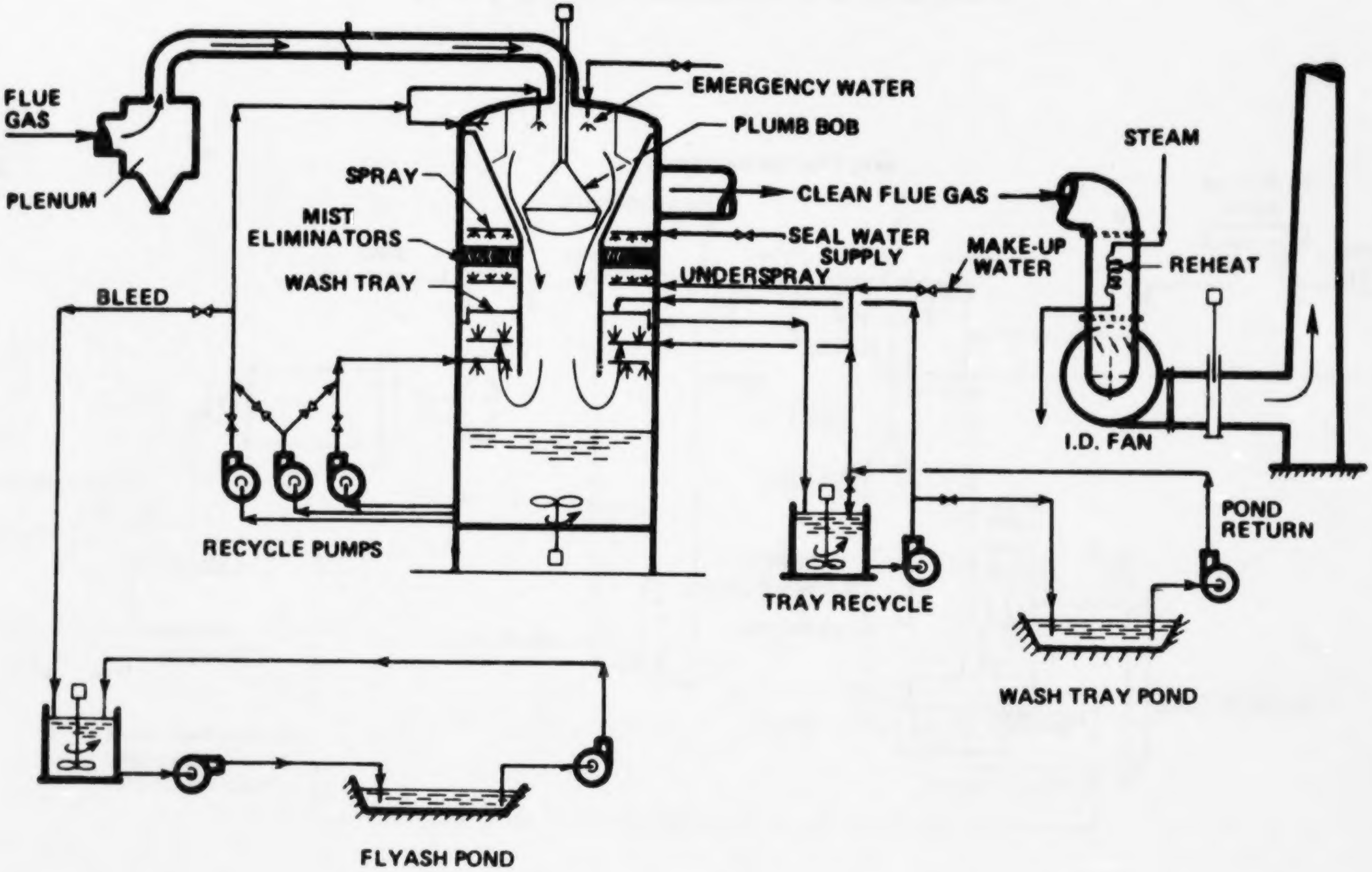
FLUE GAS
PLENUM
EMERGENCY WATER
PLUMB BOB
SPRAY
MIST ELIMINATORS
WASH TRAY
CLEAN FLUE GAS
SEAL WATER SUPPLY
UNDERSPRAY
MAKE-UP WATER
STEAM
REHEAT
I.D. FAN
BLEED
RECYCLE PUMPS
TRAY RECYCLE
POND RETURN
WASH TRAY POND
FLYASH POND

Figure 5 Demister wash scheme at Colstrip Station

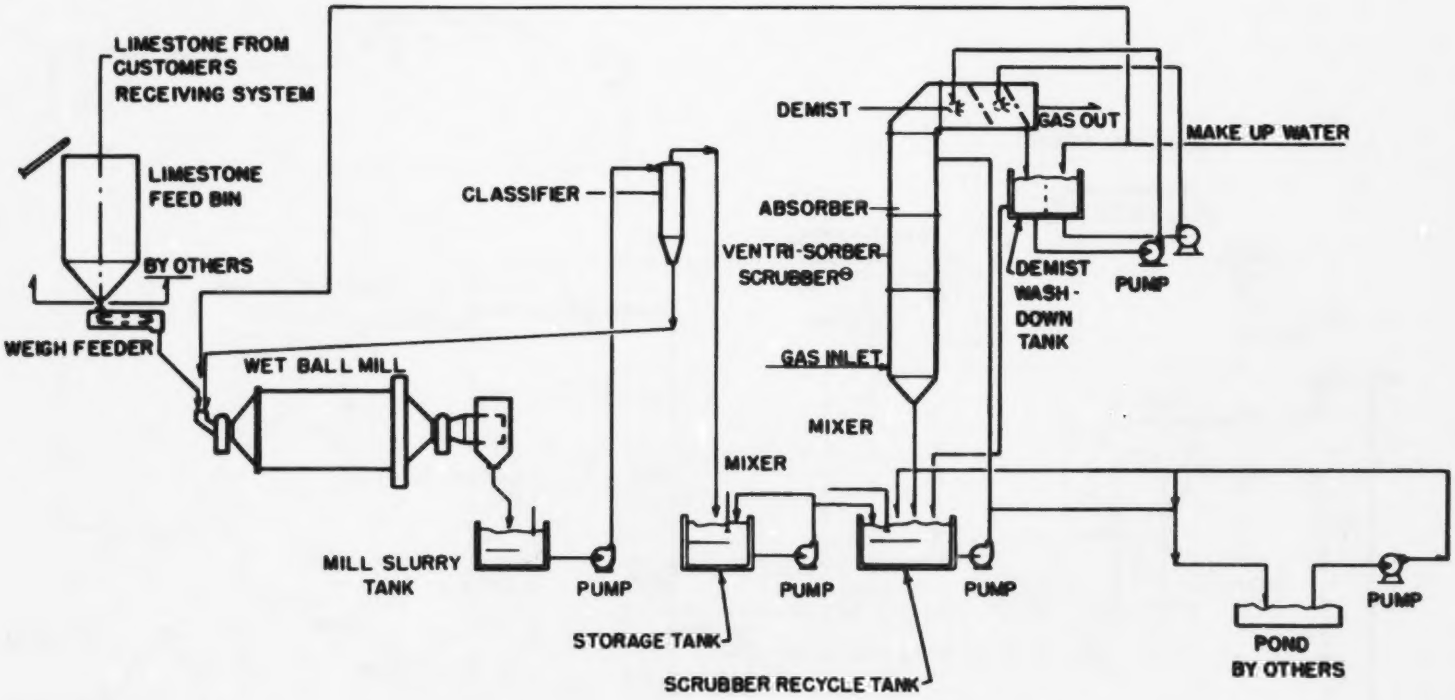
LIMESTONE FROM CUSTOMERS RECEIVING SYSTEM
LIMESTONE FEED BIN
BY OTHERS
WEIGH FEEDER
WET BALL MILL
MILL SLURRY TANK
PUMP
CLASSIFIER
MIXER
STORAGE TANK
PUMP
DEMIST
ABSORBER
VENTRI-SORBER SCRUBBER®
GAS INLET
MIXER
SCRUBBER RECYCLE TANK
PUMP
GAS OUT
MAKE UP WATER
DEMIST WASH-DOWN TANK
PUMP
POND BY OTHERS
PUMP

Figure 6 Demister wash scheme at Duck Creek Station

In TVA's extensive Colbert pilot test program with horizontal-flow chevron demisters soda ash (sodium carbonate) reagent feed was utilized to effectively control demister scaling which occurred in use of such recirculating wash water systems.[10] (Figure 7.) Level of $CaSO_4$ saturation of the wash stream was reduced to approximately 20% with 0.05 molar (gram mole/liter) sodium concentration. TVA's full-scale limestone FGD system at Widows Creek Unit 8 has experienced substantial fouling of the demister with slurry and fly-ash type deposits during an initial 4½ month on-line operating period in 1977.[14] The circulating wash water system, which was installed without sodium carbonate treatment facilities, is being evaluated in anticipation of making modifications so as to maintain clean chevron surfaces.

The significant effect of demister inlet liquor loading on demister washing duty and effectiveness is illustrated by TVA's report on pilot plant performance of high-velocity cocurrent FGD scrubber design.[15] In experimental FGD operation with downflow superficial velocity raised to 24 ft/sec., gas exiting the absorber section was turned 180° through a wet elbow separator while impacting a pool of slurry at the bottom of the scrubber, reducing entrained water content of gas later entering the horizontal-flow mist eliminator to 0.054 grain/SCF, (0.1 lb water/10^6 Btu), as compared to approximately 4 grain/SCF, (10 lb water/10^6 Btu), measured in an earlier arrangement with only a simple 90° turn. (See Figure 8 and 9.) At the very low level of scrubbing slurry carryover to the demister in the first mentioned arrangement, fouling was readily controlled merely by intermittent spraying of available fresh water on the face of the mist eliminator.

Sekhar[16] reports details of Ontario Hydro's demister system development activity. Small pilot plant testing of a two-stage horizontal-flow chevron demister in coal-fired limestone FGD service has shown the adequacy in fouling prevention of utilizing a recirculating scrubber slurry stream as a baffle washing medium when applied to the first demister stage. Comparison of test results against those with a clarified scrubbing-liquor washing medium demonstrated that the slurry solids provide critical seed-crystal surface that limits $CaSO_4$ supersaturation conditions at demister surfaces and thereby prevents scaling. In pilot tests performed at 9 ft/sec. gas velocity[17], vertical introduction of this wash slurry, positioning the feed directly above the baffles of the first demister stage, decreased outlet mist emissions at the stack to approximately half that measured in the absence of first-stage washing. Common washing practice for horizontal-flow mist eliminators utilizing horizontal sprays upstream of the demister elements would not be expected to accomplish the collection of mist entrainment to this degree. Due to the importance of baffle irrigation in maintaining clean surfaces, Ontario Hydro defined washing efficiency in each mode of operation of a full length demister-baffle air-water test model as the percentage of plate area wetted by the washing medium. Washing efficiency was improved by optimal tilting of the vertical vanes counter to gas-flow direction and by maximizing the included angle between adjacent inter-connected zig-zag chevron blades.

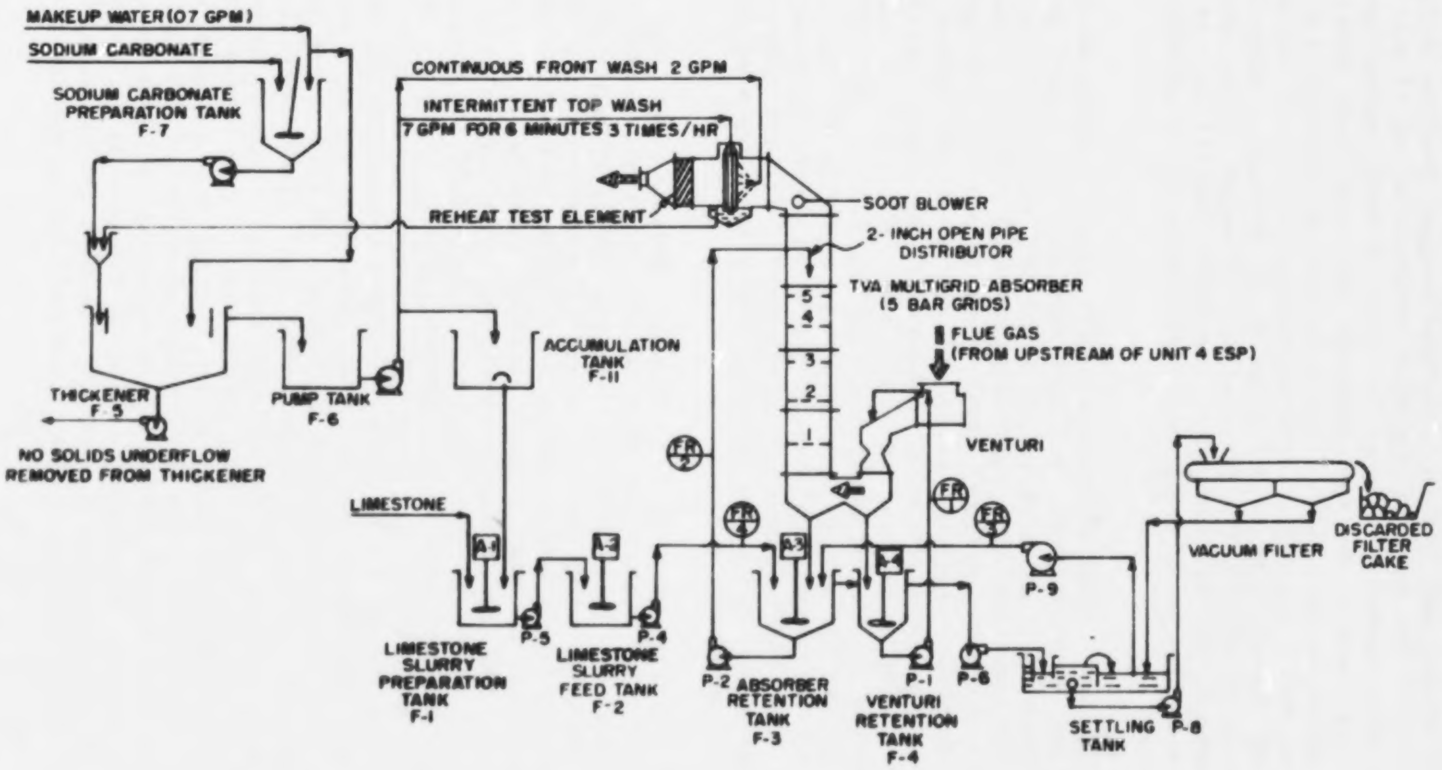
MAKEUP WATER (0.7 GPM)
SODIUM CARBONATE
SODIUM CARBONATE PREPARATION TANK F-7
CONTINUOUS FRONT WASH 2 GPM
INTERMITTENT TOP WASH
7 GPM FOR 6 MINUTES 3 TIMES/HR
REHEAT TEST ELEMENT
SOOT BLOWER
2- INCH OPEN PIPE DISTRIBUTOR
TVA MULTIGRID ABSORBER (5 BAR GRIDS)
5
4
3
2
1
FLUE GAS (FROM UPSTREAM OF UNIT 4 ESP)
VENTURI
ACCUMULATION TANK F-11
THICKENER F-5
NO SOLIDS UNDERFLOW REMOVED FROM THICKENER
PUMP TANK F-6
LIMESTONE
A-1
A-2
A-3
A-4
FR
LIMESTONE SLURRY PREPARATION TANK F-1
P-5
LIMESTONE SLURRY FEED TANK F-2
P-4
P-2
ABSORBER RETENTION TANK F-3
P-1
VENTURI RETENTION TANK F-4
P-6
P-9
SETTLING TANK
P-8
VACUUM FILTER
DISCARDED FILTER CAKE

Figure 7 Sodium carbonate feed to TVA pilot plant demister wash circuit

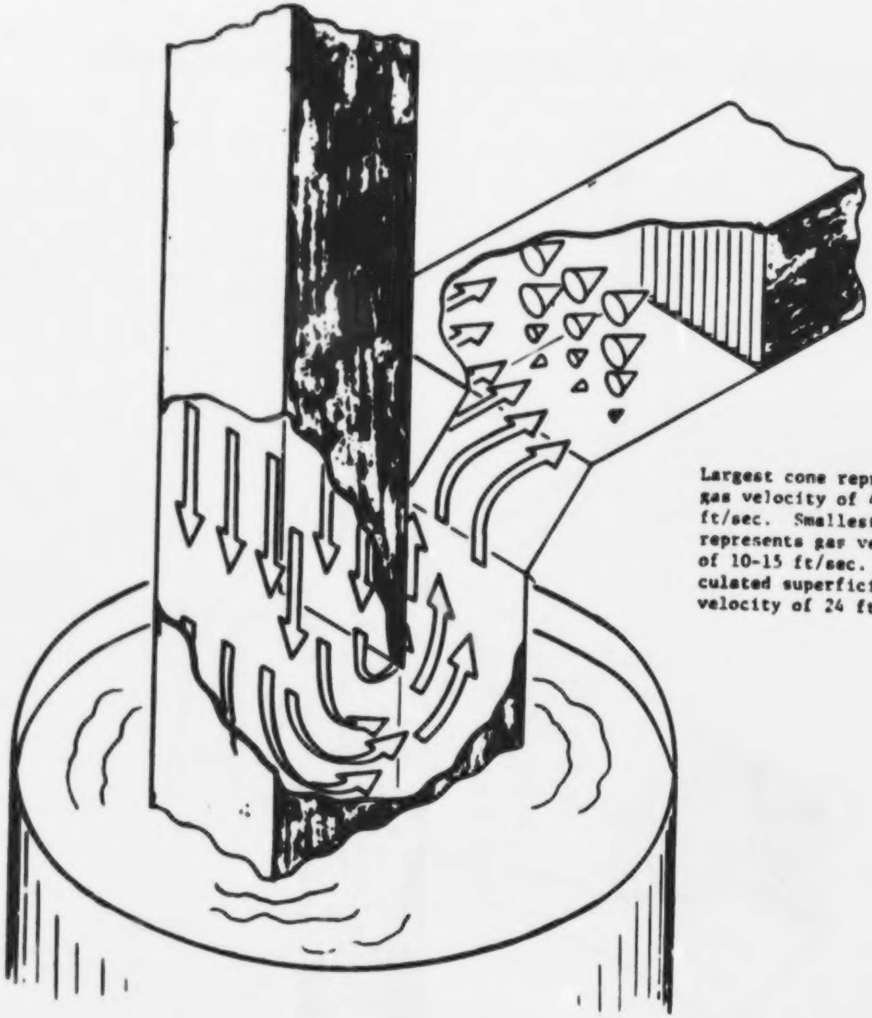

Largest cone represents gas velocity of 40-45 ft/sec. Smallest cone represents gas velocity of 10-15 ft/sec. Calculated superficial gas velocity of 24 ft/sec.

Figure 8 Wet-elbow gas discharge configuration of cocurrent absorber

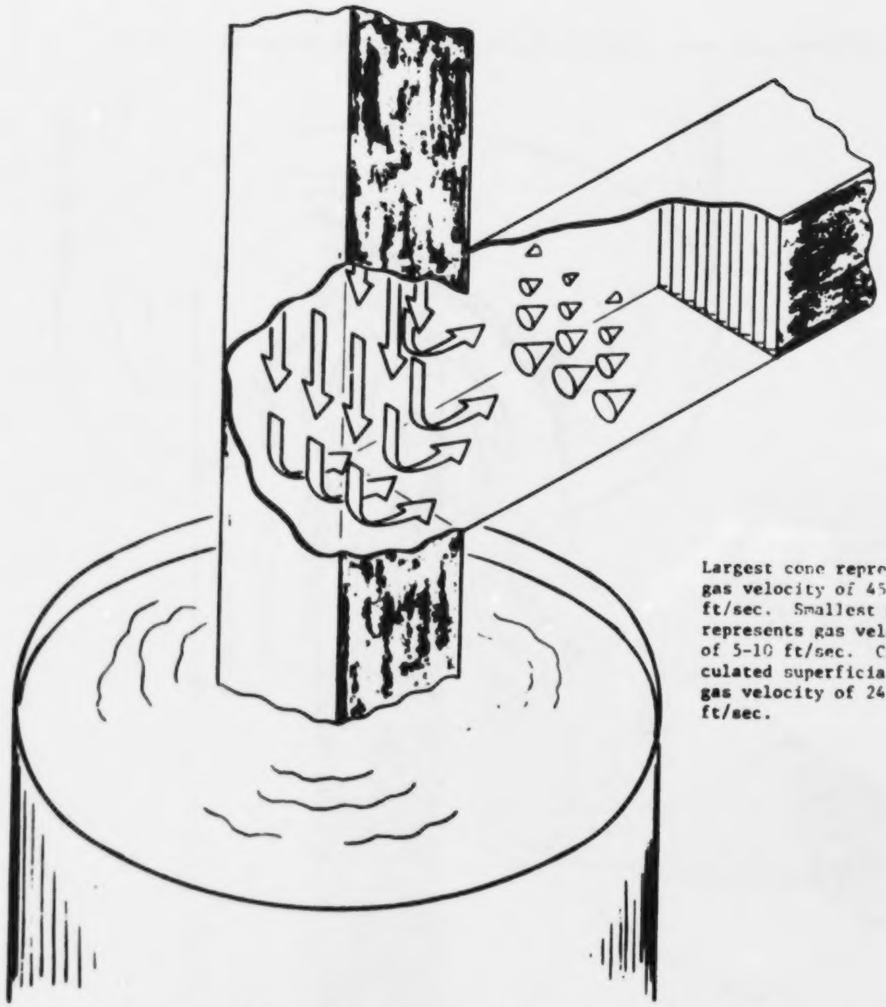

Largest cone represents gas velocity of 45-50 ft/sec. Smallest cone represents gas velocity of 5-10 ft/sec. Calculated superficial gas velocity of 24 ft/sec.

Figure 9 90 degree configuration of cocurrent-absorber discharge

DEMISTER DESIGN ADVANCEMENTS

General

A number of proprietary designs furnished by suppliers of demister elements and demister equipment appear to offer improved performance and reliability. Based on available information several specific examples may be described.

Euroform Design

The Euroform[3] type mist eliminator in vertical-flow configuration (Figure 10) utilizes design velocities as high as 20 ft/sec. This unit provides advantageous slanting in two directions in that the total gas stream is deflected from its straight course by a series of zig-zag shaped channel walls. Slanted chevron-shaped airfoils on the eliminator walls collect and drain liquid droplets removed from the gas stream. This type design incorporated in the FGD installation at Arizona Public Service Company's Cholla Station is the only existing commerical mist eliminator installation indicated in the recent EPRI FGD-status-report[5] to be free of reliability and performance impairing problems. In addition, the Cholla system was referenced by EPA in their above noted field data study,[6] and ranked among the group of FGD installations which were found to have the lowest total solids emission levels.

Heil Design

Battelle's mist eliminator report for EPRI[18] references a variety of high velocity type mist eliminator designs which incorporate special reentrainment prevention features in the form of disengaging columns. (Figure 11.) The sinuous-form pocketed baffle configuration by Heil utilizes design velocities up to 20 feet/sec. in vertical gas flow and 25 feet/sec. in horizontal flow. It is incorporated in the previously noted vertical-flow installation at Montana Power Company's Colstrip Station which is also included in the above EPA listing of FGD installations with low particulate emission levels. In addition a horizontal-flow Heil demister was used in the large Weir-scrubber FGD demonstration system at Southern California Edison's Mohave Station. The EPA study[6] particularly focuses on the favorable field data from this FGD system installation which indicates that outlet particulate solids emission concentrations were lower than inlet particulate solids levels over a range of inlet solids loadings extending to as low as 0.01 lb/10^6 Btu.

Matsuzaka Design

Battelle[18] also references Matsuzaka's utilization of the high-velocity pocketed-baffle system by Klockner-Humboldt-Deutz. Following

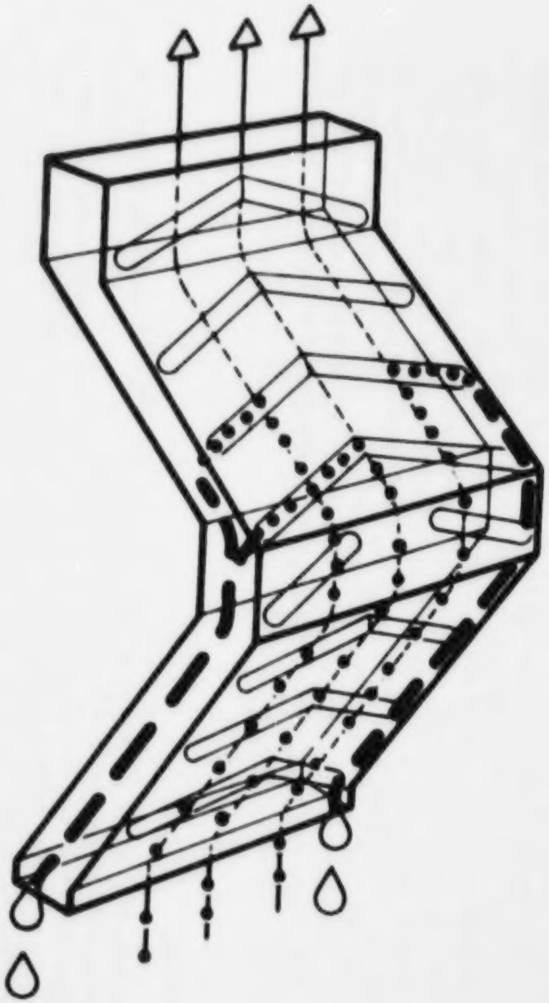

Figure 10 Demister drainage by multi-directional slanting

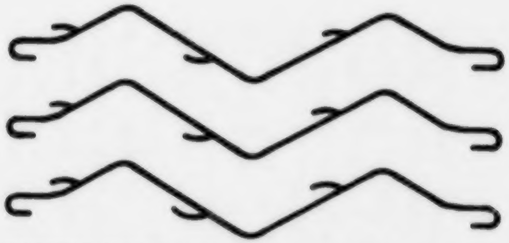

HEIL CHEVRON MIST ELIMINATOR WITH COLLECTION HOOKS

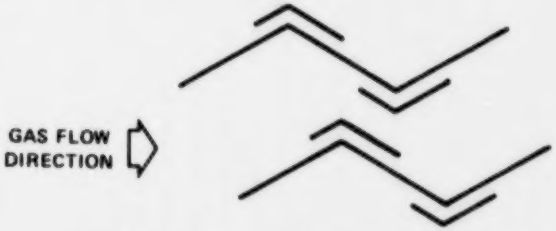

PEERLESS CHEVRON MIST ELIMINATOR WITH COLLECTION POCKETS

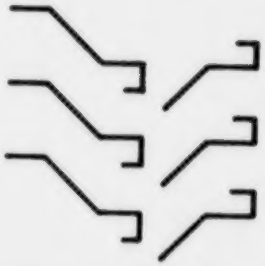

MATSUZAKA MIST ELIMINATOR WITH COLLECTION POCKETS

Figure 11 Mist eliminator design advancements

from extensive commercial application of this horizontal-flow design for FGD service in Japan in slurry scrubbing and clear-liquor double alkali applications, Central Illinois Public Service Company's 575 MW double alkali FGD-absorber system, which will start up in 1979 at Newton Station, has been equipped with this configuration and designed for a 20 ft/sec. superficial velocity to reduce solids emission to 0.01 grain/ACF (approximately 0.02 $lb/10^6$ Btu) with inlet liquid loading of approximately 1 gpm/sq. ft. of demister face area. An isolated pre-scrubber stage limits entry of chloride to the absorber. It is equipped with a two stage Humboldt demister designed for 20 ft/sec. with approximately 1½ in WG gas pressure drop to reduce liquid droplet entrainment to 0.02 grain/ACF, (representing only 0.002 $lb/10^6$ Btu total solids carryover to the FGD absorber), at inlet liquid loading of approximately 2 gpm/sq.ft. of demister face area, and is particularly noteworthy for its impending advancement of commercial high-efficiency demister design art in the utility industry.

CONCLUSION

Demister operational problems have been a major factor detracting from reliability of common throwaway-waste type flue gas desulfurization facilities in the utilities industry. Characteristically large gas-flow volumes as well as complex and substantially concentrated process-liquid conditions in coal-fired utility service have introduced major problems in utilizing prior art in mist eliminator design. Emerging system-technology advancements in application of wet process chemistry as well as mist-eliminator equipment development and mechanical engineering of systems for removal of liquid entrainment offer a broad opportunity for significant improvement in arrangement, design and operation of this key FGD system component. Pollution control performance in current expansion of scrubber-equipped coal-fired electric generating capacity in the United States will be furthered by application and ongoing commercial development of methods for improvement of carryover emissions control that will serve to depress demister fouling; achieve uniform cross-sectional distribution of gas flow; utilize gas flow system configurations for high-efficiency separation of droplet sizes that have significant bearing on the solids emission rate; and provide adequately for prevention of reentrainment under varying modes of operation of the boiler unit.

REFERENCES

1. Moen, D. A. et al, Coal Creek Station Air Quality Control System. (Presented at 29th Annual Conference of the Association of Rural Electric Generating Cooperatives. Vail, Colorado. June 11-14, 1978.) p 6, 7.

2. Calvert, S. Guidelines for Selecting Mist Eliminators. Chemical Engineering. p. 110, February 27, 1978.

3. Tennyson, R. P. Mist Eliminator Design and Application. (Presented at 70th Annual Meeting of the Air Pollution Control Association. Toronto, Ontario, Canada. June 20-24, 1977.) p 77-25.4.

4. Laseke, B. A., and T. W. Devitt. Status of Flue Gas Desulfurization Systems in the United States. (Presented at 29th Annual Conference of the Association of Rural Electric Generating Cooperatives. Vail, Colorado. June 11-14, 1978.) p 33-35.

5. Balzhiser, R. E. R&D Status Report, Fossil Fuel and Advanced Systems Division, EPRI. EPRI Journal. 3:3 - 45 to 47, April 1978.

6. Copeland, J. O. Data from Unpublished EPA Report, Industrial Studies Branch, Emission Standards and Engineering Division, Office of Air Quality Planning and Standards, U. S. Environmental Protection Agency, Research Triangle Park, North Carolina, 1977.

7. Hollinden, G. A. et al, TVA's 1-MW Pilot Plant: Final Report on High Velocity Scrubbing and Vertical Duct Mist Elimination. Environmental Protection Agency, Washington, D. C. Publication EPA-600/7-77-019, PRS-19. March, 1977. 50 p.

8. Grimm, C. et al, Particulate and SO_2 Removal at the Colstrip Station of the Montana Power Company. In: Proceedings of the Second Pacific Chemical Engineering Congress (Pachec '77), Volume 1, Smith, C. L. (Tech Prog Chairman). Denver Colorado, American Institute of Chemical Engineers, 1977. p. 324, 7, 8.

9. Willett, H. P. Communication from Peabody Process Systems, Inc., Stamford, Connecticut, June 6, 1978.

10. Hollinden et al, Performance of Entrainment Separators in Slurry Scrubbing Processes. Tennessee Valley Authority, Muscle Shoals, Alabama. Bulletin Y-93. June 1975. 39 p.

11. Head, H. N. EPA Alkali Scrubbing Test Facility: Advanced Program, Second Progress Report. Environmental Protection Agency, Research Triangle Park, North Carolina. Publication EPA-600/7-76-008. September 1976. p 8-28 to 8-30.

12. Balakrishnan, N. S. Riley Scrubber Performance at CILCO. (Presented to Committee on Power Generation, Association of Edison Illuminating Companies. Minneapolis, Minnesota. September 14, 1977.) 6 p.

13. Cheng, G. H. Communication from Environeering, Inc., Schiller Park, Illinois, July 7, 1978.

14. Tennessee Valley Authority. Widows Creek Unit 8 Limestone Wet Scrubber with 4.5 Months Operating Experience. Office of Power, Energy Research, Chattanooga, Tennessee. October 1977. 59 p.

15. Robards et al, TVA's Cocurrent Scrubber Evaluation. (Presented at Winter Annual Meeting, The American Society of Mechanical Engineers. Atlanta, Georgia. November 27 - December 2, 1977.) p 4-9.

16. Sekhar, N. Demister Design for Limestone Slurry Scrubber (Presented at 70th Annual Meeting of the Air Pollution Control Association. Toronto, Ontario, Canada. June 20-24, 1977.) p. 3-5.

17. Sekhar, N. Data from Unpublished Report, Ontario Hydro, Toronto, Ontario, Canada, 1978.

18. Battelle Columbus Laboratories. Guidelines for the Design of Mist Eliminators for Lime/Limestone Scrubbing Systems. Electric Power Research Institute, Palo Alto, California, EPRI Report FP-327 Project 209. December, 1976. 102 p.

IMPROVED MIST ELIMINATOR PERFORMANCE THROUGH ADVANCED DESIGN CONCEPTS

Richard P. Tennyson
Sheldon F. Roe, Jr., P.E.
Robert H. Lace, Sr.
The Munters Corp.
Euroform Products Div.
P.O. Box 6428
Fort Myers, Fl. 33901

ABSTRACT

This paper is directed to those engineers or operating personnel concerned with scrubber systems design and/or emissions standard achievement. A review of impingement mist eliminator types, mode of operation and degree of efficiency is presented. Practical considerations based on mist eliminator experience on several major chemical processes for SO_2 removal from flue gas and other industrial particulate scrubbing systems are presented. Some items reviewed include: vertical flow vs. horizontal flow, liquid loading capacity, maximum velocity, suggested washing practices, retrofits and materials of construction. A summary of typical installation arrangements, velocity/pressure drop, and droplet size removal charts are presented.

INTRODUCTION

Mist eliminators separate liquid drops (containing suspended or dissolved solids) from effluent gas streams. The basic equation and theory for advanced design eliminators are presented below.

Formula for calculation of limit drop size:

$$d_T = K \left[\left(\frac{PG}{PT} \ Vg \right) \left(\frac{ra-ri}{p} \right) \left(\frac{1}{C_A} \right) \right]^{-2}$$

d_T = Limit drop size, defined as the smallest diameter droplet presented in the most unfavorable position, which will be essentially 100% separated from the gas stream.

K = Constant related to specific profile shape or drag coefficient.

PT = Liquid density.

PG = Gas density.

Vg = Kinematic viscosity of gas.

ra,ri
+ p = Geometric relationship of profiles.

C_A = Gas velocity through profiles.

Most important for a given profile geometry, are gas density and velocity. For example, velocities through advanced design eliminators may vary from 100 fpm for very heavy gases to 10,000 fpm for very light gases.

With the above as background, the advantages of various geometric configurations are presented for optimizing pressure drop, gas velocity, limit drop size, and non-fouling performance - particularly important with SO_2 scrubbers using limestone slurries or other applications high in suspended solids.

GEOMETRIC CONSIDERATIONS

Horizontal vs. Vertical Gas Flow

Horizontal flow generally provides higher efficiency at slightly higher pressure drop. In horizontal flow the profiles split the gas flow into single streams. The profiles turn the gas stream, but liquid drops cannot make the short radius as easily as the gas molecules. Therefore, inertia forces the liquid drop against the wall where the drops agglomerate and fall by gravity in areas of low velocity. When a drop contacts the profile surface, it is transformed into a liquid film, which is pushed along and drained as a film. Drop reformation is prevented. The liquid film drains at 90° relative to the gas flow.

Since the drops do not have to flow back against the gas flow, the liquid draining capacity is greater, the allowable velocities are greater, and the limit drop size is smaller. Because the drag coefficient is low, higher velocities are permissible without excessive pressure drop. At higher velocity smaller drops are removed due to the increased inertial force. This results in greater overall efficiency. (Figure 1)

On the other hand, in vertical flow, the liquid must flow back against the gas stream - countercurrent flow.

FIGURE 1

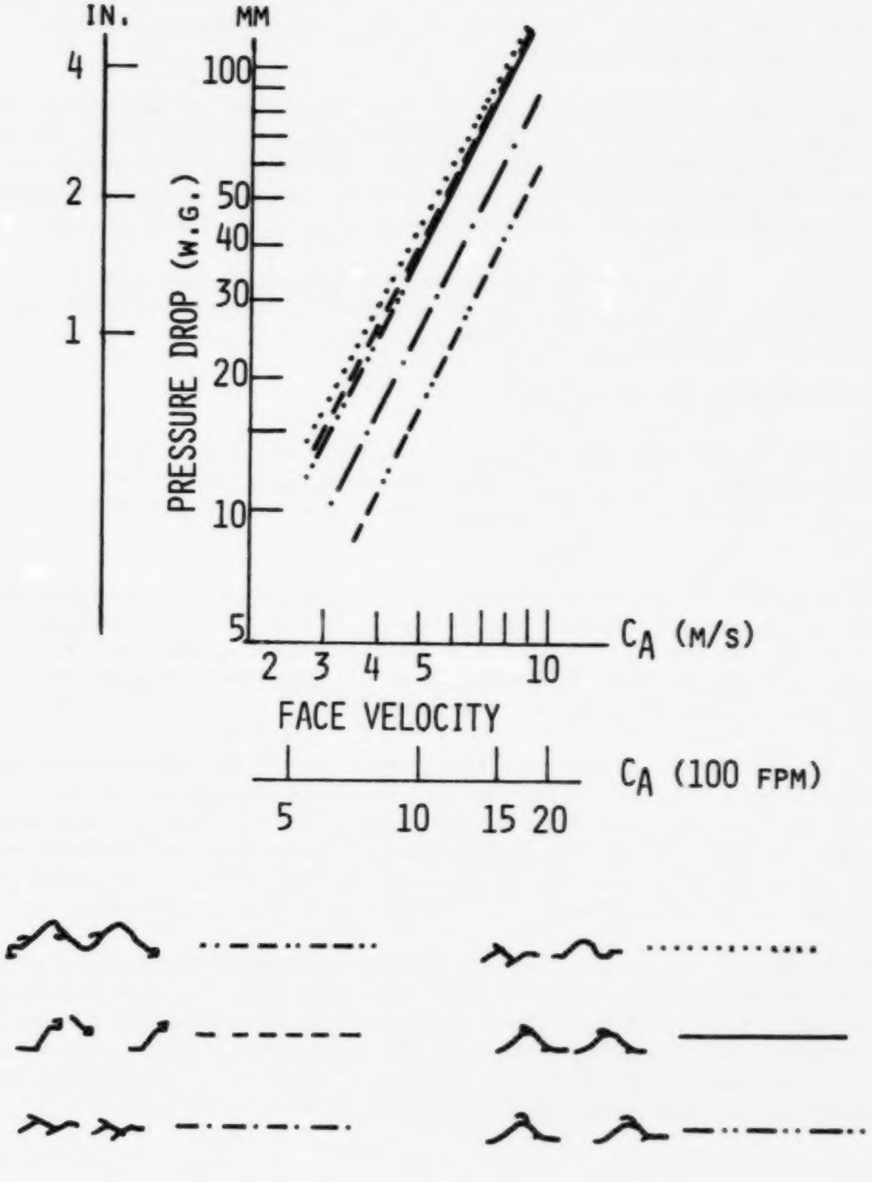
IN.
4
2
1
MM
100
50
40
30
20
10
5
PRESSURE DROP (W.G.)
C_A (M/S)
2
3
4
5
10
FACE VELOCITY
C_A (100 FPM)
5
10
15
20

In conventional socalled chevron or zig-zag eliminators drops collect in a similar fashion, however, reentrainment will occur above 600-700 fpm because droplets draining off the flat surface will be picked up by the force of the gas. To drain against the gas stream, the liquid film must be channeled into profile areas of low gas velocity, and subsequently drain into streams of large drops or continuous streams. The gas velocity for vertical flow must be lower to accommodate this draining. The profile design used for vertical flow cannot be the same as that for horizontal flow, without losing both efficiency of removal and critical velocity (reentrainment point).

Generally, the gas velocities for vertical flow eliminators, even of advanced design, are under 1200 fpm at standard conditions, while velocities may be 2000 fpm or as high as 3000 fpm for horizontal flow. Thus, the remainder of this information will concentrate on horizontal flow representing the maximum performance in a mist eliminator.

Vertical flow may be converted into horizontal flow either by modification to the discharge ducting or within the vessel itself, through mechanical arrangement modification.

PROFILE GEOMETRIC CONSIDERATIONS

Because velocities are higher in horizontal flow, the profile configuration becomes increasingly important. Profile shape and spacing control the angular acceleration and local gas velocity within the mist eliminator.

Performance of the more streamlined shapes is also superior because, in general, it is possible to space the profiles closer together, thereby increasing the velocity and the resulting inertia imparted to the drop. However, extra care in design must be exercised to prevent losing the liquid film off the rear of the profile.

Profile spacing illustrates the precision of an advanced design mist eliminator. If, for instance, profiles are spaced at 20 mm, a change in spacing of only 5 mm can produce a 100% change in the velocity within the profile. Thus, it is imperative that close tolerances be held. Part of the cost of a mist eliminator is the maintenance of close tolerances over large duct areas; i.e. 30 x 30 ft. cross section.

Performance resulting from optimizing the above factors is shown in Figure 2. It can be seen that the various constructions cover a range approximately five fold in limit drop size. As gas velocity is increased, an eliminator will lose its film off its down-stream edge and the performance will be destroyed. This can be seen in Figure 3 as well as the trade-off of pressure drop vs. limit drop size.

FIGURE 2

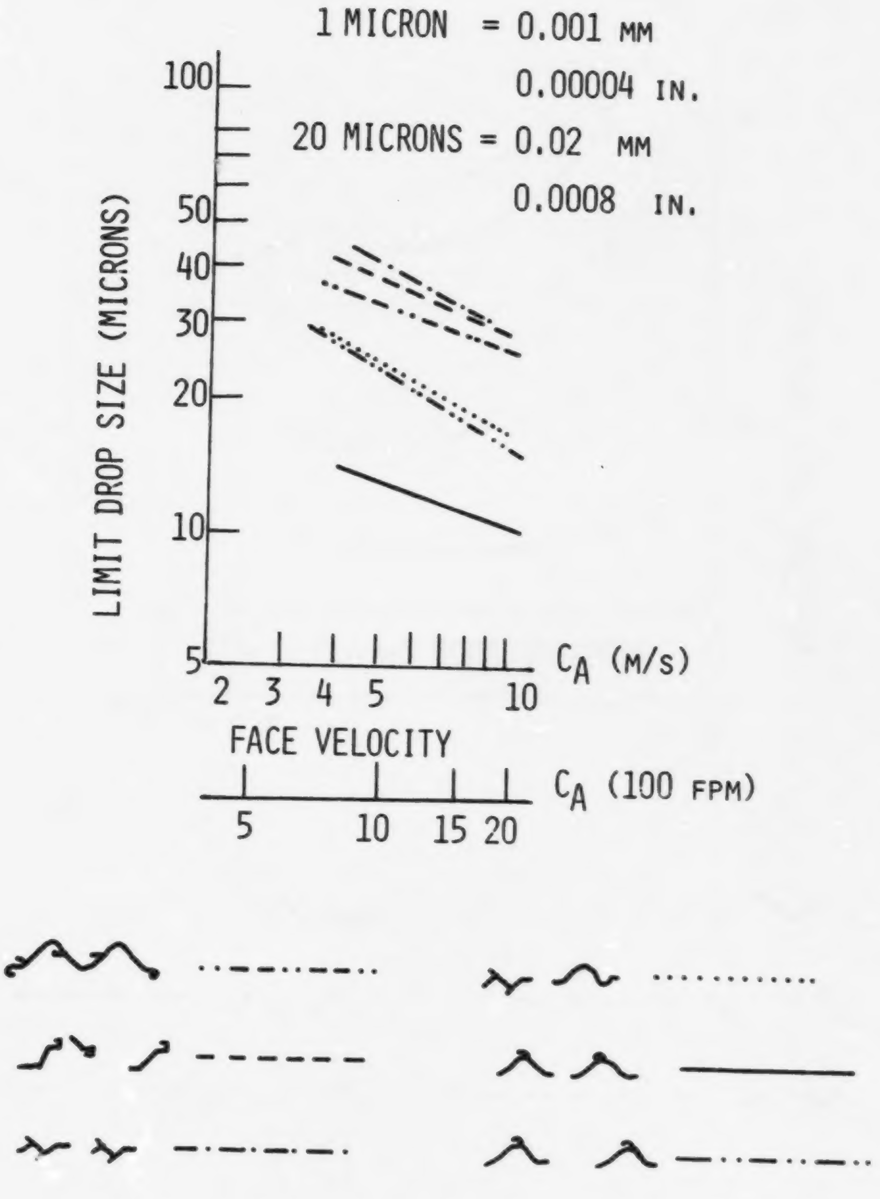
1 MICRON = 0.001 MM
0.00004 IN.
20 MICRONS = 0.02 MM
0.0008 IN.
LIMIT DROP SIZE (MICRONS)
100
50
40
30
20
10
5
2
3
4
5
10
C_A (M/S)
FACE VELOCITY
5
10
15
20
C_A (100 FPM)

FIGURE 3

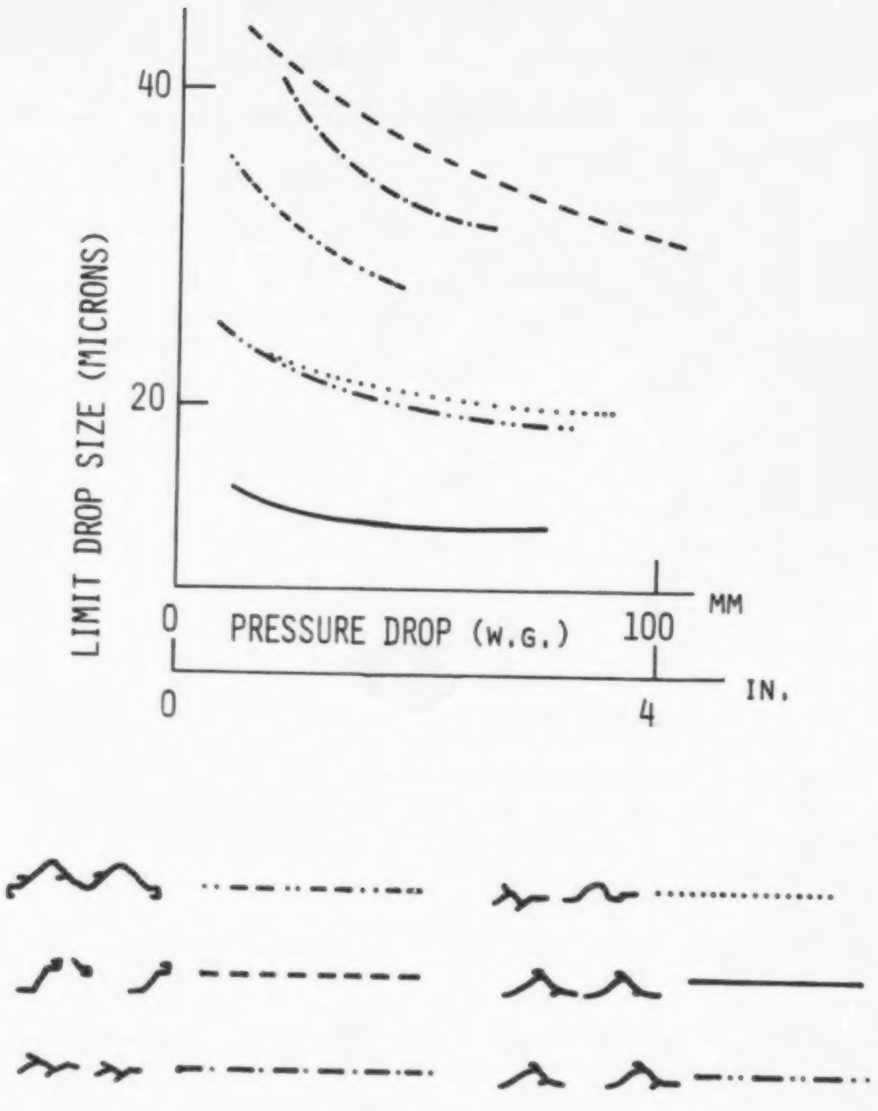

SLURRIES AND PLUGGING

Slurries, of course, present plugging problems if not handled correctly. More streamlined profiles will have less build-up because of their streamlined shape, but because they are more efficient, they dry the gas stream so much that the solids do come out on the rear sides. Adequate spray systems are then necessary.

As a gas proceeds through an eliminator, the water is literally wrung out until the gas becomes so dry, that there is no longer liquid enough to rinse off the profiles. If three or four 90° turns are arranged consecutively, it may be that build-up starts to occur by the time the down-stream turn is reached.

Thus, it is sometimes desirable to separate the turns into two banks as shown in Figures 1 - 3. The final two shapes are identical, but the last one is separated, while in the one immediately above (solid line curve) the two banks are adjacent. Separation of banks of shapes is also evident in designs 2, 3 and 4. These permit the use of higher volume sprays to insure rewetting and slurry removal, whether spraying is continuous or intermittent. There is no need to interfere with continuous operation of the eliminators while spraying. Sprays for large and small systems can be so programmed as to operate while the scrubber is on stream without significant carryover of the spray itself. The most effective wash spray utilizes a full cone nozzle operating in a 30 - 60 psi range. The cone angle will vary with the practical nozzle spacing from 60° - 120°. To be effective, a rate of 1.5 - 3 gpm/ft^2 of eliminator face area is required. The duration is a function of the system scaling potential and wash water quality.

Design of a separate bank system is shown in Figure 4 showing the mist eliminator modules 3 rows high in 28 x 28 ft. duct. Note the intermediate sprays. Figures 5 and 6 show the construction of the bottom and upper modules, in this case of polypropylene. Note the steep drain structure on the upper module to prevent solids build-up from the slurries or sludges.

CONCLUSION

An understanding of the details of shape factors in mist eliminators leads to improved performance. Engineering of the mist eliminator portion of a scrubbing system requires a total integration, considering performance required, pressure drop available and good washing practice. The success or failure of any scrubbing system is the proper function of the eliminator.

FIGURE 4

T-100 MIST ELIMINATOR

DUCT SIZE 28 X 28 FT.

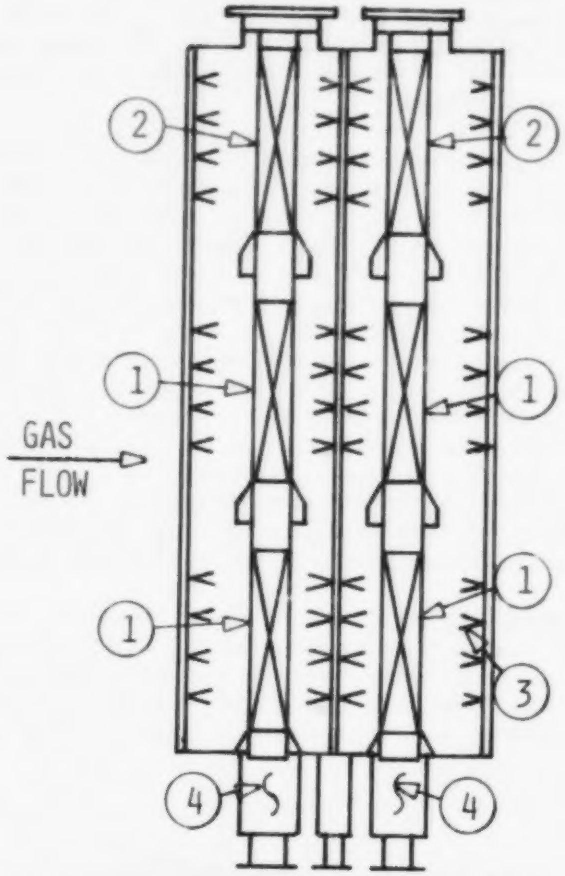
2
2
1
1
GAS
FLOW
1
1
3
4
4

1 BOTTOM MIST ELIMINATOR MODULE
2 UPPER MIST ELIMINATOR MODULE
3 SPRAY NOZZLES
4 DRAIN SUMP

Figure 5

BOTTOM MIST ELIMINATOR MODULE

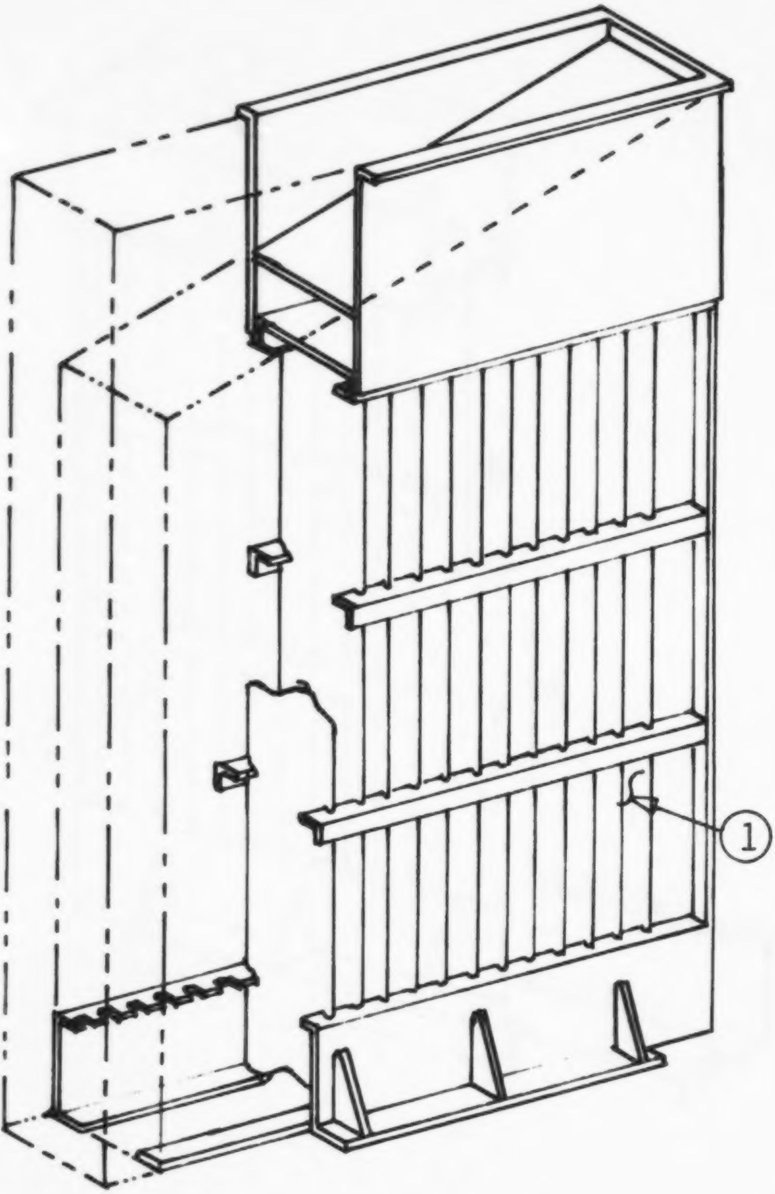

FIGURE 6

UPPER MIST ELIMINATOR MODULE

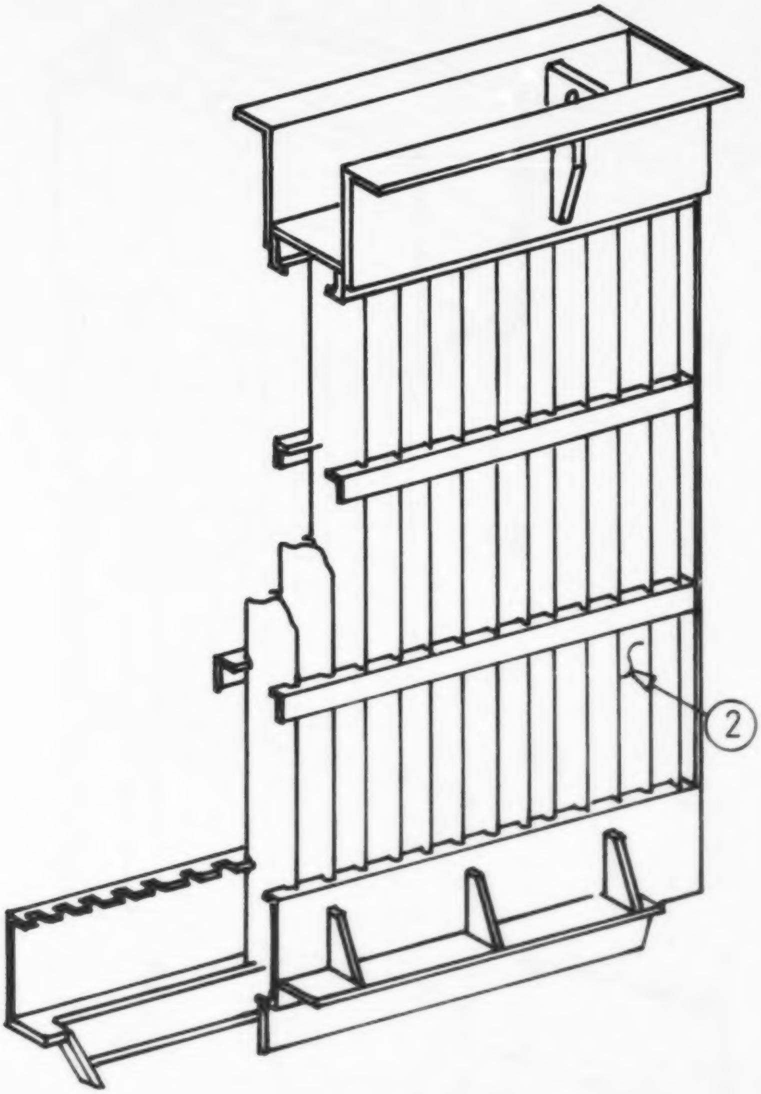

Figure 7

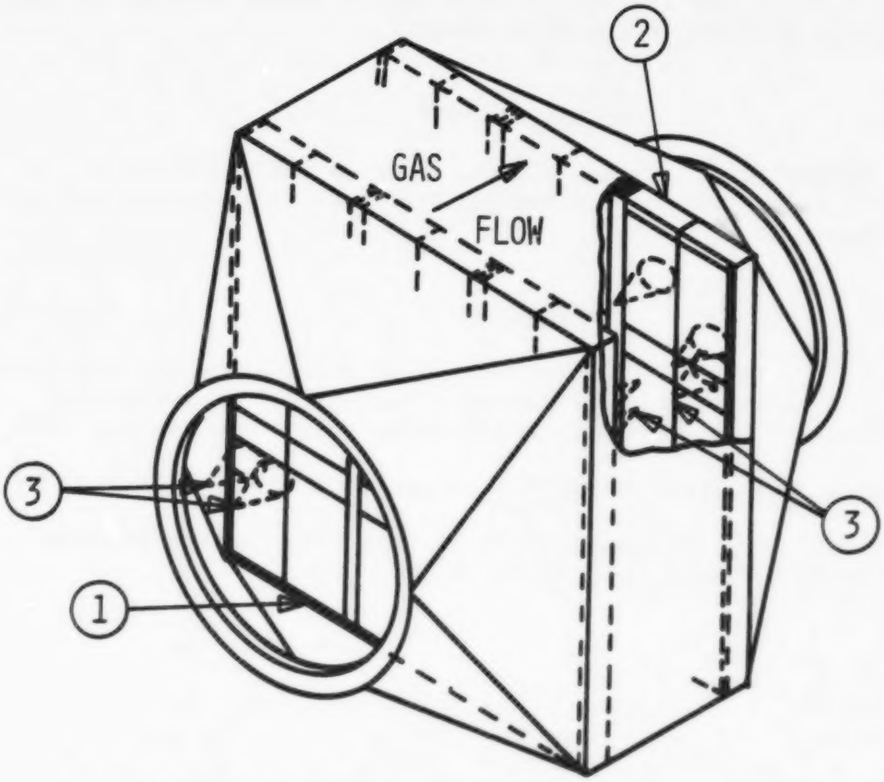
2
GAS
FLOW
3
3
1

1 BOTTOM MIST ELIMINATOR MODULE
2 UPPER MIST ELIMINATOR MODULE
3 SPRAY NOZZLES

Specific cost benefit design considerations for FGD systems employing socalled throwaway lime/limestone process technology should utilize two stages of horizontal flow eliminators. Each separated row should be provided with intermittent wash on both upstream and downstream sides.

In order to reduce equipment size without sacrifice in pressure drop, the eliminators should function at 7 m/s (1400 fpm) with a pressure drop no greater than 10-15 mm (.4-.6 inch) w.c. and separate all droplets 25 micron and greater in order to maintain minimum reheat energy and particulate emission requirements. For regenerative solution scrubbing systems, the eliminator stages may be moved adjacent to each other without need for intermediate sprays.

ACKNOWLEDGEMENT

The authors wish to thank Messrs. M. Maeda and K. Fukuta of NGK Insulators, Ltd., Chemical Engineering Division who performed much of the work reported herein.

REFERENCES

1. Regehr, Dr. Ing. U., Calculation of Mist Eliminators for Industrial Gases, p. 135-144 of Environmental Engineering, G. Lindner and K. Nyberg, D. Reidel Publishing Company, Dordrecht, Holland, 1973.

2. Tennyson, R.P., Mist Eliminator Design, APCA, 77:25.4, June 1977.

3. Lace, R.H., Sr., Maximizing Economic and Environmental Benefits Through Mist Elimination, TAPPI, April 1978.

FINE PARTICLE COLLECTION IN A MOBILE BED SCRUBBER

S. Yung, R. Chmielewski, S. Calvert
Air Pollution Technology, Inc.
San Diego, California

D. Harmon
U.S. Environmental Protection Agency
Industrial Environmental Research Laboratory
Research Triangle Park, North Carolina

INTRODUCTION

The mobile bed scrubber is a three-phase contacting device which consists of several packed beds stacked inside a vessel shell. The gas flowing upward with a high velocity, fluidizes the packing; the liquid simultaneously flows toward the bottom of the column. The packing commonly used is 2.5 cm or 3.8 cm diameter lightweight spheres even though other materials such as lightweight plastic rings, have been used.[1] The packing is supported and retained by non-flooding grids sufficiently far apart to permit turbulent and random motion of the spheres. The static packing depth is 0.15-0.60 m (0.5-2 ft).

Mobile bed contactors have been used as gas absorption towers for many years. In recent years, they are also being used in the removal of sulfur dioxide and particulates from stack gases by a lime or limestone slurry. Fundamental studies on the mechanics of mobile beds such as hydrodynamics, pressure drop, liquid holdup, minimum fluidization velocity and axial liquid mixing have been conducted by a number of investigators[2-7]. There is no carefully performed study on the particle collection in a mobile bed scrubber. The work reported here has been supported by the EPA and its objectives are to investigate the particle collection in a mobile bed scrubber and the feasibility of using it as a flux force condensation (FF/C) scrubber. This paper deals with the particle collection efficiency of the mobile bed without FF/C effects.

EQUIPMENT

The schematic flow diagram of the mobile bed FF/C scrubber pilot plant is shown in Figure 1. It consists of a gas burner, furnace, quencher, the mobile bed scrubber, entrainment separator, cooling tower, and liquid and gas movers.

The mobile bed scrubber shell was made from reinforced fiberglass duct with an inside diameter of 0.51 m (20 in). The overall height of the scrubber was 6.1 m (20 ft) of which 2.75 m (9 ft) was reserved for the mobile beds. A maximum of three stages can be housed within this space. There was an empty space of 0.92 m (3 ft) above the top retaining grid. This space was provided for the settling out of large entrainment drops. Three Plexiglas windows were also installed for the observation of bed movement and the measurement of fluidized bed height.

The mobile bed packings were hollow polypropylene spheres. Three sphere sizes, 2.5 cm, 3.8 cm, and 5.1 cm diameter, were studied. The average weight for each sphere was 1.5 g, 4.5 g and 8.0 g for the 2.5 cm, 3.8 cm, and 5.1 cm diameter spheres, respectively.

The spheres were supported and retained by means of non-flooding grids. Two types of bed supporting and retaining grids have been used in the mobile bed scrubber. They were hardware screens and plastic nets. The wire diameter of the hardware screen was 0.16 cm (1/16 in.) and the openings were 1.1 cm x 2.4 cm (7/16 in. x 15/16 in.). The open area was about 82%. The plastic net was made of polypropylene ribbons. The width of the ribbon was about 0.4 cm (5/32 in.) and the openings were 0.6 cm x 0.75 cm (15/64 in. x 19/64 in.). The open area was about 40%. The grids rested on square frames. The frames were made of 2.5 cm aluminum angles and each side measured 33 cm. The effective open areas of the hardware screen support and the plastic net support were 68% and 34%, respectively.

In the particle collection experiment, air and water at ambient conditions were used. The burner, furnace, quencher, and the cooling tower were idle for these experiments. Water was distributed evenly to the mobile bed just above the third stage top retaining grid through PVC pipes drilled with 1.27 cm (0.5 in.) holes. The air and water flowrates were measured by means of calibrated venturi meters. Pressure drop across the mobile bed was measured with calibrated gauges.

EXPERIMENTAL PROCEDURES

The purpose of the experimental program was to measure the mobile bed scrubber performance under typical industrial conditions. Air and water rates would cover common operating ranges. In starting the experiments, the water pump and blower were turned on and the flowrates were adjusted to desired levels. After steady conditions were obtained, test aerosols were injected just after the quencher. Four types of aerosols were used in the study. They were titanium dioxide, red iron oxide, power plant fly ash and grey iron cupola dust.

Particle size distribution and concentration at the scrubber inlet and outlet duct were sampled simultaneously with cascade impactors. The overall collection efficiency and the grade penetration curve were calculated from the impactor data.

EXPERIMENTAL RESULTS AND DISCUSSIONS

Pressure Drop

For a fully fluidized mobile bed, the pressure drop is made up of the sum of those due to the dry retaining grids, the weight of the dry packings, the liquid holdup in the bed, liquid froth retained on the grid, and the wall friction[2,4]; i.e.:

$$\Delta P = \Delta P_b + \Delta P_L + \Delta P_f + \Delta P_c + \Delta P_{Lh} \qquad (1)$$

Except for grids with small openings and small fractional open area, the losses due to wall friction and supporting grid friction are small. There is also little liquid retained on the supporting grids. The pressure drop across the mobile bed, then, can be considered equal to the sum of the weights of the packing and the liquid holdup in the bed [4,6].

Chen and Douglas[3] and Kito, et al.[4], experimentally measured the liquid holdup in a mobile bed. They found that the liquid holdup related to the fixed bed volume is approximately independent of gas flowrate. Since the weight of dry packing does not depend on gas flowrate, the pressure drop across a fully developed mobile bed should not depend on gas flowrate.

The pressure drop across the three stage mobile bed with hardware screen support is plotted against superficial gas velocity with liquid flowrate as parameter in Figure 2. As can be seen, pressure drop is almost independent of gas flowrate when the liquid rate is low. At higher liquid rates, pressure drop is slightly dependent on gas flowrates. These findings are consistent with Wozniak[7], Blyakher[2], Barile and Meyer[8], and Epstein[9], et al.'s results. Wozniak found that the pressure drops increase proportionally to the linear gas velocity to the 0.2 power.

Figure 3 is the pressure drop data of the plastic net supported mobile bed. Under the same operating conditions, plastic net support causes a higher pressure drop than the hardware screen. The increase in pressure drop is not solely due to the high frictional loss of the plastic net support.

There are two possible causes of the high pressure drop with the plastic net support. The first one is that liquid holdup in the bed increased with the plastic end support. In Chen and Douglas' experiment, they used only one type of supporting grid: parallel rods. Therefore, in their correlation the effects of the supporting grid geometry on liquid holdup were not accounted for. Kito, et al. used three different grids (8 mesh, 5 mesh, and metal screen with 1.2 cm openings and 84% opening ratio) in their experiments. They found that the geometry of the supports has great effect on the amount of liquid holdup. Grids with smaller openings give higher liquid holdup which in turn causes the pressure drop to rise.

A second factor which contributes to higher pressure drop with the plastic end support is the liquid froth retained on the grid. Some Russian researchers[2] have observed that a liquid froth was retained on the grids which had small openings. It is possible that grids with small openings and small fractional open area act as sieve plates.

Figure 4 is the pressure drop across the three stage plastic net supports; i.e., three stage mobile bed with packing removed. Thus, the measured pressure drops are due to the liquid retention on the grids.

The difference in pressure drop with and without packing for the plastic net supported mobile bed is equal to the pressure drops due to the weights of packings and liquid holdup. The calculated $\Delta P_b + \Delta P_{Lh}$ for the plastic net support is independent of gas flowrate up to the flooding velocity and is lower than that for the hardware screen support.

Particle Collection

Particle collection data were reduced to plots of particle penetration versus particle diameter for all experimental runs. Scrubber performance depended only on the overall pressure drop across the scrubber stages. The grade penetration curve of a one-stage mobile bed would have been the same as that of a two-stage mobile bed if they had had the same overall pressure drop.

Under the same operating conditions and with the same bed geometry, the particle collection of a three-stage mobile bed scrubber cannot be predicted from the collection of a one-stage scrubber; i.e., $Pt_3 \neq Pt_1{}^3$.

Different mobile bed scrubber geometries and operating conditions result in different scrubber performances and pressure drops. It is very difficult to evaluate and compare the scrubber capability based only on the grade penetration curves. A mobile bed scrubber with plastic net supports has a higher collection efficiency than a hardware screen supported mobile bed with the same bed geometry and operated under the same parameters. It is not true that a plastic net supported bed is better than a hardware screen supported bed since the pressure drop of the plastic net supported mobile bed is higher than that of the hardware screen supported bed.

A useful correlation called the cut/power relationship has been developed by Calvert[10] for scrubber evaluation purposes. Calvert has shown that the scrubber performance cut diameter is a very convenient parameter for describing the performance capability of a particle scrubber. Cut diameter is the particle diameter collected with 50% efficiency. The cut diameter is obtained from the experimental grade penetration curve. The cut/power relationship is a plot of the cut diameter given by the scrubber against pressure drop or power input.

Figure 5 is a plot of the measured performance cut diameter of the mobile bed scrubber versus measured pressure drop for various scrubber configurations and operating conditions. The data fall on a straight line on log-log paper. The equation describing the straight line is:

$$d_{pc} = 1.66 \times 10^{4} (\Delta P)^{-1.225} \qquad (2)$$

Figure 6 compares the published mobile bed performance data with that of the present study. As can be seen, data reported by Epstein, et al.[9], Johnson, et al.[11], and Rhudy and Head[12] agree with that of the present study. Data of Ensor, et al.[13], show slightly high efficiencies.

Ensor, et al.[13] conducted a performance test on a mobile bed scrubber which was installed in a coal burning power plant. The scrubber was installed to supplement the particulate control by the electrostatic precipitator. There was a presaturator just ahead of the mobile bed and a flue gas reheater after the scrubber.

Particle samples were taken before the presaturator and after the reheater. Thus, the particle sample might not be a representative sample of what actually existed in the scrubber; especially since there was a presaturator and a heater in between. Particle growth and evaporation might occur in the presaturator and in the reheater, respectively.

Each scrubber type has a unique cut/power relationship which describes the dependency of scrubber performance on pressure drop. The uniqueness of the cut/power relationship offers a simple method to evaluate the capabilities of different scrubber types. Figure 7 is a plot of the cut/power relationship for several scrubber types.

Of the four scrubber types, gas atomized spray, mobile bed, packed bed, and sieve plates, the gas atomized spray scrubber has the best performance capability. At a pressure drop of 20 cm W.C., the gas atomized spray scrubber can achieve a performance cut diameter of 0.75 μmA. At the same pressure drop the performance cut diameters are 1.6 μmA, 1.7 μmA, and 1.2 μmA for the mobile bed, packed bed, and sieve plate with 0.32 cm hole diameter, respectively. Industrial mobile beds usually operate at pressure drops around 30 cm W.C. The performance cut diameter is about 0.9 μmA which is better than packed beds and sieve plates but less efficient than venturi scrubbers.

DESIGN EQUATIONS

Pressure Drop

There are several empirical correlations reported in the literature for the prediction of pressure drop across the mobile bed. Table 1 lists four of the correlations for the calculation of pressure drop due to the weights of dry packing and liquid holdup. There are other correlations, mostly by Russian researchers,[1,2] which contain constants which have to be determined experimentally for each application.

Predictions by these correlations were compared with the experimental data obtained in this study for the hardware screen supported mobile bed. The comparison revealed that predictions by Uchida, et al.'s[6] correlation are much higher than that actually measured. Predictions by Kito, et al.'s[4] correlation and by Wozniak's[7] correlation are better than Uchida, et al.'s correlation; but they still are higher than that measured.

Chen and Douglas'[3] prediction agrees with the data only for the hardware screen support. However, Chen and Douglas' correlation did not predict the correct dependence of pressure drop on liquid flowrate. Compared to the pressure drop data on the plastic net supported mobile bed, Chen and Douglas' predictions are much lower than measured.

An empirical correlation was derived in this study for the prediction of pressure drop due to liquid holdup. The correlation is:

$$\Delta P_{Lh} = 8.04 \times 10^{4} \rho_G u_G^2 \left(\frac{H_s}{d_b}\right)^{0.84} \left(\frac{d_b \rho_G u_G}{\mu_G}\right)^{-1.75} \left(\frac{d_b \rho_L u_L}{\mu_L}\right)^{0.96} \left(\frac{\rho_b}{\rho_L}\right)^{0.4} \tag{3}$$

An empirical correlation was also derived in this study for the prediction of pressure drop due to the liquid froth retained on the grid:

$$\Delta P_L = 8.80 \times 10^{-2} \left(\frac{D_c}{f_s d_e}\right)^{2.6} u_G^{0.5} u_L^{2.0} \tag{4}$$

If the friction losses are neglected, the pressure drop across one stage of the mobile bed is:

$$\Delta P = g\ (1-\varepsilon)\ \rho_b\ H_s + \Delta P_{Lh} + \Delta P_L \tag{5}$$

The predictions by equation (5) are compared with data reported by Epstein, et al.[9], Barile and Meyer[8], Kito, et al.[4], Blyakher, et al.[2], Ticky, et al.[5], and Douglas, et al.[14] in Figure 8. As can be seen, the agreement between prediction and data is good.

Particle Collection

There is only one model available in the literature for particle collection in a mobile bed. It is a semi-empirical relationship presented by Bechtel Corporation[15] in a June 1971 report on the Shawnee project for EPA. This correlation is based on the premise that collection efficiency is due to inertial impaction on balls.

The predictions by this equation did not agree with the data obtained in this study. The drawback of this equation is that it did not include the effect of supporting grids on particle collection. As mentioned earlier the efficiency of a plastic net supported mobile bed is higher than that of a hardware screen supported mobile bed with the same bed geometry, and liquid and gas flowrates.

Particle collection in a mobile bed scrubber may be due to inertial impaction on the atomized liquid drops. Thus, particle collection can be predicted if the atomized drop diameter and amount of liquid in drop form can be calculated. However, the hydrodynamics of a three phase fluidized bed are extremely complex. It is impossible to derive the theoretical equations for drop size and quantity of drops. Therefore, an empirical equation is proposed for particle collection in a mobile bed scrubber. The empirical equation is:

$$Pt_d = \exp \left| -1.23 \times 10^{-7}\ (\Delta P)^{1.96}\ \ d_{pa}^{\ 1.6} \right| \tag{6}$$

In predicting the performance of a mobile bed, one first predicts the pressure drop by means of equation (5) and then, the performance cut diameter by means of equation (2) or (6). The penetration for other particle diameters can be calculated from equation (6).

CONCLUSIONS

The particle collection capability of the mobile bed scrubber has been determined experimentally and design equations have been derived in this study. The particle collection efficiency was found to be a strong function of the gas phase pressure drop. The pressure drop can be increased by using heavier balls and support grids with higher pressure drops. The pressure drops of most industrial mobile bed scrubbers are about 30 cm W.C. At this value of pressure drop, the particulate collection capability of the mobile bed scrubbers is less than that of venturi scrubbers. However, mobile bed scrubbers offer advantages over the venturi scrubbers. The mass transfer capability of mobile bed scrubbers is higher than that of venturi scrubbers. Thus, mobile bed scrubbers may be used to control particulate emissions as well as gaseous emissions.

ACKNOWLEDGEMENT

The work described in this publication was performed under Contract No. 68-02-2124 with the U.S. Environmental Protection Agency.

REFERENCES

1. Levsh, I.P., N.I. Krainev, and M.I. Niyazov. Calculation of the Pressure Drop and Heights of Three-Phase Fluidized Beds. Int'l Chemical Engineering. 8: 311-312, 1968.

2. Blyakher, I.G., L. Ya Zhivaikin, and N.A. Yurovskaya. Investigation of Hydrodynamics and Mass Transfer in Equipment with Movable Packing. Int'l Chemical Engineering. 7: 485-490, 1967.

3. Chen, B.H. and W.J. M. Douglas. Liquid Holdup and Minimum Fluidization Velocity in a Turbulent Contactor. The Canadian Journal of Chemical Engineering. 46: 245-249, August 1968.

4. Kito, M., T. Monma, Y. Kayama, T. Sagai, and S. Sugiyama. Pressure Drop and Bed Expansion in a Mobile Bed. Kagaku Kogaku Ronbunshu. 2: 276-479, 1976.

5. Tichy, J., A. Wong, and W.J.M. Douglas. Pressure Drop in a Mobile Bed Contactor. The Canadian Journal of Chemical Engineering. 50: 215-220, 1972.

6. Uchida, S., C.S. Chang, and C.Y. Wen. Mechanics of a Turbulent Contact Absorber. The Canadian Journal of Chemical Engineering. 55: 392-396, 1977.

7. Wozniak, M. Pressure Drop and Effective Interfacial Area in a Column with a Mobile Bed. Int'l Chemical Engineering. 17: 553 559, 1977.

REFERENCES, cont.

8. Barile, R.G., and D.W. Meyer. Turbulent Bed Cooling Tower. Chemical Engineering Progress, Symposium Series. 67: No. 119, 134-143, 1971.

9. Epstein, M., et al. EPA Alkali Scrubbing Test Facility: Summary of Testing Through October 1974. EPA-650/2-75-047, NTIS No. PB 244-901, June 1975.

10. Calvert, S. Engineering Design of Fine Particle Scrubbers, Journal of APCA. 24: 929-933, 1974.

11. Johnson, J.M., D.G. Jones, A. Weir, W.C. Martin, and S. Calvert. Scrubber Experience at Mohave, Paper No. 11. In Proceedings: Conference on Particulate Collection Problems in Converting to Low Sulfur Coals. EPA-600/7-76-016, NTIS No. PB 260-498/AS, October 1976.

12. Rhudy, R.G. and H.N. Head. Results of Flue Gas Characterization Testing at the EPA Alkali Wet Scrubbing Test Facility, Paper No. 13. In Proceedings: Second EPA Fine Particle Scrubber Symposium. EPA-600/2-77-193, NTIS No. PB 273-828/AS, September 1977.

13. Ensor, D.S., et al. Evaluation of a Particulate Scrubber on a Coal Fired Utility Boiler. EPA-600/2-75-074, NTIS No. PB 249-562/AS, November 1975.

14. Douglas, H.R., I.W.A. Snider, and G. Tomlinson. The Turbulent Contact Absorber. Chemical Engineering Progress. 59: 85-89. December 1963.

15. Calvert, S, J. Goldshmid, D. Leith, and D. Mehta. Scrubber Handbook, Wet Scrubber System Study, Volume I. EPA-R2-72-118a, NTIS No. PB 213-016, August 1972 (p. 5-156).

NOMENCLATURE

Latin

D_c = column diameter, m

D_c' = equivalent diameter of the grid, m

d_b = packing diameter, m

d_e = equivalent diameter of the grid opening, m

d_{pa} = aerodynamic particle diameter, μmA

d_{pc} = cut diameter, μmA

f_s = fractional open area of the retaining grid

g = acceleration of gravity, m/s^2

H_d = dynamic or operational bed height, m

H_s = static bed height, m

h_b = holdup of packing, m^3/m^3

h_{bo} = packing holdup related to fixed bed, m^3/m^3

h_L = liquid holdup in bed, m^3/m^3

h_{Lo} = liquid holdup in bed related to fixed bed, m^3/m^3

L = liquid mass velocity, kg/m^2-hr

n = number of mobile bed stages

Pt_d = particle penetration for diameter d_p, fraction

Q_L = liquid volumetric flow rate, ℓ/min

u_G = superficial gas velocity, m/s

u_L = superficial liquid velocity, m/s

Greek

ρ_b = packing density, kg/m^3

ρ_G = gas density, kg/m^3

ρ_L = liquid density, kg/m^3

ε = porosity of static bed, fraction

μ_G = gas viscosity, Pa.s

μ_L = liquid viscosity, Pa.s

ΔP = overall pressure drop, Pa

ΔP_b = pressure drop due to the weight of dry packings, Pa

ΔP_c = pressure drop due to wall friction, Pa

ΔP_f = pressure drop due to friction of the dry retaining grids, Pa

ΔP_L = pressure drop due to liquid froth retained on the grid, Pa

ΔP_{Lh} = pressure drop due to liquid holdup in the bed, Pa

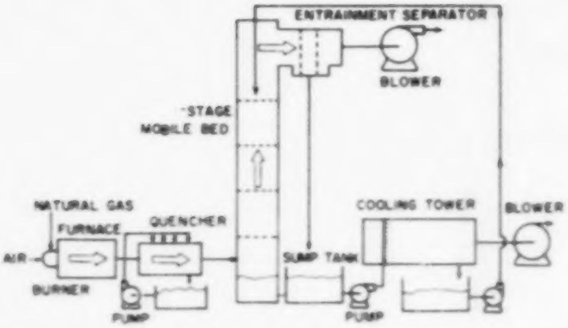
ENTRAINMENT SEPARATOR
BLOWER
-STAGE
MOBILE BED
NATURAL GAS
FURNACE
QUENCHER
COOLING TOWER
BLOWER
AIR
BURNER
SUMP TANK
PUMP
PUMP

FIGURE 1. PROCESS FLOW DIAGRAM OF MOBILE BED FF/C SCRUBBER SYSTEM.

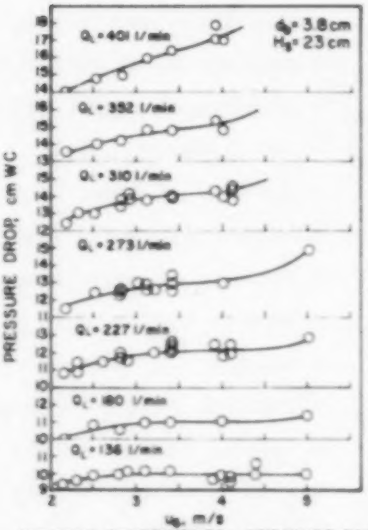

FIGURE 2. EXPERIMENTAL PRESSURE DROP OF A 3-STAGE MOBILE BED WITH HARDWARE SCREEN SUPPORT

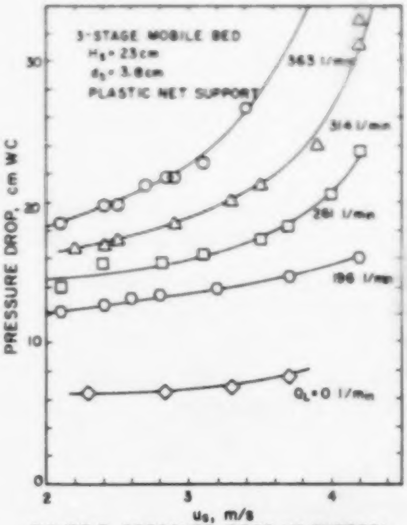

FIGURE 3. PRESSURE DROP VS SUPERFICIAL GAS VELOCITY FOR 3-STAGE MOBILE BED WITH PLASTIC NET SUPPORT.

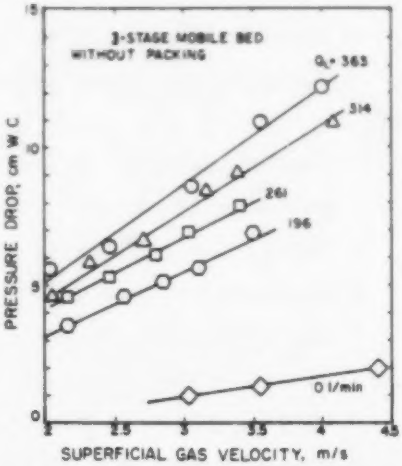

FIGURE 4. PRESSURE DROP ACROSS FOUR PLASTIC NET SUPPORTS

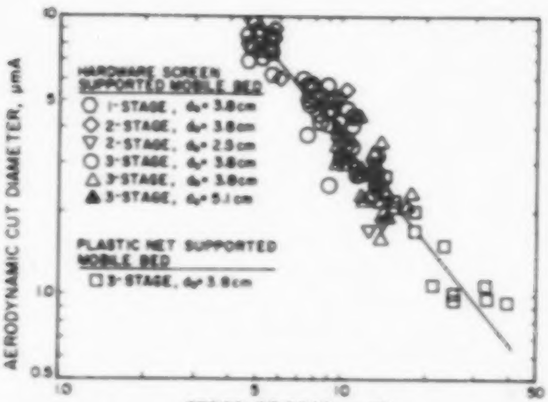

FIGURE 5. EXPERIMENTAL CUT/POWER RELATIONSHIP FOR MOBILE BED SCRUBBER.

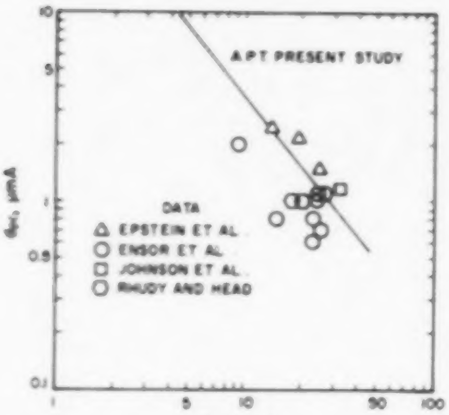

FIGURE 6. COMPARISON BETWEEN PUBLISHED MOBILE BED PERFORMANCE DATA WITH PRESENT STUDY DATA.

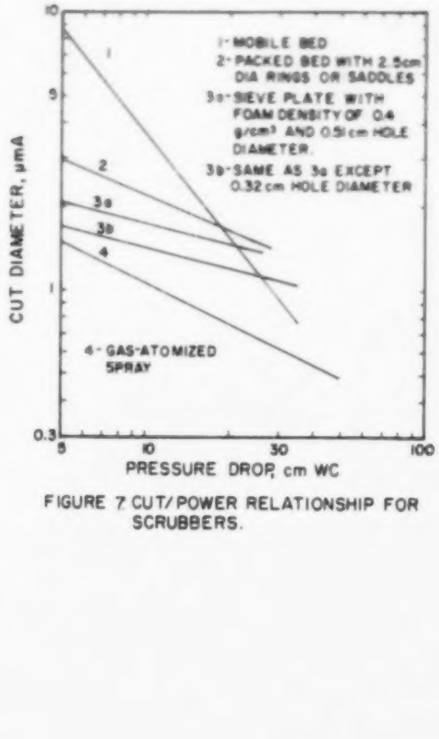

FIGURE 7 CUT/POWER RELATIONSHIP FOR SCRUBBERS.

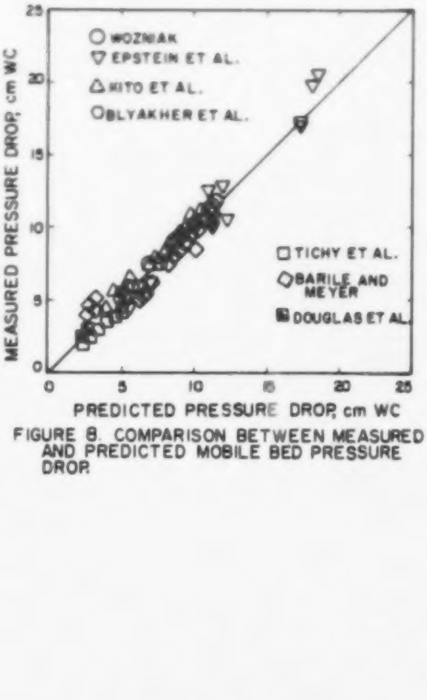

FIGURE 8. COMPARISON BETWEEN MEASURED AND PREDICTED MOBILE BED PRESSURE DROP

CONTROL OF PARTICULATE EMISSIONS WITH U.W. ELECTROSTATIC SPRAY SCRUBBER

Michael J. Pilat and Gary A. Raemhild
Department of Civil Engineering
University of Washington
Seattle, Washington 98195

ABSTRACT

The UW Electrostatic Scrubber system has been installed into two field portable pilot plants, each in a 40 ft. trailer. The UW Electrostatic Scrubber involves the use of electrostatically charged water droplets to collect air pollutant particles charged to a polarity opposite from the droplets. The Mark 1P UW Electrostatic Scrubber pilot plant has been tested at a coal fired boiler, a magnesium sulfite recovery (pulp mill), and a hog fuel (wood waste) boiler. The Mark 2P UW Electrostatic Scrubber pilot plant has been tested on dioctyl phthalate aerosol, on the emissions from a pulverized coal-fired boiler, and on the emissions from an electric arc steel furnace. Measured overall particle collection efficiencies range from about 25 to 99.8% depending upon the electrostatic scrubber operating conditions and the inlet particle size distribution. The test results illustrate that the addition of electrostatic charging of the aerosol particles and/or the spray liquor droplets can substantially enhance the collection efficiency for fine particles by wet scrubbers.

INTRODUCTION

Objectives of Research Project

The objectives of this on-going research project are to demonstrate

Preceding page blank

the effectiveness of the UW Electrostatic scrubber in controlling fine particle emissions from various industrial sources and use the information obtained as a basis for system modifications to improve the scrubber performance. Data from field tests is also to be used for preliminary designs and economic analyses of full-scale electrostatic scrubber systems.

Review of Previous Work

Penney (1944) patented an electrified liquid spray test precipitator involving particle charging by corona discharge and droplet charging by either ion impaction or induction. Penney's system consisted of a spray scrubber with electrostatically charged water droplets collecting aerosol particles charged to the opposite polarity. Kraemer and Johnstone (1955) reported theoretically calculated single droplet (50 micron diameter droplet charged negatively to 5,000 volts) collection efficiencies of 332,000% for 0.05 micron diameter particles (4 electron unit positive charges per particle). Pilat, Jaasund, and Sparks (1974) reported on theoretical calculation results and laboratory tests with an electrostatic spray scrubber apparatus. Pilat (1975) reported on field testing during 1973-1974 with a 1,000 acfm UW Electrostatic Scrubber (Mark 1P model) funded by the Northwest Pulp and Paper Association. Pilat and Meyer (1976) reported on the design and testing of a newer 1,000 acfm UW Electrostatic Scrubber (Mark 2P model) portable pilot plant funded by the EPA. Pilat, Raemhild, and Harmon (1977) reported on tests of the UW Electrostatic Scrubber pilot plant (Mark 2P model) on collecting laboratory generated DOP aerosols and emissions from a coal-fired boiler and an electric arc steel furnace. The UW Electrostatic Scrubber (patent pending) has been licensed to the Pollution Control Systems Corporation (of Renton and Seattle, Washington) for production and sales.

DESCRIPTION OF UW ELECTROSTATIC SPRAY SCRUBBER

General Description

The UW Electrostatic Scrubber involves the use of electrostatically charged water droplets to collect air pollutant particles electrostatically charged to a polarity opposite from the droplets. A schematic illustration of the UW Electrostatic Scrubber system is presented in Fig. 1.

The particles are electrostatically charged (negative polarity) in the corona section. From the corona section the gases and charged particles flow into a scrubber chamber into which electrostatically charged water droplets (positive polarity) are sprayed. The gases and some entrained water droplets flow out of the spray chamber into a mist eliminator consisting of a positively charged corona section in which the positively charged water droplets are removed from the gaseous stream.

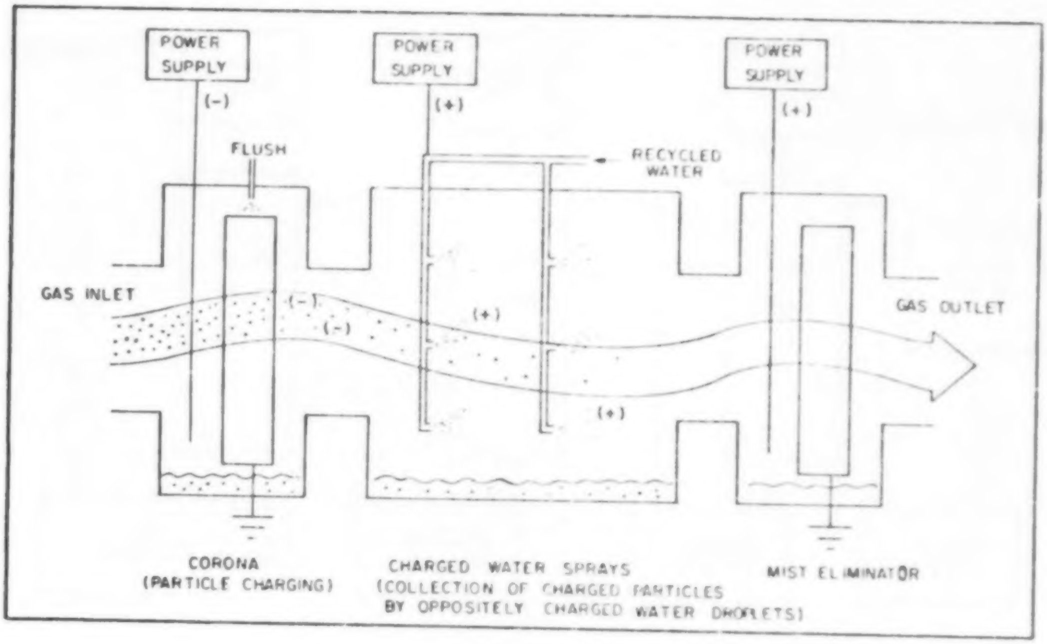
POWER SUPPLY
(−)
POWER SUPPLY
(+)
POWER SUPPLY
(+)
FLUSH
RECYCLED WATER
GAS INLET
(−)
(−)
(+)
(+)
GAS OUTLET
CORONA
(PARTICLE CHARGING)
CHARGED WATER SPRAYS
(COLLECTION OF CHARGED PARTICLES
BY OPPOSITELY CHARGED WATER DROPLETS)
MIST ELIMINATOR

Figure 1. UW Electrostatic Scrubber

Mark 1P UW Electrostatic Scrubber

A general schematic of the model Mark 1P is shown in Fig. 2. Incoming gases first pass through a stainless steel cooling tower for gas cooling and conditioning. The inlet sampling port follows the cooling tower (in the direction of gas flow). The gases then pass through three vertical particle charging and scrubbing sections. Following the last scrubbing section is a tube type mist eliminator after which the outlet sampling port is located. The gas stream is then exhausted to the atmosphere.

A model Mark 1P uses a "once through" scrubbing liquor for the spray towers. A continuous supply of fresh water is therefore necessary for operation.

Mark 2P Electrostatic Scrubber

The general layout of the UW Electrostatic Scrubber pilot plant (Mark 2P model) is shown in Fig. 3. The system (in the direction of gas flow) includes a gas cooling tower, an inlet test duct with sampling port, a particle charging corona section (corona no. 1), a charged water spray tower (tower no. 1), a particle charging corona section (corona no. 2), a charged water spray tower (tower no. 2), a positively charged corona section to collect the positively charged water droplets, an outlet test duct with sampling port port and a fan.

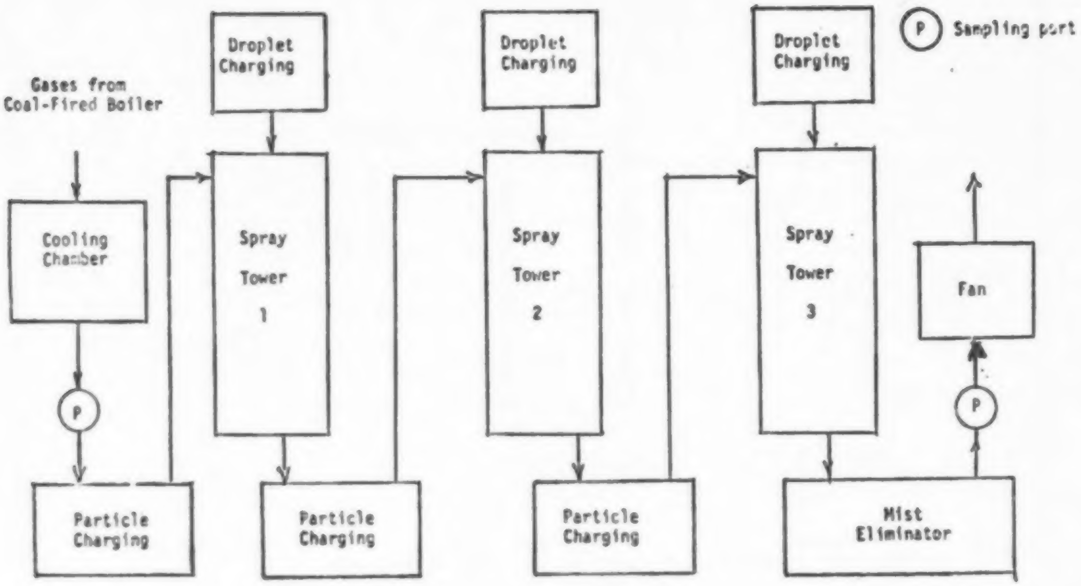

Sampling port
Gases from
Coal-Fired Boiler
Cooling Chamber
P
Particle Charging
Droplet Charging
Spray Tower 1
Particle Charging
Droplet Charging
Spray Tower 2
Particle Charging
Droplet Charging
Spray Tower 3
Mist Eliminator
P
Fan

Figure 2. Flow Diagram of UW Electrostatic Spray Scrubber
(Model Mark 1P)

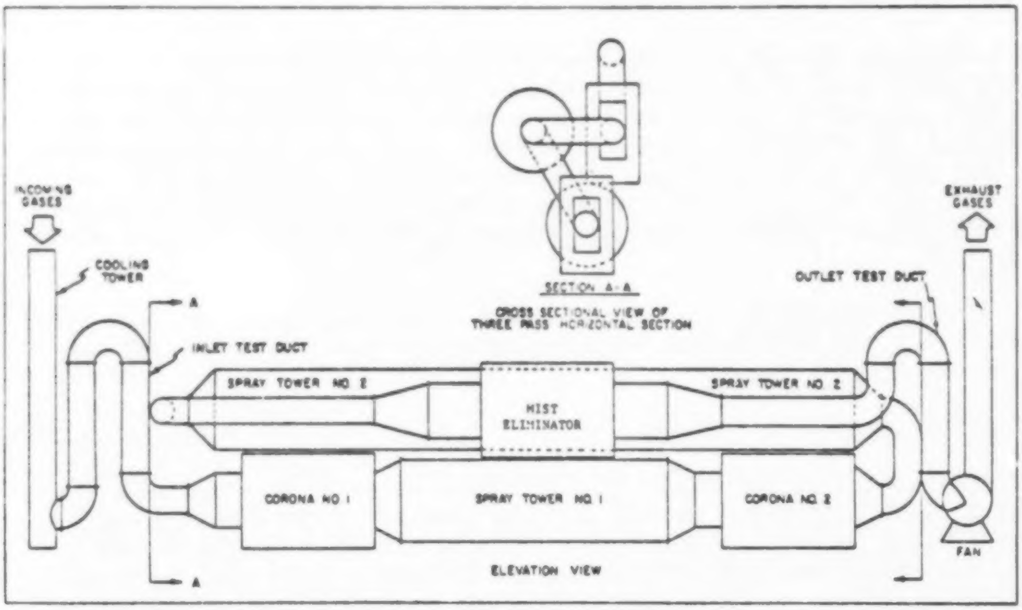

SECTION A-A
CROSS SECTIONAL VIEW OF
THREE PASS HORIZONTAL SECTION
INCOMING GASES
COOLING TOWER
A
INLET TEST DUCT
SPRAY TOWER NO 2
MIST ELIMINATOR
SPRAY TOWER NO 2
CORONA NO 1
SPRAY TOWER NO 1
CORONA NO 2
EXHAUST GASES
OUTLET TEST DUCT
FAN
ELEVATION VIEW
A

Figure 3. General Layout of Electrostatic Scrubber Pilot Plant
(Model Mark 2P)

The model Mark 2P has a scrubbing liquor recycle system. This system utilizes an electrically isolated pump, insulated hosing and a current limiting spray system for current containment and safety.

The primary differences between the Mark 1P and Mark 2P models are the number of particle charging and scrubbing sections (three for the Mark 1P and two for the Mark 2P), the orientation of these sections (vertical for the Mark 1P and horizontal for the Mark 2P) and the "once through" water system for the Mark 1P as compared to a recycle system for the Mark 2P.

FIELD TESTING AND RESULTS

Mark 1P Pilot Plant

During 1973-1974 the model Mark 1P UW Electrostatic Scrubber was constructed in a 40 ft. trailer for field tests on controlling particulate emissions from pulp mill operations. Initial tests were performed on the no. 3 boiler at the U.W. coal-fired power plant. With particle charging voltages of 37 kv (-) and water charging voltages of 2 kv (+) the overall particle collection efficiency was measured at about 98.5% (inlet 0.15 grains/sdcf and outlet 0.0028 grains/sdcf) at a water flow of 2.2 gpm and gas flow of 880 acfm (L/G of 2.5 gal./1000 acf). Submicron particle collection efficiencies were improved with an increase in water to gas flow rate ratio, and an increase in the gas residence time. Following these tests, the particle charging sections were modified to include voltages of 60 kv.

Upon completion of these modifications, the pilot plant was shipped to a sulfite pulp mill where tests were conducted on the emissions from an SO_2 absorption tower treating the exhaust gases from a magnesium sulfite recovery boiler. Particle collection efficiencies ranging from 60 to 99% by weight were measured depending on the scrubber operating parameter levels. At high particle collection efficiencies, energy requirements were found to be about 0.5 hp/1000 acfm (350 watts/1000 acfm) considering gas pressure drop, water pressure drop and electrostatic charging requirements.

The Mark 1P pilot plant was then moved to a hog fuel (wood waste) boiler for particle collection measurements. All tests were performed at maximum flow rates (1000 to 1200 acfm) with a measured range of inlet particle mass mean diameters ranging from 1.12 to 1.88 microns. Overall collection efficiencies varied from 67.4% (no particle or droplet charging) to 98.2% (fully charged condition).

Mark 2P Pilot Plant

The newly constructed Mark 20 UW Electrostatic Scrubber was initially tested using a generated dioctyl phthalate (DOP) aerosol. The spray liquor for these tests was fresh water (no recycling of the liquor).

Overall particle collection efficiencies for these tests varied from 25.0% (uncharged condition) to 99.7% (fully charged condition). The particle collection efficiency measured as a function of particle size for charged and uncharged conditions is illustrated in Fig. 4.

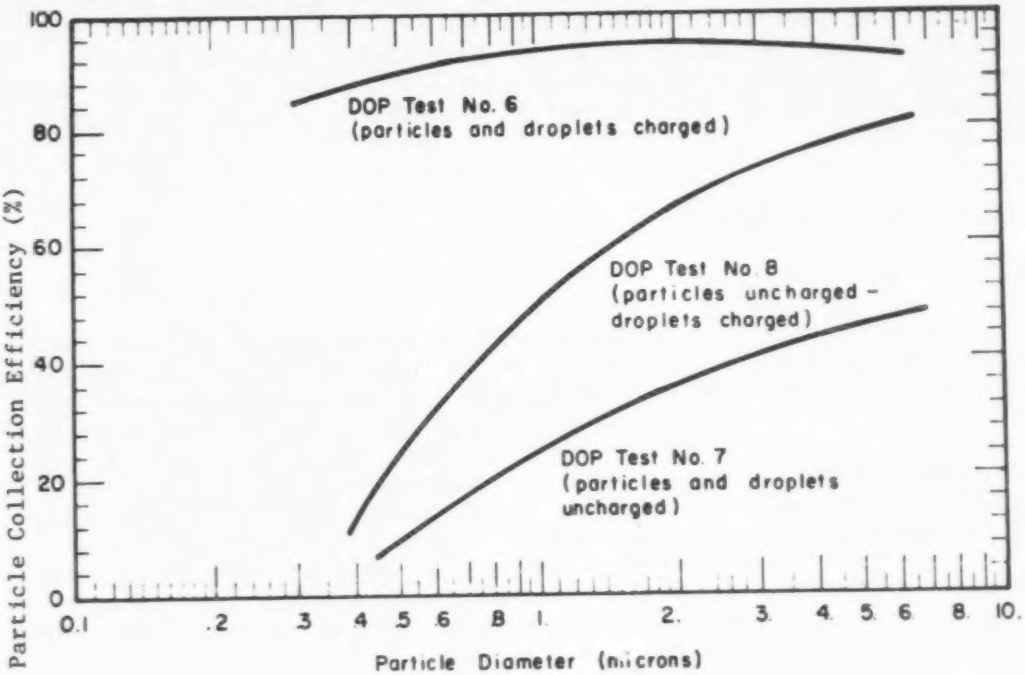

Figure 4. Particle Collection Efficiency at Various Charging Conditions

A water recycle system was designed and installed with a maximum liquor flow at 30 gal/min. The pilot plant was then moved to a steel plant in Seattle and connected to a duct exhausting from two electric-arc steel furnaces. This source was selected for the tests because the emission particles contain a large portion in the submicron size range. The particle collection efficiencies as a function of particle size (as measured with UW Source Test Cascade Impactors, Mark 5 model at the inlet and Mark 3 model at the outlet) for a range of liquor to gas ratio (L/G) and of the corona section plate's specific collection areas (SCA) are presented in Fig. 5. The highest particle collection efficiencies occurred with the higher magnitudes of L/G (about 32 gal/1000 acf) and SCA (about 94 ft^2/1000 cfm) and corresponded to outlet particle collections in the 0.004 grains/scf range.

Figure 6 illustrates the effect of the magnitude of the corona (particle charging) and the liquor spray voltages on the particle collection efficiencies at relatively constant SCA and L/G. The higher particle collection efficiencies (and correspondingly the lowest penetrations) occur at the highest corona voltage (70 kv) and liquor spray

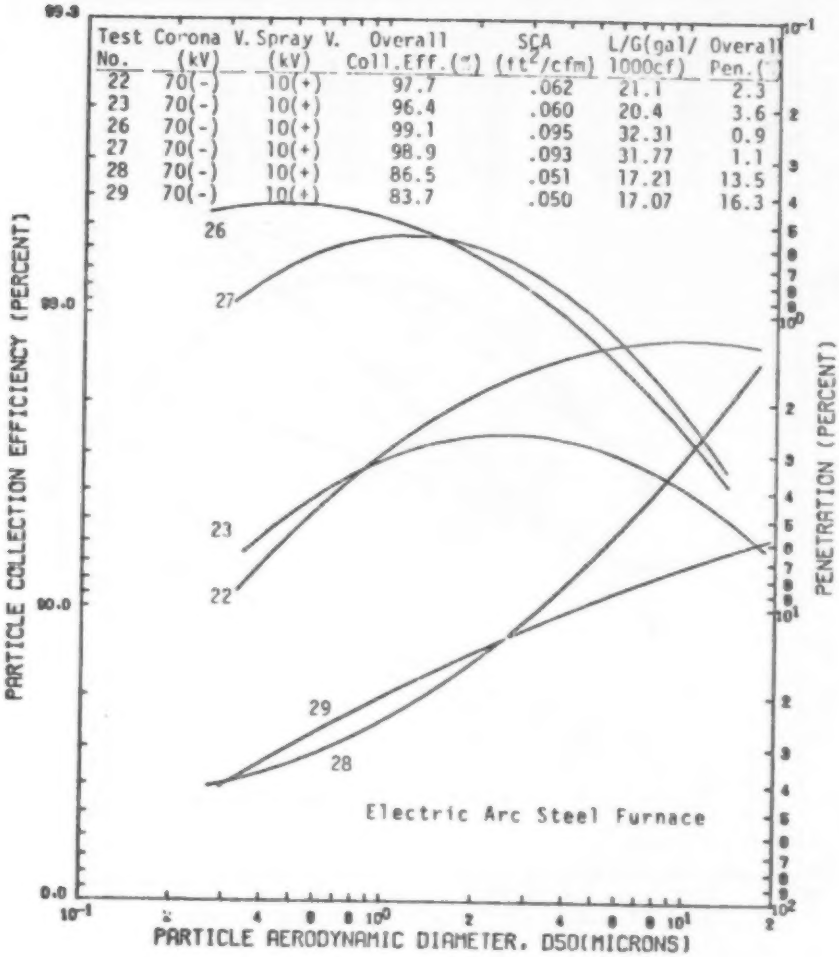

Test No.	Corona V. (kV)	Spray V. (kV)	Overall Coll.Eff.(%)	SCA (ft^2/cfm)	L/G(gal/ 1000cf)	Overall Pen.(%)
22	70(-)	10(+)	97.7	.062	21.1	2.3
23	70(-)	10(+)	96.4	.060	20.4	3.6
26	70(-)	10(+)	99.1	.095	32.31	0.9
27	70(-)	10(+)	98.9	.093	31.77	1.1
28	70(-)	10(+)	86.5	.051	17.21	13.5
29	70(-)	10(+)	83.7	.050	17.07	16.3

Figure 5. Effect of SCA and L/G on Efficiency

voltages (+2 kv). Detailed results of these are reported by Pilat, Raemhild and Harmon (1977).

In October 1977, the UW Electrostatic Scrubber pilot plant (Mark 2P model) was transported to the Centralia Steam-Electric Project (two 665 megawatt pulverized coal fired boilers) operated by Pacific Power & Light Co. A sample gas stream was trapped from the outlet of boiler no. 2. Prior to testing, the pilot plant was modified by: (1) installing pointed spikes onto the discharge frames on the corona sections, (2) installing a corona section plate water flush system (continuous wall flush), and installing a new NWL high voltage power supply (90 kv and 30 millamp) with spark rate controller for corona section no. 2 (thus coronas no. 1 and 2 have their own power supply), and (3) installing a scrubbing liquor system with the capability of adding alkaline substances

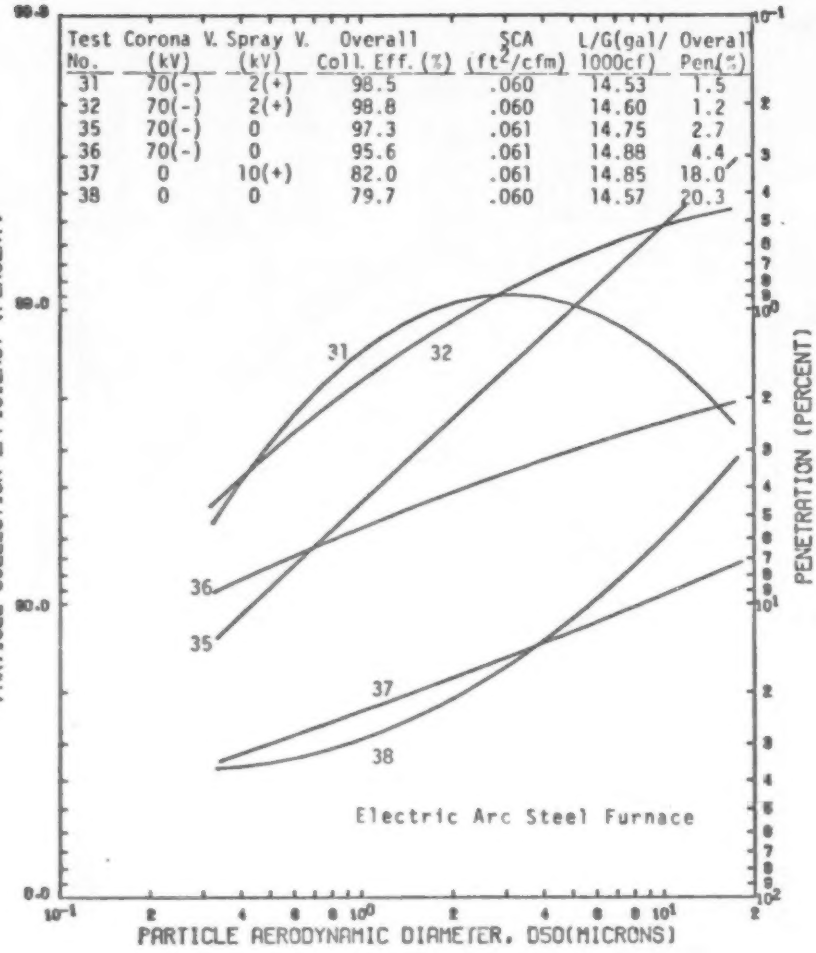

Test No.	Corona V. (kV)	Spray V. (kV)	Overall Coll. Eff. (%)	SCA (ft^2/cfm)	L/G(gal/ 1000cf)	Overall Pen(%)
31	70(-)	2(+)	98.5	.060	14.53	1.5
32	70(-)	2(+)	98.8	.060	14.60	1.2
35	70(-)	0	97.3	.061	14.75	2.7
36	70(-)	0	95.6	.061	14.88	4.4
37	0	10(+)	82.0	.061	14.85	18.0
38	0	0	79.7	.060	14.57	20.3

Figure 6. Effect of Charging Voltages of Particle Collection Efficiencies

(sodium carbonate was used) for sulfur dioxide absorption.

The results of particle collection efficiency tests using two stages (two corona sections and two spray towers) is shown in Fig. 7. The outlet particle concentration for tests 3-8 ranged from .00029 to .00099 grains/sdcf.

At one stage mode (with only corona #2 and spray tower #2 in use) the gas residence time in the corona sections is reduced 50% and in the spray chambers is reduced by 29%. The cooling tower and electrostatic mist eliminator was used in both the one and two stage modes. The

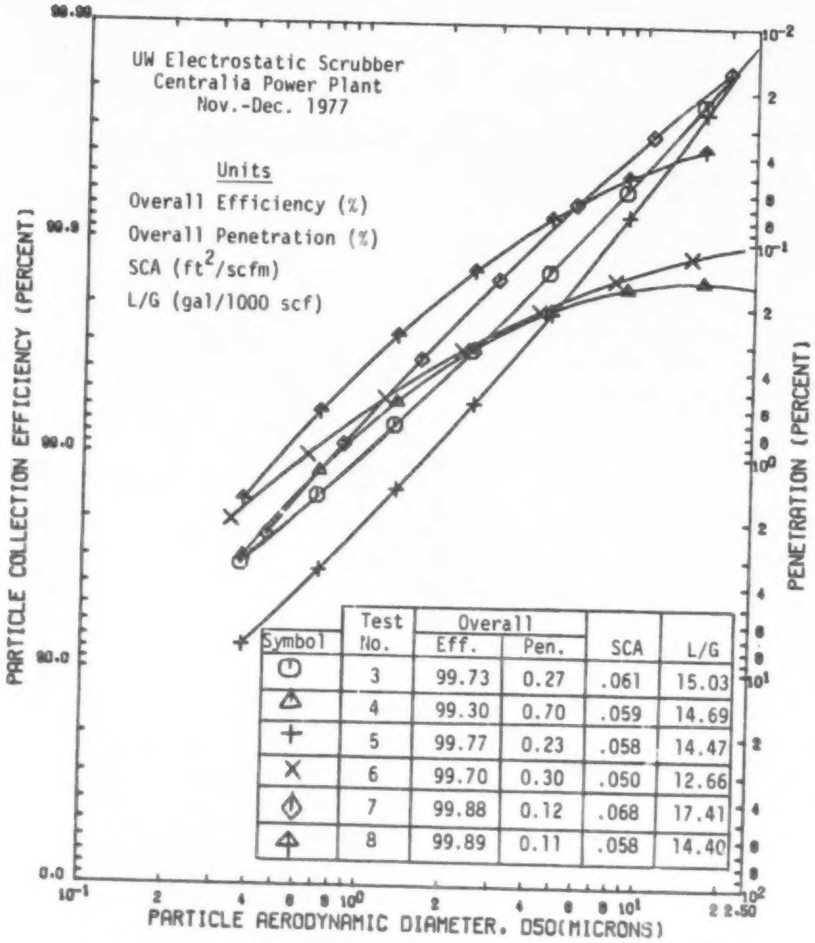

Symbol	Test No.	Overall Eff.	Overall Pen.	SCA	L/G
○	3	99.73	0.27	.061	15.03
△	4	99.30	0.70	.059	14.69
+	5	99.77	0.23	.058	14.47
×	6	99.70	0.30	.050	12.66
⌽	7	99.88	0.12	.068	17.41
⍋	8	99.89	0.11	.058	14.40

Figure 7. Particle Collection Efficiency as a Function of Particle Size (Two Stage System)

results of particle collection efficiency tests are presented in Fig. 8. The outlet particle mass concentration ranged from .00042 to .00088 grains/sdcf.

A comparison of the particle collection efficiency as a function of particle size between the two stage and one stage system is shown in Table I. The incremental particle collection efficiencies shown are the mean values for all the cascade impactor tests performed in either the one stage or two stage modes. The particle diameter is represented by the midpoint of the increment.

The reduction of certain operating parameters (SCA, L/G, gas resi-

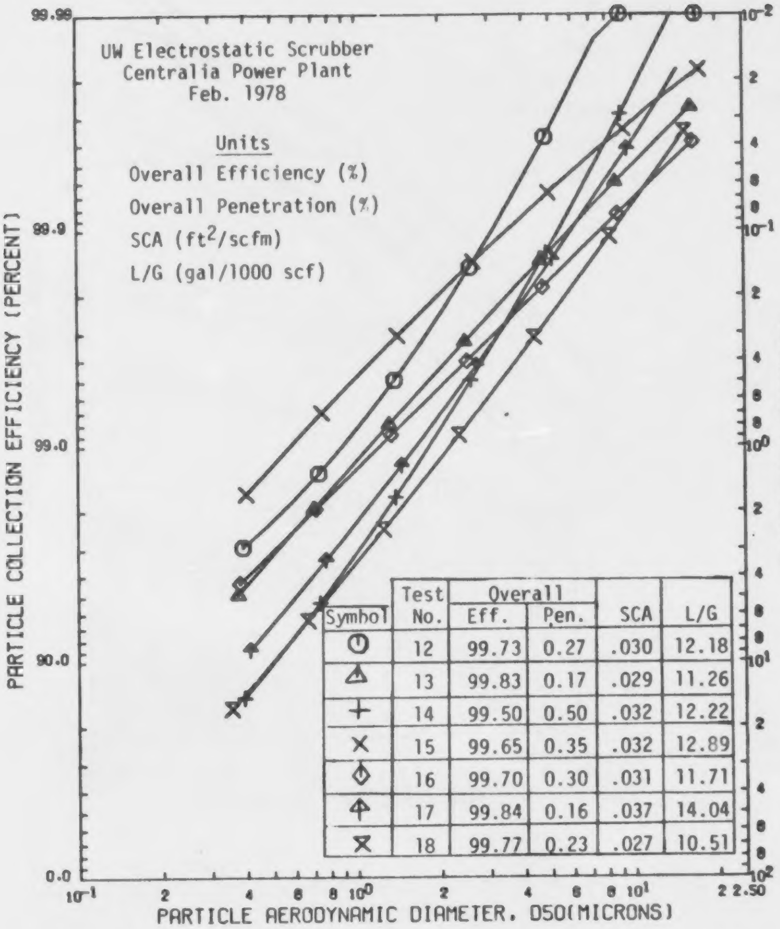

Symbol	Test No.	Overall Eff.	Overall Pen.	SCA	L/G
⦶	12	99.73	0.27	.030	12.18
△	13	99.83	0.17	.029	11.26
+	14	99.50	0.50	.032	12.22
×	15	99.65	0.35	.032	12.89
◊	16	99.70	0.30	.031	11.71
⍋	17	99.84	0.16	.037	14.04
⧗	18	99.77	0.23	.027	10.51

Figure 8. Particle Collection Efficiency as a Function of Particle Size (One Stage System)

Table 1. COMPARISON OF PARTICLE COLLECTION EFFICIENCIES BETWEEN THE TWO STAGE AND ONE STAGE SYSTEM

Particle Diameter (microns)	Two Stage		One Stage	
	Coll. Eff. (%)	Penetration (%)	Coll. Eff. (%)	Penetration (%)
0.4	96.65	3.35	92.71	7.29
0.5	97.60	2.40	94.76	5.24
0.6	98.13	1.87	96.02	3.98
0.75	98.60	1.40	97.17	2.83
0.95	98.97	1.03	98.04	1.96
1.20	99.24	0.76	98.60	1.40

dence time) on charging for the two stage to one stage mode resulted in an increase in the particle penetration from 3.35% to 7.29% at 0.4 microns diameter and from 0.76% to 1.4% at 1.2 microns diameter. In general the particle penetration for these submicron particle sizes doubled on going from two stage to one stage operation.

CONCLUSION

The results of testing of both the Mark 1P and Mark 2P pilot plants of the UW Electrostatic Scrubber illustrate the system's capability for high efficiency fine particle collection at a relatively low gas pressure drop (about 1 inch of water). For the tests at an electric utility coal fuel power plant, a 37% reduction in the active length of the electrostatic scrubber still provided overall particle collection efficiencies in excess of 99%. It has been demonstrated that the addition of electrostatic charging of the aerosol particles and/or the scrubbing liquor spray droplets can substantially enhance the collection efficiency for fine particles by wet scrubbers.

ACKNOWLEDGEMENTS

This research has been supported by US EPA (IERL) research grants (EPA Grants Nos. R-804393 and R-806035). The support and cooperation from the University of Washington, Alaska Lumber & Pulp Co. (Sitka, Alaska), Ketchikan Pulp Co. (Ketchikan, Alaska), the Northwest Pulp & Paper Assoc., Bethlehem Steel Corp. (Seattle, Wash.), and Pacific Power & Light Co. (Portland, Oregon) is greatly appreciated.

REFERENCES

1. Kraemer, H.F. and H.F. Johnstone (1955) "Collection of aerosol particles in the presence of electric fields" Ind. Eng. Chem. 47 2426.

2. Penney, G.W. (1944) "Electrified liquid spray dust precipitator" U.S. Patent No. 2,357,354.

3. Pilat, M.J., S.A. Jaasund, and L.E. Sparks (1974) "Collection of aerosol particles by electrostatic droplet spray scrubbers" Envir. Sci. & Tech.

4. Pilat, M.J. (1975) "Collection of aerosol particles by electrostatic droplet spray scrubber" APCA Journal 25 176-178.

5. Pilat, M.J. and D.G. Meyer (1976) "University of Washington Electrostatic Spray Scrubber evaluation" Final Report on Grant No. R-803278, EPA Report No. EPA-600/2-76-10 (NTIS No. PB 252653/AS).

6. Pilat, M.J., G.A. Raemhild, and D.L. Harmon (1977) "Fine particle control with UW Electrostatic Scrubber" presented at Second Fine Particle Scrubber Symposium, May 2-3, 1977, New Orleans.

7. Pilat, M.J., G.A. Raemhild, and D.L. Harmon (1977) "Tests of University of Washington Electrostatic Scrubber at an Electric Arc Steel Furnace" presented at Conference on Particle Collection Problems in the Use of Electrostatic Precipitators in the Metallurgical Industry, June 1-3, 1977, Denver.

Metric Conversion Factors

Readers more familiar with the metric system are asked to use the conversion factors tabulated below:

Non-metric	Multiplied by:	Yields metric
ft	30.48	cm
ft^3	28.32	liter
grains/scf	2.288	1 gram/m^3
gal.	3.79	liter
gal./1000 acf	0.1337	liter/m^3
ft^3/min	1.699	m^3/hr
ft/sec	0.3048	m/sec

UNION CARBIDE'S HIGH INTENSITY IONIZER* APPLIED TO ENHANCE A VENTURI SCRUBBER SYSTEM

By
M. T. Kearns, et al
Air Pollution Systems, Inc.
Kent, Washington 98031

And

C. M. Chang
Union Carbide Corp.
Linde Division
Tonawanda, New York 14150

INTRODUCTION

The impact of fine particulate emissions (<3μ in diameter) on man and the environment has induced the air pollution agencies and the government, the Environmental Protection Agency (EPA), to promulgate the current stringent control requirements and opacity regulations. It has been the function of the EPA in establishing particle emission standards, to also seek economical and technological means for submicron particulate abatement for industry. The Industrial Environmental Research Laboratory (IERL-RTP) branch of the EPA has had a program for several years to identify, evaluate and test novel fine particulate collection devices. This undertaking by the government was performed to provide industry with "...the best available control technology". As a result of the tests, the EPA requested and received numerous proposals for the demonstration of a novel fine particulate collection system, on an industrial source emission. Their purpose for this solicitation was "...to locate and demonstrate at pilot or small full scale the technical and economic feasibility for the most promising existing novel particulate collection system for control of fine particulate emissions from industrial sources". Air Pollution Systems, Inc. received a contract award as a result of this procurement to demonstrate the APS high intensity ionizer followed by a venturi scrubber system. This report discusses the technology, program and developments to date.

BACKGROUND DEVELOPMENT

There exists an almost unlimited variety of air pollution control devices for the separation of particles and gases from industrial emission sources. Fine particulate collection (<3μ in diameter) is presently limited however, to equipment which is either very large and/or has high operating costs. The selection includes equipment such as electrostatic precipitators and fabric filters which are large and have high capital costs, or venturi scrubbers, which are lower in both initial and maintenance costs but require relatively high energy consumption. Venturi scrubbers are advantageous in those applications that call for the collection of adherent or flammable submicron particulate, and/or wet or corrosive gases.

The venturi scrubber system, which represents the smallest and consequently the cheapest capital cost, has been improved by Air Pollution Systems, Inc. by reducing the operational costs. The system incorporates the APS high intensity ionizer (HII) which imposes a high electrostatic charge on the particles in a gas stream before they enter the inlet of a conventional low-energy venturi scrubber. This system, which had a wet anode configuration, was termed the Scrub-E by APS. The system now has a dry anode configuration and is called the UCC-HII* Scrubber Enhancement System. (See schematic diagram Fig. 1.) This combination lowers energy requirements to approximately one-half to two-thirds that of conventional scrubber systems while providing highly efficient removal of submicron particles, (see Fig. 2). The design of the ionizing unit provides for a relatively small add-on device to precharge the particulate. The commercialization of the system, as well as other particulate collection systems involving high intensity ionization, are being pursued by Linde Division, Union Carbide Corporation.

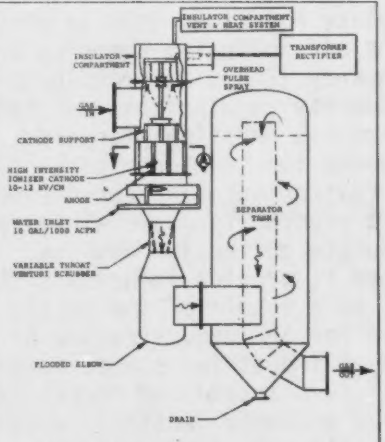
INSULATOR COMPARTMENT VENT & HEAT SYSTEM
TRANSFORMER RECTIFIER
INSULATOR COMPARTMENT
OVERHEAD PULSE SPRAY
GAS IN
CATHODE SUPPORT
HIGH INTENSITY IONIZER CATHODE 10-12 KV/CM
ANODE
WATER INLET 10 GAL/1000 ACFM
SEPARATOR TANK
VARIABLE THROAT VENTURI SCRUBBER
FLOODED ELBOW
GAS OUT
DRAIN

UNION CARBIDE'S HIGH INTENSITY IONIZER-ENHANCED SCRUBBER (20,000 ACFM)

FIGURE 1

*Licensed from Air Pollution Systems, Inc. by Union Carbide Corporation, Linde Division.

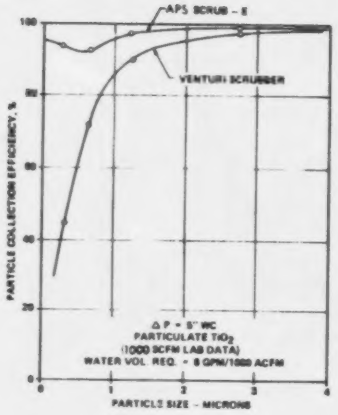

FIGURE 2 - PARTICLE REMOVAL EFFICIENCY

APS HIGH INTENSITY IONIZER

Air Pollution Systems, Inc. began its development of the Scrub-E as a result of investigating and applying high electrical field technology to new techniques and equipment for air pollution control. As an engineering research and product development firm, APS developed a new electrode geometry+, which was successful in establishing a highly stable, intensified electrostatic field. (+Patented.)

From classical theory, the amount of charge acquired by a particle in an electric field depends on the strength of the field, the density of charge present as ions (or in some case electrons), the particle radius and dielectric qualities of its constituent material, and the amount of time available for charging. The ion density in turn is a function of the supply current, electric field and the ionizer geometry. Further charging of a particle beyond its field saturation value can be accomplished by diffusion charging resulting from the thermal motion of ions. This process is most effective for particles in the submicron range, specifically with the $r < 0.25\mu$.

The APS electrode configuration produces a substantially uniform three dimensional field which is a principal factor in the greater electrical stability. The cathode is a solid metal disc supported by a structurally reliable tube section maintained in a cylindrical anode arrangement. Typical operating field strengths are around 10-15 kV/cm compared to levels of 3-6 kV/cm for wire electrode geometries. Figure 3 shows a typical EI curve for the ionizer.

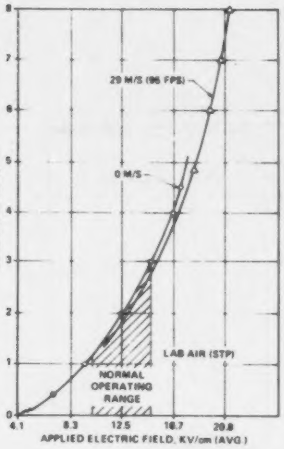

FIGURE 3 – TYPICAL E–I CHARACTERISTICS

In addition to the very high fields, the electrode geometry produces a concentrated field with ion densities many times that obtained conventionally. As noted above, the charge obtained on small particles is dependent on the ion density and is therefore increased with the higher ion density in the APS ionizer. This increases the diffusional charging of the fine particulate. As a result of the higher fields and ion densities, both the level of charge acquired by the particulate and the rate of charging are significantly higher. Particle charges approaching half an order of magnitude higher than conventional is currently being achieved. Particle charging efficiency was studied as a function of velocity (residence time). Figure 4 illustrates the effective charging of TiO2 dust (mmd = 0.5μ) in charge to mass measurements Q/m, versus velocity for normal design ranges. The plotted theoretical and experimental data points show a good correlation in expected efficiency decrease with the increase in velocity. The saturation charge (per unit mass) was calculated to be 87μ coul/gram for an 11.6 kV/cm field. This degree of charging at higher fields was greater than predicted based on cascade impactor size distribution analysis. The charge levels above the calculated saturation charge have been theorized to be the result of direct electron charging due to the very high field strengths.

The APS high intensity ionizer effectively charges the particulate at velocities of 7-10 times higher than more conventional electrostatic electrode configurations. Velocities in excess of 100 FPS can be maintained past the ionizer with charging times of a few milliseconds. Figure 5 shows the velocity regime of prime concern for the ionizer versus percent saturation charge. Charging efficiency was found to be between 80% and 90% for normal operating velocities. The high current densities are also principally responsible for the capability to efficiently charge the particulate at velocities in excess of 100 FPS. This means that the particles can be charged to a higher level in a smaller volume, and as can

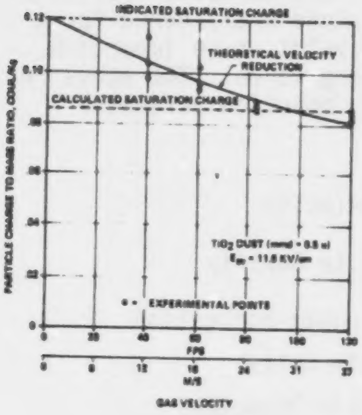

FIGURE 4 – EFFECT OF GAS VELOCITY ON CHARGING EFFICIENCY

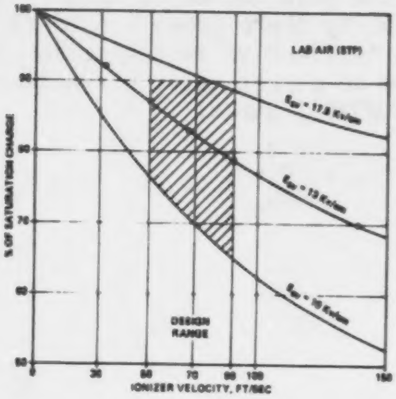

FIGURE 5 – CALCULATED PARTICULATE CHARGING EFFICIENCY

be seen in Figure 1, the ionizer section is small compared to the overall size of the equipment.

VENTURI SCRUBBER

The efficiency of the venturi scrubber is determined by the summation of the efficiencies of the individual droplets. There are many mechanisms which predominate in the venturi scrubber that affect these efficiencies, but the essential forces are inertial or impaction and diffusional forces. The droplet efficiencies, therefore, are limited by parameters which affect those forces. These parameters are the relative velocity between the particles and droplets, the velocity distribution of the gas stream flowing around the droplet, the trajectory of the particle, the mass of the particulate and its geometric shape as it relates to its air resistance (aerodynamic diameter), and the number of collector droplets.

Because one of the predominant forces of collection in the basic scrubber is impaction on water droplets, the conventional approach to increasing the efficiency has been to increase the relative velocities between the particle and droplet and/or to increase the number of droplets. Increasing the number of droplets has limited value because the efficiency of each drop is still limited by the relative velocity effect. In addition, increasing the number of droplets increases the total water flow and thus the size and cost of both the water treatment and recycle equipment. Increasing the relative velocity is the best means of overcoming the aerodynamic forces on the particulate and thus increasing the efficiencies. The aerodynamic (drag) forces act on the fine particles, tending to draw them around obstructions (such as water droplets) in the gas stream. In opposition to the drag forces are inertial forces which resist any sudden change of direction. Since the aerodynamic drag force is proportional to the plane projected area of the particle and the inertial forces are proportional to the mass, which is a product of density and volume, there is a strong size dependence over which force will predominate. For fine particulate, the mass decreases faster than the plane area, hence for a given gas velocity there comes a natural cut off point where impaction forces become ineffective in comparison to the drag force. The above relationship can be expressed as a function of the impaction parameter $\sqrt{\Psi}$ (RANZ & WONG[1]) where:

$$(1)\quad \sqrt{\Psi} = \left(\frac{C P_p V_g}{18 \eta D_c}\right)^{1/2} dp$$

V_g = Gas Velocity
P_p = Particle Density
C = Cunningham Correction
η = Air Viscosity
dp = Particle Diameter
D_c = Collector Diameter

The efficiency of collection is a function of the impaction parameter $\sqrt{\Psi}$. Equation (1) illustrates the dependence of collection efficiency on particle size since the particle diameter dp is proportional to $\sqrt{\Psi}$. It is also dependent on the collector size and the differential velocity $\sqrt{\Psi} \propto V_g/D_C$. Therefore, decreasing the collector size, or increasing the gas velocity, will also improve collection efficiency. However, the system pressure drop increases as the square of the relative velocity, and the power, or operating costs, increases rapidly as a result. A limit is reached when the incremental efficiency gains cannot be justified because of its high energy costs and/or the additional expense of the larger liquor control system.

UCC-HII* SCRUBBER ENHANCEMENT SYSTEM

In the Scrubber System (Fig. 1), the total force for particle collection is the vector sum of the inertial (Eq. 1) and electrostatic forces acting on a particle. The total electrical force is the sum of all individual electric forces acting on a particle. Strauss[2] considers the total force Fe_1 as the total of four electrical forces between a charged aerosol particle and a charged spherical collector. This force is given by $Fe_1 = Fe_C + Fe_I + Fe_m + Fe_S$. Theoretically, these forces plus the inertial impaction force (Eq. 1) provide the mechanism for collection in the Scrubber System. The formulas for these forces are not included here, but are defined as:

(2) Fe_C = Coulombic force between a charged particle and charged collector

(3) Fe_I = Image force of induced charge on uncharged particle by charged collector

(4) Fe_m = Image force of induced charge on uncharged collector by charged particulate

(5) Fe_s = Space charge force of repulsion from surrounding like charged particulate toward a relative charge void (the collector)

Since the electrostatic forces are additive, the more forces that can be utilized, the higher the force of collection. Each force that can be increased in magnitude should also add to the maximum. In the HII section the ionizer imparts an unusual high charge to the particulate. High levels of charging are attained by field charging (10-15 kV/cm) with diffusion charging and electron charging components additive. The repulsive force of the space charge adds to the coulombic attraction between charged particles and droplets. Combined with the two image forces above, the net electrostatic force is the sum of all four forces. Since the overall force is equal to the impaction force (Eq. 1) plus the electrostatic forces (Forces 2-5), the net collection efficiency becomes a complex function of all five forces.

The Scrubber System with the utilization of electrostatic forces and inertial forces, maintains an improved efficiency on fine particulate while requiring far less energy consumption than a conventional scrubber. The APS ionizer module requires the input of electrical energy equivalent to only about 0.15 HP/1000 ACFM to convert a low energy venturi scrubber into the equivalent of a very high energy scrubber. The electrostatic charges are applied directly to the suspended particles by the ionizer module. The attractive force between the charged particle and droplet is additive to the inertial and all other forces acting in the scrubber. The electrostatic forces act to overcome both the inertial and drag forces. As a result of the electrostatic forces, the effective target area of the collector droplet can extend beyond its physical size. This is in contrast to the non-electrostatically enhanced situation where the effective target area is less than the projected area of the droplet. See Figure 6 for the simulated representation.

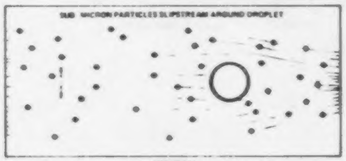

SCRUBBER

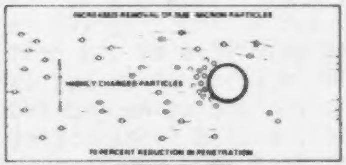
INCREASED REMOVAL OF SUB - MICRON PARTICLES
HIGHLY CHARGED PARTICLES
70 PERCENT REDUCTION IN PENETRATION

SCRUBBER WITH PRECHARGER

FIGURE 6 MECHANISMS OF COLLECTION IN SCRUBBERS

FIELD PILOT TESTING

Results of APS laboratory and field testing have shown that the ionizer typically reduces the penetration through the venturi scrubber by approximately 70% or more, without changing any other parameter. These results have been verified by Air Pollution Technology (APT), of San Diego, California. They are an independent testing organization which evaluated the Scrub-E under EPA Contract Number 68-02-1496. These results are reported in Publication No. EPA 600/2-76-154a[3]. Typical results of the APT tests are shown in Figure 7 which compare favorably with APS lab results in Figure 2. The two curves show fractional efficiency results with and without the ionizer energized. The fractional efficiencies of particulate were determined using both cascade impactors and diffusion batteries. As can be seen in Figure 7, fractional efficiencies are very high on submicron particulate with the ionizer on. The test aerosol used was titanium dioxide with an aerodynamic mass mean diameter of 1 micron. As can be seen, the fractional efficiencies for particles < 0.8 μm and > 2.0 μm were > 92% and > 99% respectively.

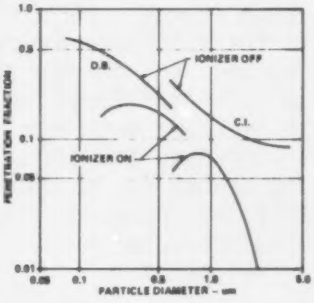

FIGURE 7 - PENETRATION VS. PARTICLE DIAMETER USING BOTH DIFFUSION BATTERY AND CASCADE IMPACTOR, RUN 28, A.P.T. TEST DATA

Another significant demonstration of the Scrub-E was on a urea (carbonyl diamide) prilling tower. The particulate size distribution was 80 to 90% by weight in the 0.4 to 1.0 micron interval range with an inlet grain loading of 0.04 gr/scf. The objective of the test program was to reduce the visible emissions to a zero level which was estimated to be about 0.0015 gr/scf. Collection efficiencies ranged from 90.75 to 96.25% performed by the plant personnel, with a final outlet grain loading of 0.0015 gr/scf. The pressure drop required to obtain this level was 7.5" w.g. at a flow volume of 750 ACFM. There were no tests conducted with the ionizer off, but visual observations revealed a dense opaque plume without the electrostatics and a zero opacity at 0.0015 gr/scf with the ionizer on.

EPA PROGRAM DEVELOPMENTS

Air Pollution Systems, Inc., in their progress on EPA Contract No. 68-02-2666, is currently in the design phase (Task 2) of the demonstration system. Task 1 in the EPA contract "scope of work" was to select "...an industrial source which constitutes an important source of fine particulate emissions". Major sources of fine particulate ($<3\mu$ in diameter) are usually high temperature operations such as metallurgical processes and fossil fuel combustion processes.

APS in their selection, chose two copper smelter operations (a reverberatory furnace and an electric furnace) and a magnesium recovery furnace operation, respectively. The EPA made a recommendation for the magnesium recovery furnace operation. The furnace is operated at Teledyne Wah Chang Albany (TWCA) Albany, Oregon. TWCA is a large production facility for zirconium and hafnium metals, columbium and tantalum alloys and a research center for the refractory metals.

Essentially, the magnesium recovery process recovers non-spent magnesium metal after it has reacted to reduce $ZrCL_4$ to pure zirconium. The spent magnesium, as $MgCL_2$, is shipped to another plant for reduction to pure magnesium metal. The magnesium furnace produces emissions of MgO and traces of $ZrCL_4$ and $MgCL_2$ as the pure magnesium is ladled from the furnace. Scanning electron microscope photographs (SEM) performed on the magnesium furnace emissions has indicated the greatest proportion of particulate to be less than 1.0 μm in diameter. Cascade impactor size distribution analysis of the particulate verified the SEM data with a D_{50} by weight of 1.48 microns. This D_{50} had a standard geometric deviation of 3.0 with a linear regression correlation coefficient of 0.995.

Objectives for the demonstration program are to remove 90% of all particulate from 0.01 to 3 μm in diameter from the source gas stream. Figure 8 shows the demonstration system schematic flow diagram for the EPA project to achieve these results.

The particulate gas stream originates at four sources. Two of these are the magnesium recovery furnaces described above. The $MgCL_2$ furnace is a concentrator operation to recover whatever remaining magnesium is left in pure form. Finally, the smokehouse emission is where the $MgCL_2$ crucibles are heated in a burnout operation. All of these furnace emission sources emit primarily MgO fume. The majority of the fume emission MgO is attributed to the magnesium recovery furnaces when the doors are opened for the ladeling process. The process is batch operation occuring at nine periods per day for an interval of about 45 minutes each. The MgO fume particles become highly charged in the ionizer array before they enter the inlet of the venturi scrubber. A variable damper is included in the venturi throat design to maintain constant flow volume at varying pressure drops. This design in conjunction with a high pressure drop fan, will allow APS to demonstrate the effectiveness of the HII versus venturi pressure drop on fine particulate. The gas stream leaving

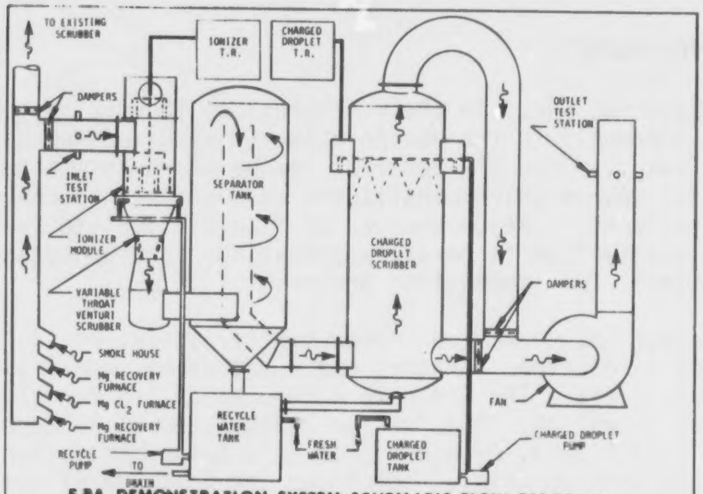
TO EXISTING SCRUBBER
IONIZER T.R.
CHARGED DROPLET T.R.
DAMPERS
OUTLET TEST STATION
INLET TEST STATION
SEPARATOR TANK
IONIZER MODULE
CHARGED DROPLET SCRUBBER
VARIABLE THROAT VENTURI SCRUBBER
DAMPERS
SMOKE HOUSE
Mg RECOVERY FURNACE
Mg CL_2 FURNACE
Mg RECOVERY FURNACE
RECYCLE WATER TANK
FAN
FRESH WATER
CHARGED DROPLET TANK
CHARGED DROPLET PUMP
RECYCLE PUMP
TO DRAIN

EPA DEMONSTRATION SYSTEM SCHEMATIC FLOW DIAGRAM

Figure 8

the venturi then enters a conventional separator where the particulate is removed. From the separator, the gas stream can either by-pass or enter a positive polarity charged droplet scrubber. The addition of this system was a proposed option for the demonstration system submitted to the EPA. Testing performed in the APS laboratory has resulted in a method of applying a substantial charging level to the water drops through the use of higher fields. The relative charge measured by APS indicated significantly higher charging to the water droplets opposed to the charge measured without using this unique charging configuration. In addition, visual observations showed a considerable finer droplet formation as the high voltage was applied.

The purpose of the charged droplet scrubber will be to investigate the feasibility of further reducing the pressure drop requirements of the venturi scrubber, while maintaining the high efficiency levels, by the introduction of charged droplets. The reduction of the liquid to gas ratio and/or the throat velocity will control the amount of charged particulate passing through the venturi into the charged droplet section for comparative efficiency measurements. Theoretically, the addition of a positive charge on the scrubbing droplets would not only increase the coulombic forces, but image and field forces of attraction as well (Forces 2-5). It is believed that these forces will be especially effective on the smaller particulate fraction. The versatility of the system will provide the means to determine how efficient charged drops are in comparison to the aerodynamic forces in the venturi.

The performance of the complete demonstration system will be tested and documented by an independent subcontractor. Tentative scheduling for the demonstration system start-up and initial tests are planned for early 1979. A final report documenting performance, collection efficiencies and system reliability will be released in late 1979.

HII RETROFITTABILITY - CONCLUSION

The specialized APS electrode geometry applies an intense electrostatic field. In addition, high ion densities promote near saturation charging of particulate within a few milliseconds, thus allowing use of high gas flow rates. It is because of the short charging times that the physical size requirements of the charging system can be greatly reduced. This means that the particles can be charged to a higher level in a smaller volume and easily retrofitted to existing collection equipment.

The present uses of the ionizer are: precharging the particulate entering a venturi scrubber, significantly reducing the pressure drop required to obtain a specific collection efficiency (the UCC-HII Scrubber Enhancement System); to precharge particulate entering a dry ESP, thus significantly reducing the overall size; and to be integrally incorporated into a wet ESP device, called the UCC-WIS (Wet Ionization System). The UCC-WIS is a pipe type ESP which is effective where the resistivity or stickiness of the dust prohibits the use of a conventional unit. Emissions with these characteristics are often found in iron-and-steel, metallurgical, chemical, pulp-and-paper, and the mining industries.

The utilization of electrostatics with venturi scrubbers as incorporated in the UCC-HII Scrubber System is expected to expand the scrubbers use into many application areas which have fine particulate emissions. As the mass mean diameter of the particulate to be controlled decreases, the Scrubber System becomes a more attractive alternative. (See Figure 7.) This is due to its small size and the high efficiencies which can be obtained on fine particulate ($<3\mu$ in diameter) at low energy levels. Traditional control equipment which can obtain high efficiencies on submicron particulate is very large and, therefore, has a high capital cost as well as utilizing a large portion of valuable plant space. The small size and relatively low capital costs, combined with the low energy requirements, favor the use of the Scrubber System for fine particle control. The EPA demonstration system will provide the necessary design criteria from data collection for an HII retrofit to any conventional venturi scrubber system. Among the market applications expected to be attracted to the Scrubber System are the mining, metallurgical, chemical and paper industries, salt soaked hog fuel boilers, phosphate rock dryers, coal dryers, urea prilling towers and electric arc furnaces.

ACKNOWLEDGMENTS

The preparation of this paper was supported by the EPA (IERL, RTP) Contract No. 68-02-2666.

REFERENCES

1. Ranz, W. E. and Wong, J. B., Impaction of Dust and Smoke Particles on Surface and Body Collectors, Industrial Engineering Chemistry. Vol. 44, No. 6, pp 1371-1381.

2. Strauss, W., Industrial Gas Cleaning, Pergamon Press, Sydney, 1974.

3. Calvert, S. et al, APS Electrostatic Scrubber Evaluation, June, 1976, EPA-600/2-76-154a.

PERFORMANCE TESTS OF THE MONTANA POWER COMPANY COLSTRIP STATION FLUE GAS CLEANING SYSTEM

Joseph D. McCain
Southern Research Institute
2000 - 9th Avenue South
Birmingham, Alabama 35205

This paper describes performance tests of a scrubber used for joint collection of sulfur oxides and particulate matter produced by coal combustion at a large coal fired electrical generating station. This novel system utilizes the alkalinity of the flyash produced by the boiler for the major portion of the sulfur dioxide removal. The scrubber was designed and constructed by Combustion Equipment Associates (New York, NY, USA) in cooperation with the Bechtel Power Corporation and A. D. Little, Inc., for the Montana Power Company. The system is in commercial operation on units 1 and 2 of the Colstrip Station of the Montana Power Company. Performance data are given for both SO_2 and flyash removal by the system.

INTRODUCTION

The flue gas cleaning system (Figure 1) now in operation on the two Colstrip 360 MW units is unique in that a wet scrubbing system is used for both particulate and SO_2 control and that captured ash provides the alkalinity for the SO_2 removal. This paper provides a summary description of the operation of the scrubber and the results of performance testing carried out to determine the SO_2 and fly ash cleaning efficiencies achieved by the system. A more complete report of the tests may be found in EPA publication 600/7-78-094.[1]

DESCRIPTION OF THE SCRUBBER[2]

The system currently installed on the two 360 MW Units 1 and 2 is

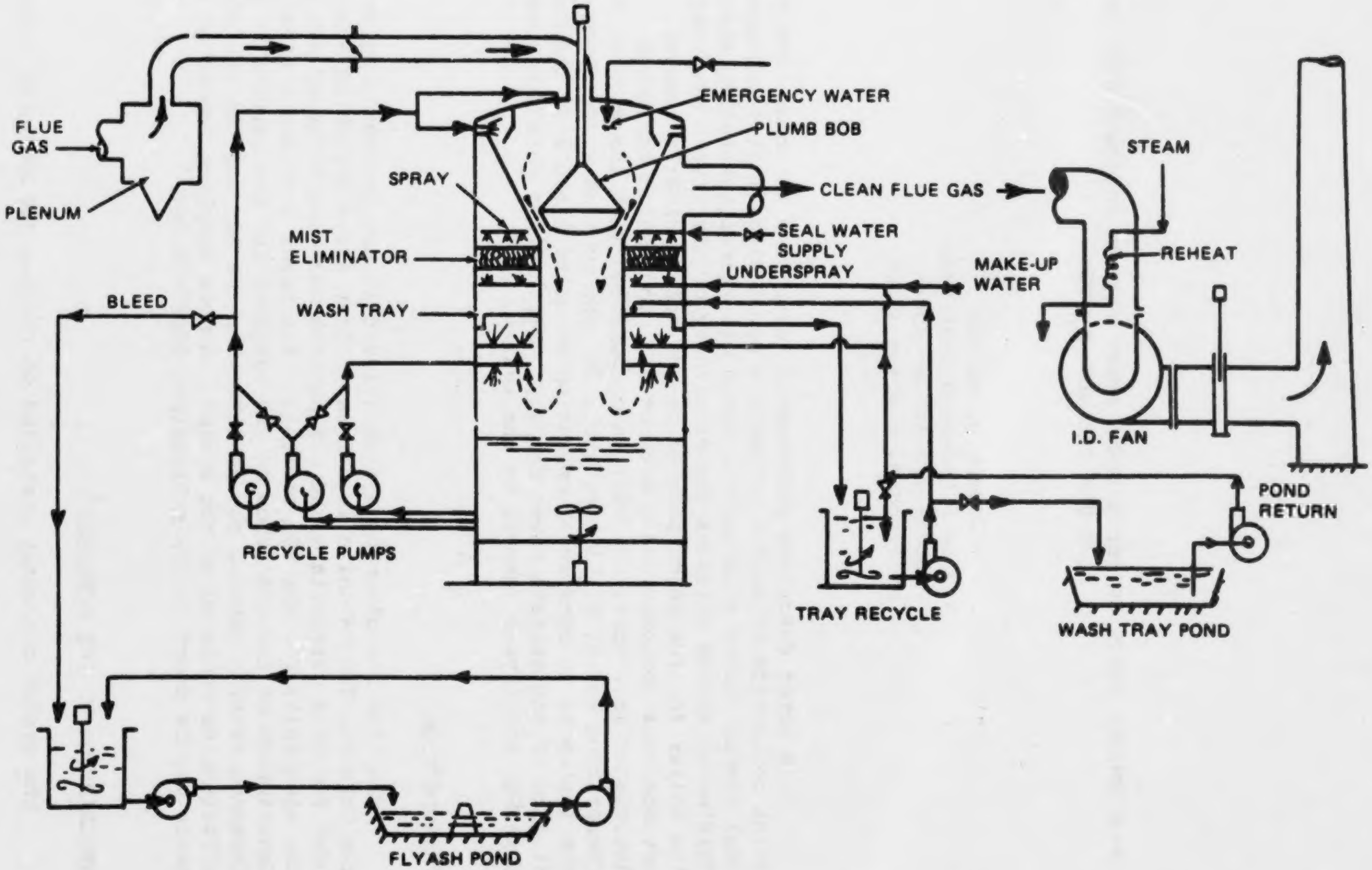
FLUE GAS
PLENUM
EMERGENCY WATER
PLUMB BOB
SPRAY
MIST ELIMINATOR
WASH TRAY
BLEED
CLEAN FLUE GAS
SEAL WATER SUPPLY
UNDERSPRAY
MAKE-UP WATER
STEAM
REHEAT
I.D. FAN
POND RETURN
RECYCLE PUMPS
TRAY RECYCLE
WASH TRAY POND
FLYASH POND

FIGURE 1. THE MOTANA POWER CO. – PUGET SOUND AND LIGHT COLSTRIP UNITS 1 AND 2 – (360 MW EACH) FLUE GAS CLEANING SYSTEM.

illustrated in Figure 1. The hot flue gas leaving the boiler is cooled in the heat recovery air heater and enters the flue gas scrubbing system at about 300°F to 150°C. The scrubbing system consists of three identical modules operating in parallel. Each scrubber module consists of a down-flow venturi scrubber centered within an upflow spray tower contactor. The venturi is equipped with a variable throat to maintain constant pressure drop at variable loads. In the venturi the scrubbing liquid is finely dispersed by the high velocity flue gas and serves to efficiently wet and trap the particulate fly ash. In the spray tower the gas contacts a recycle spray of absorption slurry. The slurry from the venturi and the spray contactor is collected and held in the base of the scrubber and recirculated at an L/G ratio of 2 ℓ/m^3 (15 gal/1000 ft^3) for venturi and 2.4 ℓ/m^3 (18 gal/1000 ft^3) for the absorber spray. An agitator in the scrubber base serves to maintain suspension of the fly ash and solid reaction products. Slurry is bled from the recycle to maintain a 12% suspended solids concentration. Slaked quick lime is added as lime slurry only if needed to augment the fly ash alkali and maintain the desired slurry pH.

Each scrubber module is designed to clean 120 MW of equivalent gas flow under normal conditions (i.e., when one module is down, the two in operation will clean the amount of flue gas generated at 80% of boiler design load.)

The treated gas leaving the spray section passes through the water washtray which serves to trap and dilute the entrainment. The gas leaving the washtray passes through a chevron demister followed by a mesh pad demister and leaves the absorption section water-saturated at a temperature of about 50°C. (120°F).

To preclude condensation in the fan and stack, and improve the gas bouyancy, the cooled gas from the scrubber is reheated 30 to 40°C (50 to 75°F.) by a steam heat exchanger. The warmed gas then passes through the dry induced draft fans and is discharged to the atmosphere from the top of a 152m (500 foot) stack.

As shown in Figure 1 the slurry discharged from the absorption loop is passed to an intermediate retention pond where the solids settle and from which the clarified water is returned to the absorption system. At intermittent intervals (currently only during the warm summer months), a floating dredge is used to reclaim the settled solids from the intermediate settling pond and transport them as a 30% slurry by pipeline to the remotely located permanent disposal pond. Decanted water (supernate) from the disposal pond is returned, also intermittently, through the same slurry pipeline to the intermediate pond for recycle to the absorption system. No stabilization of the sludge is required and a closed water loop is maintained.

Fresh water is added to the absorption system in an amount equivalent to that evaporated into the warm gas stream plus that retained in the waste sludge. This makeup water is introduced to the system as dilution water for minimizing the calcium saturation level in the mist eliminator washwater. This washwater is trapped by and withdrawn from the washtray and circulated to a small pond where entrained solids are separated. A portion of the water from this pond is returned and used to wash the undersurface of the washtray. Another portion of the flow is diluted with the fresh makeup water, and used for bottom wash of the mist eliminator.

A detailed chemical analysis of the fly ash (see Table 1) revealed that it contained alkali metal oxides in an amount theoretically sufficient to react with and adsorb the sulfur dioxide produced by the coal combustion. Laboratory experiments simulating absorption conditions revealed that this alkalinity was only usable under low pH absorption conditions (<5.6). It also revealed that absorption under these low pH conditions would result in extensive oxidation of the absorbed SO_2 producing calcium sulfate rather than calcium sulfite as the predominant reaction product.

The conditions selected were a pH of 5 to 5.6, low enough for alkali utilization and high enough for adequate SO_2 absorption capability. The other, and perhaps the key operating factor, was the use of a high level of suspended solids in the absorption slurry (12 to 15% by weight, of which some 3-4% is calcium sulfate formed in the absorption). This provided a high concentration of calcium sulfate seed crystals to promote desupersaturation. A long residence time for the recycle slurry in a stirred tank external to the scrubber was also proposed to ensure alkali utilization and to provide crystallization of calcium sulfate under controlled and non-scaling conditions. A slurry holdup of 8-10 hours was selected. The parameters for the final scrubber design are given in Table 2.

PERFORMANCE EVALUATION

The scrubber performance was evaluated by Southern Research Institute (SoRI) for the Industrial Environmental Research Laboratory of the U.S. Environmental Protection Agency during the month of May 1977.

This evaluation was one of a series of studies being conducted by the Industrial Environmental Research Laboratory of the Environmental Protection Agency to identify and test novel devices which are capable of high efficiency collection of particulates. The test methods used may not have been consistent with compliance-type methods, but were state-of-the-art techniques for measuring mass and fractional efficiency using standard mass train and inertial, electrical, and optical methods.

The tests were conducted on one of the three identical scrubber modules which are operated in parallel to control SO_2 and particulate emissions from the power boiler. The three modules are independently controlled with respect to liquor flows and venturi pressure drop. Pressure drops across the venturis are regulated by adjusting the position

Table 1. FUEL AND ASH AS DESCRIBED IN SPECIFICATIONS

COAL:	Average, As Received
Moisture	23.87%
Volatile Matter	28.59%
Fixed Carbon	38.96%
Ash	8.59% (Max. 12.58%, Min. 6.1%)
Heating Value	8843 Btu/lb. (Min. 8162 Btu/lb.)
Sulfur	.777% (Max. 1.0%, Min. 0.4%)

ASH: (Estimated composition, sulfur trioxide-free basis)

SiO_2	41.60%
Al_2O_3	22.42%
TiO_2	0.79%
Fe_2O_3	5.44%
CaO	21.90%
MgO	4.95%
Na_2O	0.31%
K_2O	0.13%
P_2O_5	0.41%

Table 2. DESIGN PARAMETERS FOR THE CEA VARIABLE THROAT VENTURI SCRUBBER (COLSTRIP APPLICATION)

Venturi Pressure Drop	43.2 cm w.c. (17 in.)
Venturi L/G	2 ℓ/m^3 (15 gal/1000 ACF, saturated
Absorption Spray L/G	2.41 ℓ/m^3 (18 gal/1000 ACF, saturated)
% suspended solids in recirculating slurry, by weight	12%
Residence time in the recycle tank	8 minutes
Gas velocity in mist eliminator zone	2.65 m/sec (8.7 ft./sec)
Wash tray pressure drop	9.65 cm w.c. (3.8 in.)
Mist eliminator pressure drop	2.5 cm w.c. (1 in.)
Reheat pressure drop	5.6 cm w.c. (2.2 in.)
Total system pressure drop (including reheat)	64.8 cm w.c. (25.5 in.)
Total scrubber pressure drop (less reheat)	55.4 cm w.c. (21.8 in.)

of the "plumb bob" shown in Figure 1, thereby increasing or decreasing the cross sectional area of the venturi throat. Throughout these tests, with the exception of one brief period, the pressure drop across the venturi on the module being tested was held at 46 ± 2 cm w.c.. Gas temperatures at the scrubber inlet ranged from 129°C to 137°C. The scrubber exit gas temperatures ranged from 57°C to 60°C and temperatures at the outlet test plane ranged from 94°C to 99°C. The temperature rise between the scrubber exit and the outlet mass sampling location results frm a flue gas reheat system and the action of the fan, both of which are located between the scrubber outlet and the sampling plane. The gas flow handled by the scrubber throughout the tests was approximately 130 DNCM/sec (280,000 DSCFM). A complete summary of the scrubber operating conditions during the tests conducted by SoRI are given in Table 3.

TEST METHODS AND RESULTS

A total of five measurement techniques were used during the tests. These were: (1) electrical mobility techniques using a Thermosystems Model 3030 Electrical Aerosol Analyzer for determining concentrations and size distributions on a number basis for particles having sizes between 0.01 µm and 0.3 µm, (2) optical techniques to determine concentrations and size distributions for particles having diameters between approximately 0.5 µm and 2.0 µm, (3) inertial techniques using cascade impactors for determining concentrations and size distributions on a mass basis for particles giving sizes between approximately 0.5 µm and 5.0 µm, (4) standard mass train (Method 17) measurements for determining total inlet and outlet mass loadings and emission rates, and (5) determinations of SO_2 concentrations by absorption of the SO_2 vapor in a solution of hydrogen peroxide followed by titration for the sulfuric acid reaction product.

The data obtained by Method 17 are summarized in Table 4 which includes the overall collection efficiencies for each of the pairs of tests.

The overall collection efficiency of the scrubber on this source under the conditions of operation tested was thus found to be approximately 99.4 percent.

The results of the SO_2 concentration measurements at the scrubber inlet and outlet are given in Table 5. Table 5 also includes SO_2 collection efficiencies derived from the concentration measurements.

Inertial sizing was accomplished using modified Brink impactors for inlet measurements and University of Washington Mark III impactors for outlet measurements. All impactors used in this program were calibrated at SoRI using the methods described in EPA publications 600/2-76-280[3] and 600/2-77-004.[4]

The impactor data are summarized in Figures 2 and 3 which present averaged inlet and outlet size distributions, respectively, on a cumulative percentage (by mass) basis versus aerodynamic particle diameter. Figure 4 shows the fractional efficiency curve as a function of aerodynamic particle diameter as derived from the inlet and outlet data that were presented in the previous figures. The fractional efficiency curve is shown again in Figure 5 as a function of Stokes diameter together with the efficiency curves derived from the ultrafine particulate data. The scrubber was operating at a venturi pressure drop of about 46 cm w.c. throughout the impactor test periods.

Measurements of the concentration and size distribution of ultrafine particulates were made using a Thermosystems Model 3030 Electrical Aerosol Analyzer (EAA) and a Royco Model 241 Optical Single Particle Counter.

The EAA provides size distribution and concentration data on a number basis for particles having diameters between approximately 0.01 μm and 0.3 μm. The optical counter provides similar data in the range from approximately 0.3 to 2 μm. Both instruments require extensive sample dilution and conditioning when used to sample flue gases. The sample extraction and dilution system used in these tests is described in a forthcoming EPA report on Contract 68-02-2114, Task VIII. Dilution factors of about 150:1 were used at both the inlet and outlet during these tests.

SUMMARY

The overall collection efficiency of the CEA variable throat venturi scrubber, determined by conventional (Method 17) techniques on a pulverized coal fired power boiler producing particulate having a mass median diameter of about 20 μm, ranged from 99.12 to 99.50 during three days of testing. The venturi pressure drop ranged from 44.5 cm w.c. to 48.3 cm w.c.. Measured fractional efficiencies were about 5% at 0.06 μm, 25% at 0.1 μm, 40% at 0.20 μm, 50% at 0.5 μm, 98.4% at 1.0 μm, and 99.99% at 2 μm. The system energy usage during the tests was approximately 7200 joules/DNCM. SO_2 collection efficiency ranged from 76.5% to 85.6%.

ACKNOWLEDGEMENTS

Appreciation is expressed to B. Knutson, D. Berube, and C. Grimm of The Montana Power Company for their cooperation during the test program. Appreciation is also expressed to I. A. Raben of Combustion Equipment Associates, Inc. for supplying the information on the design and operation of the scrubber. The test program was conducted under Contract 68-02-2181 for the Industrial Environmental Research Laboratory of the U. S. Environmental Protection Agency. Mr. Dale L. Harmon was the project officer responsible for the technical effort under this contract.

Table 3. SCRUBBER OPERATING CONDITIONS

		Module Gas Flow DNCM/s		Gas Temperatures, °C			
Date	Unit Load, MW	Inlet	Outlet	Scrubber Inlet	Scrubber Outlet	Reheat Outlet	Fan Outlet
5/17	330	110	128	132	60	79	94
5/18	350	132	140	129	58	78	96
5/18	355	133	162	129	57	78	96
5/19	355	130	137	131	59	78	96
5/19	355	124	139	133	57	74	96
5/20	290	106	113	129	56	82	93
5/20	348	127	136	129	52	82	93

	Liquor Flows, ℓpm					
Date	Upper Spray	Middle Spray	Absorption Spray	Mist Elim. Under Spray	Wash Tray Under Spray	Wash Tray Feed
5/17	15900	10200	22700	570	1170	3600
5/18	15000	9370	24400	570	1060	2900
5/18	18200	11360	19870	570	1170	2800
5/19	17600	10790	24600	625	1170	3220
5/19	17500	10600	24200	625	1190	2840
5/20	17800	10600	25700	530	1170	3220
5/20	17600	11700	25000	570	950	3220

Date	Liquor pH	% Suspended Solids	Plumb Bob Position, % of Travel	Venturi P, cm w.c.
5/17	4.3	11.4	54	44.5
5/18	4.7	15.2	58	46.4
5/18	4.7	16.4	62	46.4
5/19	4.7	14.3	61	46.4
5/19	4.6	13.4	61	47.0
5/20			53	45.7
5/20			65	45.1

Table 4. CEA VARIABLE THROAT VENTURI TEST MASS DATA

Run Number	1	2	3	4	5	6
Date	5-16-77	5-17-77	5-18-77	5-18-77	5-19-77	5-19-77
			INLET			
Moisture, %	10.30	11.62	10.25	10.87	11.86	12.26
Concentration, grams/DNCM	3.6145	5.1701	5.8663	6.2079	6.4512	6.5546
			OUTLET			
Moisture, %	14.01	19.45	17.37	16.53	18.70	18.15
Concentration, mg/DNCM	42.79	45.31	33.58	36.28	41.90	33.04
Efficiency (%)	98.82	99.12	99.43	99.42	99.35	99.50

Table 5. SCRUBBER SO_2 REMOVAL EFFICIENCY

Date	Inlet SO_2 Concentration (ppm)	Outlet SO_2 Concentration (ppm)	SO_2 Removal Efficiency (%)
5-17-77	658	130	80.2
5-18-77	525	103	80.4
5-19-77	553	130	76.5
5-20-77	625	90	85.6

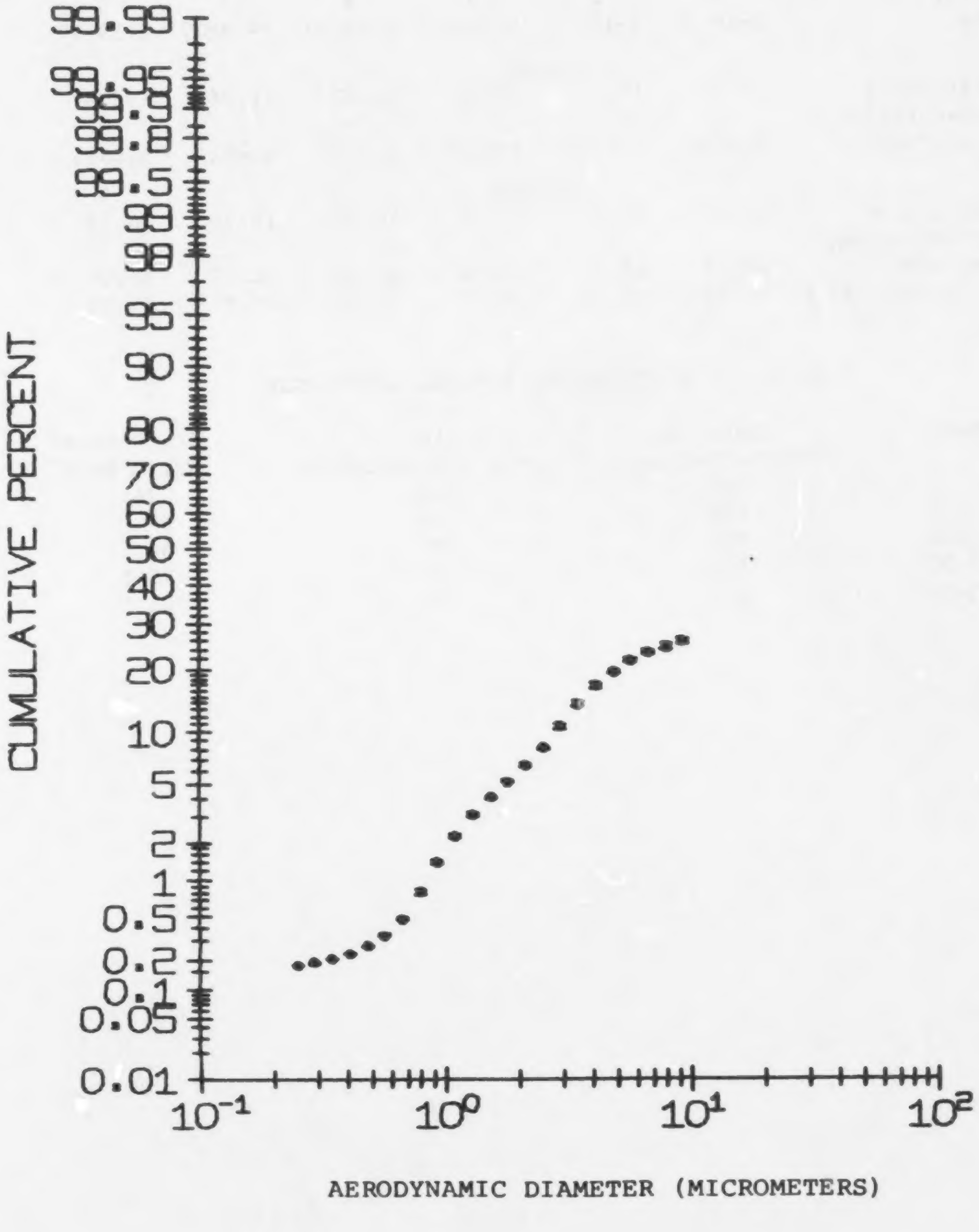

Figure 2. Average inlet particle size distribution from cascade impactor data on a cumulative percent by mass basis.

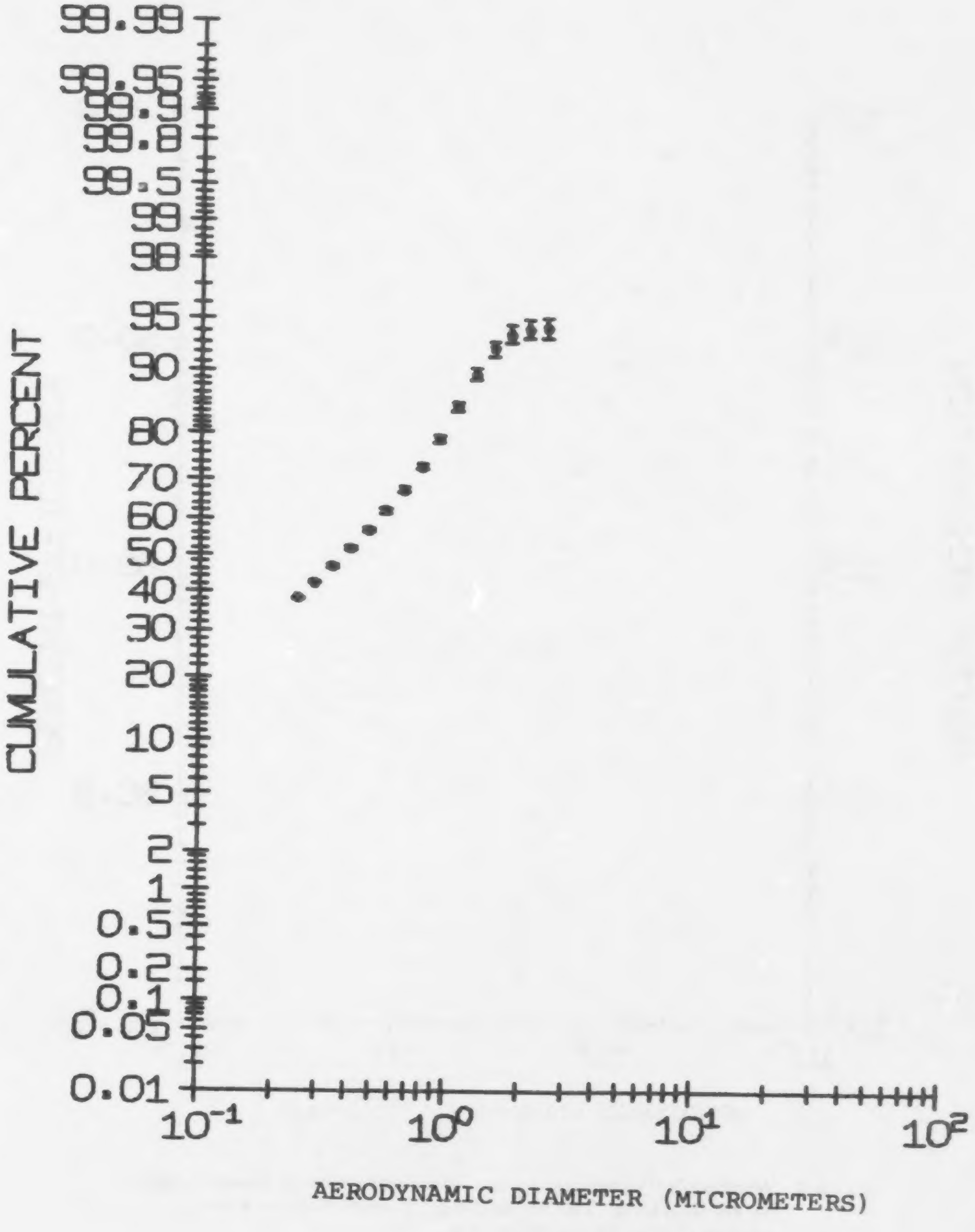

Figure 3. Average outlet particle size distribution from cascade impactor data on a cumulative percent by mass basis.

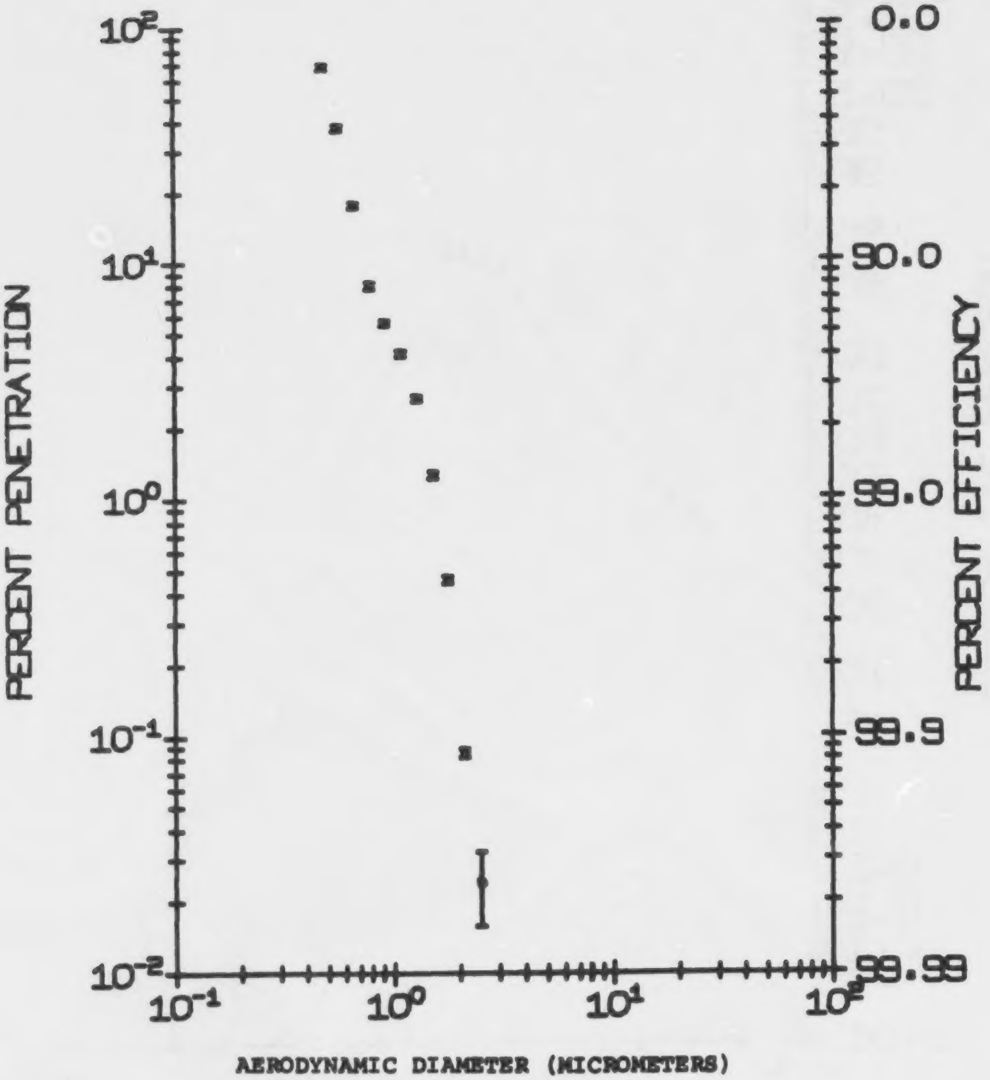

Figure 4. Fractional efficiency curve on an aerodynamic particle diameter basis for the CEA variable throat venturi scrubber operating at a venturi pressure drop of 48 cm (19 in.) w.c..

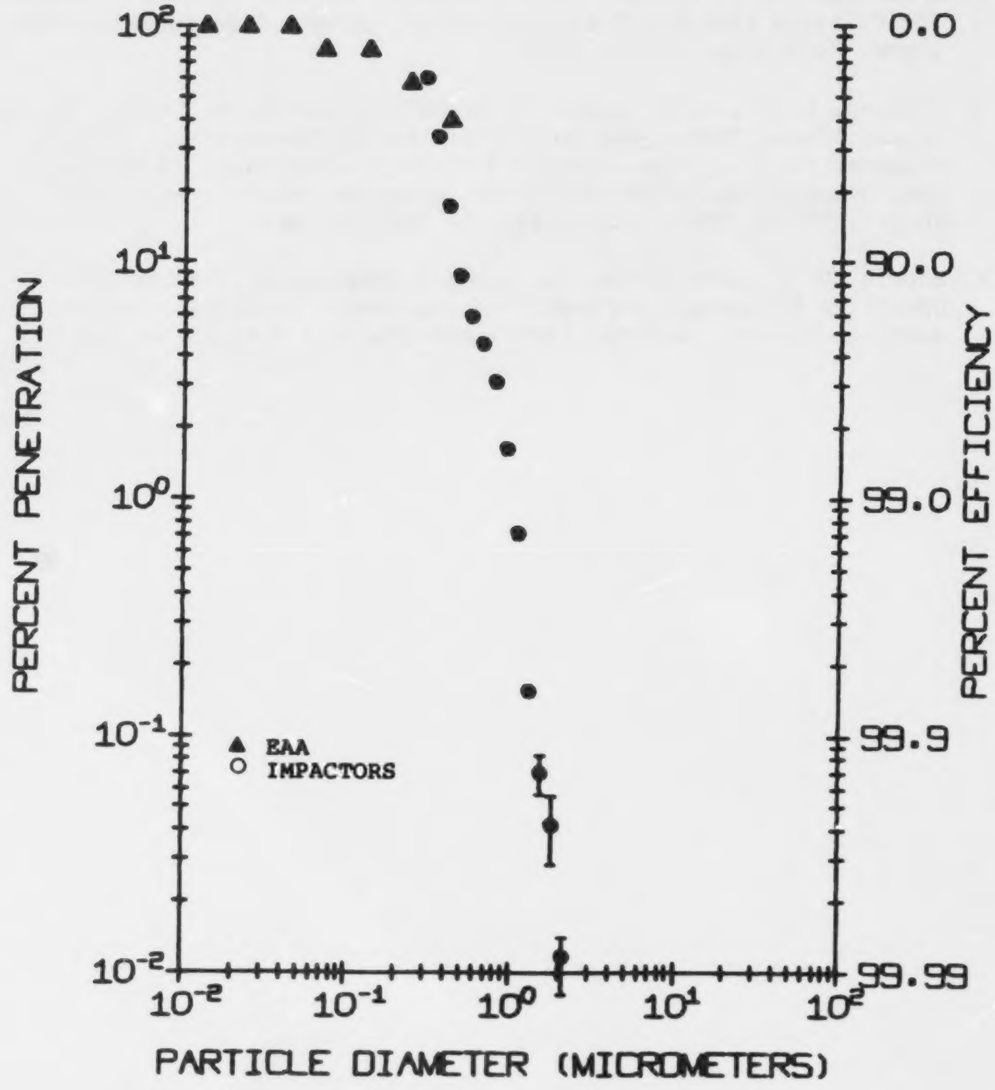

Figure 5. Fractional efficiencies based on electrical mobility and optical methods shown on a "physical" diameter basis. Also shown are fractional efficiencies from the cascade impactor data on a basis of Stokes diameters.

REFERENCES

1. McCain, J. D., CEA Variable Throat Venturi Scrubber Evaluation. Southern Research Institute, Industrial Environmental Research Laboratory, Research Triangle Park, N.C. 76 pp. 1978. EPA-600/7-78-097.

2. Grimm, C., J. Z. Abrahms, W. W. Leffman, I. A. Raben and C. LaMontia. The Colstrip Flue Gas Cleaning System. Chemical Engineering Progress, 74(2), pp. 51-57, 1978.

3. Cushing, K. M., G. E. Lacey, J. D. McCain, and W. B. Smith. Particulate Sizing Techniques for Control Device Evaluation: Cascade Impactor Calibrations. Southern Research Institute, Industrial Environmental Research Laboratory, Research Triangle Park, N.C. 96 pp., 1976. EPA-600/2-76-280, PB 262 849/3BE.

4. Harris, D. B. Procedures for Cascade Impactor Calibration and Operation in Process Streams. Environmental Protection Agency, Washington, D.C. 123 pp. 1977. EPA-600/2-77-004, PB 263 623/1BE.

RESULTS OF THE TEST PROGRAM
OF THE WEIR HORIZONTAL SCRUBBER
FOUR CORNERS STEAM ELECTRIC STATION
UNIT NO. FIVE

Glen Bratzler
Bechtel Corporation

G. T. Gutierrez
Arizona Public Service

C. F. Turton
Arizona Public Service

INTRODUCTION

In 1976, Arizona Public Service Company initiated testing of a full scrubber module at the Four Corners Power Plant near Farmington, New Mexico. The test was to demonstrate the feasibility of complying with SO_2 and particulates air quality emission regulations adopted by the State of New Mexico. These regulations required 90% SO_2 removal, limited total particulate emissions to 0.05 $lbs/10^6$ BTU heat input and limited minus two micron particulate to 0.02 $lbs/10^6$ BTU heat input.

Since APS had previously encountered problems with scale up of scrubber systems, it was felt prudent to test a scrubber of the size which would be used on a permanent system. The Weir Horizontal Scrubber which had the best operating record of all scrubber systems in service at the time was chosen for the test. The 160 MW Weir Horizontal Module, used in the test program and which has previously been reported on by others, was moved from the Southern California Edison Mohave Generating Station and installed on Unit No. Five at the Four Corners plant.

The objectives for the test program were as follows:

1. Demonstrate the Horizontal Module capabilities to meet the adopted emission regulation for particulate and SO_2 at Four Corners with the loading peculiar to the station.

2. Demonstrate the Horizontal Module and major subsystems performance and reliability.

3. Obtain information to determine the operating conditions and process control procedures necessary to achieve the desired performance.

SYSTEM DESCRIPTION

The scrubber module has a rated flue gas flow of 480,000 scfm, which corresponds to 800,000 acfm at 253F and 12.08 psia. The module system has five stages of horizontal spray chambers each 12 feet long, 28 feet wide and 17 feet high with five sets of spray nozzles, forced draft booster fan, flue gas presaturator section, mist eliminator, lime storage and slaker, and a slurry thickener.

Figure 1 is a basic flow diagram of the scrubber system. Flue gas from the Unit Five south precipitator enters the presaturator section (via the gas booster fan) at about 230F and is cooled by a spray of 300 gpm of water to the adiabatic saturation temperature of about 120F. The cooled flue gas then passes through the scrubber stages to a chevron type mist eliminator where entrained scrubber slurry is removed from the gas. The gas is then mixed with the heated ambient air from the indirect steam coil reheat system to increase the gas temperature by about 30F prior to being exhausted through a steel stack to atmosphere.

As the flue gas passes through the scrubber spray stages, it is contacted with slurry. The spray nozzles are arranged in rows of six clusters containing six to nine nozzles each, across the top of each stage. The slurry sprays downward crosscurrent to the gas flow and collects in hoppers at the bottom of each stage. Slurry from the reaction mix tank is pumped to the fourth stage and then, in a cascade system, is pumped from stage to stage counter to the gas flow. The spent slurry drains from the first stage hopper to the mix section of the reaction mix tank. The SO_2 absorbent $Ca(OH)_2$ is introduced into the system at this point at approximately 15% by weight lime slurry. The reaction section is designed for approximately four minutes of retention at the design flow rate of 9600 gpm.

SO_2 is removed from the flue gas by reaction with the lime slurry. Fly ash is removed from the gas phase in the scrubber by intimate physical contact between the spray droplets and the fly ash particles. Slaked 1/4 inch pebble lime was used as the reagent in this system.

A purge of slurry was fed to the thickener from the first stage hopper to remove the SO_2 sludge and fly ash as fast as they were formed. The thickener underflow containing about 30% by weight of suspended solids was pumped to the ash disposal ponds. The thickener overflow was collected in four equalized tanks and used as process water.

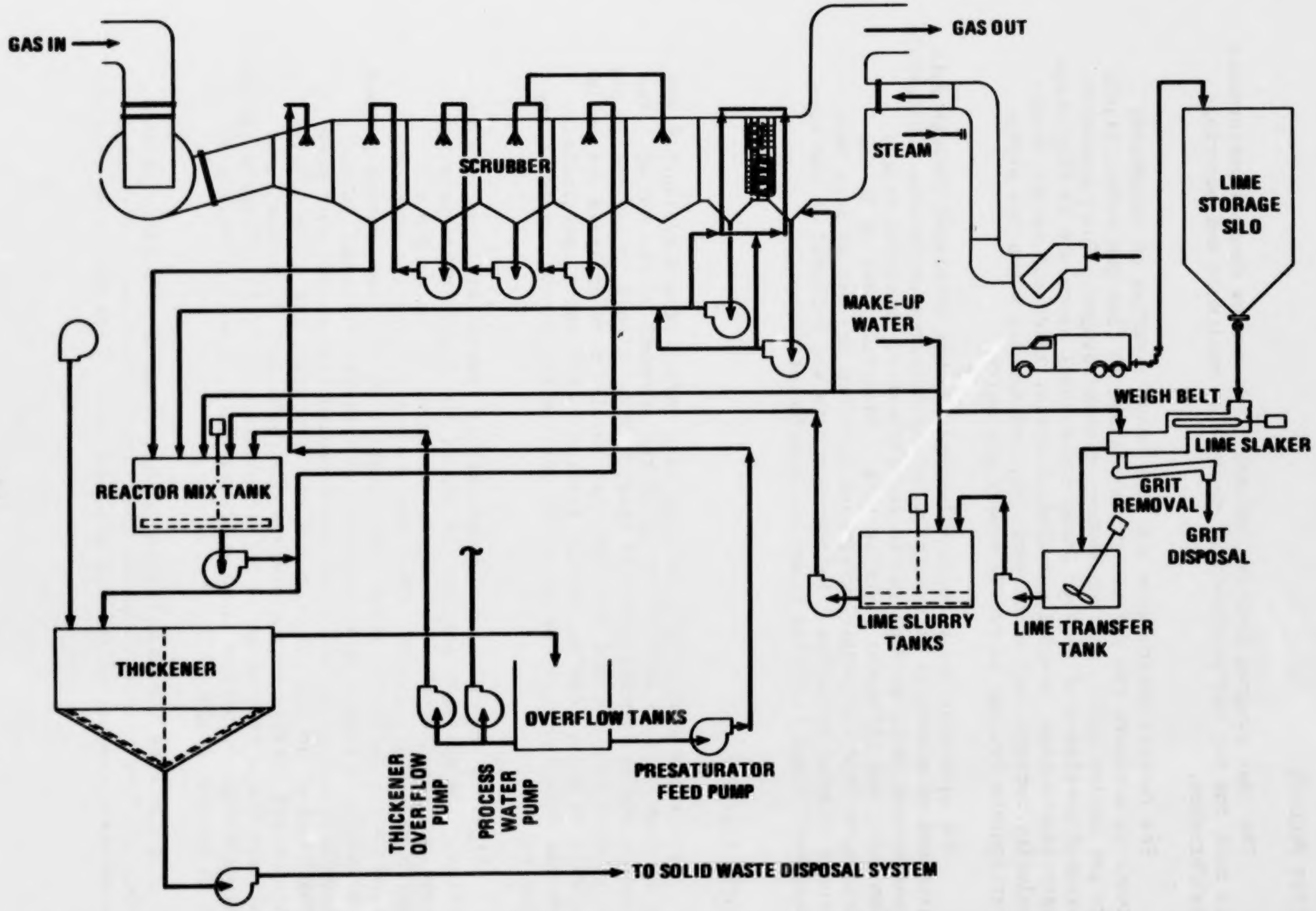
GAS IN
GAS OUT
STEAM
SCRUBBER
LIME STORAGE SILO
MAKE-UP WATER
WEIGH BELT
LIME SLAKER
GRIT REMOVAL
GRIT DISPOSAL
REACTOR MIX TANK
LIME SLURRY TANKS
LIME TRANSFER TANK
THICKENER
OVERFLOW TANKS
THICKENER OVER FLOW PUMP
PROCESS WATER PUMP
PRESATURATOR FEED PUMP
TO SOLID WASTE DISPOSAL SYSTEM

11373-900 F52 T1532
JUNE 1978

TEST PROGRAM

The test program included testing to determine removal performance fo both the SO_2 and particulate, as well as equipment and materials performance.

The removal performance was done using a series of parametric tests to evaluate the affects of variations in flue gas rates, liquid to gas ration (L/G), and the number of spray stages. The parametric program consisted of 54-Four Stage operational tests and 18-Five Stage operational test, special entrainment tests, inlet and outlet stack velocity surveys, wet stack sampling, and special minus two micron particulate testing to verify sampling results.

The equipment and materials information was developed through data gathered on materials of construction and maintenance records. Materials test coupon racks were placed in the preheater, scrubbing stages, demister, and thickener overflow tank. Materials testing in the thickener feed and underflow streams involved the use of pipe test spools mounted in series. Maintenance data was gathered on the key equipment items including pumps and instrumentation.

TOTAL PARTICULATE

The total particulate loadings were varied from 0.42 lbs/10^6 BTU to as high as 2.95 lbs/10^6 BTU (with the approval of the NMEIA). The average during testing was 0.98 lbs/10^6 BTU. Liquid to gas ratios per stage were ten, 20, and 30. The test results were analyzed for outlet loading vs inlet loading, outlet loading vs L/G ratio, particulate removal efficiency vs L/G ratio and particulate removal vs inlet gas flow rate.

Figure 2 is a plot of the particulate removal efficiency vs L/G ratios. The straight line at the top of the figure represents the average percent removed for an average inlet concentration of approximately 1.0 lbs/10^6 BTU. The percent particulate removal was found to vary with the inlet concentration so that the average percent removal curve cannot be used to extrapolate the different inlet concentrations. The effect of inlet concentrations was much more pronounced at 10 L/G per stage ratio. Comparing the given inlet particulate loading on the average, approximately 30 percent less emission would be seen at 20 L/G per stage than at 10 L/G per stage and approximately 60 percent less emission would be seen comparing 30 L/G to 10 L/G per stage.

In plotting the data for particulate removal efficiency against inlet gas flow rate for each of the three L/G's tested, no trend in particulate removal efficiency could be seen. This indicates that the

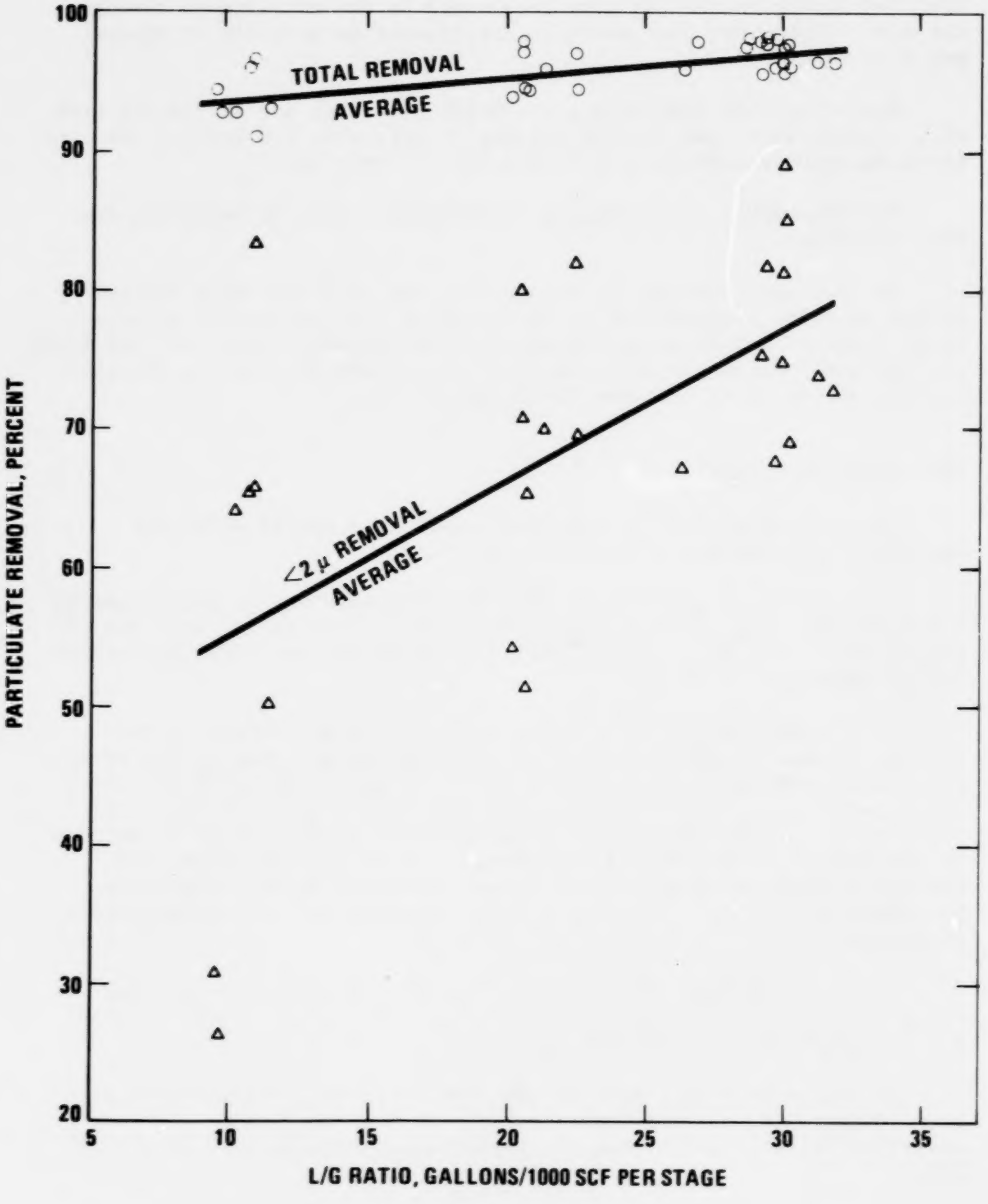

Figure 2

EFFECT OF L/G RATIO ON
PARTICULATE REMOVAL, FOUR STAGES

limiting factor on the gas flow rate would be the entrainment through the mist eliminators that would be experienced as a result of higher gas flow rates.

Operating with four stages at 30 L/G per stage and at 750,000 acfm with a total inlet particulate loading of less than 1.8 lbs/10^6 BTU, the total emission standards of 0.05 lbs/10^6 BTU were met.

The EPA method five sampling technique was used in obtaining the test results.

At the same time the EPA method five was used, the ASTM instack method was also performed as a comparison of the two testing methods. These tests show that using EPA method five sampling technique, the total particulate loading was approximately twice those obtained by the ASTM instack method under the same conditions.

LESS THAN TWO MICRON

No test method for the fine particulate was specified by the agencies, so a conservative method was used.

The percent of particulate less than two microns, as determined by the Andersen eight plate impactor, was used in conjunction with the EPA method five total particulate loading to calculate the minus two micron outlet loading.

Increasing the L/G ratio has a more significant effect on the average removal of the minus two microns particulate than on the total particulate removal. Increasing from 10 L/G per stage to 30 L/G per stage caused a variation to approximately three percent in the total particulate removal compared to an increase of approximately 22 percent in the average fine particulate removal. At 10 L/G per stage, the average removal of the minus two micron particles was approximately 53 percent, while at a 30 L/G per stage, the removal was approximately 75 percent.

It was found that removal efficiency decreases with decreasing particles size reaching a minimum at about 0.5 microns, then increased for the particles smaller than 0.5 micron.

As can be seen in Figure 2, the fine particulate data had significant scatter. Because of this scatter, the minimum fine particulate emissions reliably achievable at the conditions tested is 0.04 lbs/10^6 BTU.

SO_2

During the most of the testing, the outlet slurry pH was maintained at 5.5 as an optimum operating condition. Operation below pH 5.0 caused excessive hard scale on the scrubber surfaces and demister blades. Operation at higher than pH 7.0 tended to cause buildup of soft solids inside the scrubber and excessive use of lime.

Figure 3 shows the effect of pH and L/G on SO_2 removal. The two factors affecting the removal of SO_2 are the pH of the slurry and the L/G ratio. At 30 L/G per stage, the SO_2 removal was 82.5 percent at a slurry pH 5.0 and 98.6 percent at a slurry pH 6.0.

At slurry pH 5.5, 82 percent SO_2 removal was achieved at 10 L/G per stage and 98.6 percent SO_2 removal was achieved at 30 L/G per stage.

SO_2 removal did not change at gas flow rates between 500,000 and 750,000 acfm.

FIVE STAGES

As previously mentioned the scrubber was tested with five stages operating. The fifth stage was inserted for the test only and insufficient disengagement space between the fifth stage and the demister was available. As a result, the data for particulate removal was inaccurate due to entrainment from overloading the demister. Only a slight improvement in SO_2 removal was seen over four stages for operation at all L/G's tested. This would indicate at the higher L/G's and a given pH the peak efficiency of the scrubber for SO_2 removal had been reached with the four stage operation.

POWER CONSUMPTION

Increasing gas flow rates and L/G ratios increased pressure drops in the scrubber system. An increase from 10 to 30 L/G per stage increased the pressure across the scrubber fro 1.0 to 2.0 inches of water at a as flow rate of 750,000 acfm. Increasing scrubber pressure drops of 0.08 to 0.28 inches of water for 10 and 30 L/G per stage respectfully.

Power consumption of the FD fan represented 24 to 30% of the total power consumed by the scrubber system. The module operating with four stages and 30 L/G per stage consumed approximately 3.6 megawatts.

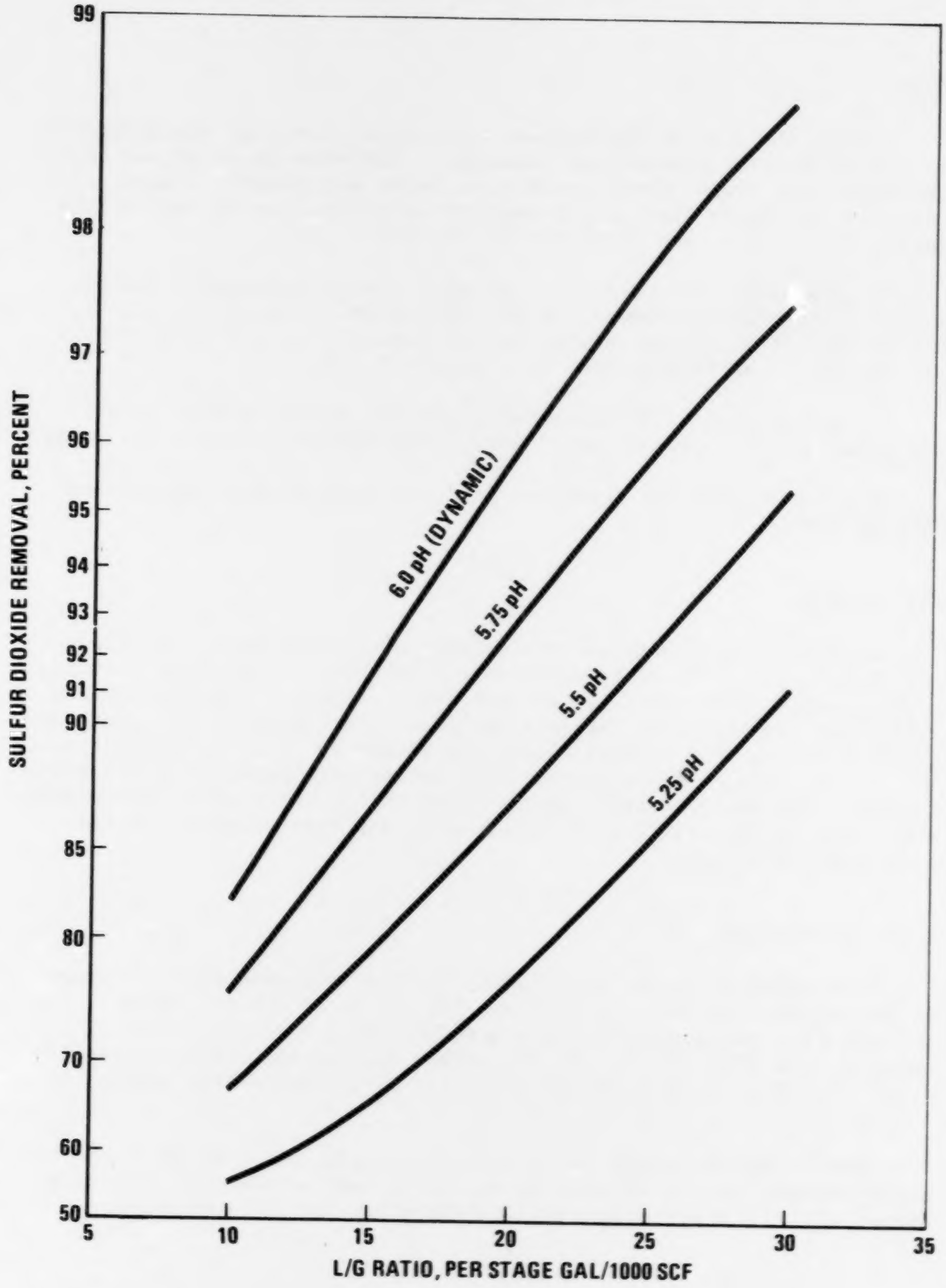

Figure 3

EFFECT OF L/G RATIO ON SO_2 REMOVAL FOR SLURRY pH OF 5.25-6.0, FOUR STAGES, 600-800 PPM INLET SO_2

MATERIALS OF CONSTRUCTION

The presaturator shell was 316L SS as a guard against excessive corrosion from the sulfuric and sulfurous acid formed in this section. Only minor shallow corrosion/erosion occurred on the shell. The uncoated carbon steel duct work downstream of the fan and upstream of the presaturator shell experienced serious corrosion due partly to the presaturator spray backflowing into the flue gas. The spray system for the presaturator was a network of internal 316L SS spray headers and nozzles. This sytem showed no appreciable wear.

The interior walls, hoppers and ceiling of the first stage of the scrubber were rubber lined, while flake glass or silica polyester resins were used as lining for the second, third, fourth, and fifth stages. At the end of the test program the rubber lining was in good condition. The flaked glass linings were in fair condition except for some edge and corner failures in every stage where the spray contacted the surface of the scrubber.

The test courpons in the presaturator section showed carbon steel to be severely corroded in 1200 hours at a rate of 100 mils per year. 304 SS corroded at a rate of approximately three mils per year. While 316L SS showed only light corrosion of 0.3 mils per year. Inconel and incoloy showed excellent wearing with corrosion in the range of 0.1 mils per year. Flake glass or silica polyester resin coating on the coupons showed excellent wear in the presaturator section.

In the scrubber and demister stages the test courpons of low carbon steel was corroded away in 1200 hours with a rate of 500 mils per year. Both 304 and 316 stainless showed mild corrosion at a rate of five to seven mils per year. Inconel and incoloy both exhibited mild corrosion at the rate of three to five mils per year. Chlorbutyl rubber in the scrubber stages showed excellent wear, while natural rubber and the flaked glass and polyester resins showed good to very good wear characteristics. Three inorganic plastic coating in these areas were found to be unsatisfactory when contacted with the high velocity spray droplets. However, these coatings were found to hold up satisfactorily when the spray droplets did not impinge directly on the surface.

Low carbon steel in the outlet duct and stack exhibited severe wear, 54 mils per year. While 304 stainless showed light corrosion at a rate of approximately 0.3 mils per year. The 316L SS showed excellent results with less than 0.1 mils per year loss. Three organic coatings in the stack showed excellent wear with losses of one to two percent by weight. Four different inorganic coatings exhibited failure rates considered poor to fair with one coating completely failing.

The uncoated carbon pipe spool in the thickener feed slurry lines showed severe corrosion/erosion, while soft rubber and hard chlorobutyl rubber linings showed excellent wear. Spools of PVC, FRP and polypropylene lined pipe showed good results with no wear and only small amounts of solids buildup. The uncoated steel, solid PVC and FRP pipe in the thickener underflow all showed minor scaling and were considered to be good, while both the soft natural rubber and hard chlorobutyl rubber lining showed excellent wear. The elyL SS, inconel and plastic coatings in the thickener overflow tank showed excellent results, while type 304 Stainless exhibited slight corrosion and the mild steel showed serious corrosion.

SPRAY NOZZLES

Two type of nozzles were used in the spray system. For the basic design conditions of operating at 20 L/G per stage ceramic nozzles were installed. When operating 30 L/G per stage and operating with the fifth stage, additional 316L SS nozzles were installed. The ceramic nozzles showed no appreciable wear after 1900 hours of operation. The stainless steel nozzles showed severe wear after approximately two months of operation. In many cases holes caused by erosion appeared in the metal nozzle body and the spinner at the location of the nozzle orifice.

SLURRY RECIRCULATION PUMPS

Pumps from four different manufacturers were installed as the main slurry pumps, with three pumps on each of the first four stages for a total of 12 pumps. Seven of the pumps were rubber lined with various linings as recommended by the manufacturers. Two pumps were precipitation hardened stainless steel, two were 28 percent high chrome all metal pumps and one was 22.6 percent chrome 2.8 percent molybdium and 1.69 percent carbon. Pumps with properly fabricated rubber liners between 40 and 60 durometer provided the best service life. The high chrome pumps showed minor wear on the wear plates and impellers. The stainless steel pumps exhibited serious erosion problems most notably on the wear plates and suction throat.

VALVES

Butterfly valves of two disc types were installed at the facility; Ryton coated ductile iron and 316L SS. Approximately 90 percent of the Ryton coated valves failed while all the stainless steel valves appeared to be in good condition with no erosion wear. The rubber seats of all the valves appeared to be in good condition. Rubber lined pinch valves with anti-flutter design features were utilized in the thickener feed, lime addition and lime return lines. These valves were in good condition at the end of the program with only slight discoloration of the rubber and some creasing and limited surface checking present on the valves. Plug and ball valves used functionally only as on/off valves were installed in different locations throughout the system. Ball valves of 304 SS used to regulate sample flow failed in approximately two months of service due to erosion of the ball. All the rubber lined plug and ball valves were in good condition.

MIST ELIMINATOR

The mist eliminator section consisted of ten modules of plastic chevron type blades arranged five wide by two high. The wash system for the mist eliminator was comprised of 15 vertical rows of three spray nozzles evenly spaced across the mist eliminator on both the inlet and outlet sides. The inlet side wash system was constructed of stainless steel piping with brass nozzles, while the outlet side wash system was constructed of carbon steel piping and a mixture of carbon steel and brass nozzles. The carbon steel headers and nozzles were badly corroded in this service. One to two minutes per header every six hours proved to be effective in reducing and controlling scale formation on the demister blades. The overall performance of the demister system was effective in removing entrained droplets. The demister wash pumps were ni-hard II metal. These pumps performed satisfactorily in the service, however, were starting to show erosion wear on both the suction and gland side liners and the impeller.

THICKENER

The 60 foot diameter thickener was in fair condition at the end of the test program and had provided satisfactory operation throughout the program. The thickener shell was uncoated carbon steel and was badly rusted by the end of the test program. The thickener performance was strongly effected by the amount of calcium sulfite present in the solids. With the typical ratio of calcium sulfite to calcium sulfate of three to one relatively poor setting characteristics were found with the absences of flocculants. The addition of both ionic and anionic, flocculants improved the settling rate from 12 feet two/ton day to 40 feet two/ton day, and was effective in improving the clarity of the overflow.

Both the thickener feed pump and the thickener overflow pump were molded rubber lined of 42 and 63 durometer rubber. The overall operation of these pumps was satisfactory. Tests indicated that a harder rubber lining should be used for the thickener feed pump and that a 316L SS pump could be used for the thickener overflow system. The thickener underflow pumps were varidriven positive displacement worm type pumps. This worm type pump operated satisfactorily but required much maintenance due to foreign objects passing through the pumps, and on several occasions sheared the drive pins and on two occasions the rotor itself sheared.

BOOSTER FAN

The booster fan was principally constructed of high strength, low alloy, manganese, vanadium steel. The fan is a forced draft fan to the scrubber and is subject to handling the fly ash entering the system. After about 1500 hours of operation the highly abrasive fly ash of the

Four Corners Plant caused pin holes to develop on the leading edge blade/center plate welds. The hollow airfoil blades filled with fly ash and caused excessive vibrations. After removing the fly ash from the blades and welding the leading edges, the fan continued to operate satisfactorily.

LIME SYSTEM

The lime system included the lime unloading system, pebble lime storage, two agitated slaked lime slurry storage tanks and a paste type lime slaker with mix tanks. The lime system operated satisfactorily. There were some problems when a powdery lime instead of a 1/4" nominal pebble lime was delivered to the plant. The powder lime vertical feeder gate and alarm system would not operate properly and it adhered to the silo cone walls and would not discharge properly into the feeder. The slaker was a moderate maintenance item that required routine cleaning.

INSTRUMENTATION

The process control instrumentation and flue gas analysis required continual maintenance and attention. pH meters from five manufacturers were tested during the program. These meters were both the submersible and flowthrough types. The submersible meters incurred continual problems with solids settling out in the probe containers. Assortment of probe chambers were tried without success. The flowthrough probes while requiring maintenance attention gave good availability in the slurry service.

Magnetic flow meters were installed in the scrubbing slurry, lime slurry, make-up, slurry feed to thickener and thickener underflow system. All of the meters experienced scaling to some degree and on two installation ultrasonic cleaners were utilized but proved to be ineffective in preventing scale.

The SO_2 analyzers were sample type systems drawing flue gas from three different duct locations and analyzing these samples in one of two instruments. One instrument draws a gas sample from the inlet duct and the other instrument alternately draws from the demister area and the stack. By providing daily calibration and leak testing the analyzer systems were acceptably accurate. The sample lines were constructed of electrically heated teflon tubing. Although easy to install this proved to be a high maintenance item. The ferruled type metal fittings were inadequate in providing air tight connections due to the relaxation characteristic of teflon. The solenoid valves in the system failed as a result of solid deposits in the sample lines. These were replaced with electrically operated ball valves which operated trouble free.

The SO_2 analyzer system was a sampling system drawing gas sequentially from three different duct locations via a timer solenoid valve arrangement. The sample locations were in the inlet duct, demister section and in the stack. With regular maintenance, calibration and periodic replacement of the analyzer cells this system performed adequately.

Double pass light absorption opacity instruments were provided in the gas inlet and outlet streams. With only minor maintenance, moderate recalibration and rezoning and periodic window cleaning the instruments performed with a high data retrival percentage.

SUMMARY

Although the Weir Scrubber Module used was not intended to operate beyond the original test program at Mohave, all of its systems operated satisfactory. Test objectives were generally met with one major exception, 0.02 lbs/10^6 BTU was not achieved.

MATERIALS PERFORMANCE PROBLEMS ASSOCIATED WITH THE SCRUBBING OF COKE OVEN WASTE HEAT FLUE GAS

M. P. Bianchi and L. A. Rosales
TRW Systems and Energy Group
Redondo Beach, California, U.S.A.

INTRODUCTION

A coke oven waste heat flue gas corrosion study has been performed as part of the Charged Droplet Scrubber (CDS) program funded jointly by the EPA and TRW at the Kaiser Steel plant in Fontana, California, (see Figure 1).

The objectives of the study were to:

- Obtain quantitative data on the performance of 316 CRES (austenitic stainless steel) of which the main structure and components are constructed.
- Investigate the feasibility of coatings as a means of improving the performance of materials exposed to coke oven flue gas environments.
- Investigate the feasibility of metallic and non-metallic liners for scrubber construction.
- Investigate alternate materials, both metals and non-metals, for CDS component and structure applications.

The approach was to use a combination of materials test coupons, coated portions of the CDS structure and components and electronic corrosion probes to assess the performance of the test materials under actual scrubber operating conditions.

Preceding page blank

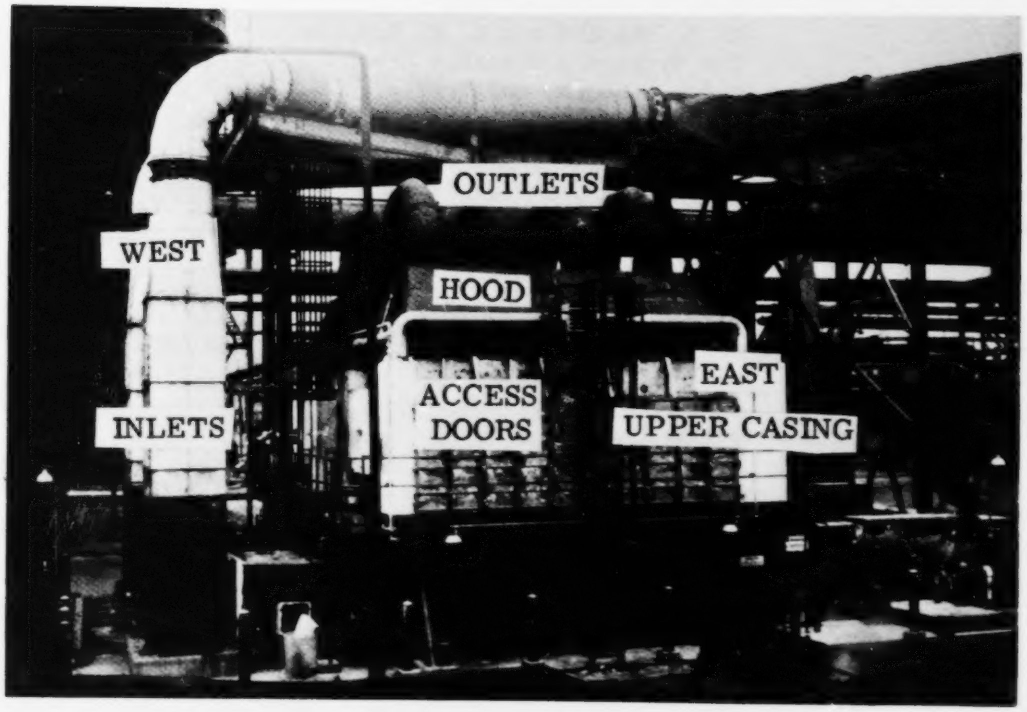
OUTLETS
WEST
HOOD
EAST
ACCESS DOORS
INLETS
UPPER CASING

Figure 1. TRW Charged Droplet Scrubber

Briefly, the charged droplet scrubber (CDS) works in the following manner. A spray of electrically charged water droplets are accelerated through an electrostatic field between a spray tube and collector plate. The contaminated discharge gases pass through this field, and dust particles are attracted to the liquid droplets by means of direct collisions or indirect charging encounters. The dust particles are carried to the collector plate where they are continuously drained off with the liquid. Figure 2 is a schematic representation of the CDS operating principles.

Coupon test samples (metal and non-metal) were installed in the upper casing (hood) and in the lower casing under the baffles of the CDS. The lower casing location produced the most severe service since the temperatures of the samples can reach that of the incoming gas stream and the wash water is only partially effective due to the screening caused by the baffles. Some of the samples were coated or lined with organic materials.

Coatings were applied to the electrode access doors, electrodes, wash couplings, upper casing (hood) surfaces, and lower casing surfaces as well as test coupons.

The electronic corrosion meter (Corrosometer, Magna Corp.) probes were used to serve as an in-process indicator/monitor for corrosion behavior. In addition, the Corrosometer data was compared to corrosion data from test coupons.

Figure 3 is a schematic of the Kaiser CDS showing the locations where the corrosion test samples and coatings were placed as well as the locations for the corrosion probe ports.

Analysis techniques employed included visual inspection, weight change determinations, metallographic examination, and hardness measurements.

TEST

Several candidate metallic and non-metallic materials were selected. The metallic materials included 316 CRES (the material of which the units are constructed), 304 CRES, titanium, and several nickel-base superalloys. In addition, mild steel coupons were selected as a substrate for candidate coating systems. The 304 CRES alloy was chosen as a candidate since it is more sensitive to chloride pitting attack than 316 CRES and would give an indication of excessive chloride build up in the system. The nickel alloys were chosen for their resistance to sulfuric acid attack. Several alloys were chosen for study which include various Cr-Mo-Fe compositions. Commercially pure titanium is known to possess outstanding corrosion resistance to most media and has performed well in sulfuric acid environments. It is not affected by the presence of chlorides.

Figure 2. CDS operating principles

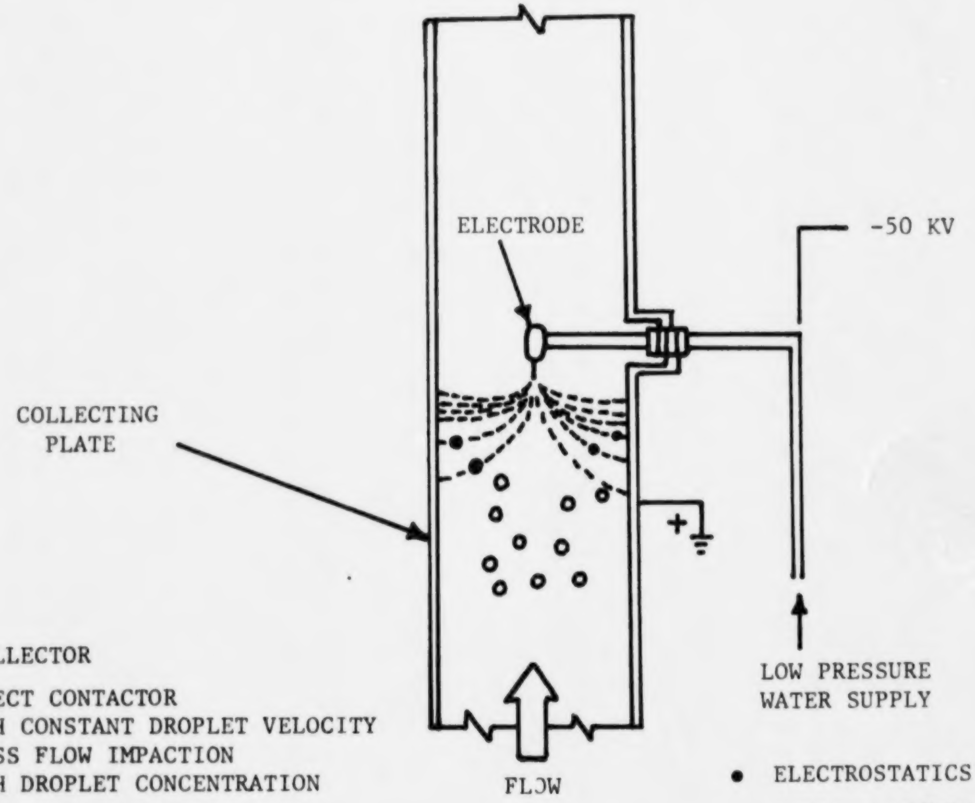
ELECTRODE
-50 KV
COLLECTING PLATE
+
LOW PRESSURE WATER SUPPLY
FLOW

- HYBRID COLLECTOR

WET - DIRECT CONTACTOR
    - HIGH CONSTANT DROPLET VELOCITY
    - CROSS FLOW IMPACTION
    - HIGH DROPLET CONCENTRATION

DRY - DIRECT CORONA CHARGING
    - INDIRECT CORONA CHARGING

- ELECTROSTATICS FOR ALL FUNCTIONS
  - WATER ATOMIZATION
  - DIRECT WATER DROPLET CHARGING
  - SELF DEMISTING

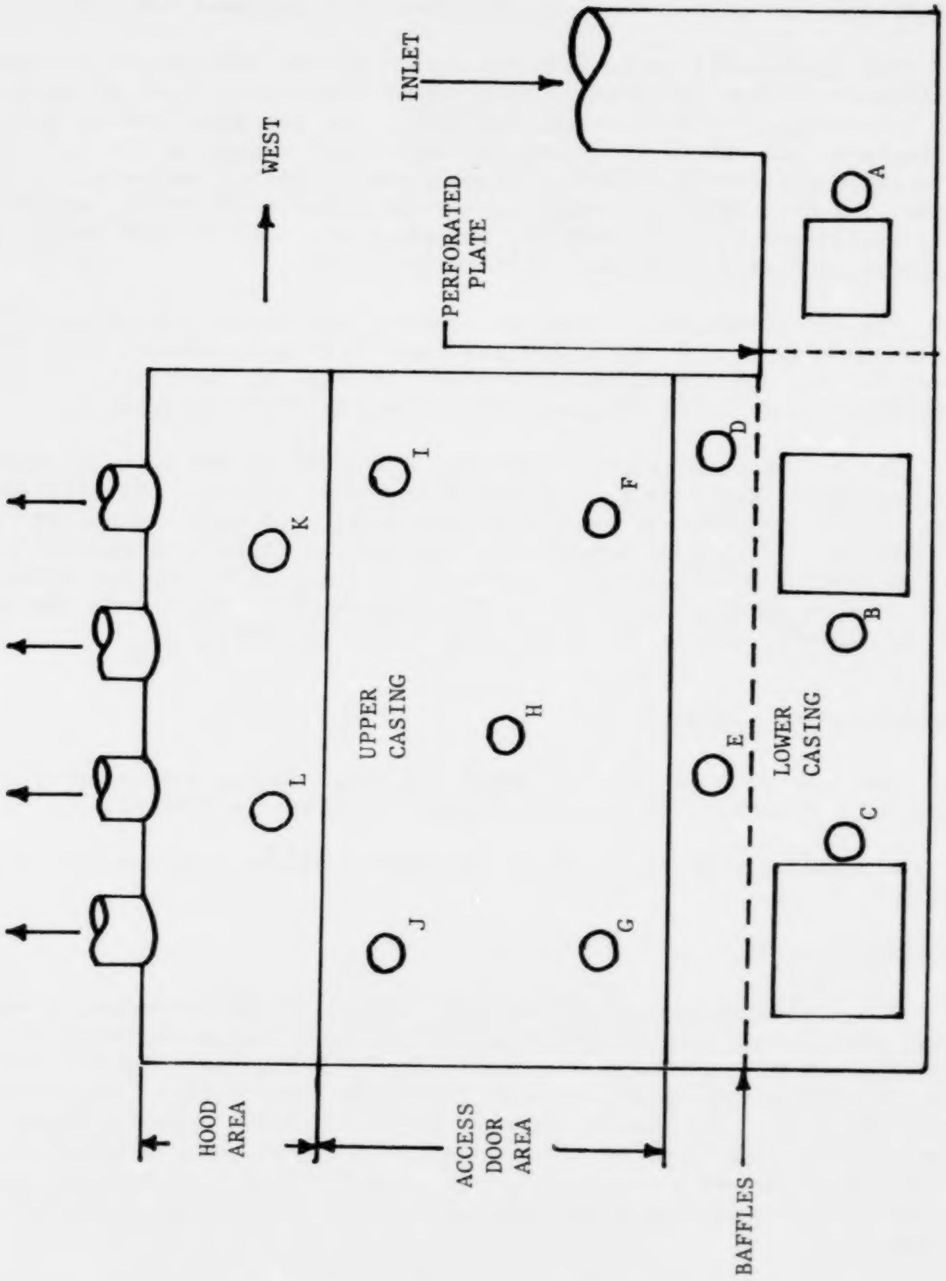
OUTLETS
WEST
INLET
PERFORATED PLATE
UPPER CASING
LOWER CASING
HOOD AREA
ACCESS DOOR AREA
BAFFLES
A
B
C
D
E
F
G
H
I
J
K
L

Figure 3. Location of corrosion test samples, coatings, and probe ports.

Two titanium alloys which possess outstanding crevice corrosion resistance, Ti-0.2 Pd and Ti Code 12, were also included in the test. Chemical lead, widely used in sulfuric acid applications, was included for test.

The non-metallic materials selected for test were chosen for their resistance to chemical attack, temperature resistance, ease of application and fabrication, as well as availability. The thermoset resins were the polyesters, and epoxy, vinyl esters, and furans either in the form of fiberglass reinforced structural composites or filled and unfilled coatings. The thermoplastic resins were polyvinylchloride (PVC), alkyds, polyvinyllidene fluoride (KYNAR), polyphenylene sulfide, and Teflon as coatings, shrink tubing, and a reinforced liner.

The elastomers were neoprene, Hypalon, and Viton as coatings, liners, seals and shims. The substrates for the liners and coatings were mild steel and 304 and 316 stainless steels. A complete tabulation of the materials and coatings selected for testing is shown in Table 1.

Two inch square coupons were made from most of the test materials. Some of these were coated using the appropriate methods. In addition, some of the non-metallic materials were fabricated into coupons by the suppliers. All coupons were coded, weighed and visually inspected prior to testing. The coupons were installed in the unit by hanging using 316 CRES wire or Teflon coated wire. The coupons were situated in the west end of the hood and in the lower area under the baffles.

INSPECTION AND ANALYSIS

The test coupons from the upper and lower casing were removed and analyzed. A summary of the observations is given in Table 2.

A detailed discussion of the appearance of the test coupons is given below.

Stainless Steels

The corrosion resistant stainless steels (CRES) subjected to the lower casing environment exhibited pitting and crevice corrosion attack. 304 CRES was more severely attacked than 316 CRES, see Figures 4 and 5. The 304 CRES specimens showed attack ranging from small multiple pits to cracking of the specimen in the most heavily pitted regions, Figure 4. Some 316 CRES specimens were only lightly attacked, or not attacked at all, while others showed extensive pitting over the entire coupon surface, Figure 5. Crevice attack was normally present around the attachment bolt holes.

The CRES sample in the upper casing showed similar behavior with the 304 CRES pitting over most of the exposed surface and the 316 CRES showing some pitting and crevice attach near the attachment holes.

Table 1. TABULATION OF MATERIALS AND COATINGS SELECTED FOR TESTING

A) Metals and Alloys

Designation	Composition	Supplier
1010 Mild Steel	Fe - .01C - 0.45 Mn	--------
304 CRES	Fe - 18 Cr - 8 Ni - 1.5 Mn	--------
316 CRES	Fe - 18 Cr - 8 Ni - 3 Mo - 1.5 Mn	--------
Ti 50 A	C. P. Ti	Timet
Ti - Code 12	Ti - 0.3 Mo - 0.8 Ni	Timet
Ti - 0.2 Pd	Ti - 0.2 Pd	Timet
Hastelloy C	Ni - 15.5 Cr - 16 Mo - 5 Fe - 2.5 Co	Huntington Alloys
Hastelloy C276	Ni - 15.5 Cr - 16 Mo - 5.5 Fe - 3.7 W - 2.5 Co	Huntington Alloys
Hastelloy B	Ni - 28 Mo - 2.5 Co - 1.0 Cr - 5 Fe	Huntington Alloys
Incoloy 825	Ni - 30 Fe - 21.5 Cr - 3 Mo - .9 Ti	Huntington Alloys
Inconel 601	Ni - 23 Cr - 14 Fe - 1.35 Al - 0.5 Mn - 0.5 Cu	Huntington Alloys
Inconel 617	Ni - 22 Cr - 12.5 Co - 9.0 Mo - 1.0 Al - .07 C	Huntington Alloys
Nickel	Ni (pure)	Huntington Alloys
Chemical Lead	Pb - 0.05 Cu - 0.005 Ag	--------

B) Non-Metallic Structural Panels

Atlac 382/Flex Bend 4010A	Bisphenol Polyester FRP	ICI United States
Atlac 711-05A	Fire Resist. Polyester FRP	ICI United States
Atlac 382-05A	Bisphenol Polyester FRP	ICI United States
Atlac 580-05A	Bisphenol Vinylester FRP	ICI United States
Polylite 33-402	Polyester FRP	Reichhold Chemical
Corralite 31-345	Polyester FRP	Reichhold Chemical
7241-6	IPA Polyester FRP	Ashland

Table 1. TABULATION OF MATERIALS AND COATINGS SELECTED FOR TESTING (Continued)

B) Non-Metallic Structural Panels

Designation	Composition	Supplier
72L + 5b-1	Fire Retarded Polyester FRP	Ashland
7240-4	IPA Polyester FRP	Ashland
197/3 + AT-8	Polyester FRP	Ashland
800/801L-68	Furan FRP	Ashland
197/3-400	Polyester FRP	Ashland
800 FR-10	Flame Retarded Furan FRP	Ashland
Neoprene Elastomer	Polychloroprene	Gacoflex Western
Viton Elastomer	Fluorocarbon	Dupont
Shrink Tubing - PVC	Polyvinylchloride	--------
6793 Hystl	Polybutadiene	TRW

C) Non-Metallic Coatings

Designation	Composition	Supplier
850-321/855-255	Polytetrafluoroethylene	Dupont
EA 919	Bisphenol-polyamine cured epoxy	Hysol
Ryton	Polyphenylene sulfide	Phillips
Compound W	Vinyl Plastisol	TRW
960/659	Alkyd Resin	Rust-Oleum Corp.
Ceilcote 252	Glass Flake Filled Polyester	Ceilcote
Kynar	Polyvinylidene Fluoride	Pennwalt
N11R/N29 Neoprene	Polychloroprene	Gacoflex Western
Hypalon Elastomer	Polychlorosufonated Rubber	Gacoflex Western
4020	Filled Vinylester	Plasites
4030	Filled Vinylester	Plasites
4092	Filled Vinylester	Plasites

Table 2. SUMMARY OF MATERIALS PERFORMANCE - MIDTERM INSPECTION - CDS

LOWER CASING - GAS STREAM

Material	Excellent	Good	Fair	Poor
Metals	Titanium C/P Ti - .2 Pd Ti - Code 12 Hastelloy C-4 Incoloy 825	Chemical Lead Inconel 617	316 CRES (P) Hastelloy B	304 CRES (P) Nickel (P) Inconel (I) 601
Coatings				Teflon (A) Kynar (A) Polyphenylene Sulfide (A) Epoxy (A) (T) Vinyl (A) (T) Alkyd (A) (T) Hypalon (A) (T) Neoprene (A) (T)
Liner			Neoprene (T)	
Reinforced and Filled Coatings				Ceilcote 252 (T)(C) Plasites: 4020 (T) (C) (A) 4030 (T) (C) 4092 (T) (C)

Table 2. SUMMARY OF MATERIALS PERFORMANCE - MIDTERM INSPECTION - CDS (Continued)

Material	Excellent	Good	Fair	Poor
Fiberglass Reinforced Plastic	Hystl 6793-132		Ashland 197/3 (T)(C) Ashland 800 (T)(C)	Ashland 7240 (T)(C) Ashland 72 (T)(C) Atlac 382 (T)(C) Atlac 711 (T)(C) Atlac 580 (T)(C) Corralite 31-345 (T)(C)
LOWER CASING - WALLS				
Coatings				Hypalon (A) Neoprene (A)
Baffle Shims	Viton			
UPPER CASING - DOORS				
Coatings			Epoxy (A)	Alkyd (A) Vinyl (A)
Liner	Armalon Teflon/Glass Fabric			
Seals	Viton			

Table 2. SUMMARY OF MATERIALS PERFORMANCE - MIDTERM INSPECTION - CDS (Continued)

Material	Excellent	Good	Fair	Poor
ELECTRODE HEADERS				
Coatings			Epoxy (A)	Vinyl (A) Alkyd (A)
Sleeving	Vinyl Shrink Tubing			
Seals	Viton "O" Rings			
UPPER CASING (HOOD)				
Seal (Upper Casing Hood)	Neoprene			
Coatings				Hypalon (A) Neoprene (A) Vinyl (A) Alkyd (A)(T)
UPPER CASING - GAS STREAM				
Metals	Ti (C.P) Ti-0.2 Pd	Incoloy 825	Inconel 617 316 CRES	304 CRES (P) Nickel (P) Inconel 601 (I) Ti - Code 12 Hastelloy C

Table 2. SUMMARY OF MATERIALS PERFORMANCE - MIDTERM INSPECTION - CDS (Continued)

Material	Excellent	Good	Fair	Poor
Coatings				Teflon (A) Polyphenylene Sulfide (A) Epoxy (A)(T) Vinyl (A)(T) Alkyd (A)(T)

Key: (P) Pitting corrosion attack
(I) Intergranular corrosion attack
(A) Adhesion failure
(T) Temperature induced attack
(C) Chemical attack

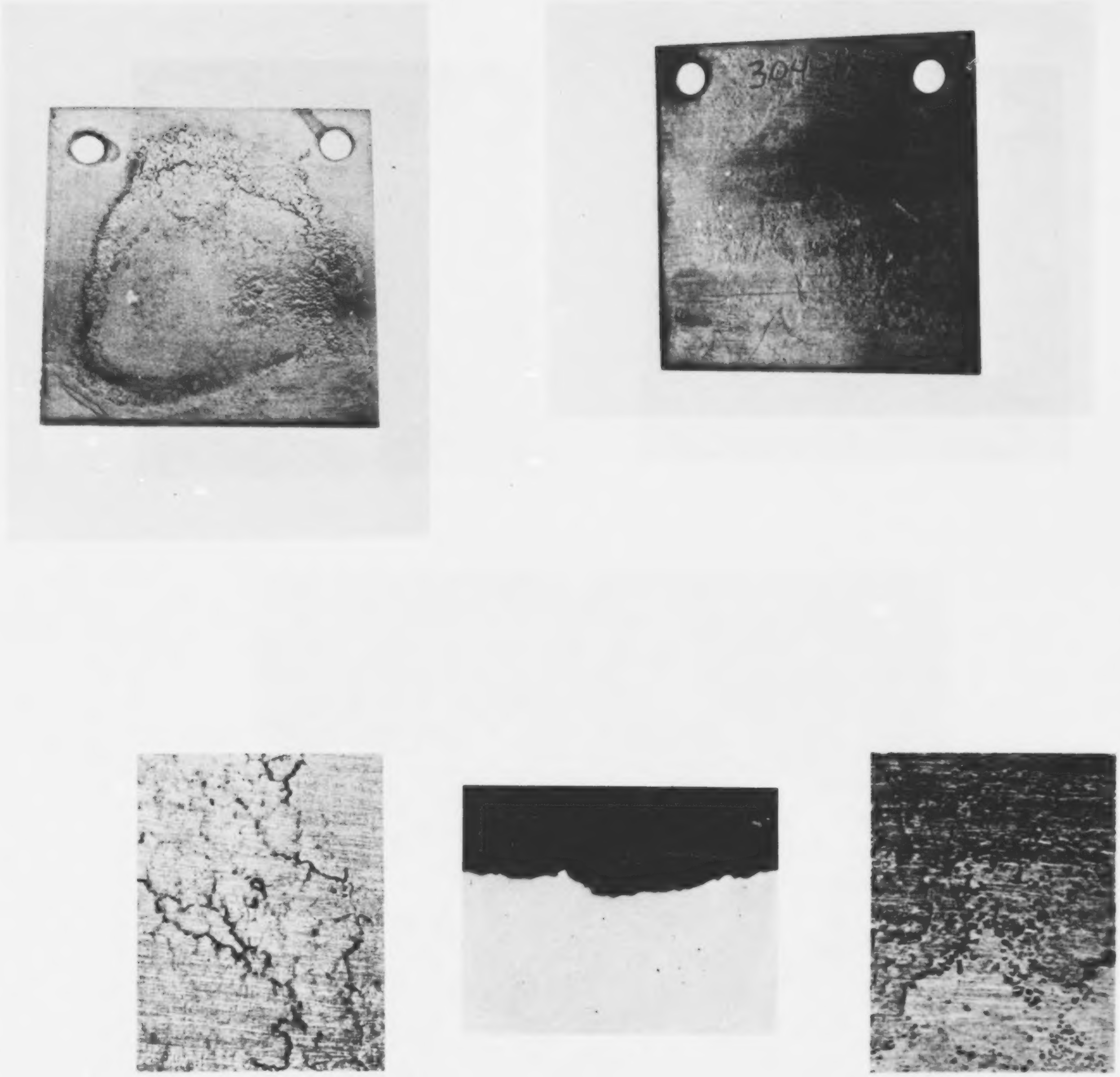

Figure 4. Coupon 304-17 (left) and 304-18 (right). Severe pitting attack with 304-17 showing cracks in heavily pitted regions. Micrograph showing section through pitted area. Lower casing.

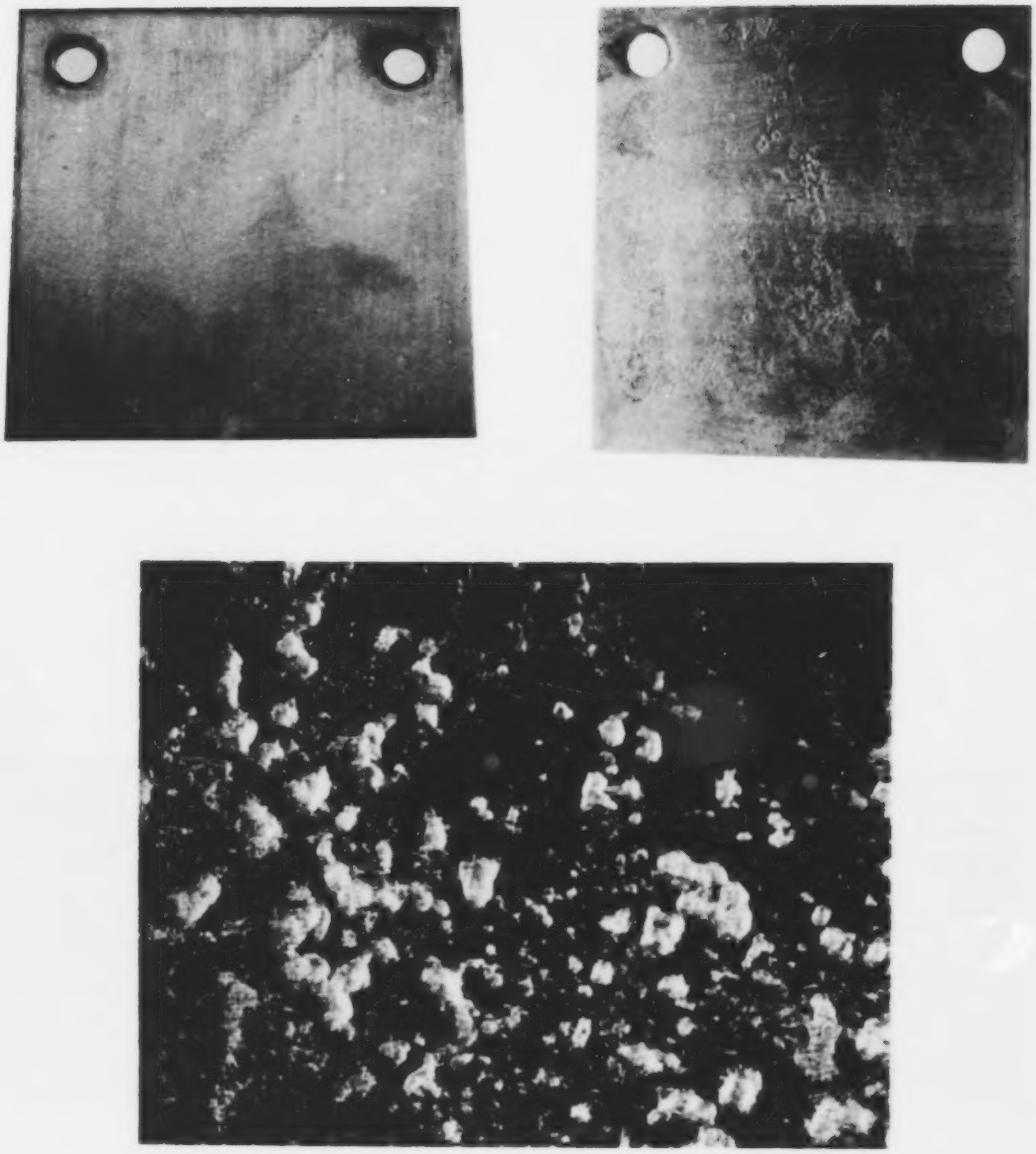

Figure 5. Coupons 316-23 (left) showing mild attack and 316-16 (right) which has extensive pitting attack. Lower casing.

Nickel Alloys

Pure nickel samples were severely attacked by the CDS environment. Extremely heavy pitting and crevice corrosion was noted on all lower casing specimens, Figure 6. The Inconel 601 specimens also showed severe attack. Intergranular corrosion caused grains to spall off the surface which resulted in multiple pits, Figure 7. The bolt attachment areas were attacked by crevice corrosion. The nickel alloys containing high amounts of molybdenum, Inconel 617, Incoloy 825, Hastelloy C-4 and Hastelloy B, were not attacked, although some discolorization was noted on the Hastelloy B coupon, Figure 8.

The nickel and Inconel 601 specimens exposed to the upper casing environment were pitted over their surfaces as shown in Figure 9. In contrast to their performance in the lower casing, Incoloy 825 and Inconel 617 all showed evidence of pitting attack in the upper casing, see Figure 10. The Hastelloy C sample was badly pitted even though it showed excellent resistance to attack in the lower casing, see Figure 11.

Titanium Alloys

The commercially pure titanium coupons and the Ti-0.2 Pd and Ti-Code 12 coupons all showed good resistance to attack in the lower casing. Some slight surface etching was noted, Figure 12. Otherwise, the surfaces appeared normal except for some staining which was removable with a non-metallic brush and detergent. The Ti and Ti-0.2 Pd coupons in the upper casing also exhibited excellent resistance to attack, Figure 13. However, the Ti-Code 12 coupon was pitted after exposure to the upper casing environment.

Lead

The chemical lead specimens were discolored due to the formation of a surface film but had not sustained pitting or crevice attack. The film was adherent and very difficult to remove by brushing and washing. All specimens were mounted in the lower casing.

Non-Metallic Coatings

All of the coatings tested showed some degradation, either of the coating itself or of the coating/substrate bond. The EA919 epoxy (E), vinyl plastisol (W) and alkyd (RO) all failed by coating attack, blistering and peeling, see Figure 14. In some cases the coating disappeared from the surface of the coupons during exposure to the CDS environment. The polyphenylene sulfide (PS), FEP Teflon (T), and polyvinylidene fluoride (K) coatings failed by adhesion as evidenced by

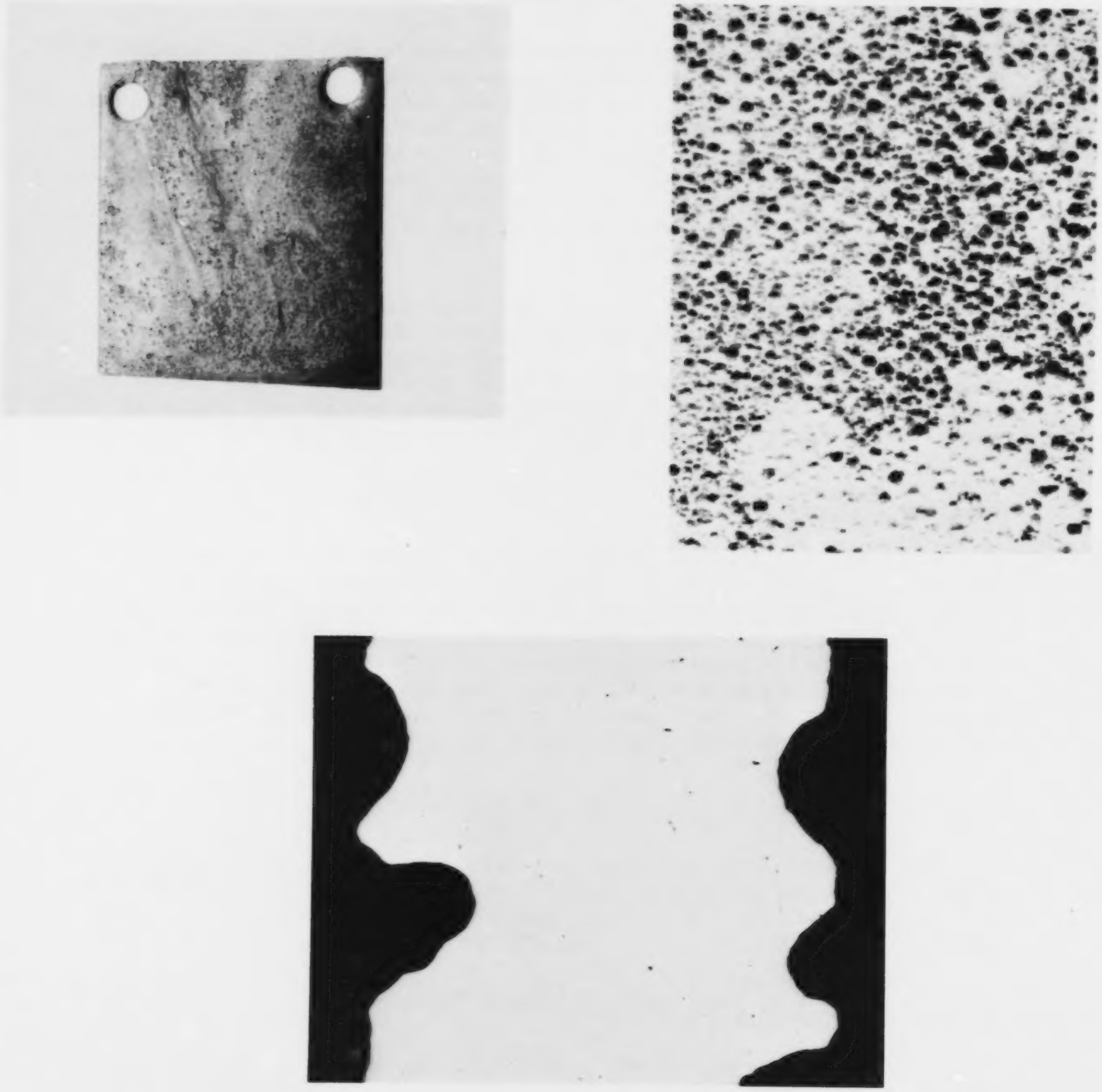

Figure 6. Coupon Ni-1. Severe pitting attack has occurred over entire surface. Lower casing.

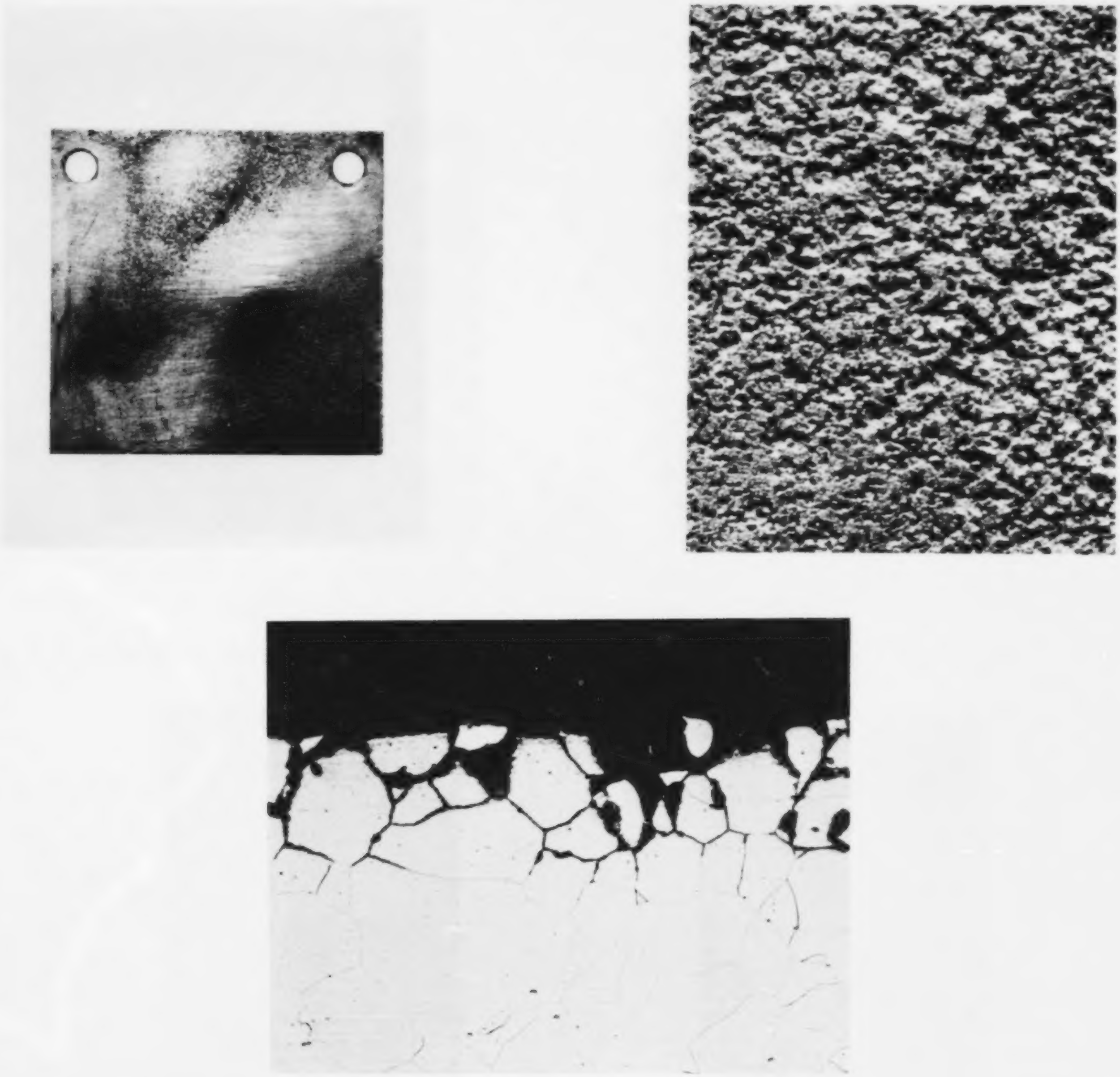

Figure 7. Coupon I601-2. Extremely severe intergranular attack with spalling of surface grains. Lower casing.

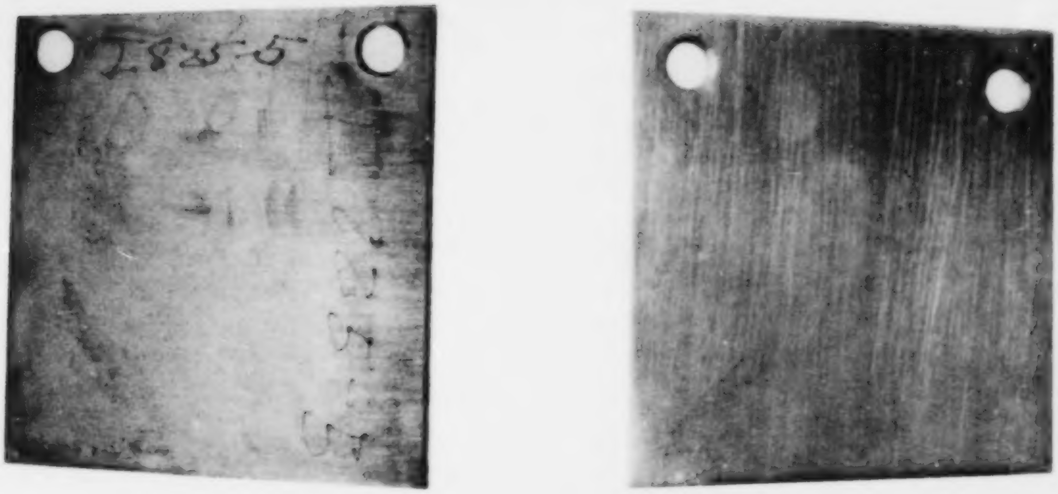

Figure 8. Coupons I825-2 (left) and I825-5 (right). No indications of corrosive attack. Lower casing.

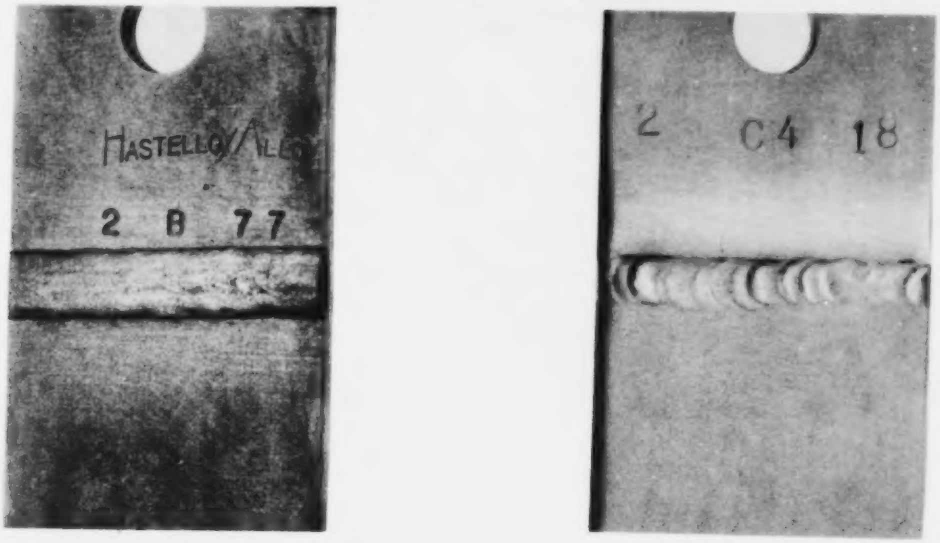
HASTELLOY/ALL
2 B 77
2 C4 18

Figure 8. Coupons Hast. B-1 (left) and Hast C-1 (right). Some discoloration of the Hastelloy B specimen. Hastelloy C-4 not attacked. Lower casing.

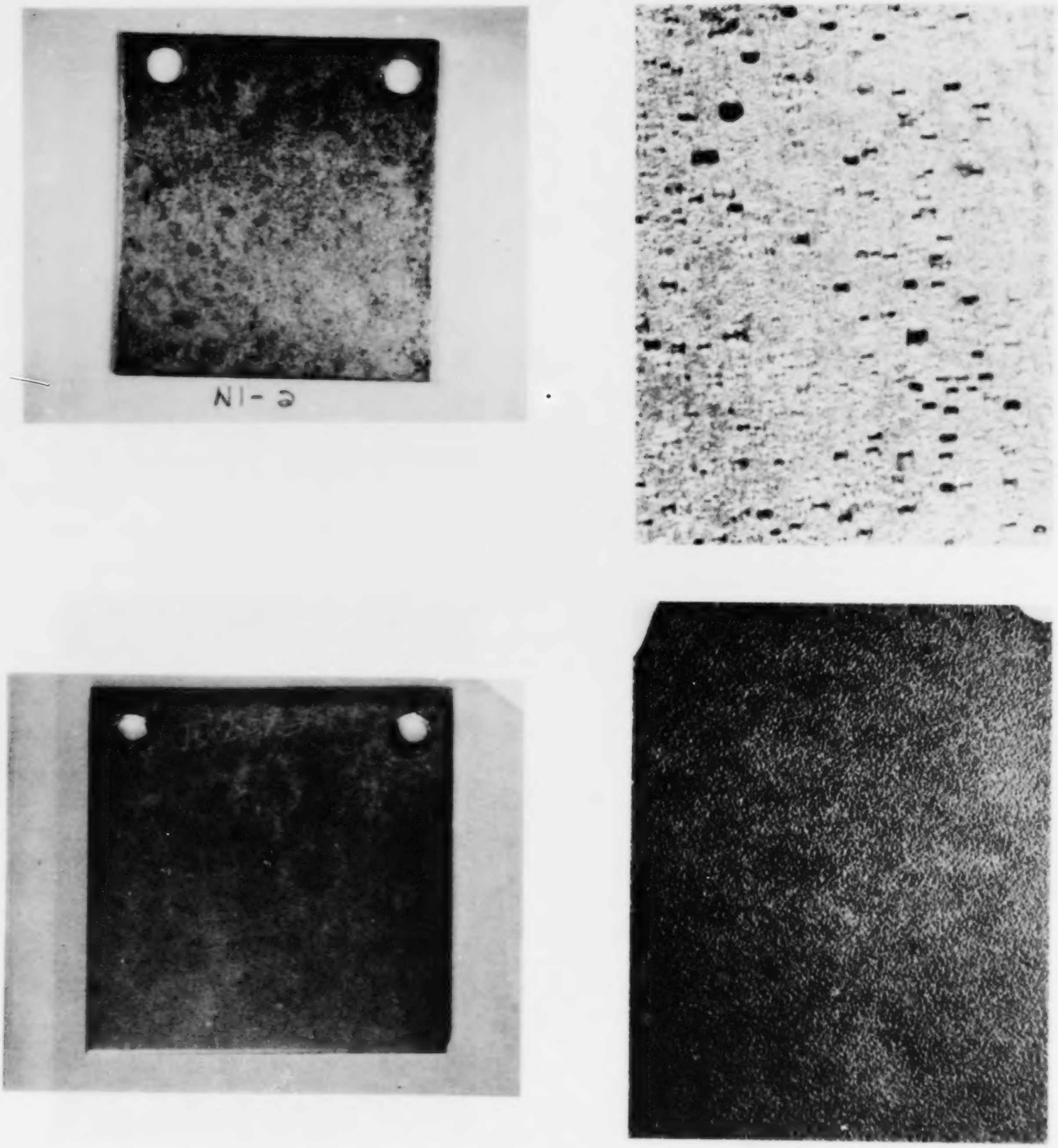

Figure 9. Coupon Ni-2. Severe pitting attack. Upper Casing. Upper photos.
Coupon I601-3. Pitting attack on surface. Upper Casing.
Lower photos.

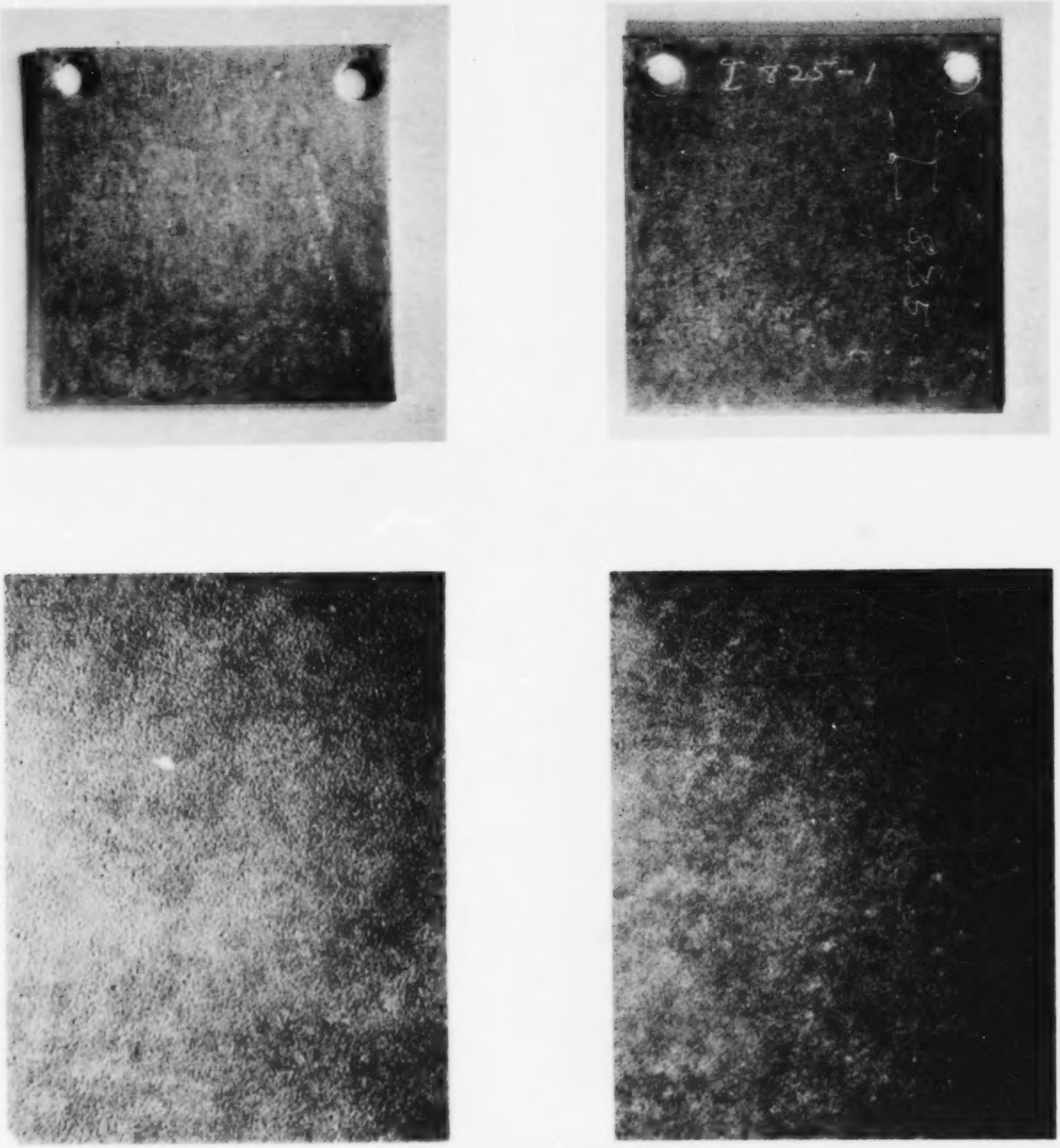

Figure 10. Coupons I617-2 (left) and I825-1 (right). Surface roughened (incipient pitting). Upper casing.

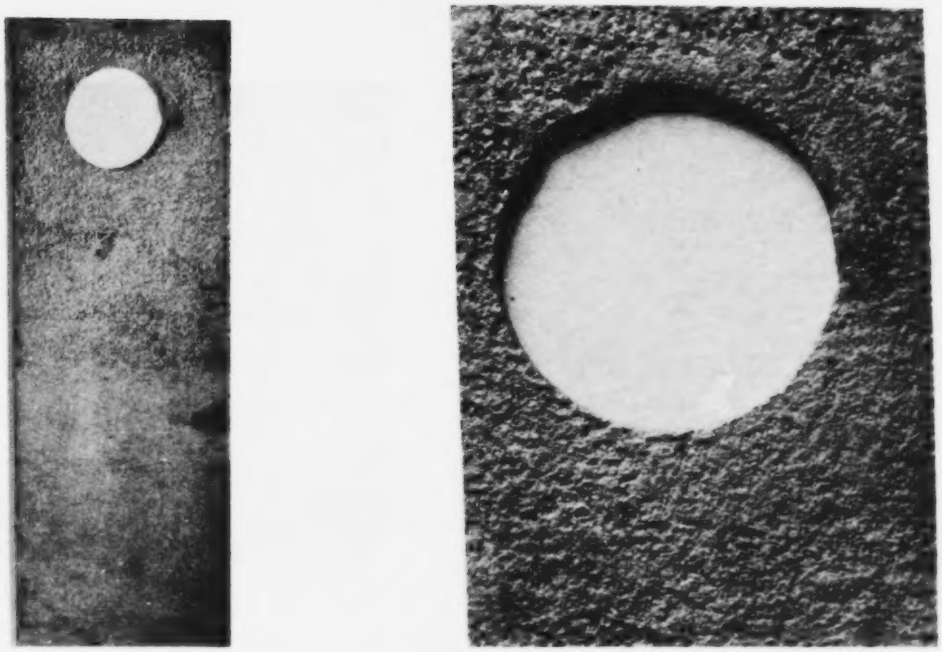

Figure 11. Hastelloy C coupon. Severe pitting attack. Upper casing.

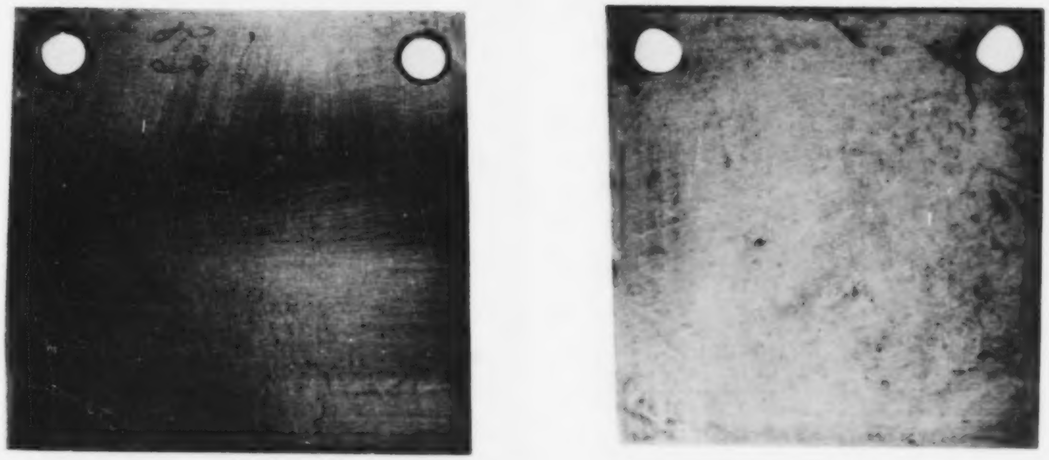

Figure 12. Coupons Ti-1 (left) and TiPd-1 (right). Some surface etching of titanium specimen. Lower casing.

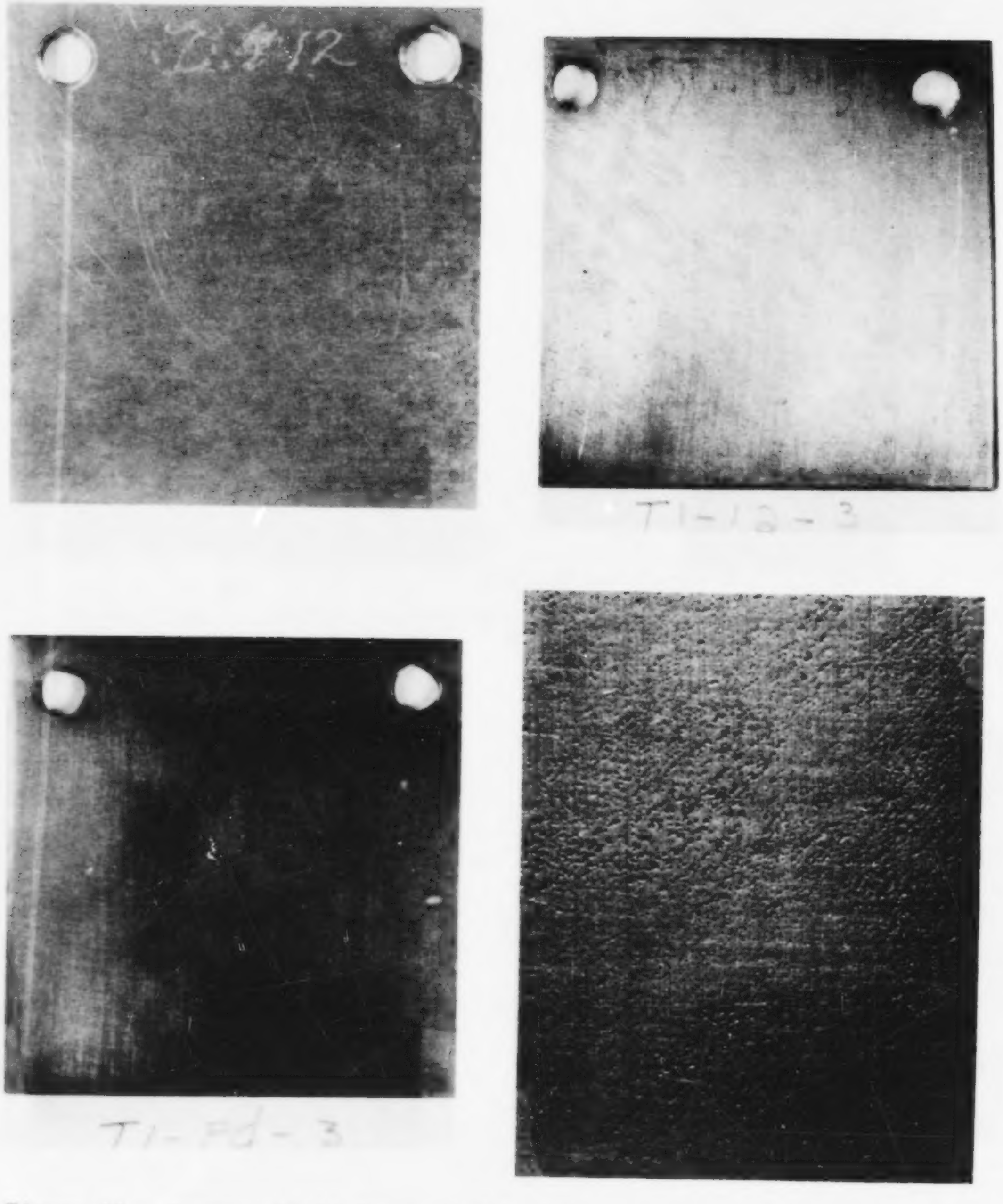
Ti 12
TI-12-3
TI-Pd-3

Figure 13. Coupons Ti-12 (upper left), TiPd-3 (lower left) and Ti-12-3 (upper and lower right). The Ti-12-3 coupon has pitted. Upper casing.

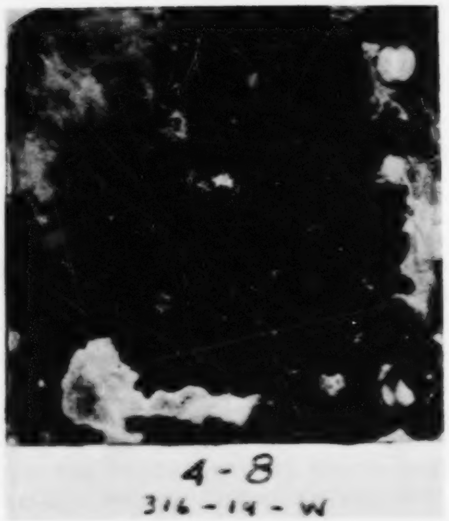

Figure 14. Vinyl plastisol coated 316 S/S coupon from lower casing showing typical failure mode for epoxy, alkyd and vinyl coatings.

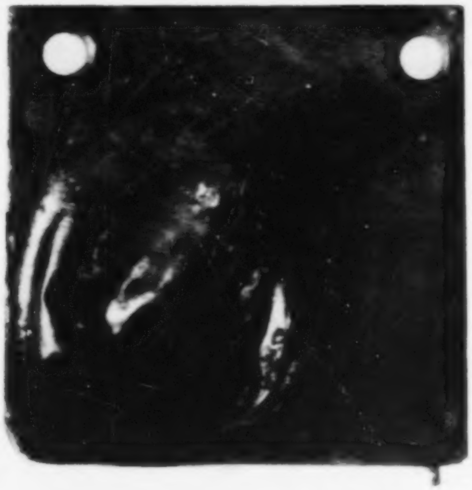

Figure 15. Polyphenylene sulfide coated 316 S/S coupon from lower casing showing typical failure mode for FEP Teflon, polyphenylene sulfide, and polyvinylidene fluoride coatings.

blistering and peeling of the coating from the substrate, Figure 15. However, the coating materials themselves appeared to be unaffected by exposure. Both the polychloroprene (N) and polysulfonated rubber (H) coatings were attacked and cracking was noted, Figure 16.

The glass flake filled polyester (Ceilcote) and filled vinylester coatings showed surface etching and, in one case, portions of the coating flaked off.

Twelve water spray nozzle couplings in the upper casing were coated with epoxy, alkyd, vinyl, and polyphenylene sulfide (3 each) and exposed to the normal operation environment. The epoxy, vinyl, and alkyd coatings failed while the polyphenylene sulfide coating was still intact when the test was terminated (the PS coating was damaged during the coupling removal operation).

Coatings were applied to lower casing walls (Hypalon and neoprene elastomers), upper casing doors (epoxy, alkyd and vinyl), the electrode headers (epoxy, vinyl and alkyd) and the upper casing walls (Hypalon, neoprene, vinyl and alkyd). Only the epoxy coatings on the upper casing doors and electrode headers did not fail, although they discolored and exhibited some blistering. All of the other coatings failed, usually in the bond. It should be noted that substrate preparation was not possible and the coatings were applied in the field after solvent cleaning with acetone. Therefore, good adhesion would not be expected.

The bonded polychloroprene (neoprene) (NB) liner material showed surface checking, and cracking, Figure 17. The elastomer hardened from a shore A of 70 to 90 indicating chemical attack.

An Armalon (Teflon/glass fabric) liner applied to an upper casing door showed excellent resistance to attack.

Non-Metallic Structural Panels

Fiber reinforced polyesters, vinylesters, furans, and polybutadiene were tested in panel form in the lower casing. In addition, polyvinylchloride (PVC) was tested as shrink tubing and polyhexafluoropropylene (Viton) as gasketing material.

The polyesters showed various degrees of degradation ranging from surface etching to delamination as shown in Figures 18 through 20. The vinylester panel showed some surface etching and edge attack, Figure 21. The furans also showed surface etching and edge attack, Figure 22. The polybutadiene panel discolored and showed some minor pitting near the edge, Figure 23.

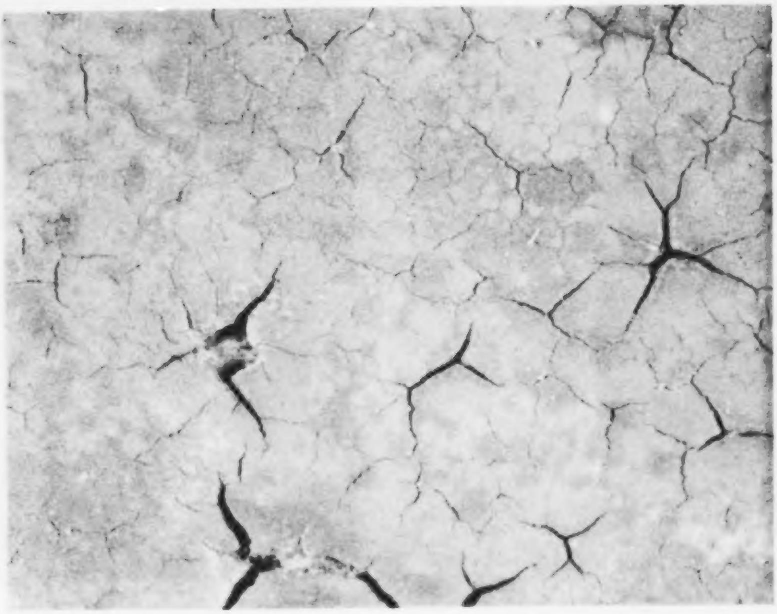

Figure 16. Chlorosulfonated polyethylene rubber coated 316 S/S from lower casing coupon showing typical cracking and surface etching of this and neoprene rubber coatings.

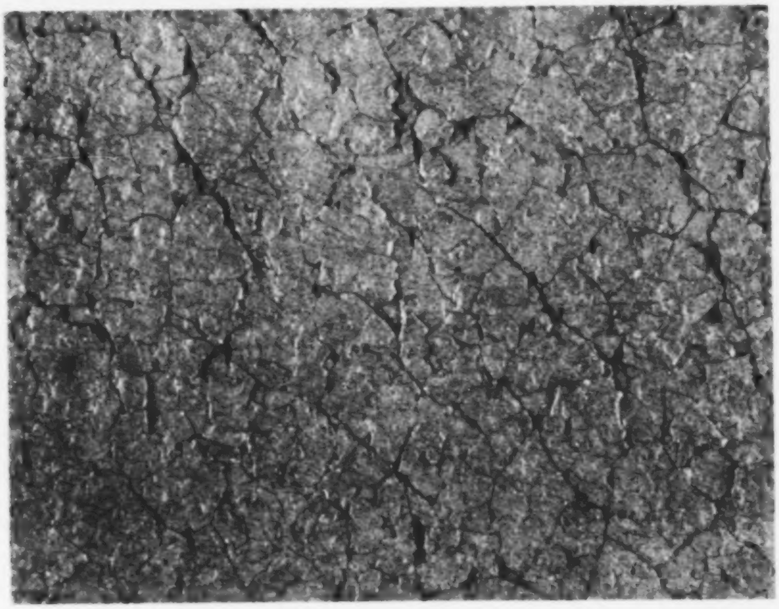

Figure 17. Neoprene elastomer liner showing surface cracking. Lower casing.

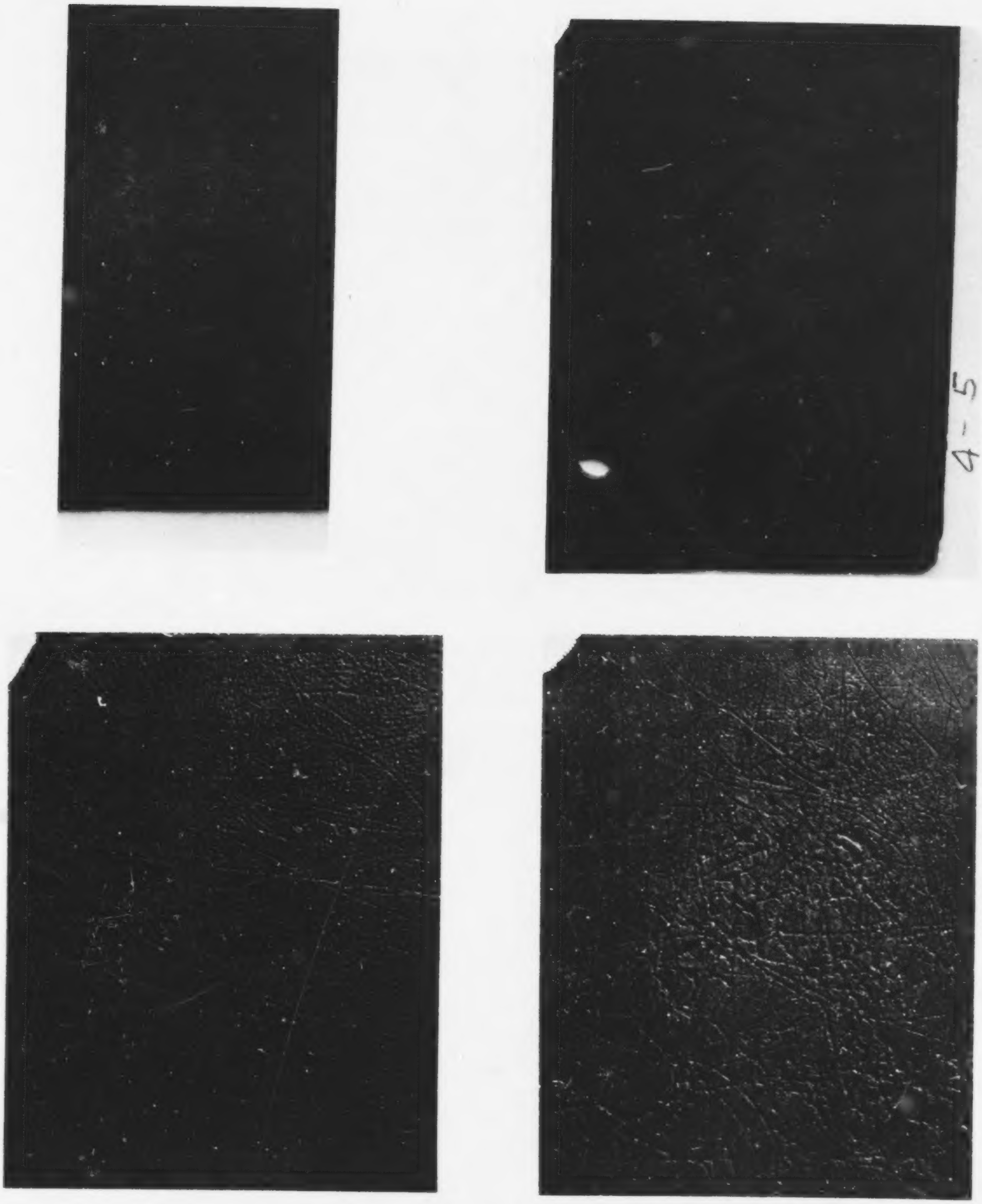

Figure 18. Coupons AT382-1 (left) and AT382/05 (right) bisphenol polyesters. Surface checking and cracking. Lower casing.

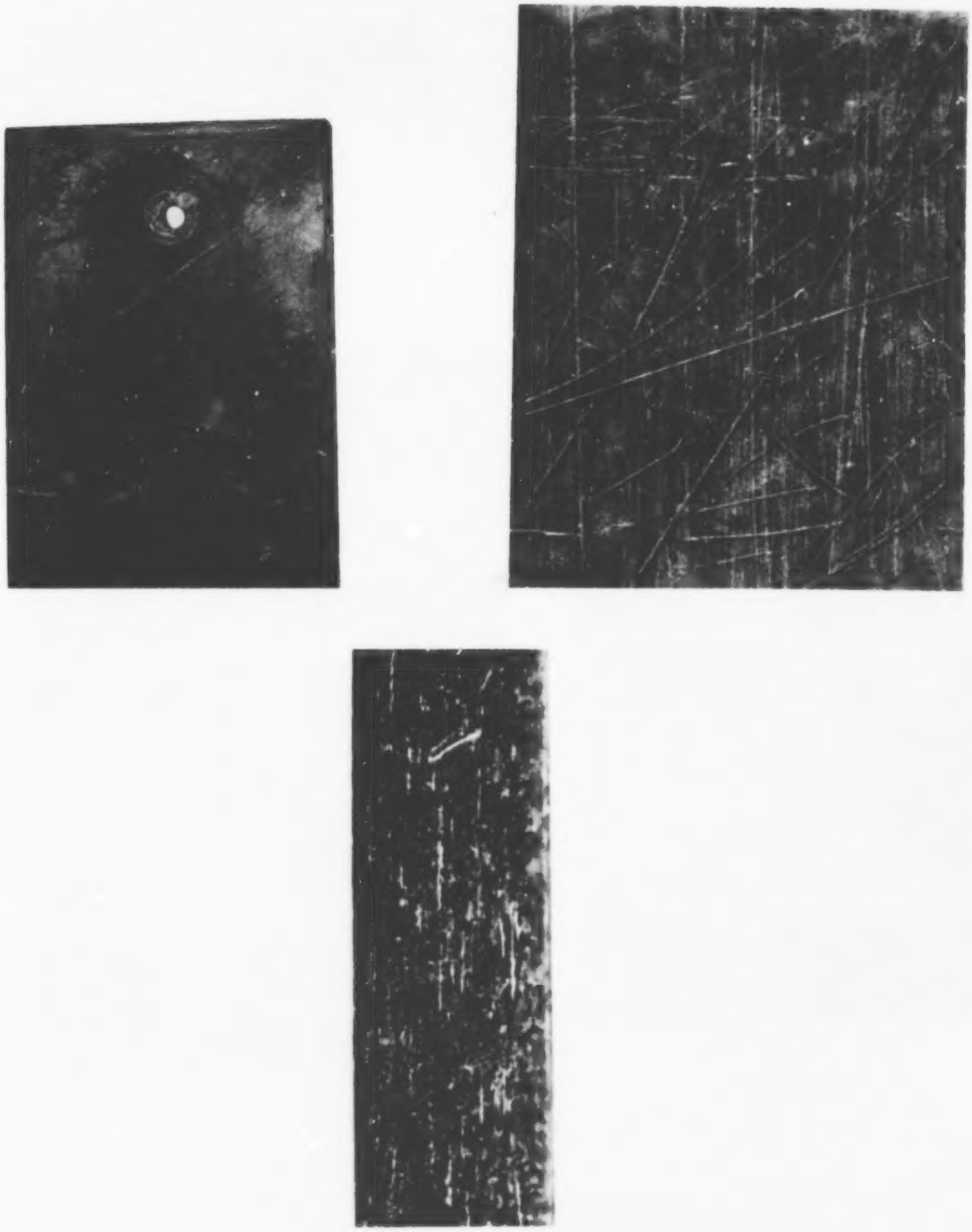

Figure 19. Coupon ASH 7241-29 IPA polyester. Surface etching, cracking and pitting. Lower casing.

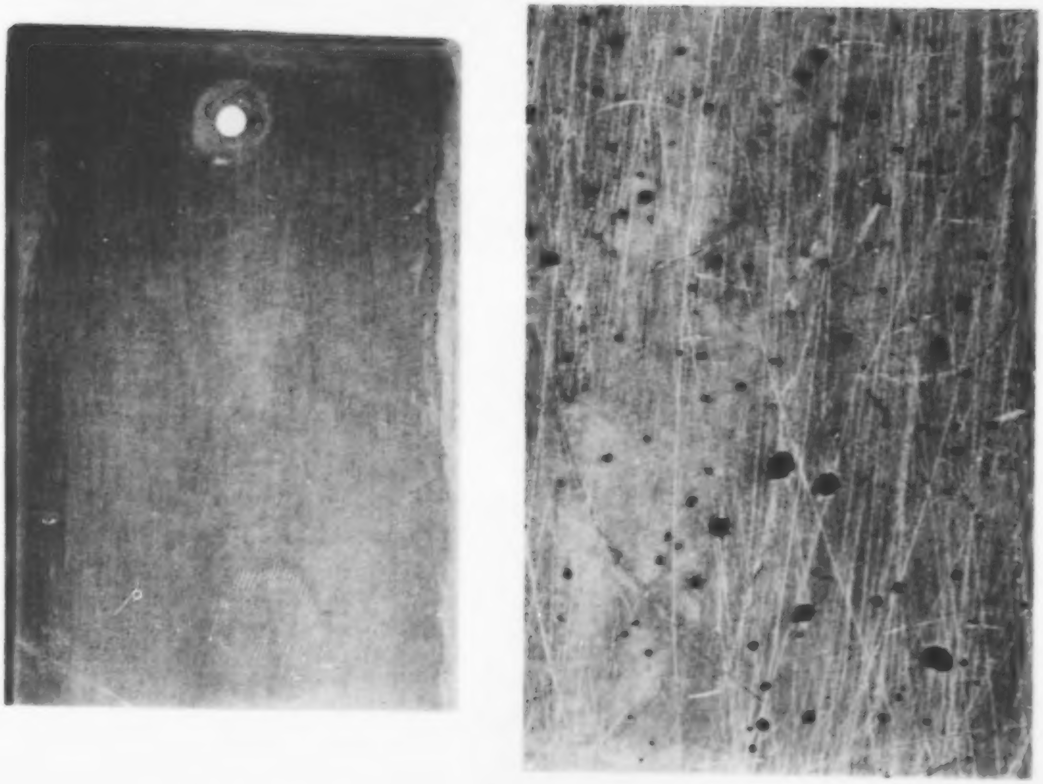

Figure 20. Coupon ASH 197/3 polyester. Surface etching, pitting and crazing. Lower casing.

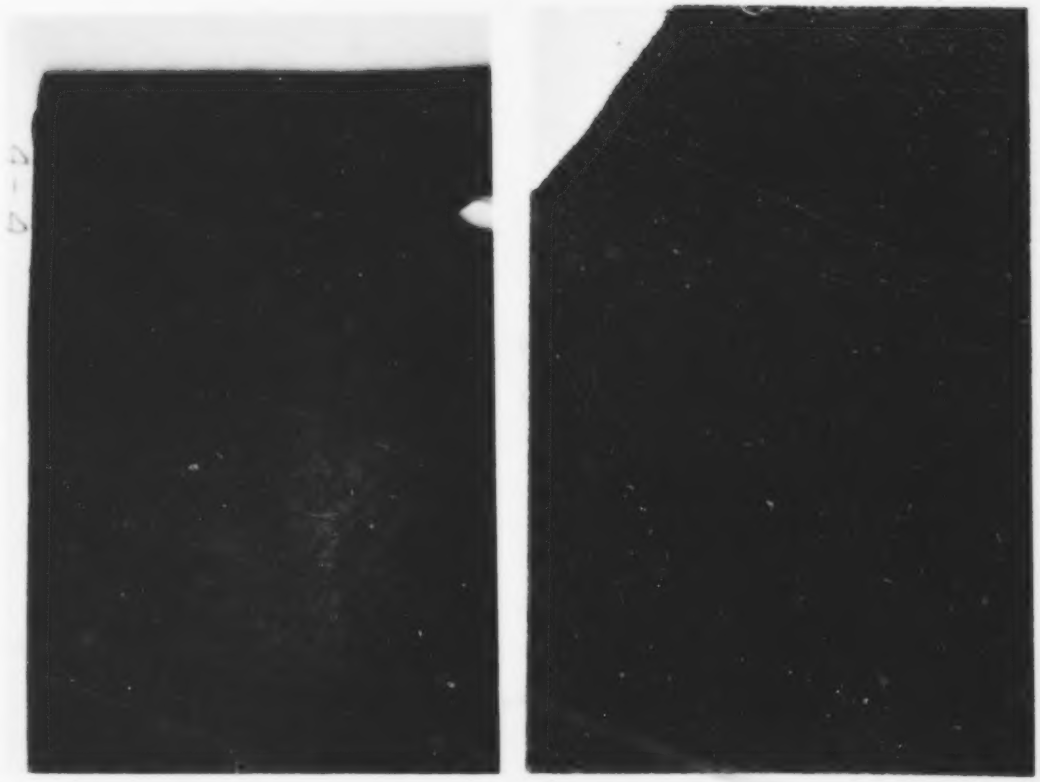

Figure 21. Coupon AT580-1 bisphenol vinylester. Surface cracked and etched. Lower casing.

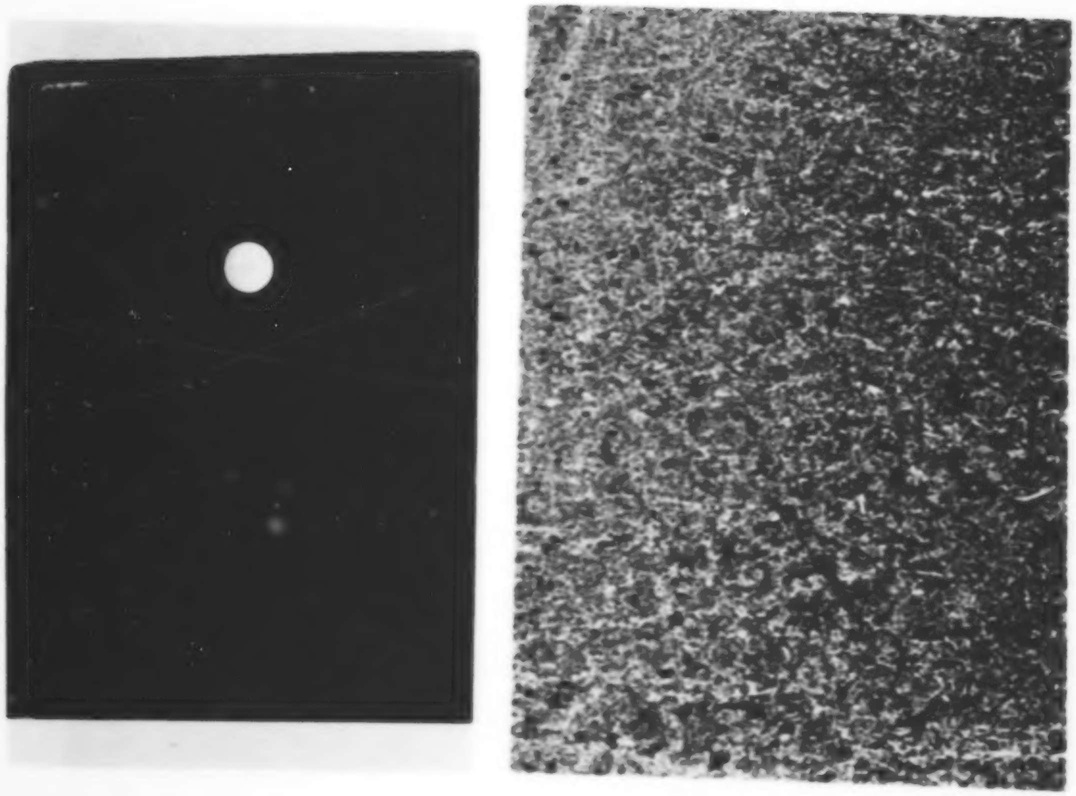

Figure 22. Coupon ASH800-28 furan showing surface cracking, checking and pitting. Lower casing.

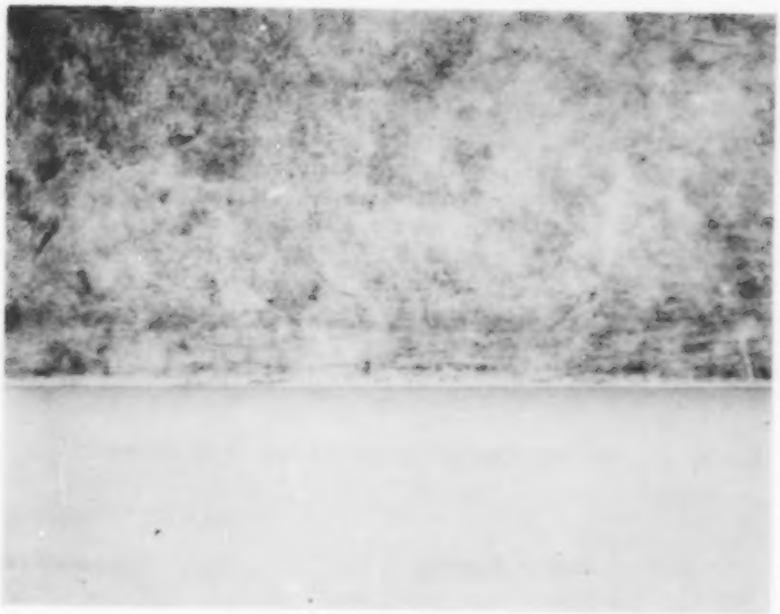

Figure 23. Coupon HY132 polybutadiene. Some pitting attack at edge. Lower casing.

The PVC shrink tubing was installed over water spray couplings and electrode couplings and showed no visible signs of degradation. The temperature of the shrink tubing was low due to water flow. Some signs of crevice corrosion of the stainless steel was noted under some of the shrink tubing liners.

The Viton seals showed no degradation due to exposure to the CDS operating conditions.

Weight Change Measurements

The metallic specimens were weighed before and after exposure to determine weight change. These data are shown in Table 3. In this Table, uniform corrosion rates are shown which were calculated from the weight change data. Note that the nickel and Inconel 601 samples pitted badly so that the uniform corrosion value given for these metals should not be used except for a qualitative comparison. The uniform corrosion rate for 316 CRES was determined from specimens which showed little or no pitting attack. The best resistance to attack was exhibited by titanium, Inconel 617 and Incoloy 825. The data were collected after an exposure of only about 470 hours of operation and certainly cannot be extrapolated with any assurance to very long periods of operation. However, the results can act as a screening test and rough comparisons can be made between the alloys tested.

Table 3. WEIGHT CHANGE OF METALLIC TEST COUPONS

	Lower Casing			Upper Casing		
Material Tested	No. of Coupons	Ave. Wt. Loss (g)	Uniform(1) Corrosion Rate (mpy)	No. of Coupons	Ave. Wt. Loss (g)	Uniform(1) Corrosion Rate (mpy)
316 CRES	5	.2950	5.3	2	.5361	9.5
Nickel	3 (P)	12.1532	228 (P)	1 (P)	9.0497	145 (P)
Inconel 601	2	1.1154	19.7 (P)	1 (P)	.9463	7.9 (P)
Inconel 617	2	.3828	6.5	1	.7537	12.9
Incoloy 825	2	.1798	3.1	1	.5064	8.9
Hastelloy B	1	3.397	46.7	-	-	-
Hastelloy C-4	1	.1807	2.4	1 (P)	1.6599	55.4 (P)
C.P. Titanium	2	.0794	2.5	1	.2329	7.4
Chemical Lead	2	.3311	9.6	-	-	-

(1) 467 hours of operation.

(P) Pitting attack - uniform corrosion rates should be used for qualitative comparison only.

Electronic Corrosion Meter Data

Five electronic corrosion probes (Magna Corporation 21434/W40/8020 with 316 CRES elements) were installed on the north side of the north CDS unit. The data taken after 467 hours of operation are shown below in Table 4.

Table 4. CORROSOMETER DATA

Probe No.	Location	Uniform Corrosion Rate (mpy)
1	A - CDS Inlet Duct	.47
2	C - Lower Casing - East End	3.67
3	D - Lower Casing - West End, Above Baffles	12.17
4	L - Upper Casing - East End	1.63
6	K - Upper Casing - West End	1.50

THERMAL/CHEMICAL ENVIRONMENT

Inlet gas temperature for the north unit was recorded at the same time that Corrosometer readings were taken. The temperature probe located near port A indicated that the inlet gas temperature ranged from 348°F to 375°F. In order to assess the wall temperatures of different parts of the unit, a thermal profile was run by inserting probes into the Corrosometer ports in the lower casing and the stage area. In addition, upper casing wall temperatures were taken at three points on the south side of the unit. The results are shown in Table 5.

Carbonaceous deposits were found on walls, doors, internal structures, baffles and test coupons. An analysis of the deposit indicates up to 1.7 weight percent chloride is present. When water was added to the deposit, the resulting solution exhibited a pH of between 1 and 2.

The coke gas stream contains C, SO_2, H_2S, O_2, NOs, CH_3, H_2, HCN, S, CO, CO_2, N_2 and possibly other hydrocarbons. Water reacted in the gas stream to form sulfuric acid and, to a lesser extent, carbonic acid, nitric acid and other corrosive fluids.

Wastewater and domestic feed water samples were analyzed to establish the chemistry before and during CDS operation. The key changes included:

a) The chloride content dropped from 60 ppm (domestic water) to about 25 ppm (wastewater).

b) The sulfate content increased from approximately 10 ppm to 220 to 286 ppm.

c) The pH decreased from 7.96 to 2.43 to 2.53.

d) The specific conductivity at 25°C increased from 290 micromhos/cm to 1200 to 1400 micromhos/cm.

Table 5. WALL TEMPERATURES OF NORTH CDS UNIT

Port	Location	Temperature (°F)
A	Inlet Duct	288
B	Lower Casing-West End (Below Baffles)	277
C	Lower Casing-East End (Below Baffles)	183
D	Lower Casing-Midpoint (Above Baffles)	206
I	Stage Area-West End, (Upper (Door #2)	122
F	Stage Area-West End, (Lower (Door #2)	113
H	Stage Area-Midpoint, (Middle (Door #5)	150
G	Stage area-East End, (Lower (Door #9)	127
—	Upper Casing-West End (Above Door #2)	155
—	Upper Casing-Midpoint (Above Door #4)	174
—	Upper Casing-East End (Above Door #9)	139

DISCUSSION AND CONCLUSIONS

Of the metallic coupons tested, the commercially pure titanium, Ti-0.2 Pd and Incoloy 825 alloys performed best. Hastelloy C-4, Ti - Code 12, and Inconel 617 had very good corrosion resistance when exposed to the lower casing gas stream but were attacked in the upper casing gas stream. The chemical lead samples performed satisfactory in the lower casing and lead lining of the casing appears to be a strong candidate for a long life design. The 316 CRES samples showed fair corrosion resistance in both the upper and lower casing gas streams.

The pitting/crevice behavior of the stainless steels and nickel alloys roughly follows the molybdenum content. Thus, the relative performance in order of increasing corrosion resistance would be predicted to be:

Ni (0% Mo), 304 CRES (0% Mo), Inconel 601 (0% Mo), 316 CRES (3% Mo), Incoloy 825 (3% Mo), Inconel 617 (9% Mo) and Hastelloy C (16% Mo).

This sequence held quite well for the samples tested in the lower casing gas stream except that Incoloy 825 performed better than Inconel 617. However, in the upper casing gas stream, the Hastelloy C coupon was severely attacked with its relative performance falling between that of pure nickel and Inconel 601. No explanation for this behavior has been identified at this time.

In general, the corrosive attack was more severe for metallic coupons exposed to the upper casing gas stream than those in the lower casing. The upper casing coupons were not exposed to the amount of water as were coupons in the lower casing since they were above the electrode headers. Therefore, the coupons were in a moist atmosphere with temperatures in the 150°F to 200°F range, but did not get the cleaning/diluting effect which the lower casing samples experienced. Therefore, the chloride concentration would be expected to be higher on the upper coupons which would tend to promote pitting and crevice corrosion in the stainless steels and nickel alloys. In addition, the moisture clinging to the coupons would tend to collect and concentrate sulfuric acid. That is, as water evaporated the higher boiling point of the sulfuric acid causes the concentration to increase. It is not clear which factors caused the pitting attack of the Ti-Code 12 coupon in the upper casing. This alloy is specifically formulated to retard pitting and crevice attack.

The sulfuric acid concentration on coupons in the lower casing would be expected to be high. However, wetting and washing of the samples did occur even though the baffles partially screened the coupons from the water flow, so that some dilution did occur. In cases where dilution did not occur, sulfuric acid concentrations of the order of 70 percent are possible.

The wall temperatures run cooler than the gas temperatures and, all other parameters being equal, the corrosion rates would be expected to be lower than for the coupons. This was borne out by the corrosion meter measurements in the upper casing and in the lower casing below the baffles for the 316 CRES. The probe located in the lower casing above the baffle showed a higher rate, Table 4, but no coupons were mounted in this region so that a direct comparison could not be made.

None of the coating systems tested were able to survive the CDS environment. The combination of temperature, gas velocity, and chemical environment caused blistering, debonding or cracking. The epoxy EA919 coating gave some degree of protection to the electrode headers (which run cool due to the internal water flow) and the upper casing doors. However, long term survival is unlikely.

The elastomeric liner materials subjected to the gas stream checked or cracked. However, some of the elastomeric materials performed well as gaskets, seals and baffle shims. Viton rubber showed excellent resistance in these configurations and neoprene elastomer performed well as a seal in the upper casing. A Teflon/glass fabric (Armalon) liner was applied to an upper casing door and showed no signs of degradation. Vinyl shrink tubing performed well over electrode header connectors since the temperature in these regions was quite low due to water flow inside the electrodes.

Of the fiberglass reinforced plastic panels, only the polybutadiene showed acceptable resistance. Again the combination of temperature (up to 350°F) and concentrated sulfuric acid was too aggressive an environment. It is possible that some of these materials, specifically Ashland 197/3 and Ashland 800, would perform satisfactorily on the walls where the temperatures are lower and the washing action of the water would prevent high concentrations of sulfuric acid to form.

VENTURI SCRUBBER DESIGN MODEL

S. Yung, H. Barbarika, S. Calvert
Air Pollution Technology, Inc.
San Diego, California

L. Sparks
U.S. Environmental Protection Agency
Industrial Environmental Research Laboratory
Research Triangle Park, North Carolina

INTRODUCTION

Venturi scrubbers are a type of gas-atomized spray scrubber and are commonly used for the collection of fine particles. The performance and hydrodynamics have been subjected to extensive study both theoretically and experimentally, by numerous investigators[1-11]. Most of the investigators concluded that particle collection by liquid drops is the predominant occurrence in the venturi scrubber and the basic equations governing the particle collection and pressure drop are those developed by Calvert[1,2] and Boll[8].

Several researchers[9,10,11] have solved these equations on a digital computer and presented graphical results. In a venturi scrubber, most of the particle collection occurs in the venturi throat. Calvert[1,2] and Calvert, et al.[7] have applied these equations to the venturi throat section and obtained explicit equations for approximating the particle collection and pressure drop. Yung, et al.[12,13] modified Calvert's equation as follows:

$$\frac{\ln Pt}{B} = \frac{\ln (c_1/c_o)}{B} = \frac{1}{K_{po}\ (1-u^*_{d1}) + 0.7}$$

$$\left| 4\ K_{po}\ (1-u^*_{d1})^{1.5} + 4.2\ (1-u^*_{d1})^{0.5} - 5.02\ K_{po}^{\ 0.5} \right.$$

$$\left. \left(1-u^*_{d1} + \frac{0.7}{K_{po}}\right) \tan^{-1}\left(\frac{(1-u^*_{d1})K_{po}}{0.7}\right)^{0.5} \right| - \frac{1}{K_{po}+0.7}$$

$$\left| 4\ K_{po} + 4.2 - 5.02\ K_{po}^{\ 0.5} \left(1 + \frac{0.7}{K_{po}}\right) \tan^{-1}\left(\frac{K_{po}}{0.7}\right)^{0.5} \right| \qquad (1)$$

$$\Delta P = - \frac{2\ \rho_L\ u_{Gt}^2\ u^*_{d1}}{g_c} \left(\frac{Q_L}{Q_G}\right) \qquad (2)$$

$$u^*_{d1} = 2\ [1-x^2 + (x^4-x^2)^{0.5}] \qquad (3)$$

$$x = L/8 + 1 \qquad (4)$$

$$L = \frac{3\ \ell_t\ C_{Do}\ \rho_G}{2\ d_d\ \rho_L} \qquad (5)$$

$$B = \frac{Q_L\ \rho_L}{Q_G\ \rho_G\ C_{Do}} \qquad (6)$$

$$K_{po} = \frac{d_{pa}^{\ 2}\ u_{Gt}}{9\ \mu_G\ d_d} \qquad (7)$$

$$K_{pg} = \frac{d_{pg}^{\ 2}\ u_{Gt}}{9\ \mu_G\ d_d} \qquad (8)$$

$$K_{p50} = \frac{d_{p50}^{\ 2}\ u_{Gt}}{9\ \mu_G\ d_d} \qquad (9)$$

where d_d is the Sauter mean diameter calculated from the Nukiyama-Tanasawa relation[14].

The predictions by these equations are in good agreement with available experimental data. Thus, these equations can be utilized to design and select venturi scrubbers to meet control requirements. This paper presents discussions of the factors that affect the performance of a venturi scrubber, design techniques, and the optimization of the venturi scrubber design. The discussions are based on the previous equations.

DESIGN PROCEDURE

In designing a venturi scrubber, three steps are usually involved. The first step is to determine what efficiency is required. This step is relatively simple. For example, if the uncontrolled emission rate is 2,310 kg/hr and the allowable rate is 25 kg/hr the venturi scrubber should have a minimum collection efficiency of 98.9%, or a maximum overall penetration of 1.1%.

The second step is to design a venturi scrubber that can achieve the requirement. Usually, there is more than one scrubber design that will meet the requirement.

The third step is optimization; i.e., pick the best configuration.

This paper will elaborate on the second step.

DESIGN PARAMETERS

Several factors have an influence on the performance and the design of a venturi scrubber. Some of these factors are:

1. Throat length of the scrubber.
2. Throat velocity and liquid-to-gas ratio.
3. The size distribution of the particles to be collected.
4. Liquid drop size distribution.
5. Liquid drop distribution across the throat.

In the derivation of the equations, liquid drops were assumed to be uniformly distributed across the throat and the liquid drop diameter was the Sauter mean diameter predicted by the empirical correlation of Nukiyama and Tanasawa[14]. These two assumptions simplify the calculations and give reasonable results.

Throat Length of the Scrubber

Under a specific operating condition, the performance of the venturi scrubber depends on the throat length as revealed by equation (1) and Figure 1. The longer the throat, the more efficient the scrubber.

This dependence is more profound for larger particles; i.e., larger K_{po}. Thus, in designing a venturi scrubber, we should use a long throat. However, we should not use a longer throat than necessary because the pressure drop will increase with increasing throat length. The final choice of throat length should be a compromise of the two. A close inspection of Figure 1 reveals that a dimensionless throat length, L, of 2-3 would be sufficient. Further increase in dimensionless throat length will increase pressure drop with little gain in scrubber performance.

Figure 2 is a plot of B, the liquid-to-gas mass flow rate ratio, versus K_{p50}, the inertial parameter for the performance cut diameter, with L, the dimensionless throat length, as parameter. For an industrial size venturi scrubber, B is usually larger than 1. For large B, the performance K_{p50} is almost the same for L equal to 2 and infinity. Therefore, in predicting penetration for venturi scrubbers with L larger than 2, the first term in equation (1) can be neglected.

Throat Velocity and Liquid-to-Gas Ratio

The effects of throat velocity and liquid-to-gas ratio are interrelated, as shown in Figure 3. Performance cut diameter is plotted against liquid/gas ratio with throat velocity as parameter. Air and water at standard conditions were used.

Cut diameter is the particle diameter collected at 50% efficiency. The smaller the performance cut diameter, the more efficient the scrubber. It can be seen from Figure 3 that, for a constant throat velocity cut diameter decreases with increasing liquid/gas ratio, goes through a minimum, and then increases again.

The explanation for this phenomenon lies in the atomized liquid drop size. At low liquid-to-gas ratio, the atomized drops are smaller in diameter and their target efficiency is high. However, they accelerate faster with the result that the relative velocity between the drops and the particles goes to zero sooner. Zero velocity means zero collection. At large Q_L/Q_G, the resulting drop size is larger. The larger drops have lower target efficiency; but they accelerate more slowly.

If the required scrubber performance cut diameter is known, one can select throat velocity and liquid/gas ratio from Figure 3. For example, if the required cut diameter is 0.5 μmA, one can use a throat velocity of 150 m/s coupled with $Q_L/Q_G = 0.3\ \ell/m^3$; or a throat velocity of 75 m/s and $Q_L/Q_G = 1\ \ell/m^3$. The pressure drop for the two selections is roughly the same, approximately 40 cm W.C.

In selecting the final Q_L/Q_G, one should make sure that liquid rate provides sufficient drop coverage to completely sweep the gas stream. Insufficient liquid will decrease the efficiency of large particles.

Effect of Inlet Particle Size Distribution on Performance

The particle penetration predicted from equation (1) is for one particle size. However, the control requirement specified in step 1 is the overall penetration for the whole population of particles, which usually are not of uniform size. To arrive at the overall penetration, one must integrate the penetration over the size distribution. This may be tedious if the size distribution cannot be represented by mathematical functions. Most industrial particulate follow a log-normal size distribution, for which one can perform the integration numerically according to the following equation:

$$\overline{Pt} = \int_0^\infty Pt \; f(d_p) \; d\, d_p \qquad (10)$$

where Pt is given by equation (1) and $f(d_p)$ is the log-normal particle distribution density. Equation (10) is solved on a digital computer and the results are plotted in Figures 4 through 6. From these figures the overall penetration or overall collection efficiency can be determined by knowing the size distribution and liquid-to-gas flow rate ratio. These figures are also presented in Chapter 7 of reference 11.

VENTURI SCRUBBER DESIGN

The information presented in this paper allows one to design a venturi scrubber to meet a required $\overline{Pt}$, using the cut diameter approach developed by Calvert[15]. The general procedure is as follows:

1. Determine the required performance curve: First, find the aerodynamic geometric mass mean diameter of the incoming dust, d_{pg}, at a temperature expected in the venturi. Then, construct a plot of K_{pg} versus d_{p50} (required) for the required $\overline{Pt}$ by,

   a. Obtaining several K_{pg}-B pairs using Figures 4 through 6 (depending on σ_g) at the required Pt.

   b. Knowing d_{pg} obtain d_{p50} for each of the K_{pg}-B pairs using Figure 7.

2. Determine the available performance curves: First determine viscosities, and Nukiyama-Tanasawa coefficients for the venturi conditions. Then construct a number of performance curves corresponding to different Q_L/Q_G ratios as follows:

   a. Select a u_{Gt}.
   b. Calculate drop diameter from Nukiyama-Tanasawa relation.
   c. Calculate drop Reynolds number and drag coefficient.
   d. Calculate B from equation (6).
   e. Obtain K_{p50} from Figure 1 or calculate it from equation (1).

f. Calculate d_{p50} from equation (9).
g. Calculate K_{pg}.

Repeat steps (a) through (g) for several velocities. Plot performance K_{pg} vs. d_{p50} curves on the same plot as the requirement curve from step (1).

3. Determine required pressure drops: The intersections of the requirement and performance curves determine the proper design points. The corresponding pressure drops required can then be found from equations (2), (3), and (4) for the desired L.

4. Determine throat cross-section area: Calculate throat cross-sectional area for each design point as follows:

a. From the design K_{pg} and the definition of K_{pg} obtain d_d as a function of u_{Gt}.

b. Substitute this function for d_d into the Nukiyama-Tanasawa relation and solve for u_{Gt}.

c. Divide Q_G by u_{Gt} to obtain the throat cross-sectional area.

5. Determine the throat length: Using the design velocity and the desired L, calculate throat length ℓ_t from equation (5).

6. Determine convergence, divergence angles: These have little effect on particle collection but they do have some effects on pressure drop. Of the two, divergence angle is more important. Divergence angle should be designed such that:

a. Boundary layer separation does not occur.
b. Momentum recovery occurs in the divergent section.

7. Select an optimum. This involves trading off liquid usage, pressure drop, and size.

DESIGN EXAMPLE

The problem of designing a venturi scrubber to control dust from a typical asphalt plant dryer is illustrated.

The dust has a log-normal distribution of diameters described by a geometric standard deviation, $\sigma_g = 5.0$ and a geometric mass mean particle diameter, $d_{pg} = 18$ µm (physical). The particle density is 2.6 g/cm^3. The flue gas flow rate is 567 Am^3/min with a gas temperature of 116°C. The uncontrolled emission rate is 2,310 kg/hr.

Based on a local Air Pollution Control District rule for the amount of weight processed, the emission should not exceed 25 kg/hr.

The required efficiency is then: (2,310-25)/2,310 x 100 = 98.9%. Thus, the design should meet an efficiency requirement of 99% or an overall penetration of 1%.

Specify the required performance curve: First, find the aerodynamic geometric mean diameter. For air at 116°C the Cunningham slip correction factor for 18 μm particles is C' = 1.013. Thus,

$$d_{pg} = 18\ (1.013 \times 2.6)^{0.5} = 29.2\ \mu mA \qquad (11)$$

Next, plot the required cut diameters (d_{p50}) for an overall penetration of 0.01, using Figures 5 and 7. The points which are shown in Figure 8 as circles are listed below:

B	K_{pg}	d_{p50}, μmA
4.3	1,000	0.64
2.8	1,500	0.58
2.2	2,000	0.55
1.6	5,000	0.41
1.4	10,000	0.30

Specify the available performance curves: Calculate the cut diameters for Q_L/Q_G ratios of 1, 1.5, and 2 ℓ/m³. Results are plotted on Figure 8.

Determine the required pressure drops: The intersections of the performance lines with the requirement line in Figure 8 determine the cut diameters (both required and performance). The required pressure drops corresponding to these cut diameters for L = 2.7 are then,

Q_L/Q_G, m³/m³	d_{p50}, μmA	ΔP, cm W.C.
0.001	0.42	67
0.0015	0.57	40
0.002	0.675	32

Determine throat cross-sectional area: Calculate the throat cross-sectional area for the third design point; i.e., $Q_L/Q_G = 0.002$ and $d_{p50} = 0.675$ μmA. From Figure 8 the required $K_{pg} = 980$; i.e.,

$$K_{pg} = \frac{d_{pg}\ u_{Gt}}{9\ \mu_G\ d_d} = 980 \qquad (12)$$

By combining the above equation with the Nukiyama and Tanasawa correlation, the throat velocity was calculated to be 5,300 cm/s. The required throat cross-sectional area is then 1,783 cm².

Determine throat length: From equation (5), ℓ_t = 20.4 L cm. If designed for L = 2.7, the throat length = 55 cm.

CONCLUSIONS

A primarily graphical method has been developed for designing venturi scrubbers. The method is easy to use as presented.

ACKNOWLEDGEMENTS

This study was supported by the EPA under Contract No. 68-02-1328, Task No. 13.

REFERENCES

1. Calvert, S. Source Control by Liquid Scrubbers. In: Air Pollution, Stern, A. (ed). Chap. 46. New York, Academic Press, 1968.
2. Calvert, S. AIChE. 16: 392-396, 1972.
3. Ekman, F.O., H.F. Johnstone. Ind. Eng. Chem. 43: 1358-63, 1951.
4. Morishima, N., T. Yoshida, Y. Kosoka, Y. Nonaka. Funtai Kogaku Kenkyr Kaishi. 9: 357-62, 1972.
5. Dropp, L.T., A.J. Akbrut. Tepoloenergetika. 1:63-8, 1972.
6. Behie, S.W., J. M. Beeckmans. Canadian J. of Chem. Eng. 51:430, 1973.
7. Calvert, S., D. Lundgren, D. Metha. APCA J., 22: 529-32, 1972.
8. Boll, R.H. Ind. Chem. Fundamentals. 12: 40-50, 1973.
9. Goel, K.C., I.G. Hollands. Ind. Eng. Chem. Fundamentals. 16: 186-192, 1977.
10. Hollands, K.G., I. Goel. Ind. Eng. Chem. Fundamentals. 14: 16-22, 1975.
11. Yung, S., S. Calvert, H.F. Barbarika. Venturi Scrubber Performance Model. EPA-600/2-77-172, NTIS No. PB 271-515/AS, August 1977.
12. Yung, S., H.F. Barbarika, S. Calvert. APCA J. 27: 348-50, 1977.
13. Yung, S., S. Calvert, H.F. Barbarika. Environmental Science and Technology. 12: 456-58, 1978.
14. Steinmeyer, D.E. In: Chemical Engineer's Handbook, 4th ed. R.H. Perry and C.H. Chilton (eds). Pg. 18-64, New York, McGraw-Hill, 1973.
15. Calvert, S. APCA J. 24: 929, 1974.

NOMENCLATURE

Latin

B = dimensionless parameter characterizing liquid-to-gas mass flow rate ratio

C_D = drag coefficient for spheres, dimensionless

C' = Cunningham slip correction factor, dimensionless

c = particle mass concentration, g/cm^3

c^* = c_1/c_o, dimensionless

d_d = drop diameter, cm or μm

d_{pa} = particle aerodynamic resistance diameter, μmA or cmA

d_{pg} = mass median diameter, μmA or cmA

d_{p50} = aerodynamic cut diameter, μmA or cmA

K_{pg} = inertial parameter of mass median diameter, dimensionless

K_{p50} = inertial parameter of cut diameter, dimensionless

K_{po} = inertial parameter at throat entrance dimensionless

L = $(3\ C_{Do}/2\ d_d)(\rho_G/\rho_L)(\ell_t)$, dimensionless throat length

ℓ_t = venturi throat length, cm

Pt = particle penetration for particles with diameter d_p, fraction or percent

$\overline{Pt}$ = overall particle penetration, fraction

Q_G = volumetric flow rate of gas, cm^3/s

Q_L = volumetric flow rate of liquid, cm^3/s

u_{d1} = drop velocity at the throat exit, cm/s

u^*_{d1} = (u_{d1}/u_{Gt}), dimensionless drop velocity

u_{Gt} = gas velocity in the throat, cm/s

x = $(L+8)/8$

z = axial coordinate, cm

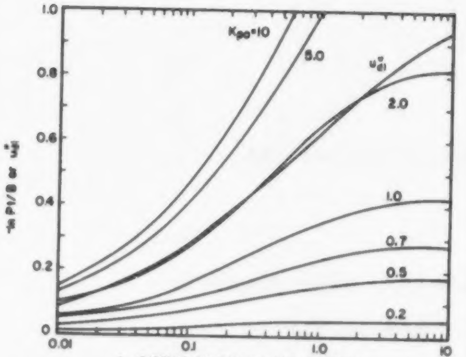

FIGURE 1. THEORETICAL PARTICLE PENETRATION AND DROP VELOCITY

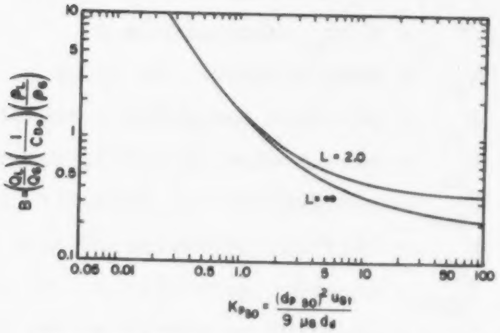

FIGURE 2. PREDICTED VENTURI SCRUBBER PERFORMANCE K_{p50} VS B

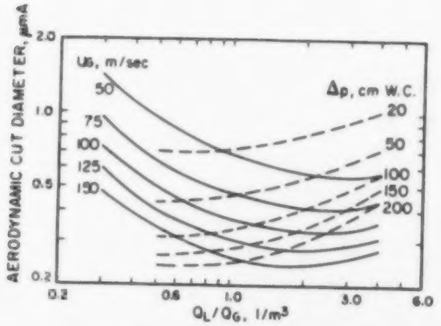

FIGURE 3. PREDICTED VENTURI PERFORMANCE, d_{p50} VS Q_L/Q_G WITH u_G AND ΔP AS PARAMETERS. (L = ∞)

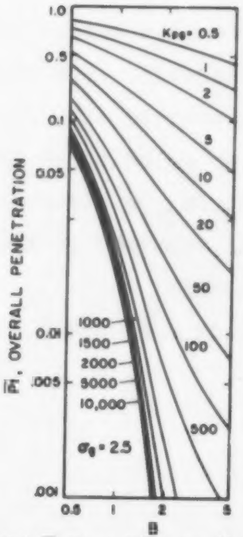

FIGURE 4. $\overline{Pt}$ VS B WITH K_{pg} AS PARAMETER

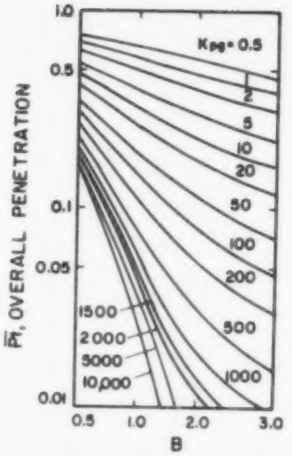

FIGURE 5. $\overline{Pt}$ VS B WITH K_{pg} AS PARAMETER. (σ_g = 5.0)

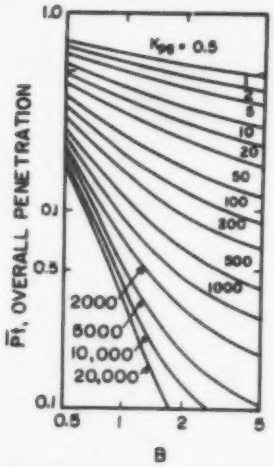

FIGURE 6. $\overline{Pt}$ VS B WITH K_{pg} AS PARAMETER, (σ_g = 7.5).

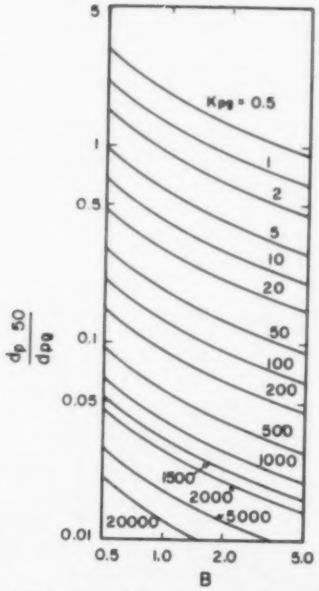

FIGURE 7. $\frac{d_p\ 50}{d_{pg}}$ VS B WITH K_{pg} AS PARAMETER

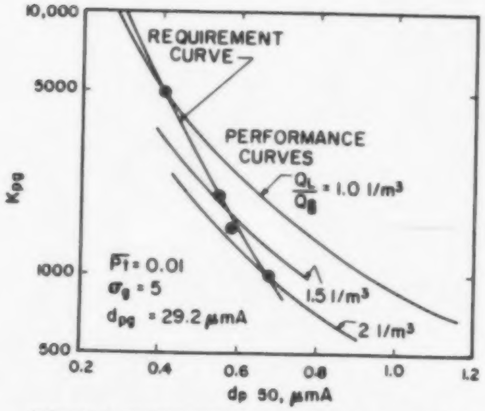

FIGURE 8. IMPACTION PARAMETER VS AERODYNAMIC CUT DIAMETER FOR A VENTURI DESIGN.

EXPERIMENTAL STUDY OF PARTICLE COLLECTION BY A VENTURI SCRUBBER DOWNSTREAM FROM AN ELECTROSTATIC PRECIPITATOR

G. H. Ramsey, L. E. Sparks and B. E. Daniel
Particulate Technology Branch
Industrial Environmental Research Laboratory
Environmental Protection Agency
Research Triangle Park, N. C.

ABSTRACT

The results of pilot plant experiments of particulate collection by a venturi scrubber downstream from an electrostatic precipitator (ESP) are presented. The data, which cover a range of scrubber operating conditions and ESP efficiencies, show that particle collection by the venturi scrubber is not affected by the upstream ESP; i.e., for a given scrubber pressure drop, particle collection efficiency as a function of particle diameter is the same for both ESP on and ESP off. The experimental results are in excellent agreement with theoretical predictions.

INTRODUCTION

The use of electrostatic precipitator (ESP)/scrubber systems for particulate collection in coal fired utility boilers has generated considerable interest. At least one utility plans to use a moderately efficient ESP followed by a scrubber to meet emission standards for a new boiler. The recent revisions to the Clean Air Act which require SO_x removal for most plants are likely to increase interest in ESP/scrubber systems.

There are numerous undocumented reports that a scrubber downstream of an ESP works better than expected. Theoretical and experimental studies of particle collection by drops indicate that there is no reason

Preceding page blank

to expect a scrubber downstream from an ESP to have different performance characteristics from a scrubber alone.[1] But data on ESP/scrubber combinations is insufficient to allow one to determine if the results from drop collection theory apply to scrubbers.

This experimental study of an ESP/scrubber system was undertaken to provide the necessary data. Also a theoretical study was conducted to determine which ESP/scrubber configurations are capable of meeting the proposed particulate New Source Performance Standard for utility boilers of 13 ng/J (0.03 lb/10^6 Btu).

The objectives of the program were to:

1. Determine the effect of an ESP on the particle penetration (1 minus efficiency) of a venturi scrubber as a function of particle diameter characteristics.
2. Determine the overall mass penetration and particle penetration as a function of particle diameter for the ESP/scrubber system.
3. Determine, with the aid of mathematical models, the ESP/scrubber configurations capable of meeting an emission standard for fly ash of 13 ng/J.

EXPERIMENTAL EQUIPMENT

The scrubber system tested in conjunction with the ESP system consisted of a venturi scrubber, an entrainment separator, and a blower and motor. The venturi scrubber had a round cross section with a throat length of 25.4 cm. The throat section could be removed so various throat diameters could be tested. The ESP/scrubber tests involved only two throat diameters: 7.62 and 10.16 cm. Larger diameters could not be installed due to the limiting size of the opening at the throat bottom flange. The water was added tangentially at two points at the top of the scrubber. The water flow rate could be varied up to a maximum of 6.43 X 10^{-2} m^3/min. The scrubbing water was not recirculated.

Following the venturi scrubber, the gas stream entered a cyclonic entrainment separator. The separator had a diameter of 50.8 cm and was 1.22 m in height. The gas entered the separator at the bottom and exited tangentially at the top. The gas was moved through the system by a blower powered by a 15 HP motor.

The scrubber installation is shown in Figure 1.

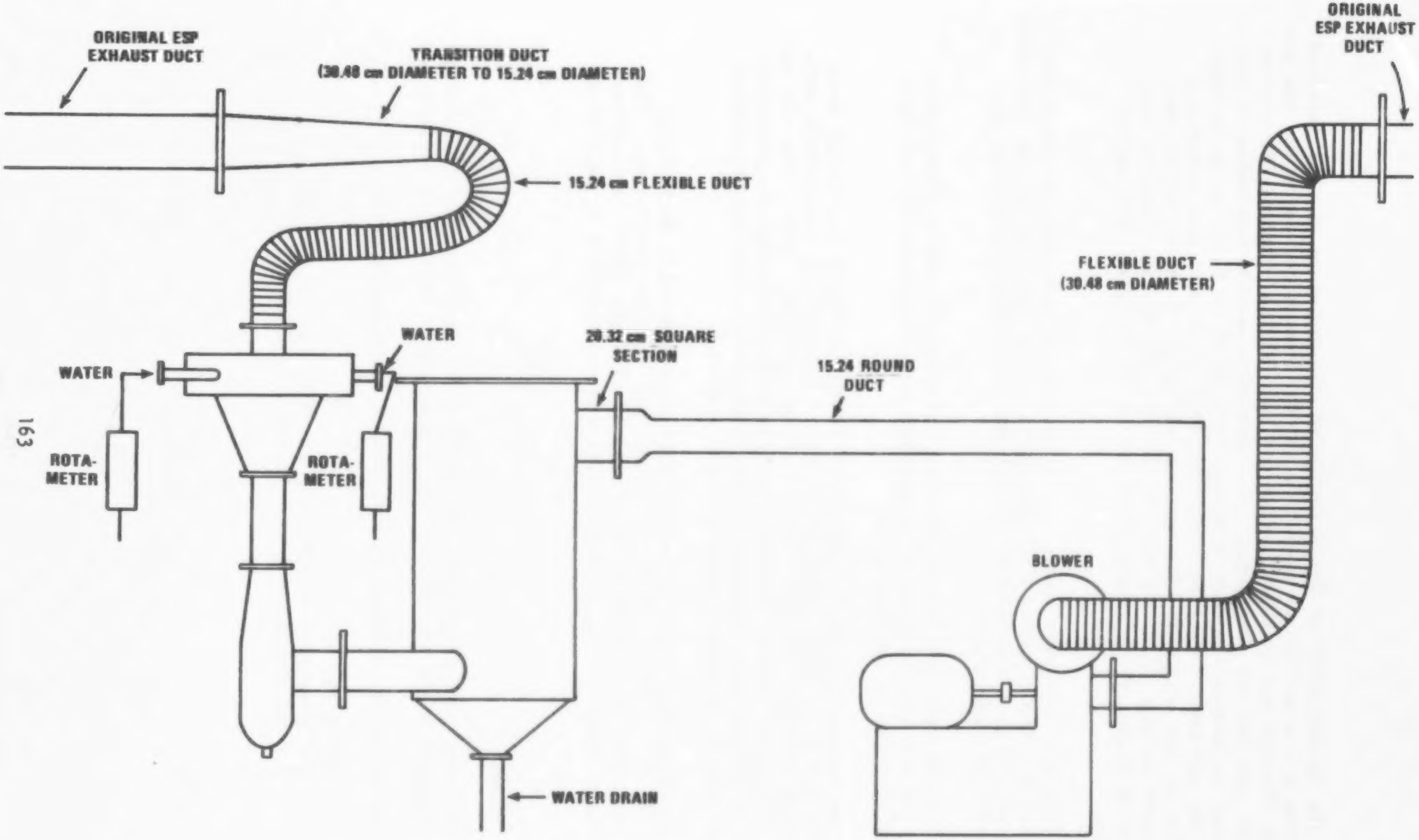
ORIGINAL ESP EXHAUST DUCT
TRANSITION DUCT (30.48 cm DIAMETER TO 15.24 cm DIAMETER)
15.24 cm FLEXIBLE DUCT
ORIGINAL ESP EXHAUST DUCT
FLEXIBLE DUCT (30.48 cm DIAMETER)
WATER
WATER
20.32 cm SQUARE SECTION
15.24 ROUND DUCT
ROTA-METER
ROTA-METER
BLOWER
WATER DRAIN

Figure 1. Scrubber system added to ESP outlet.

The installation of the scrubber to the outlet of the ESP involved removing a 3 m section of duct from the ESP system and rerouting the gas stream through the scrubber system and back to the original ESP system between the ESP and the blower. A transition section was added to the ESP duct to reduce the duct diameter from 30.48 to 15.24 cm to accommodate the scrubber. Flexible duct was used to connect the transition section to the scrubber. The gas was exhausted from the entrainment separator through 15.24 cm duct to the fan and through flexible duct (30.48 cm diameter) to connect the fan to the original ESP exhaust system.

Pressure taps were added to the duct at the entrance to the scrubber, between the scrubber and separator, and at the exit of the separator. The pressure taps allowed for measurement of pressure drop over the scrubber and separator.

The ESP used for this experiment was EPA/IERL-RTP's pilot-scale ESP. The ESP was designed by Denver Research Institute and has been described fully by Lawless et al.[3]

The aerosol generator consisted of two sandblast guns which were fed fly ash by a vibrating screw feeder. Preliminary experiments were conducted with fly ash fed directly to the sandblast guns. The fly ash from the feeder passed through a cyclone before entering the sandblast guns, to prevent dust fallout in the inlet duct. Previous experience showed that this aerosol generator was stable.[3]

All size distribution measurements were made with Meteorology Research, Inc. (MRI) cascade impactors with greased substrates. The impactors were calibrated by personnel of EPA/IERL-RTP's Particulate Technology Branch (PATB), using the procedure described by Calvert et al.[4]

TEST PROGRAM

The experimental program was divided into two phases: Phase 1 was a preliminary study and Phase 2 was a systematic study with replication.

The variables studied in the Phase 2 experiments were:

ESP on or off
ESP penetration 1 to 0.037 (efficiency 0 to 96.3%)
Liquid/gas ratio 6.65 X 10^{4} to 2.66 X 10^{3} m^{3}/Am^{3}

EXPERIMENTAL RESULTS

The particle size distribution into the scrubber depends on the penetration through the ESP. Thus, the overall penetration results must not be used to determine the effect of the ESP on scrubber performance. The particle penetration as a function of particle diameter (the graded penetration) curves for the scrubber must be used to determine the effect of the ESP. (The graded penetration curve for a scrubber is independent of the inlet particle size distribution.)

The graded penetration curves for Phase 1 are shown in Figure 2 as a plot of penetration versus aerodynamic particle diameter, d_a. ($d_a = d\sqrt{\rho C}$ where d is the physical particle diameter, ρ is the density of the particle and C is the Cunningham factor.) The predicted graded penetration curve is also shown in Figure 2.

The results of all the Phase 2 tests are shown in Figure 3. The average graded penetration curves for each of the Phase 2 tests are shown in Figure 4.

As is obvious from the data shown in Figures 2 and 4, scrubber performance is dominated by the pressure drop across the scrubber; and the ESP has no effect on the performance of the scrubber. Figure 2 shows clearly that the predicted graded penetration curve is in excellent agreement with the experimental data.

Statistical analysis of the data showed that:

1. There was no effect on scrubber performance due to the ESP.
2. Particle collection in the venturi was dominated by pressure drop.
3. Changes in throat diameter (i.e., changes in gas velocity in the throat) had more effect than changes in L/G.
4. The uncertainty in the experimental graded penetration curves was about 20%.

ESP/Scrubber System Performance

Typical graded penetration curves for the ESP/scrubber system are shown in Figures 5 and 6. These curves indicate that the ESP/scrubber system is capable of meeting the proposed revised New Source Performance Standard. In other words, a particle collection system operating with the characteristics shown in Figures 5 and 6 can collect fly ash with a typical size distribution with penetrations less than 0.003 (efficiencies greater than 99.7%).

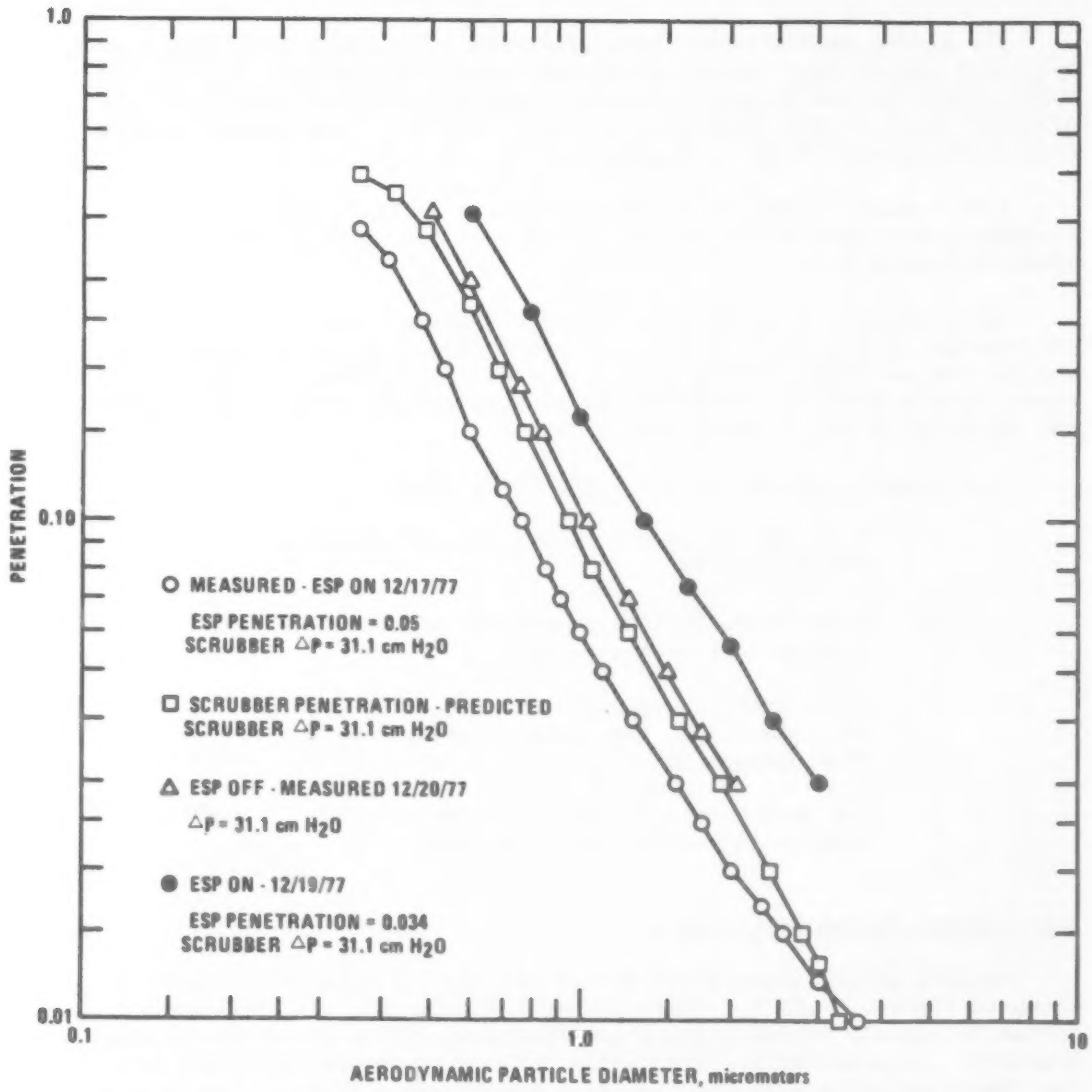

Figure 2. Graded penetration curves for venturi scrubber - phase 1 experiments.

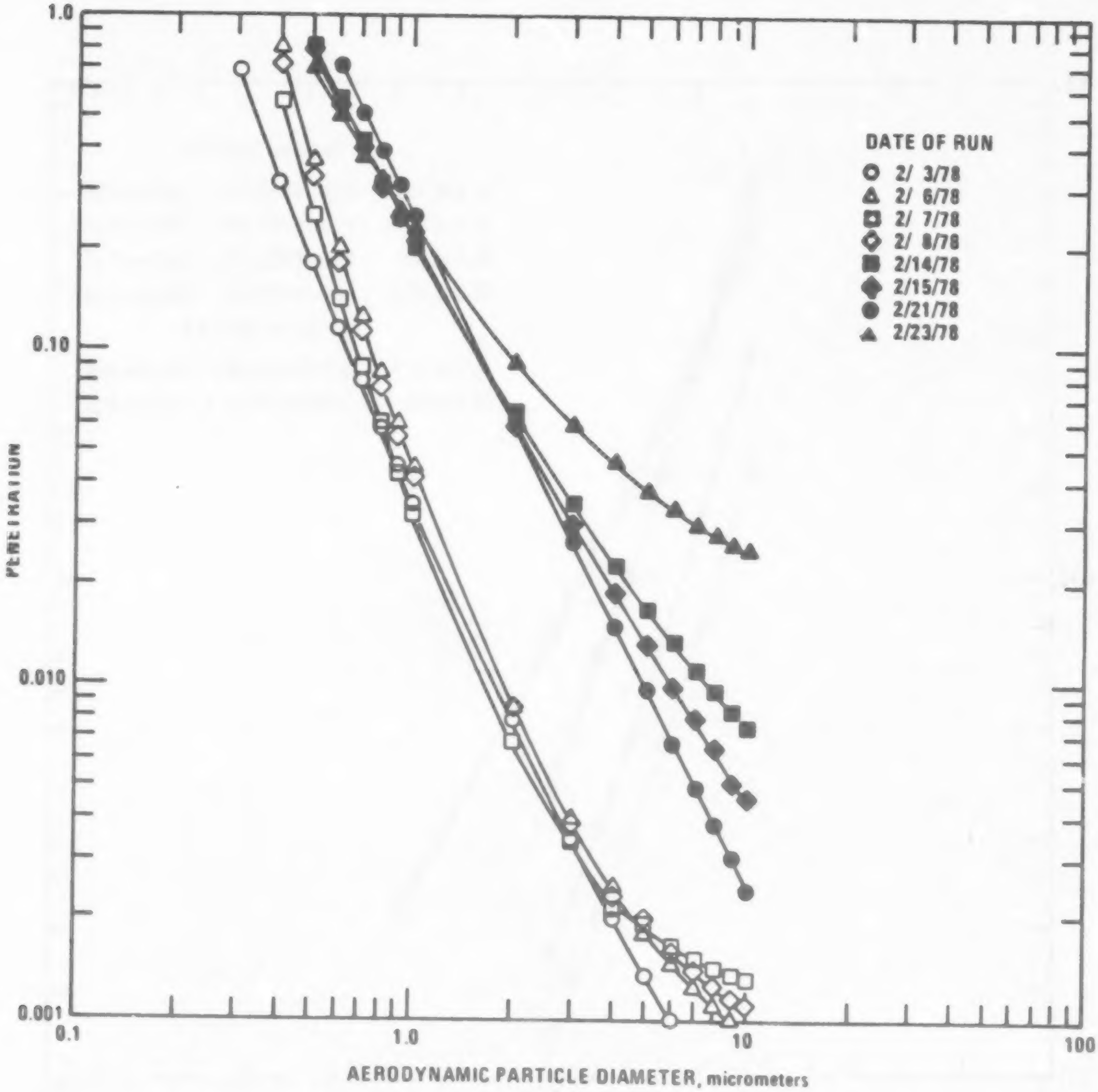

Figure 3. Graded penetration curves for venturi scrubber - phase 2 experiments.

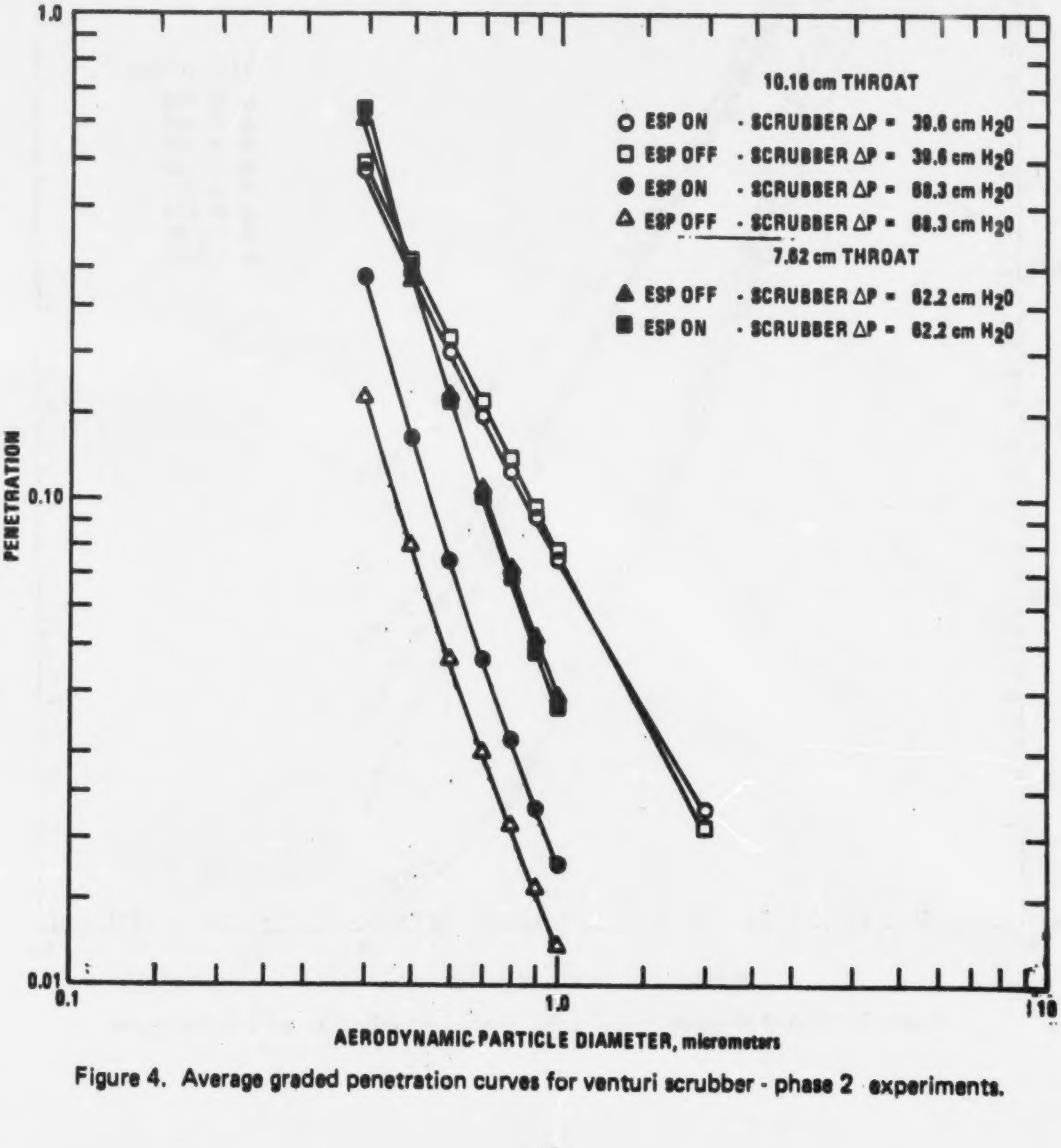

Figure 4. Average graded penetration curves for venturi scrubber - phase 2 experiments.

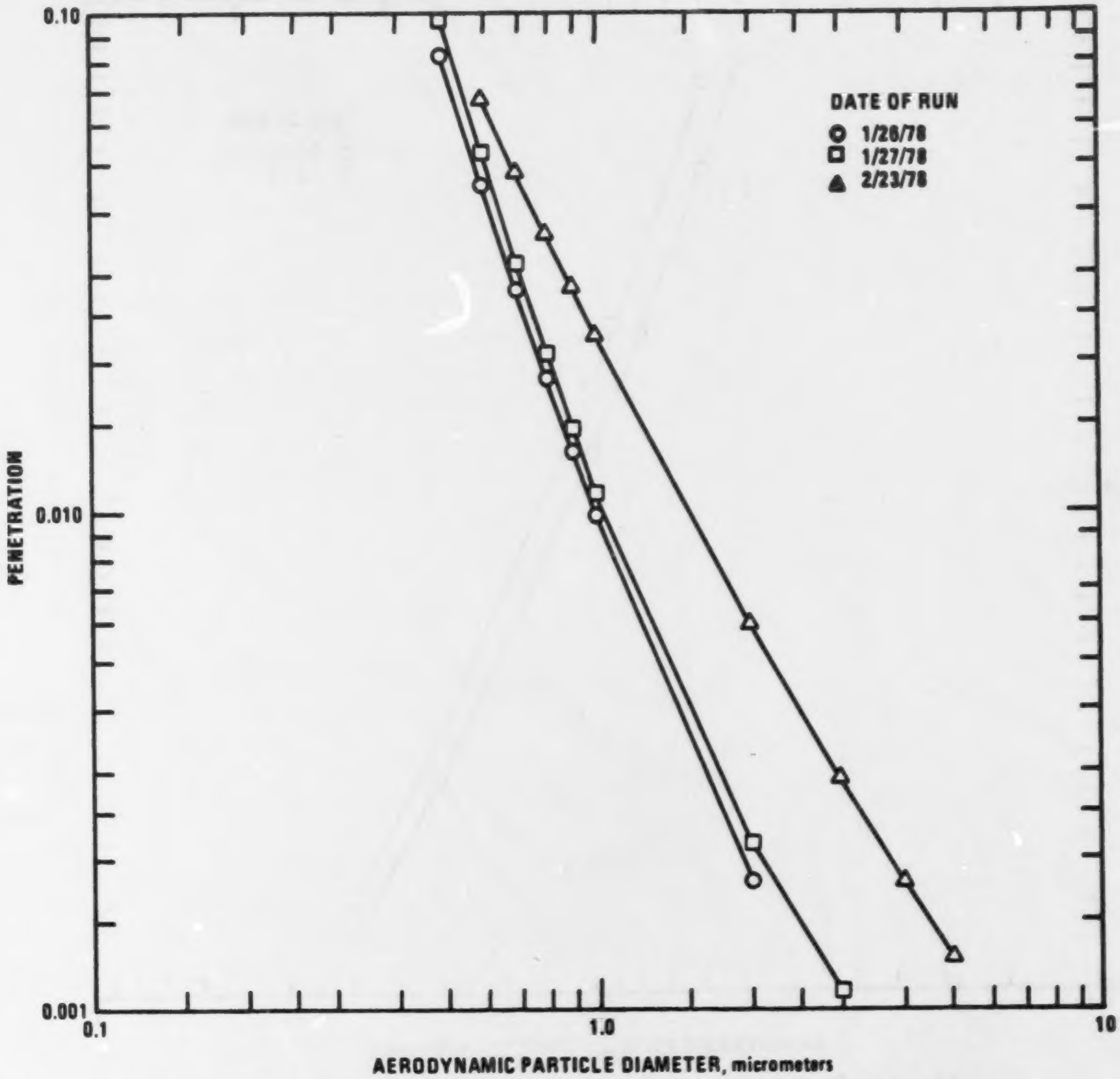

Figure 5. Graded penetration curves for the ESP - scrubber system.

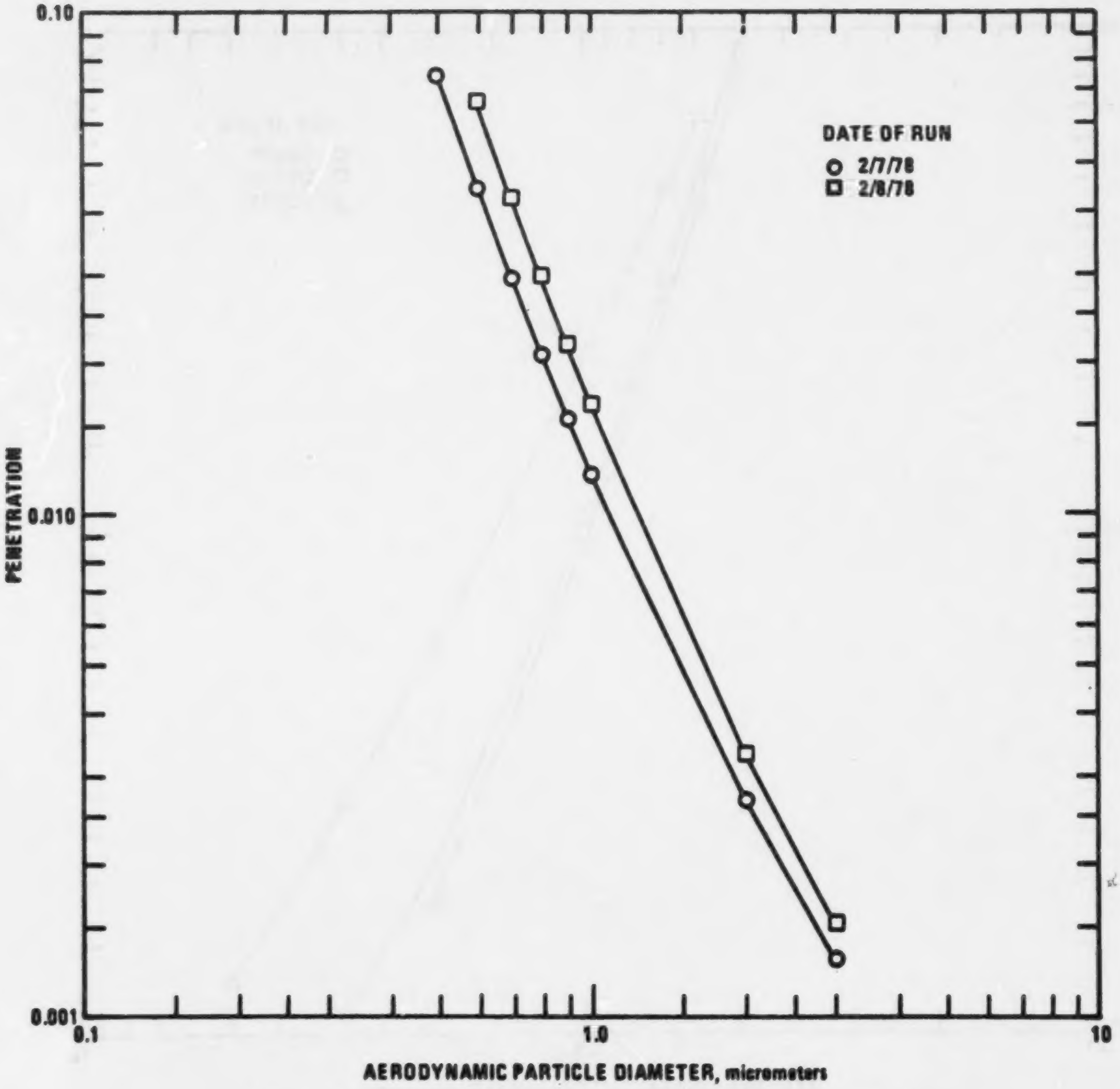

Figure 6. Graded penetration curves for the ESP - scrubber system.

In all cases the overall mass penetration is quite low. The overall mass collection efficiency is quite high.

THEORETICAL ANALYSIS OF COMBINED ESP/SCRUBBER SYSTEMS

The data presented in previous sections clearly show that particle collection by a scrubber is adequately modeled by Calvert's Venturi Scrubber Model. ESP particle collection data show that the EPA/Southern Research Institute ESP Model[5] adequately predicts ESP performance. Therefore, the performance of a combined ESP/scrubber system should be adequately predicted by a combination of the two models.

The predictions of the two models were combined to obtain order of magnitude estimates of the performance and economics of using an ESP/scrubber system as opposed to either an ESP or a scrubber alone. In essence such a system represents a tradeoff between scrubber pressure drop and ESP plate area.

Two cases were examined:

A low current density case which corresponds to a fly ash with high electrical resistivity ($\sim$5 X 10^{11} ohm-cm) such as produced by low sulfur coal.

A moderate current density case which corresponds to a fly ash with moderate electrical resistivity ($\sim$3 X 10^{10} ohm-cm) such as produced by moderate sulfur coals ($\sim$1.5-2%).

The following assumptions were made:

1. The fly ash size distribution was log-normal with mass mean diameter of 20 m and geometric standard deviation of 4.5.
2. Fly ash density was 2.4 g/cc.
3. Gas flow distribution in the ESP was characterized by a normalized standard deviation of 0.25.
4. The factor for sneakage and nonrapping reentrainment in the ESP was 0.1.
5. Rapping losses were typical as described by McDonald.[5]

The results of the calculations show that the scrubber pressure drop, ΔP, is a function of the penetration through the ESP, $\overline{Pt}_{ESP}$, and is essentially independent of the current density. The pressure drop/ $\overline{Pt}_{ESP}$ relationship is:

$$\Delta P = 85\ \overline{Pt}_{ESP} \tag{1}$$

where ΔP is in cm of water and $\overline{Pt}_{ESP}$ is a fraction.

Because the specific collector area, SCA, required for a given $\overline{Pt}_{ESP}$ is a function of the current density, the relationship between ΔP and SCA is different for the two current densities:

$$\Delta P = \exp\ (3.95 - 0.0536\mathrm{SCA}) \tag{2}$$

for the high current density case, and

$$\Delta P = \exp\ (3.91 - 0.0220\mathrm{SCA}) \tag{3}$$

for the low current density case. ΔP is in units of cm of water and SCA is in units of $m^2/Am^3/s$.

The calculated results show that the SCA can be reduced by about a factor of 2 for both moderate and high resistivity cases, for a scrubber pressure drop of about 10 cm of water.

DISCUSSION

The initial reaction to the calculated and experimental results is one of disbelief. One does not expect a fairly inefficient ESP and a moderate to low pressure drop scrubber to perform as well as both the experimental data and the calculated results in the next section show. An examination of the particle penetration versus particle diameter curves (the graded penetration curve) for both devices acting alone and the combined graded penetration curve can explain the results.

The calculated graded penetration curve for an ESP with a penetration of 0.0771 is shown in Figure 7. Note that the ESP curve has a broad peak from about 0.4 to 1 μm and then drops fairly rapidly on both sides of the peak. On the other hand the graded penetration curve, Figure 8, for a scrubber needed to produce an emission of 13 ng/J in combination with the ESP drops rapidly from essentially 1.0 at 0.1 μm to less than 0.01 at 3 μm. The scrubber is seen to be efficient in particle diameter regions where the ESP is inefficient and the ESP is efficient in particle diameter regions where the scrubber is inefficient. The two devices complement each other.

The graded penetration of the ESP scrubber system can be obtained by multiplying the two separate graded penetration curves; i.e.,

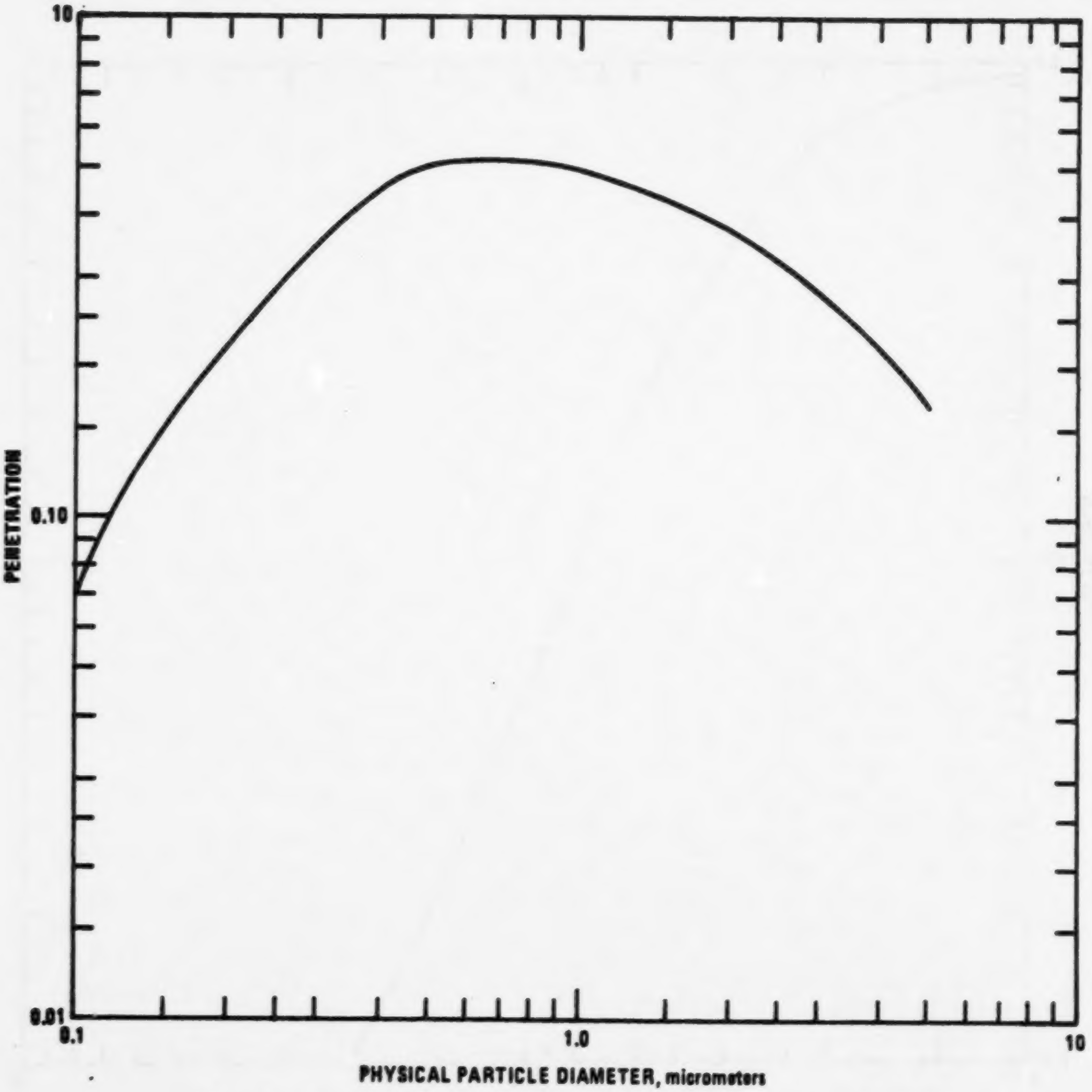

Figure 7. Graded efficiency curve for ESP with penetration of 0.0771.

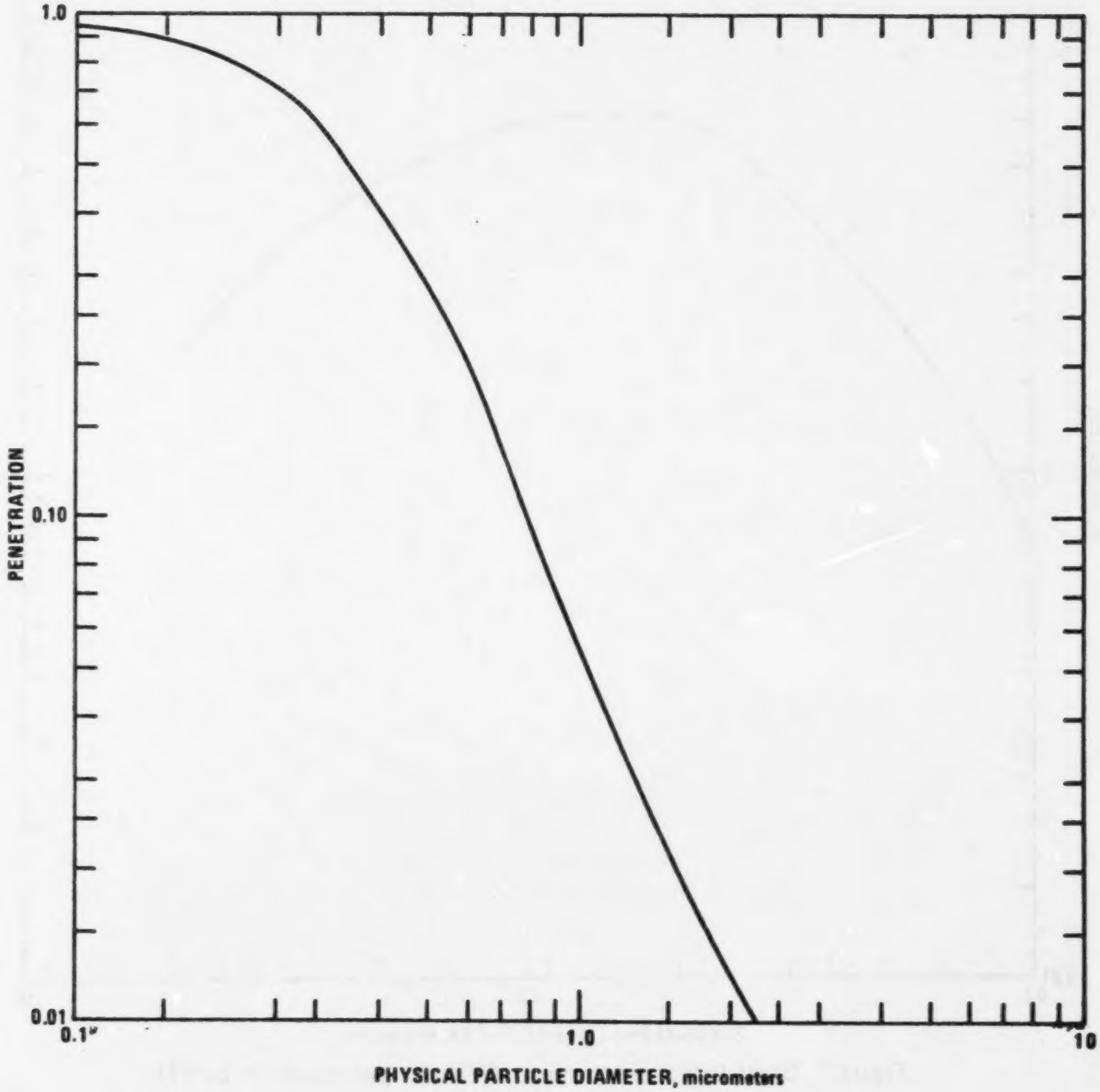

Figure 8. Penetration versus particle diameter for scrubber with pressure drop = 23 cm H_2O, density - 2.4 g/cc.

$$\overline{Pt}(d)_{ESPS} = \overline{Pt}(d)_{ESP} \times \overline{Pt}(d)_{s} \quad (4)$$

where

$\overline{Pt}(d)_{ESPS}$, $\overline{PT}(d)_{ESP}$, and $\overline{PT}(d)_{s}$ are the penetration of particles with diameter d for the ESP/scrubber system, the ESP alone, and the scrubber alone, respectively. The resulting graded penetration curve is shown in Figure 9. Note that the curve has a sharp peak at about 0.3 μm and drops rapidly on both sides. This sharp peak is characteristic of the ESP/scrubber system and, as discussed in the section on plume opacity, may cause problems with respect to plume opacity limits. (Note that the curves in Figures 7, 8, and 9 are for penetration versus physical particle diameter, not aerodynamic particle diameter as in Figures 2, 3, 4, 5 and 6.)

CONCLUSIONS

The results of the experimental and theoretical studies support the following conclusions:

1. The performance of a venturi scrubber is not affected by the ESP; i.e., the particle penetration versus particle diameter characteristics of the scrubber are the same whether the ESP is on or off.

2. The performance of the scrubber is adequately modeled by the SR-52 programmable calculator model described by Sparks.[2]

3. An ESP/scrubber system can achieve an emission of 13 ng/J.

REFERENCES

1. Sparks, L. E., "The Effect of Scrubber Operating and Design Parameters on the Collection of Particulate Air Pollutants." Ph.D. Dissertation, University of Washington, 1971.

2. Sparks, L. E., "SR-52 Programmable Calculator Programs for Venturi Scrubbers and Electrostatic Precipitators," EPA-600/7-78-026 (NTIS PB 277-672/AS) March 1978.

3. Lawless, P., G. Ramsey, and B. Daniel, "Characterization of the IERL/RTP Pilot Scale Electrostatic Precipitator." EPA report in press, 1978.

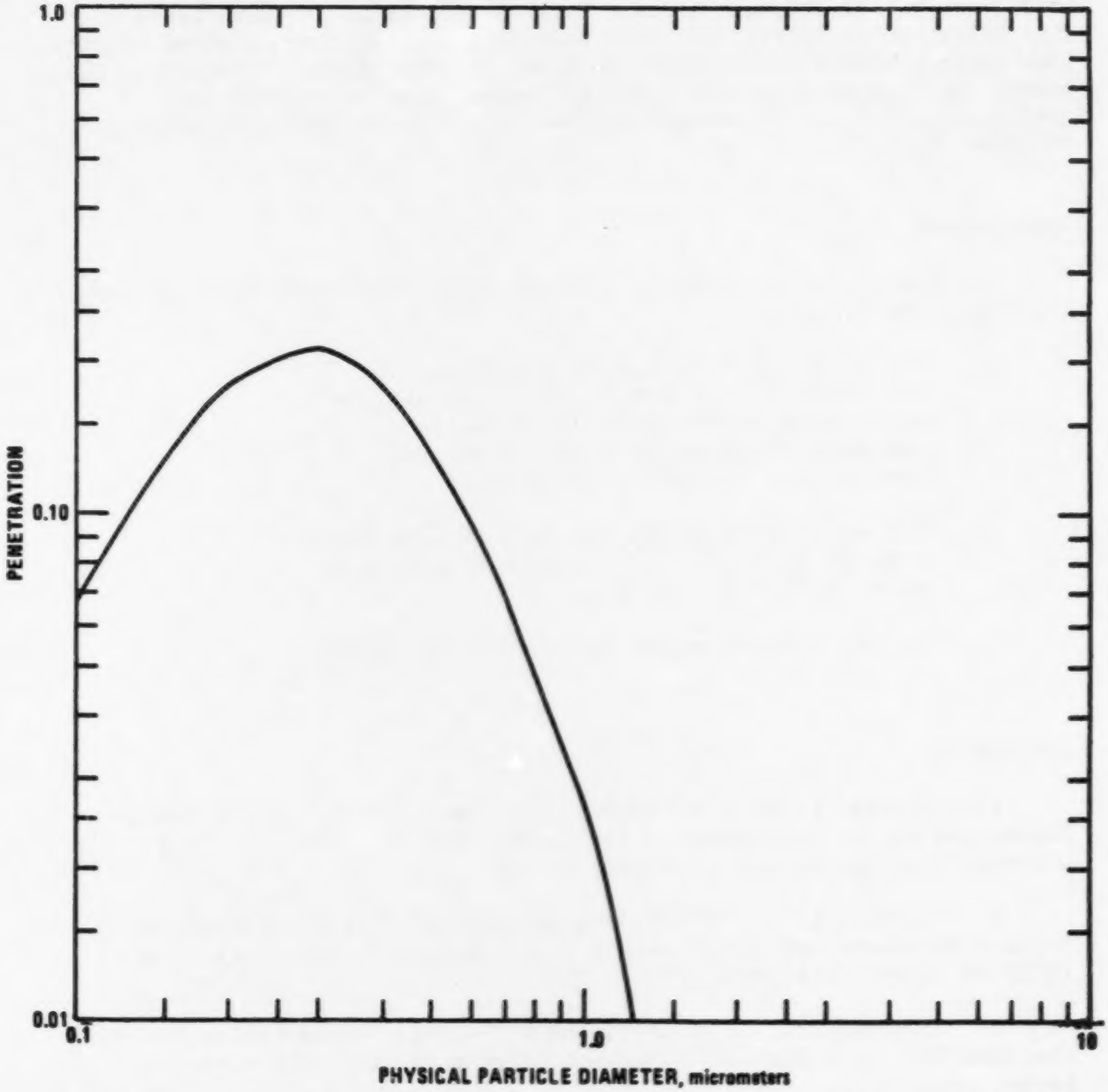

Figure 9. Graded penetration curve for ESP scrubber system - ESP penetration = 0.0771 scrubber pressure drop = 23 cm H_2O.

4. Calvert, S., C. Lake, and R. Parker, "Cascade Impactor Calibration Guidelines." EPA-600/2-76-118 (NTIS PB 252-656/AS), April 1976.

5. McDonald, J. R., "Modeling and Programming the Electrostatic Precipitation Process." EPA report in press, 1978.

6. Ensor, D. S., B. S. Jackson, S. Calvert, C. Lake, D. V. Wallon, R. E. Nilan, K. S. Campbell, T. A. Cahill, and R. G. Flocchini, "Evaluation of a Particulate Scrubber on a Coal-Fired Utility Boiler." EPA-600/2-75-074 (NTIS PB 249-562/AS), November 1975.

7. Ensor, D. C., "Smoke Plume Opacity Related to the Properties of Air Pollutant Aerosols." Ph.D. Dissertation, University of Washington, 1972.

EFFECTS OF SURFACE TENSION ON PARTICLE REMOVAL

George J. Woffinden
Gregory R. Markowski
David S. Ensor
Meteorology Research, Inc.
464 West Woodbury Road
Altadena, California 91001

ABSTRACT

Surface tension of scrubber water can affect particle removal efficiency of the scrubber. The predominant effect of reducing surface tension is to reduce the spray droplet sizes. There is an optimum droplet size for each scrubber system. If reduction in droplet size due to addition of a surfactant approaches the optimum size then a slight improvement in scrubber performance might be expected due to the surfactant addition.

INTRODUCTION

Can particle collection efficiency of a wet scrubber be improved by addition of detergent or other surfactant to the scrubber water? MRI conducted theoretical studies and limited laboratory experiments to show the effects of surface tension on the collection efficiency of particles by water droplets. Scrubber operation requires generation of liquid droplets, capture of the effluent particles by these droplets, recovery of the droplets from the flue gas stream and separation of particles from the liquid so the liquid.

CAPTURE MECHANISMS

Perhaps the most obvious effects of surface tension are demonstrated during particle capture. Particle capture by water droplets is a two step process:

1. Collision of the particle with the droplet, and
2. Coalescence or adhesion after collision.

Surface tension of the scrubber water can influence both steps.

COLLISION OF PARTICLES WITH DROPLETS

Collision efficiency depends on the number, size, and relative velocity of droplets encountered by a particle as it passes through a scrubber. When water is sprayed to form droplets, a reduction in surface tension normally reduces droplet sizes.[1,2] The amount of reduction depends on the water surface tension:

$$D = C\sigma^{1/2} \tag{1}$$

where,
D = Resultant droplet diameter
C = Constant
σ = Surface tension of the water

Smaller droplets provide more exposed surface area for particle collision, but collision efficiency is reduced. Small droplets are also more difficult to remove from the gas stream by drift eliminators so some of the particles, even after capture by droplets will pass through the scrubber system. This analysis implies that there is an optimum droplet size for a given scrubber system. Theoretical calculations were made to show the optimum droplet size based on the Scrubber Handbook model.[3] Results are shown in Figure 1. A gas flow rate of 80 m/sec was assumed. The optimum droplet sizes for other flow velocities are given in Figure 2.

It can be seen from the figures that changing the droplet diameter can improve or degrade scrubber performance depending on the initial droplet diameters and the size of particles to be removed. An example is shown in Table 1, using the Scrubber Handbook model to determine penetration.

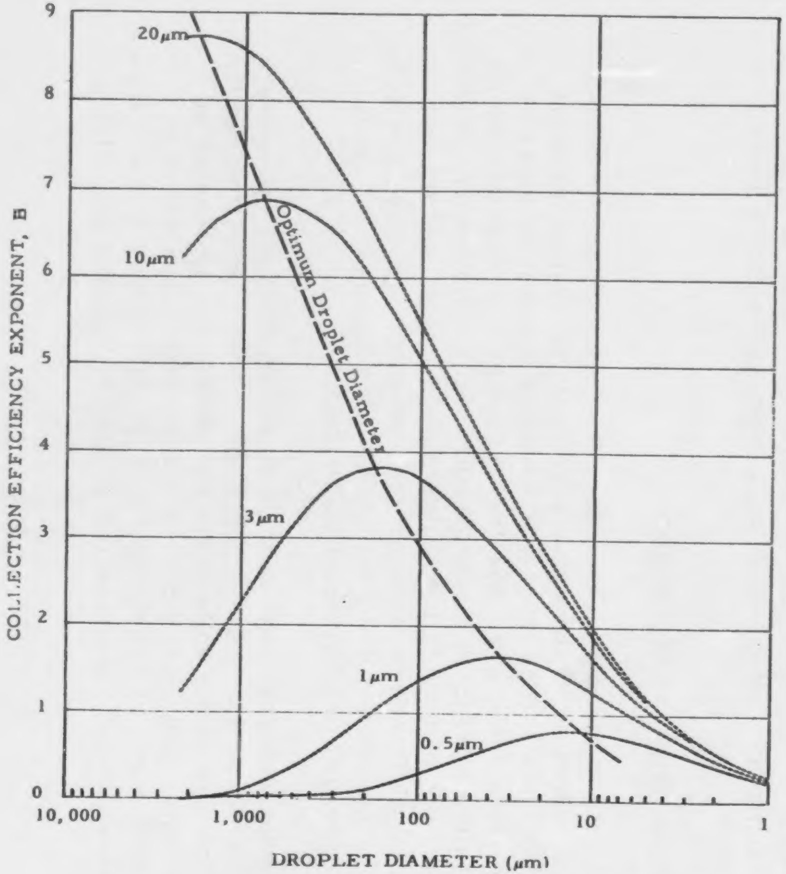

Figure 1. Scrubber droplet size for maximum collection efficiency, based on model 80 m/sec

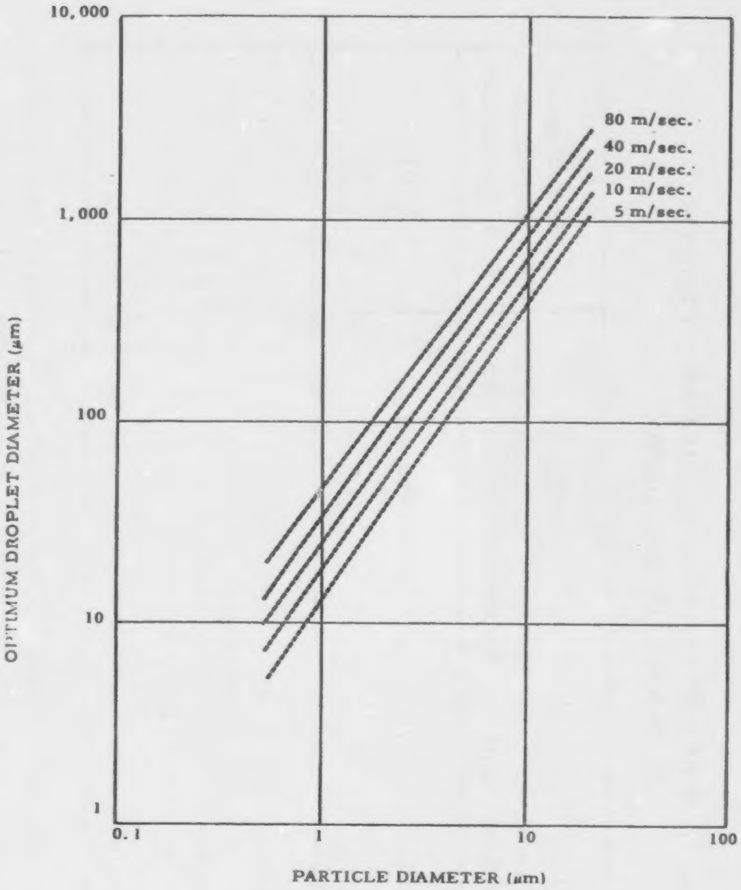

Figure 2. Scrubber droplet size for maximum collection efficiency, based on model, 5-80 m/sec

Table 1. EFFECT OF WATER SURFACE TENSION ON PARTICLE REMOVAL

D (Droplet Diameter Without Surfactant, μm)	D_s^* (Droplet Diameter With Surfactant Added, μm)	P_s Scrubber Penetration With Surfactant
205	144	0.011
144	102	0.013
51	36	0.021

Particle diameter, d = 1 μm
Gas velocity, V = 80 m/sec
Penetration without surfactant, P_o=0.02

* Assumes surface tension reduction from 72 to 30 dyne-cm.

These results indicate that if the droplets are initially larger than optimum, a reduction in size by addition of surfactant will improve particle removal efficiency. If the initial droplet size is optimum or smaller then optimum, addition of surfactant may actually reduce removal efficiency.

COALESCENCE AFTER COLLISION

After a particle and droplet collide, they may adhere or bounce apart. Adhesion requires attractive forces at the droplet-particle interface. Adhesive forces can be supplied by interfacial surface tension, other intermolecular forces (e.g., dipole or Van der Waals forces), chemical bonds, or electrostatic forces. Normally, particles being removed are relatively nonreactive chemically, and the net average electrostatic charge is near zero (even though some particles may be highly charged). Of the intermolecular forces that remain, surface tension appears to be most influential.

Reducing the surface tension of the water droplet may produce competing mechanisms that can affect coalescence. It will normally increase wettability of the solid particle, intuitively increasing adhesion probability, just as addition of detergent to wash water improves soil wettability and removal. It will also reduce the resistance to penetration by a particle (consider a particle striking an inflated balloon; a partially deflated balloon, equivalent to reduced surface tension, will allow deeper penetration).

The film thinning theory represents one model of the coalescence process. When a particle impacts a liquid droplet, the air film between them prevents immediate coalescence. The particle penetrates the droplet, being slowed by the surface tension and viscosity of the droplet. The particle then rebounds just as it might from the surface of a balloon, as long as the separating air film remains intact. If the film thins and ruptures before rebound, coalescence occurs and the particle is captured by the droplet.

The film thinning process is controlled by the viscosity of the air film and the time required for the particle to rebound after collision. Rebound time is influenced to some extent by surface tension of the droplet. Reduced surface tension produces lower elastic restoring force, greater particle penetration depth and therefore a longer, more circuitous escape path for the trapped air film. Reduction of surface tension could therefore lead to longer, not shorter, coalescence delay times, and therefore under some conditions, to reduced particle collection efficiency.

COALESCENCE EXPERIMENTS

The droplet-particle coalescence process was observed through a microscope using a high speed movie camera, Figure 3. The camera was a Beckman and Whitley Dynafax model, operated at a framing rate of 26,000 pictures/sec, with exposure times of 2.5 μsec/frame. Illumination was supplied by a xenon flash lamp through a fiber optic light pipe. Liquid droplets approximately 1000 μm diameter were suspended on a metering hypodermic syringe needle. Impacting particles were made by drawing a thin glass fiber from a rod and forming a bead on the end. Beads ranged from 10 to 4000 μm diameter and were supported by the thin fiber and rod, Figure 4. The rod was mounted on a motor driven carriage, Figure 5. Impact velocity was varied from 6 to 42 cm/sec by changing the motor gear ratio.

A 10 μm diameter particle moving at 42 cm/sec (0.42 μm/μsec) will move 10% of its diameter in approximately 2.5 μsec. Because a 10% movement will cause a blurred image during a photographic exposure, an exposure time of 2.5 μsec or less is required. A high intensity light source is required to provide sufficient illumination at these short exposure times, and a microscope is required to resolve the 10 μm diameter particles. Droplet surface tension was varied from

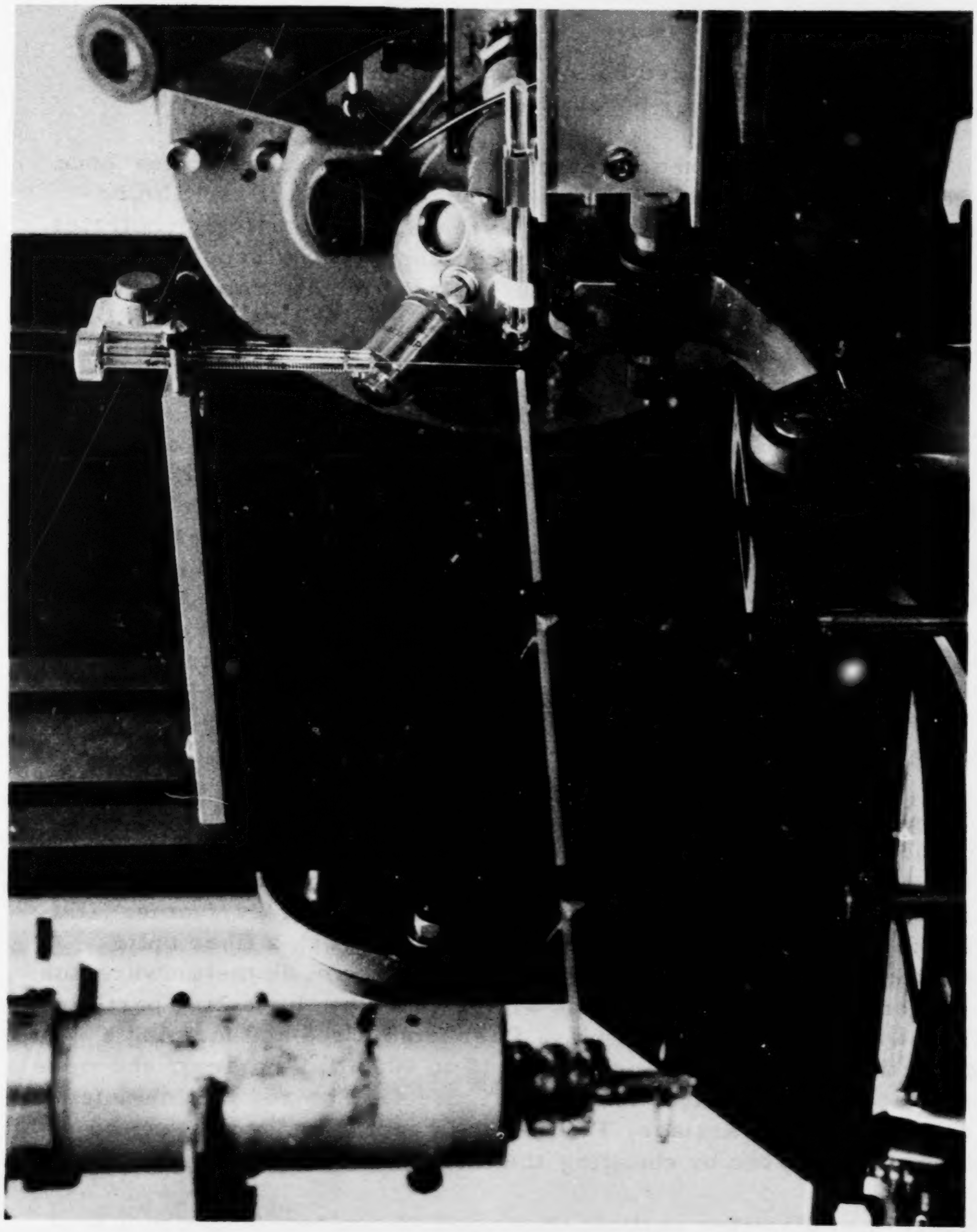

Figure 3. High speed camera used for coalescence delay time measurements

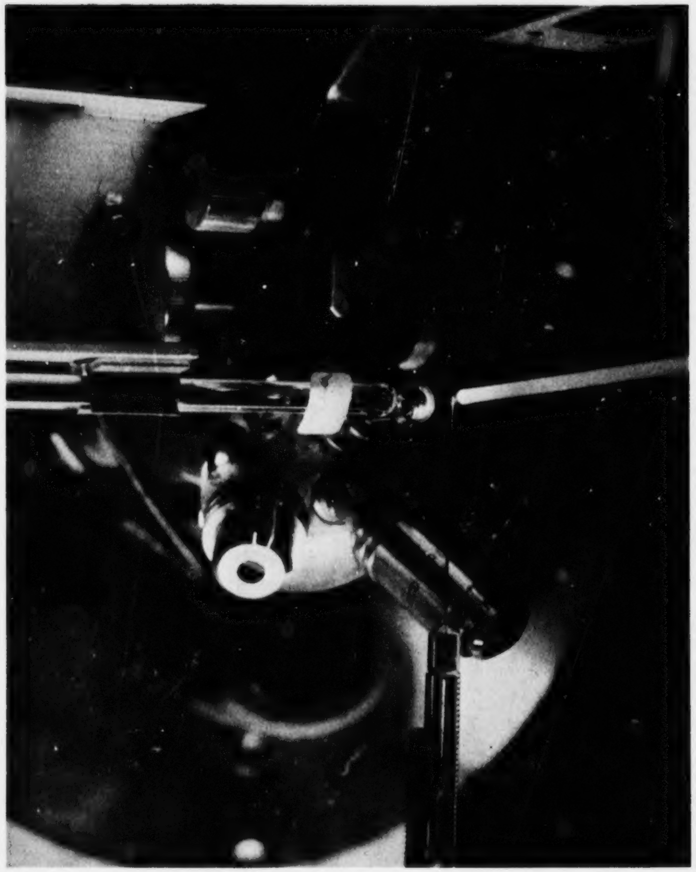

Figure 4. Glass support rod with simulated flyash particle mounted on traversing bed

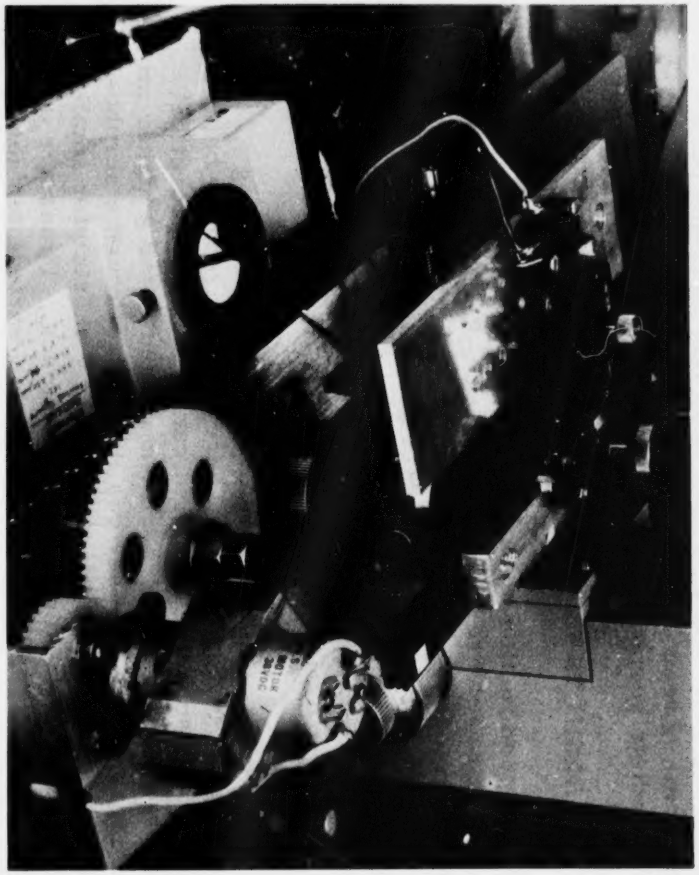

Figure 5. Motor driven particle traversing mechanism

17 to 72 dynes/cm by selecting a variety of liquids including pure water (72 dynes/cm), Freon TF (17 dynes/cm), and water-surfactant solutions (intermediate surface tensions).

EXPERIMENTAL RESULTS

Typical high speed motion picture sequences showing coalescence after impact at 42 cm/sec are given in Figures 6-9. Coalescence delay time was used as a measure of coalescence probability. Delay time is defined as the time between first contact and the time a liquid meniscus is first detectable. Formation of the meniscus is an indication that coalescence (wetting) has begun. It has been assumed that after wetting the particle will remain captured by the droplet.

Experimental results are compared with the film thinning theory[4,5] predictions in Figure 10. There is a discrepancy between the theory and the measured results, indicating that the theoretical model is probably incomplete. Experimental results for a higher impact velocity, representing a higher gas flow rate through a scrubber, are given in Figure 11. Delay times are slightly shorter for small particles, indicating improved collection efficiency. Times are unchanged for large particles. Results using a low surface tension liquid, Freon TF, are illustrated in Figure 12. There is a much wider random experimental variation in delay times when using Freon TF but average delay times are shorter, indicating slightly improved capture efficiency. Average delay times from Figures 10, 11, and 12 are compared in Figure 13.

CONCLUSIONS

Results indicate that under some conditions reduction in scrubber water surface tension can improve particle removal efficiency. The most direct effect is the reduction in spray droplet sizes. In cases where droplets are larger than optimum, some improvement in collection efficiency could be expected. In cases where droplets are already smaller than optimum, scrubber performance may be degraded. To determine whether an improvement can be made will require determination of existing droplet and particle sizes and operating conditions within the scrubber.

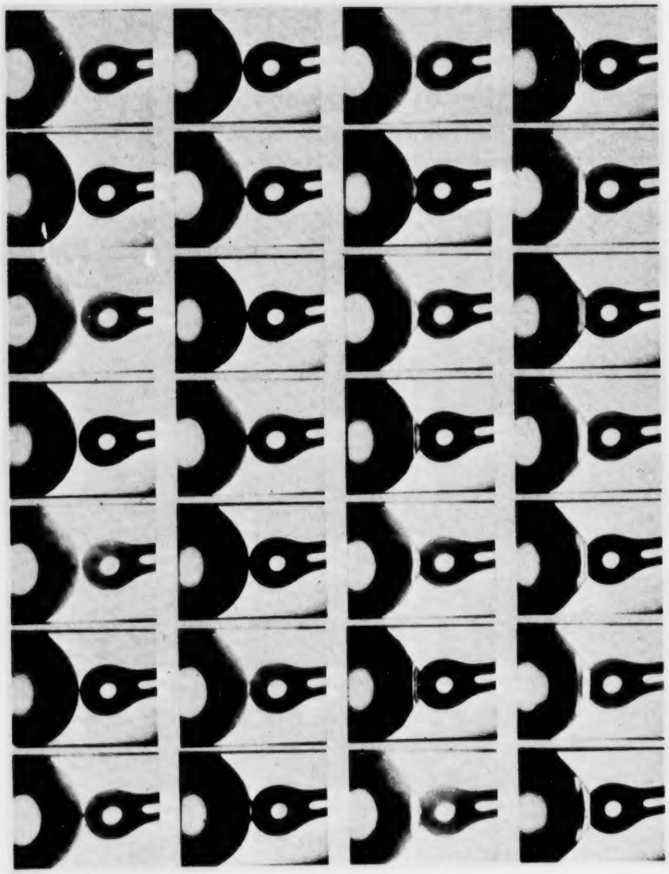

Figure 6. Coalescence of 725 μm diameter glass bead with water droplets, 234 μsec coalescence delay time

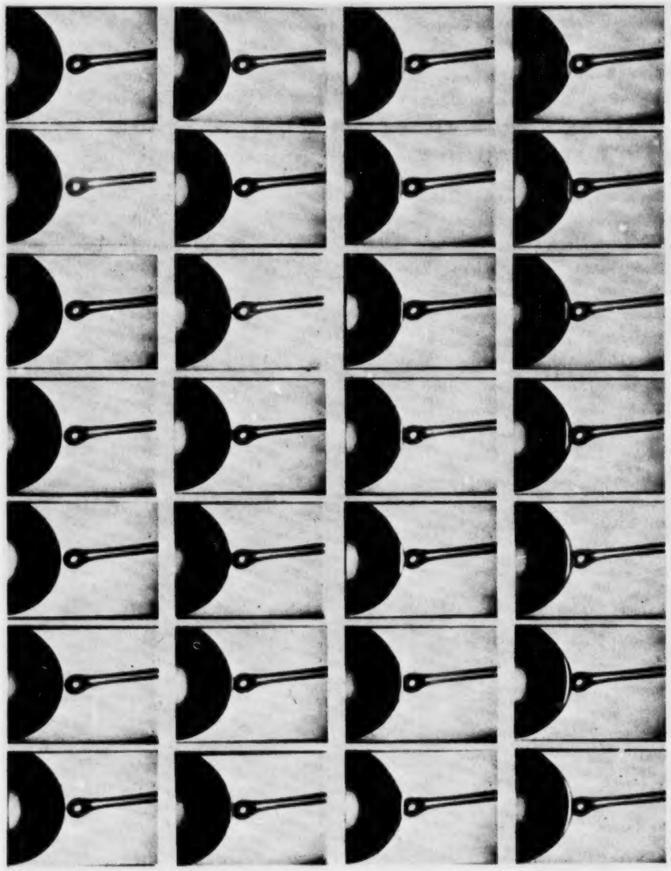

Figure 7. Coalescence of 275 μm diameter glass bead with water droplet, 117 μsec coalescence delay time

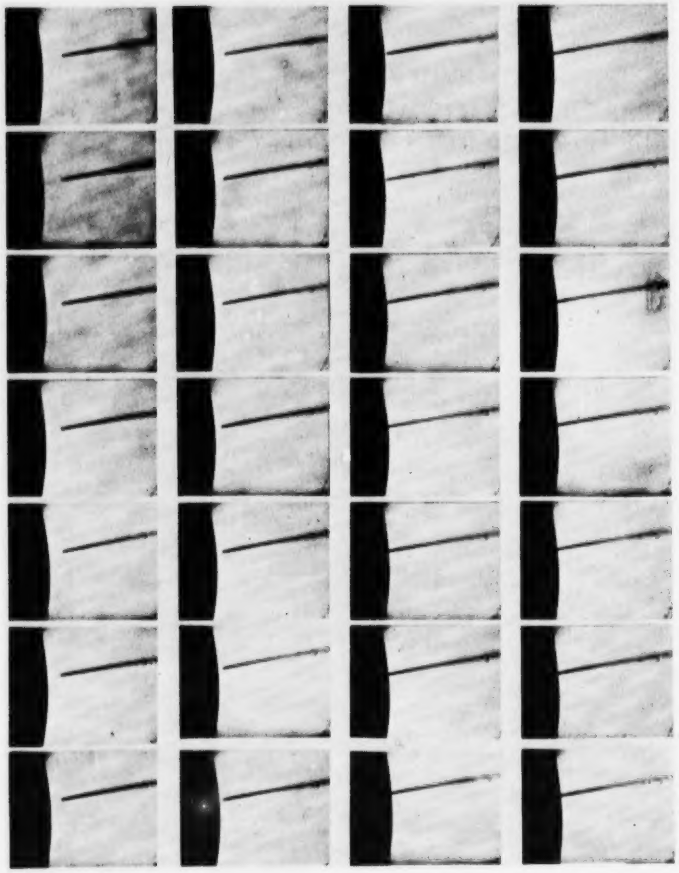

Figure 8. Coalescence of 10 μm diameter glass fiber with water droplet, <39 μsec coalescence delay time

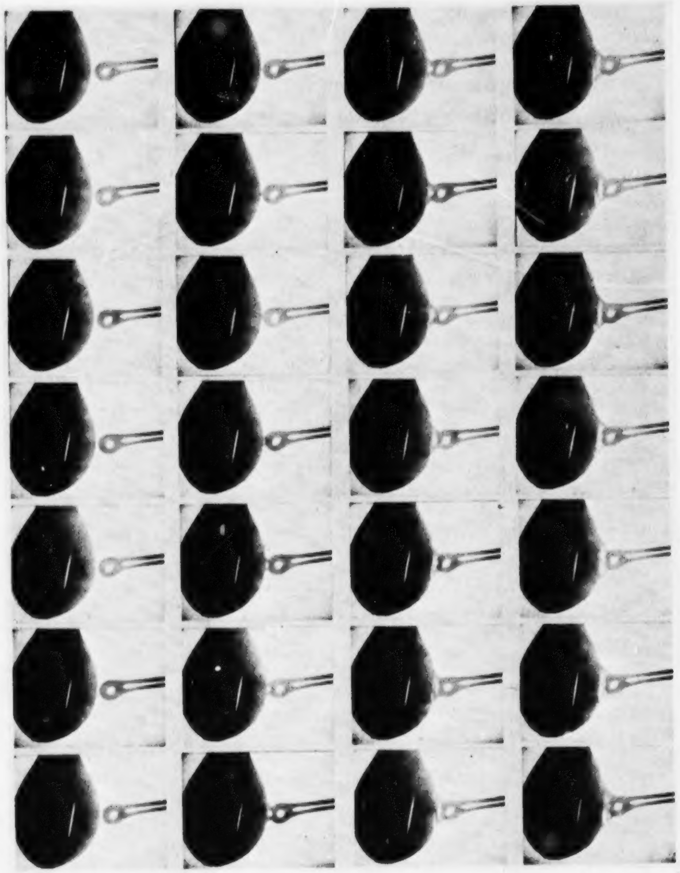

Figure 9. Coalescence of 275 μm diamter glass bead with Freon TF droplet <39 μsec coalescence delay time

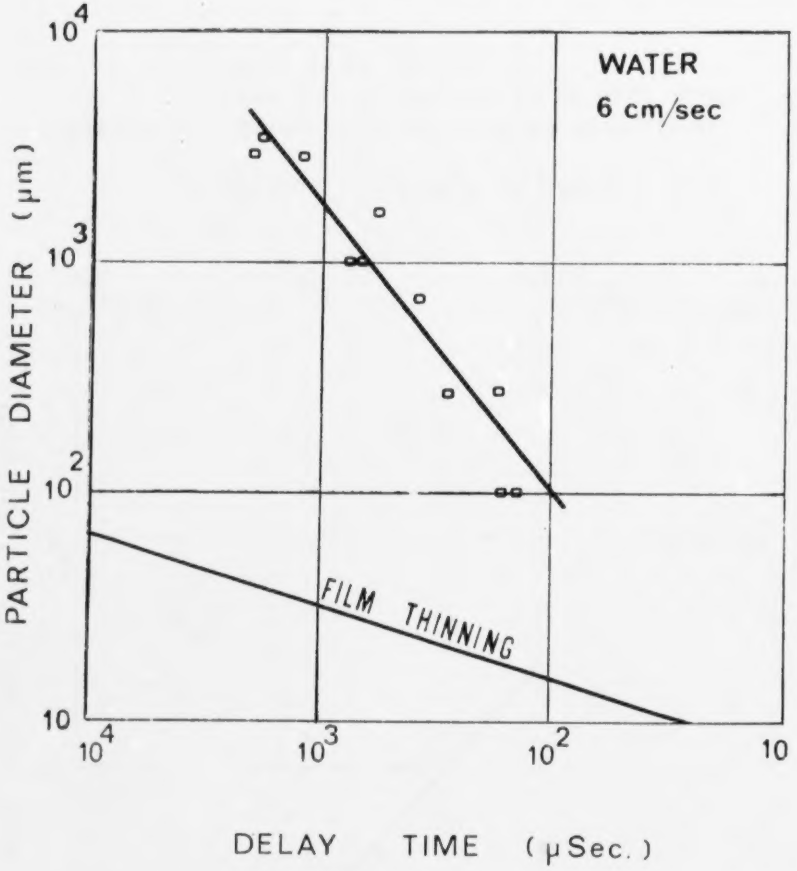

Figure 10. Comparison of film thinning theory predictions with experimental measurements for water with an impact velocity at 6 cm/sec

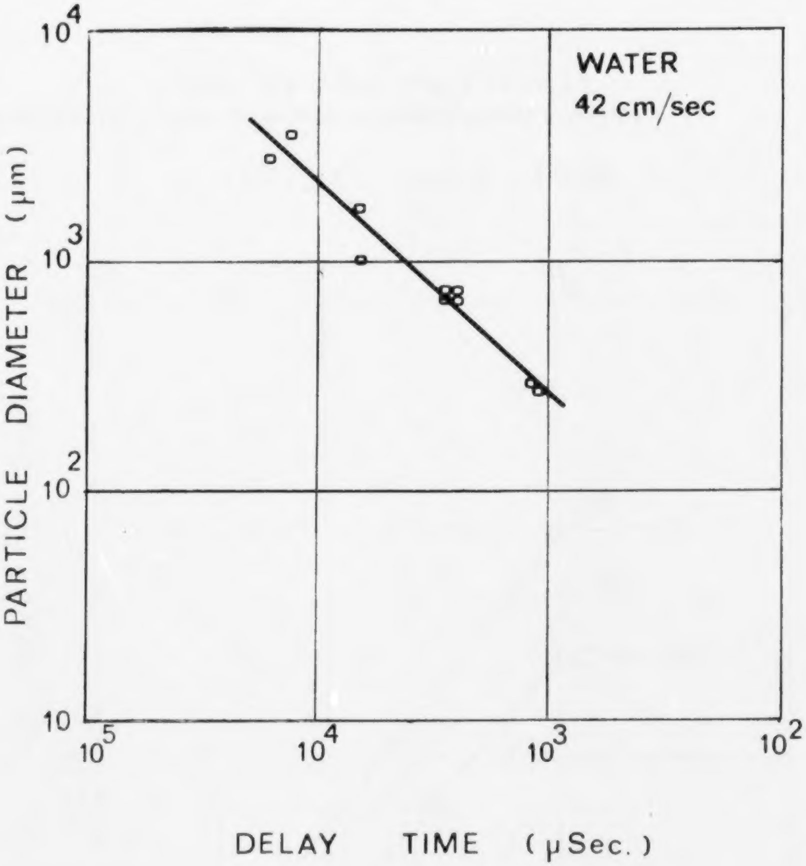

Figure 11. Measured coalescence delay times for water with an impact velocity at 42 cm/sec

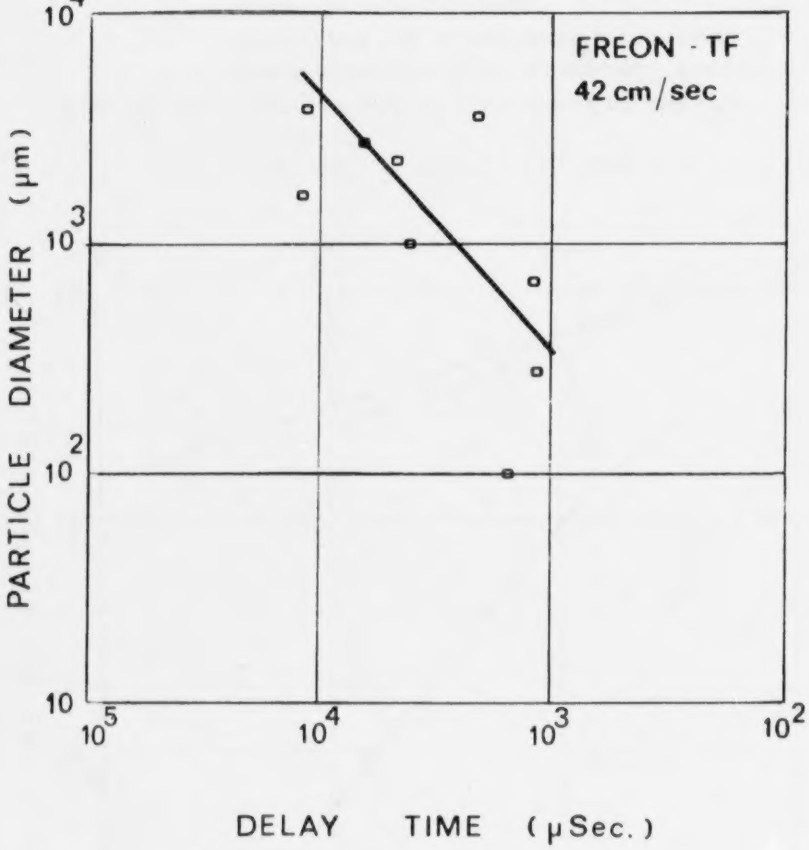

Figure 12. Measured coalescence delay time for Freon TF with an impact velocity at 42 cm/sec

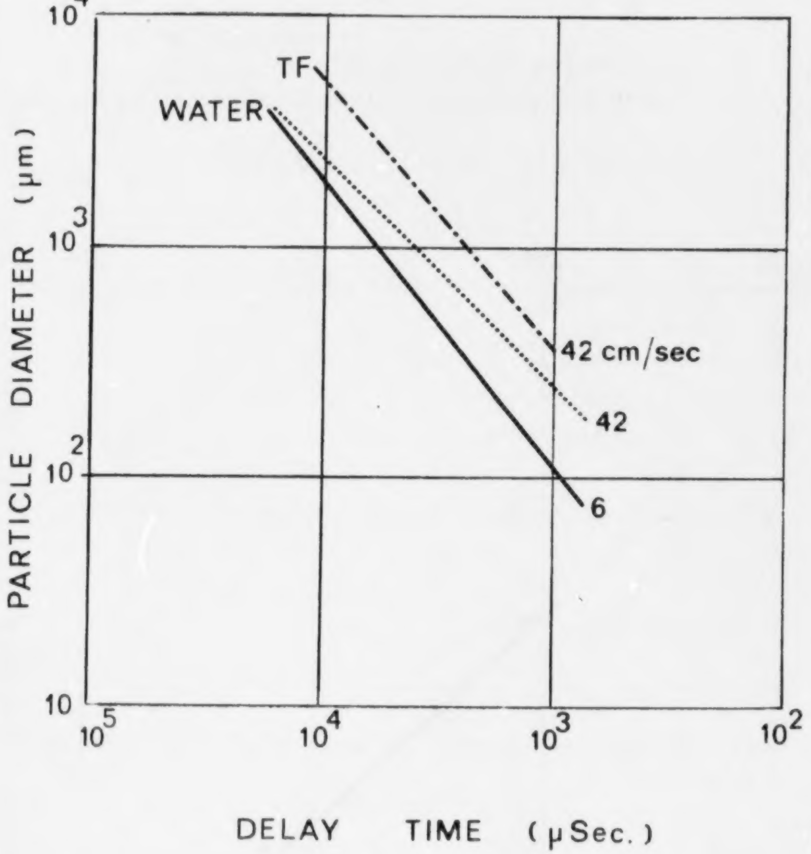

Figure 13. Comparison of coalescence delay times for water and Freon TF

REFERENCES

1. Nukiyama, S., and Y. Tanasawa, Trans. Soc. Mech. Eng. (Japan). 4, 86, 138 (1938); 5, 62, 68 (1939); 6, II-7 II-15 (1939); 6, II-18 (1940).

2. Wolfe, H. E., and W. H. Andersen, Kinetics, Mechanism, and Resultant Droplet Sizes of the Aerodynamic Breakup of Liquid Drops. Aerojet-General Corporation Report No. 0395-04 (18) SP, 1964.

3. Calvert, S., J. Goldschmid, D. Leith, and D. Mehta. "Scrubber Handbook." A. P. T., Inc. Riverside, California. EPA Contract No. CPA-70-95. NTIS # PB 213 016. August 1972.

4. Woffinden, G. W., G. R. Markowski, and D. S. Ensor, Effects of Interfacial Properties on Collection of Fine Particles by Wet Scrubbers, EPA Report No. 60017-78-097, June 1978.

5. Reynolds, O., Phil. Trans. Roy. Soc., A(177):157 1886.

CONCLUSIONS FROM EPA SCRUBBER R&D

Dale L. Harmon
Leslie E. Sparks
Particulate Technology Branch
Industrial Environmental Research Laboratory
Environmental Protection Agency
Research Triangle Park, N. C. 27711

ABSTRACT

The Particulate Technology Branch of the Industrial Environmental Research Laboratory of the Environmental Protection Agency has been engaged in a wet scrubber R&D program since 1970, beginning with a Wet Scrubber Systems Study which produced a thoroughly documented engineering handbook (Scrubber Handbook) suitable for scrubber design. This study was also designed to aid in future program development by setting forth the state-of-the-art. For the past several years, the broad objectives of the fine particle scrubber program has been to develop low pressure drop (30-50 cm water pressure drop) scrubber systems capable of collecting at least 90% by mass particles smaller than 3 μm in diameter. The major thrust of EPA's scrubber program has been aimed at development and demonstration of Flux Force/Condensation scrubbers. Development of improved entrainment separators and development of scrubber performance models are also major program areas. Most of the research and development planned for scrubber systems by EPA has been completed. This paper presents conclusions from the EPA wet scrubber R&D program.

INTRODUCTION

In 1970, the Environmental Protection Agency initiated a Wet Scrubber Systems Study to: evaluate current engineering technology, evaluate existing scrubber systems, investigate present usage problems,

Preceding page blank

determine potential new applications and develop specific research recommendations. The results of this study was the publication in 1972 of the "Scrubber Handbook"[1] and a "Final Report and Bibliography".[2] The Handbook was widely recognized as the most extensive and authoritative engineering text on the subject. The Final Report included research recommendations aimed at overcoming the identified deficiencies in the state-of-the-art. The proposed research plan reflected the need for better particulate capture efficiency of existing scrubbers, improved capabilities of future scrubbers, lower costs, and optimum application to specific processes.

Although the research plan was modified over the years, much of the research recommended in 1972 has been funded by EPA. The EPA-funded wet scrubber research generally falls into the following six areas:

Basic Scrubber Technology Development
Flux Force/Condensation Scrubber Development
Scrubber Performance Data Generation
Entrainment Separator Development
Novel Fine Particulate Control Device Evaluation and Development
Scrubber Performance Model Development

The EPA Wet Scrubber Research Program is approaching its final goal. The ongoing programs are maturing so that final reports covering EPA-funded research for most of the areas listed above have been issued or are in preparation.

DISCUSSION

The purpose of this paper is to summarize the conclusions from the EPA-funded research program which has been conducted from 1970 to the present. Conclusions from each of the above listed program areas will follow in the succeeding discussion and, in the summary, overall conclusions based on the total scrubber program will be given.

Basic Scrubber Technology Development

Theoretical bench scale experimental investigations[3,4,5] were carried out to investigate:

1) The ways in which energy consumption, liquid-to-gas ratio, and condensation of water vapor affect the collection efficiency of a conventional cocurrent-contact particulate scrubber of the orifice type.

2) The comparative performance of particulate scrubbers that draw contacting power for gas/liquid contacting from the gas stream and from the liquid stream.

3) The effects of surface tension on scrubber particle removal efficiency.

The test aerosol for the bench-scale experimental investigation for study 1) was composed of spherical particles of ammonium fluorescein with a mass median diameter of approximately 0.6 μm. The collection efficiency of the scrubber was determined and correlated as a function of the effective friction loss across the scrubber. In the absence of condensation or evaporation effects, the scrubber efficiency was dependent only upon effective friction loss, with no independent influences of gas velocity, liquid-to-gas ratio, or contactor orifice size, except possibly in the range of very low gas velocities, liquid-to-gas ratios, and pressure drops. Evaporation of large amounts of water reduced collection efficiencies, but scrubbing hot humid gas with cold water to produce condensation significantly increased the collection efficiency. The most favorable results were obtained by presaturating the hot humid gas stream before contacting it with cold water.

Three synthetic polydisperse test aerosols were used for the small pilot-scale experimental investigation for study 2). They had similar size distributions but different mass median particle diameters of 1.05, 0.68, and 0.42 μm, respectively. Different contactors were compared on the basis of collection efficiencies obtained at given levels of contacting power (power per unit of volumetric gas flow rate), using the performance of an orifice contactor as a reference level. The gas/liquid contactors investigated are summarized in Table 1.

A series contactor consisting of staggered multiple orifices in series, gave essentially the same performance as the single-orifice contactor at the higher contacting power levels but tended to give poorer performance at the lower power levels. This behavior was accentuated as the aerosol particle size decreased.

Five different pressure spray nozzles were tested, as was a sixth spray nozzle in combination with a single orifice. All these contactor configurations gave poorer performance than did the reference orifice scrubber at the same total contacting power. However, the deviation of the efficiency from the reference level proved to be a function of the fraction of the total contacting power that was derived from the liquid stream. The relative deviation of the spray scrubber efficiency from the reference level increased as the aerosol particle size decreased.

All the spray contactors but one gave very similar performances at comparable conditions despite radical differences in spray nozzle designs and spray configurations.

Table 1. GAS/LIQUID CONTACTORS[A]

Contactor	Orifice Diameter, cm	Spray Nozzle Type	Nozzle Position in Gas Line	Spray Orientation	Angle, °
Orifice	2.54 3.81				
Multiple orifices in series	3.36[B]				
Spray		Perforated tube (multiple perforations)	Concentric	Radial, crossflow	0
Spray		Flat spray	Sidewall	Crossflow	95
Spray		Full cone, wide angle	Concentric	Cocurrent	100
Spray		Deflected, hollow cone	Concentric	Radial, crossflow	180
Spray		Full cone, injector type	Concentric	Cocurrent	30
Spray and orifice	2.54 3.81	Full cone	Concentric	Cocurrent	60

[A] Gas line diameter is 5.84 cm.

[B] Diameter of circle having same area as semicircular orifice.

Study 3) was primarily a theoretical study with some bench scale tests for experimental verification. Results of the theoretical study indicate that changes in surface tension of wet scrubber liquids can either improve or degrade particle impaction efficiency, depending on particle size and scrubber operating conditions; however, changes are expected to be small.

Flux Force/Condensation Scrubber Development

One of the major areas of R&D recommended in the Wet Scrubber System Study[2] was to determine the improvements in fine particle capture which could be affected by application of diffusiophoretic and thermophoretic forces and by particle growth by condensation. Theories and equations describing these forces were found in the literature, but good reliable experimental data, to verify these theories, were meager.

The first EPA-funded Wet Scrubber R&D project following the Wet Scrubber System Study was a feasibility study of flux force/condensation (FF/C) scrubbing[6] for fine particle control. FF/C scrubbing includes the effects of diffusiophoresis, Stephan flow, thermophoresis, and particle growth due to the condensation of water vapor, and is not restricted to any specific scrubber configuration.

The results of the feasibility study showed that FF/C scrubbing is capable of high particle collection efficiency on fine particles and that, within some limitations, it is more economical than other means of particle collection. Mathematical modeling of the many simultaneous phenomena taking place in a FF/C scrubber was accomplished for some important unit mechanisms, although several coefficients remained to be fitted to experimental data.

Diffusiophoresis and inertial impaction enhancement by particle growth were found to be the two most important particle collection mechanisms involved in FF/C scrubbers; particle growth was the more important of the two.

Economic considerations define the most favorable area of application for FF/C scrubbing as those situations in which the enthalpy of vaporization is available from the gas to be cleaned, when high collection efficiencies are required for fine particles, when future capacity expansion is anticipated, or a combination of the three.

It appeared from this study that the most suitable scrubber types for FF/C application appear to be multi-stage or continuous contact.

Following the feasibility study, laboratory pilot-scale evaluations were completed for a multiple sieve plate scrubber[7] and a horizontal spray scrubber.[7,8]

The experimental study confirmed previous predictions of the technical feasibility of FF/C scrubbing. High collection efficiencies (95%) for fine particles can be achieved with a condensation ratio of about 0.15 g vapor condensed/g dry gas, in a FF/C scrubber.

Based on the experimental data, mathematical models and empirical design equations were described which can be used to scale-up FF/C scrubbers similar to those tested for specific industrial applications.

Following the laboratory pilot-scale evaluation, a pilot-scale demonstration of FF/C scrubbing for fine particle control was carried out on a secondary metal recovery furnace.[9] The scrubber was sized to treat the entire effluent stream, a maximum flow rate of 200 Am^3/min (7,000 ACFM) at temperatures up to 800°C. Demonstration plant performance was consistent with the preceding laboratory bench-scale and pilot-scale studies.

The nature of the source emissions entering the scrubber depended greatly on the type of scrap wire (being incinerated to remove the insulation from the copper wire and other metal scrap) and on the operating conditions. A conventional high energy scrubber would be incapable of controlling emissions at a practical pressure drop from anything but the premium grade of scrap. An FF/C scrubber system would be feasible for the control of lower (more polluting) grade scrap, the type of scrap which has more commercial importance.

The system was generally capable of about 90% to 95% efficiency on particles with a mass median aerodynamic diameter of 0.7 to 0.8 μmA (about 0.3 μm physical diameter for particles with a density of 4.0 g/cm^3). This efficiency was achieved with a 68 cm (27 in.) W.C. gas phase pressure drop. A conventional high energy scrubber without FF/C effects would require pressure drops of roughly 250 cm (98 in.) W. C. for 90% and 535 cm (210 in.) W.C. for 95% particle collection efficiency. Figure 1 shows a typical fractional penetration curve.

Because the efficiency and economics of FF/C scrubbing are sensitive to specific source characterizations, a second pilot-scale demonstration on an iron cupola is in process.

Scrubber Performance Data Generation

The EPA has tested at least 13 scrubbers of conventional design on a variety of particulate sources.[10,11,12,13,14,15,16] In general, the performance or efficiency of a scrubber drops off rather rapidly as the particle size decreases. The efficiency is directly related to the energy consumed by the scrubber. Table 2 summarizes the performance test program results.

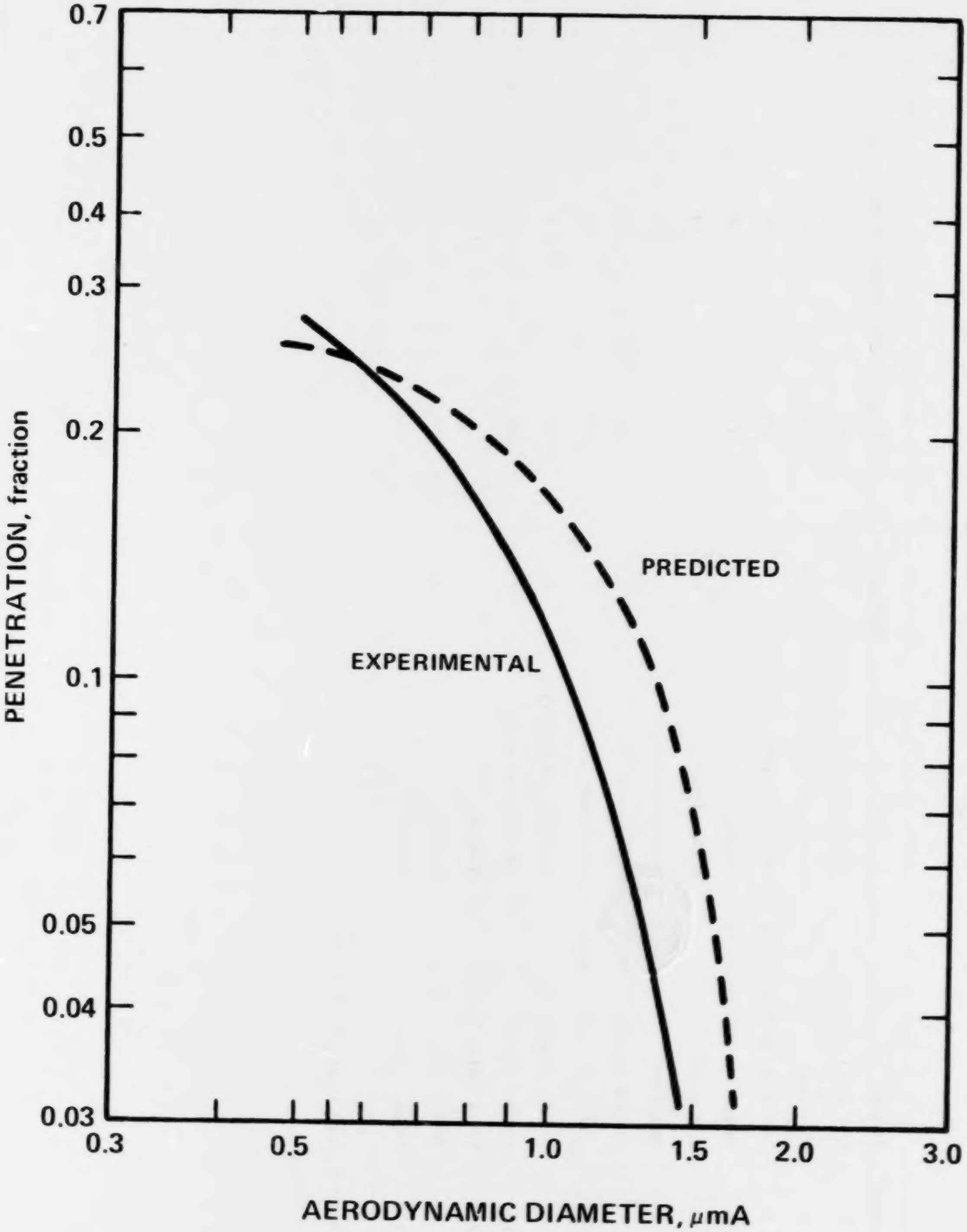

Figure 1. Particle penetration vs. aerodynamic diameter.

Table 2. PERFORMANCE TEST RESULTS

Number[A]	Source	Scrubber	Penetration, %	ΔP, cm	Mass Median Diameter, μm
1	Urea prilling tower	Valve tray	54	30	1.1
2	KCl dryer	Vaned centrifugal	3	8	> 100
3	Coal fired utility boiler	Mobile bed (TCA)	6	30	3.0
4	Coal fired utility boiler	Venturi	2.7	25	3.8
5	NaCl dryer	Wetted fiber	2.7	19	10
6	NaCl dryer	Impingement plate	10	30	> 100
7	Foundry cupola	Venturi rod	0.4	273	1.0
8	Coal fired utility boiler	Mobile bed (TCA)	8.1	22	9.0
9	Foundry cupola	Variable rod venturi	1.5	180	0.8
10	Foundry cupola	Gas-atomized spray	9.0	100	0.4
11	Borax fusing furnace	Venturi	2.5	110	1.0
12	Coal fired utility boiler	Venturi	0.7	46	20
13	Asphalt batch plant	Venturi	0.3	66	10

[A] Numbers cited in Figures 7 and 8.

Most of the scrubber tests were conducted to obtain reliable performance data for the validation of mathematical models for scrubber design. Scrubbers of several types on a variety of sources, including three very large power plant boilers, were studied: the results add significantly to our engineering ability. It is now possible to predict performance for fine particle collection with much more confidence than was possible prior to these evaluations.

Entrainment Separator Development

Because entrainment separation is as important as particle collection in a wet scrubber system, EPA funded a system study to define and advance the state-of-the-art of entrainment separator design and operation. Results of the study have been published.[17,18] Important conclusions from the study are given below.

The study indicates that available entrainment separators have various shortcomings. Examples are: overdesign, which necessitates large equipment size; low operating velocities due to flooding or reentrainment; unpredictable performance due to lack of reliable industrial operating data; and plugging by solids.

Mathematical models were developed for determining:

1) Primary collection efficiency in zigzag baffle type entrainment separators.
2) Pressure drop in zigzag baffle type separators.
3) Primary collection based on either complete turbulent mixing or no mixing.
4) Reentrainment in vertical zigzag baffles.
5) Reentrainment in horizontal zigzag baffles.
6) Reentrainment in a cyclone.
7) Solid deposition in zigzag baffles.

At low gas velocities (under industrial conditions), primary collection efficiency of knitted mesh, packed bed, tube bank, and cyclone entrainment separators can be predicted reasonably well, using mathematical models presented in the literature. The efficiency is not affected by the presence of solids in the entrainment as long as the solids deposited do not change the separator geometry significantly. The orientation of the separator has no effect on primary collection efficiency despite its effect on the liquid drainage capability and onset of reentrainment.

The capacity of an entrainment separator is limited by reentrainment which is a function of gas velocity, entrainment flow rate, and drainage. Thus, capacity can be defined in terms of these variables. Maximum gas velocity and liquid flow for negligible reentrainment have been determined experimentally for knitted mesh, tube bank, packed bed, and zigzag baffles. The liquid drainage capability of an entrainment separator has great effect on reentrainment velocity.

At high gas velocities, reentrainment is a definite problem. Reentrainment may take place by various mechanisms such as: a) transition from separated flow to separated-entrained flow, b) rupture of bubbles, c) creeping of liquid on the entrainment separator surface, and d) shattering of liquid drops resulting from splashing. Transition from separated flow to separated-entrained flow depends upon gas velocity, liquid Reynolds number, and liquid properties. The transition does not depend upon the duct dimensions. The drop size distribution is independent of the duct dimensions. The average drop diameter resulting from this transition is about 250 μm. The reentrainment velocity is considerably reduced if jets of air strike the liquid film at an angle. Therefore, sharp angles should be reduced to avoid reentrainment.

The mechanism of reentrainment in zagzag baffles is tearing of the liquid sheets (caused by high gas velocities) and shattering of liquid drops. Reentrainment in cross flow baffles with horizontal gas flow should be less than in baffles with vertical gas flow. Zigzag baffles inclined at 30° from gas flow direction should have less reentrainment than baffles inclined at 45° from horizontal gas flow direction. The reentrainment mechanisms in packed bed and mesh pad are shattering of drops and rupture of bubbles. Reentrainment resulting from small drops (less than 40 μm) due to rupture of bubbles is insignificant. The mass median drop diameter due to reentrainment was determined to vary between 80 μm and 750 μm. Large drops (above 200 μm) are present due to shattering of drops.

The pressure drop in zigzag baffles can be determined from drag coefficients for inclined plates held in the flow. The effect of liquid load on pressure drop is small. Pressure drop in tube banks can be predicted, using correlations from published literature relating to heat exchanger tube bundles. Generalized pressure drop correlation for packed beds predicts a higher pressure drop across the bed than that measured in this study. Pressure drop for knitted mesh depends on liquid velocity and gas velocity. The orientation of the separator has little effect on pressure drop and, except for knitted mesh, liquid entrainment increases the pressure drop only slightly.

The solids deposition rate depends largely on drop size and entrainment flow rate. Small drops cause a higher deposition rate than large drops. Deposition rate is higher on an inclined surface due to the increased settling rate of suspended solids. The empirical correlation of solid deposition rate, derived from small scale experiments, agrees fairly well with observations for baffles.

Additional work was funded to develop a superior entrainment separator and to better define solids deposition and washing needs. Although this current work is not complete it has progressed to the point that:

1. Mist carryover can be eliminated with a properly designed entrainment separator; i.e., scrubber performance is not limited by entrainment separation.
2. Solids buildup can be eliminated by proper washing.
3. Scaling can be eliminated by paying attention to system chemistry.

Novel Fine Particulate Control Device Evaluation and Development

Devices or dust collection systems based on new collection principles or on radical redesign of conventional collectors are sometimes offered by private developers. In the fall of 1973, EPA initiated a novel device evaluation program to identify, evaluate, and develop (where necessary) devices or systems which showed the most promise for high efficiency collection of fine particulate. (A novel particulate collection device is a device or a dust collection system--based on new collection principles or on radical redesign of conventional collectors--which is available for testing on pilot or full scale.)

More than 40 novel particulate collectors have been identified. About half of the devices identified have been of sufficient interest to justify a technical evaluation. To date, 13 devices have been either field or laboratory tested. Of the 13, 9 are scrubbers:[19,20,21,22,23,24,25,26,27,28]

Lone Star Steel - Steam Hydro Scrubber
R. P. Industries - Dynactor Scrubber
Aronetics - Two-Phase Wet Scrubber
Purity Corporation - Pentapure Impinger
Entoleter - Centrifield Scrubber
Andersen 2000 - CHEAF
Air Pollution Systems - Electrostatic Scrubber
Air Pollution Systems - Electro-Tube
Century Industrial Products - FRP-100 Low Energy Wet Scrubber

In addition, to these evaluations: a laboratory pilot scale evaluation of foam scrubbing has been completed;[29,30] a pilot scale

TRW Charged Droplet Scrubber has been designed, built, and demonstrated on a steel mill coke oven;[31,32,33] and a mobile University of Washington electrostatic scrubber has been built for tests on a variety of industrial sources.[34]

The only novel device scrubbers tested which have demonstrated a major improvement over conventional scrubbers are the electrostatically augmented scrubbers. Figure 2 compares fractional penetrations for the devices tested. The Steam-Hydro and Aronetics scrubbers have very high collection efficiencies but are also very high energy consumers. However, these two units can use waste heat to provide the required energy as was the case for both EPA sponsored tests.

Scrubber Performance Model Development

Performance models for several types of particulate scrubbers were developed by Calvert et al.[1] These models can predict scrubber pressure drop, particle penetration as a function of particle diameter, Pt(d), and overall penetration, Pt_o, for a given aerosol. The overall penetration is calculated by:

$$Pt_o = \int_0^\infty Pt(d)\ f(d)dd \tag{1}$$

where f(d) is the particle size distribution function.
Calvert et al. showed by solution of equation (1) for a log-normal size distribution that:

$$Pt_o = f(d_{50},\ d_g, \sigma) \tag{2}$$

where d_{50} is the scrubber cut diameter (the diameter with penetration of 50%),

d_g is the geometric mass mean diameter of the size distribution, and

σ is the geometric standard deviation of the size distribution.
Calvert et al. also showed that:

$$d_{50} = f\ (\Delta p) \tag{3}$$

where Δp is the pressure drop across the scrubber.
As discussed later, plots of d_{50} versus Δp are a convenient way of comparing the performance of different scrubbers.

Sparks has published an SR-52 programmable calculator program[35] based on Calvert's venturi scrubber model.[1] Yung et al.[36] have published a new venturi scrubber model which accounts for scrubber geometry and eliminates the need for empirical factors.

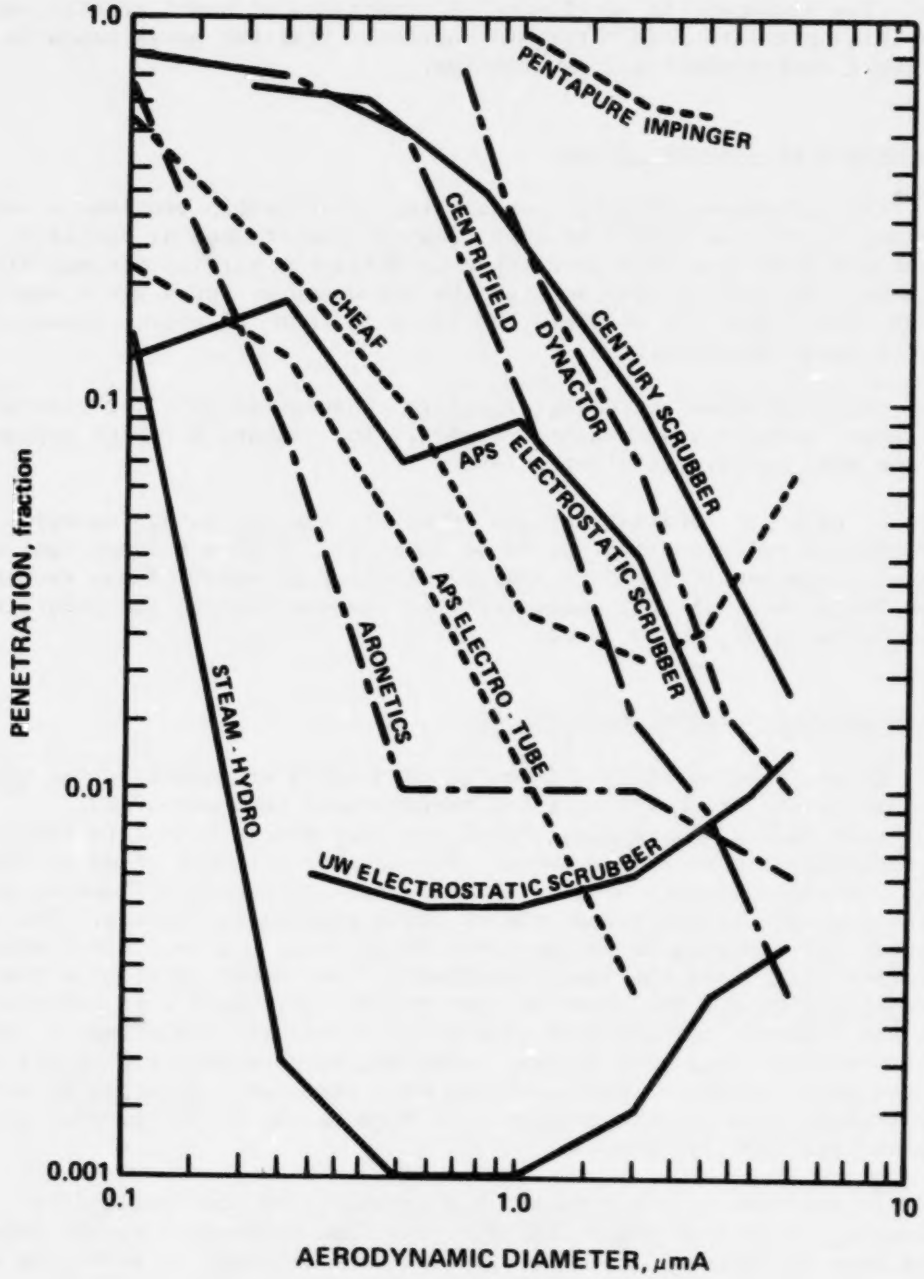

Figure 2. Penetration vs. particle size for novel devices tested by EPA.

In general, the scrubber models predict scrubber performance very well. Figures 3, 4, 5 and 6 compare the graded penetration curves predicted by the SR-52 venturi scrubber model with scrubber data for fly ash. The agreement is excellent. A comparison of model predictions for very high pressure drop scrubbers indicates that the model tends to slightly over-predict the penetration.

Comparison of Scrubber Types

The cut diameter/energy consumption relationship provides a convenient, first cut method of comparing the performance of different scrubbers even when data were taken on different particulate emission streams. In general, the smaller the cut diameter for a given energy input, the better the scrubber, at least in terms of energy consumed to give a given emission.

Figure 7 shows cut diameter/energy consumption data for several different scrubbers as measured by EPA. The venturi scrubber appears to be the most energy efficient scrubber.

If very low penetrations are required, the d_{90} or d_{95} energy consumption relationships should be compared. Figure 8 shows that the venturi scrubber is the most energy efficient scrubber. These results from field tests of full scale scrubber systems confirm the laboratory scale results of Semrau et al.[4]

Miscellaneous Scrubber Research

An engineering study and design of methods of scrubbing the exhaust of experimental rocket propulsion systems have been performed.[37,38] The study included an evaluation of the cost and technical feasibility of scrubbing the rocket exhausts. The exhaust products of major concern were hydrogen chloride and, to a lesser extent, hydrogen fluoride gases which result from the combustion of solid propellant rockets. The best process for removing these gases was found to be a gas-atomized spray scrubber which used the power supplied by the rocket to atomize the scrubbing liquid. Two types of gas-atomized scrubbers were designed: one was a conventional design similar to a venturi; the other, a low-cost unconventional open design, using neither pressure piping nor a ducted spray chamber. Cost analyses were made for both types of scrubbers for rockets with thrusts between 0.02 meganewtons (4,500 pounds) and 2 meganewtons (450,000 pounds).

In addition to the scrubber R&D sponsored by the Particulate Technology Branch of EPA's IERL-RTP, two Fine Particle Scrubber Symposia have been sponsored.[39,40] The symposia were intended to stimulate and generate new ideas for fine particle control using wet scrubbers, and to promote the transfer of technology to users.

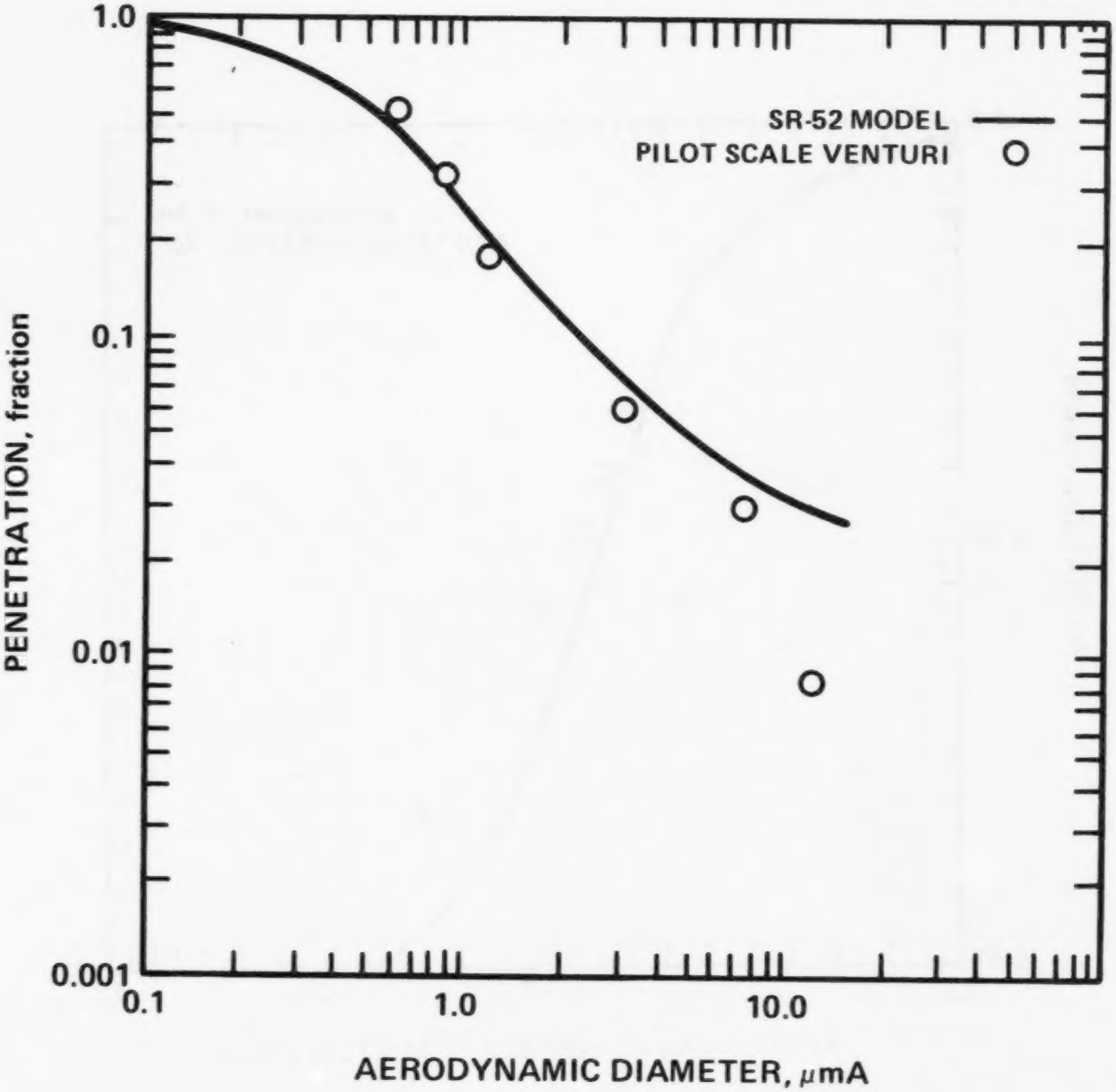

Figure 3. Comparison of graded penetration curve with a pilot scale venturi operating at a pressure drop of 27 cm w.c.

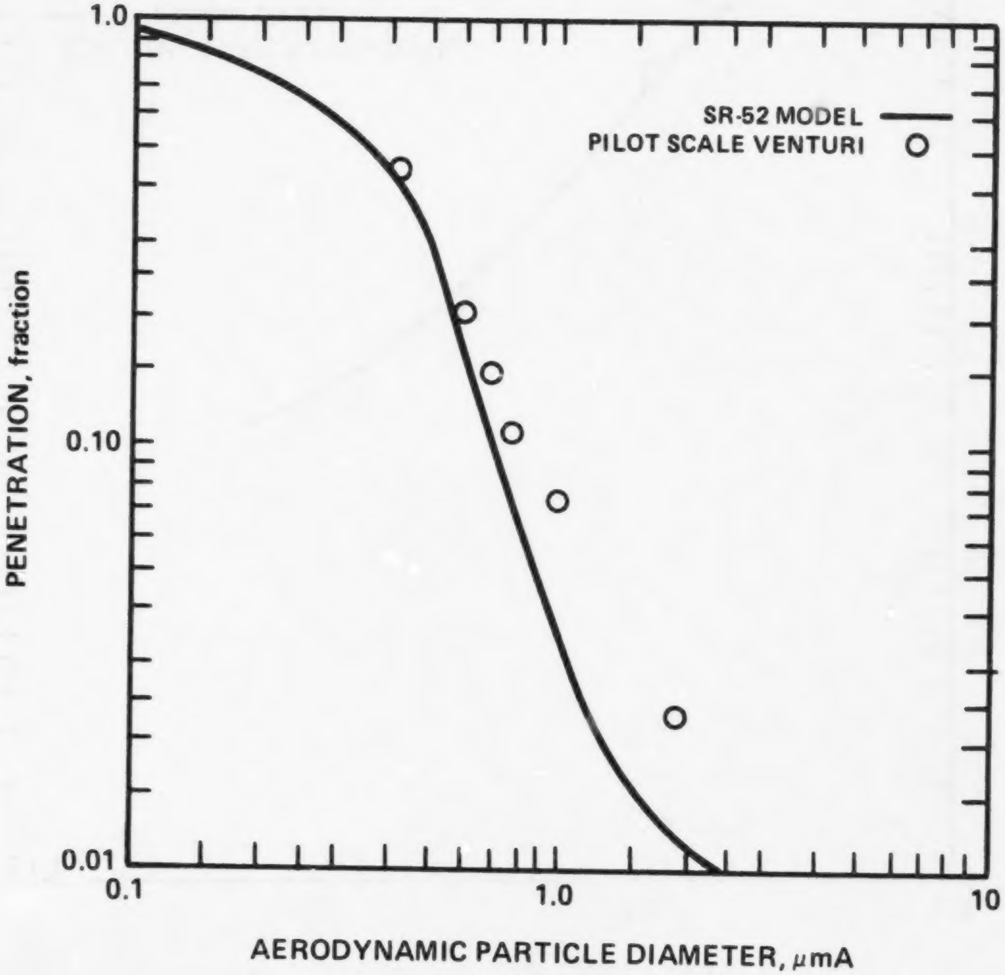

Figure 4. Comparison of graded penetration curve with a pilot scale venturi operating at a pressure drop of 40 cm w.c.

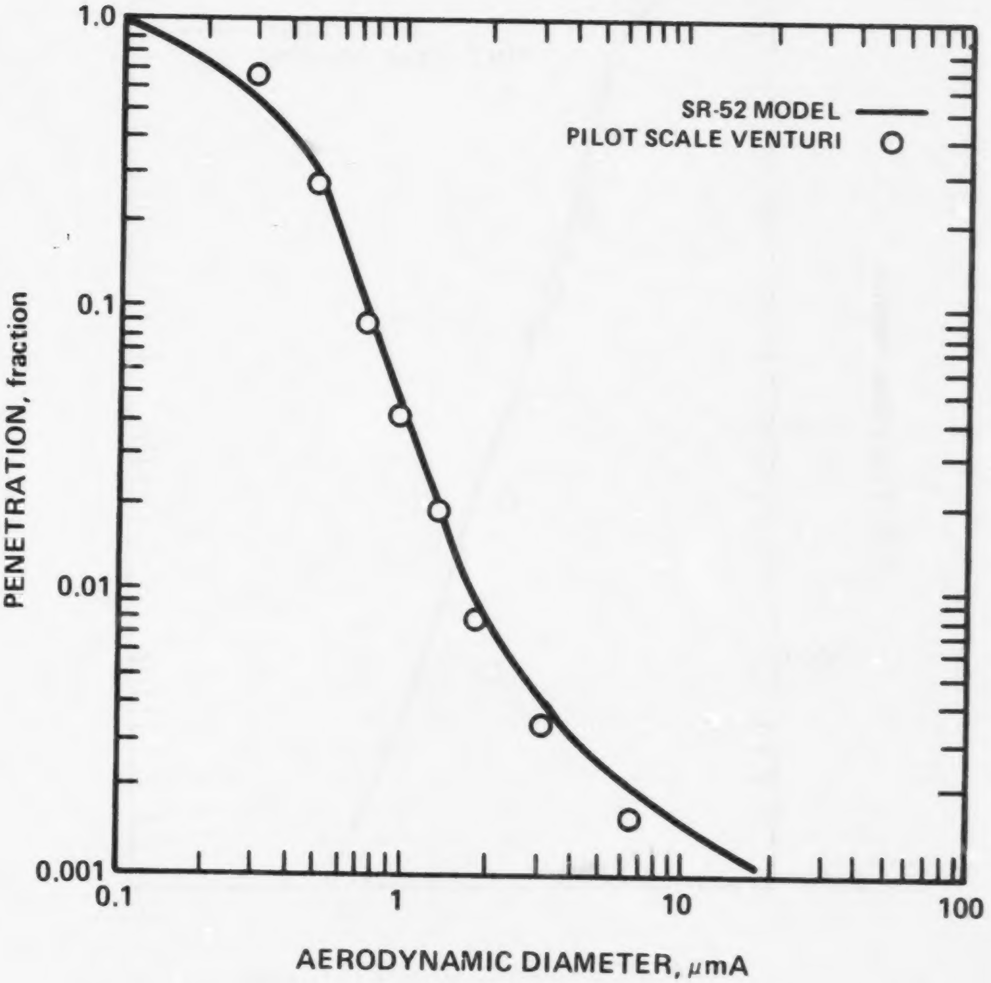

Figure 5. Comparison of graded penetration curve with a pilot scale venturi operating at a venturi pressure drop of 62 cm w.c.

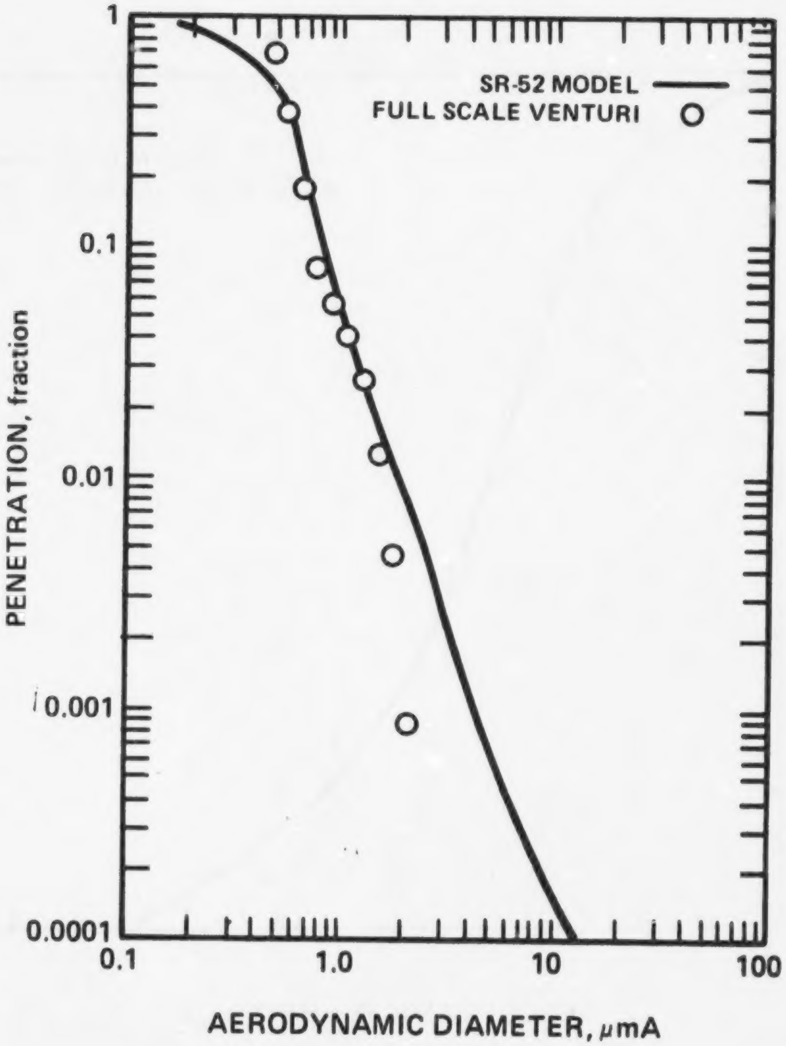

Figure 6. Comparison of graded penetration curve predicted by SR-52 program with field data for a variable throat venturi scrubber operating at a venturi pressure drop of 48 cm w.c. collecting fly ash.

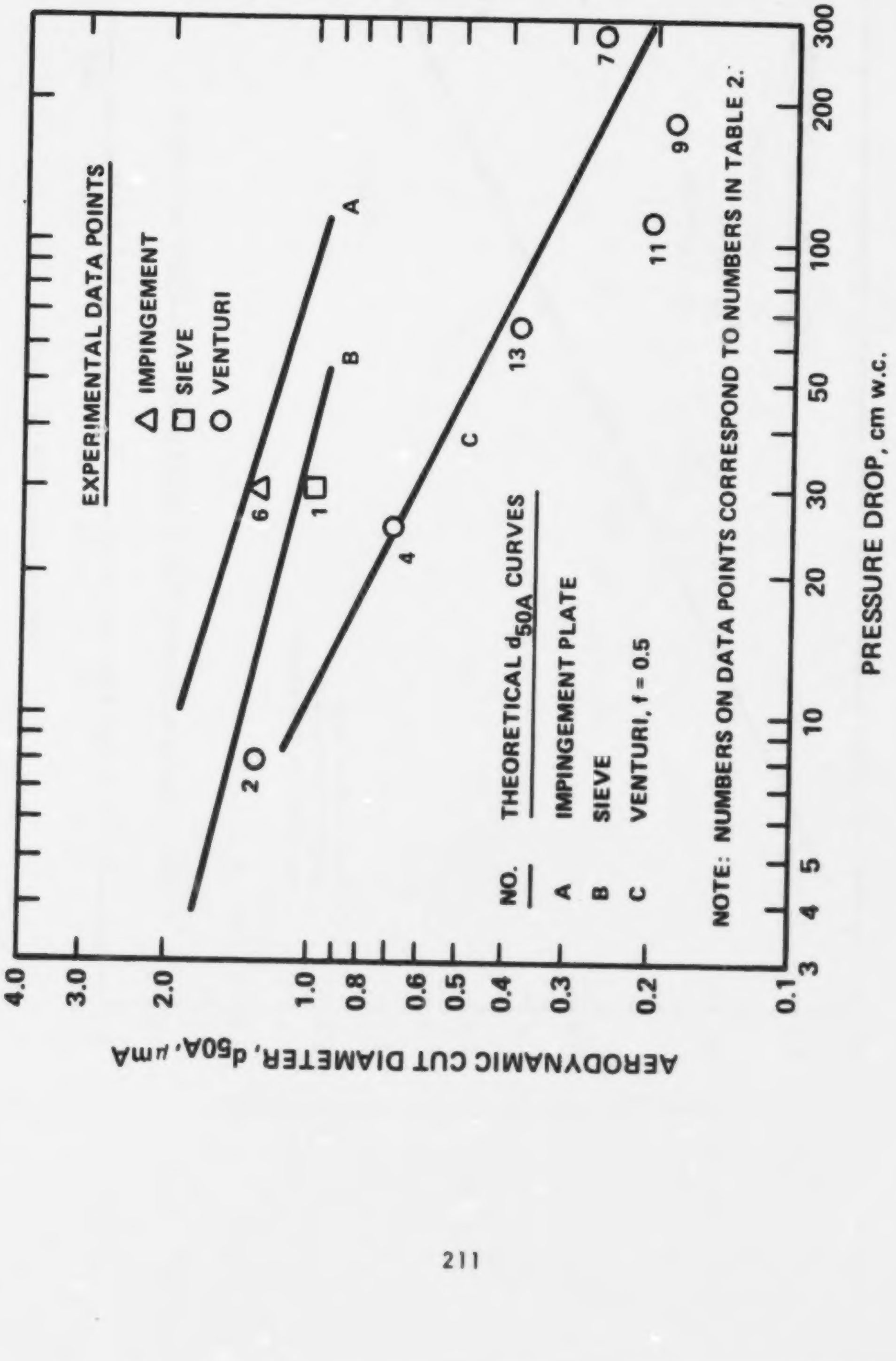

Figure 7. Theoretical and experimental cut diameters as a function of pressure drop for several scrubber types.

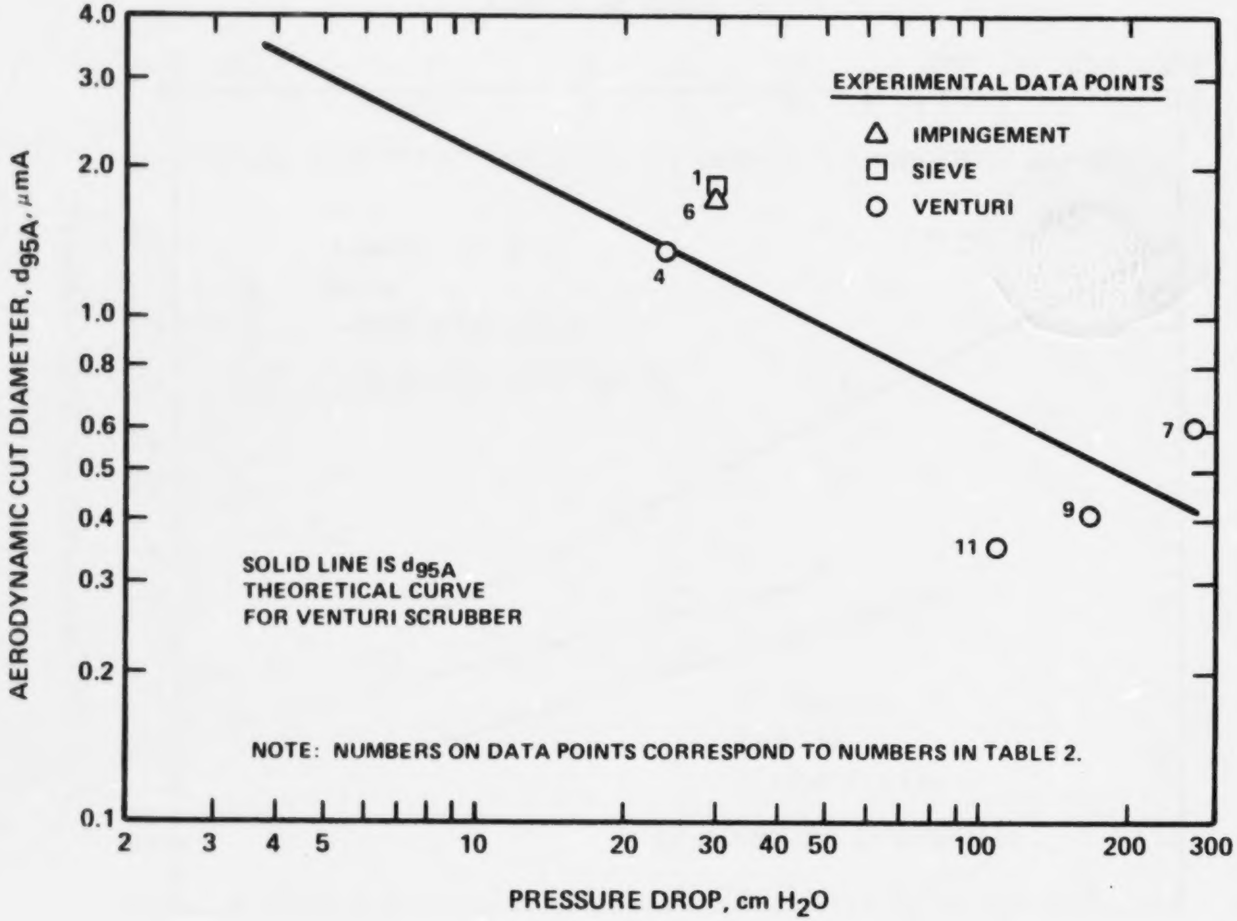

Figure 8. Theoretical and experimental cut diameters as a function of pressure drop for several scrubber types.

SUMMARY

The results of all EPA-sponsored particulate scrubber R&D support the following overall conclusions:

1) Particle collection in a scrubber is a function of both particle size distribution and the energy consumed by the scrubber.

2) Venturi types are the most energy efficient scrubbers.

3) Energy for particle collection should be introduced in a single stage for maximum energy efficiency.

4) Particle properties other than particle aerodynamic diameter have little, if any, effect on particle collection by a scrubber.

5) Scrubber performance is not limited by entrainment separation.

6) The scrubbing energy required to meet a given emission standard for a given particulate stream can be reduced only if the particles are grown or if forces other than inertial impaction are used to collect the particles.

7) Flux force/condensation scrubbing is a feasible way of introducing additional forces and of increasing particle size.

8) Electrostatic augmentation is an attractive method for introducing additional forces.

9) Available models are adequate for predicting scrubber system performance.

ACKNOWLEDGMENTS

The conclusions presented in this paper are based on EPA-supported work by numerous contractors. The authors express their appreciation to these contractors, particularly Air Pollution Technology, Inc. of San Diego, California, Stanford Research Institute of Menlo Park, California, and Meteorology Research, Inc. of Altadena, California, who were responsible for the major portion of the EPA R&D program.

REFERENCES

1. Calvert, S., Goldshmid, J., Leith, D. and Mehta, D., "Wet Scrubber System Study (Handbook) Vol. I," EPA-R2-72-118a, (NTIS No. PB 213-016), August 1972.

2. Calvert, S., Goldshmid, J. Leith, D. and Mehta, D., "Wet Scrubber System Study (Final Report and Bibliography) Vol. II," EPA-R2-72-118b, (NTIS No. PB 213-017), August 1972.

3. Semrau, K. and Witham, C. L., "Wet Scrubber Liquid Utilization," EPA-650/2-74-108, (NTIS No. PB 237-749/AS), October 1974.

4. Semrau, K. T., Whitham, C. L. and Kerlin, W.W., "Energy Utilization by Wet Scrubbers," EPA-600/2-77-234, (NTIS No. PB 276-435/AS), November 1977.

5. Woffinden, G. J., Markowski, G. R., and Ensor, D. S., "Effects of Interfacial Properties on Collection of Fine Particles by Wet Scrubbers," EPA-600/7-78-097, June 1978.

6. Calvert, S., Goldshmid, J., Leith, D., and Jhaveri, N. C., "Feasibility of Flux Force/Condensation Scrubbing for Fine Particulate Collection," EPA-650/2-73-036, (NTIS No. PB 227-307), October 1973.

7. Calvert, S., Jhaveri, N. C. and Huisking, T., "Study of Flux Force/Condensation Scrubbing of Fine Particles," EPA-600/2-75-018, (NTIS No. PB 249-297/AS), August 1975.

8. Calvert, S. and Yung, S. C., "Study of Horizontal-Spray Flux Force/Condensation Scrubber," EPA-600/2-76-200, (NTIS No. PB 262-669/AS), July 1976.

9. Calvert, S. and Gandhi, S., "Fine Particle Collection by a Flux Force/Condensation Scrubber: Pilot Demonstration," EPA-600/2-77-238, (NTIS No. PB 277-075/AS), December 1977.

10. Calvert, S., Jhaveri, N.C., and Yung, S., "Fine Particle Scrubber Performance Tests," EPA-650/2-74-093, (NTIS No. PB 240-325/AS), October 1974.

11. Ensor, D. S., Jackson, B. S., Calvert, S., Lake, C., Wallon, D. V., Nilon, R. E., Campbell, K. S., Cahill, T.A., and Flocchini, R.G., "Evaluation of a Particulate Scrubber on a Coal-Fired Utility Boiler," EPA-600/2-75-074, (NTIS No. PB 249-562/AS), November 1975.

12. Calvert, S., Barbarika, H. F., and Lake, C. F., "National Dust Collector Model 850 Variable Rod Module Venturi Scrubber Evaluation," EPA-600/2-76-282, (NTIS No. PB 263-617/AS), December 1976.

13. Calvert, S., Barbarika, H. F., and Monahan, G. M., "Gas-Atomized Spray Scrubber Evaluation," EPA-600/2-77-209a, (NTIS No. PB 274-449/AS), October 1977.

14. Calvert, S., Barbarika, H., and Monahan, G.M., "American Air Filter Kinpactor 10 X 56 Venturi Scrubber Evaluation," EPA-600/2-77-209b, (NTIS No. PB 276-716/AS), November 1977.

15. Calvert, S., Barbarika, H. F., and Monahan, G. M., "Evaluation of Three Industrial Particulate Scrubbers," EPA-600/2-78-032, (NTIS No. PB 279-572/AS), February 1978.

16. McCain, J. D., "CEA Variable-Throat Venturi Scrubber Evaluation," EPA-600/7-78-094, June 1978.

17. Calvert, S., Jashnani, I. L., Yung, S., and Stahlberg, S., "Entrainment Separators for Scrubbers - Initial Report," EPA-650/2-74-119a, (NTIS No. PB 241-189/AS), October 1974.

18. Calvert, S., Jashnani, I.L., Yung, S., and Stahlberg, S., "Entrainment Separators for Scrubbers-Final Report," EPA-650/2-74-119b, (NTIS No. PB 248-050/AS), August 1975.

19. McCain, J. D. and Smith, W. B., "Lone Star Steel Steam-Hydro Air Cleaning System Evaluation," EPA-650/2-74-028, (NTIS No. PB 232-436/AS), April 1974.

20. McCain, J. D., "Evaluation of Aronetics Two-Phase Jet Scrubber," EPA-650/2-74-129, (NTIS No. PB 239-422/AS), December 1974.

21. Cooper, D. W. and Anderson, D. P., "Dynactor Scrubber Evaluation," EPA-650/2-74-083a, (NTIS No. PB 243-365/AS), June 1975.

22. McCain, J. D., "Evaluation of Centrifield Scrubber," EPA-650/2-74-129a, (NTIS No. PB 243-626/AS), June 1975.

23. Cooper, D. W., Wang, R., and Anderson, D. P., "Evaluation of Eight Novel Fine Particle Collection Devices," EPA-600/2-76-035, (NTIS No. PB 251-621/AS), February 1976.

24. Calvert, S., Rowan, J., Yung, S., Lake, C., and Barbarika, H., "A.P.S. Electrostatic Scrubber Evaluation," EPA-600/2-76-154a, (NTIS No. PB 256-335/AS), June 1976.

25. Calvert, S., Christensen, C., and Lake, C., "A.P.S. Electro-Tube Evaluation," EPA-600/2-76-154b, (NTIS No. PB 258-824/AS), July 1976.

26. McCain, J. D., "Evaluations of Novel Particulate Control Devices," EPA-600/7-78-093, June 1978.

27. Ensor, D. S. and Hooper, R. G., "Century Industrial Products FRP-100 Wet Scrubber Evaluation," EPA-600/7-77-116, (NTIS No. PB 276-520/AS), October 1977.

28. Calvert, S., Yung, S. C., Barbarika, H., and Patterson, R.G., "Evaluation of Four Novel Fine Particulate Collection Devices," EPA-600/2-78-062, (NTIS No. PB 281-320/AS), March 1978.

29. Ctvrtnicek, T. E., Moscowitz, C. M., Walburg, T. F., and Yu, H.H.S., "Application of Foam Scrubbing to Fine Particle Control, Phase I," EPA-600/2-76-125, (NTIS No. PB 261-075/AS), May 1976.

30. Ramsey, G. H., "Evaluation of Foam Scrubbing as a Method for Collecting Fine Particulate," EPA-600/2-77-197, (NTIS No. PB 271-549/AS), September 1977.

31. Melcher, J. R., and Sachar, K. S., "Charged Droplet Scrubbing of Submicron Particulate," EPA-650/2-74-075, (NTIS No. PB 241-262/AS), August 1974.

32. Lear, C. W., "Charged Droplet Scrubber for Fine Particle Control: Laboratory Study," EPA-600/2-76-249a, (NTIS No. PB 258-823/AS), September 1976.

33. Krieve, W. F. and Bell, J. M., "Charged Droplet Scrubber for Fine Particle Control: Pilot Demonstration," EPA-600/2-76-249b, (NTIS No. PB 260-474/AS), September 1976.

34. Pilat, M. J. and Meyer, D. F., "University of Washington Electrostatic Spray Scrubber Evaluation," EPA-600/2-76-100, (NTIS No. PB 252-653/AS), April 1976.

35. Sparks, L. E., "SR-52 Programmable Calculator Programs for Venturi Scrubbers and Electrostatic Precipitators," EPA-600/7-78-026, (NTIS No. PB 277-672/AS), March 1978.

36. Yung, S. C., Calvert, S., and Barbarika, H. F., "Venturi Scrubber Performance Model," EPA-600/2-77-172, (NTIS No. PB 271-515/AS), August 1977.

37. Calvert, S. and Stalberg, S., "Evaluation of Systems for Control of Emissions from Rocket Motors-Phase I," EPA-600/2-75-021a, (NTIS No. PB 245-590), August 1975.

38. Barbarika, H. F. and Calvert S., "Design Criteria for Rocket Exhaust Scrubbers," EPA-600/7-78-057, (NTIS No. PB 282-255/AS), March 1978.

39. "EPA Fine Particle Scrubber Symposium (San Diego, 5/28-30/74)," EPA-650/2-74-112 (NTIS No. PB 239-335/AS), October 1974.

40. Calvert S., and Parker, R., "Second EPA Fine Particle Scrubber Symposium," EPA-600/2-77-193 (NTIS No. PB 273-828/AS), September 1977.

FINE PARTICLE EMISSION CONTROL BY HIGH GRADIENT MAGNETIC SEPARATION

Charles H. Gooding
Energy and Environmental Research Division
Research Triangle Institute
Research Triangle Park, N.C 27709

and

Dennis C. Drehmel
Industrial Environmental Research Laboratory
U.S. Environmental Protection Agency
Research Triangle Park, N.C. 27711

INTRODUCTION

Several widely used industrial processes, primarily in the iron and steel and ferroalloy industries, emit large quantities of waste gas containing magnetic particles. Particulate emissions from these processes are presently controlled with varying degrees of success by conventional technologies such as electrostatic precipitation, wet scrubbing, and fabric filtration. In the last decade research and commercial applications have demonstrated that high gradient magnetic separation (HGMS) is an effective and economical method of removing small, weakly magnetic particles from selected liquid streams.[1] Generalized theory and pilot-scale experimental results indicate that the process should also be applicable to the control of fine, magnetic particle emissions from industrial stacks.

BASIC CONCEPT OF THE PROCESS

In essence HGMS is an enhanced filtration process. The fundamental concept is the collection of small particles on ferromagnetic fibers that are immersed in a uniformly applied magnetic field. The ferromagnetic

Preceding page blank

fibers induce regions of highly non-uniform magnetic field intensity, and the particles are attracted to the fibers' surface by magnetic force.

In its most simple practical form, the high gradient magnetic separator consists of a canister packed with a fibrous, ferromagnetic material such as steel wool (Figure 1). The canister is located in a magnetic field that is normally generated by a solenoid, and the magnetic tractive force provides high-efficiency collection of particles as the gas passes through the canister. When the collection matrix becomes fully loaded, the magnetic force is removed and the particles may be flushed from the matrix with a pulse of air. This can be accomplished by using a system of several modules, each similar to the one depicted in Figure 1, in parallel-flow, cyclic operation. That is, each module provides filtration for a predetermined time interval. Then the flow is diverted to other modules; the magnetic field of the loaded module is deenergized; the matrix is cleaned; the field is reenergized; and the module is ready for reuse. An alternative scheme, which results in zero downtime of the available magnetized volume, is to construct the magnet and matrix so that the loaded matrix can be removed from the magnetized region into a non-magnetized cleaning region and continuously replaced by a clean matrix without interrupting the filtration process. Both cyclic and continuous systems are now commercially available.

High gradient magnetic separation is widely used on a commercial scale in the clay industry to remove fine paramagnetic color bodies from slurries of kaolin.[1] Laboratory and pilot-scale investigations have been conducted by several groups to assess other liquid system applications in mineral processing[2,3], wastewater treatment[3], and coal cleaning.[4,5,6] Several of these programs are current, and other commercial applications of HGMS seem likely to occur over the next few years.

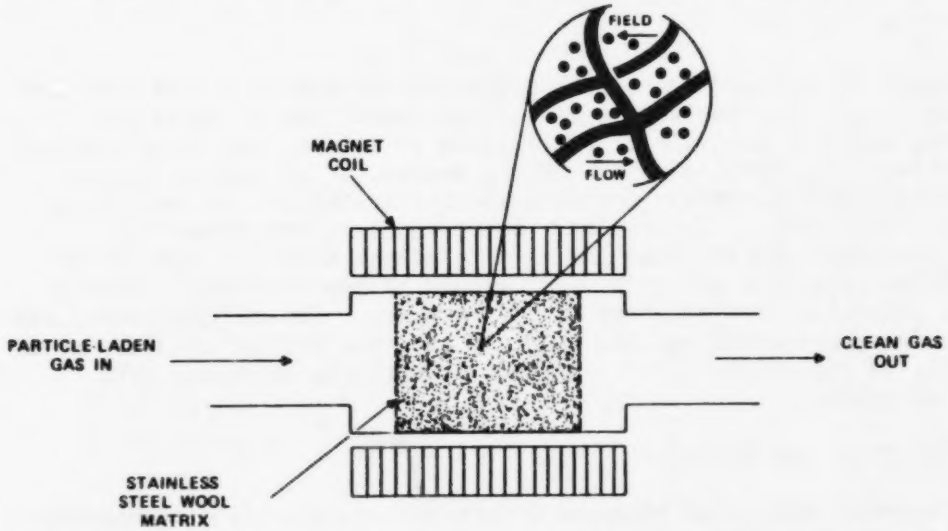

Figure 1. Schematic representation of a high gradient magnetic separator.

POTENTIAL APPLICATIONS FOR FINE PARTICLE CONTROL

With current magnet technology the capital costs and power requirements of large solenoids make HGMS potentially competitive with other particulate control methods. Since the filtration process is enhanced by the magnetic force, the void volume of the collection matrix can be much larger than in a conventional filter, allowing very high gas velocities at relatively low pressure drops. This combination translates into a potential reduction in energy requirements compared to conventional particulate control techniques, even though production of the magnetic field requires some energy. High operating velocities help to reduce both the capital costs and space requirements of the equipment. Furthermore, because the process as developed up to this stage is completely dry, it should avoid the water pollution problems associated with some scrubber installations. Magnetic stainless steels of the 400 series can be used as a collection matrix to make the process compatible with high temperature and corrosive environments. The absence of any sparking mechanism in the collection process should allow its application in combustible gas streams.

The magnetic susceptibility and size distribution of the dust particles are the key parameters that will determine the practicality of fine particle emission control applications, although other gas characteristics could affect economics to a lesser extent. Magnetic susceptibility of particulate matter cannot be predicted quantitatively from composition data alone, but the percentage of iron is a qualitative indicator. With relatively high iron concentrations even submicron particles can be collected efficiently and economically. Reported data on the particle size distribution and composition of dusts emitted from several processes in the iron and steel industry are shown in Table 1. Emissions from ferroalloy processes are much more diverse, but the production of several alloys (including silicomanganese, ferromanganese, and ferrochrome) results in the emission of particulates containing significant quantities of iron as well as other strongly magnetic species. All of these processes should be considered potential candidates for HGMS fine particle control.

DESCRIPTION OF COMPLETED EXPERIMENTAL WORK

The competitive methods of particulate emission control delineate practical constraints on the design of an HGMS device for stack gas applications. Technology currently is available to control particulate emissions from most industrial sources with a capital investment for uninstalled primary equipment no greater than \$8500 per cubic meter of gas flow per second (\$4/cfm). Power consumption is normally less than 3.2 kJ/m^3 (2.0 hp/1000 cfm) in precipitators and fabric filters, but can be many times greater in difficult applications where high-energy wet scrubbers must be employed. These general criteria and the cost and power requirements of conventional HGMS equipment indicate that an HGMS control device would most likely have to operate satisfactorily with a

Table 1. EXPECTED CHARACTERISTICS OF UNCONTROLLED GAS STREAMS FROM SEVERAL PROCESSES

Process	Dust Concentration g/m^3	Mass Median Diameter μm	Iron Compsition % Total Fe	Noteworthy Gas Characteristics
Sinter Machine				
Windbox	1-2	10	25-50	5-15% H_2O, hydrocarbons, flourides, SO_x, 120-180°C
Discharge End	5-12	10	25-50	120-180°C
Blast Furnace	10-25	100	35-50	20-40% CO, 2-6% H_2, 200-300°C
Basic Oxygen Furnace				
Open System	10-25	1	55-70	250-300°C
Closed System	40-70	15	55-70	75% CO, 250-300°C
Electric Arc Furnace	0.2-7	1	15-40	40-120°C
Open Hearth Furnace	4-7	5	55-70	7-15% H_2O, 250-350°C
Scarfing Machine	0.5-1	0.5	50-70	H_2O saturated, 50-60°C

superficial gas velocity of at least 5 m/s (1000 ft/min), a pressure drop of less than 2.0 kPa (8 inches H_2O), and an applied magnetic field of less than 1.0 T in order to be competitive with other control methods in most applications.

At the beginning of this study bench-scale experiments were conducted to gain a preliminary evaluation of the practicality of the process. Dust from an industrial basic oxygen steelmaking furnace (BOF) was dispersed in an air stream and passed through a loosely packed steel wool matrix in an 8.9-cm diameter canister in the bore of an iron-bound solenoid. With the unit operating with superficial gas velocities up to 10.6 m/s (2100 ft/min), high efficiency collection of dust was achieved with applied fields of 0.3 T or lower. Pressure drop through the matrix was normally less than 2.5 kPa (10 inches H_2O). Figure 2 shows the dramatic reduction in the penetration of particles through the matrix when relatively low magnetic fields were applied. These preliminary experiments confirmed that the HGMS process could be successfully applied to collect gas-borne particles and provided data from which a larger unit and a more systematic experiment were designed.

The layout of the second-phase, pilot-scale HGMS system is depicted schematically in Figure 3. Dust from a BOF was dispersed into a wind tunnel, and a 2500 m^3/hr (1500 cfm) slipstream was drawn off and processed through the HGMS pilot plant. A low efficiency cyclone, upstream of the HGMS, removed uncharacteristically large agglomerates that were not adequately broken up by the dispersion system. The magnetic separator consisted of an iron-bound solenoid surrounding a 30-cm diameter canister of loosely packed 430 stainless steel wool. Ranges of the experimental operating parameters are given in Table II. Tests were also conducted with dust from an electric arc steelmaking furnace (EAF) and most recently with dust from a sinter plant. The BOF and EAF experiments were systematically designed so that the effects of individual parameters could be studied. Experimentally determined magnetization curves for the three dusts are shown in Figure 4.

TABLE II. RANGES OF OPERATING PARAMETERS IN HGMS EXPERIMENTS.

Applied Field	0-0.5 T
Matrix Packing Density	0.005-0.010
Matrix Length	15-30 cm
Superficial Gas Velocity	4.9-11.1 m/s (970-2185 ft/min)
Gas Temperature	25-130°C

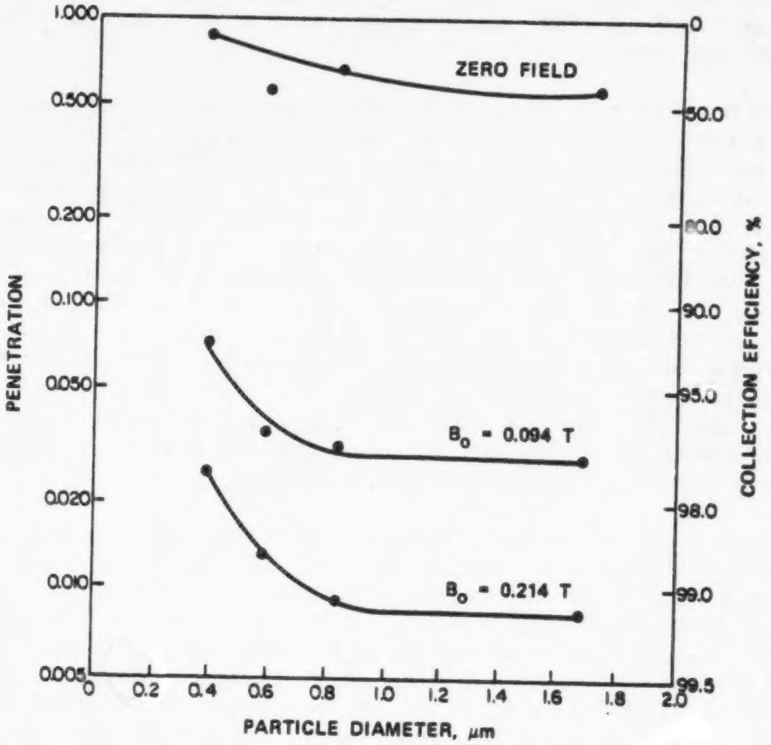

Figure 2. Bench-scale collection of BOF dust with a gas velocity of 8.4 m/s (1650 ft/min) and a pressure drop of 1.7 kPa (6.7 inches water).

After the operating conditions were established for a particular run, the fractional penetration of dust particles through the HGMS was determined as a function of particle size by using cascade inertial impactors to measure the concentration and size distribution of the dust upstream and downstream of the matrix. Since the impactors required approximately 90 minutes to collect an adequate sample, an optical (light-scattering) particle sizing device was also used to ensure that no significant upsets or transients occurred during the impactor sampling period.

PILOT-PLANT EXPERIMENTAL RESULTS FOR TWO DUSTS

The experimental efficiency with which the BOF and EAF dusts were collected under identical operating conditions is shown in Figure 5. As expected, the more strongly magnetic BOF dust was collected more efficiently than the EAF dust. The curves of Figure 5 are predictions of a theoretical model. Basically the model predicts single-fiber collec-

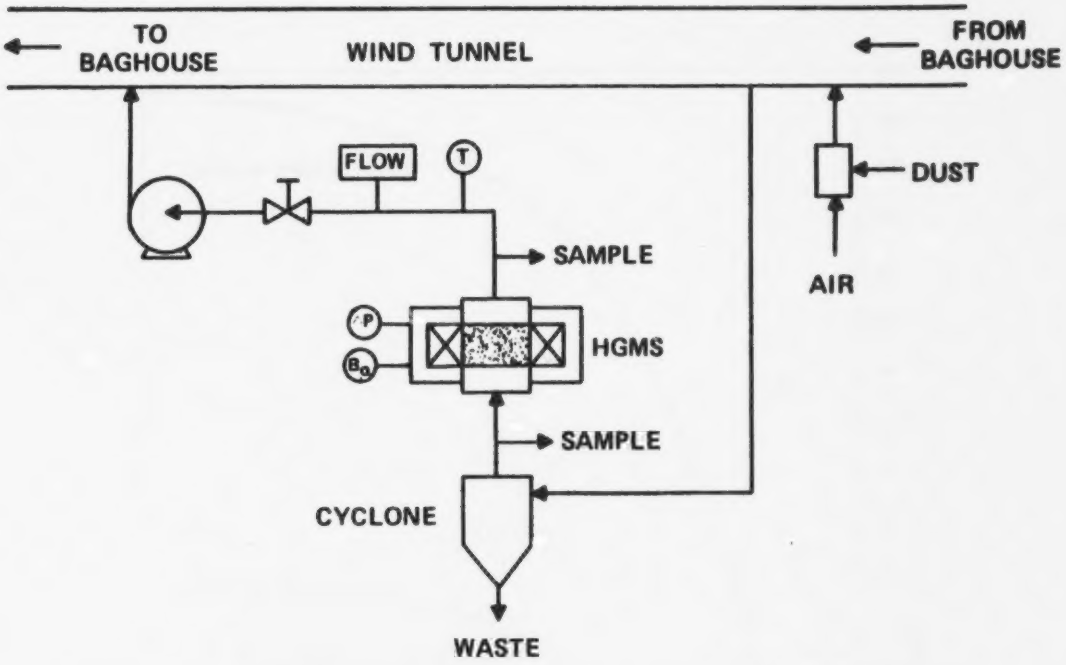

Figure 3. Schematic representation of pilot-scale HGMS facility.

tion efficiencies from a solution of the equations of motion that yields particle trajectories. The single-fiber efficiencies, R_c, are then extended to predictions of total matrix penetration, P, using the equation

$$P = \exp[-EFLR_c/a(1-F)] \qquad (1)$$

where F = matrix packing density,
L = matrix length,
a = fiber radius,
E = effectiveness factor (allows for deviations from idealized assumptions of the model).

Reasonable assumptions and geometric arguments predict the value of E to be $4/\pi^2$ ($\simeq$ 0.41), but reduction of experimental data from all of the runs showed the BOF and EAF data to be better fit by E values of 0.09 and 0.07, respectively. It should be noted that the single-fiber collection efficiency can be greater than 1.0 because of the magnetic tractive force. The development of the model is described in more detail elsewhere.[7,8]

The effects of individual parameters on particle collection were found to be in reasonable agreement with theoretical expectations. The

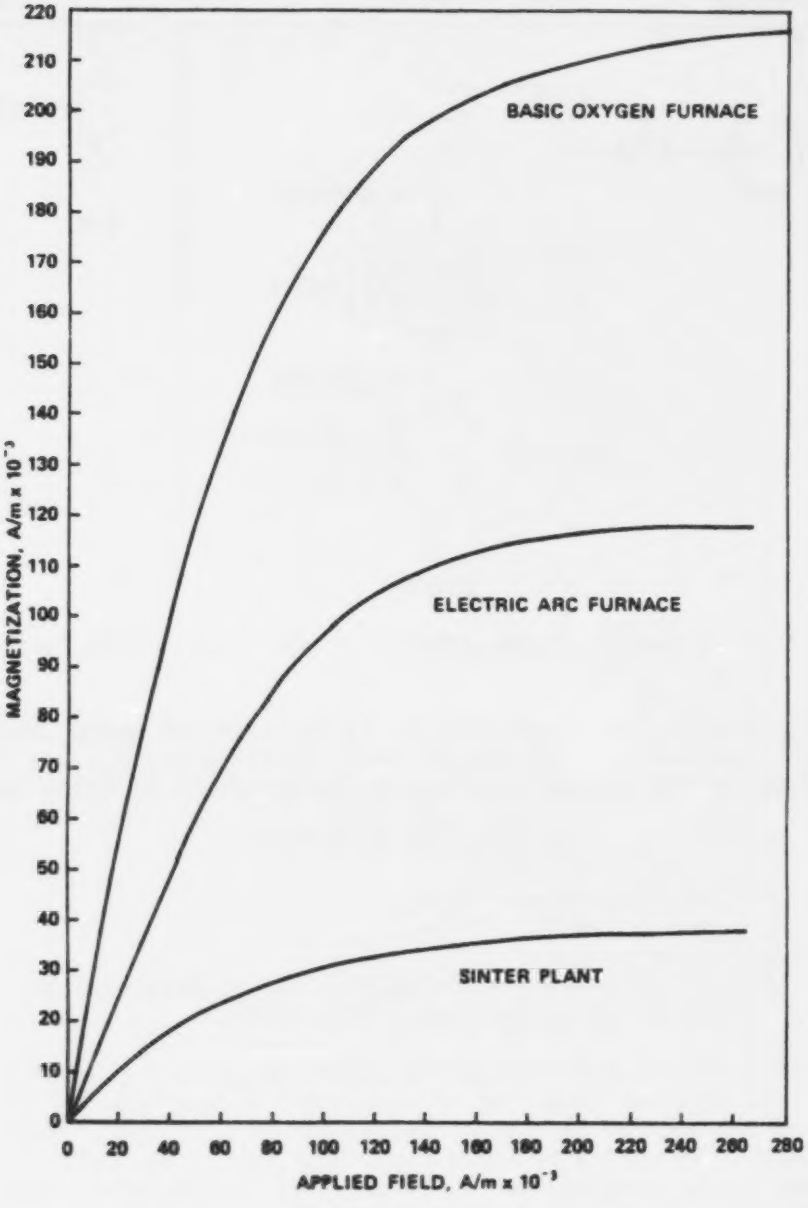

Figure 4. Magnetization curves of three steel industry dusts.

particle size and magnetic susceptibility effects are illustrated in Figure 5. At lower fields and higher velocities, the penetration of larger particles tends to be greater than predicted. The reason for this observation, although not yet fully understood, may be due to detrimental inertial effects that contribute to particle bounce and reentrainment. Gas velocity has a relatively small effect on the collection of submicron particles; higher velocities actually may be beneficial by enhancing inertial impaction in cases in which the single-fiber collection efficiency is less than 1.0.

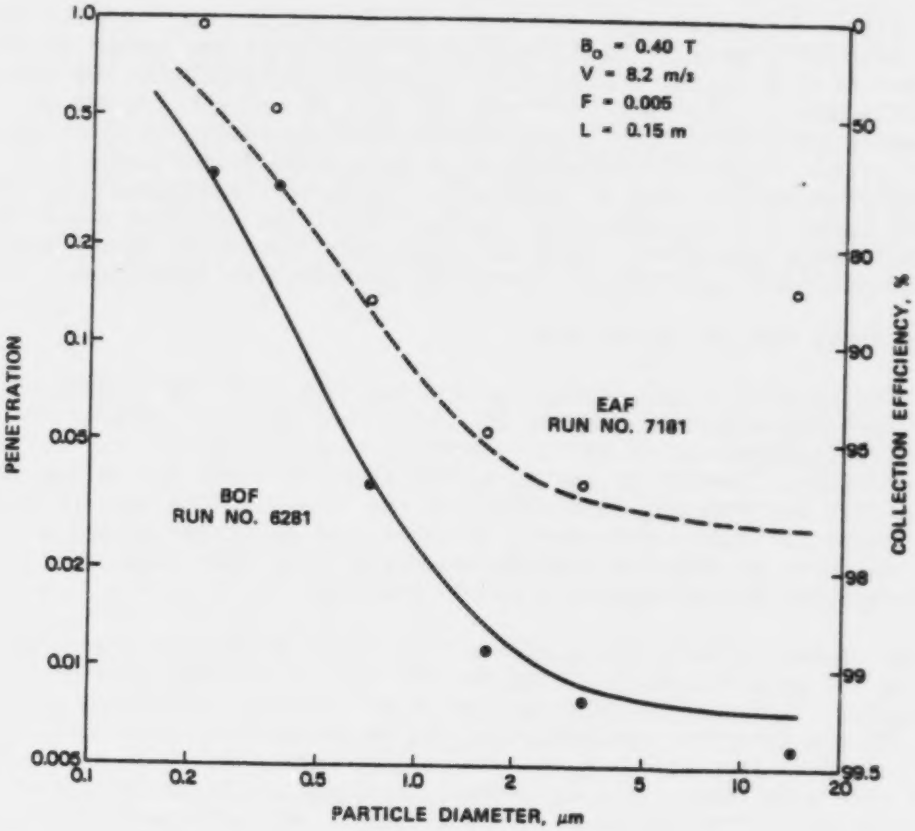

Figure 5. Experimental data and theoretical predictions of HGMS collection of two dusts under identical conditions.

Higher magnetic fields enhance the collection of particles, but the effect is diminished as both the particles and matrix approach magnetic saturation. With dusts exhibiting magnetic properties similar to those shown in Figure 4, collection efficiency can probably be improved more economically by increasing the density or length of the collection matrix rather than increasing the applied field beyond 0.4 to 0.5 T. The experimental data confirm the effects of matrix density and length expressed in Equation (1).

Increasing the operating temperature could adversely affect particle collection since the gas viscosity (and hence the drag force on the particles) would be increased, and magnetization of the particles and matrix may be diminished. However, no significant effect of temperature could be discerned from the few experimental runs that were made at the higher temperature level used in this study.

Figure 6 demonstrates that both the BOF and EAF dusts can be collected with high efficiency. The collection efficiency of the larger particles was not as high as the present model predicts (particularly the high-velocity BOF run) but was still greater than 99 percent. Based on currently available, continuous-cleaning HGMS equipment, projections for a full-scale, high-efficiency BOF dust collection device predict an uninstalled capital cost of $\$8200/m^3/s$ ($3.86/cfm) and power requirements of $3.2\ kJ/m^3$ (2.0 hp/1000 cfm). Collection of the EAF dust would be slightly more expensive. These estimates were projected from a specific design and could possibly be lowered by optimization techniques.

CONCLUSIONS AND CONTINUING WORK

The results of this investigation indicate that HGMS may be an efficient and economical method of particulate emission control in selected applications in which relatively high susceptibility dust must be collected. Several processes in the iron and steel and ferroalloy industries are possible candidates for the fine particle control by HGMS. The theoretical model provides a valuable tool to screen potential applications, to evaluate alternative designs, to plan experiments, to analyze data, and to conduct economic analyses.

Our latest pilot-plant work has focused on the sinter plant, which may be the most likely candidate for application of HGMS control. Many companies are presently experiencing unsatisfactory collection of sinter dust by electrostatic precipitation due to resistivity problems. Fabric filtration is reported to have been applied successfully in one installation with oily feed materials being restricted to circumvent potential problems with condensation of hydrocarbons.[9] Wet scrubbers require high pressure drops to achieve good collection and may introduce the undesireable side effect of a discharge stream containing arsenic, phenols, ammonia, and other potential water pollutants.

We have recently conducted pilot-plant tests with sinter dust and achieved good collection as shown in Figure 7. The relatively low magnetization of sinter dust makes it more difficult to collect than BOF or EAF dust, but preliminary estimates indicate uninstalled capital costs in the range of \$6400 to $\$12,800/m^3/s$ ($3 to $6/cfm) and power requirements of 3.2 to $4.8\ kJ/m^3$ (2 to 3 hp/1000 cfm), depending on the choice of operating gas velocity. In general, the power requirements increase

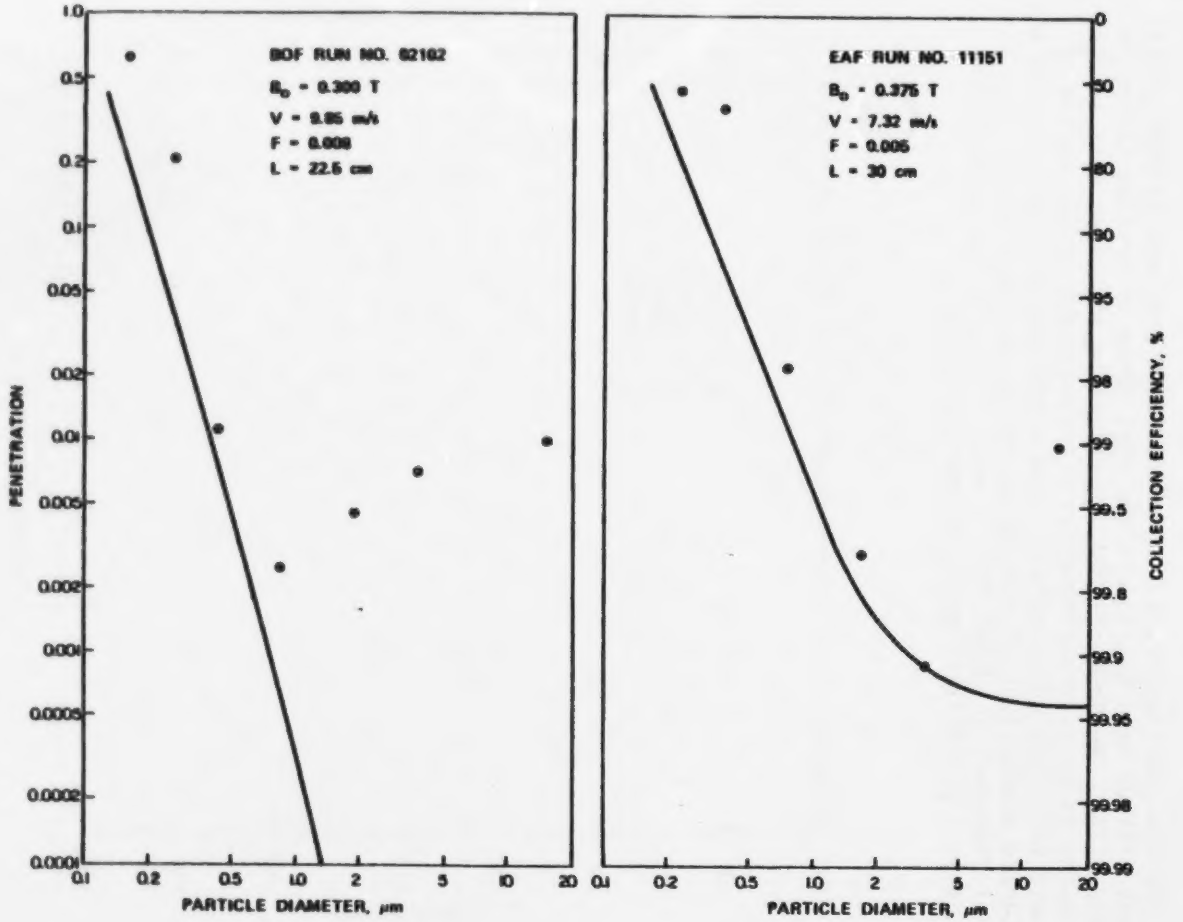

Figure 6. High-efficiency collection of BOF and EAF dusts: theory and experimental data:

with increasing gas velocity as the capital investment decreases. Since the sinter dust is fairly coarse, the potential effects of large-particle reentrainment are more significant than with finer dusts, and this phenomenon may have a bearing on the selection of optimum operating conditions.

We are now constructing a 5100 m^3/hr (3000 cfm) mobile HGMS pilot-plant that will be used to conduct the next phase of testing at one or more field sites. We have reached a preliminary agreement with a major steel company to begin these tests at a sinter plant in the spring of 1979. Data collected under actual field conditions will allow us to make more accurate projections of process economics and to identify the industrial processes in which HGMS is most likely to find commercial acceptance as a particulate emission control method.

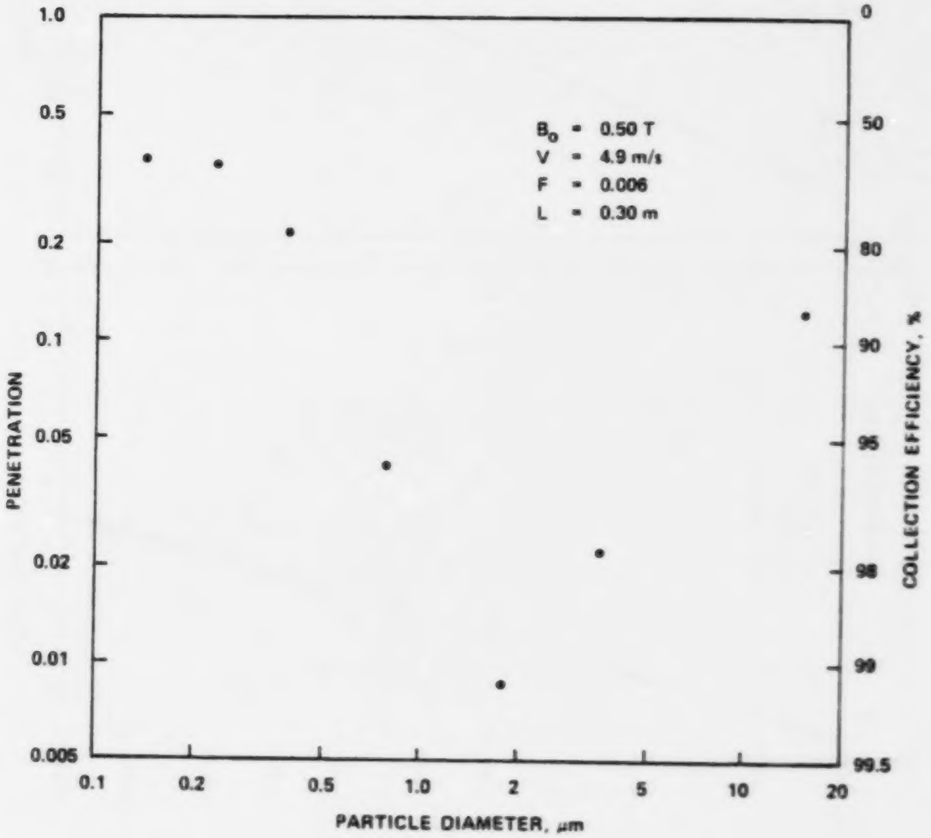

Figure 7. Collection of sinter dust.

REFERENCES

1. Oder, R.R. High Gradient Magnetic Separation Theory and Applications. IEEE Trans. Magn. Vol. MAG-12(5). pp. 436-443, Sep 1976.

2. Murray, H.H. Beneficiation of Selected Industrial Minerals and Coal by High Intensity Magnetic Separation. IEEE Trans. Magn. Vol. MAG-12(5). pp. 498-502, Sep 1976.

3. Oberteuffer, J.A. Engineering Development of High Gradient Magnetic Separators. IEEE Trans. Magn. Vol. MAG-12(5). pp. 444-449, Sep 1976.

4. Oder, R.R. Magnetic Desulfurization of Liquefied Coals: Conceptual Process Design and Cost Estimation. IEEE Trans. Magn. Vol. MAG-12(5). pp. 532-537, Sep 1976.

5. Liu, Y.A., and C.J. Lin. Assessment of Sulfur and Ash Removal from Coals by Magnetic Separation. IEEE Trans. Magn. Vol. MAG-12(5). pp. 538-550, Sep 1976.

6. Maxwell, E., D.R. Kelland, and I.Y. Akoto. High Gradient Magnetic Separation of Mineral Particulates from Solvent Refined Coal. IEEE Trans. Magn. Vol. MAG-12(5). pp. 507-510, Sep 1976.

7. Lawson, W.F., W.H. Simons, and R.P. Treat. The Dynamics of a Particle Attracted by a Magnetized Wire. J. Appl. Phys. Vol. 48(8). pp. 3213-3224, Aug 1977.

8. Gooding, C.H., T.W. Sigmon, and L.K. Monteith. Application of High Gradient Magnetic Separation to Fine Particle Control. EPA-600/2-77-230 (NTIS No. PB 276633/AS). Nov 1977. 149 pp.

9. Nowak, T.T. Ironmaking Proc. Vol. 31. p. 75, 1972.

THE USE OF ACOUSTIC AGGLOMERATORS FOR PARTICULATE CONTROL

J. Wegrzyn, D.T. Shaw and G. Rudinger
State University of New York at Buffalo
Buffalo, New York 14226

ABSTRACT

Recent experimental data obtained at State University of New York at Buffalo using a 10 hp mechanically driven vibrating piston acoustic generation reaffirms the use of sonic agglomeration as a means of particulate control. In this paper the current theories of sonic agglomeration processes are briefly reviewed, with special emphasis being placed on the extrapolation of these theories (whenever possible) to a high temperature and pressure environment. In particular, calculations on the orthokinetic inertial capture of particulate matter show at a temperarure of 1800°C and a pressure of 20 atm, a reduction in collection efficiencies by less than an order of magnitude. Other capture mechanisms are also discussed for the possible use of sonics in the industrial applications of particulate matter clean up of a corrosive high temperature, pressure environment.

INTRODUCTION

It is a bit ironic that in a 1978 Symposium on Particulate Control, papers dealing with acoustic treatment of particulate matter are being presented in the Advanced Technology Session, for when the need for particulate control became apparent in the late forties and early fifties, acoustic agglomeration was considered to be the prime candidate for the job. The first results, however, of the large-scale testings carried out on sonic agglomerators during these early years were very discouraging in terms of the specific energy consumption (defined as the energy required for the generation of the sound field per 1000 cfm) when compared to the other pollution abatement equipment available

Preceding page blank

at that time - such as, filters, scrubbers, and electrostatic precipitators. Besides economics, the basic fact that sonic agglomeration merely controls the size distribution of the suspended matter and does not directly remove any particulate matter, also had indirectly, a chilling effect among the early researchers for the use of acoustics as a mechanism for suspended particulate matter control.

Recent developments in the energy-environmental research area created a critical need for a non-conventional particulate emission control device which can operate effectively in a combined high temperature pressure and corrosive environment. This need along with other nonconventional applications has sparked renewed interest[1] in the use of acoustic agglomerators for particulate control.

The East Europeans never really lost interest in the many types of acoustic interactions and summaries of their works are given in two monographs[2,3].

Although the mechanisms of sonic agglomeration are not completely understood, results from our experients show a strong coupling of sonic and aerosol flow fields, giving the particulate matter both translational and vibration motion. It is the aim of the SUNY/Buffalo research group to understand better the forces resulting on the particles, from an applied high intensity source, so that the optimization of the agglomeration process can be achieved. That is to say, we are looking at the frequency, sonic intensity, particle size distribution, and particle mass loading dependence on the agglomeration constant in both the traveling and standing wave mode. As far as the economics are concerned, once a relibale model is developed on the performance of sonic agglomerators (on the large scale) a more realistic cost effectiveness can be determined.

THEORY OF ACOUSTIC AGGLOMERATION

Acoustic agglomeration is a growth process caused by the collision and subsequent sticking of two suspended particles. A strong acoustic field gives rise to an oscillating motion to an airborne particle suspended in this field. The oscillating motion of an airborne particle is described in the following equation first derived by Stokes in 1851 (discussed on parge 84 of reference 5)

$$m'\frac{du_p}{dt} = -6\pi C\eta a(u_p-u_g)-6\pi C\eta a\left(\frac{\omega a^2}{2\nu}\right)^{1/2}$$

$$\left[(u_p-u_g)+\frac{1}{\omega}\;\frac{d}{dt}(u_p-u_g)-\frac{2}{3\omega}\left(\frac{\omega a^2}{2\nu}\right)^{1/2}\;\frac{du_g}{dt}\right] \qquad (1)$$

The physical meaning of the terms in the brackets are: the first and second terms are the inertial part of the resistance of the gas medium and the last term represents the reaction of the gas medium to the particle acceleration.

Equation (1) can be cast into a more useful form by introducing here the following two terms

$$\tau = \frac{2}{9}\,\frac{\rho_p a^2}{C\eta} \qquad \text{and} \qquad y = (\omega a^2/2\nu)^{1/2}$$

and rewriting Eq.(1) as:

$$\tau\,\frac{du_p}{dt} = -(u_p-u_g)-y\left[(u_p-u_g)+\frac{1}{\omega}\,\frac{d}{dt}(u_p-u_g)-\frac{2}{3\omega}\,y\,\frac{du_g}{dt}\right] \qquad (2)$$

Where τ is the dynamic relaxation time and $y = a/\Delta$, where Δ is the boundary layer thickness of an oscillating flow. The solution of Eq. (2) was first obtained by Konig[4] and is discussed in more detail by both Fuchs[5] and Mednikov[2], and is given as,

$$\mu_p = \frac{U_p}{U_g} = \frac{X_p}{X_g} = \left[\frac{\delta^2[4y^4+12y^3+9(2y^2+2y+1)]}{\frac{16}{9}y^4+8\delta y^3+9(2y^2+2y+1)\delta^2}\right]^{1/2} \qquad (3)$$

where μ_p is called the degree of the entrainment of the particle. U_p is the maximum particle velocity and U_g is the maximum gas velocity, and finally the particles amplitude of vibration is given by X_p and the gases amplitude of vibration is given by X_g. For $y << 1$ Eq.(2) reduces to the more recognizable form,

$$\tau\,\frac{du_p}{dt} = -(u_p-u_g) \qquad (4)$$

The solution of the above equation for the case when $u_g = U_g \sin wt$ has the form

$$\mu_p = \frac{U_p}{U_g} = \frac{X_p}{X_g} = (1+\omega^2\tau^2)^{-1/2} = [1+(2\pi\tau/T)^2]^{-1/2} \qquad (5)$$

For normal temperature and pressure the difference between equations (3) and (5) has been shown by Fuchs to be negligible. However, as was pointed out by Mednikov and Sirotin[6], under a high gas-medium pressure this difference is no longer negligible because the inertial terms of Eq.(1) can no longer be neglected, since $y \eqsim 1$.

A plot according to Eq.(5) of the variations of u_p versus the particle radius for various frequencies is given in Fig. 1.

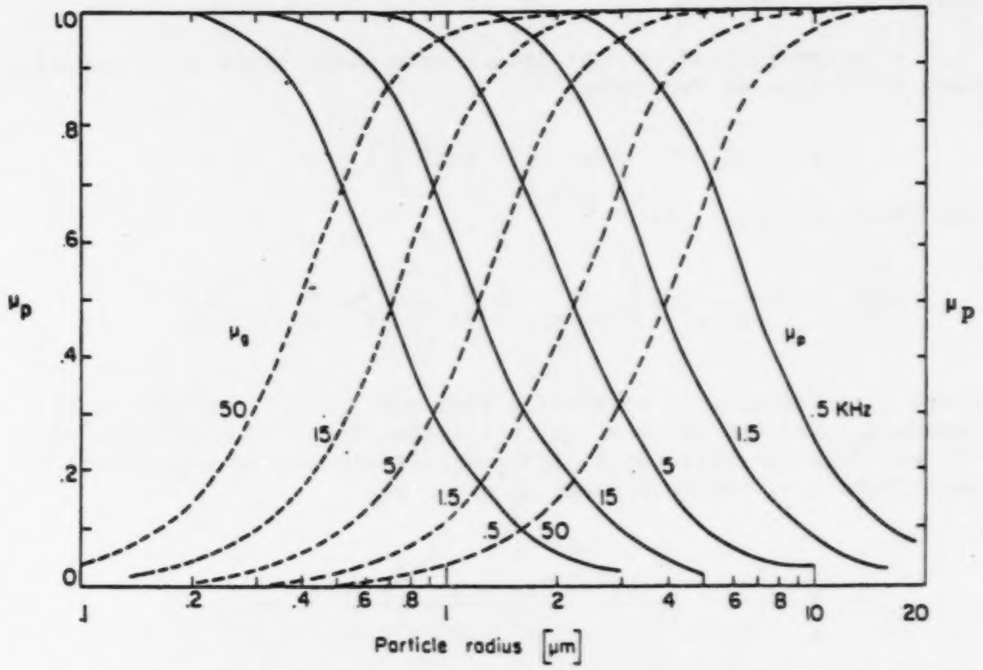

Fig. 1 Degree of entrainment μ_p versus particle radius at different frequencies (ρ_p = 1g/cm^3)

Figure 1 is very illustrative of the three types of particles interactions that can occur in an acoustic agglomeration experiment. Consider if you will, two sizes of particles for a monotone system. Those particles whose radius is relatively small (r_s) so that their entrainment factor μ_p is nearly one, and those particles whose radius are much larger (r_L) and have a near zero value of entrainment factor. In this simplified model there exists three types of interaction:

r_s with r_s, turbulent diffusion

r_s with r_L, inertial orthokinetic

r_L with r_L, hydrodynamical.

(These models are discussed more fully in Mednikov's book.)

In the past it has been the inertial orthokinetic mechanism that was considered to be the most promising interaction for acoustic agglomeration. The reasoning is quite simple, since the large particle is nearly stationary and the smaller particles vibrating with nearly

100% of the gas vibrational velocity, there is a large differential velocity between the two particles. Theoretically it has been shown[7] that there can be as large as 10^6 increase in coagulation of inertial orthokinetic over a purely gravitation coagulation model. This at first glance seems indeed very attractive, but coagulation between small and large particles does not shift the mean size distribution of the aerosol to any great extent. Inertial orthokinetic coagulation merely removes the fine particles without much change to the mass mean (the mass mean is mainly a function of the size distribution of the large particles). In the past most agglomeration experiments were analyzed by determining the change in the mass size distribution and this is part of the reason why the past results on acoustic agglomerators have been determined to be ineffective.

The hydrodynamical interaction, that is the larger particles attraction-interaction between each other, is then very important if one is to shift the mass size distribution to a larger mass size, so that it can later be effectively removed (this is the idea of acoustic preconditioning). As an example, a collision between two 20 micron particles is comparable in mass to 10^6 collisions of .2 micron size particles with a 20 micron particle.

Because of the reasoning outlined above, the third type of interaction, that is the turbulent diffusion interaction between small particles, is also not of great importance in the preconditioning of an aerosol. To reinforce this conclusion preliminary data from the vibrating piston shows that when only small particles are present the stability of the aerosol is quite good, as compared with the rapid agglomeration that is observed when larger particles are also present. (Again, the terms small and large are relative to the entrainment factor.)

One last word on acoustic-particulate matter interaction is the ability of a strong acoustic field to focus an aerosol.

The levitation and focusing power of an acoustic field has been known and observed for some time. This type of phenomena is potentially important because now the acoustics can serve directly as the removal mechanism rather than just a preconditioner.

INERTIAL ORTHOKINETIC COAGULATION AT HIGH TEMPERATURE AND PRESSURE

Coinciding with the theme of this Symposium on particulate control at high temperatures and pressures, the inertial orthokinetic model of acoustic agglomeration was extended into the high pressure and temperature region. This was done by using the complete solution of Eq.(1) which is Eq.(3) and by adjusting the constants of this expression to account for a high temperature and pressure environment.

Figure 2 is a plot of the ratio of the particle velocities

$(U_p/U_{p,NTP})$ to the particles radius for a sound intensity of $1W/cm^2$ and for various temperatures and frequencies. Where $(U_{p,NTP})$ is the particles amplitude velocity at the condition of normal temperature and pressure. It is seen from this figure that there is an increase in U_p over $U_{p,NTP}$, and since the agglomeration rate is proportional to U_p, there has to be a corresponding increase in the inertial orthokinetic acoustic coagulation rate at high temperatures. Things are not quite as fortunate when additional considerations are made of the effects of high pressure on the particles velocity. Figure 3 is a plot of the ratio of the particle velocities $(U_p/U_{p,NTP})$ for the same sound intensity of $1W/cm^2$, but now in a combined high pressure and temperature environment for the three frequencies of 10, 1 and .1 kilohertz. This graph illustrates the point that the gain in the magnitude of the particles velocity at high temperatures is more than offset by the loss in amplitude velocity at high pressure. This is further pointed out on Fig. 4, which is a plot of the ratio of the particles velocities versus the ambient pressure for the two temperatures 300°K and 1200°K. From Fig. 4 there exists a decrease in the velocities (inertial orthokinetic coagulation) by a factor of four for a 1200°K temperature environment at a pressure of 30 atm. These results agree with Calverts[8]

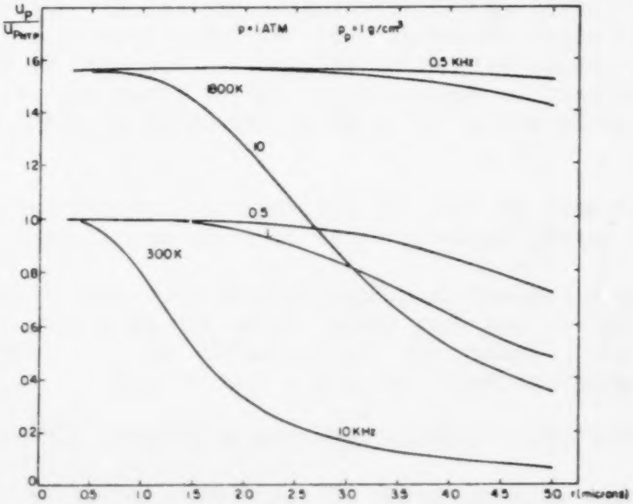

Fig. 2 The effect of temperature and frequencies on particle velocities versus radius.

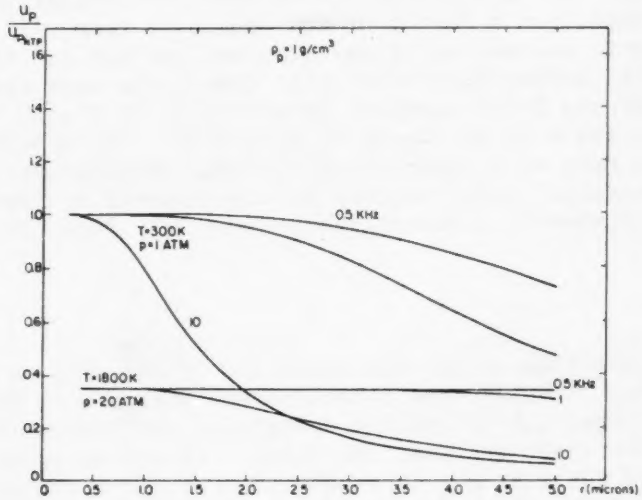

Fig. 3 The effect of temperature pressure and frequencies on particle velocities versus radius

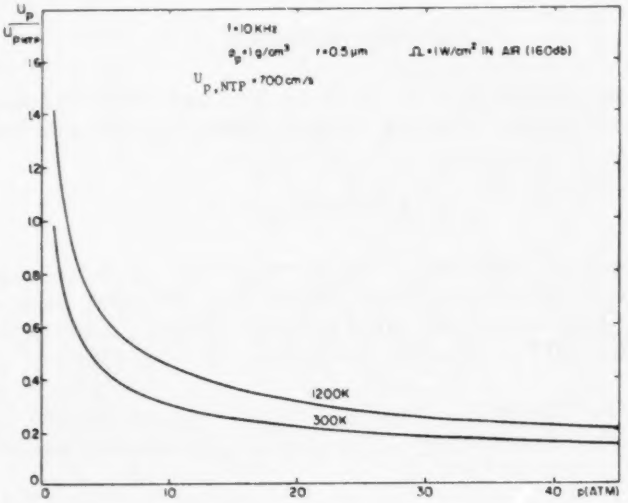

Fig. 4 The effect of temperature and pressure on particle velocities versus pressure.

review paper on the effects of high temperature and pressure on the various collection mechanisms for the sonic agglomeration case. However as was pointed out earlier, this orthokinetic coagulation process is extremely rapid, and a factor of four decrease then will have only a minimal impact, because as it was also pointed out earlier it is the hydrodynamical attractions which will change the mass size distribution. The extent of the hydrodynamical interactions in a high temperature and pressure field is not known at this time. The effectiveness of shifting the mass size distribution at high temperatures and pressures awaits experimental verification, but the removal of fine particles by inertial orthokinetic interactions is certainly feasible by acoustical means.

CONCLUSION

The bottom line on the applicability of any process is its cost effectiveness. A valid cost effectiveness analysis is dependent upon three parameters; (1) an optimum design, (2) an encompassing theory, and (3) a consistent mathematical model. As far as sonic agglomerators are concerned there exists in publication, at least at the time of this writing, no clear cut optimum design nor any all encompassing theory for the complete acoustic-particle interaction process. It is then the research aim of the SUNY/Buffalo group to fill this gap in design and theory of a large industrial scale acoustic agglomerator or removal system. A legitimate cost effectiveness statement can then be made, once these goals are reached.

ACKNOWLEDGEMENTS

This work was supported in part by the National Science Foundation, the Department of Energy and the French Commissariat a L'Energie Atomique.

REFERENCES

1. Shaw, D.T. and J. Wegrzyn, The Application of Sonic Agglomeration for the Control of Particulate Emissions, EPA/DOE Symposium of High Temperature High Pressure Particulate Control, Washington, D.C. September 20, 1977, EPA 600/9-78-004, pp. 325-354.

2. Mednikov, E.P, Acoustic Coagulation and Precipitation of Aerosols, translated from Russian by C.V. Larrick, Consultants Bureau, New York, 1965.

3. Rozenberg, L.D. (ed.), Physical Principles of Ultrasonic Technology, Plenum Press, New York, 1973.

4. Konig, W. Ann. Phys. and Chem., 42 (3):353, 1891.

5. Fuchs, N.A., The Mechanics of Aerosols, translated from Russian by R.E. Daisley and M. Fuchs, Pergamon Press, New York, 1964.

6. Mednikov, E.P. and A.M. Sirotin, Soviet Phys.-Acoustics, 13, 393, 1968.

7. Rajendran, N., Acoustic Agglomeration of Aerosols, Ph.D. Dissertation, State University of New York at Buffalo, 1977.

8. Calvert, S. and R. Parker, Effects of Temperature and Pressure on Particle Collection Mechanisms: Theoretical Review, EPA 600/7-77-022, 1977.

ANALYTICAL AND EXPERIMENTAL STUDIES ON GRANULAR BED FILTRATION

C. Gutfinger, G. I. Tardos, and N. Abuaf*
Department of Mechanical Engineering
Technion, Israel Institute of Technology
Haifa, Israel

ABSTRACT

This paper reviews the models developed for the granular bed dust filtration theories and compares some of the predictions with experimental data. The emphasis is concentrated on granular bed filters and on dust particles in the size range 0.01 to 10 μm.

The application of the various dust deposition mechanisms, i.e., inertia, interception, diffusion, electrical forces, etc., to both single sphere elements and whole filter beds are discussed. The relevance of the flow regime and the field around a single sphere both in an infinite fluid and in a swarm of particles, to the filtration models are also presented and reviewed. Some of the latest methods of combining the different filtration mechanisms are discussed, and some of the problem areas of the models are pointed out. Experimental data obtained with granular bed filters from existing literature are presented and compared with theoretical predictions for single sphere and total granular bed filtration efficiencies.

---

*Present Address: Brookhaven National Laboratory, Upton, NY, USA

Preceding page blank

INTRODUCTION

The so-called "granular bed filters" are dust separation devices using granules as filter media: the contaminated gas stream containing small solid or liquid particles (droplets) is passed through a dense bed of granular material where the particulates are separated. This procedure has been known for a long time and was used extensively in water filtration. The use of this technique for airborne material is relatively new. The growing interest in the development of industrially feasible granular dust filters is due to the possibility of constructing these devices as continuously operating units in which the bed material is circulated continuously through the filter in such a way that clean particles (granules) are introduced and dirty granules are discharged from the bed. Dust covered granules are cleaned outside the filter and reintroduced into the system.

With the recent developments in such filtration devices as the panel bed (Squires and Pfeffer [1], Paretsky [2], Lee [3]) and the fluidized bed filters (Cook, et al [4], Rubine and Margolin [5], Krupp-Koppers [6], Tardos, et al [7], Jugel, et al [8]), both of which are capable to operate continuously, the application of granular bed filters to removal of dust and other particulate matter from flue gases in industrial processes has become feasible. Consequently, dust separation from a gas stream by means of a granular bed has been lately the subject of a sizeable number of theoretical and experimental studies. The experimental investigations deal mainly with the overall filtration efficiency of a granular bed and its improvement by changing the filter parameters and physical construction. Most of the fundamental studies are limited to experiments with single spherical collectors. The theoretical work appearing in the literature ranges from the analysis of the flow field and collection efficiency of single filter elements to overall efficiency computations for complete filters.

The effects considered to contribute to filtration of dust are those of inertia, diffusion, electrical forces, gravity and adhesion. Going through the literature on dust filtration by granular beds one encounters fragmented information in papers usually covering one or two filtration mechanisms without providing the broader scope of the problem. In the present paper, we bring together the most important works relevant to granular bed dust filtration concerning the theoretical and experimental aspects of the problem.

THE FILTER MODEL - LIMITATIONS OF THE THEORETICAL APPROACH

The filtration of dust in a bed of granules is a complicated physical process. A long list of assumptions and simplifications must be introduced into the theoretical approach before a mathematically tractable problem is obtained. These assumptions and simplifications must be verified, in turn, by experimental means. The main assumptions as used in granular bed filtration theory are presented below.

In the analysis of the filtration process, the granular bed filter is usually assumed to be a homogeneously porous bed of uniformly sized spherical particles. Commonly used filter material such as sand, glass, plastic, etc., has granules which do not deviate markedly from the assumed spherical shape. The mean bed porosity, ϵ, has a strict physical meaning only in densely fluidized and eventually in a packed bed of granules. In a bubbling fluidized bed, the above assumption is not valid.

Filtration of the particulates is due to their sticking to the filter elements. It is assumed that a particle which approaches a filter element, the collector, to a distance comparable to its radius will collide with it and stick to it. (Stechkina and Fuchs [9], Dorman [10], Loffler [11]). The classical assumption of the "sticking" particles as presented above, is the most drastic simplification introduced into the filtration theory because it excludes the effect of the surface properties of the two substances which come into contact, on the filtration phenomenon. Experimental studies on dust filtration carried out with electron microscopes show (Dorman [10]) that the dust particles prefer to stick on one another instead of on the collector, forming so-called "trees". These experiments also show that contact conditions between the dust and the collector granules may be favorable, or not, thus increasing or decreasing the filtration efficiency. Moreover, the extent of the favorable sticking is highly dependent on the gas relative humidity. Furthermore, the filtration process in moving and fluidized beds is complicated by dust particle buoyancy and especially by reentrainment. During these processes, particles colliding with a collector or even retained in a previous stage of filtration are carried downstream by the gas flow, thus reducing the actual separation efficiency. These phenomena are mainly apparent when the collection media is saturated with dust particles, (Loffler [11]). Very little attention has been given to these subjects to date. Therefore, in the theoretical approach presented in the literature, the classical assumption of the sticking particles is used, with the understanding that this simplification requires additional justification.

It is further assumed that the dust particle concentration in the gas stream is low enough so as not to influence the flow field around the filter elements. In a "clean air filter," this assumption is very close to reality. In a gas stream of high dust concentration, it is usually the practice to employ a cyclone in order to remove the bulk of the dust upstream the filter. Thus, the assumption of a dilute suspension is not expected to introduce any considerable errors in the theoretical model.

Another assumption is that the filtration process is time independent, thus each filter element and the whole filter has always the same filtration efficiency. This last assumption is good for the case of continuously regenerated granular bed filters and less correct for static packed bed filter.

The works on granular bed filtration generally follow the classical assumption that every filter element within the granular bed experiences similar filtration phenomena and, therefore, a "single filter element efficiency" can be defined. In other words, the filtration efficiency of an actual filter can be computed by summing up the effects of all elements in the filter. Thus, the theoretical computation of the filtration efficiency of a whole filter bed is subdivided into the prediction of single filter element efficiencies and their summation by integration. The single filter element efficiency, E, is defined as the total amount of dust particles captured by the filter element (granule), divided by the total number of particles flowing toward it in a cylinder of the same diameter, 2a, oriented along the flow direction:

$$E = \frac{J}{n_o U_o \pi a^2} \qquad (1)$$

Here, J is the total dust particle flux toward the collector surface, n_o, the dust concentration and U_o the gas superficial velocity. If one assumes that the captured particles all flow toward the collector in a co-axial cylinder of diameter, 2b, (see Fig. 1):

$$J = n_o U_o \pi b^2 \qquad (2)$$

the single filter element efficiency, E, can be defined also as:

$$E = b^2/a^2 \qquad (3)$$

The computation of E, consists essentially of the knowledge of either the total flux, J, or the distance b the so-called distance of the limit (or grazing) trajectory (Fig. 1). The first procedure is usually used when diffusional deposition is considered and the latter for all remaining mechanisms.

The method of computing the total efficiency, η, of a given filter bed from single element efficiencies, E, was reported by Tardos, et al. [7]:

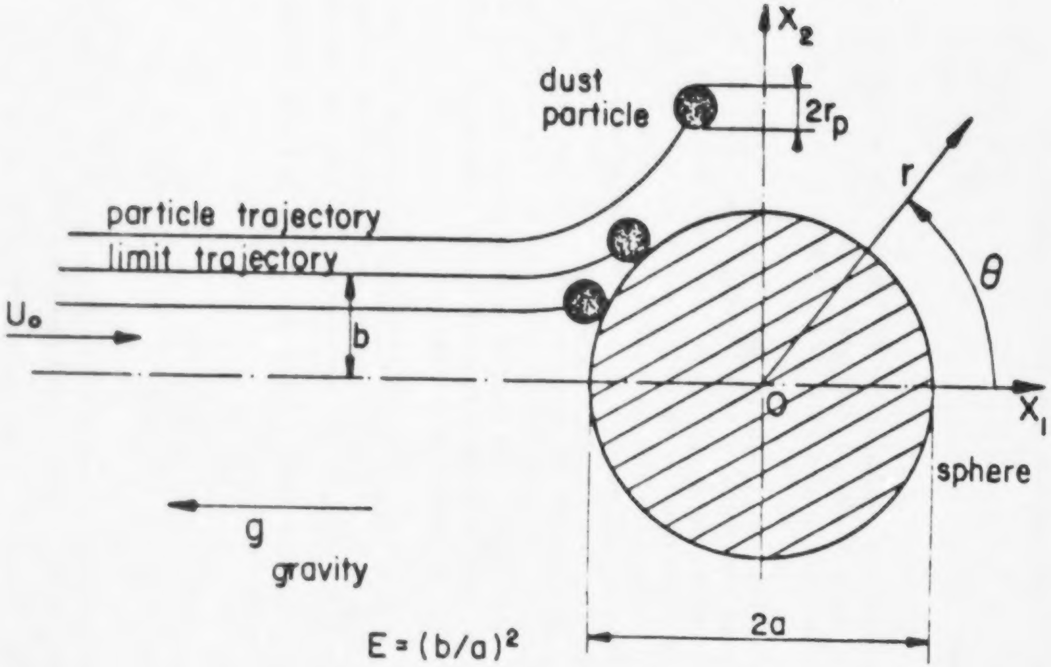
X_2
dust particle
$2r_p$
particle trajectory
limit trajectory
U_o
b
r
θ
O
X_1
sphere
g
gravity
$E = (b/a)^2$
2a

Figure 1: Inertial Deposition of Particles

$$\eta = 1 - \frac{n_{final}}{n_{initial}} = 1 - \exp\left[-1.5 \cdot \frac{1-\varepsilon}{\varepsilon} \cdot \frac{L}{2a} \cdot E\right] \quad (4)$$

Here n_{final} and $n_{initial}$ are the dust concentrations downstream and upstream the filter. Using this procedure, the computation of the total efficiency, η, of a granular bed filter of given thickness, L, porosity, ε, and filter element (granule) diameter, 2a, is reduced to the computation of the single element efficiency, E.

THE FLOW FIELD MODEL

The first step in the calculation of the filter efficiency, E, is to determine the flow field of the gas in the filter. This field is usually so complicated that a simplified model must be adopted.

One model considers the filter elements as obstacles to an otherwise straight flow of the fluid without taking into account the mutual influence of the elements on each other. In this case, one considers the filter elements (spheres) as being situated in a fluid which extends to infinity. This is the so-called "loose filter model". Although it does not fit the packed bed, it may sometimes approximate the flow in a fluidized bed filter. Moreover, any flows solved for an actual granular bed should converge to the solution for the flow around the sphere in an infinite fluid when the bed porosity, ε, approaches unity. Therefore, the single sphere solutions may be used in checking the more complicated solutions for the granular beds usually obtained only by numerical methods.

The simplest of the single sphere solutions is that of the creeping flow, corresponding to negligibly small Reynolds numbers, ($Re_o \leq 0.01$). The flow pattern can be computed using the expression for the stream function for this case (Lamb [12]) and the relations for the velocity components:

$$U_r = -\frac{1}{R^2 \sin\theta} \frac{\partial\psi}{\partial\theta} \; ; \; v_\theta = \frac{1}{R \sin\theta} \frac{\partial\psi}{\partial R} \quad (5)$$

Some other well-known solutions for flow around a sphere, are those of Oseen ($Re_o < 2$), Proudman and Person [13] ($Re_o < 5$), Pearcey and McHugh [14] ($Re_o \leq 10$), Jenson [15], Hamielec, et al [16], Le Clair, et al. [17] (Re_o = 0.01 - 400), Rimon and Chang [18], Dennis and Walker [19], and Seeley, et al [20]. Some of these solutions are summarized in Table 1.

At higher Reynolds numbers (Re_o > 200....500), the flow field can be obtained by the boundary layer theory. For the case of a rigid sphere in an unbounded fluid, the problem was solved by Schlichting [21], Scholkemeier [22], and Frossling [23]. In order to obtain the boundary layer thickness, an approximate method can be used (Goldstein [24] and Tomotika [25]).

Obviously, the single sphere flow model is a rather poor approximation for the flow field in an actual granular bed. On the other hand, due to the complexity of the packing arrangement, the flow patterns in the bed are very complicated indeed and except for a few isolated cases of symmetrically arranged packings, (Sorensen and Stewart [26] cannot be solved accurately. Fortunately, for cases where the main interest is the integrated filtration efficiency of a whole filter, the detailed knowledge of the local flow field can be dispersed with and substituted by some average flow approximation.

One of the ways to approach the flow field in a granular bed is by introducing the concept of the "unit cell". The unit cell model used to describe the flow field in a lattice of equal spheres was first proposed by Uchida in 1949 and developed later by Happel [27] and Kuwabara [28]. The unit cell solution was recently extended into the range of intermediate Reynolds numbers by Le Clair and Hamielec [29]. A solution for potential flow in a unit cell is also possible (Lamb [12]).

A different approach to solve the flow field through a bed of granules is to consider it as a random cloud of similar particles and to use statistical methods of analysis. A typical example is the work of Tam [30], where the flow must be interpreted as the most probable one around one of the spheres. Creeping flow and no particle - particle interaction were assumed. A similar approach has been successfully applied by Batchelor [31] in describing the motion of a dispersion of spheres in sedimentation.

Neale and Nader [32] have attacked the problem of flow through a granular bed from a slightly different point of view. They have assumed that the sphere around which the flow field is computed is surrounded by a spherical fluid envelope and by a large exterior porous mass which represents the entire sphere swarm. The equations of creeping flow are solved for the cell region and a modified form of Darcy's law (the so-called Brinkmann's equation) for the porous matrix. Matching the boundary conditions for these two equations the flow pattern in the whole bed is obtained in the form of inner and outer stream functions. This flow model was tested against drag measurements and very good agreement was obtained for flows up to Reynolds numbers $Re_o \leq 10$. The flow solutions described above were brought together in Table 2.

TABLE 1

SOLUTIONS FOR FLOWS TO A SINGLE SPHERE IN AN INFINITE FLUID

Name	Reference	Steam Function	Range	Remarks
1. Creeping Flow	Lamb [12]	$\psi = -\frac{1}{4}\left(2R^2 - 3R + \frac{1}{R}\right)\sin^2\theta$	$Re_o < 0.01$	
2. Oseen Flow	Goldstein and Batchelor [24]	$\psi = -\frac{1}{4}\left(2R^2 + \frac{1}{R}\right)\sin^2\theta +$ $\frac{3}{2Re_o}\left(1 + \cos\theta\right)\left[1 - e^{\frac{1}{2} Re_o R(1 - \cos\theta)}\right]$	$Re_o < 2$	
3. Intermediate Reynolds No. Flow	Hamielec and Johnson [80]	$\psi = -\left(\frac{1}{2} R^2 + \frac{A_1}{R} + \frac{A_2}{R^2} + \frac{A_3}{R^3} + \frac{A_4}{R^4}\right)\sin^2\theta$ $-\left(\frac{B_1}{R} + \frac{B_2}{R^2} + \frac{B_3}{R^3} + \frac{B_4}{R^4}\right)\sin^2\theta\cos\theta$	$10 < Re_o < 100$	
4. Intermediate Reynolds No. Flow	Hamielec et al. [16] Le Clair et al. [17]	- - - - - - - -	$0.01 < Re_o < 400$	Numerical Solution
5. Potential Flow	Lamb [12]	$\psi = -\left(\frac{1}{2} R^2 - \frac{1}{2}\frac{1}{R}\right)\sin^2\theta$	$Re_o \to \infty$	

TABLE 2

SOLUTIONS FOR FLOWS IN SWARM OF PARTICLES (GRANULAR BEDS)

NAME	REFERENCE	STREAM FUNCTION	RANGE	REMARKS
1. Creeping Flow	Happel [27] Kuwabara [28]	$\psi = \left(\frac{A}{R} + BR + CR^2 + KR^4\right) \sin^2\theta$	$Re_o \leq 0.01$	
2. Intermediate Reynolds No. Flow	Le Clair and Hamielec [29]	Numerical Solution	$Re_o \leq 500$ $\epsilon \geq 0.4$	
3. Very High Reynolds No. Flow	Lamb [12]	$\psi = -\frac{1}{2\epsilon}\left(R^2 - \frac{1}{R}\right)\sin^2\theta$	$Re_o \to \infty$	Potential Flow
4. Low Reynolds No.	Tam [30]	$\psi = -\frac{R^2}{2}\sin^2\theta - \frac{B}{R}\sin^2\theta + \frac{A}{p^2R}\sin^2\theta[e^{-pr}(1 + pR)-1]$	$Re_o \leq 1$ $\epsilon > 0.33$	Statistical Model
5. Low Reynolds No. Flow	Neale and Nader [32]	$\psi = -\frac{1}{2}\left(\frac{A}{\alpha^3}\frac{1}{R} + \frac{B}{\alpha}R + CR^2 + F\alpha^2R^4\right)\sin^2\theta$ $\bar{\psi} = 1\,\frac{1}{2}\left[\frac{H}{\alpha^3}\frac{1}{R} + R^2 + \frac{G}{\alpha^2}e^{-R\alpha}\left(1 + \frac{1}{R\alpha}\right)\right]\sin^2\theta$	$Re_o \leq 10$	Inner Flow Outer Flow
6. Low and Intermediate Reynolds No.	Payatakes and Muira [81] Muira and Payatakes [82]	Collocation Solution	$Re_o \leq 1$	Constricted Tube Model
	Payatakes, et al [34]	Numerical Solution	$Re_o \leq 75$	

At this stage one may conclude that at the present state of knowledge, the statistical and the unit cell flow models describe reasonably well the flow in loosely packed granular beds with the statistical models providing a slightly more accurate picture and the unit cell models having an edge of simplicity and ease of applicability to dust filtration studies. For the low porosities, typical of granular bed filters, it seems like Neale and Nader's flow model provides in terms of accuracy and simplicity the best results available to date.

An entirely different model for fluid flow within a dense swarm of granules, is the so-called "pore model" described in detail by Scheidegger [33]. Here, the fluid is supposed to flow through a bundle of straight tubes whose dimensions and orientation is a function of bed porosity, ε. Many different combinations of tubes were proposed but, none of these models gave satisfactory results when tested against measurements. Different corrections had to be introduced for each specific case. Based on these ideas, Payatakes (Payatakes, et al [34]) proposed lately the "constricted tube" model. Here the tube section has a variable cross sectional area along the flow direction. The tube length and curvature can be adjusted as a function of bed porosity and granule size. The model was applied to filtration in deep beds (Payatakes, et al [35]).

It is hoped that simple models based on these and similar ideas will be extended in the future for the range of low porosities and intermediate Reynolds number flows, typically encountered in industrial granular filters.

DUST DEPOSITION MECHANISMS IN THE GRANULAR BED

The filter model discussed above allows to treat the dust removal problem mathematically. The main simplifying assumptions considered in order to obtain the model were:

1) The filter elements are spheres identical in size
2) The porosity of the bed is uniform
3) The dust is spherical, monodisperse, and much smaller than the filter elements
4) The fluid flow through the bed is slow, and Darcy's law is valid for the flow in the porous matrix
5) The particles concentration in the fluid is low enough to neglect their influence on each other and on the momentum of the carrier gas
6) The dust particles that touch a filter element stick to it and are not re-entrained by the flow
7) Each filter element (collector, granule) has similar filtration properties
8) The filtration process is time independent.

The main question to be answered remains what are the forces that must be taken into account when the collision mechanism between dust particles and a filter element is analyzed. Classical assumptions consider diffusional (Brownian), inertial, gravitational, electrical and adhesional forces. The different mechanisms are presented in detail in this section.

Diffusional Deposition

The movement of the fine dust particles relative to that of the gas stream, at normal temperatures and pressures, is mainly governed by Brownian effects. For particles in the submicron size range, their Brownian motion is sufficiently intense to produce collisions with a large surface located in the flow. If this surface retains the particles either by adhesion or some other effects, they may diffuse from the stream to it and deposit thereon. This process is called diffusional deposition. With decreasing particle size, the intensity of Brownian movement increases and so does the diffusional flux to the surface.

The derivation of the characteristic diffusion equation from the theory of Brownian motion was presented by Chandrashekhar [36] in the following form:

$$\frac{Dn}{Dt} = \mathcal{D}\,\nabla^2 n \qquad (6)$$

where $\mathcal{D}$ is the particle diffusion coefficient and, n, the dust concentration.

Assuming steady state diffusion to the sphere surface and spherical symmetry, one gets the simplified diffusion equation in dimensionless form:

$$U_r \frac{\partial N}{\partial R} + V_\theta \frac{1}{R}\frac{\partial N}{\partial \theta} = \frac{2}{Pe}\left[\frac{\partial^2 N}{\partial R^2} + \frac{2}{R}\frac{\partial N}{\partial R} + \frac{1}{R^2 \sin\theta}\cdot\frac{\partial}{\partial\theta}\left(\sin\theta\,\frac{\partial N}{\partial\theta}\right)\right] \qquad (7)$$

where N is the dimensionless dust concentration, $N = n/n_o$, R the dimensionless radius, $R = r/a$, $Pe = 2aU_o/\mathcal{D}$, the Peclet number, and U_r and V_θ are the velocity components as obtained from the flow field model, Eq. (5). The boundary conditions of Eq. (7), (Levich [37], Friedlander [38], Stechkina [9]) are:

$$\left.\begin{aligned} N(\infty,\theta) &= 1 \\ N(1,\theta) &= 0 \\ N(L,\pi) &= 1 \end{aligned}\right\} \qquad (8)$$

A generalized analytical solution of Eq. (7) with boundary conditions (8) for some of the flow models presented in Table 2 and for the particular case of one sphere in an infinite fluid [Table (1 obtained lately by Tardos, et al. [39]. This solution applies for the case of low Reynolds number flow and for high values of the Peclet number, Pe > 100. The last condition is not a restrictive one for dust filtration theory because of the small values of the particle diffusion coefficient, $\mathcal{D}$. The single filter element efficiency E_D (due to diffusion only) as obtained in the above work is:

$$E_D = \frac{4Sh}{Pe} = 4\ g(\varepsilon)\ Pe^{-2/3} = 4 \sqrt[3]{\frac{2}{3\sin^2\theta} \cdot \left|\frac{\partial^2\psi(1,\varepsilon,\theta)}{\partial R^2}\right|} \cdot Pe^{-2/3} \qquad (9)$$

where Sh is the Sherwood number, $g(\varepsilon)$ is a correction factor and $\psi(R,\varepsilon,\theta)$ is the stream function (Table 2). This equation was first obtained by Levich [37] for the case of diffusion to a free failing solid sphere situated in an infinite fluid [$g(1) = 1$]. The same solution was also obtained by Friedlander [40] and Lochiel and Calderbank [41], and approximately by Zebel [42], while a second order correction to this expression was indtroduced by Acrivos and Goddard [43]. Levich's solution was applied to a sphere situated in a multi-particle system (granular bed) by Pfeffer [44] for the case of the Happel [27] flow model, by Sirkar [45] for the Tam [30] model, and by Tardos, et al. [39] for the Kuwabara [28] and Neale and Nader [32] flow fields. Expressions of $g(\varepsilon)$ for different flow models given in Table 2 are presented in Table 3, (Gutfinger and Tardos [46]).

The finite size of the dust particles, i.e., the Interception effect, was not taken into account in Eq. (9). In order to consider this effect together with diffusion, the boundary conditions (8) of Eq. (7) must be modified accordingly:

$$\begin{aligned} N(\infty,\theta) &= 0 \\ N(1 + R_p,\theta) &= 0 \qquad\qquad (10) \\ N(1 + R_p,\pi) &= 1 \end{aligned}$$

where, $R_p = r_p/a$ is the Interception parameter. The boundary conditions in the form of Eq. (10), is the mathematical expression of assumption (6), which states that dust particles approaching the filter element (collector) to a distance equal to its size, are separated from the flow. Eq. (9) with boundary conditions (11) was solved using a numerical scheme and the Kuwabara flow model [Table (2)] by Tardos, et al.[47].

All the above presented solutions for the single filter element efficiency, E_D, are valid for low and very low Reynolds number flows, where creeping motion can be assumed. Pfeffer's solution, Table 3 (1). was extended for small values of the Reynolds number Re < 1 by El-Kaissy and Homsy [48] using a small perturbation technique.

For the case of circulating bubble swarms, Le Clair and Hamielec [49], obtained expressions for the overall Sherwood number for all values of the Reynolds number. These results may be used in a wetted (lubricated) granular bed. No similar solution for beds of solid elements was obtained to date.

For the sake of completeness, the different solutions for diffusion to one single sphere in an infinite fluid at intermediate and high Reynolds numbers are presented in Table 4. These solutions cannot be applied directly to granular bed filtration.

In conclusion, it may be stated that in spite of the great number of theoretical studies on mass transfer to a sphere (solid or fluid), the problem of filtration in a dense granular bed of solid granules is far from being solved. The only reliable data are those for low Reynolds number flows (creeping flows, Table 3) when the flow and the transport phenomenon can be modeled by a relatively simple model. More effort is necessary to extend this solution for high Reynolds number flows.

Interceptional Deposition

Interception occurs due to the fact that a certain amount of particle laden fluid passes in the vicinity of a collector through the concentric annulus with radii a, and $a + r_p$. Particles carried by the fluid through this space touch the filter element because of their size, r_p. This effect takes place even when inertial, diffusional and other deposition effects are negligible.

Interception can be taken into account in the fashion presented by Tardos, et al. [7, 47]. However, for small values of the interception parameter, $R_p = r_p/a \le 0.01$, an analytical solution is possible (Gutfinger and Tardos [46]). The single filter element

TABLE 3

VALUES OF CORRECTION FRACTOR $g(\varepsilon)$ FOR MASS TRANSFER IN A GRANULAR BED

Author	Flow field used	$g(\varepsilon)$	Range	Remarks
1. Pfeffer [44] Cookson [83]	Happel [27]	$\left[\frac{2[1-(1-\varepsilon)^{5/3}]}{2-3(1-\varepsilon)^{1/3}+3(1-\varepsilon)^{5/3}-2(1-\varepsilon)^{2}}\right]^{1/3}$	$Re_o < 0.01$ $Pe \geq 1000$	Theoretical
2. Tardos et al [39]	Kuwabara [28]	$\left[\frac{\text{[illegible]}}{2-\varepsilon-\frac{9}{5}(1-\varepsilon)^{1/3}-\frac{1}{5}(1-\varepsilon)^{2}}\right]^{1/3}$	$Re_o < 0.01$ $Pe \geq 1000$	Theoretical
3. Sirkar [45, 84]	Tam [30]	$\left[\frac{2+1.5(1-\varepsilon)+1.5[8(1-\varepsilon)-3(1-\varepsilon)^{2}]^{1/2}}{\varepsilon[2-3(1-\varepsilon)]}\right]^{1/3}$	$Re_o \leq 1$ $\varepsilon > 0.33$ $Pe \geq 1000$	Theoretical
4. Tardos et al. [39]	Neale & Nader [32]	[illegible]	$\gamma = \frac{\varepsilon}{(1-\varepsilon)^{1/3}}$ $Re_o \leq 10$ $Pe \geq 1000$	Can be approximated by: $g(\varepsilon) = 1.31/\varepsilon$ $0.35 \leq \varepsilon \leq 0.7$
5. Tardos et al. [47]	Kuwabara [28]	$1.07 + 3.43\,(1-\varepsilon)$	$Re_o < 0.01$ $Pe \geq 1000$	Numerical solution
6. Tan et al. [78]	—	$1.1/\varepsilon$	$Re_o < 1$ $0.35 < \varepsilon < 0.7$	Experimental
7. Wilson and Geankoplis [79]	—	$1.09/\varepsilon$	$Re_o < 10$ $0.35 < \varepsilon < 0.7$	Experimental
8. Thoenes & Kramers [85]	—	$1.448/\varepsilon$	$Re_o < 10$ $\varepsilon = 0.476$	Experimental (regular packing)
9. Karabelias et al. [69]	—	$1.19/\varepsilon$	$Re_o < 10$ $\varepsilon = 0.26.$	Experimental (regular packing)
10. Sorensen & Stewart [85]	Sorensen & Stewart [26]	$1.104/\varepsilon$ $1.17/\varepsilon$	$\varepsilon = 0.476$ $\varepsilon = 0.26$	Theoretical (regular packing)

TABLE 4

DIFFUSIONAL DEPOSITION ON ONE SPHERE

Author	Flow Field Used	Result	Remarks
1. Levich [37]	Creeping Flow Table 1 (1)	$Sh = 0.997\ Pe^{1/3}$	Solid Spheres
2. Acrivos & Goddard [43]	Creeping Flow Table 1 (1)	$Sh = 0.991\ Pe^{1/3} + 0.922$	Solid Spheres
3. Yao in Prieve & Ruckenstein [61]	Creeping Flow Table 1 (1)	$Sh = 0.995\ Pe^{1/3} + \frac{3}{8}\ \frac{Pe}{Rp^2} + \frac{1}{9}\ StGaPe$	Solid Spheres London and Gravity Forces Considered
4. Levich [37]	Creeping Flow Table 1 (1)	$Sh = 0.65\ Pe^{1/2}$	Spherical Circulating Bubble
5. Woo & Hamielec [86]	Intermediate Reynolds No. Flow Table 1 (4)	Numerical Solution	Drops
6. Lochiel & Calderbank [41]	Boundary Layer Theory	$Sh = 0.84\ Re_o{}^{1/2} Sc^{1/3}$	Solid Spheres*
7. Suneja [87]	Potential Flow Table 1 (5)	$Sh = 0.768\ Pe^{1/2} + 0.5\ R_p\ Pe$	Drops, Considering Interception Effects
8. Boussinesq in Chao [88] Le Clair, Hamielec [49]	Potential Flow Table 1 (5)	$Sh = 1.13\ Pe^{1/2}$	
9. Watts [89]	Potential Flow Table 1 (5)	$Sh = 1.156\ Pe^{1/2} + 4.73$	
10. Winnikow in LeClair and Hamielec [49]	Potential Flow (High Re_o No.)	$Sh = \frac{2}{\sqrt{\pi}}(1 - 2.89\ Re_o{}^{-1/2}) Pe^{1/2}$	$Re_o \geq 100$

*The Schmidt number is defined as $Sc = \frac{\mu_A}{\rho_A D}$. Thus $Pe = Re_o \cdot Sc$.

Remark: This table is not complete due to the enormous number of theoretical studies of mass transfer to a sphere or spherical bubble.

efficiency E_R (due to interception only) is given by:

$$E_R = 1.5\ g(\varepsilon)^3\ R_p^{\ 2} \tag{11}$$

A similar expression for the special case of the Happel flow model [27] was first obtained by Paretsky [2] and lately by Rajagopalan and Tien [50] In Eq. (11) $g(\varepsilon)$ is the correction given in Table 3.

Inertial Separation

The motion of dust particles larger than about 2-3μm in a gas stream is governed by such forces as inertia and drag. These effects may determine the collision of the particles with a filter element (collector), situated in the flow. If the surface of this collector retains the dust particles, they are separated from the stream and the process is called inertial deposition. This may be explained as follows: the existence of the collector in the flow causes a curvature of the gas stream lines near the surface. In the vicinity of the surface, the particles cannot follow the curvature of the streamlines and due to their inertia, are projected against it and separated from the stream. It is obvious, that the impact is conditioned by the shape and size of the collector, the characteristics of the flow pattern, and the properties of the dust particles. In order to find the conditions for the impact between the dust particles and the collector, the trajectory of the particles must be known.

The general equations of motion of one small particle in the filter bed were presented by different authors (Paretsky [2] and Pilat, et al. [51]) in the form:

$$\frac{d^2\vec{X}}{dT^2} = \frac{1 + R_p}{St}\left(\vec{U} - \frac{d\vec{X}}{dT}\right) + \frac{\vec{F}_{ext}\ a(1 + R_p)}{m_p U_o^2} \tag{12}$$

Here, $\vec{X}$ is the position vector, $\vec{U}$ is the dimensionless gas velocity whose components are given in Eq. (5), $St = 2C\rho_p U_o r_p^{\ 2}/(9\mu a)$ is the so called Stokes number, $R_p = r_p/a$ is the Interception parameter and $\vec{F}_{ext}$, the external force acting on the particle (excluding drag). The stream funciton, ψ, as presented in Tables 1 and 2 may be used directly in Eq. (12) to compute the gas velocity $\vec{U}$. The equation of motion as written above is general enough to incorporate any effect that influences the motion of the dust particle. This is accomplished by introducing the proper effect through the external force $\vec{F}_{ext}$. If several effects coexist, they may be added together at this point.

The procedure by which a single element efficiency, E, is computed goes through the following sequence:

- Eq. (12) is solved for a given dust particle, resulting in the particle trajectories, Fig. 1.
- Of these, the limiting trajectory, i.e., the trajectory that just misses the collector, is taken, and its distance, b, from the line of symmetry is recorded. The single filter element efficiency is computed from the relation of definition (Eq. 3).

If in the general equation (12), the value of the external force is taken zero ($\vec{F}_{ext} = 0$), the resulting equation yields particle trajectories when only inertial effects are considered. The initial conditions for Eq. (12) are:

$$\left.\begin{array}{l} \vec{X}\,(o) = \vec{X}_o \\ \dfrac{d\vec{X}}{dT}\,(o) = \vec{e}_{Uo} \end{array}\right\} \qquad (13)$$

where $\vec{e}_{Uo}$ is the unit vector in the direction of gas flow, and $\vec{X}_o$ is the position vector of the trajectory starting point.

The dimensionless quantity $St = 2C\rho_p U_o r_p^2/9\mu a$ in eq. (12) is the Inertial parameter or, the so-called Stokes number. The value of this parameter characterizes pure inertial deposition of dust on a collector and therefore, computed values of the inertial single filter element efficiency, E_I, are given as a function of this quantity.

The simplest solutions for the collection efficiency, E_I, are those when one considers creeping or potential flow around a single sphere. This is done by substituting the appropriate expressions for the velocity, $\vec{U}$, and solving for the limiting trajectory. The difference between this solution and those for more complicated cases will be only in the expressions for the velocity of the fluid substituted into Eq. (12). Any fluid velocity profile listed in Tables 1 and 2 is appropriate for this purpose. Table 5 summarizes the theoretical results for various conditions available in the literature. All the solutions listed are numerical solutions and except for the results of Michael and Norey [52] are presented in graphical form. The first seven works listed in Table 5 provide efficiences, E_I, for a single sphere situated in an infinite fluid under various flow conditions, while the remainder of the works are for a sphere inside a granular bed at various flow conditions and various simplifying assumptions.

TABLE 5

INERTIAL DEPOSITION OF PARTICLES

Author	Deposition On	Range	Flow Field Used	Remarks
1. Herne [54]	one sphere in infinite fluid	Creeping Flow Potential Flow	Table 1 (1) Table 1 (5)	
2. Hocking [90]	one sphere	Creeping Flow	- - -	
3. Michael & Norey [52]	one sphere	Potential Flow	Table 1 (5)	$E = 1 - \frac{1}{St} + \frac{1}{St^2}$ for $St \geq 5$
4. Pearcey & Hill	one sphere	$Re_o = 1,4,10$	- - -	
5. Present Fig. 2,3	one sphere	$Re_o = 0.01\text{-}80$	Table 1 (2),(3)	
6. Beard & Grover [60]	one sphere	$Re_o = 1\text{-}400$	Table 1 (4)	Valid for drops
7. Pilat et al. [51]	one sphere	Potential Flow	Table 1 (5)	Diffusion effects considered
8. Paretsky et al [74]	packed bed	Creeping Flow (Happel Model)	Table 2 (1)	
9. Tardos et al. [7]	fluidized bed	Creeping Flow (Kuwabara model)	Table 2 (1)	Interception and gravity effects considered
10. Rajagopolan and Tien [50]	Packed bed	Creeping Flow (Happel Model)	Table 2 (1)	London forces, gravity and interception effects considered $E = 0.72\ g^3(\varepsilon)\ Lo^{118}\ R_p^{1518} + 2.4\ 10^{-3}\ g(\varepsilon)^3\ (GaSt)^{1.2}\ R_p^{-0.4}$ for $R_p < 0.18$
11. Gutfinger et al. [58]	fluidized bed	Potential Flow	Table 2 (3)	Interception effects considered
12. Gutfinger & Tardos [46]	packed & fluidized beds	Heale & Nader flow model $Re_o < 10$	Table 2 (5)	Diffusion and interception effects considered

$$\frac{d^2\vec{X}}{dT^2} = \frac{1 + R_p}{St}\left(\vec{U} - \frac{d\vec{X}}{dT} + Ga \cdot St \cdot \vec{e}_g\right) \tag{14}$$

Here, $Ga = ga/U_o^2$ is the so-called Gallileo number and, $\vec{e}_g$ is a unit vector oriented in the direction of the gravity field. Equation (6) with initial conditions (15) was solved by Tardos, et al. [7] using the Kuwabara flow model and a Runge-Kutta integration scheme. An analytical expression for pure gravitational deposition efficiency (the special case $St \rightarrow 0$) was lately obtained by Prieve and Ruckenstein [61] and Rajagopalan and Tien [50] in the form:

$$E_G = St \cdot Ga \tag{15}$$

Particle Deposition due to Electrical Effects

Electrical forces may occur in a granular bed either due to an external electric field, E_o or due to induced electrostatic effects. The electrostatic effect usually appears in fluidized beds of dielectric materials because of the mutual friction between the granules or because the charge carried by the dust particles entering the filter. Electrical forces usually affect strongly the separation efficiency of a filter bed because of the high potentials which are generated between the granules.

The mathematical treatment of the electrical deposition follows closely the presentation in the previous paragraphs. The external force in the general trajectory, Eq. (12), must be computed accordingly:

$$\frac{d^2\vec{X}}{dT^2} = \frac{1 + R_p}{St}\left(\vec{U} - \frac{d\vec{X}}{dT} + K_e\,\vec{f}\right) \tag{16}$$

Expressions for the last term of the above equation, $K_e\vec{f}$, are given in Table 6 (after Nielsen and Hill [62]). Equation (16) takes into account explicitly the effects of inertia, fluid drag and electrical force on the motion of a dust particle. The trajectory equation in this form was solved only for the case of a single spherical or ellypsoidal collector situated in an infinite fluid [Kraemer and Johnston [63], Zebel [42], Knutson [64], Nielsen and Hill [62]).

A similar problem of electrical deposition of dust particles in a granular bed was not yet solved. The difficulty arises when the electric charge on the collector, Q_C, or the particle, Q_p, must be measured or evaluated. No general model of the charged granular bed

TABLE 6

ELECTRICAL FORCE EXPRESSIONS (NIELSEN & HILL, [62])

e	Force F_e	Description	Parameter K_e	Radial Component f_r	Angular Component f_θ
c	Coulombic force	Both collector and particle are charged.	$K_c = \frac{CQ_cQ_p}{24\pi^2\epsilon_f r_p a^2 \mu U_o}$	$1/R^2$	0
ic	Charged-particle image force	Particle only is charged. Charge separation induced in collector.	$K_{ic} = \frac{\gamma_c CQ_p^2}{24\pi^2\epsilon_f r_p a^2 \mu U_o}$	$-[R/R^2 - 1)^2 - k/R^3]$	0
ip	Charged-collector image force	Collector only is charged. Charge separation induced in particle.	$K_{ip} = \frac{\gamma_p CQ_c^2 r_p^2}{12\pi^2\epsilon_f a^5 \mu U_o}$	$-1/R^5$	0
ex	External electric field force	Particle only is charged. Charge separation in collector induced by external electric field	$K_{ex} = \frac{CQ_pE_o}{6\pi r_p \mu U_o}$	$(1 + 2\gamma_c/R^3)\cos\theta$	$-(1 - \gamma_c/R^3)\sin\theta$
icp	Electric dipole interaction force	Neither body is charged. Charge separation in both bodies induced by external electric field	$K_{icp} = \frac{2\gamma_c\gamma_p\epsilon_f Cr_p^2 E_o^2}{a\mu U_o}$	$-[2(1 + 2\gamma_c/R^3)\cos^2\theta]$ $-(1 - \gamma_c/R^3)\sin^2\theta]/R^4$	$\frac{-[(2 + \gamma_c/R^3)\sin\theta\cos\theta]}{R^4}$

In Figs. 2 and 3, single filter element efficiencies, E_I, for the case of inertial deposition on a sphere situated in an infinite fluid at Reynolds numbers $Re_o = 0, 0.01, 0.1, 10, 40, 80, 100, \infty$ are presented. For this purpose, the flow fields, as obtained by Goldstein (Oseen flow, Table 1) and Hamielec, et al. [53] (Table 1) were used. The results of Herne [54], Michael and Norey [52], Langmuir (Pich [55] and Fuchs [56]), Tardos [7,57], and Gutfinger, et al. [58], with some experiments of Walton and Woolcock [59] are also presented in the Figures. As seen, for the two limiting cases of Stokes flow ($Re_o \to 0$) and potential flow ($Re_o \to \infty$), the solutions are in good agreement. Furthermore, single sphere efficiencies obtained by considering the Oseen flow round the sphere, are identical to those obtained from the Stokes flow considerations for $Re_o = 0.01$ and $St > 1.5$.

Values of single sphere efficiency obtained by considering the approximate Hamielec flow field as given in Figure 3 are between the two limits (potential and Stokes flow model) for Reynolds numbers $Re_o = 10 - 80$. A rather unexpected result is that of $Re_o = 100$, which gives higher collection efficiencies than those of potential flow. This probably indicates that the Hamielec flow solution breaks down at $Re_o > 100$. Some recent numerical results for the flow field as obtained by Le Clair, et al. [17] were used by Beard and Grover [60] to compute single sphere collection efficiencies at intermediate Re numbers which do not suffer from this deficiency.

In all the works presented above only pure inertial deposition was dealt with. The effect of interception, i.e., the finite size of the dust particles, may be introduced during the computational process in the following way: any particle having a trajectory that passes the collector surface closer than a distance equal to its radius, r_p, is intercepted. This is equivalent to increasing the effective radius of the filter element by one particle radius, $R_{ef} = 1 + R_p$. Computations of this kind were first carried out by Tardos, et al. [7] and lately by Gutfinger and Tardos [46].

Gravitational Deposition

As pointed out previously, the general trajectory equation (12) incorporate any effect that may influence the motion of a dust particle within the granular bed. If the external force in the equation is taken as $\vec{F}ext = m_p g \vec{e}_g$ gravitational separation (settling) of particles is obtained together with inertial effects. The trajectory equation in this case becomes:

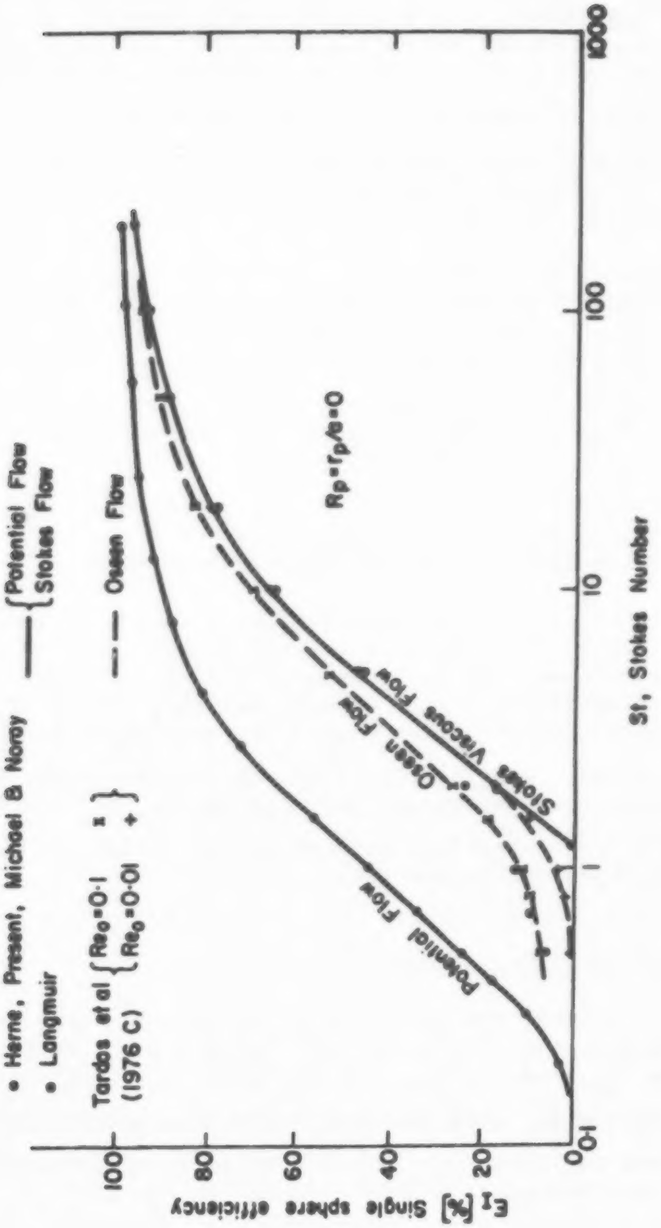

Figure 2: Single sphere efficiency at Re_o = 0.01–0.1

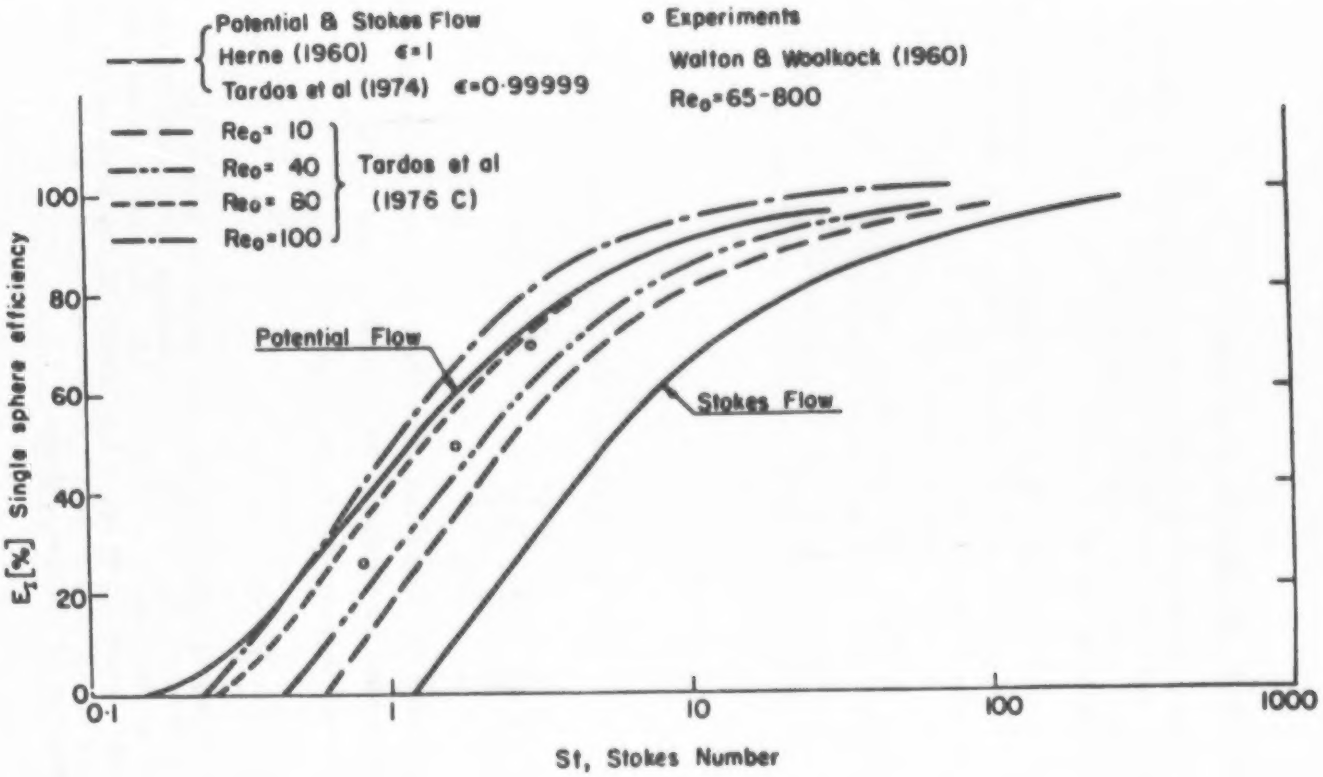

Figure 3: Single sphere efficiencies at Re_o = 10-100

was yet developed, neither was a granule charge measuring technique established. However, an approximate solution was presented lately, by Zahedi and Melcher [65] for dust filtration in a bubbling fluidized bed with external electric field produced with the help of two electrodes.

Combined Diffusional and Inertial Deposition

In cases where inertia and diffusion did interact, a common way of computing the combined filtration efficiency is to add the separate efficiencies due to these two effects (Payatakes, et al [35], Yao, et al [66], Rajagopalan and Tien [50]).

In order to consider the effect of diffusion in combination with inertial effects, $\vec{F}_{ext}$ in Eq. (12) must be computed so that it will account for the concentration gradient between the flue gas stream, n_o, and the filter element surface where the concentration is taken as zero. One may consider this process as caused by a "diffusion force" whose effect is a relative particle-gas velocity, $\vec{V}_B$, due only to diffusion. The "diffusion force" is assumed to be a Stokes type force and can be computed using the Stokes equation (Paretsky [2] and Pilat, et al [51]:

$$\vec{F}_{ext} = \frac{6\pi\mu \vec{V}_B r_p}{C} \qquad (17)$$

Introducing Eq. (17) into Eq. (12), one obtains for the trajectory equation:

$$\frac{d^2\vec{X}}{dT^2} = \frac{1 + R_p}{St}\left(\vec{U} - \frac{d\vec{X}}{dT} + \frac{\vec{V}_B}{U_o}\right) \qquad (18)$$

In order to evaluate the diffusion velocity V_B/U_o, the corresponding diffusion problem must be solved. The diffusion velocity V_B can be computed as follows (Bird, Stewart and Lightfoot [67]:

$$\frac{V_B}{U_o} = -\frac{2}{Pe}\cdot\frac{1}{N}\cdot\frac{dN}{dR} \qquad (19)$$

Here, N is the dimensionless particle concentration dN/dR, the concentration gradient and, Pe, the Peclet number. Equation (18) was solved recently by Gutfinger and Tardos [46]. The computations show that in the region where inertial and diffusional depositions are weak, the efficiencies obtained are close to the ones calculated by a simple arithmetic summation of the two effects.

A generalized form of Eq. (18) including inertial, diffusional, electrical and gravitational effects can now be written easily using the notations of the previous chapters as:

$$\frac{d^2\vec{X}}{dT^2} = \frac{1 + R_p}{St}\left(\vec{U} - \frac{d\vec{X}}{dT} - \frac{2}{Pe}\ \frac{1}{N}\frac{dN}{dR}\,\vec{e}_r + K_e\vec{f} + Ga \cdot St\ \vec{e}_g\right) \qquad (20)$$

In order to solve Eq. (20), the flow field, $\vec{U}$, must be specified as in Tables 1 and 2. The diffusional term 2/NPe • dN/dR, has only a radial component, whereas, the last term on the right hand side, has a component directed parallel to the gravity field (see Fig. 1). Values for the term characterizing electrical effects are available only for spheres situated in an infinite fluid (Table 6). The solution of Eq. (20) for a granular bed has not been achieved to date.

EXPERIMENTAL WORK ON GRANULAR BED FILTRATION

A review of experimental works on fluidized bed filtration was presented by Jackson [68] and Payatakes, et al [35] and on mass transfer in packed beds by Karabelas, et al [69] and recently by Hsiung and Thodos [70]. Some of the more important experimental works on granular beds are listed below.

Meissner and Mickley [71] carried out their experiments on a fluidized bed of 1.85 in. diameter containing microspheres of different materials, such as cracking catalyst, activated alumina, silica gel, glass, etc., with diameters 74-147 μm. These beds were used to remove sulfuric acid mists from an air stream; mist concentrations used were 0.3 - 2 mg/l, mist droplet size was 2-14 μm. In these conditions, they obtained filter bed removal efficiencies from 40-90 percent.

Similar experiments were conducted by Black and Boubel [72] for removal of sublimated ammonium chloride particles (mean size 0.52 μm and concentration 0.03-8.3 mg/m^3) from air with a fluidized bed of glass shot in a 2 in. column. They obtained removal efficiencies of 50-90 percent.

Thomas and Yoder [73] and Paretsky, et al [74] reported experiments with low concentration latex aerosols filtered through sand beds at different gas velocities. Deposition efficiencies of 40-100 percent were obtained.

Recent experimental results of filtration in fluidized bed filters were obtained by Knettig and Beeckmans [75] and McCarthy, et al [76] The experiments by Knettig and Beeckmans [75] were carried out in order to demonstrate the very pronounced influence of the supporting screen or grid on the overall efficiency of the filter. Methylene blue and uranine aerosols of 0.8, 1.6, and 2.9 μ were passed through

425 μ diameter glass shot beds of different heights. Packed and fluidized beds were considered. The filter bed was supported by a screen (30.3 percent open area) or a grid (0.569 percent open area). It was clearly demonstrated that in the case of the grid supported bed, the superficial velocity, U_o, computed on the empty bed cross section, was meaningless for the efficiency computations. The fluid jets produced by the supporting device increase the filtration efficiency especially of the first layers.

Careful efficiency measurements of DOP (di-octyl-phtalate) aerosols in a five-stage fluidized bed were carried out by McCarthy, et al [76]. The gas velocity varied between 1.5-4.5 cm/sec and the aerosol particle diameters between 0.06-1.4 μm, placing these experiments in the diffusional deposition region. The filter bed material was 135 μm diameter alumina granules. Filtration efficiencies were measured after each one inch of bed height. High total efficiencies were obtained.

In Fig. 4, a comparison of theoretical data as obtained by Tardos, et al [39,47.77] with experimental filter bed efficiencies, η, of Paretsky, et al [74] and Knetting and Beeckmans [75] is presented. The fit between the computed and experimentally obtained results is reasonable. Recent filtration experiments performed by Gutfinger and Tardos [46] with several electrically neutral systems are plotted in Fig. 5 together with theoretical curves. Also here the fit is quite good.

Experimental mass transfer data and analytical correlations for packed beds which are applicable to submicron filtration are in a great abundance. Recently, Tan, et al [78] demonstrated once more the validity of the experimental relationship established initially by Wilson and Geankoplis [79] for the case of mass transfer at low Reynolds numbers ($Re \leq 1$) and high Peclet numbers ($Pe \geq 1000$) in packed beds of spherical elements:

$$Sh = g(\varepsilon)\ Pe^{1/3} = \frac{c}{\varepsilon}\ Pe^{1/3} \qquad (21)$$

Here, c, is a constant which must be determined experimentally. Different values for this constant, obtained by various authors, are presented in Table 5, together with expressions deduced from theory. The agreement between the experimental values of c = 1.09-1.98 and the theoretical values c = 1.31 obtained by Tardos, et al [39] is very good indeed.

Summary

In the present paper, the state of the art of dust deposition in granular bed filters was presented. First the flow fields used in modeling such filters were listed, then the collection efficiency of

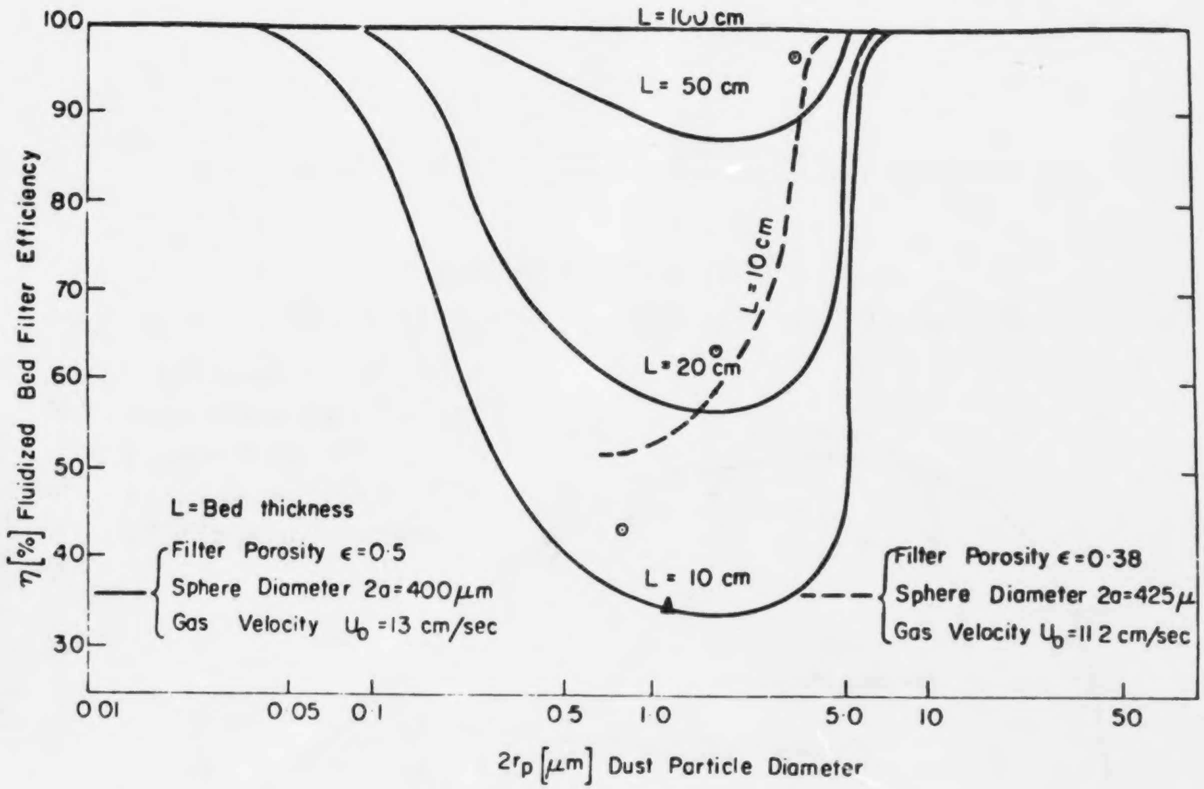

▲ Experimental, Paretsky et. al. [74] - U_o = 13.3 cm/sec, L = 8.2 cm, 2a = 500 - 1850 μm, ε = 0.43

⊙ Experimental, Knetting and Beeckmans [75] - Screen supported bed, U_o = 11.2 cm/sec, L = 10 cm, 2a = 425 μm, ε = 0.38

Figure 4: Fluidized bed filter efficiency vs. dust particle diameter.

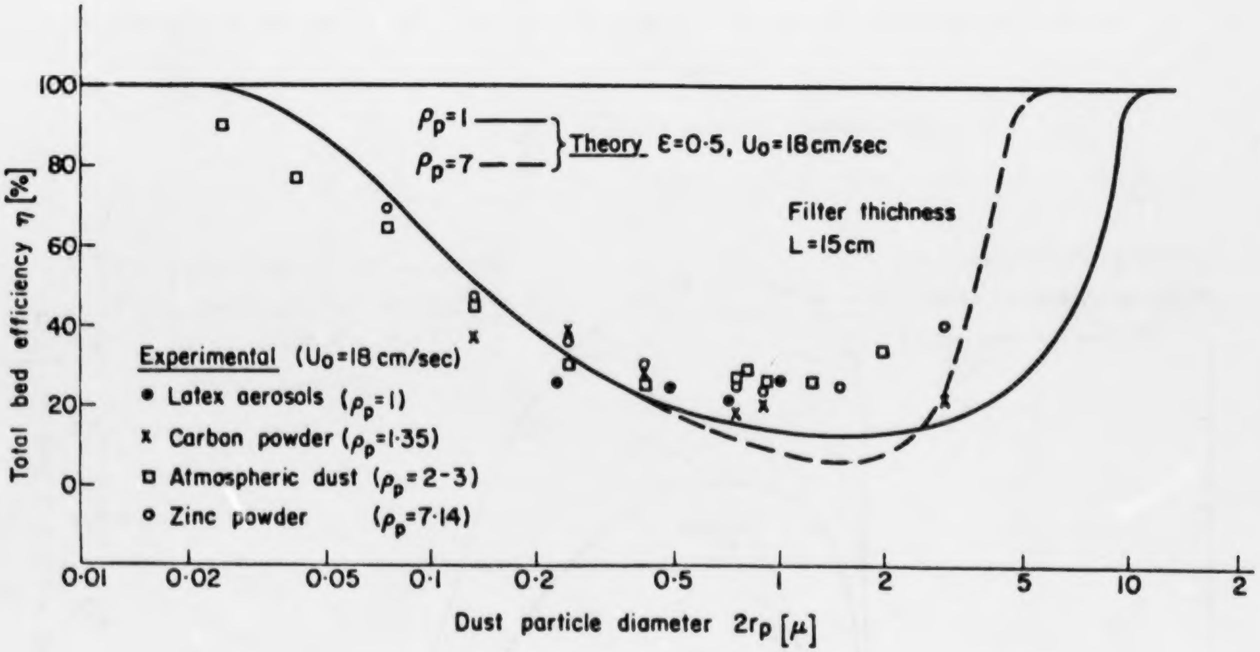

Figure 5: Total Filter Efficiency versus dust particle diameter in a tin bed of 690μ granules (porosity $\varepsilon = 0.5$)

single elements and whole filters for inertial, diffusional and interception mechanisms were defined. Experimental data obtained with such filters were compared with theoretical predictions.

As a conclusion, one can state that although the granular bed has proven itself, both theoretically and experimentally, as a very efficient filter for micron and submicron particles, there is still considerable work to be done in order to explain the operation of granular filters. This includes theoretical models that will take into account electrostatic forces, the entrainment of dust from the collector's surface, unsteady characteristics of the filter, and lastly, comparison of these theoretical results with well-designed experiments.

ACKNOWLEDGEMENTS

This research was supported by a grant from the National Council for Research and Development, Israel, and the KFA Julich, Germany.

REFERENCES

1. Squires, A. M. and R. Pfeffer. JPACA. 20: 534, 1970.
2. Paretsky, L. Ph.D. Thesis, City Univ. of New York. 1972.
3. Lee, K. C. PH.D. Thesis, City University of New York. 1975.
4. Cook, C. C., G. R. Swany and J. W. Colpitts, J.A.P.C.A., 21: 479, 1971.
5. Rubin, Yu. M. and Yu. A. Margolin. Coke & Chem. (USSR). 17: 3, 1974.
6. Krupp-Koppers, British Patent No. 1921684, 1974.
7. Tardos, G., C. Gutfinger and N. Abuaf. Deposition of Dust Particles in a Fluidized Bed Filter. Israel J. Tech. 12: 184, 1974.
8. Jugel, W. E. O. Reher, R. Grobler, und A. Tittmann. Die Abscheidung von Staubteilchen aus einem Verunreinigtem Gasstrom mit Hilfe des Wirbelschichtverfahrens. Chem. Techn. 22: 7, Juli 1970.
9. Stechkina, I. B. and N. A. Fuchs. Ann. Occup. Hyg. 9: 59-64, 1966; 10: 23-30, 1967; and 11: 299-303, 1968.

10. Dorman, R. G. Dust Control and Air Cleaning, Pergamon Press, Oxford, 1974.

11. Loffler, F. Collection of Particles by Fiber Filters. in Air Pollution Control, W. Straus, Ed., John Wiley, London. 1971.

12. Lamb, H. Hydrodynamics; 6th Ed., Cambridge University Press, Cambridge. 1932.

13. Proudman, I. and J. R. A. Pearson. Expansion at Small Reynolds Numbers for the Flow Past a Sphere and a Circular Cylinder. J. Fluid Mech. 2: 237, 1957.

14. Pearcey, I. and B. McHiugh. Phil. Mag., (7th series). 46: 783, 1955.

15. Jenson, V. G. Viscous Flow Round a Sphere at Low Reynolds Number (<40). Proc. Roy. Soc. A 249: 346, 1959.

16. Hamielec, A. E. T. W. Hoffman, and L. L. Ross. AIChE J. 13: 2, 1967.

17. LeClair, B. P., A. E. Hamielec, and H. R. Pruppacher. J. Atmos. Sci. March 1970.

18. Rimon, Y. and S. I. Cheng. Phys. Fluids. 12: 949-959, 1969.

19. Dennis, S.C.R. and J.D.A. Walker. J. Fluid Mech., 48. 4: 771-789 1971.

20. Seeley, L. E., R. L. Hummel, and J.W. Smith. J. Fluid Mech. 68, 3: 591-608, 1975.

21. Schlichting, A. Boundary Layer Theory, McGraw Hill. 1960.

22. Scholkemeier, F.W. Arch. Math. 1, 1949.

23. Frossling, N. NACA TN 1432, Washington, February 1958.

24. Goldstein, S. Modern Developments in Fluid Dynamics. Dover Publication, New York, 1965.

25. Tomotika, I. ARC Reports and Memoranda, No. 1678, 1935.

26. Sorensen, J. P. and W. E. Stewart. Computation of Forced Convection in Slow Flow Through Ducts and Packed Beds - I, II, III, IV. Chem. Eng. Sci. 29: 819, 1974.

27. Happel, J. Viscous Flow in Multiparticle Systems: Slow Motion of Fluids Relative to Beds of Spherical Particles. AIChE Journal. 4: 197, 1958.

28. Kuwabara, S. The Forces Experienced by Randomly Distributed Parallel Circular Cylinders or Spheres in a Viscous Fluid at Small Reynolds Numbers. J. Phys. Soc., Japan. 14: 527. 1959.

29. Le Clair, B. P. and A. E. Hamielec. Viscous Flow Through Particle Assemblages at Intermediate Reynolds Numbers. I & EC Fundamdentals. 7, 4: 542. 1968.

30. Tam, C.L.W. The Drag on a Cloud of Spherical Particles in Low Reynolds Number Flow. J. Fluid Mech. 38: 537. 1969.

31. Batchelor, G. K. Sedimentation in a Dilute Dispersion of Sphere J. Fluid Mech. 52, Part 2: 245. 1972.

32. Neale, H. N. and W. K. Nader. Prediction of Transport Processes Within Porous Media: Creeping Flow Relative to a Fixed Swarm of Spherical Particles. AIChE Journal. 20: 530. 1974.

33. Scheidigger, A. Fluid Flow in Porous Media. John Wiley, New York. 1960.

34. Payatakes, A. C., C. Tien and R. M. Turian. A New Model for Granular Porous Media, Part I and II. AIChE Journal. 19: 58 and 67. 1973.

35. Payatakes, A.C., C. Tien and R.M. Turian. Trajectory Calculation of Particle Deposition in Deep Bed Filtration. AIChE Journal, 20, 5: 889, 1974.

36. Chandrashekhar, S. Selected Papers on Noise and Stochastic Processes. N. Wax, ed., New York. 1954.

37. Levich, V. G. Physicochemical Hydrodynamics, Prentice Hall, New Jersey. 1962.

38. Friedlander, S. K. Particule Diffusion in Low-Speed Flows. J. Coll. Int. Science. 23: 157, 1967.

39. Tardos, G. I., C. Gutfinger and N. Abuaf. High Peclet Number Mass Transfer to a Sphere in a Fixed or Fluidized Bed. AIChE Journal. 22. 6: 1147. 1976.

40. Friedlander. S. K. A Note on Transport to Spheres in Stokes Flow. AIChE Journal. 7: 347. 1961.

41. Lochiel, A. C. and P. H. Calderbank. Chem. Engng. Sci., 19: 471-484. 1969.

42. Zebel, G. Capture of Small Particles by Drops Falling in Electric Fields. J. of Colloid and Interface Science. 27, 2; 294, 1968.

43. Acrivos, A. and J. D. Goddard, "Asymptotic Expansions for Laminar Forced-Convection Heat and Mass Transfer: Part I and Part II," J. Fluid Mech. 23, 273 (1965) and 24, 339, (1966).

44. Pfeffer, R. Heat and Mass Transfer in Multiparticle Systems, Ind. Eng. Chem. Fundamentals. 3. 1964.

45. Sirkar, K. K. Creeping Flow Mass Transfer to a Single Active Sphere in a Random Spherical Inactive Particle Cloud at High Schmidt Numbers. Chem. Eng. Sci. 29: 863. 1974.

46. Gutfinger, C. and G. I. Tardos. Theoretical and Experimental Investigations on Granular Bed Dust Filter. Ind. Eng. Chem. Fund. (submitted for publication) 1977.

47. Tardos, G., N. Abuaf, and C. Gutfinger. Diffusional Filtration of Dust in a Fluidized Bed Filter, Atmospheric Environment. 10: 389. 1976.

48. El-Kaissy, M. M. and G. M. Homsy. A Theoretical Study of Pressure Drop and Transport in Packed Beds at Intermediate Reynolds Numbers. Ind. Eng. Chem. Fundam. 12, 1: 82. 1973.

49. Le Clair, B. P. and A. E. Hamielec. Viscous Flow Through Particle Assemblages at Intermediate Reynolds Numbers - A Cell Model for Transport in Bubble Swarms. Can. J. of Chem. Eng. 49: 713. 1971.

50. Rajagopalan, R. and C. Tien. Trajectory Analysis of Deep Bed Filtration with the Sphere in Cell Porous Media Model. AIChE Journal. 22, 3: 523. 1976.

51. Pilat, M. H. and A. Prem. Calculated Particle Collection Efficiencies of Single Droplets Including Inertial Impaction, Browian Diffusion, Diffusiophoresis and Thermophoresis. Atm. Env. 10: 13. 1976.

52. Michael, D. H. and P. W. Norey. Particle Collision Efficiencies for a Sphere. J. Fluid Mech. 37, 3: 565. 1969.

53. Hamielec, A. E., S. H. Storey and J. M. Whitehead. Canadian J. Chem. Engng. December 1963.

54. Herne, H. The Classical Computation of the Aerodynamic Capture of Particles by Spheres. Int. J. Air. Pollut. 3: 26, 1960.

55. Pich, J. Theory of Aerosol Filtration by Fibrous and Membrane Filters. in Aerosol Science, (Edited by C. N. Davies), Academic Press, New York. 1966.

56. Fuchs, N. Mechanics of Aerosols, Pergamon Press, Oxford. 1973.

57. Tardos, G. M. Sc. Thesis, Technion - Israel Institute of Technology, Haifa, Israel. March 1975.

58. Gutfinger, C., N. Abuaf, and G. Tardos. Proceedings of the Sixth Scientific Conference of the Israel Ecological Society, Tel Aviv. 4-5 June. 1975.

59. Walton, W. H. and A. Woolcock. The Suppression of Airborne Dust by Water Spary. Inst. J. Air. Pollut. 3: 129. 1960.

60. Beard, K. V. and S. N. Grover. Numerical Collision Efficiencies for Small Raindrops Colliding with Micron Size Particles, J of the Atm. Sc. 37: 543. March 1974.

61. Prieve, D. C. and E. Ruckenstein. Effect of London Forces Upon the Rate of Deposition of Brownian Particles. AIChE Journal, 20, 6: 1178. 1974.

62. Nielsen, K. A. and J. C. Hill. Collection of Inertialess Particles On Spheres with Electrical Forces. I & EC Fundamentals. 15: 149, 1976.

63. Kraemer, H. F. and H. F. Jonstone. Ind. Eng. Chem. 47: 2426, 1955.

64. Knutson, E. O. Approximate Formulas for Electrostatic Collection of Aerosol Particles by Sphereoids. J. of Coll. Int. Sci. 54, 3: 453. 1976.

65. Zahedi, K. and J. R. Melcher. JAPCA. 26: 345. 1976.

66. Yao, K. M., M. T. Hahibian and C. R. O'Melia. Water and Waste Water Filtration: Concepts and Applications. Environ. Sci. Technol. 5: 1105. 1971.

67. Bird, B. B., W. E. Stewart, and E. N. Lightfoot. Transport Phenomena. J. Wiley and Sons, New York. London. 1960.

68. Jackson, M. Fluidized Beds for Submicron Particle Collection, AIChE Symp. Ser. 141: 82. 1974.

69. Karabellas, A. J., T. H. Wegner and T. J. Hanratty. Use of Asymptotic Relations to Correlate Mass Transfer Data in Packed Beds. Chem. Eng. Sci. 26: 1581. 1971.

70. Hsiung, T. H. and G. Thodos. Mass Transfer Factors from Actual Driving Forces for the Flow of Gases Through Packed Beds ($0.1 < Re_o \leq 100$). J. Heat Mass Transfer. 20: 331. 1977.

71. Meissner, H. P. and H. S. Mickley. Removal of Mists and Dusts from Air by Beds of Fluidized Solids. Ind. and Engng. Chem. 1238. 1949.

72. Black, G. H. and R. W. Boubel. Effectiveness of a Fluidized Bed in Removing Submicron Particulate from Air Stream. I & EC Process Design Development. 8: 573. 1969.

73. Thomas, J. W. and R. E. Yoder. AMA Arch. Ind. Health. 13: 545 & 550. 1956.

74. Paretsky, L., L. Theodore, R. Pfeffer and A. M. Squires. J. Air Pollut. Control Ass. 21: 204. 1971.

75. Knetting, P. and J. M. Beekmans. Capture of Monodispersed Aerosol Particles in a Fixed and in a Fluidized Bed. Canadian J. of Chem. Eng. 52: 703. 1974.

76. McCarty, C., A. J. Yankel, R. G. Patterson, and M. L. Jackson. Multistage Fluidized Bed Collection of Aerosols. Ind. Eng. Chem. Process Des. Dev. 15, 2: 266. 1976.

77. Tardos, G. I., N. Abuaf and C. Gutfinger. Dust Deposition in Granular Bed Filters - Theories and Experiments. JAPCA, (accepted for publicatio). 1976.

78. Tan, A. Y., B. D. Prasher, and J. A. Guin. Mass Transfer in Nonuniform Packing. AIChE Journal. 21, 2: 396. 1975.

79. Wilson, E. J. and C. J. Geankoplis. Liquid Mass Transfer at Very Low Reynolds Numbers in Packed Beds. Ind. Eng. Chem. Fundamentals. 5: 9. 1966.

80. Hamielec, A. E. and A. I. Johnson. Canadian J. Chem. Engng. April 1962.

81. Payatakes, A. C. and M. A. Muira. Model of the Constricted Unit All Type for Isotropic Granular Porous Media. AIChE J. 23, 6: 922. 1977.

82. Muira, M. A. and A. C. Payatakes. Collection Solution of Creeping Mewtonion Flow Through Periodically Constricted Tubes With Piecewise Continuous Wall Profile. AIChE J. 24, 1: 43. 1968.

83. Cookson, J. T. Removal of Submicron Particles in Packed Beds. Environ. Sci. Tech. 17: 348. 1970.

84. Sirkar, K. K. Transport in Packed Beds at Intermediate Reynolds Numbers. Ind. Eng. Chem. Fundamentals. 14: 73. 1975.

85. Thoenes, D. and H. Kramers. Mass Transfer from a Sphere in Various Regular Packings to a Flowing Fluid. Chem. Eng. Sci. 8: 271. 1958.

86. Woo, S. E. and A. E. Hamielec. A Numerical Method of Determining the Rate of Evaporation of Small Water Drops Falling at Terminal Velocity in Air. J. of the Atm. Sci. 28: 1448. 1971.

87. Suneja, S. K. Capture of Particles by Drops Falling at High Speeds. J. of Colloid Interface Sci. 44, 3: 509. 1973.

88. Chao, B. T. Transient Heat and Mass Transfer to a Translating Droplet. J. of Heat Transfer, Transactions of the ASME. 273, May 1969.

89. Watts, R. G. The Effect of Curvature on Heat or Mass Transfer from an Isothermal Sphere. J. of Heat Transfer, Transactions of the ASME. 1, 1972.

90. Hocking, L. M. The Theoretical Collision Efficiency of Small Drops. Int. J. Air Pollut. 3: 154. 1960.

THE EFFECTS OF ELECTRIC AND ACOUSTIC FIELDS ON THE COLLISION RATES OF SUBMICRON SIZED DOP AEROSOL PARTICLES

Paul D. Scholz, Larry W. Byrd and Phillip H. Paul
Division of Energy Engineering
The University of Iowa
Iowa City, Iowa 52242

ABSTRACT

Results are presented of the effects of an a-c electric field combined with a traveling sound field on the collision coefficient of airborne submicron sized DOP particles. The study was conducted using a continuous flow system and a moderately monodisperse DOP aerosol with a particle concentration of about 2.5×10^6 cm^{-3} and a mean particle diameter of about 0.09 μm. The direction of propagation of the sound field was coaxial to the direction of flow and the a-c electric field was directed normal to the flow. At a sound wave intensity of 145 dB and a frequency of 7624 Hz, the collision coefficient was 1.95 times the Brownian coefficient. At the same sound field conditions but with the addition of the 69.5 kV/m (at 60 Hz) a-c electric field, the collision coefficient was increased to 2.64 times the Brownian value.

INTRODUCTION

The work reported here is based on an experimental investigation to study the effects of a traveling sound wave and an a-c electric field on the collision rates between submicron sized aerosol particles. The purpose of these external fields is to increase the relative motion between the aerosol particles, thereby increasing the particle-particle collision frequency. An increase in the collision frequency implies an increase in the rate of agglomeration or coalescence, assuming that the particles stick upon contact. Increasing the collision rate is of interest because of the possibility of preconditioning dusty gases by inducing the submicron sized particles to agglomerate onto larger

Preceding page blank

particles. In an air cleaning application, the agglomerates would be subsequently removed from the gas stream in a downstream and conventional particle removal device which, without the pretreatment, would not effectively remove the submicron particle fraction. As an example, Scott[1] has proposed the use of a progressive saw-tooth acoustic wave form to precondition a dusty gas. The field configuration used in this study further augments the particle collision rate by adding an a-c electric field that is directed normal to the traveling sound field. It should be noted that, whereas acoustic coagulation requires high frequency sources (i.e., on the order of 10-30 kHz) to establish the desired differential motion between the hyperfine and larger particles in a suspension, the two-field scheme suggested here has more flexibility because the field frequencies and magnitudes may be changed independently to optimize the rate of agglomeration. In addition, because of the additional enhancement that results by adding the crossed a-c electric field to the sound field, there is the potential of utilizing lower sound frequencies and intensities to achieve the same agglomeration rates.

Summary of Past Experimental Work

There is no experimental data available on collision rates of submicron sized particles subjected to a combination of electric and acoustic fields. Some data is available on sonic agglomeration of submicron sized aerosol particles (see, for example, Mednikov[2] and Shaw and Wegrzyn[3]). There is no literature available with data on the coagulation of submicron aerosol particles in an a-c electric field. Hence, the work reported here on the use of a combined acoustic and electric field to enhance agglomeration among submicron sized particles is unprecedented.

Organization of Paper

The next major section contains a discussion of the experimental facility that was used in the investigation. The results are presented and discussed in the section that follows the discussion of the facility. The conclusions are presented in the final section.

EXPERIMENTAL FACILITY

The facility consists of three systems: the aerosol generating system; the continuous flow coagulation system; and the system for extracting and determining the particle size and concentration of the flowing aerosol. These are to be discussed in this section, along with the components used to generate the electric and acoustic fields for the study.

Aerosol Generating System

A schematic of the aerosol generating system is shown in Figure 1. The system is based on the submicron aerosol generator developed by Liu[4] and associates at the University of Minnesota. (Most of the components of the system are manufactured by Thermo-Systems Incorporated (TSI) of

St. Paul, Minnesota, and the TSI model numbers are indicated in Figure 1.) The system consists of two atomizers, an evaporator-condenser, a 1 liter damping tank, a packed bed wet scrubber, a desiccant filled diffusion dryer, and a particle neutralizer. In the tests reported here, a 0.06% dioctylphthate (DOP) in alcohol solution was fed to the atomizers from two 50 mℓ syringes driven in parallel by a syringe pump. The purpose of the damping tank is to attenuate the oscillations in the particle concentration due to very small and inherent oscillations in the carriage speed of the syringe pump. The aerosol is passed through a Kr-85 bipolar charger to remove any net electrostatic charge that may exist because of the particle generation process. The charger does not neutralize each individual aerosol particle, but it does ensure that the particles obey a Boltzmann equilibrium bipolar charge distribution.

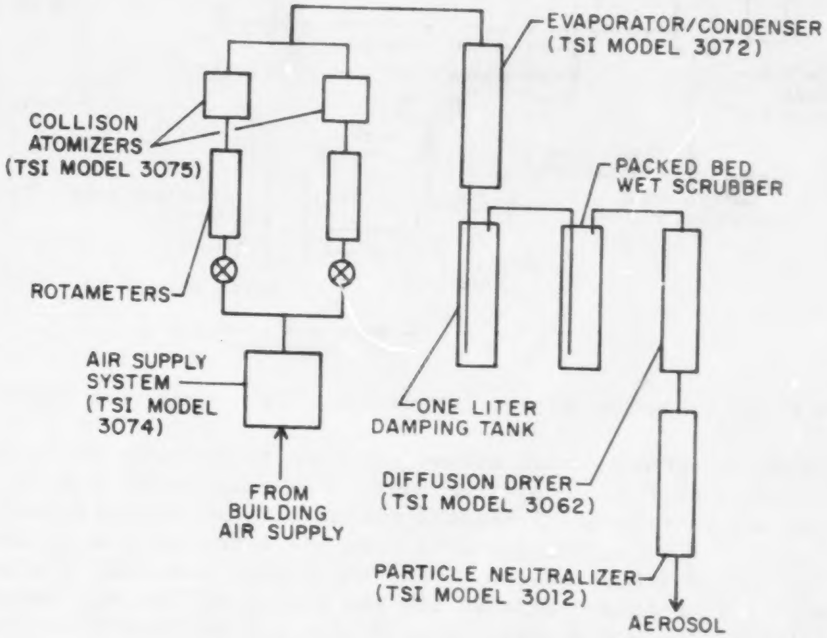
EVAPORATOR/CONDENSER
(TSI MODEL 3072)
COLLISON
ATOMIZERS
(TSI MODEL 3075)
PACKED BED
WET SCRUBBER
ROTAMETERS
AIR SUPPLY
SYSTEM
(TSI MODEL
3074)
ONE LITER
DAMPING TANK
FROM
BUILDING
AIR SUPPLY
DIFFUSION DRYER
(TSI MODEL 3062)
PARTICLE NEUTRALIZER
(TSI MODEL 3012)
AEROSOL

Figure 1. Aerosol generating system

Continuous Flow Coagulation System

A schematic of the continuous flow coagulation system is shown in Figure 2. The system consists of the entry section and the coagulation tube with isokinetic sampling probes.

The aerosol from the aerosol generating system described in the previous section is admixed with filtered air in a nozzle mixing block to give a total aerosol flow rate of 44 ℓpm. The total flow then passes through the entry section which introduces the flow uniformly and axially into the coagulation tube. A screen and a honeycomb structure

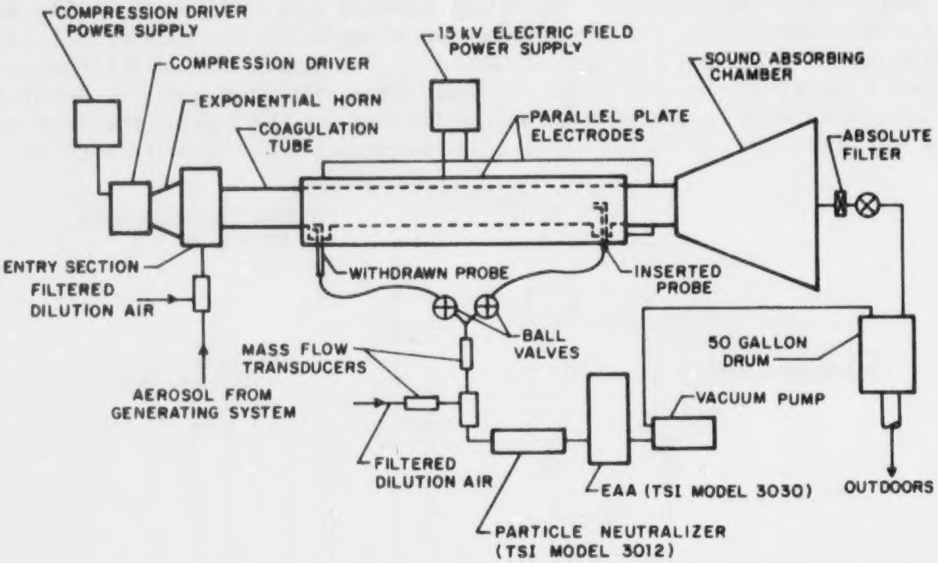
COMPRESSION DRIVER POWER SUPPLY
COMPRESSION DRIVER
EXPONENTIAL HORN
COAGULATION TUBE
15 kV ELECTRIC FIELD POWER SUPPLY
PARALLEL PLATE ELECTRODES
SOUND ABSORBING CHAMBER
ABSOLUTE FILTER
ENTRY SECTION
FILTERED DILUTION AIR
WITHDRAWN PROBE
INSERTED PROBE
BALL VALVES
MASS FLOW TRANSDUCERS
50 GALLON DRUM
AEROSOL FROM GENERATING SYSTEM
VACUUM PUMP
FILTERED DILUTION AIR
EAA (TSI MODEL 3030)
OUTDOORS
PARTICLE NEUTRALIZER (TSI MODEL 3012)

Figure 2. Schematic of the continuous flow coagulation system

made of short lengths of soda straws are used to minimize the turbulence at the entrance of the coagulation tube. The coagulation tube is about 4.9 m long and is made of Plexiglass tubing with an inside diameter of 6 in. (i.e., 15.2 cm). The distance from the entry section to the upstream isokinetic probe is 61.0 cm and the distance between the probes is 182.9 cm. (The region between the two probes is the test section for the coagulation tests discussed later.) For a flow rate of 44 ℓpm and a tube diameter of 15.2 cm, the Reynolds number is about 430. Hot wire anemometer surveys taken at the two probe stations indicate that the flow speed is nearly uniform over a central core of about 9 cm in diameter at the upstream probe and about 6.5 cm at the downstream probe.[5] The flow speed at the center of the coagulation tube is about 4 cm/sec.

Particle Sampling and Size Analysis System

Two movable isokinetic sampling probes are used one at a time to extract a continuous sample at the entrance and exit planes of the test section. The inside diameter of the glass probes is 14.5 mm and each has an inlet with a sharp beveled entrance. The time for the continuously flowing aerosol to pass from one probe to the other is 45.3 seconds. At the isokinetic condition the flow rate through the probes is 0.373 ℓpm, which is about 1/120 of the total aerosol flow. In order to provide the required flow rate of 4 ℓpm to the particle size analyzer, the aerosol flow from either probe is admixed with filtered air in a nozzle mixing block. The dilution ratio is about 1:10.6. The flow rates of the probe flow and of the dilution air are determined with mass flow transducers. The transducers are manufactured by Sierra Instruments of Carmel Valley, California, and are calibrated with an accuracy of ±1%.

After the probe flow is diluted, the aerosol is passed through another bipolar charger to reestablish an equilibrium charge distribution. The particle size distribution is determined next by an Electric Aerosol Size Analyzer (EAA). The data from the EAA is reduced by a computer program (named EATRRN) developed by Liu and Kapadia. The program is available from TSI.

Electric Field and Acoustic Field System

The electrodes for the electric field consist of two parallel sheets (one on each side of the coagulation tube) of copper screen 47 cm high by 244 cm long and separated a distance of 21.6 cm. The power supply is a 15 kV neon light transformer. Thus, the magnitude of the electric field is about 69.5 kV/m.

The progressive wave sound field is generated by a compression driver, Model 2440, manufactured by James B. Lansing Sound, Incorporated of Los Angeles. An exponential horn is used to match the throat diameter of the driver to the inside diameter of the entry section (which is the same as the inside diameter of the coagulation tube). The compression driver is powered by a 60 watt amplifier. A function generator is used to provide the input signal to the amplifier. In order to minimize the effects of standing sound waves in the coagulation tube, a large sound absorbing chamber was placed at the downstream end of the coagulation tube. The chamber has the shape of a frustrum of a right rectangular pyramid with a base of about 1.1 m by about 0.61 m. The height of the frustrum is about 0.94 m. The internal volume of the chamber contains a combination of foam rubber and fiberglass with converging passages to absorb the sound waves. The standing wave ratio at the sound frequency used in the tests discussed in the next section was about 6.5%.

EXPERIMENTAL RESULTS

The experimental conditions and the results of the tests are presented and discussed in this section. The values of the experimental variables are presented in the first subsection, the experimental procedure is discussed in the second, the results are presented in the third, and the final subsection is devoted to a discussion of the results.

Values of the Experimental variables

For the tests, the total DOP particle concentration in the coagulation tube at the upstream probe location varied from 1.86×10^6 to 2.67×10^6 cm^{-3}. The mean particle diameter ranged from 0.0801 to 0.0998 µm. These values were determined using the EAA data which was reduced using the data reduction program EATRRN mentioned before. (It was found that bimodal distributions resulted in a better curve fit in the EATRRN program and the resulting chi-square values ranged from about 5.3×10^{-3} to 1.3×10^{-2}. A typical set of curve fit parameters were: median size in the first mode = 0.0891; standard deviation of the first mode = 1.48; median in the second mode = 0.164; standard deviation in the second mode = 2.29; and fraction of particles in the first mode = 0.93.) The concentrations were corrected for the 1:10.6 dilution that occurs before the flow from either probe enters the EAA. As mentioned above, the average translation time of the aerosol through the test section was 45.3 sec. The static pressure in the coagulation tube for all the tests was +10.9 cm of water. The magnitude of the electric field for the tests was 69.5 kV/m and the frequency was 60 Hz. The sound pressure of the traveling sound waves was varied from 115 to 145 dB and the frequency was 7624 Hz. The aerosol samples during the tests were extracted with the probes located at the centerline of the coagulation tube.

Experimental Procedure

Because the aerosol generating system was not highly stable, three syringe pairs of DOP-alcohol solution were run consecutively through the system before each test. (Each syringe pair lasted about 35 minutes when using a 40 mℓ charge in the two 50 mℓ syringes.) To ensure that the system was stable during a test, the analog output voltage of the analyzer current for each of the EAA channels was recorded on a 10 inch strip chart recorder in the following manner: the output from channel 4 was recorded first, followed by the outputs of channels 5 through 11 and then back to channel 4. If the final output from channel 4 did not agree to within about 2% of the initial output, the run was discarded. In addition, the tests conducted for each field condition (e.g., for a given sound wave intensity and frequency) were sequenced as follows: the outputs from the EAA channels (starting and finishing with channel 4 as discussed above) were recorded first without the external field(s), then the EAA channel outputs were recorded with the field(s), and then without the field(s). (The runs without the field(s) were referred to as the Brownian runs.) Again, if the EAA channel outputs for the initial and final Brownian runs in a test sequence did not agree to within 2%, the series was rerun. (Because of the relatively large particle size of the aerosols used in these tests, there was no noticeable difference between the outputs of channels 1 through 4, so the outputs of channels 1, 2, and 3 were not recorded.)

Results

The reduced results of the field tests described above are listed in Table 1. The results are based on the EAA analyzer currents obtained for each test, but reduced by the computer program EATRRN and then corrected by the dilution ratio of the air flow admixed with the aerosol flow extracted by each probe. The values of the collision coefficients listed in the table are calculated from the expression

$$b = \frac{n_u - n_d}{n_u n_d \tau} ,$$

where n_u and n_d are the total particle concentrations in the coagulation tube as determined from the upstream and downstream probe data,

Table 1. TABULATION OF THE BROWNIAN AND FIELD ENHANCED COLLISION COEFFICIENTS AS A FUNCTION OF THE SOUND WAVE INTENSITY AT A SOUND FREQUENCY OF 7624 Hz

Sound Wave Intensity (dB)	Electric Field Magnitude (kV/m)	Brownian Collision Coefficient b_B (cm^3/sec)	Field Enhanced Coefficient b_f (cm^3/sec)	Collision Coefficient Ratio b_f/b_B
115	0	1.39×10^{-9}	1.39×10^{-9}	1.00
125	0	6.70×10^{-10}	7.07×10^{-10}	1.06
130	0	1.42×10^{-9}	1.61×10^{-9}	1.14
130	69.5	1.42×10^{-9}	1.73×10^{-9}	1.21
135	0	1.85×10^{-9}	2.43×10^{-9}	1.31
135	69.5	1.66×10^{-9}	2.51×10^{-9}	1.52
140	0	1.88×10^{-9}	3.05×10^{-9}	1.62
140	69.5	1.88×10^{-9}	3.51×10^{-9}	1.86
145	0	1.40×10^{-9}	2.72×10^{-9}	1.95
145	69.5	1.40×10^{-9}	3.70×10^{-9}	2.64

respectively, and τ (=45.3 sec) is the aerosol transport time between the probes. This expression is derived from the well-known zero order coagulation model for a monodisperse aerosol, which is expressed as $dn/dt = -bn^2$. This expression does not account for the fact that the aerosol particles are not perfectly monodisperse. However, the resulting values of the collision coefficient are expected to properly reflect the influence of the acoustic and electric fields (since the aerosols were moderately monodisperse).

The ratio of the field enhanced collision coefficient to the Brownian coefficient is plotted in Figure 3 as a function of the sound wave pressure (in dB). As shown in Figure 3 (and in Table 1), the collision coefficient increases from about 2 times the Brownian rate for the sound field at 145 dB to about 2.6 times for the case of the combined fields at the same sound intensity. Tests at sound wave frequencies of 2502 Hz and at 9329 Hz and at intensities of 125 and 135 dB seem to indicate that the collision coefficients are weak functions of frequency.

Discussion of Results

Due to the accuracies (i.e., ±1%) of the mass flow transducers used with the isokinetic probes, there is an uncertainty in the value of the dilution ratio used to determine the total particle concentrations, n_u and n_d, from the EAA reduced concentrations. As a consequence, there is a ±24% uncertainty in the values of the collision coefficients, b_B and b_F, listed in Table 1. The reproducibility of the results may be inferred from the variation of the values of b_B listed in Table 1. The average value of b_B is 1.50×10^{-9} cm^3/sec and the standard deviation is

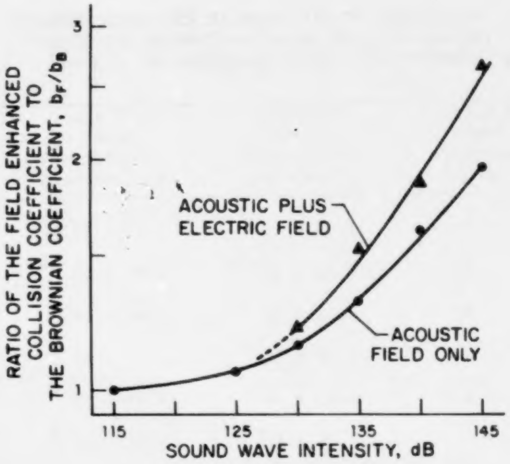

Figure 3. Ratio of the field enhanced collision coefficient to the Brownian coefficient as a function of the sound wave intensity

3.61×10^{-10} cm^3/sec, which is about the value of the ±24% uncertainty introduced above. By normalizing the field enhanced collision coefficients by the Brownian coefficients, the variations between the different field tests should be reduced. Thus, the values of b_F/b_B should correctly reflect the effects of the external fields on the collision coefficients.

As mentioned above, the average value of the Brownian collision coefficient is 1.50×10^{-9} cm^3/sec. This compares to a value of about 1.10×10^{-9} cm^3/sec from Fuchs'[6] transition regime model for a monodisperse aerosol with a particle diameter of 0.09 μm. (The particle Knudsen number in this case is about 0.7.) Hence the average value is above the value predicted by Fuchs' formula. This is not consistent with the experimental findings of Chatterjee, et al.,[8] who found somewhat lower values than predicted by Fuchs' model in the Knudsen number range from 0.8 to 1.6. The higher value indicated here may be due to the fact that the aerosol particles used in these tests obeyed a Boltzmann equilibrium charge distribution. This means that, although the aerosol was macroscopically neutral, there was a substantial number of equally, but oppositely charged particles. The effect of these oppositely charged particles would be to increase the apparent Brownian collision coefficient. (It is reasoned later that these charged particles play an important role in the increases noted in the combined field results.) It is further reasoned that the higher average value of the Brownian collision coefficient is not due to particle losses by diffusion, gravitational settling, or turbulent agglomeration. Diffusion losses in the system are minimal because probe surveys across the diameter of the coagulation tube indicated very small concentration gradients. Gravitational settling is not important because of the small particle size. Turbulent agglomeration is also negligible because the measured rms values of turbulence averaged only about 3.8% of the mean flow speed values over the uniform flow region in the coagulation tube.

The curve in Figure 3 for the acoustic field indicates that for sound intensity values above about 135 dB, the collision coefficient appears to be approaching a straight line, i.e., $b_F/b_B \propto \exp(\mathrm{dB})$. This is the relationship predicted by Mednikov's model[2] of orthokinetic interaction. However, Mednikov's model is not appropriate here because the experimental particle distribution is moderately monodisperse, whereas Mednikov's model requires that the colliding particles have different masses (i.e., different sizes). It is clear from Figure 3 that a traveling sound field can significantly increase the collision rate (even) in a moderately monodisperse aerosol.

The curve in Figure 3 for the acoustic plus electric field case indicates that the collision coefficient in a moderately monodisperse aerosol may be further enhanced by applying an a-c electric field directed normal to the direction of propagation of the traveling sound field. The curve in this case has a greater slope than the curve for the case when only the traveling sound field is applied. One way to quantify this effect is to note that at a sound wave pressure of 140 dB, the electric field adds an equivalent of about 5 dB to the ratio of the collision coefficents for the sound wave case. Because the energy density of the propagating sound wave is proportional to the exponential of the sound pressure (in dB), the 5 dB savings corresponds to about a 1/3 lower energy density. Hence in terms of the power requirement to generate the sound field, the 5 dB decrease reflects a considerable power savings. Because of the difference in the slopes of the two curves, it appears as though the effect may become even greater at higher sound intensities.

In order to postulate why the electric field significantly enhances the acoustic collision coefficient, it is worthwhile to examine the magnitudes of the particle displacements in the two oscillating fields. The amplitude of the particle displacement in the sound wave may be approximated by the expression[2]

$$|\Delta x|_A = U_g/\omega_A\left(1 + \omega_A^2\,\tau_i^2\right)^{1/2} \quad ,$$

where U_g is the amplitude of the oscillating speed of the gas molecules at the sound wave angular frequency ω_A, and τ_i is the usual particle relaxation time (multiplied by the Stokes-Cunningham correction factor). At a frequency of 7624 Hz and a sound wave pressure of 145 dB and for DOP particles with a radius of 0.045 μm, the value of the displacement is about 1.8×10^{-3} cm. The amplitude of the displacement of a charged particle in the a-c electric field is (assuming that the angular frequency of the electric field is such that $\omega_E\tau_i \ll 1$)

$$|\Delta x|_E = q_i\, B_i\, E/\omega_E \quad ,$$

where q_i is the particle charge, B_i is the particle mobility, and E is the amplitude of the oscillating electric field. The particle mobility is $B_i = S_i/6\pi\,\mu_g\,R_i$, where S_i is the Stokes-Cunningham correction factor, μ_g is the dynamic viscosity of the gas, and R_i is the particle radius. For an electric field with a frequency of 60 Hz and an amplitude of 69.5 kV/m and for singly charged DOP particles of radius 0.045 μm, the value of $|\Delta x|_E$ is 6.4×10^{-4} cm, or not quite half of the value of $|\Delta x|_A$. For a particle concentration of 2.5×10^6 cm^{-3}, which is the approximate particle concentration used for these experiments, the inverse cube root distance between the particle centers is about 7.4×10^{-3} cm, or about 4 times the value of $|\Delta x|_A$. In the case of the sound wave alone, the thermal motion of the particles combines with the motion driven by the sound wave to cause an increase in the collision rate. In the case of the electric field alone, the particle displacements are not large enough to significantly increase the collision rate above the Brownian rate. However, by combining the oscillating motion of a charged particle entrained in a sound wave with the motion of the same particle in a crossed a-c electric field, the collision cross-section increases normal to the sound wave oscillations. In essence, the charged particles appear to have a width of about $2|\Delta x|_E \approx 1.3 \times 10^{-3}$ cm, which is the same order of magnitude as $|\Delta x|_A$. It is this increase in the collision cross-section that is believed to be the reason that the collision coefficient increases with the addition of the crossed a-c electric field.

The source of the charged particles is the bi-polar charger in the aerosol generating system. As mentioned earlier, the aerosol exits from the charger with a Boltzmann charge distribution. In the case of a monodisperse aerosol with a particle diameter of 0.08 μm, a Boltzmann charge distribution means that about 48% of the particles are neutral, 46% are singly charged (half are positively charged and half are negatively charged), and 6% are doubly charged (again, half are positive and half are negative).[8] Hence 52% of the particles are charged, which is the fraction that responds to the a-c electric field.

CONCLUSIONS

The combination of the crossed fields significantly enhanced the Brownian collision coefficient. The increase with the acoustic field alone was significant; however, the addition of the a-c electric field to the acoustic field further enhanced the increase. It is expected that larger electric field magnitudes will show further increases. Thus, it has been demonstrated that combined a-c electric and acoustic fields may be used to effectively induce particle agglomeration between submicron sized particles. The crossed field configuration has merit and needs to be further explored as a possible means to pretreat dusty gases.

ACKNOWLEDGMENT

This work has been supported by a research grant from the Particulate and Multiphase Processes Program of the National Science Foundation.

REFERENCES

1. Scott, D. S. A New Approach to the Acoustic Conditioning of Industrial Aerosol Emissions. J. of Sound and Vibration. 43:607-619, December 1975.

2. Mednikov, E. P. Acoustic Coagulation and Precipitation of Aerosols. Published by Consultants Bureau, New York, 1965.

3. Shaw, D. T., and J. Wegrzyn. Application of Acoustic Agglomerators for Emergency Use in LMFBR Plants. (Presented at the 1977 American Nuclear Society Winter Meeting. San Francisco, November 27-December 2, 1977.)

4. Liu, B.Y.H., and D.Y.H. Pui. A Submicron Aerosol Standard and the Primary, Absolute Calibration of the Condensation Nuclei Counter. J. of Colloid and Interface Sci. 47:155-171, April 1974.

5. Scholz, P. D. Effects of Electric and Acoustic Fields on Particle Collision Rates in Aerocolloidal Suspensions. (Presented at the NSF and EPA sponsored Workshop on Novel Concepts, Methods and Advanced Technology in Particulate-Gas Separation. University of Notre Dame, April 20-22, 1977.)

6. Fuchs, N. A. The Mechanics of Aerosols. Pergamon Press, New York, 1964.

7. Chatterjee, A., M. Kerker, and D. D. Cooke. Brownian Coagulation of Aerosols in the Transition Regime. J. of Colloid and Interface Sci. 53:71-82, October 1975.

8. Pui, D.Y.H., and B.Y.H. Liu. Electrical Aerosol Analyzer: Calibration and Performance. (Presented at the Aerosol Measurement Workshop. University of Florida, March 24-26, 1976.)

ELECTROSTATIC SEPARATION IN CYCLONES

W. B. Giles
Corporate Research and Development
General Electric Company
Schenectady, New York

ABSTRACT

The results of cold flow experiments on a two-stage Aerodyne cyclone are presented which indicate that electrostatic forces can strongly enhance the separative efficiency and could be of special significance in achieving good gas cleaning performance in large scale cyclone units.

INTRODUCTION

The hundred year old art of gas cleaning by means of cyclone separators is well known and extensively documented. Excellent survey papers and articles exists by Porter et al(1), Jackson(2) and Caplan(3), the interior flow fields have been explored by Ter Linten(4) and Kelsall(5), standardized designs and practices have been defined by Stairmand(6), and good agreement has been realized between experiment and the relatively recent theory of Leith and Licth(7). The general rules of thumb indicate that small cyclones driven to high swirl velocity give optimal separative efficiency subject to the limitation of pressure loss, erosion, and coarse particle bouncing. Hence, multicyclones and staging have been employed in conditions where unusually high gas cleaning is mandated.

Present interest in economic coal utilization has placed a renewed and intense interest in optimum cyclone operation. This is particularly true in an application such as pressurized fluidized bed coal combustion where the downstream turbine is highly susceptible to the erosiveness of even a few coarse high velocity particles and environmental constraints must be met on the small particles - both areas where cyclone separators are not anticipated to provide adequate control. The picture is further clouded by the fact that complimentary gas cleaning equipment such as electrostatic precipitators and granular bed filters can impose a severe economic burden on the system and entail considerable development risk at coal combustion operating conditions. Further, many small cyclones operating in parallel, or multicyclones, have had a history of clogging of the outlet dust lines thus thwarting their intended function. Therefore, there remains considerable dependence on understanding and optimizing large cyclone separators as the most cost effective and reliable method of gas cleaning-particularly at high temperature and pressure conditions.

The purpose of this paper is to document the observation of strong electrostatic forces which aid, and in some cases, dominate the separative performance characteristics of cyclones.

Based on the results of cold-flow model experiments, it will be shown that performance degradation may not occur in scale-up to large cyclones due to the presence of these additional separation forces. Therefore, the existence of either naturally occurring, or induced charges on the dust burden under actual combustion condition is seen as a major hope in achieving adequate gas cleaning.

THEORETICAL CONSIDERATIONS

The underlying theoretical mechanism commonly used to describe cyclone separation is that the swirling gas flow imposes an inertial force on the dust particles causing them to migrate toward the wall against viscous drag forces, or Stokes Law. Leith and Licht(7) recognized the critical importance of turbulent mixing occurring in the cyclone which tends to negate the inertial separative action. This feature is accommodated in their analysis by assuming uniform mixing of the uncollected dust. They have also succeeded in showing excellent correlation with the work of several experimenters.

The net result expresses the ratio of collected dust to inlet dust or separative efficiency η in terms of the non-dimensional separative parameter ψ as

$$\eta = 1 - \exp - 2[C\psi]^{1/2n + 2} \qquad (1)$$

where C involves geometric parameters and,

$$\psi = \frac{\rho_p d_p^2 U_{t_2}}{18 \mu D} (n + 1) \qquad (2)$$

The separative parameter ψ, contains the terms implicit in the inertial mode of separation in which the viscous drag forces act against the inertial forces over a gas residence time. Therefore, a small scale model may be used to assess prototypical size by testing with similarity in geometric form, separative parameter, and high enough Reynolds numbers for turbulent flow conditions. For example, the performance of a six foot diameter, D, prototype could be determined from a 1-1/2 foot diameter model by testing at one fourth the wall tangential velocity, U_t, using the particles of the same mass density, ρ_p and diameter, d_p, and gas viscosity, μ.

The term, n, describes the tangential swirl velocity distribution as a function of the radius, r, as

$$U_t r^n = \text{constant} \qquad (3)$$

Typically, n is on the order of 0.5 and has been defined empirically by Alexander(8) in terms of operating temperature and cyclone diameter.* Figure 1, therefore, shows the general form of cyclone collection efficiency based on inertial theory. Hence a cyclone that exhibits a 90% collection efficiency with a four-to-one increase in size with all other operational parameters at the same condition.

By evaluating cyclones in this method, via model performance measurements at subrated flows, it was found that cyclones do not necessarily follow this theory.

TEST PROCEDURES

The cyclone evaluated in this series of experiments was a two-stage model designed and manufactured by Aerodyne Development Corporation. The first stage was sized to operate at low velocity to remove the heaviest and coarsest dust burden so as to minimize the erosion potential to the second, higher velocity stage. Figure 2 shows the relative size of this cold flow model which has a nominal diameter of three feet. The second stage was positioned concentrically in the center of the first stage so as to require only one pressure shell and insulation lining in actual application. The configuration of this second stage is patterned after the Tornado Dust Collector, under licensing from Siemens A.G., West Germany. A cross-sectional sketch is shown in Figure 3. The inlet flow enters the first stage tangentially to produce a swirling flow in the annular region between the two stages and splits with approximately 60% of the flow delivered to the primary swirl vanes which direct this flow upward. The remaining flow enters the secondary swirl vanes which

---

* A more appropriate dependence is expected to consist of Reynolds number to additionally accommodate the influence of velocity and high pressure operation.

Figure 1: Theoretical cyclone efficiency characteristic (after Leith/Licht(7))

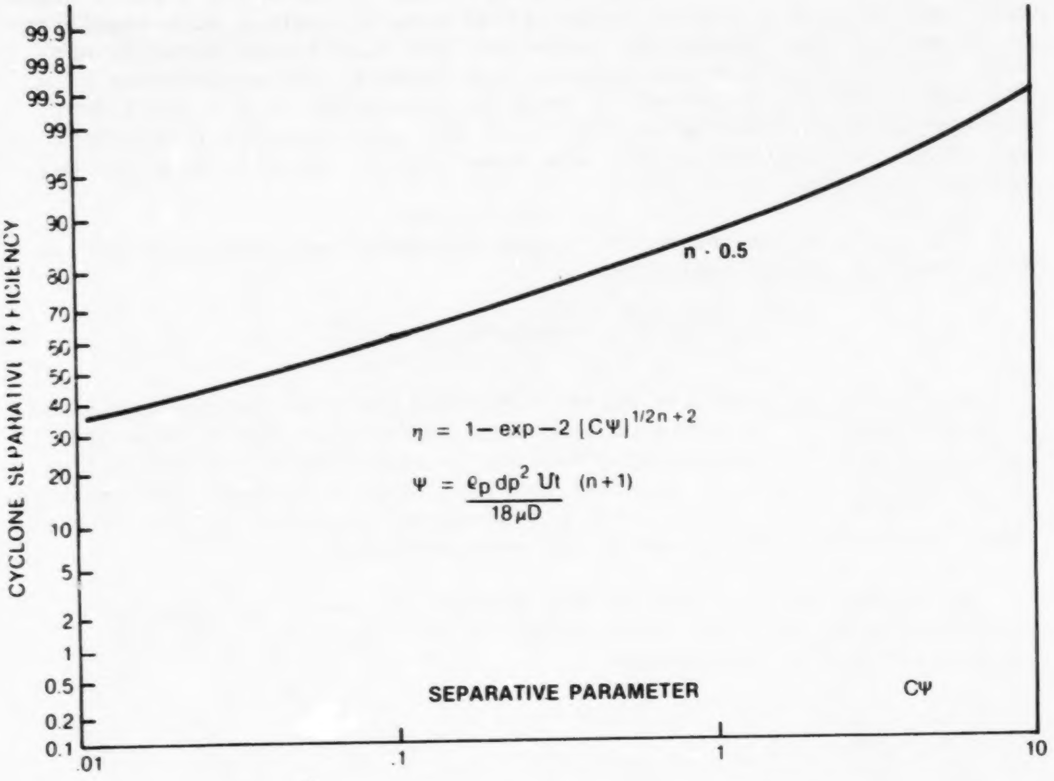

direct this flow upward. The remaining flow enters the secondary swirl vanes which direct this flow downward in an annular region adjacent to the18 inch diameter cyclone wall. Both swirl flows are, of course, co-rotational and the flow exits vertically upward through a constricting orifice which enhances spin-up of the interior vortex.

The test procedure consisted of measuring overall efficiency with pre-classified test dust. Metered, clean air was provided by a blower, as indicated in the schematic of Figure 4, with the test dust admitted at dilute concentration by a blown bed. The observation of inlet and outlet dust loads was obtained optically using two particulate Mass Concentration Monitors, PILLS V, of the Environmental Systems Corporation.

The test dusts consisted of using classified A.C. Fine Air Cleaner Test Dust (G.M.) with a specific density of 2.65, and flyash captured in the first stage cyclone of the Exxon Miniplant Pressurized Fluidized bed facility which had a specific density of 2.50. The size distribution for both are shown in Figure 5. Performance differences obtained with these two test dust can be traced to the marked difference in sizes of each.

Figure 2: Aerodyne Development Corporation two-stage test model

Abnormalities in the performance of the cyclone compared with the conventional wisdom of equations (1,2) were identified in previous work as being of electrostatic origin. Therefore, once these same abnormalities were again observed various attempts were undertaken to both eliminate and enhance electrostatic effects, and are indicated in the schematic of Figure 4. These consisted of grounding the cyclone, humidifying the dry shop air used for the dust generator, incorporating a TSI Nuetralizer on the exhaust of the dust generator, introducting a grounded aluminum honeycomb in the overhead of the dust generator, and providing a corona charger device in the inlet line to the cyclone.

TEST RESULTS

Figure 6 shows the overall separative efficiency with A.C. Fines as a function of cyclone flow rate with the shop air humidity raised to an

Figure 3: Cross-sectional sketch of Aerodyne cyclone model

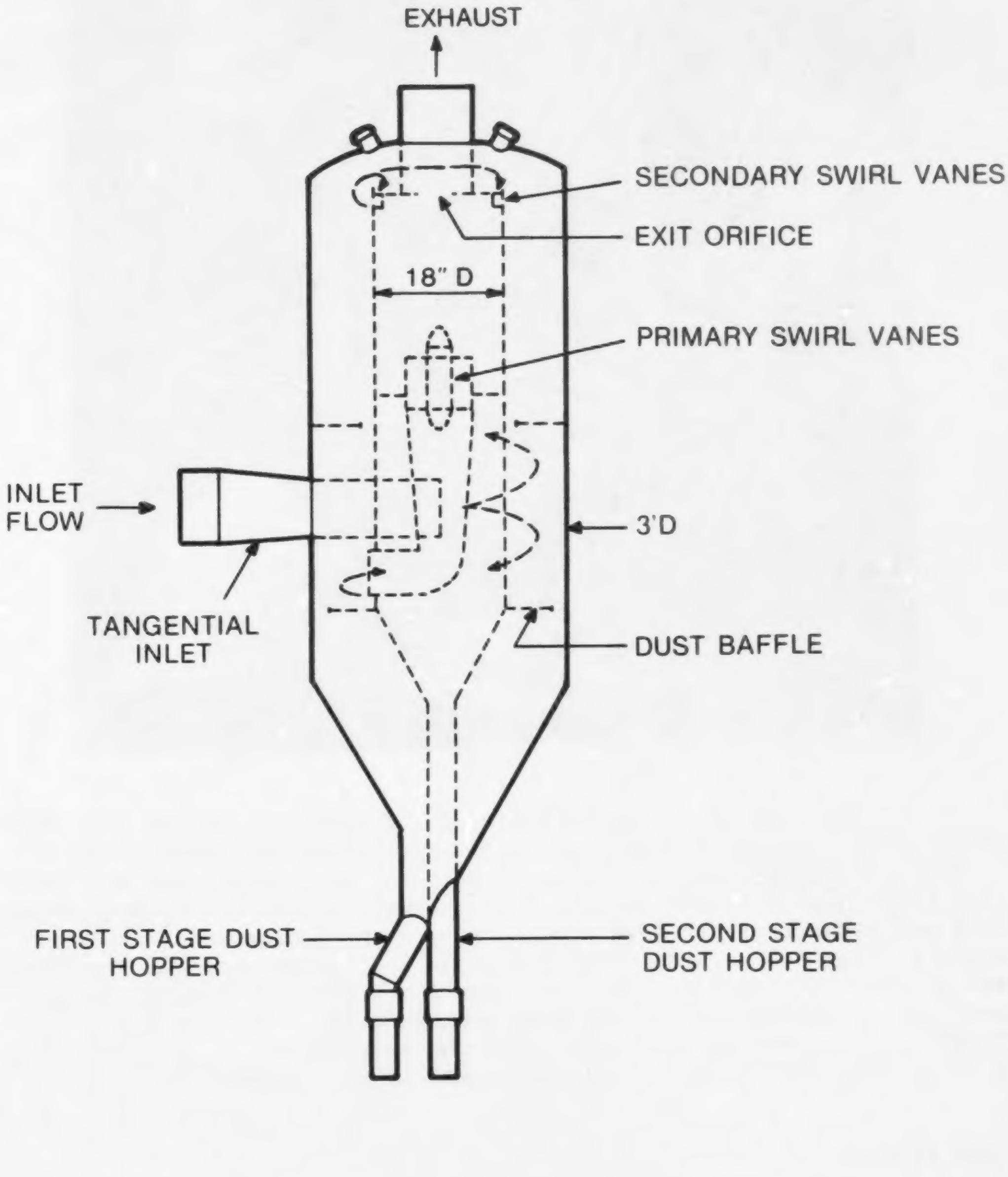
EXHAUST
SECONDARY SWIRL VANES
EXIT ORIFICE
18" D
PRIMARY SWIRL VANES
INLET FLOW
3'D
TANGENTIAL INLET
DUST BAFFLE
FIRST STAGE DUST HOPPER
SECOND STAGE DUST HOPPER

FIGURE 4: Separative efficiency test schematic

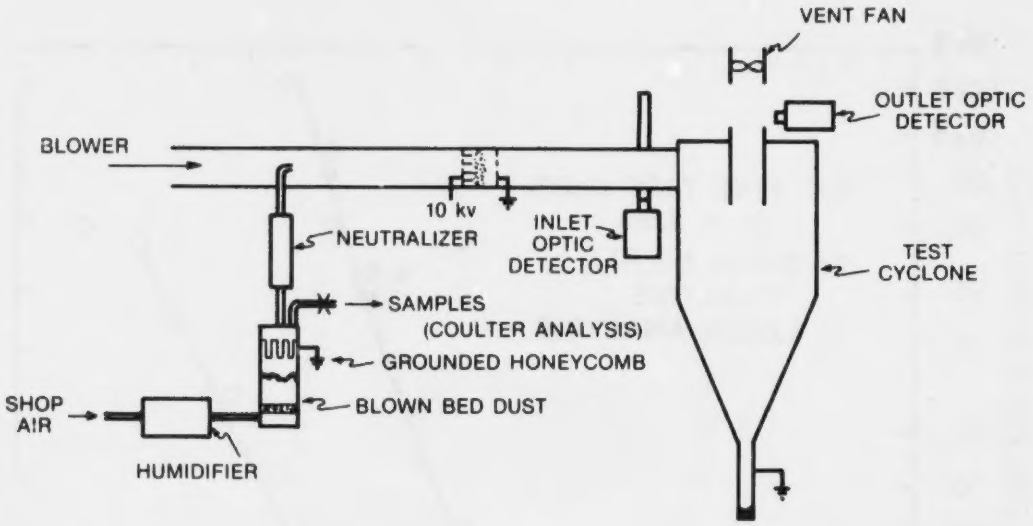
VENT FAN
OUTLET OPTIC DETECTOR
BLOWER
10 kv
INLET OPTIC DETECTOR
NEUTRALIZER
TEST CYCLONE
SAMPLES (COULTER ANALYSIS)
GROUNDED HONEYCOMB
BLOWN BED DUST
SHOP AIR
HUMIDIFIER

approximate level of 30 to 50% relative humidity. It can be noted that the performance decreases significantly as the cyclone flow rate is increased to its rated velocity condition at 1280 cfm. This is, of course, in marked contradiction to the anticipated performance expected from inertial theory as set forth in equation 1 and in Figure 1. Use of the TSI Aerosol Neutralizer resulted in a substantial lowering of performance and a flatter characteristic with flow rate, but still does not correspond to inertial theory expectation.

Similar results were also found with and without the neutralizer using the coarser flyash test dust, as shown in Figure 7. The higher overall efficiency is due to the coarser test dust.

Finally, the use of grounded honeycomb in the dust generator resulted in apparent inertial performance characteristics of the cyclone. Figure 8 contrasts these results with earlier trends with electrostatic forces.

As further verification of this electrostatic influence, the D.C. corona charger was used at +10kv and was found to further enhance collection efficiency as shown in Figure 9.

DISCUSSION

Obviously many important issues remain to be addressed. It is theorized that space charge repulsion is the most probable mechanism by

Figure 5: Test dust size distribution

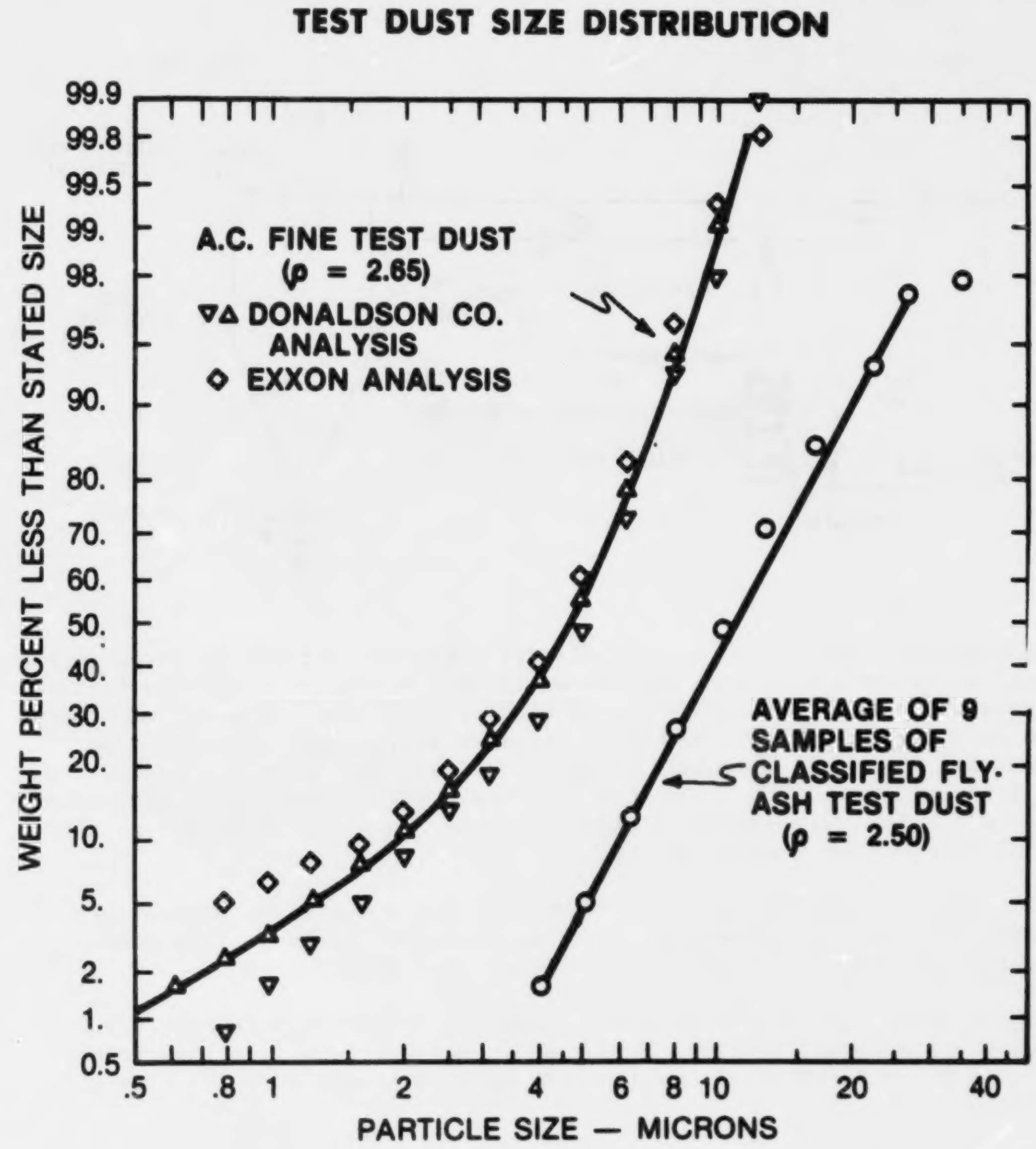

which electrostatic forces enhance cyclone collection efficiency. Therefore, the effect could be much more important with small dust particles compared to large particles; and a dependence of dust particles compared to large particles; and a dependence of dust loading level would also be expected.

Figure 6: Influence of TSI Aerosol Neutralizer on the performance of grounded Aerodyne cyclone with deswirl vanes and A.C. test dust ($\rho = 2.65$)

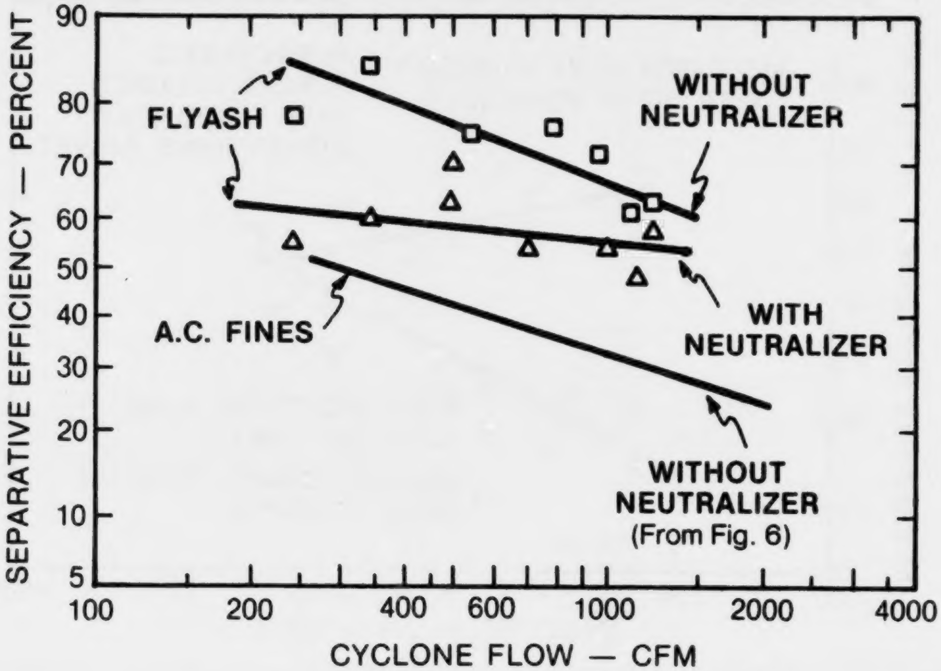

Figure 7: Influence of classified flyash dust ($\rho = 2.50$) on the performance of grounded Aerodyne cyclone with deswirl vanes

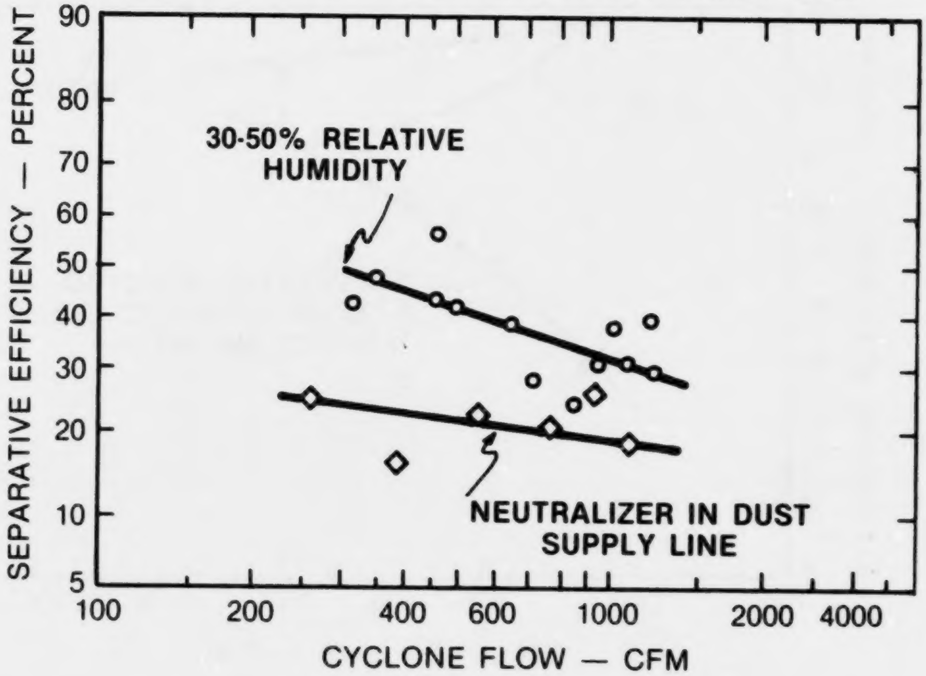

Figure 8: Performance of Aerodyne cyclone with suppressed electrostatic forces operated without deswirl vanes and with A.C. fines (ρ = 2.65) test dust

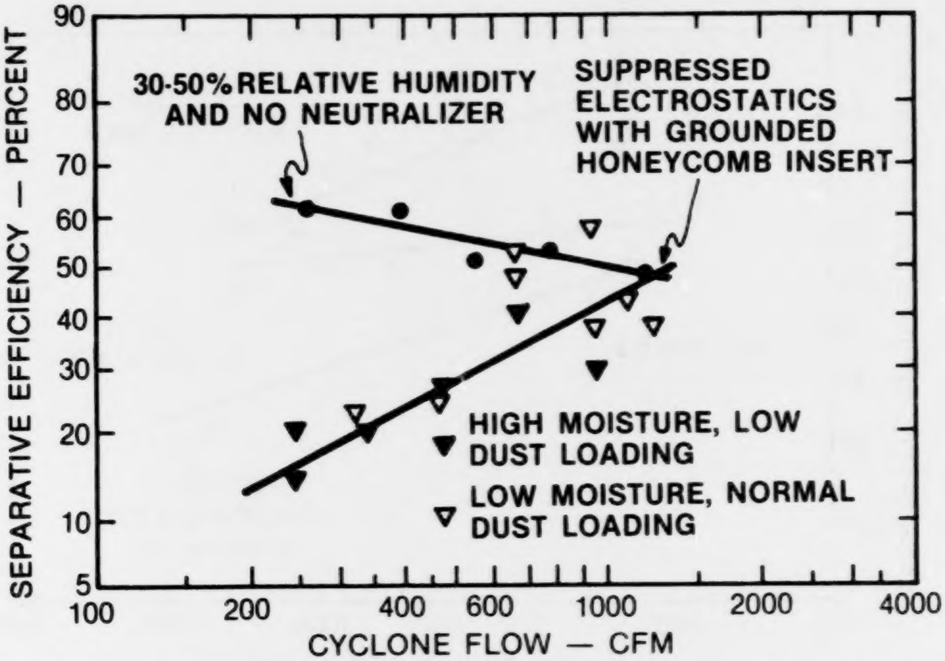

Figure 9: Influence of suppressed and enhanced electrostatic forces on Aerodyne cyclone performance operated without deswirl vanes and with classified flyash (ρ = 2.50) test dust

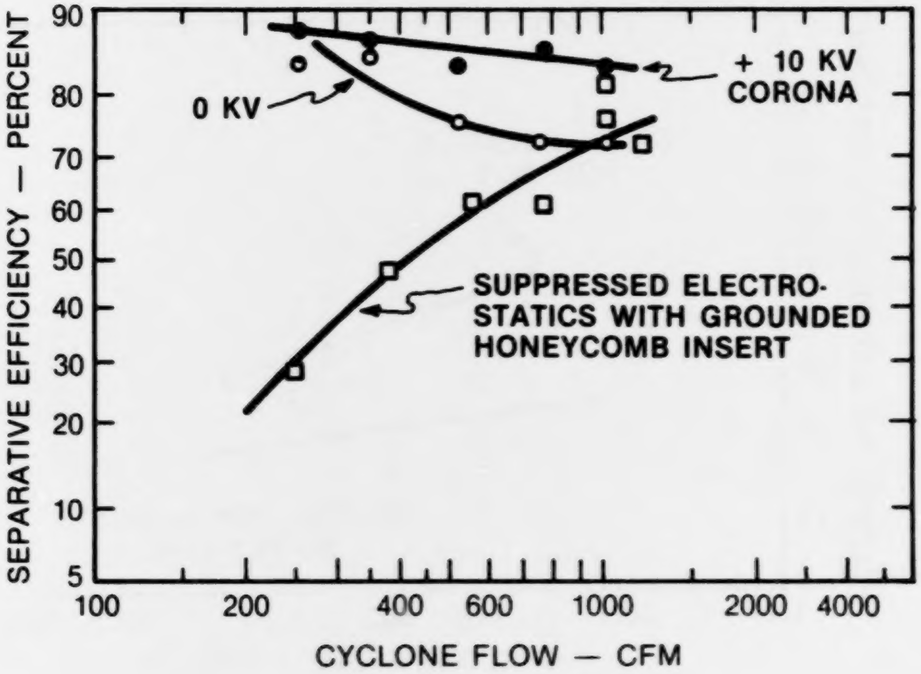

The results presented here pertain only to the two-stage Aerodyne model and one might conclude that they are unique to this special design, particularly with the very large gas residence time in the first stage. However, similar observations have been realized on models of a more conventional form. In one case, the use of grounded aluminum tape attached to the interior wall of the cyclone was sufficient to eliminate the anomalies associated with electrostatics. In another model we have, as yet, been unable to control electrostatics. The dust generator can be identified as the source of naturally-charged particles by using a conductive filter and a very high impedance ampmeter.

Electrostatics have also been found to play a dominant role in sampling for particle size analysis and can provide a major source of error in interpreting cyclone performance. If a sampling probe is inserted in a line carrying dusty gas, and electrically insulated from the duct with one or the other grounded, the resulting dust sample will be much finer than if the sampling probe and duct wall are electrically connected. Apparently the induced charge, which is dependent on both dust load and gas velocity, produces a strong voltage gradient in the vicinity of the probe to selectively attract fine particles and/or repel coarse particles.

CONCLUSION

Electrostatic forces have been found to play a major role in improving cyclone collection efficiency. Whether or not these forces can exist at coal combustion conditions remains to be seen, but at least present research on electrostatic precipitators indicates that particle charging can be realized at the temperatures and pressures of pressurized fluidized bed combustion. More specifically, as a direct result of the findings presented here, research is being directed toward assessing electrostatic cyclone behavior in recent tests at NCB/s Coal Utilization Research Laboratory. If these hot-flow experiments under actual PFB conditions are similar to this experience, then the economic burden of separate electrostatic separators may be replaced by improved full-scale cyclone performance.

ACKNOWLEDGEMENT

This work was performed under DOE Contract No. EX-76-C-01-2357 to the General Electric Energy Systems Programs Department by Corporate Research and Development.

REFERENCES

1. Porter, H. F., et al, "Gas-Solid Systems," Section 20, Perry and Chilton, Chemical Engineers' Handbook, McGraw-Hill, 5th ed. (1973).

2. Jackson, R., "Types of Return Flow Cyclones," "uni-flow Cyclones," and "The Performance of Cyclones," Brit. Coal Utiliz. Res. Assn. Bull., Revs. 224, 225, 227, (1963).

3. Caplan, K. J., "A Source Control by Centrifugal Force and Gravity," Air Pollution, Vol. III, Academic Press, New York (1968).

4. Ter Linten, A. J., "Investigations Into Cyclone Dust Collectors," Proc. Inst. Mech. Engrs. 160, 233 (1949).

5. Kelsall, D. F., "A Study of the Motion of Solid Particles in a Hydraulic Cyclone," Trans. Instn. Chem. Engrs. 30, 87-108 (1952).

6. Stairmand, C. J., "The Design and Performance of Cyclone Separators," Trans. Instn. Chem. Engrs. 29, 356-383 (1951).

7. Leith, D. and Licht, W., "Collection Efficiency of Cyclone Type Particle Collectors, A New Theoretical Approach," AI Ch. E. Symp. Ser., Air-1971(1972).

8. R. Mck. Alexander, Proc. Austral. Inst. Met (N.S.) (152), 202 (1949).

EVALUATION OF THE ELECTRIFIED BED PROTOTYPE COLLECTOR ON AN ASPHALT ROOFING PLANT

Robert M. Bradway
William Piispanen
Verne Shortell
GCA Corporation
GCA/Technology Division
Bedford, Massachusetts

ABSTRACT

A prototype electrified bed (EFB) particulate collection device was evaluated. The 500 cfm unit, which utilizes mechanical and electrical mechanisms for collection, was installed at an asphalt roofing plant during the test program. The fractional efficiency was determined with upstream and downstream impactors and the total mass efficiency was determined with glass fiber filter sampling trains.

The mean inlet loading was 0.2585 gr/dscf and the mean outlet loading was 0.0037 gr/dscf for an average efficiency of 98.57 percent. The inlet aerosol had a mass median diameter of about 1 micrometer with 90 percent less than 2 micrometers. Measurements of volatile hydrocarbons by onsite gas chromatography showed that the inlet concentration of approximately 100 ppm was reduced by 20 to 50 percent by the device.

Over the past several years GCA has been involved in several evaluations of novel control devices for EPA. This paper reports the results of a relatively brief evaluation of the Electrified Bed, or EFB, which is a registered trademark of EFB, Inc. The test series was brief because there was a minimum of parameters which could be conveniently altered at the test location and, additionally, only a limited amount of time was available for testing.

The EFB demonstration unit consists of two granular beds perpendicular to the gas flow; a 10 kV corona charger between the beds imparts an electrical charge across the gas stream. The beds are also charged at 10 kV, although the current is very low. Bed material is fed through hoppers on top and emptied into suitable containers on the bottom. The bed material is changed automatically by timers or manually. Each bed is 2 inches deep and 2 feet square. The flows encountered during testing resulted in a velocity of about 100 fpm through the bed with a pressure drop of about 8 inches of water.

The test program was conducted at an asphalt roofing plant in Massachusetts. The plant is quite old and has experienced some problems controlling fume emissions from the saturators. At present, the emissions from the saturators are collected by overhead hoods and ducted to the plant boiler.

A slipstream with a manual damper introduced the gas stream to the EFB. Whenever possible, the EFB utilizes a bed material inherent to the process being controlled. For the asphalt roofing plant, crushed slate which is added to the shingle surface was utilized. This material is spindle shaped and is 10 to 20 mesh in size.

Two types of sampling trains were used. The first was a total mass train consisting of two 42 mm glass fiber filters in series followed by a tee fitted with a septum to allow extraction of a syringe sample for gas chromatography analysis. Two filters were used in series to verify that the first filter was not being penetrated by the liquid aerosol.

The second train consisted of an Andersen impactor followed by a 42 mm glass fiber filter. Impactor flow rates were generally kept in the 0.35 to 0.40 acfm range to minimize particle bounce problems.

Four pretest runs were conducted to evaluate several parameters. First, we wanted to determine the variability in plant operations. We also wanted to evaluate the test methods, particularly seepage through glass fiber filters and anomalous weight changes of the impactor substrates. We also wanted to establish any variations in the gas volume being introduced to the unit.

Table 1 shows the results of these preliminary tests: there were major day-to-day changes in the flow to the EFB. Furthermore, rather substantial variations in the collection efficiency led us to examine the outlet filters under a microscope. Slate particles visible on some filters indicated bed slough off. These problems were resolved prior to actual testing.

Table 2 shows the results of the six tests performed during the actual test program. In all subsequent summary comments about performance, the results of run 5 have been excluded. Although inlet and outlet size distributions were fairly typical, both the inlet and outlet grain loadings differed from the mean by more than 1 standard deviation and were therefore not included.

The mean inlet grain loading was 0.2585 gr/dscf with a mean outlet loading of 0.0037 gr/dscf. This computes to an average efficiency of 98.56 percent. The EFB also reduced the concentration of volatile hydrocarbons by 20 to 50 percent as measured by onsite gas chromatography. The average inlet hydrocarbons concentration was about 100 ppm. The production rate during testing was monitored to determine the operating conditions. The line speed was nominally 400 fpm but substantial variations did occur. Twice sampling had to be temporarily interrupted because the production line went down.

The impactor measurements of the gas stream entering the EFB, shown in Figure 1, showed good agreement and the mmd was determined to be 1 μm with 90 percent of the material less than 2 μm.

Construction of inlet and outlet differential size distributions permits a determination of collection efficiency as a function of particle size. Figure 2 shows runs 5 through 10.

Note that for our tests the collection efficiency for the most abundant particle size of 1 μm was about 99.9 percent. Strangely, collection efficiency appears to decrease at larger particle sizes. There are several possible explanations for this observation. First, there may still have been some slough off of bed material, although none was visible on the filters or substrates. Another possibility is that probe and expansion chamber wall losses may have altered the size distributions. A third possibility is that particles may have agglomerated due to induced dipole moments or other agglomeration mechanisms.

In summary, the following comments can be made about our tests:

- The EFB operated on about 415 acfm
- The velocity was about 100 fpm
- The corona charger operated at 10 kV and 1 ma

Table 1. RESULTS OF PRELIMINARY EFB TESTS

Test number	Sample train	Inlet			Outlet			Efficiency (percent)
		T_{stk} (^{o}F)	Q_{stk} (acfm)	Grain loading (gr/dscf)	T_{stk} (^{o}F)	Q_{stk} (acfm)	Grain loading (gr/dscf)	
1	Impactors	-	-	-	112	204	0.0048	-
1	Filters	140	285	0.0379	112	204	0.0004	98.94
2	Impactors	145	243	0.2368	125	413	0.0134	94.34
2	Filters	145	243	0.2119	125	413	0.0281	86.74
3	Impactors	134	365	0.4105	107	540	0.0086	97.90
3	Filters	134	365	0.2604	107	540	0.0083	96.81
4	Impactors	140	439	0.1910	104	522	0.0164	91.41
4	Filters	140	439	0.1387	104	522	0.0125	90.27

Table 2. EFB TEST RESULTS

Test number	Date (1978)	Sample location	Q (scfm)	T_{stk} (^oF)	Moisture[a] (percent)	Total hydrocarbon (ppmv)	Methane (ppmv)	Grain[a] loading (gr/dscf)	Particulate efficiency (percent)
5	2/21	Inlet	391.8	142	2.0	99	n.m.[b]	0.31061	95.81
		Outlet	416.6	113	1.6	87.1	14.1	0.01301	
6	2/22	Inlet	385.0	140	2.6	97.1	6.8	0.21779	98.20
		Outlet	445.9	111	2.1	78	4.5	0.00391	
7	2/22	Inlet	390.3	136	1.9	-	-	0.25002	98.76
		Outlet	454.1	103	1.7	-	-	0.0031	
8	2/23	Inlet	372.6	145	2.1	144	n.m.[b]	0.27630	99.15
		Outlet	471.7	113	1.6	73	n.m.[b]	0.00236	
9	2/23	Inlet	377.7	135	2.4	-	-	0.26693	98.66
		Outlet	472.4	111	1.8	-	-	0.00357	
10	2/24	Inlet	295.4	129	2.7	107	20.5	0.28151	97.97
		Outlet	374.0	104	1.9	56	14.3	0.00572	

[a] From total mass trains results.

[b] No measurement available.

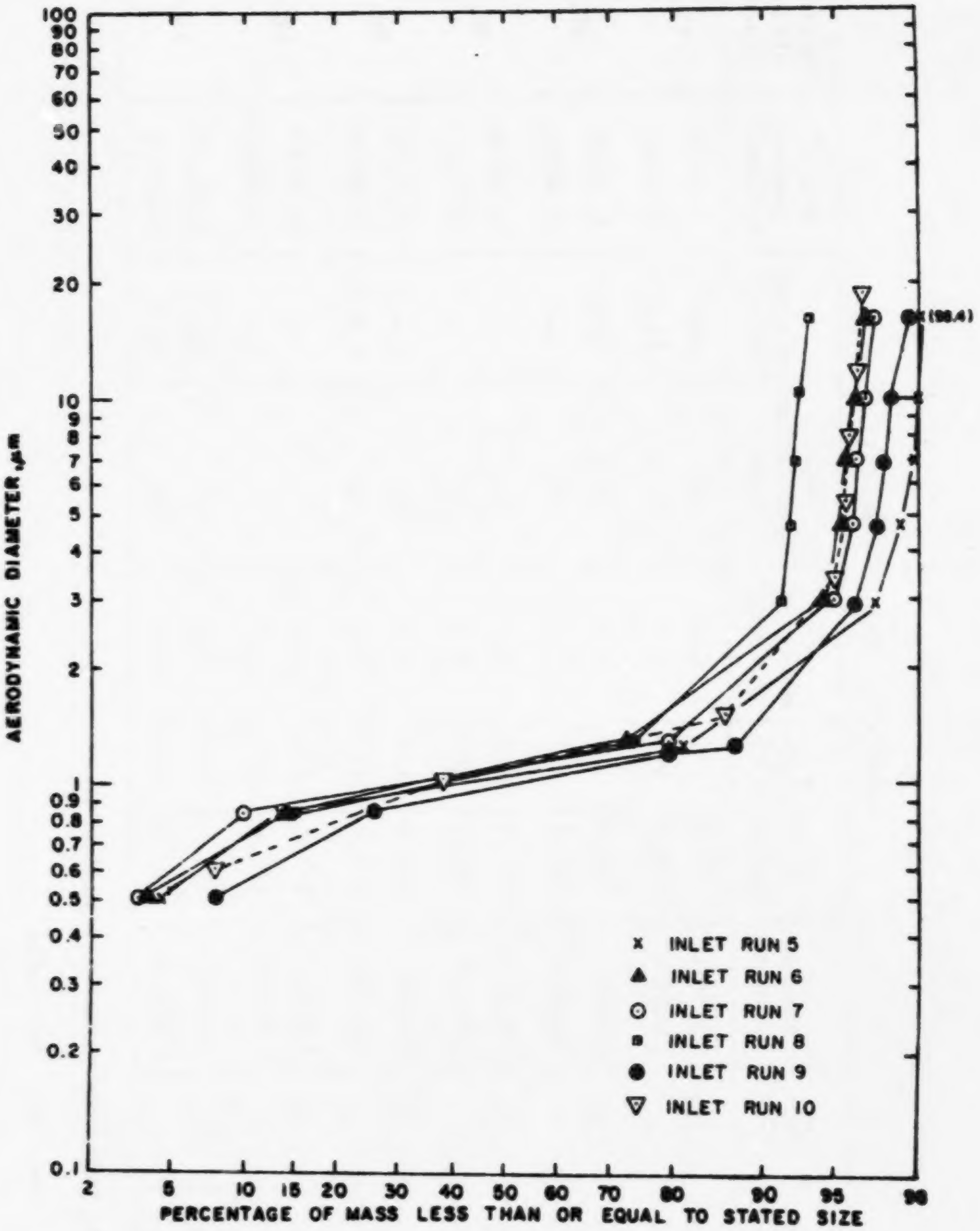

Figure 1. Fractional size distribution of EFB unit

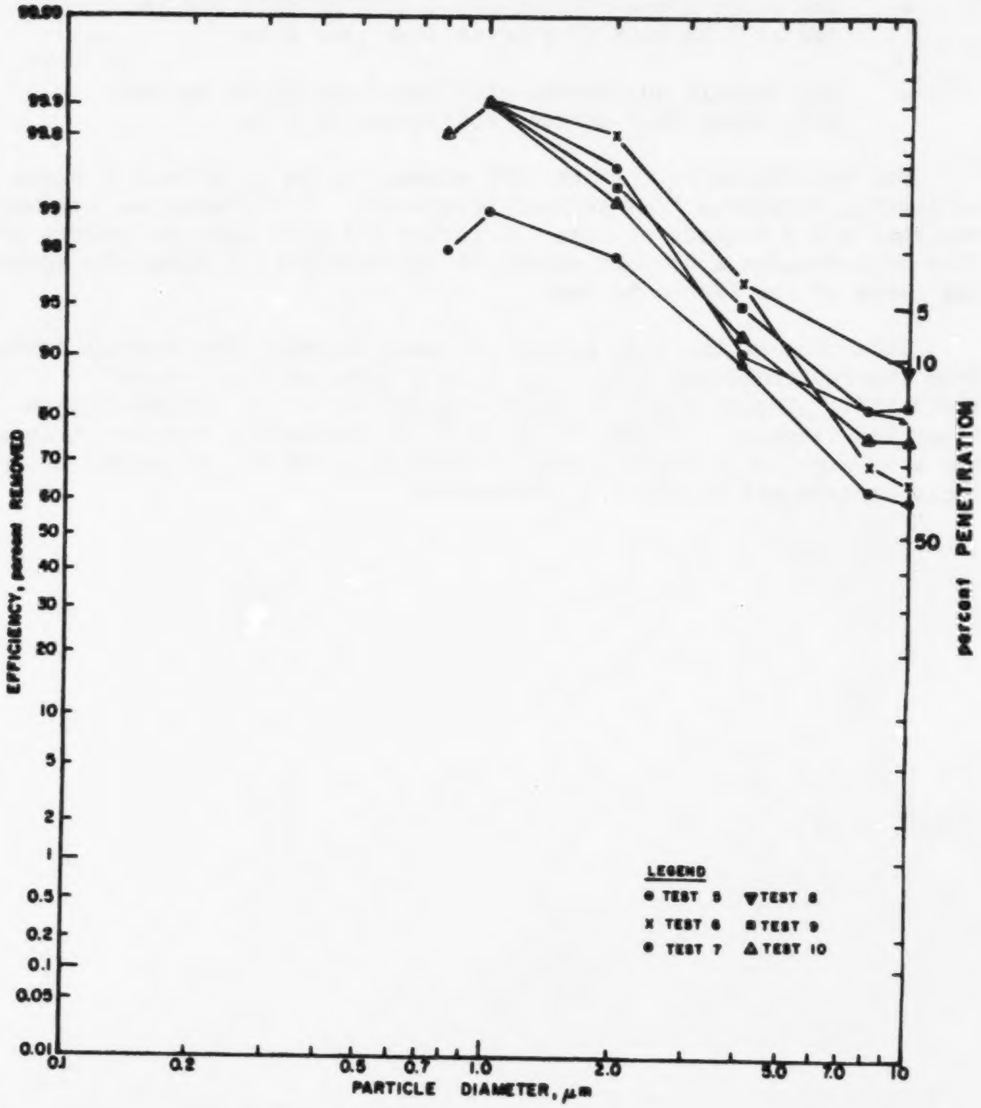

Figure 2. Fractional efficiencies of EFB unit as measured with Andersen impactor

- The beds were charged at 10 kV and 0.1 ma
- The pressure drop across the unit was about 8 inches of water
- The inlet concentration was 0.2585 gr/dscf and had a mmd of 1 μm with 90 percent less than 2 μm
- The overall collection efficiency was 98.56 percent with about 99.9 percent collection at 1 μm

Our conclusion is that the EFB appears to be an effective means of collecting emissions from asphalt saturators. A conventional venturi scrubber would require at least 70 inches pressure drop to achieve similar efficiencies and would result in approximately 8 times the operating costs of the EFB as tested.

This project has been funded at least in part with Federal funds from the Environmental Protection Agency under contract number 68-02-1487. The contents of this publication do not necessarily reflect the views or policies of the U.S. Environmental Protection Agency, nor does mention of trade names, commercial products, or organizations imply endorsement by the U.S. Government.

EVALUATION OF AN APITRON ELECTROSTATICALLY AUGMENTED FABRIC FILTER

Joseph D. McCain, Paul R. Cavanaugh, Larry G. Felix and
Randy L. Merritt
Southern Research Institute
Birmingham, Alabama 35205

ABSTRACT

This paper presents a summary of the results of tests performed to determine overall and fractional collection efficiencies of the Apitron (Apitron, Inc., Division of American Precision Industries, Charlotte, NC) dust collector. The Apitron device utilizes a wire-pipe type electrostatic precipitator as a pre-collector and particle charger immediately upstream of a conventional pulse jet fabric filter. Pilot plant units were tested at two sites, one collecting fly ash from a pulverized coal fired steam generator while the other was tested collecting redispersed silica dust. At each site tests were conducted with and without electrostatic augmentation.

INTRODUCTION

This paper presents a summary of the results of tests conducted by Southern Research Institute (SoRI) to determine the fine particle collection capabilities of the Apitron electrostatically augmented fabric filter. These tests were conducted as part of a series of tests of novel particulate control devices sponsored by the Particulate Technology Branch of the Industrial Environmental Research Laboratory of the U.S. Environmental Protection Agency. The tests were designed to determine collection efficiencies versus particle size over the range from about 0.01 μm to about 5 μm both with and without electrostatic augmentation.

DESCRIPTION OF THE APITRON DUST COLLECTOR

Figure 1 shows a cutaway view of a trailer mounted, mobile, pilot plant Apitron unit, one of the two units tested. The particular unit

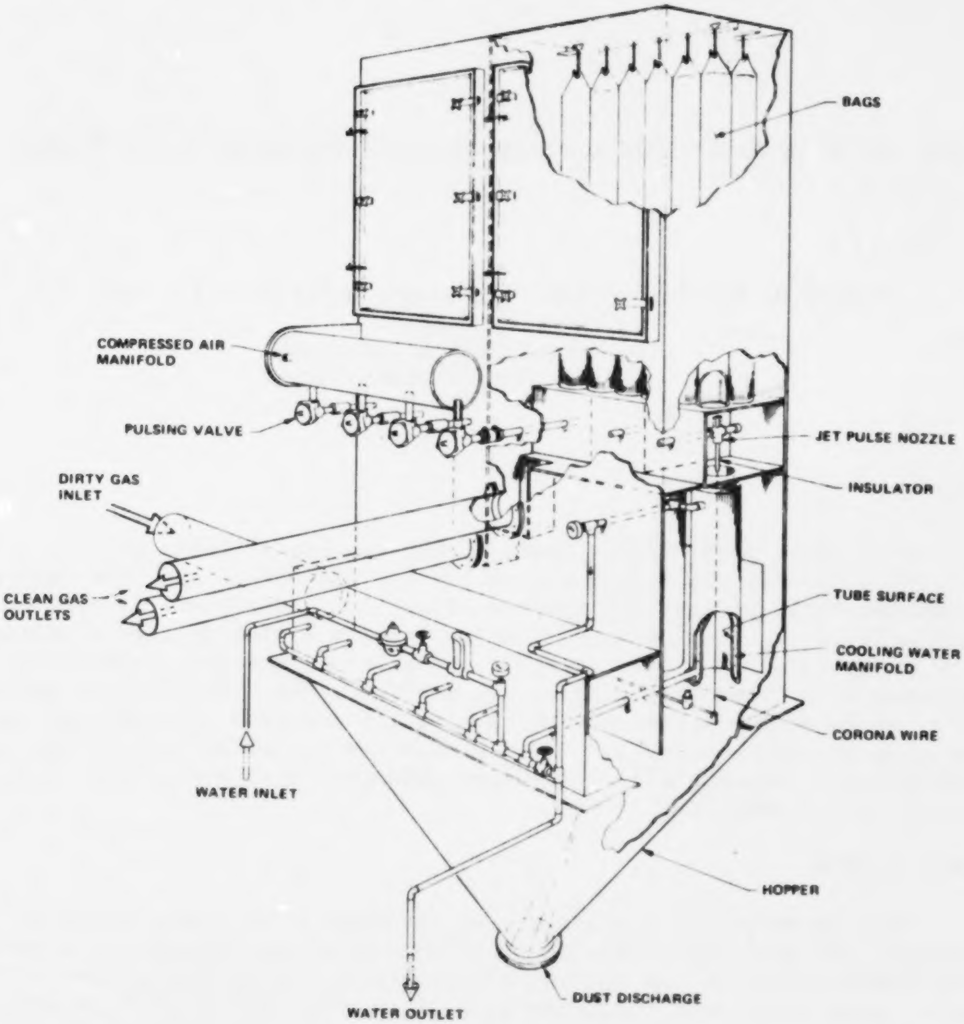
BAGS
COMPRESSED AIR MANIFOLD
PULSING VALVE
JET PULSE NOZZLE
INSULATOR
DIRTY GAS INLET
CLEAN GAS OUTLETS
TUBE SURFACE
COOLING WATER MANIFOLD
CORONA WIRE
WATER INLET
HOPPER
DUST DISCHARGE
WATER OUTLET

Figure 1. Cutaway view of a trailer mounted, mobile, pilot plant Apitron Unit.

is divided into two separate compartments which share a common inlet, hopper and power supply. Each compartment has its own exit duct and flow metering capability, thus permitting simultaneous testing of two fabrics. Only one of the two compartments was used in the testing by SoRI.

In a full scale unit, on which the second of the two test series was conducted, a single long bag is used downstream of each precipitator tube. On the mobile unit height constraints require the use of four short bags over each precipitator tube rather than a single, long bag.

The Apitron system is generally similar to a conventional pulse jet fabric filter. In the Apitron, however, the tubes used for inducing additional gas flow in the cleaning pulses over that provided by the compressed air supply are reconfigured to serve as wire-pipe electrostatic precipitators with one precipitator tube per bag. The incoming particulate laden gas flows upward through an inlet plenum and hopper and then through the precipitator tubes which remove a portion of the particulate matter. The majority of the remaining particles, which now carry significant uni-polar electrical charges, are then removed by the fabric filter. The charge carried by the particles appears to effect the formation of the dust cake on the fabric surface in such a way as to result in the cake's having a more porous, open structure. This reduces the flow resistance of the dust cake making it possible to operate the Apitron at markedly higher filtration velocities then conventional fabric filters for the same operating pressure loss. Typical design face velocities for the Apitron are in the range of 30 to 75 mm/sec (6 to 15 fpm).

The compressed air cleaning pulses are produced by nozzles located above each precipitator tube concentric with the corona discharge electrode. The cleaning pulse thus serves to clean the tube and discharge electrode as well as the bag associated with it.

The precipitator tubes can be made as double walled structures through which water can be passed as shown in Figure 1. This serves two purposes: first it permits some control of the resistivity of the dust collected on the tube by altering the temperature of the dust layer and second, it results in significant recovery of waste heat. The resistivity control can be quite important in the operation of the Apitron as it normally operates at current densities much higher than those used in most conventional electrostatic precipitators (250 to 750 nA/cm^2 as compared to 15 to 100 nA/cm^2).

The fabrics used for bag materials are felted Nomex, Teflon, or polyester depending upon the specific application.

Specifications for the two units tested are given in Table 1.

TABLE 1. SPECIFICATIONS FOR APITRON TEST UNITS

	Small Scale Mobile Unit	Full Scale Pilot Plant
Precipitator Tube ID (cm)	12.7	15.2
Precipitator Tube Length (cm)	83.8	121.9
Number of tubes per compartment	3	72
Number of compartments	2	1
Number of bags per tube	4	1
Filter area per bag (m^2)	0.293	2.23
Operating voltage full power (kV)	30	39
Operating current per compartment (mA)	7.5	325
SCA ($m^2/am^3/s$)	8.5	8.9
Cleaning Pulse Pressure (kPa)	241	552
Cleaning Pulse Duration (ms)	50	50
Cleaning Interval (min)	6	8
Nominal air flow per compartment (Am^3/s) as tested	0.118	4.72
Operating Pressure Drop (cm w.g.)	3.3	7.1
Bag Material	Teflon Felt	Polyester Felt

PERFORMANCE EVALUATION

Performance tests were conducted on a small scale mobile unit during December, 1977 and on a full scale pilot plant during June, 1978. The test methods used may not have been consistent with compliance type methods, but were state-of-the-art techniques for determining mass and fractional efficiencies.

A total of four measurement techniques were used during these tests. These were: (1) electrical mobility techniques using Thermosystems Model 3030 Electrical Aerosol Analyzers (EAA) for determining concentrations and size distributions on a number basis for particles having diameters between 0.01 µm and 1.0 µm, (2) optical, single particle, light scattering techniques to determine concentrations and size distributions on a number basis for particles over the size range from about 0.5 µm to 2 µm, (3) inertial techniques to determine concentrations and size distributions on a mass basis over the size range from about 0.5 µm to 5 µm, and (4) standard mass train (Method 17) techniques for measuring total inlet and outlet particulate loadings and emission rates.

The tests were conducted on two pilot plant units. The first, a small scale mobile unit, was tested while in operation collecting fly ash from a sidestream in the exhaust from a pulverized coal fired boiler. New Teflon bags were installed at the start of these tests. The test data were subsequently found to show generally decreasing outlet emissions throughout the test series. These decreases in emissions, which are believed to be due to conditioning of the bags, masked some of the effects which were expected to occur in comparing power on-power off operation. In addition, problems with an EAA resulted in little data being obtained in the 0.01 µm to 0.5 µm size range.

Because of the problems just described, a second test series was conducted. In this case a full scale pilot plant with well conditioned polyester bags collecting redispersed silica dust at normal atmospheric conditions was tested.

In order to permit comparisons of performance with and without electrostatic augmentation at constant filtration velocities a filtration velocity lower than the maximum design velocity was used. Operation without electrostatic augmentation at high filtration velocities resulted in system pressure losses in excess of fan and pulse jet cleaning capabilities. Operation with and without augmentation was possible at face velocities of about 30 mm/s (6 fpm) although even at this velocity the cleaning effectiveness of the pulse jets appeared to be significantly reduced. Operating conditions of both units during the respective tests are given in Tables 2 and 3.

Included in Tables 2 and 3 are the total inlet and outlet particulate loadings and overall collection efficiencies determined from them. Air infiltration at joints in the inlet ducting to the mobile unit resulted in substantial dilution of the flue gases. The data shown in

TABLE 2. SMALL SCALE MOBILE UNIT TEST CONDITIONS AND RESULTS

Date	Outlet Temperature °C	Gas Flow cm^3/min	Filtration Velocity mm/s	ESP Voltage Kv	ESP Current mA	System Pressure Loss cm w.c.	Inlet Loading mg/DNm^3	Outlet Loading mg/DNm^3	Collection Efficiency %	Total Energy Usage $joules/am^3$
12/2/77	71	8.47	40.2	30.5	7.5	0.5	4260	7.15	99.83	1670
12/5/77	74	7.42	35.2	30.0	8.0	3.0	5580	5.49	99.902	2240
12/6/77	74	7.00	33.2	29.0	8.5	3.8	5560	3.32	99.940	2500
12.7.77	74	6.91	32.8	0	0	8.9	2130	2.03	99.905	868
12/8/77	54	2.92	13.8	0	0	3.3	3090	2.21	99.928	323

Felted Teflon Bags

TABLE 3. LARGE SCALE PILOT PLANT TEST CONDITIONS AND RESULTS

6/12-14/78	20	283	29.4	27	118	6.6	12800	0.172	99.9987	1370
6/14-15/78	24	243	25.3	0	0	21.6	12600	0.480	99.9962	2125
6/15-16/78	22	261	27.0	0	0	22.9	12800	0.366	99.9971	2250
6/16-17/78	24	232	24.1	0	0	15.2	12400	0.126	99.9990	1437
6/17-18/78	24	283	29.4	27-33	118-190	10.2	12800	0.119	99.99907	1750-2400
6/18-19/78	24	283	29.4	39	325	8.5	12800	0.094	99.99927	358 5

Felted Polyester Bags

Table 2 has been corrected for the effect of this dilution. The differences in performance of the two units probably resulted from the difference in bag materials and conditioning of the bags. As shown in Tables 2 and 3, a marked difference in pressure drop was found for similar filtration velocities in the two series of tests. The higher pressure losses across the bags in the second test series and the corresponding higher efficiencies both probably resulted from a decrease in the effective filtration pore sizes and/or an increase in effective thickness of the filter cake and matte.

Inlet particle size distributions in the size range from 0.3 μm to 10 μm are shown in Figure 2 for the two sites. The two distributions are sufficiently alike that little performance difference at the two sites can be attributed to differences in particle size distribution. However, other physical factors such as particle shape, surface roughness, adhesion, etc., could have had some effect on performance.

Fractional efficiencies of the small scale mobile unit as determined by inertial methods are shown in Figure 3. The trend toward increasing efficiency in the first several days after installation of the bags is evident in this sequence of tests.

Previous testing by the manufacturer had shown that outlet emissions were significantly higher without electrostatic augmentation than with augmentation. Because it was possible that the trend of decreasing penetration with time as the bags became conditioned masked the expected effect of de-energizing the precipitator, a second test series was performed to re-examine the effect. This test was that performed on the full scale pilot plant collecting redispersed silica dust. Operating conditions, inlet and outlet particulate loadings, and overall collection efficiencies for the tests of the full scale unit are given in Table 3. Fractional collection efficiencies for the full scale unit as determined with inertial and electrical mobility methods are shown in Figure 4. In this case the expected increase in penetration when operating without electrostatic augmentation was observed.

SUMMARY AND CONCLUSIONS

The Apitron dust collector was found to operate at collection efficiencies in excess of 99% for particles larger than 0.3 μm with relatively clean Teflon bags. Efficiencies in excess of 90% for particles in the 0.01 μm to 0.3 μm size range and in excess of 99.9% for particles larger than 0.3 μm were measured for a unit using felted polyester bags. Operating pressure drops at a fixed filtration velocity (air to cloth ratio) were substantially lower with electrostatic augmentation than without. Total energy usage figures with and without augmentation were generally comparable with higher values for augmentation using the Teflon bags and lower values for augmentation using the polyester bags. Typical energy usage with augmentation is approximately 900 to 1400 joules/Am^3 (0.6 to 0.91 Hp/1000 ACFM).

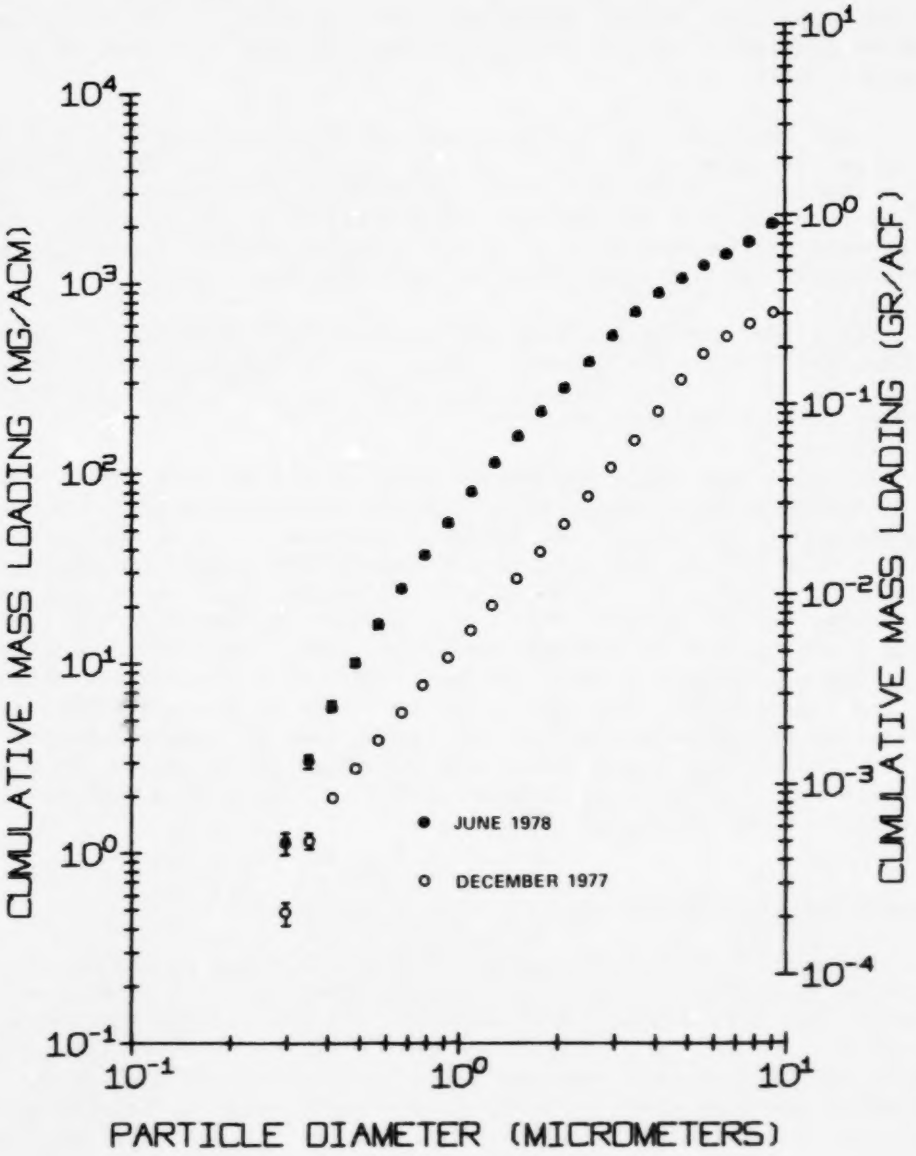

Figure 2. Inlet particle size distributions in the size range from 0.3 μm to 10.0 μm for the two sites. December 1977, small scale mobile unit, June, 1978, full scale pilot plant.

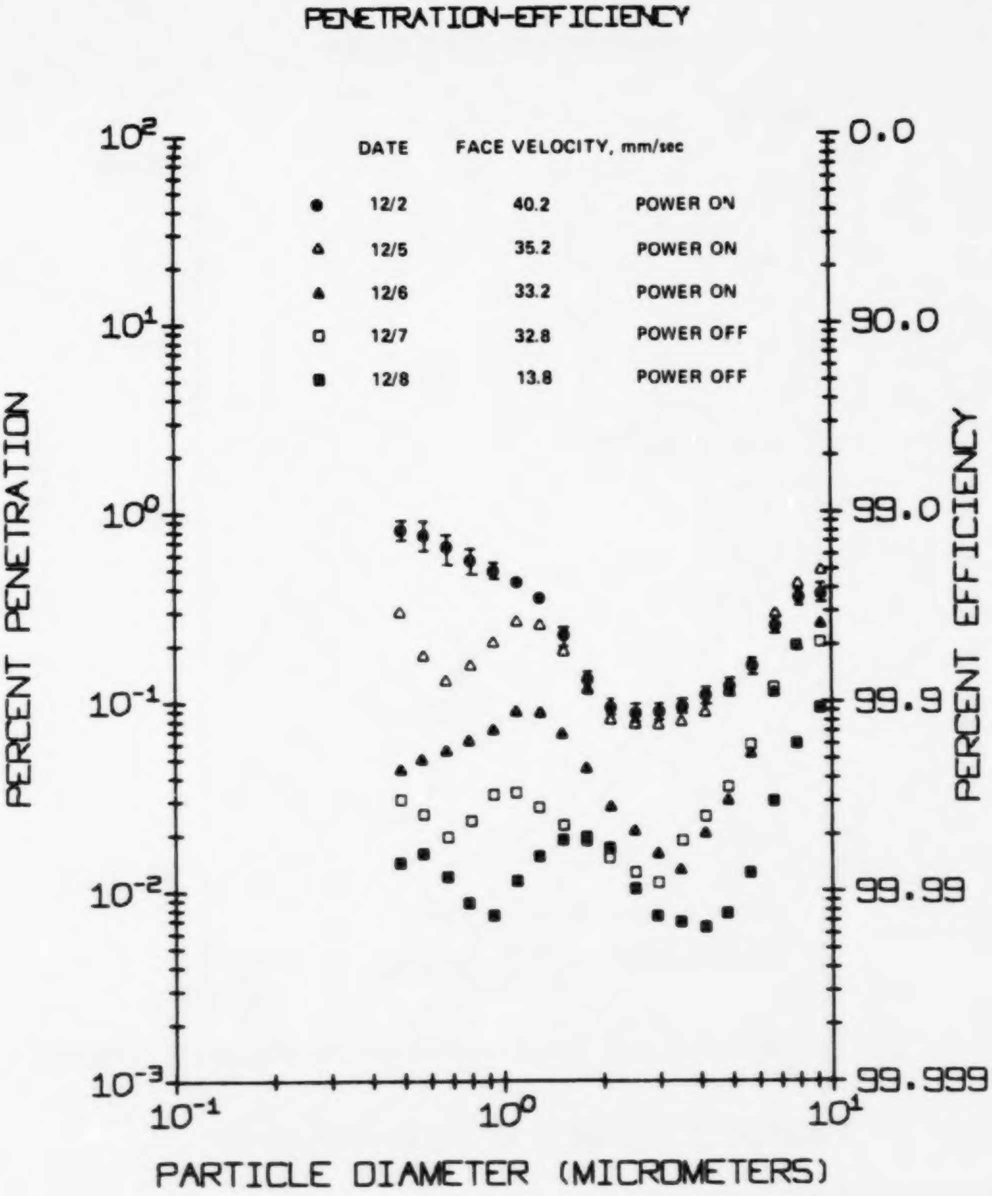

Figure 3. Fractional efficiency of small scale mobile unit as determined by inertial methods.

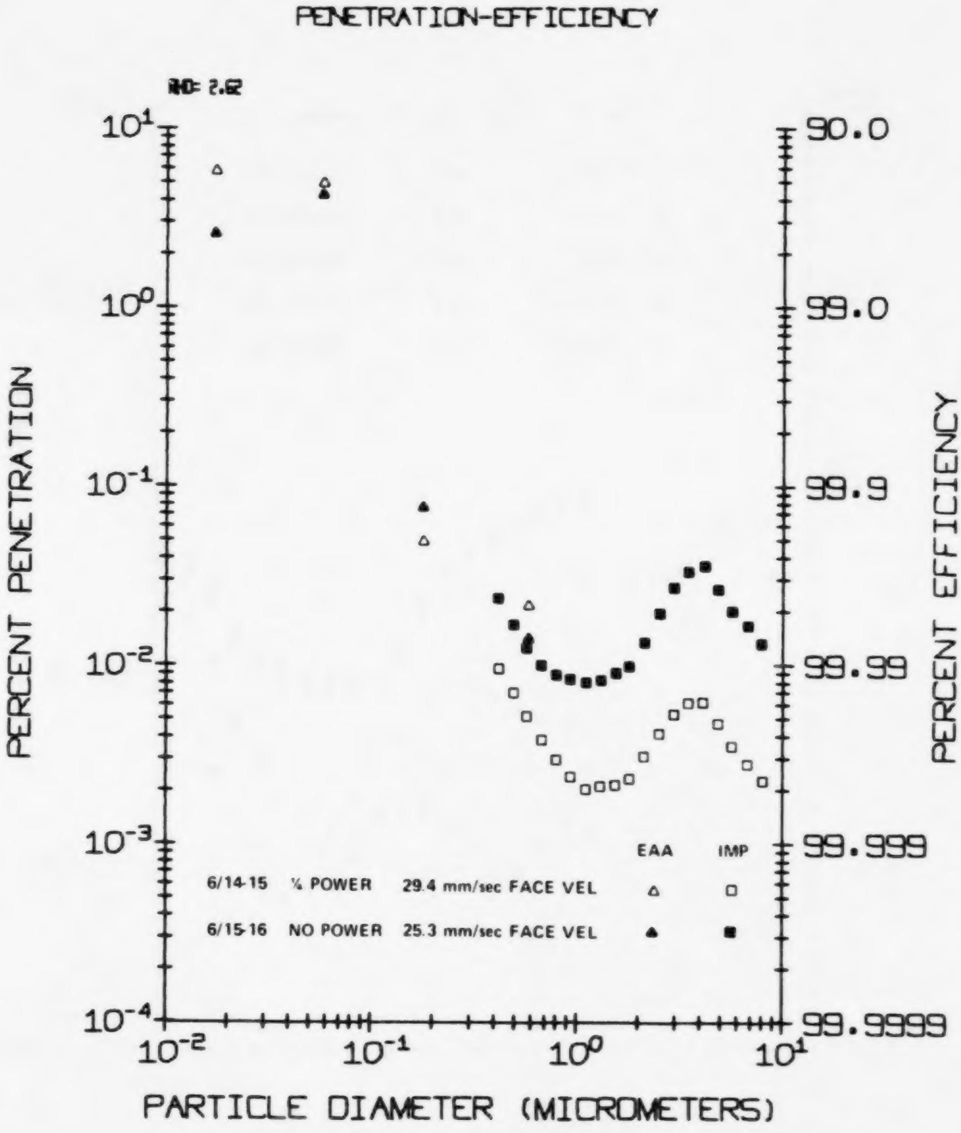

Figure 4. Fractional efficiency of full scale unit as determined by electrical mobility and inertial methods.

ACKNOWLEDGEMENTS

Appreciation is expressed to D. Helfritch, E. Gonas, and R. Tegler of Apitron, Inc. for their assistance in carrying out the test programs. The tests were performed under Contract 68-02-2181 for the Industrial Environmental Research Laboratory of the U.S. Environmental Protection Agency. Mr. Dale L. Harmon was the project officer responsible for the technical effort under this contract.

CORONA ELECTRODE FAILURE ANALYSIS

Roy E. Bickelhaupt
Southern Research Institute
Birmingham, Alabama 35205

Walter V. Piulle
Electric Power Research Institute
Palo Alto, California 94303

ABSTRACT

The goals of this project were to acquire a better understanding and to assist in the solution of the corona electrode failure problems. From a relatively large data base, it was determined that most corona electrode failures are due to: (a) electrical erosion (65%), (b) mechanical stress (15%), (c) chemical corrosion (12%), (d) combinations thereof and unknown causes (8%). The conditions required to bring about failure usually can be related to excessive over-voltage, lack of or poor maintenance, manufacturing and installation problems, improper usage, and inadequate design. An attempt is made to present the data in a form usable by plant operators to identify failure modes, to associate certain types of failure with probable locations, and to suggest remedial steps to eliminate certain types of failure.

INTRODUCTION

Corona electrode failure is a problem that affects plant maintenance and precipitator efficiency. Normally when an electrode fails, a short occurs in the specific electrical section, and the section must be removed from service. If the failure frequency is great in comparison to the frequency at which wires are replaced during normal maintenance, the overall performance of the precipitator can be poor.

Most wire failures are caused by electrical erosion, mechanical stress, chemical corrosion, or combinations thereof. The conditions

Preceding page blank

required to bring about failure usually can be related to manufacturing and installation problems, lack of or poor maintenance, improper usage, and inadequate design. The paper attempts to develop a better understanding and to assist in the solution of corona electrode failure problems. The paper is a condensation of a detailed report entitled "Corona Electrode Failure Study" executed by Southern Research Institute under the sponsorship of the Electric Power Research Institute, Contract RP413-1.

SCOPE

Information pertaining to 50 relatively new precipitators was solicited from the electric utility industry. The participating power stations were asked to supply detailed information about the construction and operation of their precipitators and to acquire corona wire failure data, including frequency and location, for a six- to twelve-month period. Also, two examples were requested for each type of failure that plant personnel observed.

All the information received was tabulated, and the statistical wire failure information was organized based on plan and elevation position in the precipitator and type or mode of failure. All failed wire specimens were visually examined, and examples were selected for photography and laboratory study. An attempt was made to correlate failure rates and modes with precipitator design and operational parameters.

OBSERVATIONS

Failure Frequency

To evaluate the severity of the problem, one must have a yardstick with which to judge. It was arbitrarily suggested that a failure rate of two wires per year per precipitator would be considered acceptable, one failure per month can be tolerated, and failure rates greater than one per month are unsatisfactory. Based on comments received from the participants along with data and wire specimens, the above scale appears reasonable. To keep the failure frequency evaluation simple, the effect of broken corona electrodes on the amount of collecting surfaces lost for any given precipitator was omitted.

Table 1 shows the percentage of power generating units having precipitators experiencing various failure frequencies. This summary indicates that the corona electrode failure rate for the precipitators from 57% of the power generating units involved is quite low. At these stations the problem is considered either insignificant or of low priority. On the other hand, 43% of the generating units have precipitators with significant corona electrode failure frequencies and 20% of these units present an intolerable situation. One concludes that the subject of corona electrode failure warrants investigation.

Table 1. CORONA WIRE FAILURE RATE

Wire Failure Rate Number/Year	Number of Power Generating Units	
0-2	15	(43%)
3-12	5	(14%)
13-52	12	(34%)
>52	3	(9%)

It is also interesting to examine failure mode in terms of failure frequency. The failure modes are electrical erosion (arcing), corrosion, mechanical problems, and unknown or combination modes. The failed wires recovered by the participating plants were catalogued according to failure mode. When possible (not all participants submitted wire specimens), the declared failure mode was substantiated in this laboratory.

To consider the various modes of failure in terms of failure rate, the number of failures were computed on an annual basis for each installation in terms of the various failure modes. These computations are summarized in Table 2. The first line of data shows that all the participating installations combined would produce 902 wire failures annually and that half of these wires would fail as a result of corrosion and about 40% as a result of arcing. Other than totaling the results for this particular study, these data do not define the general picture of the corona electrode failure problem. One installation had a catastrophic corrosion problem producing a great number of wire failures that distorts the general situation. If the data for this installation are deleted, the summation (line 2-Table 2) shows that two out of three wires fail by arcing and that the remainder fail equally divided among the corrosion, mechanical or other modes. This distribution is not appreciably altered by deleting the data from installations where only infrequent failures occur (see line 3). If one considers the installations having low rates of failure alone (line 4), it is shown that about 75% of the failures occur by arcing and that there is less ambiguity about the failure mode.

Table 2. NUMBER OF FAILURES PER YEAR PER MODE
AS A FUNCTION OF FAILURE RATE

All Installations having an annual failure rate of	Modes				
	Arcing	Corrosion	Mechanical	Other	All modes
0 to 400	332(36.8%)	456(50.6%)	73(8.1%)	41(4.5%)	902(100%)
0 to 86	327(65.0%)	62(12.3%)	73(14.5%)	41(8.2%)	503(100%)
13 to 86	294(64.2%)	55(12.0%)	68(14.8%)	41(9.0%)	458(100%)
0 to 12	33(73.3%)	7(15.6%)	5(11.1%)	0(0.0%)	45(100%)

FAILURE MODES

Chemical Corrosion

The combustion of coal containing sulfur using an excess of air produces the chemical species required to cause the electrolytic corrosion of iron and steel in the precipitator. These species include water, oxygen, and the sulfuric acid resulting from the reaction of its components, water and sulfur trioxide. Depending on the concentrations of sulfuric acid vapor and water vapor present in the flue gas, the acid dew point is usually in the range of 120 to 150°C ($\sim$250 to 300°F). It would therefore seem to be an inevitable situation that acid condensation will frequently occur in "cold-side" precipitators. One might inadvertently cause acid condensation by operating the precipitator at a temperature level considered to be marginal with respect to the dew point, and of course each time the unit goes in and out of service, the precipitator temperature passes through the dew point. It is conceivable that condensate produced during cool down and heat up will not be vaporized and removed from its position of corrosive action if the precipitator operating temperature is marginal with respect to the dew point.

Although corona electrode failure due to corrosion can occur at any position in the precipitator, it usually is found near the top of the chamber, particularly if the problem is severe as in the case of installations included in this study. This type of corrosion problem is associated with inleting of purge air at electrical feed-throughs at the top of the precipitator to inhibit deposition of particulate on support insulators.

An example of this type of corrosive failure is shown in Figure 1. The failure may or may not be characterized by obvious evidence of corrosion product. Sometimes the appearance will be one of general, overall rust color. However, this type of failure usually is characterized by: a limited vertical affected zone, a sharp demarcation between affected and unaffected regions, and wire failures that end with a sharp point on the longitudinal centerline of the wire.

It can be shown that this failure was not caused by arcing or mechanical stress by examining the microstructure of the wire from the failed region. The microstructure showed a preferred grain orientation, in the direction of wire drawing, prevailing throughout the specimen. No evidence of thermal input due to arcing or grain distortion due to mechanical stress could be found.

Another illustration of corrosive failure is one that is not necessarily associated with the upper elevation of a precipitator and may simply represent slow deterioration over a long period of time. Figure 2 shows this type of failure. The short length of wire in the center of the figure is slightly corroded but has a diameter of 0.109 in., the original diameter. At some positions along the wire shown on the right, the diameter has been reduced to 0.050 in. These wires also had ash adhering over extended lengths. The photomicrograph on the left shows the etched structure of the cold drawn 1045 steel wire and the very

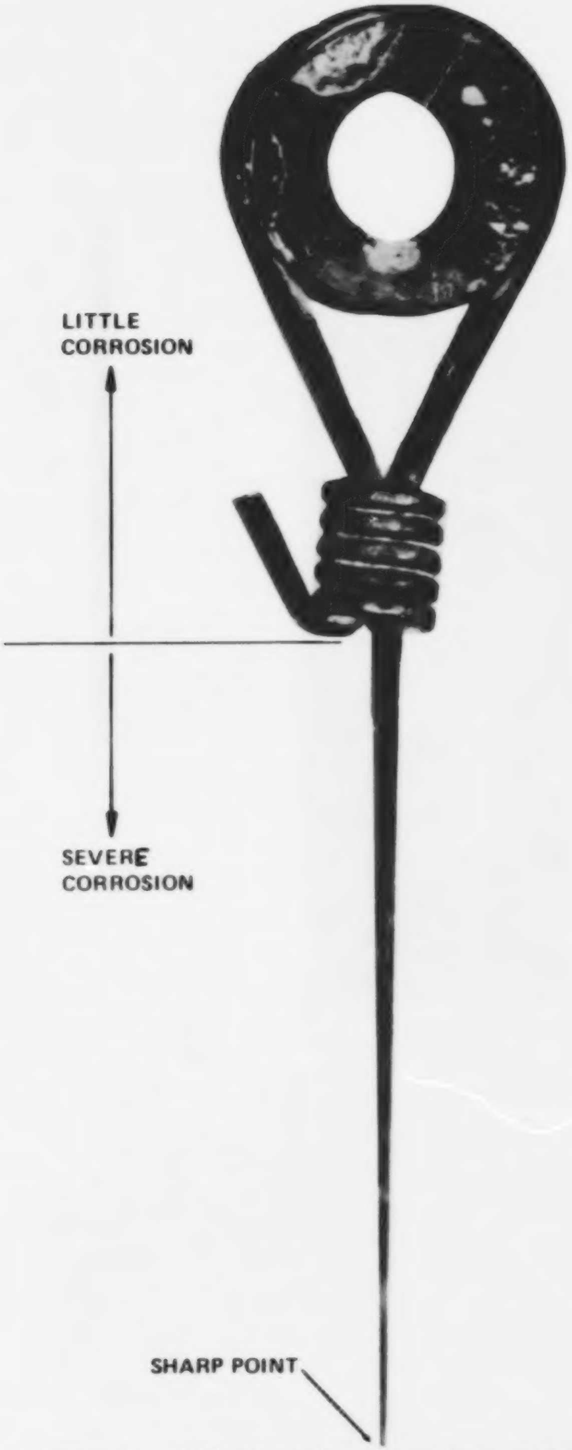
LITTLE CORROSION
SEVERE CORROSION
SHARP POINT

Figure 1. Illustration of severe corrosion in the upper elevation of a precipitator.

Figure 2. Extensive general wire diameter reduction as a result of corrosion over a long-time period.

thick deposit of corrosion product. Since these wires may have been installed for six years, the observed condition may simply be the result of long-time exposure. On the other hand, this may be an illustration of corrosion related to residual ash deposit containing condensed and/or adsorbed acid.

Since the operator today often has little control over the fuel available, one must concentrate on the flue gas temperature in the precipitator. The operator can take the following steps to reduce the corrosion problem:

- Eliminate all inadvertent in-leakages of air having a temperature lower than that of the precipitator

- Determine that purge air at feedthroughs is not driving the temperature of part of the flue gas below the dew point

- Eliminate unnecessary thermal excursions through the acid dew point

- Determine the thermal profile of the precipitator when operating in a normal, "coldest" condition. Compare this temperature profile with acid dew point information using accurate inlet gas analyses for water and sulfur trioxide. Maintain the coldest part of the precipitator above the dew point.

- Maintain a "clean" precipitator making sure that dust is successfully rapped from wires and plates and wash periodically according to precipitator manufacturer's instructions to eliminate residual deposits of acid or debris.

Precipitator manufacturers might consider electrode assembly designs that do not encourage the condensation of acid, avoid galvanic corrosion due to combinations of dissimilar metals, and design superior purge air feedthroughs. They might also determine, perhaps in conjunction with steel manufacturers, whether a superior corona electrode material is available. It was noted that several stainless steels have been used; no evidence of a trial using a low alloy steel has been observed. At present it would seem that a low carbon, hard drawn, plain carbon steel is the best material considering the influence of cost.

Electrical Erosion (Arcing)

Unlike the corrosion problem, failures due to arcing are much more common and occurred in every installation that reported a wire failure. Approximately a third of the installations that participated in this study have an arcing problem of significant proportion. The arcing problem generally is not costly with respect to number of wires lost; however, the problem is severe in that it necessitates unscheduled maintenance and can affect precipitator performance dramatically by having persistent single wire failures eliminating electrical sections of the collector.

By far the greatest number of arcing failures occur at the bottom of the precipitator, near the elevation of the bottom of the collecting plate. The next most frequent failure elevation is near the middle with the fewest occurring at the top. For those cases in which arcing is a severe problem, this type of failure occurs more often in the inlet sections. The location of the arcing failure with respect to plan and elevation positions is dependent on the situation that caused the arcing. Often the observed "arcing failure" is simply the end result of some other problem or failure.

Figure 3 shows a failure at the elevation of the bottom edge of the collector plate. It is interesting to note that the failed ends of the wire are somewhat blunt and that the deteriorated region is symmetrical about the wire centerline. It is suggested that this type of failure may have occurred due to the absence of or failure of an anti-sway device. In this condition, the wire remains taut, is free to swing, and becomes rather uniformly degraded by arcing around the entire circumference. To verify an arcing failure, the wire microstructure is again useful. Figure 4 shows the microstructure in the affected and unaffected region of this failed specimen. In the region of failure there has been considerable thermal input due to the electrical arcing. This thermal input is manifested by grain growth and the precipitation of a second phase.

Arcing failures in the bottom region of the precipitator can be caused by a variety of situations: a) plates and wires out of plumb, b) plates that have distorted out of plane, c) wire and weight alignment hardware not available, broken, or shifted from correct position, d) excess ash build-up in hoppers causing weights to fail to maintain tension on the wires, and e) faulty construction or some mechanical failure that allows an object causing high electrical stress to be in the region of a corona wire.

Arcing failure having the general appearance of those described also occur infrequently in the vicinity of the top of the collection plates. These failures are often repeatedly caused by the proximity of some structural component, a construction error, or other accidental fault.

Failures due to arcing also occur in the middle third of the corona wire and can have affected lengths varying from an inch to several feet. Often what seems to be an arcing failure near the middle of the corona wire is really a secondary effect occurring after the principal failure occurs near the bottom of the precipitator. For this reason, it is prudent to have, if possible, the entire corona wire assembly available for failure analysis.

Other than an unusual collection plate distortion, it would seem that there is only one way in which a failure could occur near the middle of the corona wire without some preliminary, partial or complete failure near the bottom. That situation is one in which the wire oscillates with

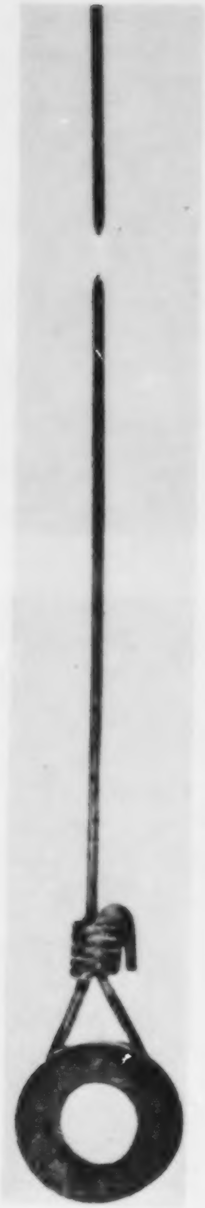

Figure 3. Illustration of electrical erosion at the lower elevation of the collection plates.

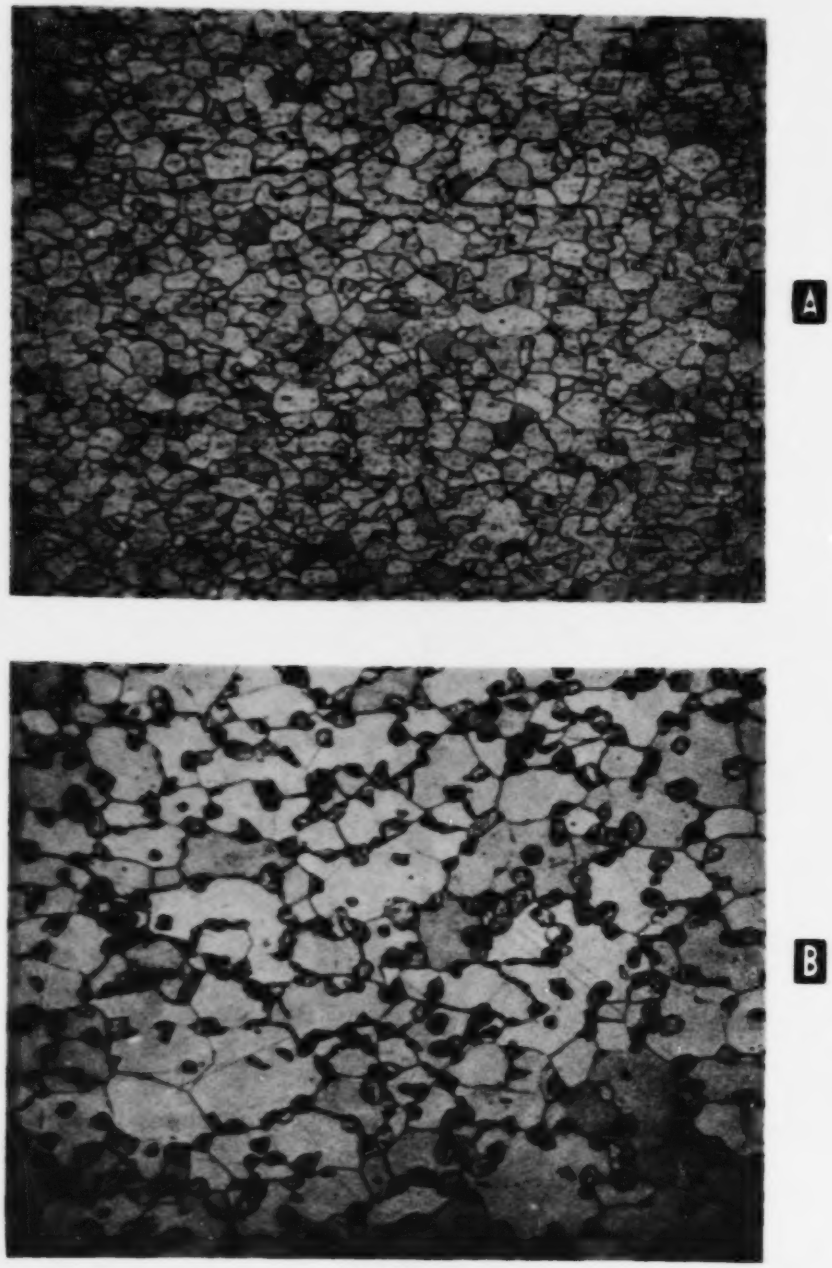

250X

Figure 4. Microstructure (250X) at the longitudinal centerline of the failed wire shown in Figure 3; A) unaffected region away from failure and B) region near point of failure.

sufficient amplitude so that at times it is close enough to the plates to cause arcing. Usually the failed wire will have an affected zone that is fairly long, up to several feet, and the wire may have developed one flat side or two flat surfaces diametrically opposed depending on whether the wire vibrated near one or both collection plates near it. In this study, no failures of this type were positively identified.

Several installations reported instances of failures occurring near the middle of the corona wire that were certainly the result of a preceding problem near the bottom of the precipitator. Failures such as these, it is reasonably certain, occur when the force holding the wire in tension is lost. This can result from excessive ash build-up in the hoppers, mechanical failure of the weight attachment, preliminary arc failure at the bottom of the wire, etc. When the source of tension in the wire is lost, the wire may tend to bow or kink. When it does, it can contact the plate or a stiffener and burn through consuming a short length of wire.

Mechanical and Combination Failure Modes

The type of failure mentioned immediately above was common for those installations using a design in which two wires support one weight. Apparently one or both of the wires can become disengaged from the weight because of unequal tension on the two wires and/or failure of the heads of the shrouds that are intended to keep the wire in the weight.

One of the reasons that the above described corona wire failure occurs is related to degradation of the ends of the shrouds. Five examples of this condition are shown in Figure 5. Various degrees of part degradation are illustrated. The cracks of the type shown in the end of the fourth part from the left, although exaggerated by use, can be observed in a new part. The head of this corona wire shroud is apparently formed by cold impact. The metal is severely distorted, folded and cracked in forming as revealed by microstructural examination. This leaves the metal with considerable residual stress and in a condition particularly susceptible to the effects of corrosion and mechanical stress. By examining the cross-sections of the shroud heads shown in Figure 5, one can see the damage caused by mechanical stress due to vibration and rapping. Also, a certain amount of wire revolution about its own longitudinal axis must take place causing various profiles due to mechanical erosion. Corrosion also plays a role in this failure process both with respect to erosion and mechanical stress problems.

Another example of failure in the mechanical mode was experienced by several installations. These failures occurred at the bottom of the precipitators in the general region where arcing failure often occurs. The wires fractured in a plane normal to the longitudinal centerline of the wire. The shrouded wires failed within a half inch of the end of the shroud, while wires attached with loop rings failed within a few inches of a ferrule. Photographs of examples of this type of failure are shown in Figure 6. Microscopically the wire failures resemble a

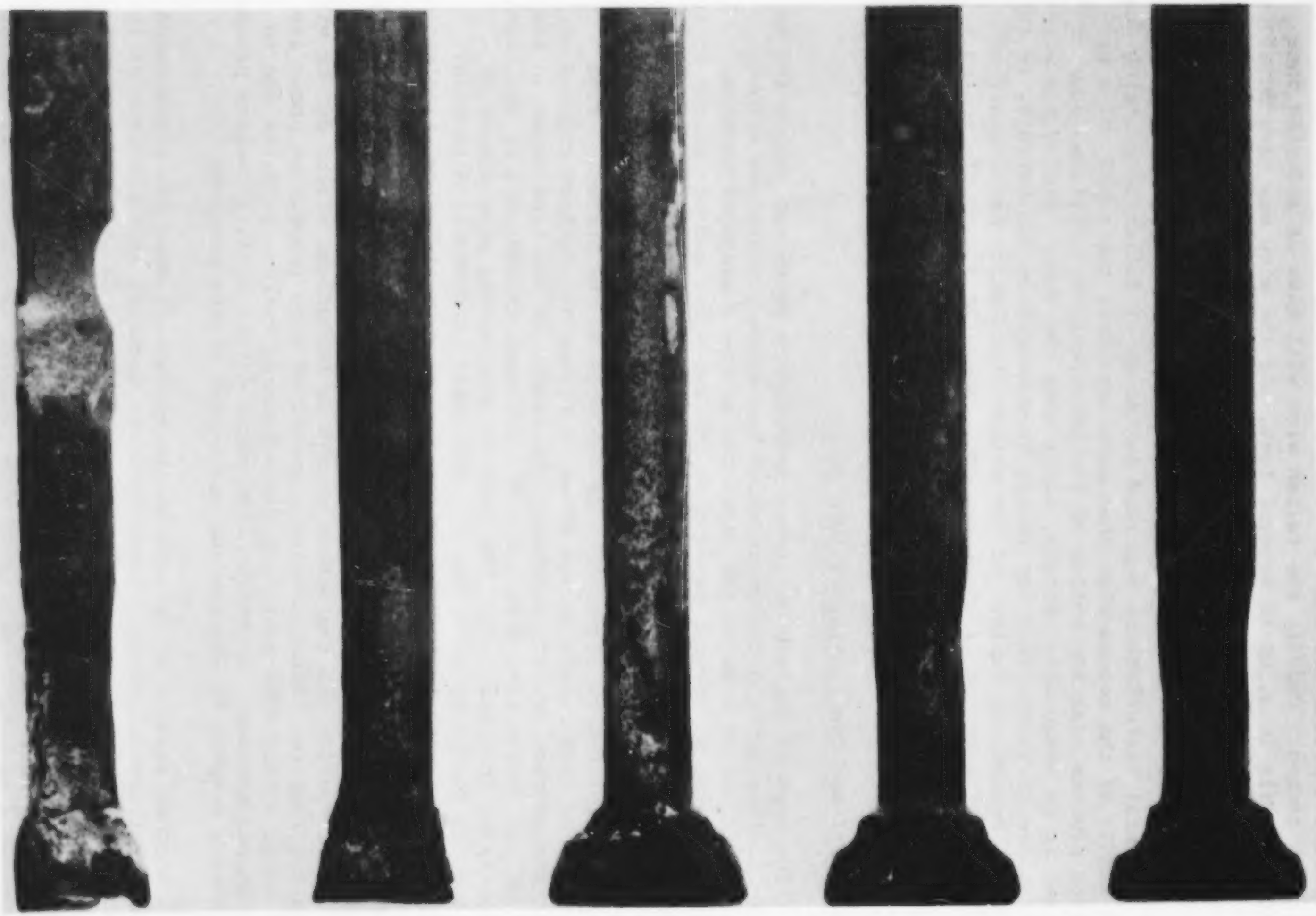

Figure 5. Illustration of degraded shroud heads.

PLANE OF FRACTURE
PLANE OF FRACTURE

Figure 6. Illustrations of brittle, mechanical failures.

fatigue fracture. Scanning electron microscopy was attempted to relate the fractography to fatigue; however, this was impossible because the fracture surfaces were old and had not been protected for subsequent examination. The region of failure is concomitant with a high incidence of arcing and is a position that would be exposed to considerable flexing as a result of rapping or wire oscillation for any reason.

Figure 7 shows a crack about 4 mils long extending into a 1045 steel wire specimen. The crack starts at the OD of the wire and propagates in the same plane as the crack that caused failure. In this case, the steel in question was moderately high in carbon which should facilitate the formation of a hard, brittle phase at the wire surface from which a crack can develop. However, high carbon concentration is not a prerequisite for this type of crack formation. Although the crack shows both an inter and transgranular path, it is generally parallel to the primary fracture path. It is quite possible that in the case of this type of wire fracture the problem was aggravated by corrosion which was in evidence.

SUMMATION

In an effort to condense the corona wire failure information acquired in this study into a form potentially useful to the plant personnel responsible for the operation of the precipitator, Table 3 was been constructed. This table is designed along the lines of a trouble shooting guide and represents an initial attempt. With additional experience, information and failed specimens, it can be improved and developed to satisfy individual utilities. The objective of the table is to allow the plant personnel to more easily recognize the mode of failure, identify the cause, and take remedial steps.

As a result of observations made during this study and remarks received from various participants, one can make several general statements which if adhered to by the operators would eliminate much of the corona wire failure problem:

a) thoroughly inspect during erection of the precipitator to insure that quality workmanship is reflected in the fabricated parts and erection technique,

b) set up an adequate maintenance schedule to ensure that design clearances are maintained,

c) map wire failures by plan position in each electrical section and by elevation to help determine the cause of failure,

d) stop inadvertent air in-leakage and adequately heat purge air used in feedthroughs, and

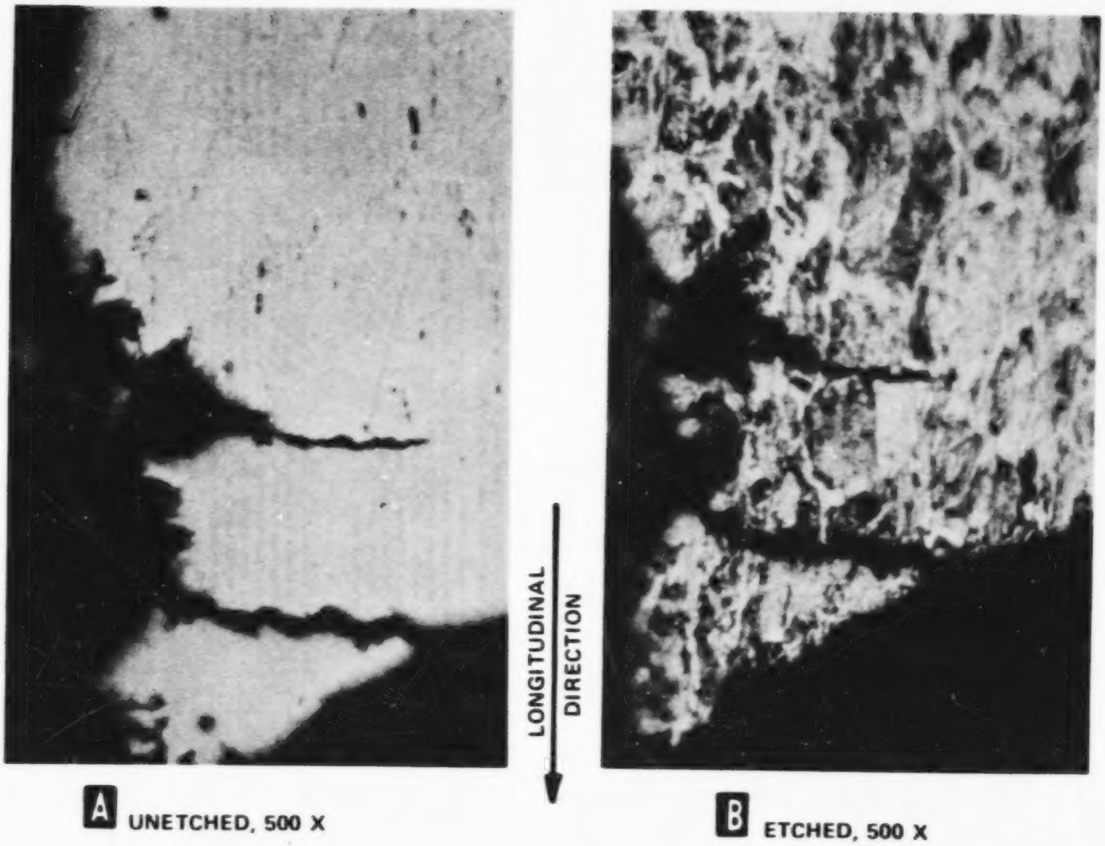
LONGITUDINAL DIRECTION

A UNETCHED, 500 X

B ETCHED, 500 X

Figure 7. Microstructure illustrating crack initiation leading to failures of the type shown in Figure 6.

Table 3

TROUBLE SHOOTING GUIDE FOR CORONA WIRE FAILURES

Failure Designation	Location		Distinguishing Features		Cause or Contributing Factors	Remedial steps
	Plan	Elevation	Macrostructure	Microstructure		
Corrosion 1	Usually middle & outlet sections	Top	Rust, scale, or other corrosion products. Failed wire forms sharp symmetrical point. many wires involved.	Pitted surface, no evidence of thermal input or mechanical distortion.	Condensation of sulfuric acid, due to cold purge air.	Heat purge air for feedthroughs.
Corrosion 2	Anywhere	Usually upper half	Rust, scale. Failed wires may be relatively few in number and may or may not be grouped. Usually occurs at contact points between electrode components. Sometimes general reduction of wire diameter over long lengths of wire.	Same as above	Condensation of sulfuric acid due to: inadvertent cold air leakage, operating precipitator at a temperature below the acid dew point, or condensation occurring during multiple temperature excursions below the acid dew point.	Stop leaks, make sure entire precipitator temperature is above the acid dew point, limit the number of times the temperature falls below the dew point to as few as possible, keep precipitator clean
Arcing 1	Usually a repetitive type of failure in a specific area.	Top	Wires and other electrode components show evidence of electrical erosion, usually quite directional. Usually a short length of wire affected resulting in tapering to somewhat of a point from one side.	Evidence of thermal input - melting, grain growth, recrystallization, formation of martensite, etc.	Loss of clearance between wires and plates or support structures. Imperfect or intermittent contact between frame and wire connectors.	Check for warped plates and general loss of clearance. Determine if continuous or excessive rapping, or some other vibration is causing loss of frame to connector contact.
Arcing 2	Anywhere	Middle	Usually long lengths of wire, >1', flattened and tapered on one or two sides. (Failures showing vigorously arced short lengths of wire are usually secondary effects from a failure in the lower elevation).	Same as above	Oscillating wires swinging close enough to the plates to arc.	Check for broken steadying device, make sure wire length is within tolerance, and consider changing wire stiffness and/or weights.
Arcing 3	Anywhere often inlet section	Bottom	Usually short length of wire affected and usually the arcing source is quite directional. Evidence of penciling, pitting and burning. Failed end usually tapered to a non symmetrical point.	Same as above	Loss of clearance between wire and plate because of: shifted alignment or steadying frame, warped plates, broken weight guides, ash build-up on wires, plates or alignment device, ash overflow in hoppers, loss of wire tension, etc.	Reestablish design clearances; make sure ash is being rapped from plates and wires and that ash removal system is operating; examine for broken guides and loss of weight. Check automatic voltage control Check low voltage tripping devices.
Mechanical 1	Anywhere	Anywhere	Fatigue type failure, flat fracture face normal to the longitudinal direction of the wire, hook, shroud, etc. General embrittlement of the wire leading to multiple fractures in handling.	Usually minute cracks are to be found at the wire O.D. in the same orientation as the fracture; sometimes evidence of arcing and/or corrosion at the surface can also be found; near the fracture face secondary transgranular cracks may be seen.	Cracks initiated due to wire imperfections resulting from fabrication, arcing, corrosion, etc. are propagated by low level stresses associated with wire vibration.	Employ any of the above suggestions to minimize arcing and corrosion. Check rapping procedure and all other conditions that influence wire vibration (wire stiffness, weights, etc.). Reduce sparking rate.
Mechanical 2	Anywhere	Top & bottom	Mechanically failed connector joining wire to frame or weight, rarely a wire, severely distorted to produce work hardening. Also mechanical erosion due to relative motion between parts.	Sometimes severely distressed microstructure can be found, often evidence of corrosion and arcing are also visible	Excessive wire vibrations both in the transverse and longitudinal directions. Situation aggravated by arcing and corrosion.	Eliminate the excessive vibration due to rapping or poor design of fit between mating parts. Minimize corrosion and improve connector design or fabrication.

e) whenever contemplating the alteration of operating conditions, consider the potential effect on corona wire stability, mechanical condition, and relative clearance with other components.

Considering all wire-weight corona wire assembly designs collectively, several features seem to warrant attention by the precipitator manufacturers:

a) contiguous components of the assembly that form acute angles and/or unite electrochemically dissimilar metals have less resistance to corrosion problems,

b) the design of and fabrication technique for some components might be reviewed with respect to developing a mechanically superior part,

c) improvement in designs so that loss of wire tension rarely occurs,

d) improvement in electrode design and/or rapping techniques so that the ends of the corona wire assembly act as connectors rather than vibratory contacts,

e) improved design for maintaining clearances, and

f) analyze designs to assure that wire oscillations are minimized to inhibit arcing and fatigue failures.

For the typical installation, the greatest number of corona wire failures are caused by electrical erosion and mechanical failures initiated by electrical stress. Sometimes these failures are due to operating the precipitator under conditions of excessive sparking. For optimum precipitator performance, it is imperative that maximum effective voltages and currents are maintained on the corona electrodes. To accomplish this, the precipitator manufacturers have instituted automatic voltage controls. All of these are variations of the principle of operating the precipitator in a carefully controlled "sparking" mode. Therefore it must be insured that these devices are not operated in excess of manufacturer's recommendations. In some cases for causes too numerous to list, even the "standard" spark rates are excessive, and electrically caused corona electrode failures can and will repeatedly result. To prevent such occurrences, a methodical evaluation of existing conditions must be made. Based on these evaluations, readjustment of automatic control devices can be made, or if this is limited due to age or type of device, replacement of the aged device with a newer, more responsive type of voltage controller should be considered.

HIGH TEMPERATURE & HIGH VELOCITY
POROUS METAL GAS FILTRATION MEDIA

Leonard J. Ortino, P. E.
Vice President & General Manager
Michigan Dynamics Division
Ambac Industries, Inc.
Subsidiary of United Technologies Corp.
Garden City, Michigan 48135

Robert M. Bethea, P. E.
Professor Chemical Engineering
Texas Tech University
Lubbock, Texas 79409

ABSTRACT

Current fabric filter problems include temperature, and velocity limitations; excessively large installations; and high maintenance and bag replacement costs. These can all be improved by suitable metal fabric media. This paper is directed towards the initial evaluation of such a medium for high temperature and high velocity gas filtration. Critical design parameters have been identified and the scope of required testing is described.

Dynapore^R porous metal laminates composed of sintered wire cloth were developed for gas filtration based on earlier experience with high pressure, high temperature liquid filtration. Several requirements for different gas stream particulate removal have been evaluated. Initial testing and application of Dynapore laminates has shown promise in areas involving high temperatures, and high velocities. Of the different cleaning methods evaluated, high velocity reverse air flow has been found most satisfactory. A system concept has been developed incorporating Dynapore laminates with high velocity reverse flow or pulse cleaning.

Preceding page blank

INTRODUCTION

If EPA goals for cleaner air over the next five year period are to be met within reasonable cost guidelines, we believe there must be a significant shift to filtration. Current limitations of fabric filter materials will require an increase in efforts to develop better filter materials for capturing sub-micron particles at high temperatures and high velocities. Applications which require immediate attention include coal-fired boilers, steel and iron furnaces, incinerators, coal gasification, etc. One method for obtaining better filter materials is to use a rigid, porous metal filter medium. This paper presents the currently available operational data, for such a medium.

LITERATURE REVIEW

Major high temperature industrial sources of fine particulates are: Iron and steel production, coal-fired power plants, lime and cement kilns, recovery furnaces in Kraft pulp mills, and municipal incinerators, Burchard, 1974. The immediate uses of metallic filter media for air contaminant control are numerous: Electric arc melting furnaces, molten metal transfers, sinter plants, lead retorts, zinc refining, copper reverberatory furnaces, secondary aluminum recovery, etc., Squires, 1973. From currently available literature, it is clear that metallic filters are superior to fabric filters in such applications because they do not require the addition of cooling air, do not burn, and provide dimensional stability.

In order to control such emissions economically, high velocity filter media are needed which will withstand service temperatures up to 1200 C. Glass fibers even when treated with silicone, graphite or polyfluorocarbon coatings are inoperable at temperatures above 300 C, except for brief surges. Porous metal filtration materials have the ability to withstand high temperatures, and resist deformation at high velocities. Although granular bed filters are operable to 550 C, their performance is not reliable, Draemel, 1974.

Metallic filters can be fabricated in several forms: sintered powdered metal, plain wire cloth, sintered wire cloth and fibre metal felt. Because of their strength and the ease with which they become blinded, sintered powdered metal filters are usually cleaned by high energy, 80-100 psig, reverse air flow through pulse jets of up to 1 sec. duration, Carls and Levitz, 1968.

Metallic wire cloth filters have been used to control emissions from iron foundry cupolas and blast furnaces, Sakaguchi, 1972. Other uses for wire cloth filter media have been the control of emissions from non-ferrous alloy production where the temperatures were 600-1000 C, Mandriko and Peisakhov, 1971. The authors noted that the filters were easily cleaned by low pressure reverse air jets and that high velocities are possible.

DYNAPORE FILTER MEDIA

It is evident from the available literature that there has been and continues to be considerable interest in metallic filter media for temperatures over 230 C and velocities over 25 FPM. In this paper we discuss Dynapore* filter media, a high strength, laminated, sintered, porous stainless steel material specifically engineered for tough requirements. It can consist of one or more layers of wire cloth with or without perforated or expanded sheet metal for added strength.

Dynapore laminates for gas filtration were developed from the experience gained in the development of a much larger group of laminates for high temperature and high pressure liquid filtration and for fluidization applications. Table 1 lists a few typical Dynapore laminates.

Table 1. TYPICAL DYNAPORE LAMINATES

APPLICATION	um RATING	FILTER CLOTH	ADDITIONAL LAMINATIONS	AIR FLOW**	WATER FLOW+
FLUIDIZ'N	-	-	12 x 64 Wire Cloth	5	.058
	-	-	30 x 250 Wire Cloth	10	.110
	-	-	12 x 64 Wire Cloth	25	.261
LIQUID FILTRATION	5	200 x 1400	60 x 60 Wire Cloth	91	.99
	10	165 x 1400	30 x 30 Wire Cloth	162	1.48
	50	400 x 120	13.5% OA Perf. Plate	361	2.77
GAS FILTRATION	15	165 x 800	72% OA Perf. Plate	360	3.39
	64	50 x 250		601	4.62
	102	30 x 150		779	5.80

** SCFM at 2 in H_2O P + GPM / sq in at 1 PSID

*Dynapore is the registered trademark of Michigan Dynamics Div., Ambac Industries, Inc., Subsidiary of United Technologies Corp., Garden City, Mich.

Dynapore laminates are normally made from types 304 or 316 stainless steels. For higher temperatures they can be Hastalloy, Inconel, Nichrome, and the Driver Harris super alloys. Any metal which can be woven into cloth, except those that contain reactive metals such as aluminum, can be used for Dynapore. The filter cloth for Dynapore can be a square weave, plain Dutch weave or twilled Dutch weave.

Dynapore laminates are bonded by the sintering process along with various degrees of compaction or calendering of the laminate to insure a satisfactory sinter bond. Sintering produces a homogeneous metal bond at each cross-over of the wires of the cloth as well as each point of contact between adjacent layers of the laminate. The sinter bond is produced by atomic diffusion at temperatures around 90% of the melting point, which is about 1200 C for stainless steel. It is generally accomplished in a reducing atmosphere or a hard vacuum. Dynapore laminates are produced in flat sheets which can be worked like sheet metal into any size or shape element, by standard fabrication techniques. Calendering is a precision rolling process which increases each point of contact to insure a more reliable and stronger sinter bond. Additionally, calendering produces a smooth surface on the outside layers which generally improves the particulate removal process.

CLEANING METHODS

Laboratory tests at Michigan Dynamics and field tests by Alabama Alloy, Inc., Birmingham, Alabama, and Michigan Boiler & Engineering Co., Detroit, Michigan, have shown that sintered wire cloth laminates can be cleaned by mechanical vibration, with or without reverse air flow and high velocity reverse gas or liquid flow either in a continuous manner by means of jets or in a pulse manner by means of accumulators or explosive techniques. Test data is accumulating which heavily favors pulse cleaning because it leaves a layer of dust to act as the true filter for fine particles.

Initial tests were performed by Michigan Dynamics in 1976 with panels of Dynapore. The dust cake was formed by shaking a ferro-silicon furnace exhaust dust, made up primarily of sub-micron particles, into the air stream going through the panel. The dust cake was removed by reverse high velocity air flow through the panel using an air nozzle with a pressure of 50 psig. Though very effective, sometimes it was too much so, and left no residual dust to help in the next cycle.

In the latter part of 1976 a Dynapore laminate was selected as the filter medium for a system for an electric arc furnace making ferro-silicon alloy ingots at Alabama Alloy. Tests performed by the system designer indicated that simple impact of the mounting structure was sufficient to remove the dust cake. Actual operational tests showed that this was not satisfactory. Laboratory tests on panels removed from the system determined that high velocity reverse air flow from a nozzle at 50 psig would clean the panels. Additional testing with indicated system design changes are now being made at Alabama Alloy.

Several years ago Michigan Boiler & Engineering designed and built a system based on a patent by D. Ostby[7] utilizing wire cloth mounted on a structural frame. Test data generated with this system produced similar results to those with Dynapore laminates. Initial tests with Dynapore laminates, in fact, indicate that they can handle higher velocities. This is due to the improved structural and fabrication characteristics of Dynapore laminates.

Initial cleaning tests were conducted on the Michigan Boiler system utilizing high sub-sonic reverse air flow. The cleaning method was then changed to a high sub-sonic to sonic velocity shock wave generated by the rapid exhaust of air from a 4.7 cu ft tank at 40 psig. The filter element had a volume of 42 cu ft. With the medium clean the initial ΔP was 0.72 in of H_2O. A dust load of 6000 grains/sq ft containing about 30% sub micron particles was introduced over a period of one hour with the velocity reaching 91 FPM. During this time the ΔP increased to 13 in of H_2O. The filter element was satisfactorily cleaned to a residual ΔP of 2 in of H_2O by the shock wave from the rapid discharge of the air tank. Many successive cycle of dust cake formation and cleaning were repeated within these limits. Typical results of this testing procedure are shown in Figure 1, as a plot of filter resistance versus deposited dust, with points plotted every 15 minutes. Velocity was increased at each 15 minute interval. The decrease in resistance at the higher velocities is attributed to some fall off of the dust cake. The efficiency was checked by measuring the dust collected at the blower exhaust, which averaged 99.8%. Dynapore laminates are currently being tested on this system.

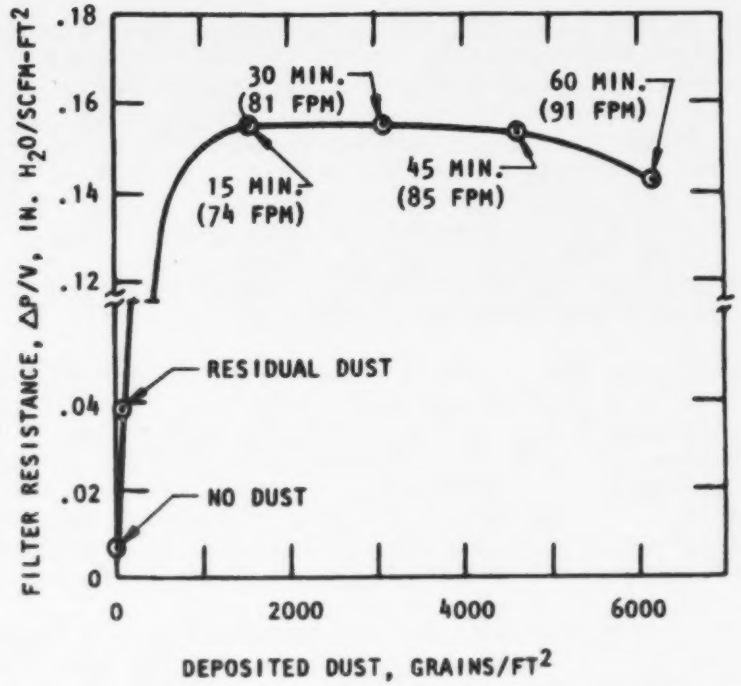

Figure 1. Dust cake formation and cleaning cycle tests.

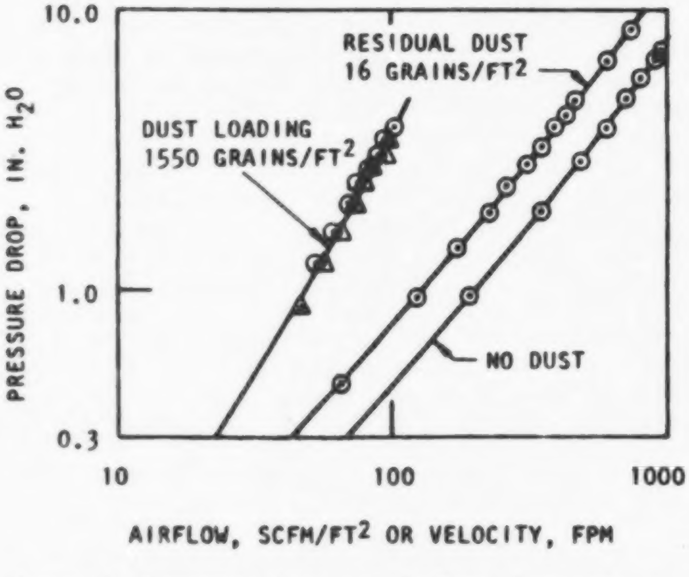

Figure 2. Pressure drop vs.airflow, Dynapore filter medium tested with Alabama Alloy dust.

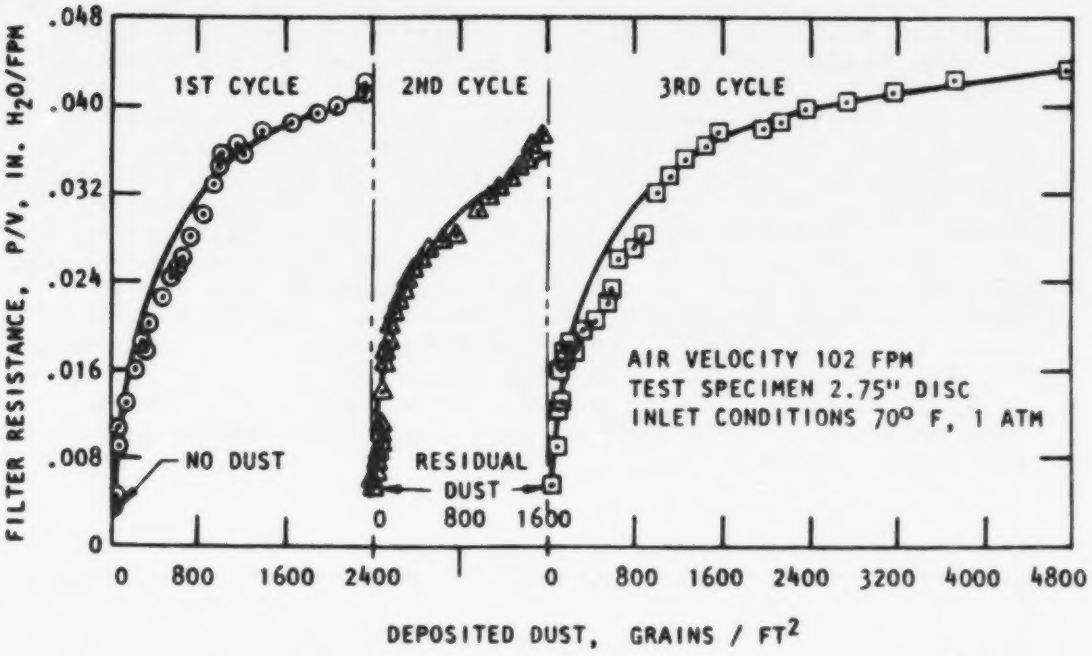

Figure 3. Filter resistance vs. dust deposit for Alabama Alloy dust on Dynapore laminate.

PERFORMANCE TESTING

Laboratory and field tests have been performed on many Dynapore laminates since early 1976 and have been conducted at an accelerated pace since late 1977. An example is the evaluation of a Dutch weave wire mesh sintered to a plate perforated with hexagonal holes. Typical test data is presented in Figures 2 & 3. Figure 2 shows pressure drop versus air flow velocity, first clean, then with a light residual dust loading of 16 grains per sq ft and finally with a heavy loading of 1550 grains per sq ft. Additional runs were made with dust loading up to 5000 grains per sq ft.

Figure 3 shows this higher dust loading relationship with data for repetitive cycles measuring filter resistance versus deposited dust with constant air velocity of 102 FPM. Of major significance, these tests show a relatively low pressure drop of 4.5 in of H_2O with a velocity of 102 FPM and dust loading of 4800 grains per sq ft. The filter was cleaned after each cycle by a short reverse air pulse generated by the rapid discharge of a 3 cu in air supply at 97 psig. No overall efficiency was measured during these tests due to the lack of suitable equipment to do so.

Further testing of Dynapore laminates was conducted by Michigan Boiler & Engineering. Figure 4 shows five dust loading cycles with a Dynapore panel using 50 x 250 Dutch weave cloth. Test results are similar to those in Figure 1. With the Dynapore laminate clean, the ΔP was 1.7 in of H_2O. During each 15 minute cycle a dust load of 100 grams (approximately 1540 grains) per sq ft was applied with an air velocity of 100 FPM. The dust was primarily silicon oxide with 30% sub-micron particles. During each cycle, the ΔP rose to about 12 in of H_2O within the first minutes then, leveled off at near 14 in of H_2O for most of the cycle. Toward the end of each cycle, portions of the dust cake would fall, causing the ΔP to drop to about 13.6 in of H_2O. Residual ΔP after each cleaning ranged from 2.3 to 2.7 in of H_2O. Cleaning was accomplished by super sonic shock wave pulses. Several cycles were run to determine collection efficiency which averaged 99.8%

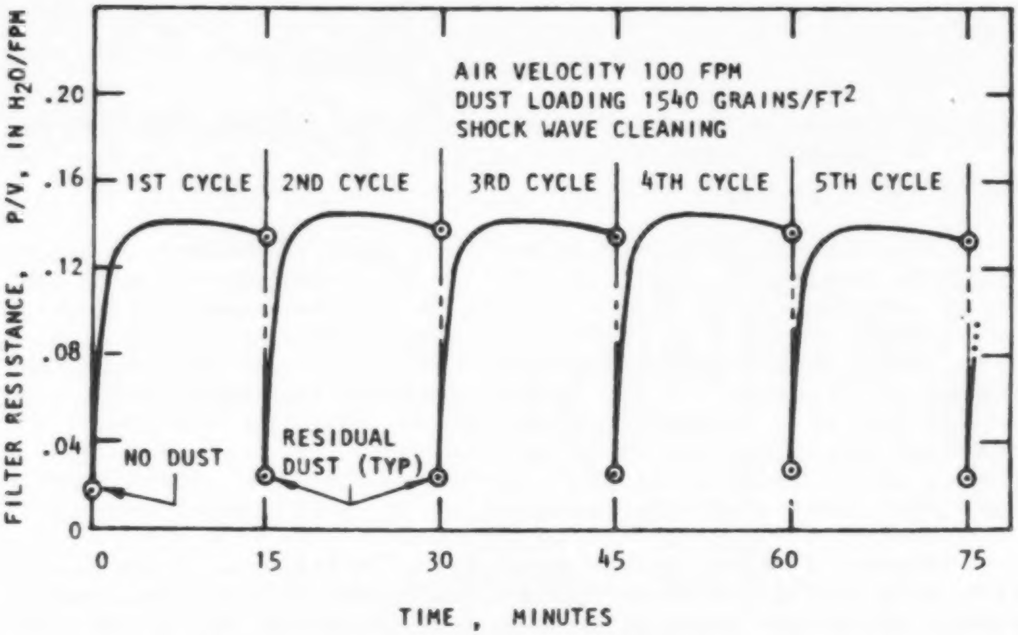

Figure 4. Filter resistance vs. time for 50 x 250 Dynapore laminate, Michigan Boiler and Engineering test facility.

FUTURE TEST REQUIREMENTS

The data presented in this paper is very limited in scope, and a great deal of quantitative data is still undetermined. Test facilities are currently being expanded and upgraded to provide for appropriate and reliable testing. This will be amplified by the tests being run and being set up to be run by companies already using or beginning to design Dynapore filters into their air pollution control systems.

Tests are currently being conducted at Michigan Dynamics and at O.E.M.'s to evaluate efficiencies of particulate removal under various pollutant and environmental conditions as well as effectiveness of various cleaning methods.

Some of the specific data which needs to be determined include:

1. Quantitative data on pressure drop versus dust cake build up and cleaning cycles over extended periods of time for various particulate compositions, velocities, temperatures, and humidities.

2. Quantitative data on collection efficiencies for different Dynapore laminates with various particulate compositions and environmental conditions.

3. Evaluation of the effectiveness of various cleaning methods as related to ratios of blowback flow rates to forward flow rates and frequency of cleaning cycles.

Although a great deal of testing is still to be done, there's sufficient basic data to serve as a guide to system designs utilizing Dynapore laminates. Towards this end, a patent has been applied for by Michigan Dynamics covering the application of Dynapore laminates for air pollution control systems. The recommended cleaning method is a reverse air jet blast or pulse, but other cleaning methods can also be used.

The task ahead of us now is to accelerate the test work being done to provide quantitative data needed to finalize suitable systems for high temperature and high velocity gas filtration with Dynapore laminates.

REFERENCES

1. Burchard, J. K., 1974. The Significance of Particulate Emissions. J. Air Pollut. Control Assoc. 24: 1141-1142.

2. Squires, B. J., 1973. New Developments in the Use of Fabric Filter Dust Collectors in the Steel, Non-Ferrous, and Foundry Industries, Proc. Int. Clean Air Congr., 3rd Dusseldorf, W. Germany, 1973. p. E27-E30.

3. Draemel, D. C., 1974. The State of the Art of High Temperature Filtration and Current Technology Developments. Proc. Symp. Control of Fine Particulates and Industrial Sources, pp. 425-454. San Francisco, CA.

4. Carls, E. L. and N. M. Levitz, 1968. Blowback of Sintered-Metal Filters: A Review of Tests and Operating Experience. Reports ANL-7392, Chem. Engr. Div., Argonne Nat'l. Lab., Argonne, IL.

5. Sakguchi, H., 1972. High Temperature Bag Filter Dust Collector Devices. Fuel and Combustion (Japan) 39(5): 475-482.

6. Mandriko, A. S. and I. L. Peisakhov: The Use of Steel Gauze for Dust Cleaning of Gases in the Iron and Steel Industry. Steel (USSR) 1(12): 993.

7. Ostby, D. H. and J. H. Smith. High Temperature Air Filtration System and Method for Foundries. U. S. Patent No. 3,948,623, Apr. 6, 1976.

DRY DUST COLLECTION OF BLAST FURNACE EXHAUST GAS
BY MOVING GRANULAR BED FILTER

H. Kohama, K. Sasaki, S. Watanabe, K. Sato
Kobe Steel, Ltd.
Kobe, Japan

INTRODUCTION

Dust collection of blast furnace gas has been carried out by a wet dust collection system which uses the following equipment in series —— dust catcher, multi-cyclone, venturi scrubber, and wet electrostatic precipitator or venturi scrubber. This process loses unexpectedly large amounts of energy, because the sensible heat contained exhaust gas is taken away by scrubbing water owing to its direct contact with gas. For the purpose of minimizing this energy loss we propose a new dry dust collection system.
Our target is

1. effective utilization of sensible heat of blast furnace gas, and

2. no need for any waste water treatment facilities.

Our new dry system is composed of the following equipment —— dust catcher, multi-cyclone, and moving bed filter. The following report of our test demonstrates the feasibility of our new facilities.

TEST FACILITIES

As Photo 1 shows, a double staged moving bed filter was put to a test. Dusty gas is filtered at the moving granular bed layer which is made up between two sheets of wire screen and filled by 1.2 mm ~ 5 mm sized granular silica sand.

Filter media moves slowly downward between the two sheets of wire

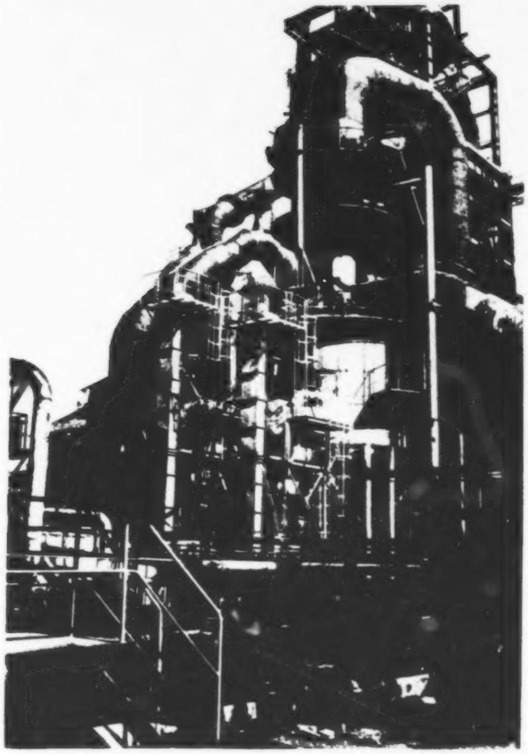

Photo 1. TEST FACILITIES

screen and is fed out by a rotating feeder which is equipped at the bottom of moving bed. After being free of collected dust in a vibrating screen, regenerated filter media is again fed at the top of the equipment. In this way filter media is circulated.

Moving bed filter shows far more stable performance than conventional dust collecting equipment even when blast furnace gas varies its temperature, volume, and dust concentration.

Specifications of test facilities are shown in Table 1. The gas tightness of our test facilities is paid special attention, because blast furnace gas contains about 20 % of carbon monoxide.

PROCESS OF TEST

Flow sheet of test equipment is shown in Fig. 1. The dust collection efficiency as well as pressure drop through filter media depend on dust load (weight ratio of collected dust to filter media amount), filtration velocity, and granular size of media.
Consequently in our test the effect of filtration velocity and granular size on dust collection efficiency is first evaluated at a single stage moving bed. Then the effect of dust load and filtration velocity on dust collection efficiency and pressure drop is investigated in a double stage moving bed. Finally necessary requirements to keep the dust concentration at the equipment outlet at the desired value are pursued and considered.

Table I. SPECIFICATIONS OF TEST FACILITIES

	FIRST STAGE	SECOND STAGE
NO. OF THE LAYER OF GRANULE	1	1
FILTRATION AREA	0.5 m^2	1 m^2
LAYER THICKNESS	200 mm	200 mm
GRANULAR SIZE	1.2 ~ 5 mm	1.2 ~ 2.5 mm
GAS CAPACITY	MAX. 1080 m^3 / hr	MAX. 1080 m^3 / hr
MOVING VELOCITY OF FILTER MEDIA	8 ~ 50 cm / hr	7 ~ 55 cm / hr

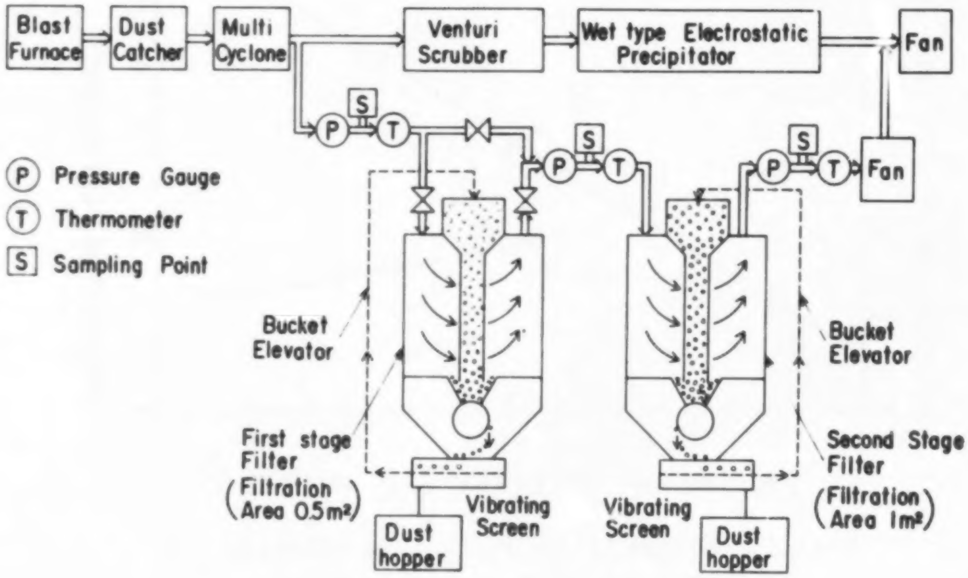
Blast Furnace
Dust Catcher
Multi Cyclone
Venturi Scrubber
Wet type Electrostatic Precipitator
Fan
S
P
T
S
P
T
S
P
T
Fan
P Pressure Gauge
T Thermometer
S Sampling Point
Bucket Elevator
First stage Filter
(Filtration Area 0.5m²)
Vibrating Screen
Dust hopper
Vibrating Screen
Dust hopper
Bucket Elevator
Second Stage Filter
(Filtration Area 1m²)

Fig 1. Flow sheet of test equipment

TEST RESULTS

The effect of filtration velocity on dust collection efficiency and pressure drop.

Fig. 2 shows the test results. Pressure drop becomes larger very quickly as the filtration velocity increases. At the velocity of 0.3 m/sec, ΔP shows about twice more than at 0.1 m/sec. Very similar results are seen in spite of the variation of dust load. Dust collection efficiency becomes a little smaller at higher filtration velocity.

The fact of lower dust collection efficiency in spite of a higher pressure drop is presumably explained by the process that some turbulence which occurs in dust layer on the surface of filter media causes pin-hole leak and makes lower dust collection efficiency.

The relation between pressure drop and filtration velocity can be expressed as follows.

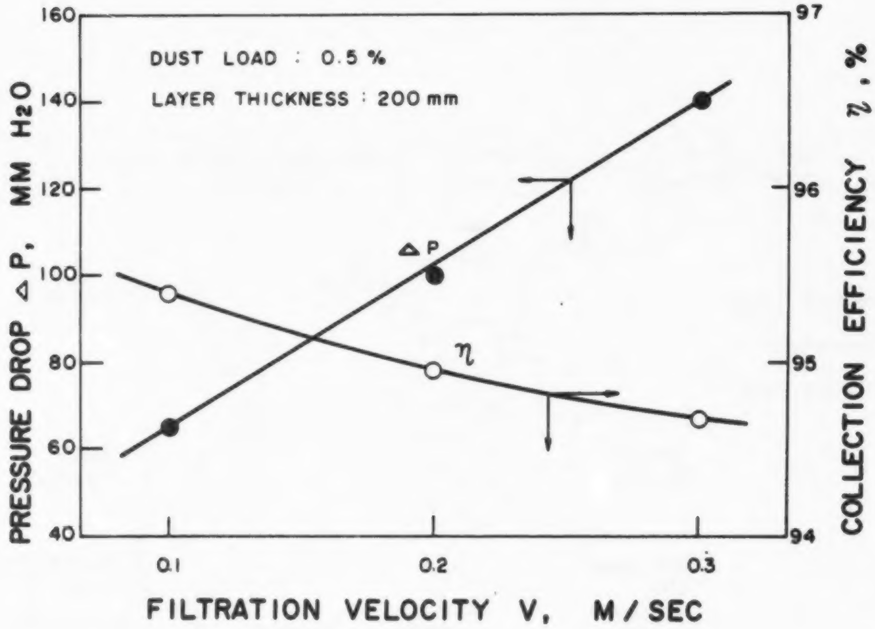

Fig. 2. Effect of filtration velocity on pressure drop and collection efficiency.

$\Delta P = 325\ V^{0.7}$ ΔP in mm H_2O
V in m/sec

During start-up pressure drop is made up by only that of filter media, because there is almost no dust deposit.

Pressure drop during start-up $\Delta P \propto V^{1.3 \sim 1.4}$

When some dust is deposited on filter media as well as on wire screens, pressure drop is shown as follows.

Pressure drop after dust deposition $\Delta P \propto V^{1.0 \sim 0.7}$

The effect of granular size of filter media on pressure drop and dust collection efficiency

Fig. 3 shows the effect of granular size. The smaller the granular size is, the bigger is the pressure drop. The dust collection efficiency increases at the same time.

This result comes from the fact that specific area of filter media per unit volume increases with the smaller size of granule and also dust deposition as well as bridging becomes easier.

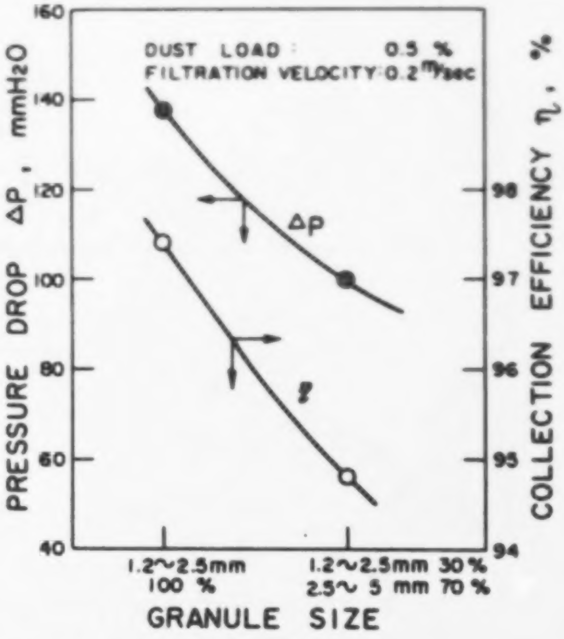

Fig. 3. Effect of granule size on pressure drop and collection efficiency.

The effect of dust load on pressure drop and dust collection efficiency.

Fig. 4 shows above effect on pressure drop. Pressure drop becomes higher with dust load increase in spite of the variation in filtration velocity. In a range where dust load is over 3 %, ΔP-increase shows very gentle one. Pressure drop depends more on filtration velocity than on dust load.

Fig. 5 shows the effect of dust load on collection efficiency. Dust collection efficiency becomes higher with the increase of dust load. But there will be the highest point in efficiency when pin-hole leak at the higher velocity range is taken into consideration.

Dust collection efficiency amounts to 99 % at 0.2 m/sec of filtration velocity and 5.5 % of dust load. Pressure drop of above example amounts to 140 mm H_2O.

Based upon above results, the best selection of a moving bed

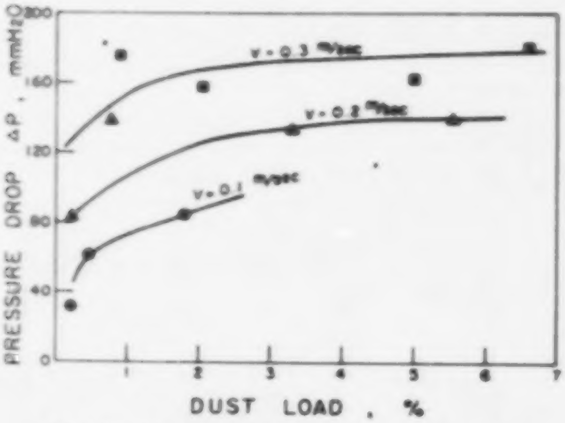

Fig. 4 Effect of dust load on pressure drop.

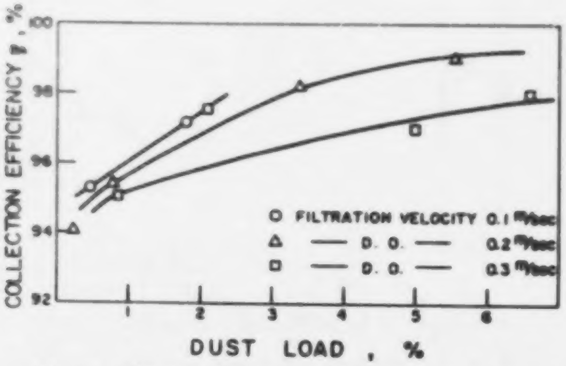

Fig. 5. Effect of dust load on collection efficiency.

filter running condition lies in finding a suitable dust load, after keeping the economically lowest possible filtration velocity and adopting rather smaller sized granule.

The effect of dust load and filtration velocity at double stage dust collection.

Based upon the test results at single stage filter, 0.2 m/sec, 0.3 m/sec filtration velocity and 1.2 mm ~ 5 mm granular size are selected as a running condition of the first stage. 0.1 m/sec, 0.15 m/sec filtration velocity and 1.2 mm ~ 2.5 mm granular size are selected as a running condition of the second stage.

Figs. 6 & 7 show the effect of dust load and filtration velocity on dust collection efficiency. Efficiency becomes higher with the dust load increase in the first as well as in the second stage. At the first stage dust collection efficiency shows lower one with higher velocity. At the second stage filtration velocity has no influence on collection efficiency.

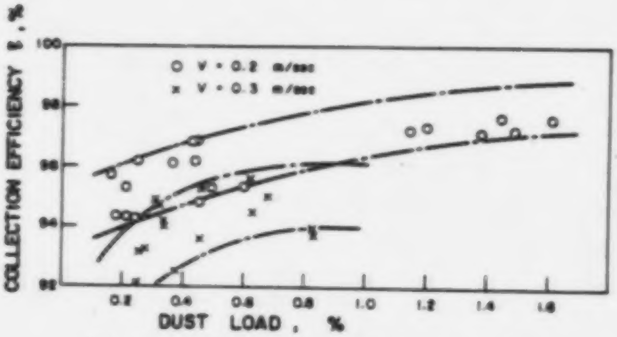

Fig. 6. Effect of dust load and filtration velocity on collection efficiency at the first stage.

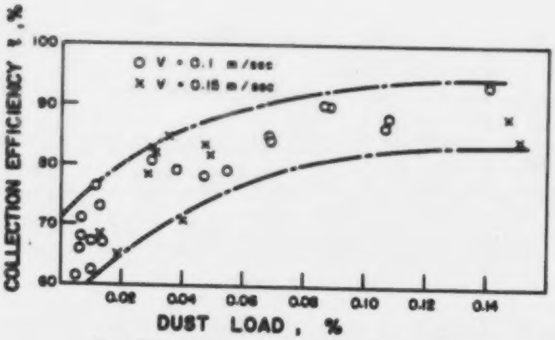

Fig. 7. Effect of dust load and filtration velocity on collection efficiency at the second stage.

This result can be explained as follows. Pin-hole leak makes lower the efficiency at the first stage. Dust load at the second stage is very low, because the amount of dust is low and sticking of dust on filter media is also very low. In the lowest range of dust load of second stage dust collection efficiency becomes higher with the dust load increase. We presume that deposited dust increase on filter media catches smaller dust by bridging.

Figs. 8 & 9 show the effect of dust load and filtration velocity on pressure drop. At the first stage pressure drop becomes higher with the increase of dust load. The increasing rate of pressure drop shows steeper climb at the higher velocity range. At the second stage there is no effect of dust load. At the velocity of 0.1 m/sec,ΔP shows 20 ~ 40 mm H_2O, and at 0.15 m/sec,ΔP shows 50 ~ 70 mm H_2O.

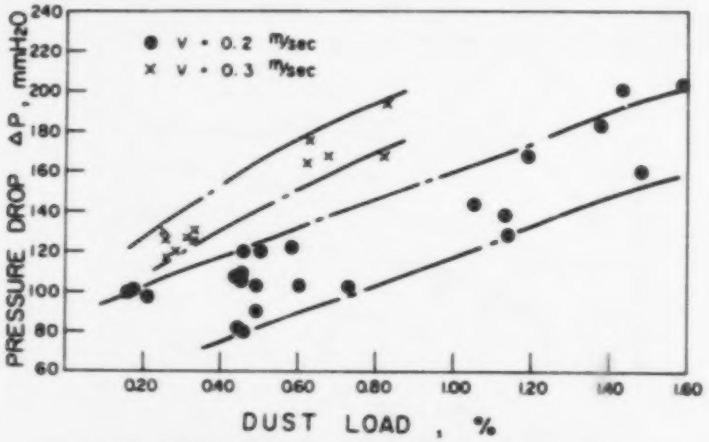

Fig. 8. Effect of dust load and filtration velocity on pressure drop at the first stage.

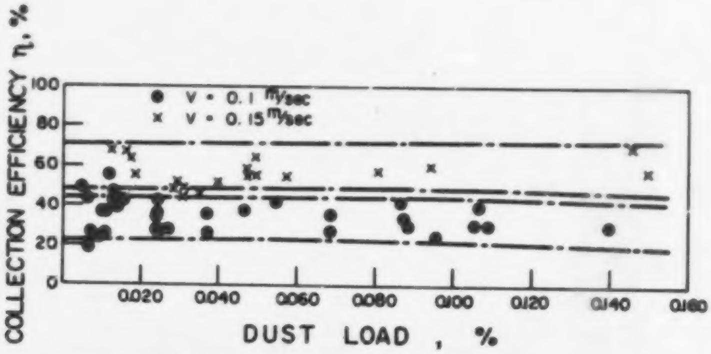

Fig. 9. Effect of dust load and filtration velocity on pressure drop at the second stage.

Moving bed filter compared to wet dust collectors

Table 2. shows the dust concentration at the outlet of conventional venturi scrubber and electrostatic precipitator compared to those of our test facilities.

This table shows that our test facilities can show better results than the conventional ones when our new facilities are put to run with filtration velocity 0.2 m/sec at the first stage, 0.1 m/sec at the second stage.

Table 2. MOVING BED FILTER COMPARED TO WET DUST COLLECTORS.

	VENTURI SCRUBBER + Wet E.P.	MOVING GRANULAR BED FILTER				
	OUTLET DUST CONCENTRATION	OUTLET DUST CONCENTRATION	FILTRATION VELOCITY		MOVING VELOCITY OF GRANULAR MEDIA	
			FIRST STAGE	SECOND STAGE	FIRST STAGE	SECOND STAGE
1	8 mg/Nm^3	19 mg/Nm^3	0.3 m/sec	0.15 m/sec	50 cm/hr	16 cm/hr
2	5	10	0.3	0.15	50	16
3	11	7	0.2	0.1	50	7
4	8	7	0.2	0.1	50	7
5	25	25	0.2	0.1	8	7
6	20	12	0.2	0.1	8	7

CONCLUSION

1. To attain the required dust concentration (0.01 gr/Nm^3) at the moving bed filter outlet, overall dust collection efficiency must be kept at about 99.5 %.
   For this specific purpose the dust collection efficiency must be kept at 97 % in the first stage and at 85 % in the second stage.
   When we keep 0.2 m/sec filtration velocity and dust load higher than 0.1 % at the first stage and 0.10 ~ 0.15 m/sec filtration velocity and dust load higher than 0.08 % at the second stage, above required efficiency can be attained by our equipment.

2. Above result of our new equipment is better than the performances of conventional venturi scrubber and wet electrostatic precipitator.

3. Test was applied to normal pressure blast furnaces.
Future test will be applied to higher pressure blast furnaces.

ACKNOWLEDGEMENTS

We would like to express our appreciation to Dr. Iinoya of Kyoto university for his advice and encouragement throughout this test, and acknowledge the permission given by Kobe Steel, Ltd. to publish this investigation.

CERAMIC FILTER, SCRUBBER, AND ESP

Robert A. Clyde
Clyde Engineering Service
Box 430820
S. Miami, Florida 33143
Tel. (305)661-1777

ABSTRACT

Polyurethane foam can be easily cut in several different shapes and then converted to ceramic the same shape which can be used as a high temperature (3000°F), corrosion resistant filter, scrubber, and possibly electrostatic precipitator collector. A catalyst support and heat exchanger is also described.

Shaping of plastic foam is done in three principle ways. Feeding a sheet horizontally into a knife with rollers on the top and bottom pushing the plastic up or down results in a wave form as shown in Fig. 1 and 8 or the egg crate form of Fig. 9. Machinery for stamping holes is similar to that used for making plastic hair curlers. Tapered holes can be burned out and an electrically heated wire will cut as in Fig. 3 and 6.

After being shaped, the plastic foam is dipped into a ceramic slurry, the plastic is burned out, and a ceramic sponge the same shape as the plastic is formed. Several different types of ceramic with different thermal shock and expansion values can be used. The sponge is made at Alfred University, Alfred, N.Y. 14802 by Messrs. William Crandall and Jeffrey Morris. If caustic is used in a scrubber nickel can be plated on the ceramic as per Mr. Clyde's patent 3,900,646. The advantage of vapor deposition is that it goes on pore free so caustic cannot attack the ceramic.

CERAMIC FILTER, SCRUBBER, AND ESP

Robert Clyde, Clyde Engineering

The ceramic sponge (10 to 80 pores per linear inch) can be used as the filter, or, if smaller particles must be retained, the sponge can hold another finer filter such as ceramic, cloth, fiber glass, etc. and provide a means of by-pass around the finer filter so excessive pressure drop is not incurred as in Fig. 6,8, and 9. The tapered holes in Fig. 4, 8, and 9 act as a Venturi to speed up the particles and facilitate impingement on the filter.

Fig. 1 shows the wave form sponge. The X's represent open spaces. When used as a scrubber, gases go horizontally and liquid drips down through the open spaces as shown in Fig. 2, an enlarged view.

Wires can be put through the open spaces of Fig. 1 where X's are and an electrostatic precipitator with a large area (10 sq. ft. per gram of sponge) collector plate provided. It could be mounted on a rotary drum with particulate pulsed or washed off at the bottom. Perovskite is a ceramic that can be grounded electrically.

Fig. 3 can also be used as a scrubber. The holes, item 31 are to accomodate a viscous material such as molten glass which can remove coal particulates before going to a turbine. The gas goes horizontally back and forth up the column.

Fig. 5 can be mounted on a rotary drum and be cleaned at the bottom by pulse jets or acid.

Fig. 6 can remove Diesel particulates.

Fig. 7 has coarse holes on the left and progressively finer holes as the gas goes from left to right.

Fig.8 and 9 have tapered holes so the gas is accelerated before going into an open space and then impingement on the filter.

Fig. 10 would make an effective auto catalytic converter or NO_x reducer for boilers. The corkscrew passageway reduces pressure drop while maintaining turbulence. Mr. Clyde's patents 3,900,646 and 3,998,758 describe methods for plating catalytic metals on sponges. As a precombustion catalyst, the sponge does an effective job of mixing fuel and air.

A high temperature heat exchanger as shown in Fig. 11 can be used to cool gases before they contact a heat sensitive filter. Silicon carbide conducts heat better than ceramic.

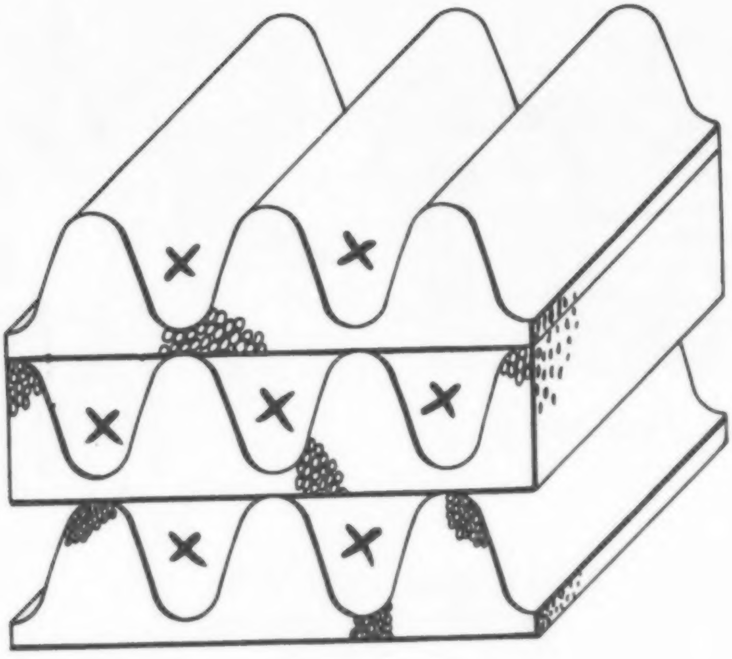

FIG. 1

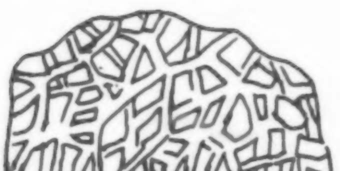

FIG. 2

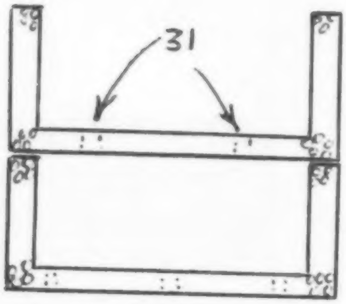

FIG. 3

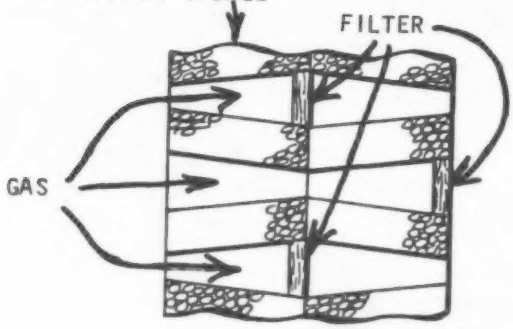
CERAMIC SPONGE
FILTER
GAS

FIG. 4

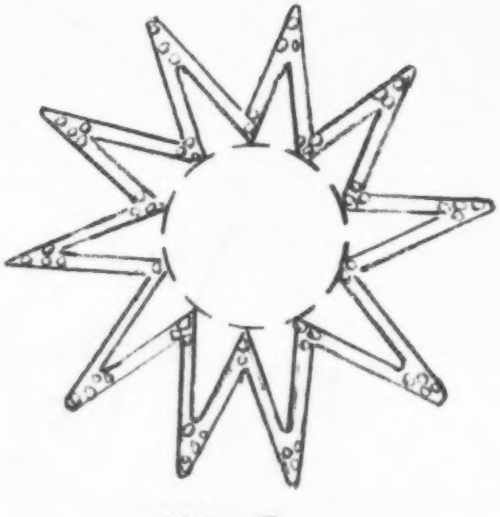

FIG 5

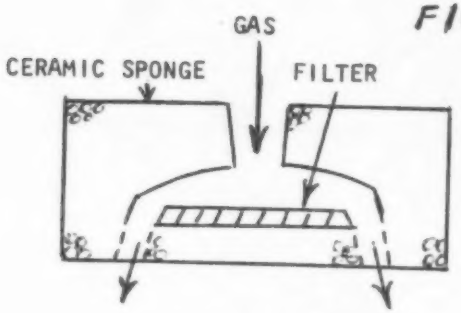
GAS
CERAMIC SPONGE
FILTER

FIG. 6

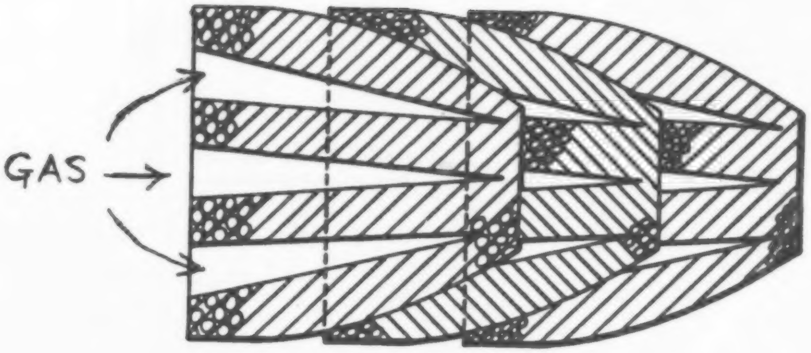

FIG. 7

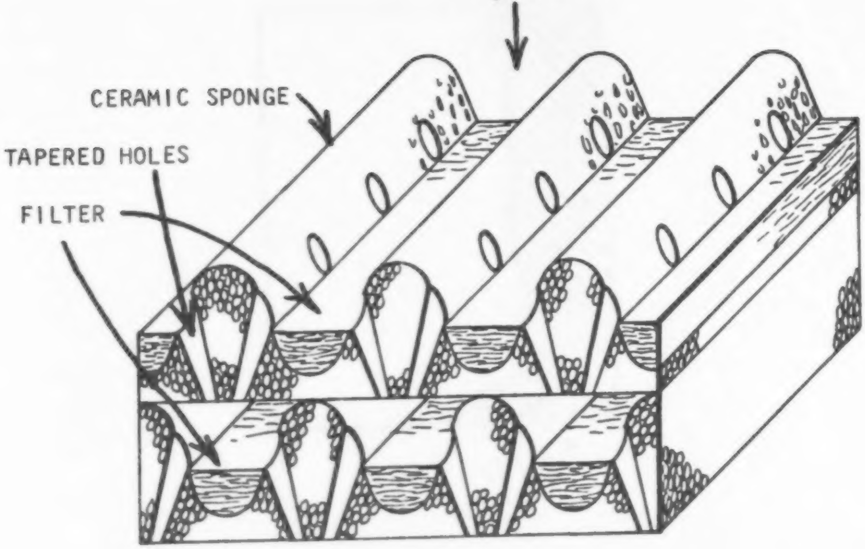
GAS
CERAMIC SPONGE
TAPERED HOLES
FILTER

FIG. 8

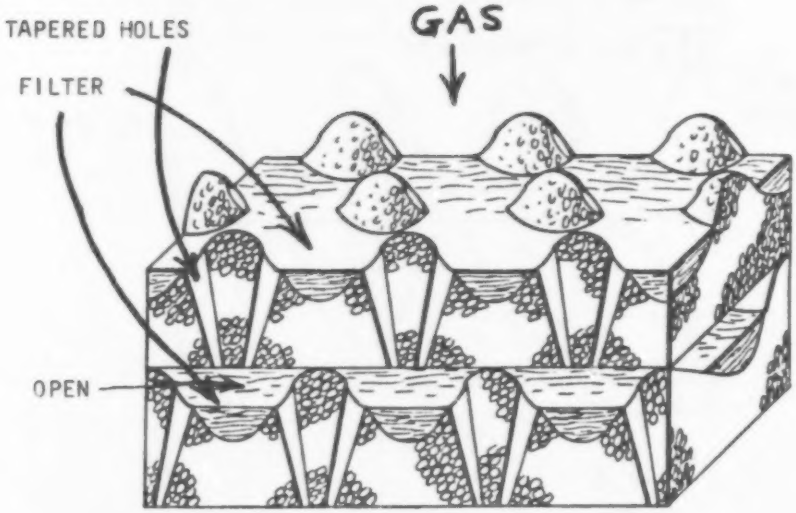
GAS
TAPERED HOLES
FILTER
OPEN

FIG. 9

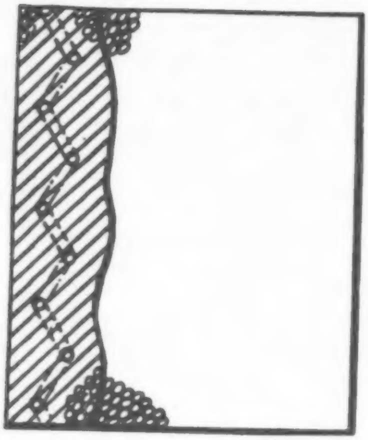

FIG. 10

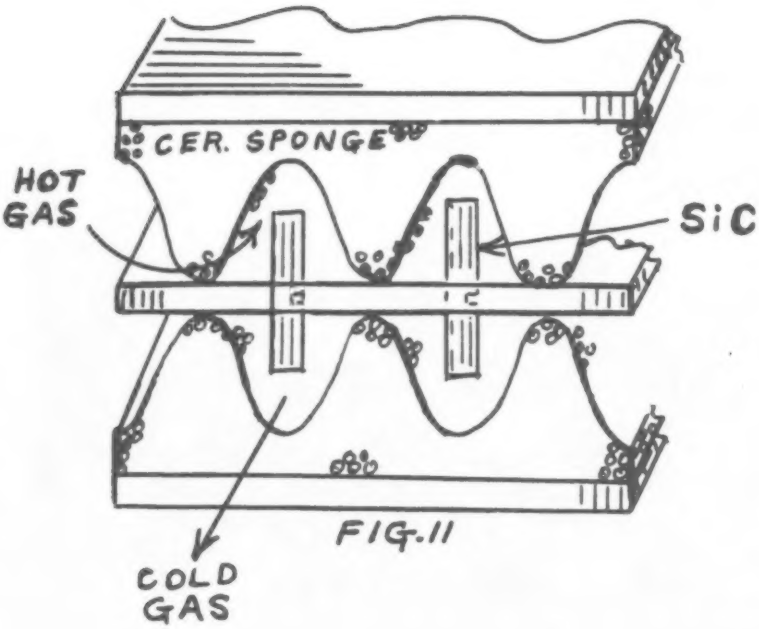

CER. SPONGE
HOT GAS
SiC
COLD GAS

FIG. 11

FUNDAMENTAL PARTICLE COLLECTION AT HIGH TEMPERATURE AND PRESSURE

R. Parker and S. Calvert
Air Pollution Technology, Inc.
San Diego, California

D. Drehmel
U.S. Environmental Protection Agency
Industrial Environmental Research Laboratory
Research Triangle Park, North Carolina

INTRODUCTION

When designing, troubleshooting, or evaluating the performance of particulate control equipment, it is important to have a firm understanding of the physical mechanisms by which the particles are removed from the gas stream. This is especially true when the control device is to be used at high temperature and pressure (HTP) conditions where current design models are unproven. In order to provide a rational basis for dealing with HTP particulate control equipment, a sound theoretical understanding of the HTP effects on particle collection mechanisms is essential.

We have made a thorough examination of the literature concerned with HTP effects on particle collection.[1] Although HTP particle collection has been of interest for over 30 years no fundamental evaluation of the theory has been attempted. In general, conventional models for particle collection (valid at low temperatures and pressures) have been extrapolated to predict performance in HTP situtations. Insufficient performance data are available to evaluate these models at HTP conditions, especially as a function of particle size.

This paper focuses on particle collection by the mechanism of inertial impaction. Theoretical uncertainties are reviewed and preliminary experimental data are presented.

THEORY

Stokes' Law

The major difference between the collection of particles at normal conditions and at high temperature and pressure is in the resistance force of the gas. For a rigid spherical particle moving through a continuous viscous gas at constant relative velocity, and for negligible inertial effects arising from the gas being displaced by the particle, the resistance force, F_r, is given by Stokes' Law:

$$F_r = - 3\pi \mu_G d_p u_r \qquad (1)$$

where μ_G is the gas viscosity, d_p is the particle diameter, and u_r is the relative velocity between the particle and the gas. The negative sign indicates that the drag force is opposite to the direction of motion of the particle.

Equation (1) must be modified for non-continuum effects when the mean free path of the gas molecules becomes significant in comparison with the particle diameter. The modified Stokes' Law becomes:

$$F_r = \frac{-3\pi \mu_G d_p u_r}{C'} \qquad (2)$$

The correction factor, C', is often referred to as the "Cunningham slip correction factor" because of the pioneering work of Cunningham.[2] The slip correction factor will be discussed in more detail later in this paper.

Equations (1) and (2) are strictly valid only for very small Reynolds numbers, N_{Re}. That is, in general,

$$N_{Re} = \frac{d_p u_r \rho_G}{\mu_G} < 1 \qquad (3)$$

where ρ_G is the gas density.

For larger N_{Re}, the drag force may be calculated as:

$$F_r = -C_D \left(\frac{\pi d_p^2 \mu_G u_r^2}{8 C'} \right) \qquad (4)$$

where C_D is the drag coefficient. The drag coefficient is shown as a function of N_{Re} in Figure 1.

Particle Reynolds numbers will increase at high pressures and will decrease at high temperatures for a given gas velocity. For example, consider a gas velocity of 10 m/s. This is representative of velocities in inertial sizing instruments such as cascade impactors. The particle Reynolds number is shown as a function of particle diameter, temperature and pressure in Figure 2. It is clear that particle Reynolds numbers greater than unity can occur at high pressures even for submicron particles.

Inertial Impaction

One of the most important mechanisms for the collection of particles larger than a few tenths of a micrometer in diameter is inertial impaction. Inertial impaction takes advantage of the particles' inertia by impinging the particles and gas against a target. Large particles impact on the target while the fine particles and gas are diverted around it.

The dimensionless parameter which characterizes the extent to which particles are removed by inertial impaction is termed the inertial impaction parameter, K_p. It is equivalent to the ratio of the particle stopping distance to the characteristic dimension of the collector.

For any particle Reynolds number, the inertial impaction parameter may be written in the form,

$$K_p = \frac{8\, d_p\, \rho_p\, C'}{3\, \rho_G\, d_c}\, f(N_{Re}) \qquad (5)$$

where d_c is any characteristic length.

The function $f(N_{Re})$ is proportional to the particle stopping distance, ℓ_i. It has been determined graphically and is presented in Figure 3.

For low Reynolds numbers,

$$f(N_{Re}) = 0.0417\, N_{Re} \qquad (6)$$

and,

$$K_p = \frac{d_p^{\,2}\rho_p\, C'\, u_r}{9\, \mu_G\, d_c} \qquad (7)$$

Slip Correction Factor

One of the major uncertainties in the use of equation (2) at high temperatures and pressures is in the Cunningham slip correction factor, C', used to modify Stokes' Law. It is an empirical factor generally based on the data of Millikan[3,4] and is given by Davies[5] as:

$$C' = 1 + N_{Kn}\, [1.257 + 0.400 \exp(-1.10/N_{Kn})] \qquad (8)$$

where N_{Kn} is the Knudsen number, defined by:

$$N_{Kn} = \frac{2\lambda}{d_p} \tag{9}$$

where λ is the mean free path of the gas molecules.

The constants in equation (8) are based on experimental data for Knudsen numbers from zero to greater than 100. The experiments were at low pressure (about 0.003 atm) and room temperature (20°C to 25°C). Therefore consideration must be given to their applicability at high temperatures and pressures.

Equation (8) may be written in the general form:

$$C' = 1 + N_{Kn} \left| A + B \exp\left(-c/N_{Kn}\right) \right| \tag{10}$$

The constants A,B, and c are empirical and thought to be a function of the momentun transfer between gas molecules and the particle.

It is the object of our experimental program to determine if equation (8) is valid at high temperatures and pressures. From the theoretical and experimental studies of the momentum accommodation coefficient (reviewed by Calvert and Parker[1]), we expect C' to be somewhat larger at higher temperatures.

EXPERIMENTAL PROGRAM

Test Facility

An experimental program to study fundamental particle collection mechanisms at high temperature and pressure is underway at A.P.T., Inc. under EPA sponsorship. The experiments will investigate the collection mechanisms of inertial impaction, Brownian diffusion, and electrical migration at temperatures up to 1,100°C and pressures up to 15 atm. Particles in the general size range of 0.5 to 10 μm are being considered.

A special high temperature and pressure test facility has been designed and constructed. This facility was described previously by Parker, et al.[6]

Inertial Impaction Tests

High temperature and pressure nitrogen loaded with fly ash is passed through a specially designed inertial impaction test section. The test section is illustrated in Figure 4. It is essentially a single stage impactor placed between two flanges. Five separate jet plates are available so that we can observe cut diameters ranging from 0.5 to 10 μm

Particles are collected on a ceramic fiber substrate which is used to minimize particle bounce at the impaction plate. The substrate is removed and weighed after each test in order to complete the mass balance of particles and to check the overall efficiency determined from the inlet and outlet samples.

Isokinetic samples are taken at the inlet and outlet of the test section. The samples are collected on filters which can be washed and analyzed for particles.

The filter samples are removed after each test and are analyzed using an electronic particle counter (Coulter Counter Model TA-11) to determine the mass and size distribution of the fly ash collected on each filter. Also the sample probes are cleaned after each test and analyzed to determine the amount and size of particles deposited in each probe.

The data obtained from analysis of the inlet and outlet samples are used to determine an experimental penetration curve. The penetration curve is used to determine an experimental cut diameter. Experiments can be run at temperatures ranging up to 1,100°C and pressures up to 15 atm.

The theory presented above can be used to determine an experimental value for the slip correction factor. That is:

$$C' \text{ (expt.)} = \frac{3\, K_{p50}\, \rho_G\, d_h}{8\, d_{p50}\, \rho_p\, f} \qquad (11)$$

where K_{p50} = calibrated value for K_p at 50% collection efficiency
ρ_G = gas density, g/cm^3
d_h = jet diameter, cm
d_{p50} = experimental cut diameter, cm
ρ_p = particle density, g/cm^3
f = function of N_{Re} (Figure 3), dimensionless

The average particle density has been determined by comparing the calibrated cut diameter with the cut diameter measured using fly ash at standard temperature and pressure. K_{p50} is determined experimentally in the laboratory and is assumed to be independent of temperature and pressure.

RESULTS AND CONCLUSIONS.

Some preliminary results are presented in Table 1. The theoretical predictions in the last column were obtained using equations (8) and (9).

Agreement between experiment and theory is quite good for the lower pressure tests, considering the experimental difficulties. The high pressure tests do not agree with theory and this most likely is a result of experimental errors.

Much more data are required before any definite conclusions can be made. However, preliminary data do not indicate that any substantial errors will be encountered if conventional impaction theory is used to predict performance for high temperature applications.

Table 1. EXPERIMENTAL RESULTS

Run #	Temperature, °C	Pressure, atm	Reynolds Number	Cut Diameter, μm	C' Experiment	C' Theory
30-12	26	1.40	2.65	1.08	1.11	1.11
30-6	27	1.41	2.81	1.16	0.994	1.10
31-6	106	1.31	1.66	1.11	1.22	1.15
31-25	202	1.34	1.27	1.21	1.19	1.18
30-11	699	1.11	0.334	1.26	1.61	1.49
30-13	816	1.10	0.294	1.32	1.56	1.53
31-1	106	4.08	8.12	1.45	0.891	1.03
31-2	100	9.84	10.37	1.32	1.32	1.02
31-4	103	5.08	5.18	0.92	2.10	1.05

REFERENCES

1. Calvert, S. and R.D. Parker. Effects of Temperature and Pressure on Particle Collection Mechanisms: Theoretical Review. Air Pollution Technology, Inc., EPA-600/7-77-002, NTIS PB 264-203. January 1977.

2. Cunningham, E. Proc. Roy Soc. (London), A83: 357, 1910.

3. Millikan, R.A. Coefficients of Slip in Gases and the Law of Reflection of Molecules from the Surfaces of Solids and Liquids. Phys. Rev. 21: 3: 217, 1923.

4. Millikan, R.A. The General Law of Fall of a Small Spherical Body Through a Gas, and Its Bearing upon the Nature of Molecular Reflection from Surfaces. Phys. Rev. 22 1: 1, 1923.

5. Davies, C.N. Definitive Equations for the Fluid Resistance of Spheres. Proc. Phys. Soc. 57 (4): 18, July 1945.

6. Parker, R.D., S. Calvert and D.C. Drehmel. High Temperature and Pressure Effects on Particle Collection Mechanisms. In: Proceedings of the EPA/DOE Symposium on High Temperature/High Pressure Particulate Control. Washington, D.C., September 20-22, 1977. EPA 600/9-78-004. CONF-770970.

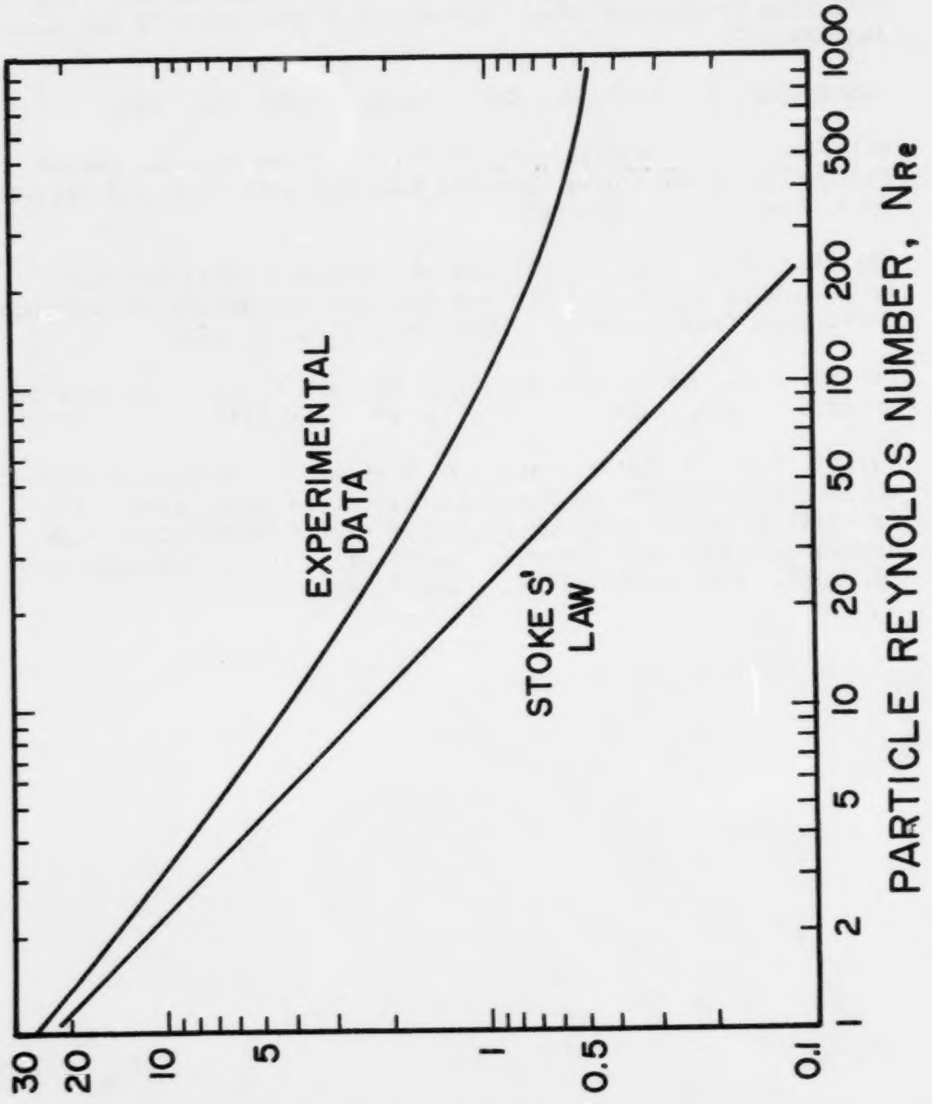

FIGURE I. DRAG COEFFICIENTS

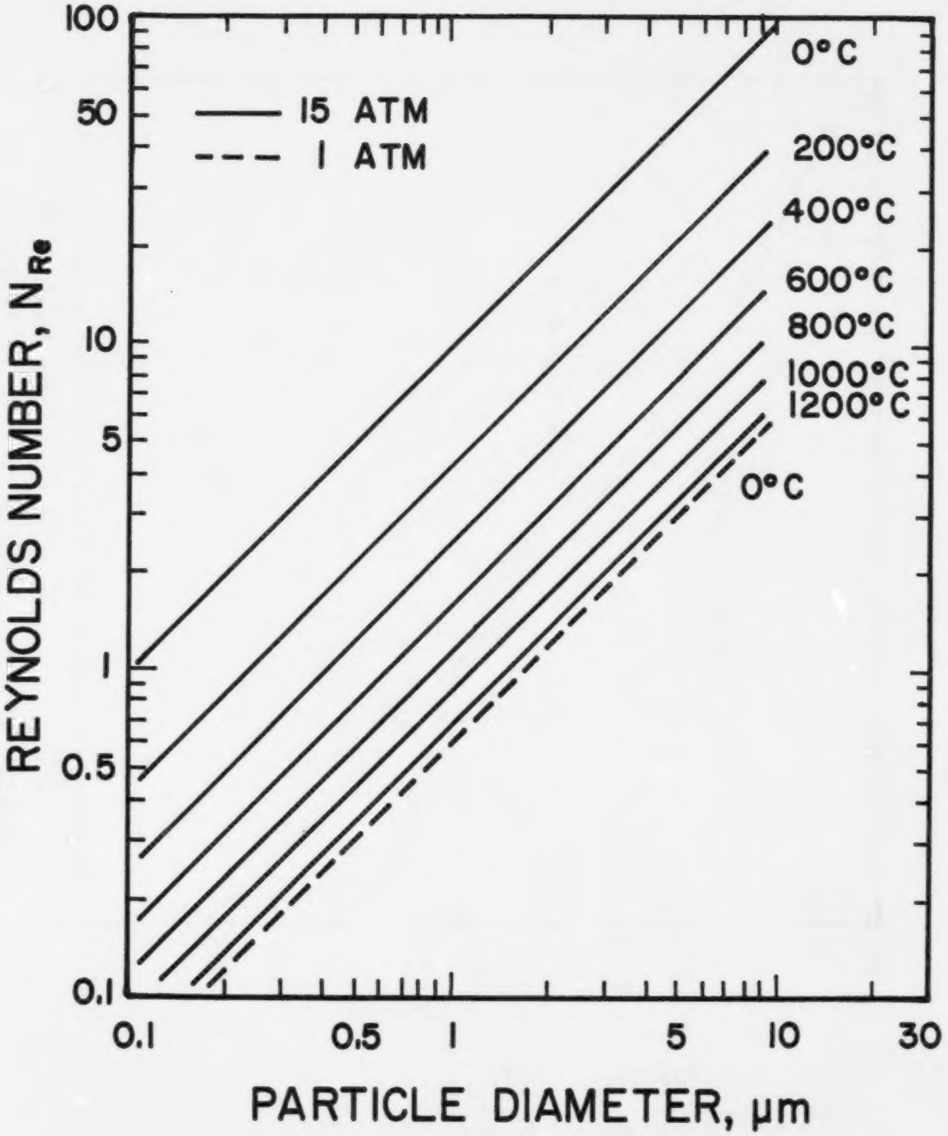

FIGURE 2. PARTICLE REYNOLDS NUMBER

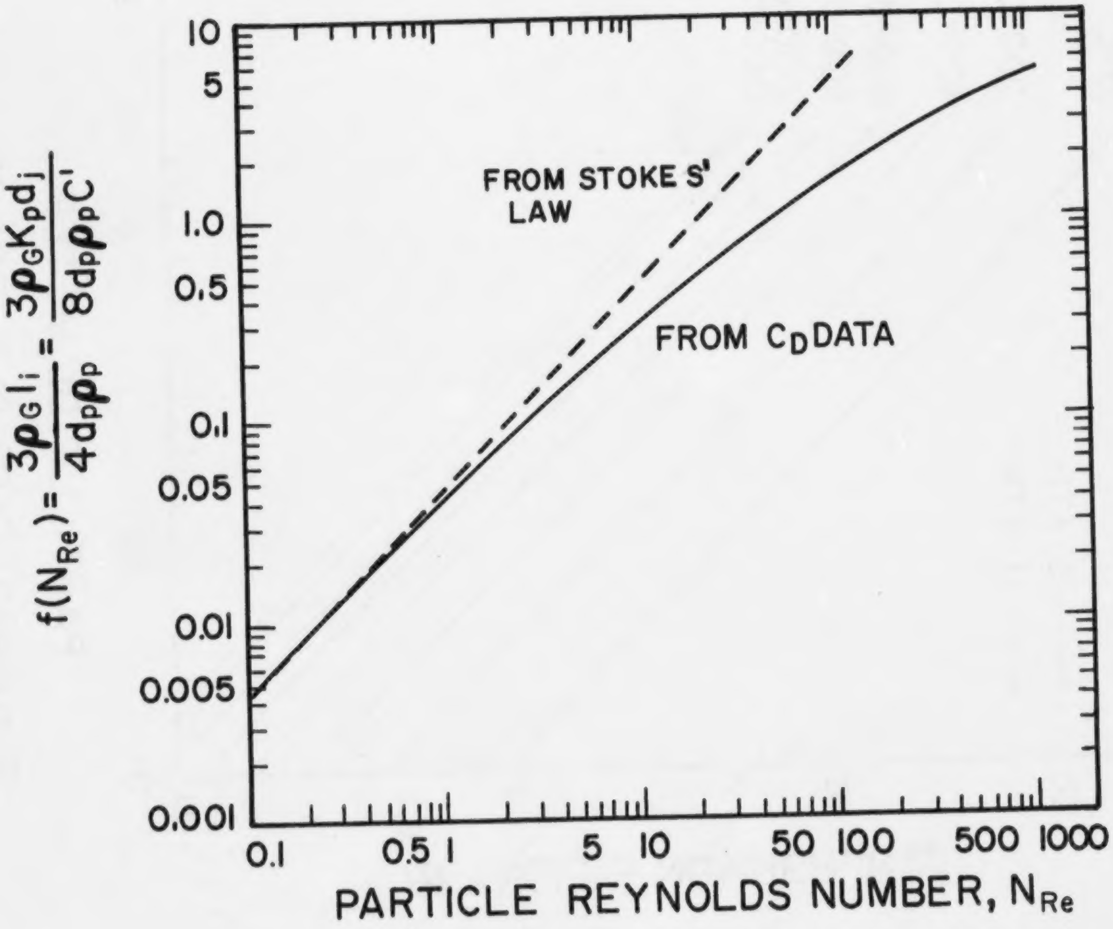

FIGURE 3. PARTICLE STOPPING DISTANCE

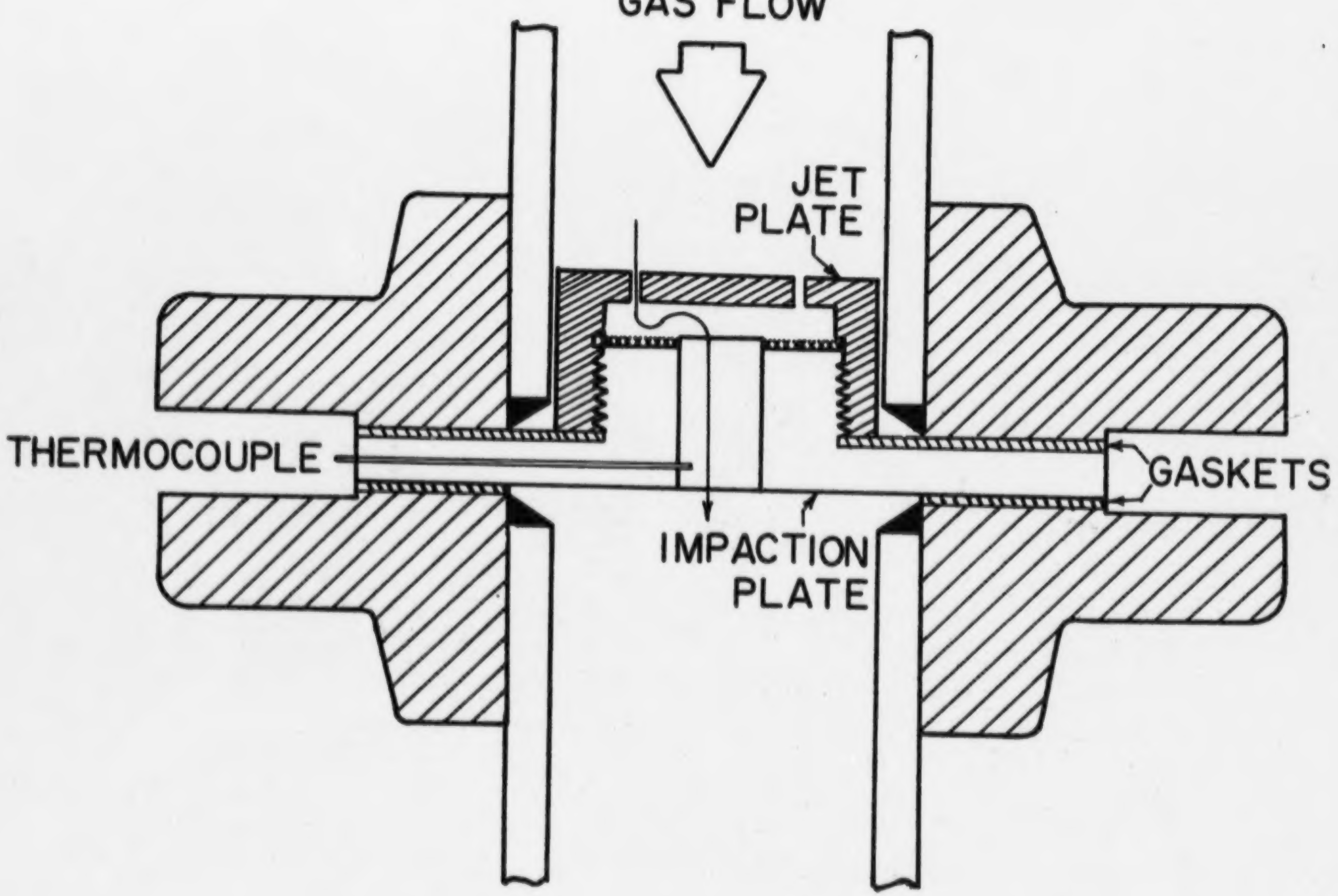
GAS FLOW
JET PLATE
THERMOCOUPLE
GASKETS
IMPACTION PLATE

FIGURE 4. IMPACTION TEST SECTION

PARTICULATE CONTROL FOR FLUIDIZED BED COMBUSTION

David F. Becker
Michael G. Klett
Gilbert Associates, Inc.

INTRODUCTION

The U.S. Department of Energy is sponsoring development of fluidized-bed combustion (FBC) technology as a promising alternative for utilization of our abundant domestic coal resources in an environmentally acceptable manner. Development of fluidized-bed combustion of coal has been underway since the early sixties in this country and in England. The original intent of the program was to reduce the size of a coal-fired boiler to make it competitive with oil and gas-fired boilers. With the advent of the Clean Air Act in 1970, increased interest was generated in FBC because of its ability to remove the coal sulfur in-situ. Continuing development efforts have produced a 30 MW_e atmospheric fluidized-bed combustion (AFBC) system currently undergoing testing at Rivesville, West Virginia and 13 MW_e and 20 MW_e pressurized fluidized-bed combustion (PFBC) systems scheduled for construction starting this year.

PARTICULATE EMISSIONS FROM FBC

Fluidized-bed combustion operates on the principal of intimate mixing of coal and a sulfur-absorbing additive in a turbulent, well-mixed bed "fluidized" by the combustion air. In the process of controlling gaseous SO_2 emissions, the particulate emissions problem is aggrevated. Particulate emissions occur as a result of elutriation of materials from the fluidized-bed. Essentially all particles below a critical size will elutriate from the bed, with this critical value increasing with increasing superficial velocity. Fine particles elutriated from the bed can originate in the coal and sorbent feed

Preceding page blank

streams, can result from attrition of the particles in the bed, or, in the case of the sorbent, can result from decrepitation of the particle during calcination and/or sulfation.

Atmospheric Fluidized Bed Combustion

Mass Loadings -

Mass loadings reported from the primary combustor of an atmospheric fluidized-bed combustion system vary over a wide range depending on bed design, feed characteristics, and operating conditions. Unfortunately, insufficient data are available over the range of design, feed, and operating conditions to correlate particulate emissions with these parameters with any precision.

The range of particulate loadings which have been measured from various sized AFB primary combustors is shown in Table 1. Also shown are the particulate loadings after the primary cyclone collector. The limited data show no clear trend for particulate loadings as a function of bed size. The particulate loadings from the primary combustor generally range from 20-70 lb/10^6 BTU, while these from the primary cyclone are in the neighborhood of 1-10 lb/10^6 BTU. Measured mass loadings from simulated Carbon Burnup Cell (CBC) runs indicate a mass loading from the combustor of 40-80 lb/10^6 BTU and from the cyclone collector of 1-20 lb/10^6 BTU[1,2].

The variation in dust loadings for a given superficial velocity can be considerable, due to the different decrepitation rates of limestones/dolomites in fluidized-bed combustors. Unfortunately, sorbent decrepitation rates cannot, at the present time, be predicted from any simple quantitative analysis. It appears that some sorbents are simply unsuitable for use in FBC because of their excessive decrepitation characteristics. This is one of the problems with particulate control inherent to fluidized-bed combustors which is not shared by conventional coal-fired boilers.

Size Distribution -

Of importance to specification of the final particulate cleanup device in an AFBC system is the size distribution of particulates in the flue gas stream leaving the primary cyclone. Figure 1 is a summary of the available size distribution data for this gas stream, as well as the gas stream leaving the CBC cyclone collector. The large variation in weight percent of material less than 3 μm for the primary cyclone should be noted, as well as, the limited data for the CBC cyclone. It is this material, of course, which is most difficult to remove in the final particulate collection device.

Chemical Characteristics -

Also of importance to the design of the final particulate control device is the chemical composition of AFBC particulate. In general, the variation in mass loadings is reflected in the variation in chemical composition of AFBC particulate. General trends are that the larger particles collected in the primary cyclone are higher in combustible material (15-50% vs 1-20%), higher in uncalcined material (2-20% vs 1-10%), and lower in products of reaction (1-5% vs 2-10%) than is the material which passes through the cyclones[3,4]. Some data exists on the composition of AFBC particulate based on infrared spectrometric techniques and is presented in Table 2[5]. The data indicates that glass, lime, and quartz are the major components which pass through the primary collector. $Ca(OH)_2$ and $CaCO_3$ are virtually absent and $CaSO_4$ is present in amounts from about 2-12% by weight. Pope, Evans, and Robbins has analyzed the particulate emitted from a simulated Carbon Burnup Cell and found that both the particulate collected in the CBC cyclone and the particulate passing through the cyclone contained 10-20% carbon by weight[2].

Electrical Characteristics -

Another area of importance with respect to collection of AFBC particulate is the electrical properties of the material since these are of critical importance to the operation of an electrostatic precipitator. The resistivity of this material should be in the range of 10^{+7} to 5 X 10^{+10} ohm-cm for good collection. For AFBC it has been found that:

1. Low SO_3 levels ($\sim$5 ppm) exist in AFB products of combustion. Almost all of the sulfur not absorbed is emitted as SO_2.
2. The additive materials ($CaCO_3$, CaO, MgO) and reaction products ($CaSO_4$) all have high resistivities (on the order of 10^{12} ohm-cm).
3. If a large amount of carbon is present, a very low resistivity could result. Carbon is a good conductor with a resistivity of 3.5 x 10^{-3} ohm-cm and could lower the resistivity below the 10^{+7} ohm-cm level for good performance.

The available information on the resistivity of material from AFBC is shown in Figure 2[6]. The in-situ points indicate that a hot-side precipitator should collect this material, although the material sampled is not completely representative of full-scale AFBC operation since effluent from the CBC was not included. The laboratory data indicates that a cold-side precipitator would not perform well; however, additional testing is required to confirm these pilot scale results.

Pressurized Fluidized Bed Combustion

Mass Loadings -

In general, data reported to date on mass loadings from PFB combustors provide only enough information to establish a systematic variation in total dust loading as a function of excess air and fluidizing velocity. This is summarized in Figure 3[7] where pilot plant data from the Exxon batch combustor[8] and BCURA[9,10] have been plotted. The Exxon and BCURA data do correlate rather well in terms of dust loadings measured at each facility, superficial velocity, and excess air. The general trend of rapidly increasing dust loading with superficial velocity is apparent.

Of importance to the final particulate cleanup device in a PFBC system is the loading and size distribution from the initial cyclones since primary, and in most cases, secondary cyclones will be used for initial particle collection. Table 3 presents a summary of the available data from various pilot plants after cleaning the combustion gases with two conventional cyclones. As indicated by this data, the best that can be achieved using small diameter conventional cyclones is a particulate carryover of 0.15-0.20 gr/scf with a median particle size of about 2-5 microns. Conventional cyclone separators alone are inadcquate for reducing exhaust loadings sufficiently to meet the Federal EPA New Source Performance Standard (equivalent to about 0.06 gr/scf at 20% excess air) or to permit long term gas turbine operation, and some other device will be needed in order to provide a viable system.

Size Distribution -

The particle size distribution data reported from pressurized fluidized-bed combustors is shown in Figure 4[7,11,12]. In general, these data were obtained by combining in a weighted fashion the individual size distributions measured from first cyclone, second cyclone, and exhaust gas captures. Because of a lack of hot gas sampling techniques, data from in-situ measurements are not available. The data from Exxon Batch/ANL and BCURA/Exxon Miniplant with recycle can be grouped into separate families. The BCURA data indicates a significantly higher proportion of fine particles than the Exxon (Batch) data. The lower superficial velocities tested at BCURA and differences in tube bundle and bed geometry probably contributed to the separation of the data.

Also shown in this figure is the current estimate of the particulate efflux distribution based on the BCURA data for particles smaller than 40 μm. If the measured particle size distributions are found to contain significantly more fines, it could severely impact the gas cleanup systems. This estimate indicates that about 25% of the particles are smaller than 10 μm and about 7% are smaller than 2 μm.

Chemical Characteristics -

PFBC particulates from the primary and secondary cyclones and exhaust gas captures have been chemically analyzed by various investigators to determine carbon, sulfur, and calcium contents and, in some cases, ash constituents. Preliminary experiments on the fate of 19 trace elements in a pressurized fluidized-bed combustor have been reported by Argonne National Laboratory[11,13] and the determination of the distribution of trace elements emissions is also in progress at Exxon[8]. The alkali content of the effluent stream (primarily Na and K) is a matter of critical concern because of the potential for fouling and hot corrosion of the gas turbine blading. The alkali present in the form of solids is subject to removal by the various hot gas particulate cleanup devices. However, alkali present in the vapor phase will not be significantly reduced by filtration devices. The experimental data on alkali metal emissions in the vapor phase from tests conducted at NCB/CURL indicate that about 0.5-8 ppm sodium and potassium are liberated into the gas phase from a FBC at about 3-6 atm pressure and temperatures of 1450°F-1750°F[9,14,15].

Physical Characteristics -

Combustor efflux particulate matter captured in the cyclone separators at BCURA and Exxon facilities indicate that the ash is a freely flowing powder with no signs of fusion. BCURA reports that, typically, the cascade section and target rods accumulate a slight leading edge deposit which is usually soft and powdery[14,15]. CPC has found that the sticky nature of the particulates in the flue gas renders small (3-1/2 inch and 6 inch) inertial separators ineffective as cleanup devices, since they are highly susceptible to plugging[16].

Recent testing at Exxon has demonstrated significant difficulties with particulate plugging in the Ducon granular bed filter. The inlet sand retaining screens plugged and blowback became possible. Part of the plugging problem was attributed to condensation on the screens during combustor start-up. Further experimental investigation is being carried out to clearly define the dimensions of this potential problem.

PARTICULATE CONTROL TECHNOLOGY FOR FLUIDIZED BED COMBUSTION

Atmospheric Fluidized Bed Combustion

The final particulate collection device for an atmospheric fluidized-bed combustion system would likely either be an electrostatic precipitator or a fabric filter. It is unlikely that a wet scrubber would be employed for final cleanup for several reasons of which, perhaps, the most important is that one of the principal advantages of the AFBC system would be negated by wet particulate collection - namely the dry collection of sulfur as $CaSO_4$. For this reason, collection of particulate matter by wet scrubbing is not considered a viable alternative for an AFBC system.

Required Removal Efficiency -

Based on the laboratory and small scale tests run to date, the combined particulate load passing through the collecting cyclones from primary and CBC combustors might be on the order of 1-10 $lb/10^6$ BTU. Thus, to meet the present EPA New Source Performance Standard for particulates (0.1 $lb/10^6$ BTU) a removal efficiency of 90-99% would be required for the final particulate collection device. While these removal efficiencies are not exceptionally high by industry standards, they must be achieved on a particulate which is primarily below 10 μm.

Electrostatic Precipitators (ESP) -

An analysis of the characteristics of electrostatic precipitators and their application to control particulate emissions in related industries such as the electric utility, portland cement, and gypsum product industries indicates that, with certain restrictions, this control technology should be capable of controlling particulates from AFBC[27]. The restrictions suggested for operation of an ESP on an AFBC system are:

1. The precipitator should be located upstream of the air preheater to operate in the 600-700°F range.

2. The precipitator should be conservatively sized.

3. Gas flow distribution studies utilizing scale models should be conducted to assure that poor gas distribution does not impede the performance capability of the ESP.

4. Adequate rapping capability should be included in the ESP system design to assure that highly resistive, adhering dust can be adequately removed from the collecting plates.

The first restriction is a result of the available particulate resistivity data for the additive and additive products. Flyash material will also exhibit a high resistivity value at low flue gas temperature in the relative absence of SO_3. The second restriction results from the operating characteristics of the ESP (that is, it tends to act as a constant % removal device), the lack of an adequate data base on the mass loading or size distribution characteristics of the particulate, and the variation in attrition/decrepitation characteristics of sorbent material. Additionally, conservatism is call for because particulate emissions may vary considerably between the experimental beds run to date and the commercial size beds. There is likely nothing inherent about the particulate loading or size distribution in the emission characteristics of an AFBC which would preclude the successful application of an electrostatic precipitator to control particulate emissions. Precipitators have been designed to handle much higher dust loadings and much finer size distributions than those anticipated (after the cyclone collectors) from an AFBC.

Another reason for conservative ESP design on an AFBC system is that ESP design today is still far from rigorously scientific. The vendor community relies quite heavily on previous operating experience with similar installations to arrive at a design effective migration velocity and, hence, precipitator size (SCA). For a new application, then, such as an AFBC system, the lack of a direct data base of effective migration velocities presents some difficulties and dictates a conservative design.

Proper gas flow distribution through model studies is required since the design of the gas ducts and inlet structure is critical to proper ESP operation. Providing adequate rapper capability arises as a result of industry experience with release of different particulate materials from ESP collecting plates. Flyash, for example, does not adhere as tenaciously to the collecting plates as does cement dust (principally CaO). Adequate rapper capacity should be designed into the ESP system to assure satisfactory collection plate cleaning over a wide range of dust adhesions to maintain ESP operating efficiency.

It should be noted that these restrictions have been followed in the design of the ESP installation for the Rivesville 30 MW_e AFB combustor. Specifically, the ESP was located hot-side (730°F inlet temperature), model flow studies were conducted of the ducting and inlet flue arrangement to assure proper gas flow distribution, and the precipitator was conservatively sized (inlet gas velocity of 3.75 ft/sec and an SCA of about 375 ft^2/1000 acfm)[17].

Fabric Filters -

Fabric filters have been used successfully in many industrial applications which produce particulate emissions similar to that expected from AFBC. Fabric filters have been used: (1) to collect $CaSO_4$ from gypsum calciners, (2) to collect CaO particulate from lime kilns, (3) to collect fly carbon in the carbon black industry, and, (4) in recent years, to collect flyash and flyash/carbon from industrial and utility coal-fired boilers. Although different fabrics have been used in the above applications, glass fabrics have been the predominant choice of filtering media. As a result, new or exotic fabrics should not have to be developed for an AFBC application.

This not withstanding, however, no direct experience data base exists for the design of a fabric filter for collection of AFBC particulate. While related industrial experience can be useful as a guide for fabric selection, collector and bag design, etc., the determination of such parameters as the specific dust-fabric filter resistance coefficient and air-to-cloth ratio needed to give acceptable bag service life and outlet emissions concentrations can only be found through experimental testing. Potential problem areas which have been identified for fabric filters on AFBC systems and which need to be addressed in the pilot testing program include tendency of AFBC particulate to bleed through the fabric collector, the abrasiveness of AFBC particulate, the hygroscopicity of AFBC particulate, and the presence of unburned carbon in the AFBC particulate[27]. It should be noted that the application of fabric filters to industrial and utility coal-fired boilers was preceded by an extensive pilot testing program.

AFBC particulate may tend to bleed through the fabric material because of its relatively small particle size and narrow size range as a result of the cyclone precleaners. (The use of cyclone precleaners may be beneficial, however, in extending bag service life for an AFBC application because they remove the coarser, more abrasive particles.) The CaO material in AFBC particulate may tend to absorb moisture from the flue gas stream and may plug the fabric media. Whether or not this will be a problem will depend on many factors such as residence time, the type, density, and size of the fabric material, etc. The problem of unburned carbon in AFBC particulate relates to spontaneous oxidation and electrostatic effects. Particulate abrasiveness relates to bag life. These potential problem areas can only be addressed with pilot testing.

The overall prognosis for control of particulates from an AFBC system by the use of fabric filters is good because of the considerable related industrial experience possessed by the vendor community and the success in recent years with fabric collectors on coal-fired boiler installations. Fabric collectors have successfully filtered gas streams with much higher grain loadings and much finer size distributions than those expected (after the cyclone collectors) from an AFB combustor. Fabric collectors are less sensitive to inlet fluctuations in particle mass loading and size distribution than are electrostatic precipitators, which is in their favor for application to AFBC systems.

Pressurized Fluidized Bed Combustion

Particulate Cleanup Requirements -

The particulate removal system must be capable of reducing the particulate loadings in the combustion off-gas to levels compatible with environmental standards and with gas turbine operating conditions. Specific problems related to the gas turbine include blade erosion, hot alkali corrosion of turbine parts, and gas turbine fouling. To define particulate cleanup requirements, PFB carryover and turbine tolerances must be quantified. Unfortunately, at this time, there are no reliable data for these criteria, so that particulate cleanup requirements are poorly defined.

Environmental -

The EPA particulate emission standard for new coal-fired steam generators is presently 0.1 pounds of particulates per mission Btu of fuel. For a pressurized boiler operating in the 20-30% excess air range (water-cooled and air-cooled respectively), this is equivalent to an exhaust emission of about 0.06-0.055 gr/scf. There is no specific restraint on particle size distribution.

Erosion -

The limits of particulate loading from PFBC for acceptable gas turbine erosion rates have not yet been determined. Gas turbine manufacturers have not yet established correlations between particle loadings and size distributions with turbine life expectancy. Turbine tolerance for particulates depends in a complex way on particle size, particle physical properties, impact velocity, impact angles, and blade materials. Smaller particles will be less erosive than large particles, so that heavier loading of fine particles may be tolerated. Some of the estimated particulate loadings and their associated size distributions for acceptable gas turbine erosion rates are presented in Table 4[18-21]. Considerable variation of opinion appears in this table as to allowable loadings and particle size, based largely on a review of the same data.

Corrosion and Fouling -

Gas turbine components exposed to the hot combustion gases are made of materials that form oxide scales to protect themselves from oxidation. In the presence of alkali metal compounds, which react with the sulfur oxides and chlorides in the combustion gas, liquid films of sulfate and sulfate-chloride mixtures can be deposited on the turbine hardware. These melts must be prevented because they can initiate hot corrosion and can lead to substantial deposit formation (fouling).

Actual experimental results to date indicate that gas temperature in terms of both level and consistancy, has a critical bearing on the extent of hot gas corrosion. CPC found that at 1600°F with or without additives no evidence of sulfidation was found in turbine blade materials. However, for temperature excursions above 1710°F for as little as one hour, detectable sulfidation was found to occur in some alloys, while for temperature excursions to 1750°F catastrophic sulfidation was found to occur in all alloys tested[16]. BCURA has found evidence of sulfidation in some of their test target rods[9].

Fouling is the accumulation of unwanted deposits on the hot turbine components due to ash constituents in the fuel. In tests conducted by the Solar Division of International Harvester Co.[22], the fouling characteristics of particulate from the CPC combustor were investigated. Solar concluded that the CPC flyash had a marked tendency to form dense deposits on impaction with hot turbomachinery surfaces. Their data, shown in Figure 5, indicate that ash deposition or fouling is a linear function of particulate loading and time for the range of variables studied. The data point to a potentially serious problem to efficient gas turbine operation.

Potential High Temperature/High Pressure Cleanup Devices -

Several approaches have been proposed and are being developed for particulate cleanup of high temperature and high pressure gases. The processes most actively being investigated, as shown in Figure 6[23], include inertial devices, granular bed filters of various designs, electrostatic precipitators, fabric filters, metal or ceramic filters, and various hybrid designs. Except for conventional cyclones, these methods must be classified as developmental hot gas cleanup techniques and require considerable effort before they can be reliably used. While some methods and processes are more advanced than others, questions of ultimate efficiency, reliability and equipment life are still unanswered and must be confirmed by both bench scale and pilot scale experiments. Only inertial devices and certain granular bed filters are presently available for pilot plant testing.

In general, particle collection efficiency is significantly reduced at high temperature and pressure for particles with diameters larger than a few tenths of a micrometer.

Conventional cyclones have been the first choice for high temperature particulate cleanup due to their relative insensitivity to temperature, and because it is proven technology. The major disadvantage of cyclones is that they have low collection efficiency for small particles. Conventional cyclones alone will not be sufficient to satisfy environmental standards or gas turbine erosion limits.

High efficiency, rotary flow cyclones which employ secondary air to improve efficiency have recently been introduced. While these cyclones offer a potential for improved performance over conventional cyclones, meeting stringent cleanup requirements has not been demonstrated. The Aerodyne model of the rotary flow cyclone, after modifications for high pressure application, will be tested at the BCURA pilot plant. This cyclone will be derated from a commercial version due to the modifications and the use of dirty instead of clean secondary air.

A promising technique under development by several groups is the use of granular beds for high temperature and pressure gas cleanup. Beds of granules should, in principle, be able to achieve the same high efficiency as beds of fibers, are somewhat easier to clean, and may be operated at high temperatures. Intensive experimental testing on large scale, hot pressurized filters is required to establish the operating performance, reliability and equipment life for the different granular bed filter designs. As a beginning, a Ducon filter has been installed in the Exxon miniplant for pilot testing. Initial testing has as yet not demonstrated that the present EPA emission standard can be met for more than a few hours of operation[24].

Electrostatic precipitators have been used successfully in a large number of industrial applications at gas temperature typically up to about 750°F and at gas pressures usually at 1 atm and generally well below 10 atm. The ability to generate stable corrona up to 2000°F and 500 psig has been demonstrated in no-flow particle-free operation[25]. The evaluation of particle collection characteristics is now needed.

Probably the most widely used method of removing dust and fumes from a gas stream is by the use of fabric filters. Several glass and metal fibers could potentially be adapted to a hot gas environment. As with other dust collection equipment, current work is aimed at increasing the operating temperature for fabric filters. Work is being done on special glass and metal fibers for use at temperatures ranging from 1100-2200°F[25]. The difficulty in raising filtration temperature does not lie with the fabrics but rather with the filter housing and cleaning mechanism. Conventional fabric filter designs probably cannot withstand temperatures in excess of those currently used for glass fibers (550°F) without radical redesign of the fabric holding structures[26].

Porous ceramic and metal filters are commercially available for filtering solids from gases and liquids at high temperatures. Both types of filters require relatively high pressure drop. Cleaning is done by periodic blowback. Entrapment of small particles requires regular (i.e., 6 months to a year) special cleaning by chemical or ultrasonic means to restore permeability. This plus the brittle nature and thermal sensitivity of the materials could limit their use[18], although recent lab scale work in this area has shown promise[25].

CONCLUSIONS

In general, there is limited data on the mass loading, size distribution, chemical, and physical characteristics of particulate emissions from fluidized-bed combustors, and more information is required for the economical design and operation of control equipment to meet environmental or gas turbine standards for particulates. Limited data is available on sorbent attrition/decrepitation rates in fluidized-bed combustors which have been found to significantly influence mass loadings and, to a lesser extent, size distribution and chemical characteristics. Test programs are presently being conducted at various installations under DOE and EPA sponsorship to provide additional data in these areas.

There are several industries, aside from the electric utility industry, which have particulate emissions similar to those expected from AFBC, and an analysis of the performance of ESPs and fabric filters in these industries indicates that, with certain adaptations and modifications, this technology should be capable of controlling AFBC particulates. For the ESP, the major unknown, at this time, appears to be the carbon content of AFBC particulate which could act to lower resistivity values below a good collection level. A firm data base on migration velocities is also lacking at this time. For fabric filters, the lack of a direct data base on gas-to-cloth ratio and specific dust-fabric filter resistance coefficient for AFBC particulates dictates that an experimental program be undertaken to establish this data base. Test programs have been developed to further these data bases.

Four problem areas with respect to particulate emissions from PFBC are environmental restrictions, gas turbine erosion, corrosion, and fouling. Present environmental standards require 70-90% removal in the final particulate collection device. Gas turbine erosion considerations, which appear to be particularly ill-defined at this time, may require 99% removal. Such a stringent removal requirement could prove very difficult to meet because, in general, particulate collection efficiency is significantly reduced at high temperatures and pressures. At the present time, there is no commercially available hot gas cleanup device which achieves these particulate removal levels, although several methods are under development.

Hot gas corrosion of turbine materials may be a potentially serious problem. Since gas phase Na+K is not subject to removal in the particulate collection device, other alternatives may have to be pursued. Some success has been reported by Combustion Power Co. with bed additives. Turbine fouling is also thought to be related to gas phase Na+K, although no criteria have yet been established to limit deposition buildup.

At this time, a great need exists for additional data to establish the seriousness of these potential PFBC problem areas. To this end, test and evaluating programs have been developed and recommended for PFBC systems to: (1) establish the distribution of Na+K among the products of PFB combustion as affected by plant operating variables; (2) establish allowable particulate loadings by size distribution to protect the gas turbine from erosion; (3) establish corrosion and fouling rates in an operating gas turbine environment; and (4) develop the hot gas cleanup equipment required to meet environmental/turbine standards.

REFERENCES

1. Robison, E. B. Study of Characterization and Control of Air Pollutants from a Fluidized-Bed Combustion Unit, The Carbon Burnup Cell. NTIS PB 210828. February 1972.
2. Pope, Evans & Robbins, Inc. Multicell Fluidized-Bed Boiler Design, Construction and Test Program, Quarterly Progress Status Report for Period October-December 1976. US ERDA FE/1237/Q-76/8. January 1977.

3. National Coal Board. Reduction of Atmospheric Pollution, Appendices: Vol. 2 of 3. U.S. Environmental Protection Agency. September 1971.
4. National Coal Board. Reduction of Atmospheric Pollution, Appendices: Vol. 3 of 3. U.S. Environmental Protection Agency. September 1971.
5. Coates, Neil H., and Richard L. Rice. Sulfur Dioxide Reduction by Combustion of Coals in Fluidized-Beds of Limestone. AICHE Symposium Series #141. Vol. 70.
6. Mesko, J. E. Multicell Fluidized-Bed Boiler Design, Construction and Test Program. U.S. Office of Coal Research. OCR 90 Interim #1. August 1974.
7. General Electric Energy Systems Program Development. CFCC Development Program, Hot-Gas Cleanup Efflux Characterization for Commercial Plant, Task 4.1.1. ERDA Contract No. EX-76-C-01-2357. August 1977.
8. Hoke, R. C., et. al. Studies of the Pressurized Fluidized-Bed Coal Combustion Process. EPA-600/7-76-011. September 1976.
9. National Research and Development Corporation. Pressurized Fluidized-Bed Combustion. Office of Coal Research. R&D Report No. 85 Interim #1. July 1974.
10. National Coal Board/Coal Utilization Research Laboratory. Pressurized Fluidized-Bed Combustion. Technical Progress Report Nos. FE-1511-18, -33, -35, -36, -37, -38 and -40. April 1975 to May 1977.
11. Vogel, G. J., et. al. Reduction of Atmospheric Pollution by the Application of Fluidized-Bed Combustion and Regeneration of Sulfur-Containing Additives. EPA-650/2-74-104. September 1974.
12. Hoke, R. C., et. al. Studies of the Pressurized Fluidized-Bed Coal Combustion Process. EPA-600/7-77-107. September 1977.
13. Vogel, G. J., et. al. Annual Report on a Development Program On Pressurized Fluidized-Bed Combustion. ANL/ES-CEN-1011. July 1975.
14. National Research Development Corporation. Pressurized Fluidized-Bed Combustion, Complete Report of Test Run No. 5. BCURA Ltd. US ERDA. September 1975.
15. National Research Development Corporation. Pressurized Fluidized-Bed Combustion, Report No. 43, Annual Report - July 1976 to June 1977. US ERDA. September 1977.
16. Combustion Power Company, Inc. Energy Conversion from Coal Utilizing CPU-400 Technology, Final Report. US ERDA FE/1536-1. March 1977.
17. Brummer, John H. Fluidized-Bed Boiler Promises Coal Burning With Less Pollution.Power. 1977 Generation Planbook.
18. Stone and Webster. Purification of Hot Fuel Gases from Coal or Heavy Oil. EPRI 243-1 Interim Report. November 1974.
19. Westinghouse Research Laboratories. Evaluation of the Fluidized-Bed Combustion Process, Vol. I, Pressurized Fluidized-Bed Combustion Process Development and Evaluation. EPA-650/2-73-048a. December 1973.
20. Westinghouse Research Laboratories. Fluidized-Bed Combustion Process Evaluation, Phase II - Pressurized Fluidized-Bed Coal Combustion Development. EPA-650/2-75-027c. September 1975.

21. General Electric Energy Systems Programs Development. CFCC Development Program, Cleanup Equipment Performance Specification for Commercial Plant, Task 4.1.2. ERDA Contract No. EX-76-C-01-2357. August 1977.

22. Corrosion and Erosion Evaluation of Turbine Materials in an Environment Simulating the CPU-400 Combustor Operating On Coal, Final Report. US ERDA FE/1536-3. April 1977.

23. Klett, M. G., et. al. Particulate Control for Pressurized Fluidized-Bed Combustion. US ERDA FE-2220-16. January 28, 1977.

24. Miniplant Studies of PFB Coal Combustion, Third Annual Report. EPA-600/7-78-0[illegible]. April 1978.

25. EPA-DOE Symposium on HTHP Particulate Control. EPA-600/9-78-004. CONF-770970. September 20-21, 1977.

26. First, N. W. New Kinds of Fabric Filtration Devices. Journal of the Air Pollution Control Association. Vol. 24. No. 12. December 1974.

27. Becker, D. F. Evaluation of Particulate Emissions and Control Equipment for Fluidized-Bed Combustors, Draft Report. U.S. DOE Contract No. EX-76-C-01-2220. May 1978.

TABLE 1

PARTICULATE LOADINGS FROM VARIOUS SIZE AFBC

	FLUIDIZING	PART. LOADINGS - LB / 10^6 BTU	
BED SIZE-FT^2	VELOC.-FT /SEC	COMBUSTOR	CYCLONE
0.196	2.0 - 3.0	5.00 - 23.6	—
1.333	11.6	27.2 - 77.2	—
3.976	6.4 - 10.9	36.9 - 61.7	0.81 - 9.58
4.5	2.1 - 8.1	15.5 - 18.3	1.10 - 2.28
9.0	11.7 - 13.4	12.7 - 35.2	1.03 - 1.67

TABLE 2

INFRARED ANALYSIS OF SOLIDS FROM AFB COMBUSTOR

		WT%					
COAL, Ca/S, AND S REMOVAL	LOCATION	$Ca(OH)_2$	$CaCO_3$	$CaSO_4$	CaO	Glass	Quartz
HVAB; Ca/S - 3.4; S REMOVAL, 94%	BED	8	3	20	40-44	-	-
	CYCLONE	-	<1	3	10-15	20-25	3-6
	FILTER	-	<1	6	20-25	20-25	3-7
HVBB; Ca/S - 1.2; S REMOVAL, 84%	BED	7	2	30	~40	-	-
	CYCLONE	-	-	12	25	25-30	~10
	FILTER	-	-	12	15-20	35-40	~15
HVCB; Ca/S - 2.5; S REMOVAL, 98%	BED	11	<5	29	40-50	-	-
	CYCLONE	-	-	5	-	40-45	10-15
	FILTER	-	-	6	-	35-40	15-20

TABLE 3
PARTICULATE LOADINGS FROM PILOT PFB CYCLONES

PILOT PLANT	AVERAGE LOADINGS GR / SCF	MEDIAN PARTICLE SIZE μM
BCURA	0.1	6 - 8
NRDC	0.14	1.4 - 5.4
NRDC	0.15	1.9 - 17.4
ANL	0.52	-
CPC	0.42	3 - 4
EXXON (BATCH)	0.6	-
EXXON (MINIPLANT)	0.8	6.9

TABLE 4
PARTICULATE LOADINGS BY SIZE FOR ACCEPTABLE TURBINE EROSION

INVESTIGATOR	ALLOWABLE LOADINGS FOR PARTICLE SIZE - Gr/SCF			
	PARTICLE SIZE	< SIZE	> SIZE (MAX. SIZE)	TOTAL LOADING
S&W (1974)	7 μM	0.0001-0.003	0 (7 μM)	0.0001-0.003
WEST (1973)	2 μM	0.14	0.01	0.15
WEST (1975)	5 μM 5 μM - -	0.00126 0.029	0.00074 0.0002 (10 μM)	0.002 0.0292 0.0004-0.02 0.005-0.04
GE (1977)	9 μM	UNLIMITED	0.1	0.1+

FIGURE 1

SIZE DISTRIBUTION DATA FOR PARTICULATES EMITTED BY PRIMARY CYCLONE FROM AFBC

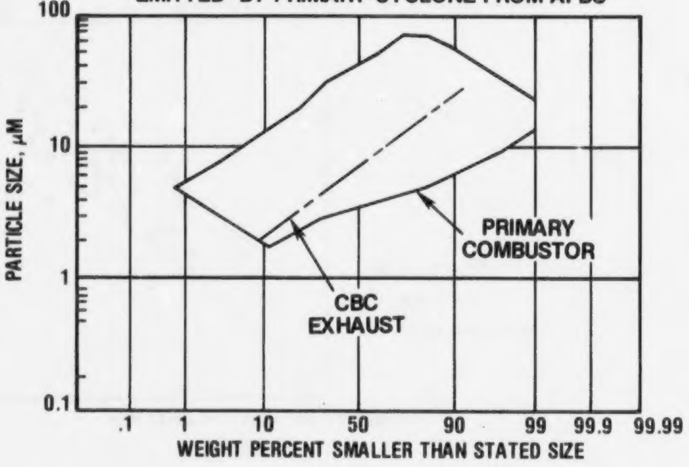

FIGURE 2

RESISTIVITY DATA FOR ATMOSPHERIC FLUIDIZED-BED COMBUSTOR

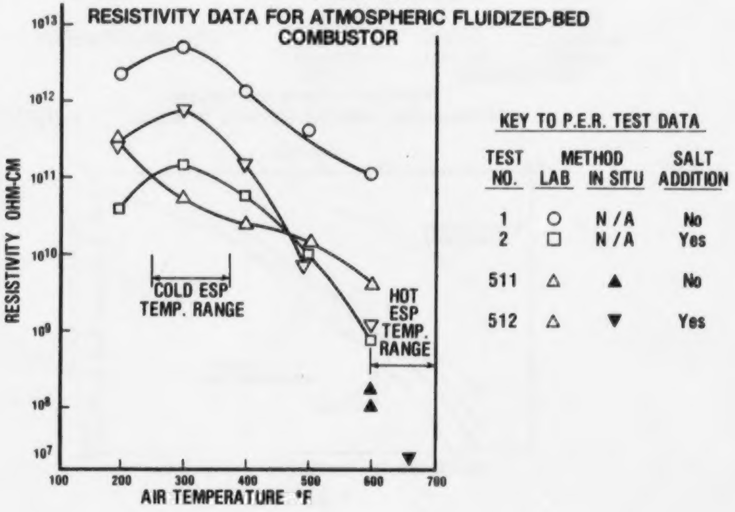

KEY TO P.E.R. TEST DATA

TEST NO.	METHOD LAB	METHOD IN SITU	SALT ADDITION
1	○	N / A	No
2	□	N / A	Yes
511	△	▲	No
512	△	▼	Yes

FIGURE 3

PFB DUST LOADING MEASUREMENTS

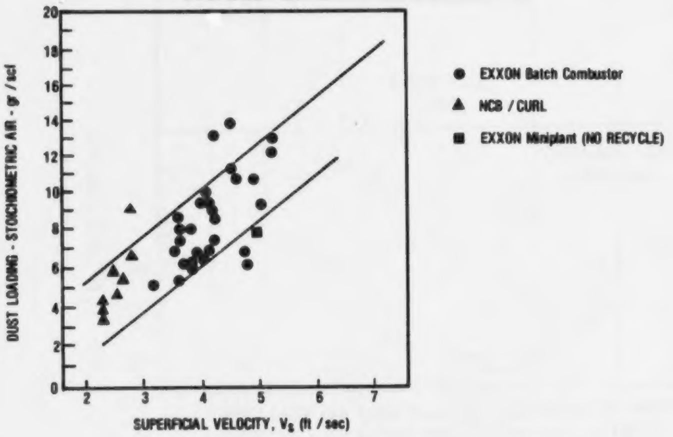

FIGURE 5

DEPOSITION OF GRANULAR FILTER ASH WITH TIME ON EROSION BARS

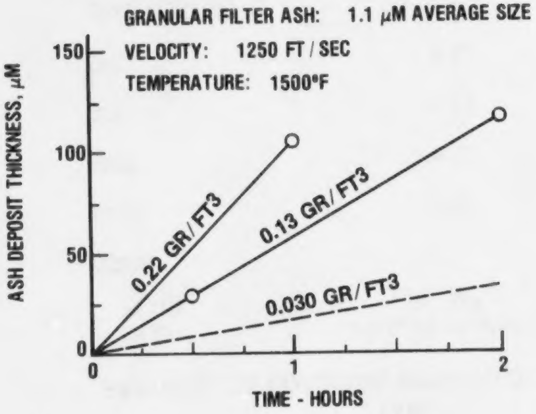

FIGURE 4

PFB OVERHEAD PARTICULATE SIZE DISTRIBUTION

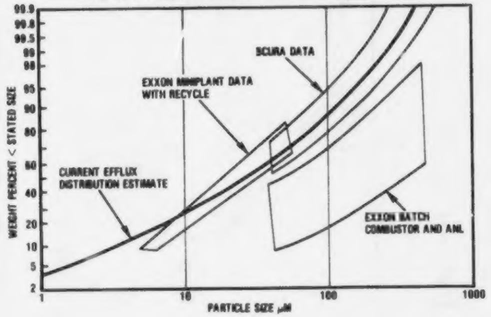

FIGURE 6 POTENTIAL HIGH TEMPERATURE, HIGH PRESSURE PARTICULATE REMOVAL SYSTEMS

APPROACH/DEVELOPER	PRESENT OPERATING CONDITIONS °F/ATM	STATUS OF TESTING TESTING STAGE	 TESTING CONDITIONS °F/ATM
I. INITIAL DEVICES CYCLONES	1750/12	PILOT SCALE	1750/10 TWO STAGES
MULTICLONE/CPC		PILOT SCALE	1450/2.7 TWO STAGES
MULTICLONE/DONALDSON		NO TESTING	
ROTARY FLOW CYCLONE/AERODYNE		PILOT SCALE	1600/10 TWO STAGES
ROTARY FLOW CYCLONE/GENERAL ELECTRIC		LAB SCALE	AMBIENT
II. GRANULAR BED FILTERS MOVING BED FILTER/CPC	1000/1	LAB SCALE	1300/1 31° SEGMENT
FIXED BED FILTER/DUCON		PILOT SCALE	1600/10
FIXED BED FILTER/WESTINGHOUSE		LAB SCALE	AMBIENT
RESTRICTED CIRCULATION FILTER/SQUIRES, CCNY		LAB SCALE	1000/1
RESTRICTED CIRCULATION FILTER/PEMMCO		CONCEPTUAL	
III. ELECTROSTATIC PRECIPITATION RESEARCH COTTRELL	900/1	LAB SCALE	1650/1
IV. FABRIC OR POROUS MEDIUM FILTERS	550/1		
METAL FABRIC FILTER/BRUNSWICK		LAB SCALE	700/1
CERAMIC FABRIC FILTER/ACCUREX-AEROTHERM		LAB SCALE	1500/10
SINTERED METAL FILTERS	900/1	NO TESTING	
POROUS CERAMIC FILTERS	3000/1	LAB SCALE	1400/1
V. HYBRID PROCESSES DYNAMIC PRECIPITATORS/MECHANICAL TECH		LAB SCALE	
CHARGED FILTERS/AMERICAN PERCISION	400/1	LAB SCALE	400/1

HIGH TEMPERATURE GLASS ENTRAINMENT OF FLY ASH

WILLIAM FEDARKO
Fossil Energy Programs
U.S. Department of Energy
Washington, D.C. 20545

ARNO GATTI AND LOUIS R. MC CREIGHT
Space Sciences Laboratory
General Electric Company
Valley Forge Space Center
P.O. Box 8555
Philadelphia, PA 19101

Hot gas clean up of coal combustion products to be used for powering gas turbines is very difficult but necessary for efficiency. A novel process analogous to water scrubbing which overcomes the ricochet/fracture/reentrainment problem and makes use of the caking/sticking tendency of fly ash at elevated temperatures has been demonstrated and is now ready for advanced testing. It utilizes waste glass in a viscous condition to trap and dissolve the particles which are first deflected against the glass coated walls of a labyrinth duct at about 1000° C and then most remaining particles and possibly some vaporized species are trapped in a bubbler of molten glass at about 1200° C. Several test runs show an efficiency of 97-99% of all particles and essentially 100% of the particles over 2 microns being removed from an Illinois No. 6 Fly Ash - Dolomite effluent which contained from 2-80 micron particles with a peak in the size distribution curve at 20-25 μm.

This process is designed to be continuous with means for adding extra glass and heat to control the viscosity as needed. Waste glass which may consist primarily of the dissolved fly ash and secondarily of the initial waste glass will be drained from the bottom of the vertical chamber. In addition to potentially providing process heat, it is expected to be useful for aggregate in paving or building materials at a value of about $2.50/ton or, as glass cullet, for other building products at as high as $8-10/ton. This is as contrasted to the present practice of paying to have the dusty, low density ash hauled away from power plants at $2.50 to $3.00 per ton.

INTRODUCTION

The clean-up of coal combustion gases, while hot, to be used as fuel for gas turbines is well recognized as a difficult problem. Several low temperature techniques are being extrapolated to higher temperatures but are encountering severe problems. Among the problems which limit the effectiveness of various particle removal processes, in some cases at both low and high temperatures, are: ricochet and fracture of the particles resulting in reentrainment, a tendency for the particles to cake or stick, and the need to back flush with again the possibility of reentrainment of the particles as well as some down time. Finally, there is potentially a still very serious problem of alkali carry over even when most of the particles are removed.

It was postulated that these problems can be minimized, if not eliminated by the use of glass to capture the particles and possibly the vaporized alkalis. At future gas turbine operating temperatures of about 1300 to 1400°C the glass could possibly be entirely composed of the fly ash in a molten condition. At the present desulfurization and gas turbine operating temperatures however, lower temperature glasses are needed to initiate and maintain the cleaning process which consists of two separate processes; (1) impaction in which a glass coating on the walls of a duct and of a labyrinth of plates serve to capture the particles from the gases and (2) scrubbing in a shallow bath of molten glass. In both steps of this continuous process, the fly ash particles are trapped and dissolved thereby adding to the glass by-products which can be drained from the collector and possibly used for numerous applications such as aggregate in paving and building materials, fiber and foam glass insulation, containers and wall tiles.

The first phase of the development of these ideas into a practical hot gas clean up system is described.

Glass Selection Studies

While the initial idea (and conceptually the simplest approach) on which this program was based is to use just the fly ash in a molten or glassy condition to capture fly ash particles, there are several good reasons why this is not practical. Principal among them are that the fly ash from various coals of interest melt at $\sim$ 1300°C to about 1500°C which is clearly too high a temperature for several other aspects of the overall process, including the desulfurization and gas turbine operation. It is therefore desirable and necessary to consider initiating and continuing the process with some low cost, lower melting materials. While these might possibly include numerous materials used in ceramics for fluxing glasses, glazes, and enamels, there would be an increased danger of alkali carry-over to the turbines with some of them. The prodigous quantities of fuel, fly ash, and therefore fluxes needed in the power generation process also dictates the use of lower cost materials or approaches. It was therefore decided after a brief review of various glasses and fly ash compositions that glass cullet at about $8-10/ton would be used in the laboratory studies while the future full scale plants might be operated on incinerator waste glass. In addition, direct electrical resistance heating in specific parts of a future plant might also be an efficient method of lowering the glass viscosity in order to induce flow just as it is becoming in many glass manufacturing operations.

Although several fly ash and glass compositions were considered, amber container glass cullet was selected to be used with 70% Illinois No. 6 fly ash 30% Dolomite effluent for the principal studies in the program. The compositions of several of these materials are shown in Table 1 and the viscosity vs. temperature for several as determined by the National Bureau of Standards (NBS) are shown in Figure 1.

Table 1. COMPOSITION IN OXIDE WEIGHT PERCENT OF FLY ASH AND GLASS MATERIALS EVALUATED FOR FLUIDITY-TEMPERATURE RELATIONSHIP

Oxide	70 Ill. #6 30 Dolomite	NBS Synthetic Fly Ash K884	NBS Container Glass SRM710	Amber Container Glass
Na_2O	1.3	-	8.7	13.9
K_2O	1.2	-	7.7	0.4
CaO	11.25*	10.6	11.6	9.9
MgO	7.25*	3.3	-	1.0
SrO	-	-	-	0.2
Al_2O_3	24.69*	21.8		2.1
Fe_2O_3	2.68*	16.6		0.3
Sb_2O_3	-	-	1.1	-
P_2O_5	-	-	-	
Si_2O	35.51*	47.8	70.5	72.2
TiO_2	-	-	-	0.1
SO_3	7.4	-		

*By Analysis, this program

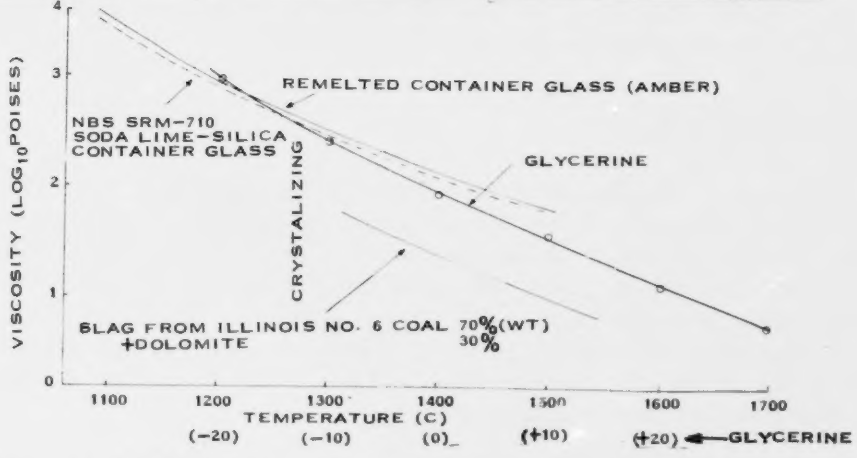

Figure 1. Viscosity vs temperature of various materials in study

Flow studies of the various fly ash/amber glass mixtures were also made by the standard flow botton test used for many years by the porcelain enamel industry. This test is a practical, quality control technique for evaluating the fluidity and feasibility of enamel frits. It is considerably less expensive and much simpler than high temperature viscosity determinations and produces reliable data if such factors as particle size of the materials, pellet forming pressure, pellet height and weight, and temperatures are controlled. Figure 2 illustrates the typical behavior of various glass-fly ash compositions flow buttons at 1000° C, 1100° C and 1250° C for 3 hours. These tests were particularly aimed at illustrating the behavior of the indicated compositions at temperatures expected to be used in the later hot duct tests. They clearly show a range of fluidities vs. temperatures and by inference the ability to capture and dissolve fly ash particles in the amber container glass.

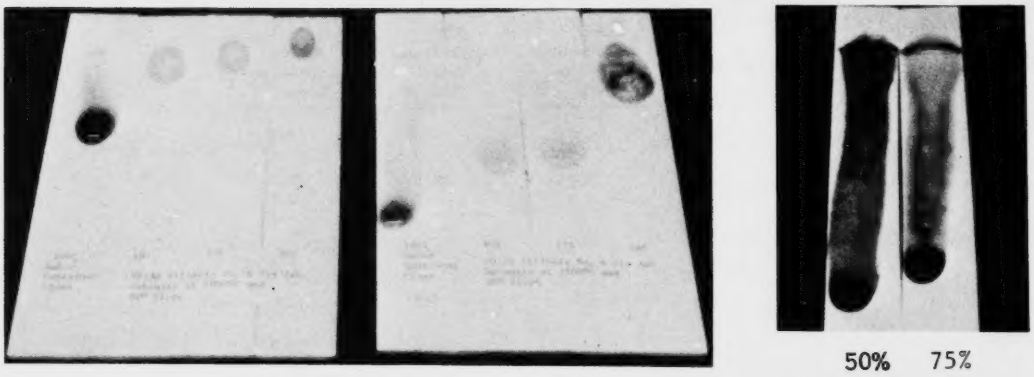

Figure 2. Flow button studies of amber container glass and indicated % additions of 70% Ill. No. 6 Fly Ash 30% Dolomite for 3 hours on 30° slope at (left to right) 1000°C, 1100°C and 1250°C.

Particle Collection Studies

The basic sticky wall concept is potentially applicable to several different configurations of particle collection devices ranging from cyclones to scrubbers. Implicit in some devices would be the necessity to circulate, flow once through or even pump the molten glass. While technically possible it would clearly be an undesirable complication to be avoided, if possible. On the other hand, the slow or sluggish reaction rates common to ceramics and glasses and the desire to have a simple yet efficient operation and utilization of starting materials leads to certain design features as follows:

1. Large wetted surface area
2. Long residence time
3. Means of adding glass or heat to control viscosity
4. Continuous operation without backflushing.

Two test apparatus' to study these parameters were therefore planned for the program. First, a horizontal flow labyrinth type duct was built using clear plastic sheets and cooled glycerine flowing vertically downward over the plates to simulate glass at various viscosities. Several tests and modifications were made in this unit and the best features were then built into a high temperature test unit.

The hot test duct was oriented vertically to simplify the additions of glass and to more easily permit the use of a bubbler type of scrubber above the labyrinth formed by sets of inclined ceramic plates.

Horizontal Flow Labyrinth Duct (Cold)

The design and variations were selected to be both practical for trapping fly ash particles and to be readily translated and operated in high temperature versions. The inlet and outlet ducts have a cross sectional area of 0.1 square feet. Within the plate area the cross sectional area is reduced by 50% to .05 square feet which should result in a two-fold increase in velocity and pressure compared to the inlet values. The combined wall and floor area provided 10 square feet of active area. Thus, the unit was designed so that scale-up parameters are simple multiples of 10.

Figure 3 shows the test unit on a stand with accompanying pressure monitoring gauges. Drain holes are provided in the scrubber floor while feed holes were provided in a top plate to regulate the flow of glycerine to the wetted plates. A reservoir volume was provided above the labyrinth of plates while a collection sump was attached below the scrubber. A vacuum cleaner bag was fixed at the exit end to capture the remaining particles which pass through the duct.

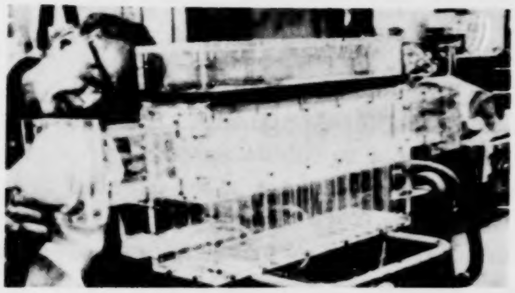

Figure 3. Plastic labyrinth test duct showing air and particle injection at left end and vacuum cleaner bag at exit on right.

The operation of the scrubber was as follows:

1. Cooled glycerine at pre-determined temperatures (and therefore pre-determined viscosities) was throttled through the slide valve onto the reflector plates.

2. Dust ladened air was passed through the scrubber at rates up to 60 SCFM and dumped into a porous paper bag (commercial vacuum cleaner bag) at the outlet end.

Particle injection was accomplished by using either a Metco plasma spray gun or, for runs of short duration, a modified hypodermic syringe was used. Montana Rosebud fly ash fed at ~ 1.2 grains per cubic foot of gas was used as a a standard loading for initial tests at 30-40 SCFM prior to the selection of the Illinois No. 6 fly ash-Dolomite for the continuing studies.

The glycerine reservoir at the top of the duct held at least 8000 cc's of glycerine and its temperature was controlled by a refrigerated cooling coil. At one poise the duct operated for over four minutes at a feed setting of 1/2 and 2 minutes at a full feed setting.

Sixteen successful runs were made in the clear plastic labyrinth duct during the program; over a range of conditions and configurations which were aimed at quickly arriving at a suitable configuration for the high temperature unit which could not be so easily modified or reconfigured. These are summarized in Table 2 and are briefly described below:

1. Three test runs with cooled glycerine to simulate various viscosities of glass are shown as the first three runs of Table 2.

2. The original 14 section labyrinth with one middle and two side mounted plates per section was modified to permit collection of the glycerine and entrained particles from each of the 14 sections in an individual sump.

Table 2. SUMMARY OF THE DATA COLLECTED USING THE PLASTIC LABYRINTH TEST DUCT

Run#	Time (min)	Particle (gms)	Particle Collected in bag (gms)	Effic. %	gr ns/ cu. ft. into duct	gr ns/ cu. ft. out of duct	SCFM air	REMARKS
-2*	2	4	.03	99.2	.771	.006	40	7.5°C, 1.5 poise
-3*	2	4	.04	99.00	.771	.008	40	20°C, 1.0 poise
-4*	2	4	.03	99.25	771	.006	40	0°C, 2.0 poise
-5*	10	16.4	.606	96.3	.843	.031	30	
-6*	10	12.4	.446	96.4	.637	.028	30	
-7*								Aborted
-8$^{(1)}$	5	10.2	.118	98.8	.605	.007	52	Crisco run
-9$^{(1)}$	5	11.2	.282	97.5*	.664	.0167	52	Crisco run
-10$^{(1)}$	5	10.6	.287	97.3	.629	.0170	52	Crisco run
-11$^{(1)}$	5	2.2	.021	99.0	.130	.001	52	Crisco run injector off
-12$^{(1)}$	5	9.5	.256	97.3	.563	.052	52	Crisco run
-13$^{(1)}$	5	9.9	.343	96.5	.567	.020	52	Crisco run
-14$^{(1)}$	5	3.3	.124	96.2	.196	.007	52	Crisco run
-15*	5	19.3	1.032	94.6	1.14	.061	52	Duct dry run
-16*	5	17.7	.325	98.2	1.06	.02	52	Slanted plates
-17*	3	9.4	.268	97.1	.93	.026	52	Slanted plates
-18*								Bubbler-Aborted
-19*	10	23.8	.297	98.8	.61	.008	60	Bubbler

* Glycerine at room temperature except as noted for the first three runs

(1) Crisco runs during which scrubber plates were coated with grease (Crisco(R)) and run for a total of 35 minutes.

3. Three perforated plates were installed at 45° in the middle of the duct to permit glycerine to flow down the plates and to bridge over the holes through which the dirty gas passes. This is one form of a bubbler style scrubber.

4. The unit was reconfigured into a total bubbler design with all of the gases forced to bubble upward through the glycerine (after passing through the labyrinth) and exit up a vertical outlet duct at the far end of the unit from the entrance.

This latter design performed with the highest efficiency and was used therefore as the basis for the hot duct design.

Ceramic Hot Duct

The plastic duct had demonstrated that the sticky wall concept was viable. A high temperature test unit was then designed and built. The most significant change in design was to vertically orient the assembly so that the bubbler and the flowing glass concepts would need a smaller fluid glass supply and could be more easily resupplied. The design chosen is shown schematically in Figure 4. This design provides both labyrinth and bubbler particle cleaning capability.

The duct was dimensioned so that it is close to the physical size of the plastic labyrinth model, except that it had 10 compartments rather than 14. The plate area per compartment was 114 square inches (both sides) and the gas passages are 12.5 square inches in cross section throughout the unit, including the mullite piping and the bubbler area, to minimize pressure drops in the system.

Materials of construction for the duct included 3200°F capability fire brick for the walls, mullite deflector plates and mullite piping. Figure 5 shows the high temperature duct ready for operation. All internal areas of the scrubber were coated with a slurry of about a 50 mils thick powdered amber glass which formed the sticky wall during operation.

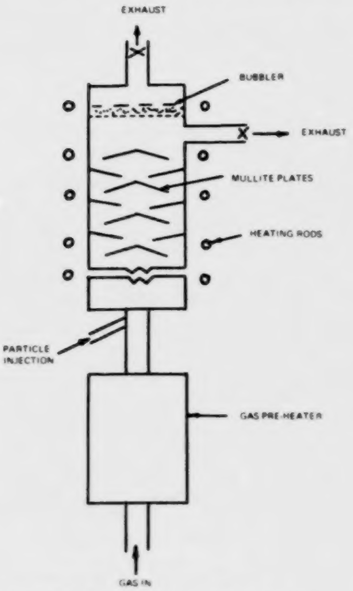

Figure 4. Schematic of high temperature test apparatus which provides both labyrinth and smaller particle cleaning capability

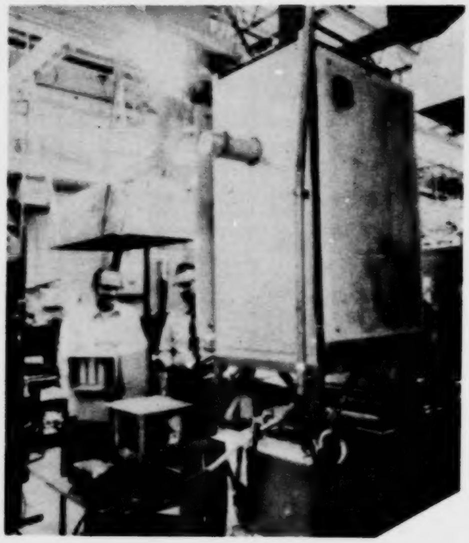

Figure 5. External view of high temperature test duct with air preheater below and particle feed apparatus in left foreground

The completed assembly stood over 9 feet in height and was about 28 inches square. The main duct body was heated by 14 silicon carbide resistance heaters while the bubbler assembly was heated by four additional heaters by a separate power supply since the viscosity of the glass in this section had to be carefully controlled and at a higher temperature.

Finally, a filter was designed and assembled which was capable of operating at high temperature for trapping all of the particulates which passed through the duct. No particulates were ever visibly seen excaping beyond the filter during operation.

Test Results

The test results are summarized in Table 3, which shows the run conditions and results, and in Figure 6, in which several types of data are presented to permit easier correlation. The latter includes: (1) a schematic diagram to indicate thermocouple locations, (2) temperature plot during a typical run, (3) a photo of the interior of the duct after 11 runs, (4) chemical analysis data and (5) estimates of the fly ash pick-up in each stage.

Table 3. SUMMARY OF DATA ON HOT DUCT OPERATIONS

Run #	Time (min)	Duct Temp (°C)	Particles Injected (gms)	Particles Collected (gms)	Efficiency (%)	Grns cu.ft. in	Grns cu.ft. out	SCFM Air (min)	REMARKS
1	3	RT	15	1.23	91.8	1.4	.11	55	
2	5	RT	24	1.81	91.4	1.4	.10	55	
3	-	900	-	-	-	-	-	55	Run aborted, filter too tight, excessive back pressure.
4	5	900	1.3	-	-	-	-	55	Feeder clogged by large particle ~ 1.6 mm dia.
5	5	900	36	1.6	95.6	2.0	.09	55	Extremely high loading, run OK, no visual dust escaping.
6	-	900	-	-	-	-	-	55	Bubbler on at 1100°C - No bubbles. Too much back pressure. Run aborted.
7	5	900	6	0	100	.34	0		Bubbler at 1150°C. Run OK. Not much fly ash put through.
8	5	900	19.5	.3	98.5	1.1	.02		Bubbler at 1150°C. Good run.
9	-	900	-	-	-	-	0		Bubbler at 1150°C using new feed device, too much back pressure. Run aborted.
10	15	900	265	8	97	5.7	.2	48	Run using new feed device. Extreme loading evident. Fly ash mixture 50%:70-30 Ill. #6-Dolomite, 50% glass + 1% Cr_2O_3.
11	15	900	170	5.7	97	3.6	.12	48	Bubbler, sealed feed device, extreme loading evident with ash mixture 50% glass.

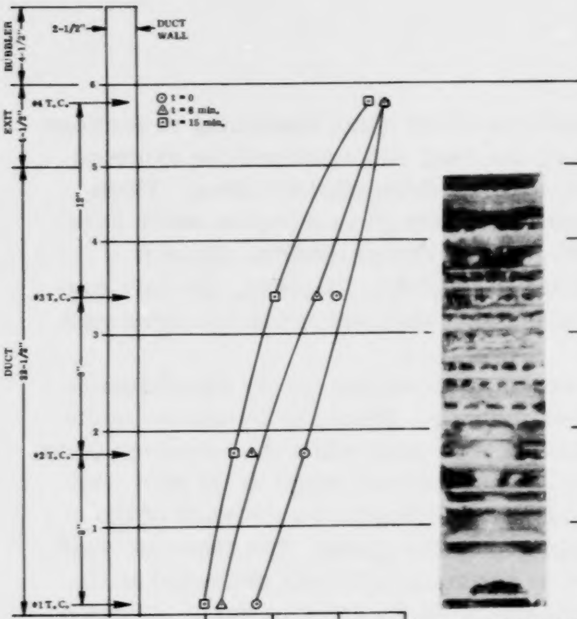

Photo of the hot duct after 11 runs totaling 58 minutes and 53 6.8 grams of 70% Illinois No. 6 Fly Ash - 30% Dolomite plus glass powder. Note that the bubbler section does not show in this photo.

Chemical Analysis

	After Test Runs				
	Fe_2O_3 %	MgO %	Nature of Sample Analyzed	Fly Ash - Dolomite Pick-up in duct	Calculated Fly Ash - Dolomite Pick-up in Glass
Area 5	.22	2.12	Glass*	3%	0%
Area 4	.28	1.11	Glass*	6.2%	4%
Area 3	.33	1.16	Glass*	12.5%	6%
Area 2	.32	1.16	Glass*	25%	6%
Area 1	4.82	7.92	Fly Ash˙	50%	Not determined

* Initial glass composition is 0.25% Fe_2O_3 and 0.96% MgO

˙ Initial Fly Ash - Dolomite mixture is 2.60% Fe_2O_3 and 7.75% MgO.

Figure 6. Schematic of Hot Test Duct showing thermocouple locations and typical temperature during a run.

Overall the operation of the duct was very satisfactory and perhaps even slightly better than expected in that the actual temperatures were found to be about 100°C lower than thought during the runs. This was found when the recorder was recalibrated. As can be noted in Figure 6 the amber container glass has flowed downward from the bubbler section (which is just out of the field of view at the top of the photo) into sections 2, 3, 4, and 5. Section 1 contains most of the injected fly ash dolomite and some additional powdered glass which was included to demonstrate the capability to add extra glass as needed by this method. Additional glass can also be added, of course, through the bubbler section by controlling viscosity and pressure to let some of it drain into the test duct sections.

Particle size studies of as-received fly ash mixture and fly ash collected at the exit port from room temperature runs were made to compare particle diameter distributions since from the plastic duct results it was shown that without sticky walls, large particles would eventually pass through the duct due to ricocheting or rebounding. This appears to be true for the hot duct also. Room temperature runs show particles have passed through which are as large as those in as-received material. It is also seen that during hot runs, large particles are effectively trapped and a more uniform smaller particle-sized effluent results.

After dismantling the hot duct, samples of the glass remaining in Sections 2 and 5 were metallographically mounted, polished and examined for evidence of fly ash pick-up by light microscopy and x-ray diffraction analysis. These show that a crystalline phase has precipitated in the glass samples which have apparently dissolved fly ash-dolomite material. The crystalline phase is a complex silicate which has proved difficult to identify. However, the data suggests that an iron-aluminum-calcium-magnesium-silicate phase has developed.

Samples of glass from the same areas as above and the fly ash-dolomite mixture were also prepared for chemical analysis. Since the fly ash-dolomite mixture contains considerable magnesia and iron oxide while the container glass does not, comparing the MgO and Fe_2O_3 content of each stage in the duct with the original fly ash-dolomite composition gave a quantitative measure of the amount of fly ash-dolomite mixture picked up by the glass. The chemical analysis results are shown in Figure 6 with an estimate of fly ash dissolved in the glass samples. As can be seen, a maximum of 8% fly ash pick-up is indicated by the data. This is not an unexpected result, due to the low temperature operation discussed earlier (and therefore less solution) and also because of the rapidly decreasing amount of fly ash within each compartment as it progresses upward through the duct.

It now appears that the basic ideas have been achieved and well demonstrated so that the process is ready for more exacting studies under more completely realistic operating conditions.

ACKNOWLEDGEMENTS

The authors are pleased to acknowledge the support of this work by the U.S. Department of Energy under contract EF-77-C-01-2608. Important contributions to the work were also made by Harry W. Rauch, Sr. in the area of glass technology, by William Laskow who performed many aspects of the experimental work, and by Webster Capps of the National Bureau of Standards who performed the viscosity determinations. Their work is particularly appreciated and acknowledged.

A.P.T. DRY SCRUBBER FOR PARTICLE COLLECTION AT HIGH TEMPERATURE AND PRESSURE

S. Calvert, R. Patterson and S. Yung
Air Pollution Technology, Inc.
San Diego, California

D. Drehmel
U.S. Environmental Protection Agency
Industrial Environmental Research Laboratory
Research Triangle Park, North Carolina

INTRODUCTION

High temperature and pressure (HTP) gas streams are encountered in developing advanced energy processes such as coal gasification and fluidized bed combustion. It is often economically desirable to utilize this gas stream directly by passing it through a gas turbine. To prevent the erosion and corrosion of turbine blades and heat exchanger tubes, it is necessary to remove the particulates before utilization. The particle collection efficiency requirements are stringent, perhaps 90 percent for 1.0 μm diameter particles and 99.5 percent overall.

The elevated temperature and pressure conditions suggest that new devices for removal of fine particles may be necessary. Typical particle collectors used in fossil-fuel-fired power plants (electrostatic precipitators, scrubbers, fabric filters) generally operate at temperatures below 260°C and at low pressures. The suitability of these components at elevated temperatures and pressures may be limited. The A.P.T. dry scrubbing system, which we call the "PxP" system (for "particle collection by particles"), is compatible with the special demands of HTP gas cleaning.

PXP SYSTEM

The PxP system for fine particle control utilizes relatively large particles as collection centers for the fine particles in the gas stream. The relatively large particles (collector particles) introduced to the gas stream can collect fine particles by mechanisms such as diffusion, inertial impaction, interception and electrophoresis. The larger size of the collector particles allows easy separation from the gas stream by devices such as cyclones and gravitational settling chambers.

Figure 1 is a functional diagram of the process steps for a representative PxP system. The functional phenomena represented on this diagram could occur concurrently or separately in several types of equipment.

The first step involves introducing the collectors to the gas stream. This process can involve pneumatic or mechanical injection into the gas stream. The second stage involves contacting the collectors with the gas in order to encourage the movement of the fine particles to the collectors. A venturi device can be used for the contactor which would be analogous to a venturi scrubber except that solid collectors are used instead of liquid drops. Alternative contactors such as centrifugal scrubbers could be used.

The next process step is to remove the collector particles after sufficient exposure in the contactor to cause capture of the initial fine particles present in the gas. At this stage the large size and mass of the collector particles is utilized to separate them from the gas. A cyclone separator could be used for this step. Two streams are shown leaving the separator: the cleaned gas leaves the process at this point, and the second stream represents the flow of dirty collector particles to the next step. The final process involves either discarding the collector particles or cleaning them for recycling and disposing of the material collected from the gas stream.

Performance Prediction

The particle collection efficiency and pressure drop for an A.P.T. dry scrubber with cocurrent flow can be predicted with the same relationships that define cocurrent wet scrubber performance. The theoretical performance of the PxP scrubber has been determined based on the venturi scrubber model of Yung et al.[1] Figure 2 is a plot of particle penetration against particle size with collector/gas flow rate ratio as a parameter and temperatures of 20°C and 820°C.

The predicted penetration curves have the following characteristics:

1. For a given set of operating conditions, the penetration decreases with increasing size of fine particles. This is expected since the collection mechanism is inertial impaction of the fine particles upon the collectors.

2. For a given size of collector particle and aerodynamic diameter of fine particle, the penetration decreases with increasing value of $(Q_c \rho_c/Q_G)$.

3. A similar dependence upon the gas velocity is apparent from the model of Yung et al.[1]

4. For the 100 µm diameter collectors and a given fine particle aerodynamic diameter, the penetration increases with increasing gas temperature. This is the result of an increasing gas viscosity with temperature which reduces the effective inertia of the fine particles.

It can also be shown that collector particle diameter affects collection efficiency when other factors are held constant. The cut diameter (i.e., the diameter of the particle which is collected at 50 percent efficiency) decreases as collector diameter decreases. Collection efficiency for particles larger than several microns diameter varies in a more complex way, depending on flow and geometric parameter combinations.

Phase I - Experimental Program

Experimental work has been done by A.P.T. at bench scale to determine fine particle collection efficiency in a PxP scrubber in order to confirm the predictions obtained from available mathematical models. Results of experiments with dibutylphthalate (DBP) aerosol at 20°C are reported in greater detail in an earlier paper, Calvert et al.[2]

The contactor and gravity separator used in these experiments is shown in Figure 3. Collectors entered the T-shaped contactor through the branch leg and were entrained by air entering through one of the "run" legs. The system gas flowed either horizontally or vertically downward into the separator. Cleaned gas flowed out of the branch of the separator tee.

Particle penetration data for all runs with nickel and sand collectors are represented in Figure 4, a "cut power plot." The cut diameter is plotted against gas pressure drop in Figure 4. The line represents the relationship which is predicted and which has been confirmed by a number of field tests on large wet scrubbers. Agreement between the data points and the line is good.

The experimental apparatus was constructed of 316 SS after completion of the low temperature experimental program. This permitted operation of the system to 820°C. Particle penetration data at 650°C with nickel collectors is shown in Figure 5. Penetration of particles less than 1.0 µmA was less than predicted, possibly due to enhanced diffusional deposition.

Phase II - Experimental Program

A pilot plant is being constructed to test the PxP system on a larger scale. The PxP pilot plant will include all of the components needed for a full-scale system. A schematic of the Phase II experimental apparatus is shown in Figure 6.

An atmospheric fluidized bed coal combustor (AFBC) has been designed and constructed for providing a particulate source representative of advanced energy sources. The AFBC is designed to provide 14.2 Am^3/min of dirty gas at 820°C. The major components of the AFBC are:

Combustor -

The combustor is a ceramic-lined, carbon steel vessel with a disengaging section to minimize the carryover of fines. The distributor grid is a perforated Inconel 600 plate with a square grid design (0.16 cm holes on 1.0 cm centers). During operation the bed consists of the components given in Table 1.

Table 1. BED MATERIAL COMPOSITION

COMPONENT	WT. %	SIZE, cm	ORIGIN	CHEMICAL COMPOSITION	
Inert Material	80	0.16-50% 0.32-50%	Ferro Corp/ Coors	Arlcite/Alumina	
Limestone	18	0.38x0.08	Colton Limestone	%Calcium Carbonate	95
				%Ash	5
Coal	2	0.64x0	Colorado Bituminous	%Moisture	6.8
				%Fixed Carbon	47.7
				%Volatile	40.6
				%Sulfur	0.5
				%Ash	4.4
				Heating Value	30 joules/kg (13,000 BTU/lb)

The bed material and combustor are initially heated above the coal combustion temperature with a natural gas burner. The hot gas from the natural gas burner enters under the grid.

Coal and Bed Material Feeder -

An auger feeder is used to control the feed rate of coal and makeup bed material from the hopper. A continuous weighing system on the hopper monitors the feed rate. The coal and bed material leaving the auger are blown into the bed with air in a transport tube.

Positive Displacement Blower -

A positive displacement blower with a capacity of 4.8 Nm^3/min at 27 kPa pressure drop provides combustion air to the AFBC.

Primary Cyclone -

The primary cyclone is designed to have 10 μmA diameter cut point for removing the large fly ash fraction, unburnt coal particles and bed material from the gas stream. The cyclone has a carbon steel shell, castable ceramic refractory and a stainless steel liner.

Gas leaving the cyclone enters a diverter valve which can be used to bypass the PxP scrubber as needed during testing. Gas bypassing the PxP scrubber is quenched and then cleaned in a venturi scrubber to meet local APCD codes.

The PxP scrubber pilot plant will be constructed as shown in the schematic of Figure 1. The bench scale experimental apparatus is presently being tested on the effluent of the AFBC.

CONCLUSIONS

The experimental data on the primary collection efficiency of the PxP system agree well with predictions based on a mathematical model which was first developed for wet scrubbers. Since the model was derived for the mechanism of particle collection by inertial impaction on spheres in a cocurrent scrubber, it is reasonable to expect it to fit the data. The PxP A.P.T. dry scrubber system has the same primary collection efficiency/power relationship as a venturi type wet scrubber.

The overall efficiency of the PxP system will depend on the reentrainment characteristics of the specific system in addition to the primary efficiency. Particle and collector properties, system geometry, flow rates, and other parameters will influence reentrainment.

Research is continuing on the experimental evaluation of the PxP system for HTP applications. The work upon which this paper is based is supported by the U.S. Environmental Protection Agency.

ACKNOWLEDGEMENT

The work described in this publication was performed under Contract No. 68-02-2164 with the U.S. Environmental Protection Agency.

REFERENCES

1. Yung, S.C., S. Calvert and H.F. Barbarika. Venturi Scrubber Performance Model. EPA-600/2-77-172. NTIS PB 271 515/AS. August 1977.

2. Calvert, S., R.G. Patterson and D.C. Drehmel. Fine Particle Collection Efficiency in the A.P.T. Dry Scrubber. Presented at the EPA/DOE Symposium on High Temperature High Pressure Particulate Control, Washington, D.C. September 1977.

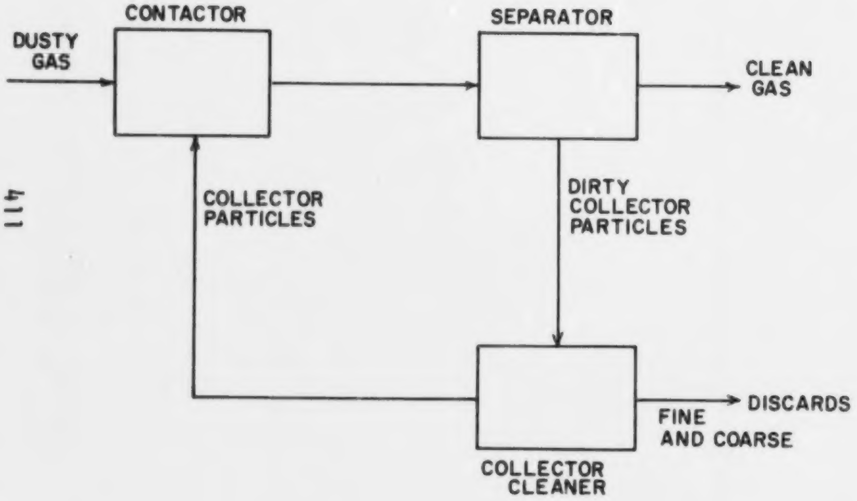
DUSTY GAS
CONTACTOR
SEPARATOR
CLEAN GAS
COLLECTOR PARTICLES
DIRTY COLLECTOR PARTICLES
COLLECTOR CLEANER
FINE AND COARSE
DISCARDS

Figure 1. Schematic diagram of A.P.T. dry scrubber system.

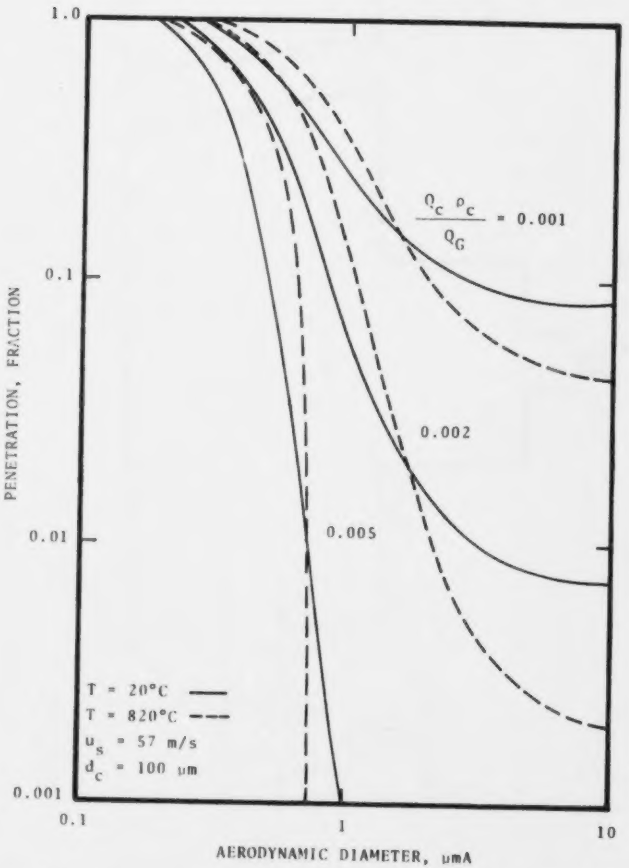

Figure 2. Theoretical particle collection characteristics of the A.P.T. dry scrubber.

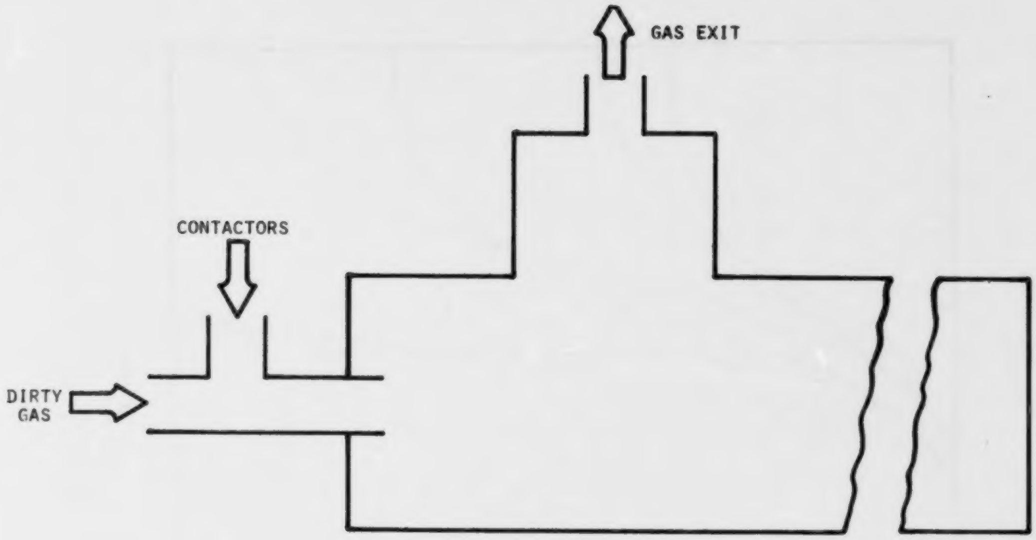
GAS EXIT
CONTACTORS
DIRTY GAS

Figure 3. Contactor and gravity separator.

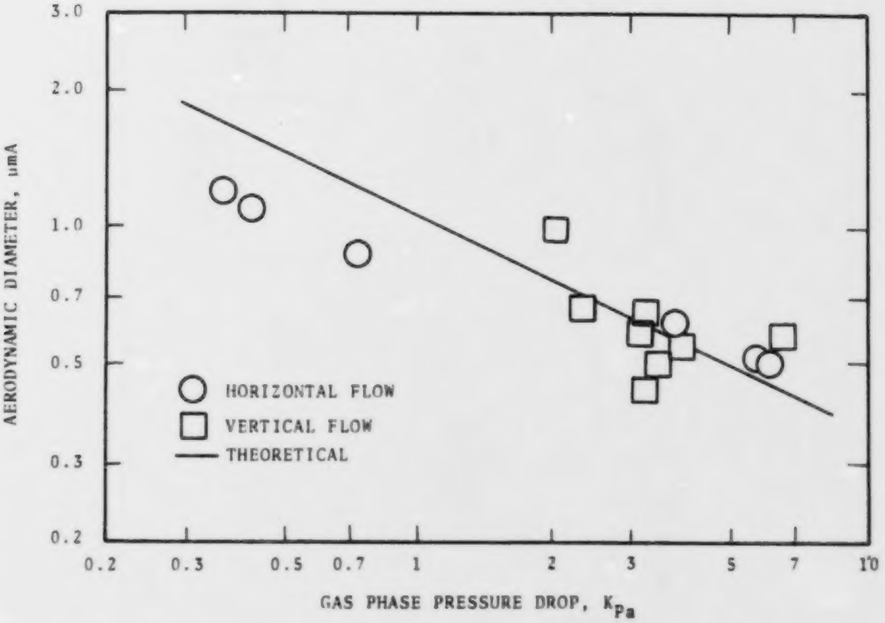

Figure 4. Comparison of particle collection characteristics of the A.P.T. dry scrubber with the A.P.T. cut/power relationship.

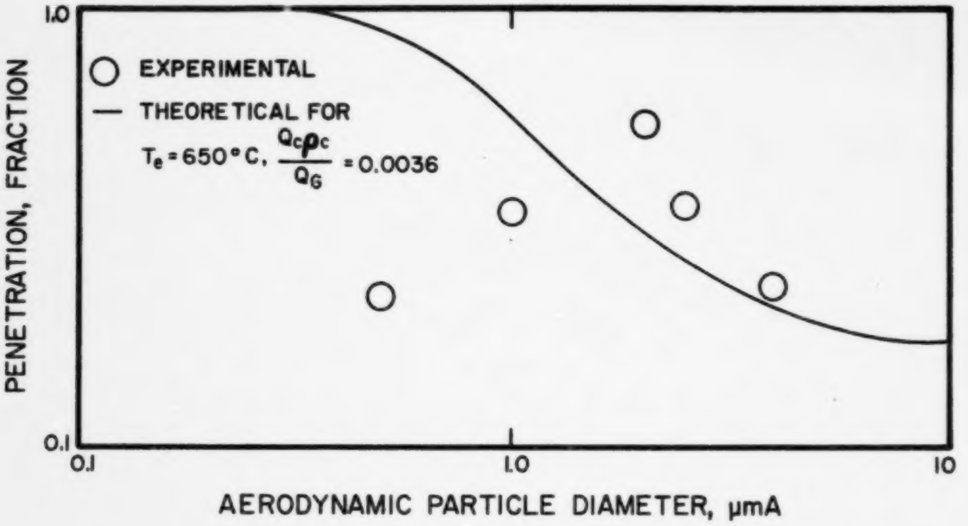

Figure 5. Particle penetration with nickel collectors.

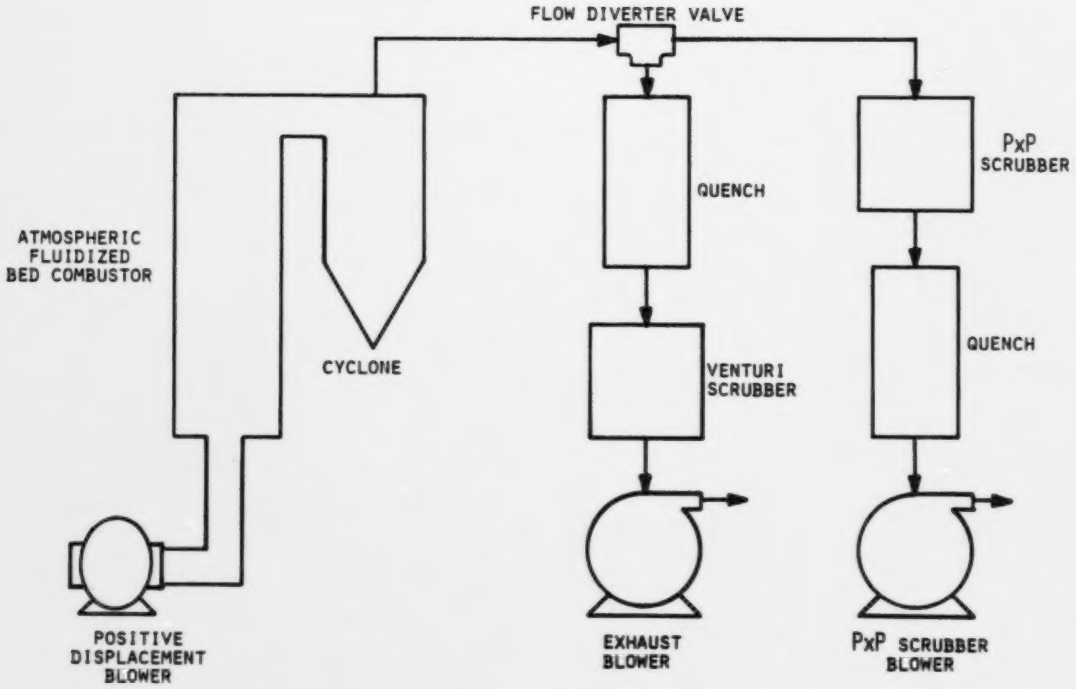
FLOW DIVERTER VALVE
QUENCH
PxP SCRUBBER
ATMOSPHERIC FLUIDIZED BED COMBUSTOR
CYCLONE
VENTURI SCRUBBER
QUENCH
POSITIVE DISPLACEMENT BLOWER
EXHAUST BLOWER
PxP SCRUBBER BLOWER

Figure 6. Phase II experimental apparatus.

ELECTROSTATIC PRECIPITATION AT HIGH TEMPERATURE AND PRESSURE: CAPABILITIES, CURIOSITIES AND QUESTIONS

Myron Robinson
Research-Cottrell
Somerville, New Jersey 08876

ABSTRACT

It is not widely appreciated - even among manufacturers of electrostatic precipitators - that precipitation is one of the more promising candidates for particle-gas separation at temperatures as high as 2000°F and pressures up to 800 psi. Corona stability and effective particle removal have been demonstrated over a broad enough range of temperatures and pressures to indicate the applicability of electrostatic gas cleanup to coal gasification and pressurized fluidized-bed combustion. Future high-temperature and pressure (HTP) R & D will properly address questions of precipitation optimization rather than feasibility. In this paper, the present state of knowledge of HTP precipitation is reviewed and salient problem areas are identified for subsequent study. These include the suppressive effect of pressure on back corona and the apparent superiority of the positive discharge for certain combinations of pressure and geometry. New high-pressure experimental data are presented.

Article not available at time of publication.

Preceding page blank

HIGH TEMPERATURE, HIGH PRESSURE ELECTROSTATIC PRECIPITATION

John R. Bush
Paul L. Feldman
Myron Robinson
Research-Cottrell
Somerville, New Jersey 08876

ABSTRACT

This **paper** presents the results of work conducted by Research-Cottrell under EPA Contract 68-02-2104.[1] The feasibility of electrostatic precipitation at temperatures and pressures varying from ambient condition to 1366 K and 3550 kPa, respectively, has been demonstrated in a laboratory wire-pipe electrode system. Stable corona discharges are obtained at all temperatures subject to appropriate choices of electrode dimension, polarity, and pressure. Current-voltage characteristics are reported for dry air, a simulated combustion gas, and a substitute fuel gas. The effects of temperature, pressure, electrode geometry and polarity on sparkover voltage, corona-starting voltage, and current are evaluated. A precipitator performance model is included to incorporate this data into a high temperature, high pressure precipitator design. This model has been evaluated for an electrostatic (HTHP) precipitator following a pressurized fluidized bed combustor at 1089 K and 920 kPa. It is recommended that prototype HTHP electrostatic precipitators be applied to pilot coal gasifiers and fluidized bed combustors to obtain detailed design data and to verify the accuracy of the performance model under actual operating conditions.

Preceding page blank

INTRODUCTION

Development of coal utilization processes, such as pressurized fluidized bed combustors or low Btu gasifiers, is considered to be of primary importance in the continuing search for alternate energy systems. The fluidized-bed combustor, for example, can be used to generate electricity using conventional steam turbines, and, when at pressure, through gas turbines. But the feasibility of particulate control at the high temperatures and pressures through electrostatic precipitation, has not been established.[2] Pressurized fluidized bed combustion, for example, requires high efficiency particulate removal ahead of the gas turbine at temperatures ranging from 950 K to 1400 K and at pressures above 700 kPa.

Of particular interest to Research-Cottrell when this research project was undertaken for the U.S. Environmental Protection Agency were the gas-cleaning requirements at extreme conditions necessary for protection of downstream equipment, such as turbines. These requirements go well beyond those for compliance with environmental emission standards.

The stated objective of the project was to determine the feasibility of electrostatic precipitators for particulate removal at the elevated temperatures and pressures associated with developing coal-conversion processes. Specifically, it was desired to:

i) Explore corona stability over temperatures and pressures ranging from ambient levels to 1366 K and 3550 kPa, respectively.

ii) Establish current-voltage characteristics (including corona starting and sparkover voltages), in terms of temperature, pressure, electrode geometry, and polarity, in a particle-free test precipitator using dry air, a simulated combustion gas, and a substitute fuel gas.

iii) Prepare preliminary design and cost data for a commercial precipitator to be used in conjunction with a pressurized fluidized bed combustor.

This study represents the first reported attempt, at any pressure, to establish a corona discharge suitable for electrostatic precipitation at as high a gas temperature as 1366 K, 1200 K being the previous maximum.[3] The highest pressure at which a precipitator has ever operated is 5500 kPa at outdoor temperature,[2] exceeding the maximum here of 3550 kPa.

FUNDAMENTALS OF HIGH TEMPERATURE, HIGH PRESSURE PRECIPITATION

The electrostatic precipitator apppears to be unique among the conventional particulate collectors such as fabric filters, cyclones, and scrubbers in that combined conditions of elevated temperature and pressure offer the potential of increased collection efficiency. Such an improvement results from the potentially higher sparkover voltages, and hence greater applied electric field strengths and particle migration velocities attainable at high relative gas densities.[4]

Until the work reported herein was completed, there existed a fundamental problem in designing a precipitator for a given high temperature, high pressure (HTHP) service. This was an incomplete knowledge of 1) the range of all variables in which a stable corona discharge can be maintained and 2) the current-voltage characteristics within that range. In particular there exists for either polarity a critical pressure, beyond which sparkover alone, without antecedent corona prevails. For positive polarity this critical pressure is sharply defined within a narrow band. For negative polarity discharge, the critical phenomena is not clearly defined and a "post-critical discharge may be found at pressures well above the critical value.

This phenomena of critical pressure is produced by two opposing effects. First, the shorter mean free paths found at elevated pressures impede ionization by collision and tend to raise the sparking level. Second, the denser packing of gas molecules renders photo-ionization more likely and reduces ion diffusion. Thus pressure facilitates streamer propogation from the anode across the gap and, at the critical pressure, sparkover results.

Another phenomena which occurs is the relatively low value of sparkover voltage for positive polarity as compared with negative polarity as pressure is increased. This can be explained as follows: Intense ionization of the gas in the high field region near the discharge electrode attracts and removes the highly mobile electrons. The remaining heavy, slow moving positive ions are repelled away from the wire towards the collecting electrode. The field on the far side of this ion cloud, affected by a positive-ion space charge distortion, is increased and, with it, the rate of ionization. These conditions are favorable for the propogation of positive streamers that continue to develop and advance towards the cathode. With negative polarity, the discharge electrode is surrounded by a positive ion space charge that shields the wire from the anode. This action reduces the effective field at the anode and thus higher voltages are required for sparking.

For HTHP precipitators, thermal ionization effects must be considered. Normally, ionization is governed by i) electronic and molecular collision processes in the presence of an electric field and ii) photon absorption. At high temperatues, thermal ionization adds new mechanisms to the system:

i) Electron-ion production by collision of gas molecules with each other. Such ionization may occur in the absence of ionized particles or of a high-intensity electric field.

ii) Photo-ionization resulting from thermal emission of the hot gas, which emits quanta in accord with the laws of black-body radiation.

The surface of the discharge electrode and of the collecting electrodes will reflect most of this radiation. Thus, photons are always available for ionization at the high temperatures.

iii) Ionization by collision with high energy electrons that have been generated by the above two processes.

Apprehensions arise for precipitation at high temperatures because significant thermal ionization rates may lead to catastrophic currents at reduced voltages. Earlier predictions that this could occur at temperatures of 1089 K have been shown experimentally to be untenable.[3] Revised work suggest that although thermal ionization may become noticeable at 1089 K, practical precipitation may be limited only by temperatures exceeding 1400-1600 K.[5] The lower limit applys to gases containing significant quantities of a component with a low ionization potential, such as potassium. Amounts of 1 atom in 10^4 could be significant to cause excessive ionization at these temperatures.

EXPERIMENTAL APPARATUS AND TEST CONDITIONS

The laboratory test precipitator used to obtain current-voltage characteristics is shown in Figure 1. This wire-pipe design was enclosed within a pressure vessel capable of operating to 3550 kPa. The top section contained a high pressure feed through bushing to connect the discharge electrode to the power supply. The lower section provided access for observations and a centering insulator support. The center section held the precipitator tube which is surrounded by a three-zone heater used to maintain the desired operating temperatures up to a maximum of 1367 K. A layer of Kaowool insulation protected the pressure vessel wall from the high temperatures.

The collection tube electrode, 7.26 cm in diameter, was made from Inconel 601 and was electrically isolated into three sections. This arrangement provided a uniform field within the center section for corona current measurements. Each end piece was flared out to prevent sparking at premature voltage levels. The discharge wire electrode also consisted of Inconel 601.

The precipitator was energized by a power supply capable of 400 kV and 60 mA. Gas was charged to the precipitator from compressed gas cylinders to obtain the desired gas compositions. Moisture levels were controlled by passing the gas through a humidifier at a specified temperature.

The experimental test plan was designed to establish ranges of stable corona generation as a function of temperature, pressure, gas composition, discharge polarity, and electrode geometry. These parameter ranges are shown in Table 1.

Temperature was varied in 278 K intervals from 533 K to 1366 K for all gas mixtures. Pressure was varied in intervals of 344 kPa from atmospheric pressure to 3550 kPa. In moving from one test condition to another, pressure was always released from the vessel to maintain thermal stability. At each pressure level, current and voltage characteristics were obtained for both negative and positive polarity.

Data were taken in the environments of three different gas compositions: air, combustion (flue) gas, and a substitute fuel gas. A substitute fuel gas mixture was chosen in place of actual fuel gas because of laboratory safety requirements. This mixture substituted helium for hydrogen and carbon dioxide for carbon monoxide. Quantities of each were controlled to simulate, as closely as possible, the important physical properties of the gas including ionic mobility and thermal conductivity. The composition for the substitute fuel gas and the combustion gas are found in Table II.

The primary data taken for each condition were current-voltage curves. Sparking voltage was determined as that voltage level maintained with light continuous sparking for a period of two minutes. Corona starting voltages were determined by two methods:

1) That voltage where the corona pips, as observed by an oscilliscope, disappeared with decreasing applied voltage; and (2) extrapolation of the current-voltage curves to very low current levels. At high temperatures where thermal ionization is present only method (2) could be used.

RESULTS

The experimental data, consisting of linear current denisty (mA/m) vs the impressed voltaged (kV) are reproduced in Figure 2 through 5 for dry air, Figure 6 for combustion gas, and Figure 7 for the substitute fuel gas. The corona starting and sparkover voltages, obtained from those curves and from independent measurements, are shown as functions of the gas density, δ, relative to ambient conditions of 278 K and atmospheric pressure, in Figures 8 and 9 for simulated combustion gas and substitute fuel gas.

The first objective, being also the most important, is to establish whether any temperature or pressure limitations exist for stable corona discharge. Such limitations may be caused by: i) excessive currents at low voltage resulting from thermal ionization and ii) the disappearance of stable corona due to the manifestation of the critical pressure.

Examination of the data shows no catastrophic currents at high temperatures under any conditions. This is evident over the full range of experimental pressures, temperatures, and polarities.

It might be expected that runaway currents at low voltages would be most likely to occur at the lowest gas densities (or highest temperature at atmospheric pressure). However, for negative corona at δ less than unity, the reverse is generally true, i.e., the pre-sparkover currents are much less than at higher densities. For positive polarity the low density currents are mixed, there are still no runaway currents. The problem of high gas conductivity associated with low densities has not arisen.

TABLE I. Test Variables

Temperature:	Ambient to 1366 K
Pressure:	Atmospheric to 3550 kPa
Discharge Electrode Diameter:	1.58 mm, 2.34 mm, 3.18 mm
Discharge Polarity:	+, -
Gas Composition;	Air, Combustion Gas, Substitute Fuel Gas

TABLE II. Gas Composition (Volume %)

Component	Substitute Fuel Gas	Combustion Gas
CO_2	23.0	9.2
He	18.5	--
O_2	--	2.8
N_2	53.5	83.0
H_2O	5.0	5.0

On the basis of earlier critical pressure studies[6], it might be supposed that the critical pressure phenomena would set an upper pressure limit to the positive corona discharge and that this critical pressure would increase with temperature. This effect can be observed in the data over the entire temperature span, for positive polarity. The negative critical pressure, as explained earlier, is expected to be higher than the positive, maintaining all other parameters constant. From the families of curves obtained, one can see that the negative critical pressure always exceeds the positive. It is further apparent that, as the critical pressure increases with temperature, a much wider range of pressures has stable corona at higher temperatures.

Evaluation of sparking voltages versus gas density for positive and negative polarity in Figure 2-5 reveals a tendency for the positive sparkover voltage to exceed the negative for temperatures above 533 K and low air densities (below ∿ 2). This effect is not unequivocal, but the trend seems clear when supported by results of earlier workers. The significantly higher negative than positive currents prevailing at a given voltage at high temperatures are unmistakable.

For the case of substitute fuel gas (Figure 9) the positive sparkover exceeds the negative, over the complete temperature range evaluated, up to a relative density of 6 or 7. For combustion gas the transition occurs at a density of 4 for temperatures above 1089 K (Figure 8).

As temperature and pressure are increased together, for all experimental situations, it is clear from the data that precipitation is possible at significantly higher voltages than at normal conditions. This is an important fact when assessing the viability of electrostatic precipitation for HTHP particulate removal applications, especially as compared to other collection devices, because the rate of particle collection is roughly proportional to the square of the electric field strength within the precipitator. Thus the net effect of higher operating voltages is either a proportionally larger increase in particle collection efficiency or a corresponding decrease in the required precipitator size for a specific efficiency. Thus precipitation becomes more efficient as temperature and pressure increase together. Other devices, such as cyclones or filters, do not benefit from high temperature and pressure due to the increasing gas viscosity and decreasing molecular mean free path. The higher voltage in HTHP electrostatic precipitation greatly overrides these effects.

MODEL PRECIPITATOR PERFORMANCE AT HIGH TEMPERATURE AND PRESSURE

The collection efficiency of a precipitator at high temperature and pressure can be modeled, provided that the properties of the gases and particulate are known for these conditions. A performance equation, based upon a modified Deutsch equation for efficiency, has been developed by P. L. Feldman,[7] as follows: The Deutsch equation can be written in expanded form.

$$1-\eta_i = \exp\ -(\varepsilon_o E_o E_p/3\mu)(A/Q)(a_i C_i d_i) \qquad (1)$$

where η_i = fraction collection efficiency for particle size d_i - dimensionless
A/Q = specific collection area $-m^2/m^3/s$
ε_o = permitivity of free space = 8.85×10^{12} F/m
E_o = charging field strength -V/m
E_p = collection field strength -V/m
C_i = Cunningham slip factor -dimensionless
$= (1 + 2.5\ \lambda/d_i + 0.84\ \lambda/d_i \exp(-0.435\ d_i/\lambda))$
a_i = parameter derived from Cochet equation for particle charging -dimensionless
$= (1 + 2\lambda/d_i)^2 + 2/(1 + 2\ \lambda/d_i)$
d_i = particle diameter -m
μ = gas viscosity at temperature and pressure -decapoise = kg/m-sec
λ = mean free path of gas molecules at temperature and pressure -m

By integrating equation (1) over the inlet particle size distribution f(i), an overall precipitator efficiency (η) can be obtained:

$$(1 - \overline{\eta}) = \int_0^{\infty} (1 - \eta_i)\ f(i)\ d\ (d_i/d) \qquad (2)$$

Letting $k = \varepsilon_o E_o E_p\ A/3\mu Q$ and $g_i = a_i C_i d_i$ in equation (1) and assuming a log-normal particle size distribution, equation (2) can be expressed as follows:

$$(1 - \overline{\eta}) = (1/2\pi\ \ln \sigma) \int_0^{\infty} \exp\ (-kg_i$$
$$-0.5\ (\ln\ (d_i/d)/\ln \sigma)^2)\ d(\ln d_i/d) \qquad (3)$$

where σ = geometric standard deviation of particle size
d= mass mean particle diameter

This expression can be solved numerically to yield values of k vs ln $(1-\overline{\eta})$ which can be plotted on log-log paper to yield a straight line, whose equation is as follows:

$$1 - \overline{\eta} = C(10^{-6}k)^{m} \qquad (4)$$

where m is slope of line = $\ln(\ln(1-\overline{\eta})/\ln(1-\eta_o))/\ln(k/k_o)$

and $C = 1-\overline{\eta}_o$ @ $k_o = 10^6\ m^{-1}$

In equation (4), k is a parameter having no terms dependent upon particle size, only on the precipitator design and gas conditions. All terms containing size dependent factors are found in the parameters C and m, which need to be determined for each particle size distribution. The term k thus relates the specific collection area directly to the charging and collecting fields at the gas conditions of temperature and pressure independent of particle size.

PRECIPITATOR DESIGN FOR PRESSURIZED FLUIDIZED BED COMBUSTION

Highly efficient particulate removal following a pressurized fluidized bed combustor is essential for minimizing effects on turbine blade erosion and for meeting environmental regulations. Temperature and pressures being planned for control of particulate have been reported as 1000 K - 1200 K and 900 to 1000 kPa.[8] For example, using the conditions found for the Exxon miniplant combustor,[8] the performance of a HTHP electrostatic precipitator can be evaluated based upon equation (4), the properties of the gas mixture, and the flue gas particulate distribution.

The gas composition from the miniplant, showing major components, is found in Table III:

Using a temperature of 1089 K and a pressure of 920 kPa, the viscosity μ and mean free paths λ are calculated to be

$\mu = 4.58 \times 10^{-5}$ decapoise
$\lambda = 3.365 \times 10^{-8}$ m

TABLE III. Exxon Miniplant Flue Gas Composition (Approximate)

Component	% By Volume
N_2	78
CO_2	13.5
O_2	3
H_2O	5.5

The particulate in the flue gas has been reported by Hoke[8] to have a mean diameter $\bar{d}$ of 6 microns with a geometric standard deviation σ of 2.72.

Using these values in equation 3, values of $1-\bar{\eta}$ and k have been computed. These are plotted on log-log paper as $-\ln(1-\bar{\eta})$ vs k ($10^6 m^{-1}$) to yield a straight line with general formula as equation (4). Finding the slope m = 0.522 and C to be 0.0055, the overall efficiency can be expressed as:

$$1 - \bar{\eta} = 0.0055^{(10^{-6} k)^{0.522}} \tag{5}$$

For 99% collection efficiency, the precipitator constant k must be $0.79 \times 10^6 \ m^{-1}$. Using the definition of $k = \varepsilon_o E_o E_p A/3\mu Q$ and assuming $E_o = E_p$ for this purpose, one can determine the specific collection area by knowing the field strength that can be applied, as estimated from Figure 6-g. For a field strength of E = 800,000 V/m, the required specific collection area is $19.5 \ m^2/m^3/s$. Assuming a velocity of 1.5 m/sec and a pipe diameter of 0.203 m, the length of pipe required would be 1.5 m.

This leaves the discharge electrode to be specified. For a wire pipe system, the discharge electrode radius will be determined using Peek's equation for establishing corona starting fields and using an expression defining the electric field at the wire surface as a function of applied voltage.

$$E_c = m\ \delta\ (A + B/(r\delta)^{1/2}) \tag{6}$$

$$E_c = V/\ r \ln (R/r) \tag{7}$$

where

A = constant, for air = 32.2×10^5 V/m
B = constant, for air = 8.4×10^4 $V/m^{1/2}$
δ = relative gas density
r = wire radius
R = pipe radius
m = surface "roughness" factor = 0.8

Using R = 0.102 m and V = 80,000 V, the two equations can be solved simultaneously to yield a value of r for the discharge electrode of 0.0026 m. The discharge electrode, whether rigid or wire, should incorporate this effective value of r into the design.

The HTHP precipitator design needs to be evaluated for cost. The pressure vessel may be of a diameter requiring field fabrication or possibly two smaller shop fabricated vessels can be considered. The insulation thickness, material, and method of installation must be considered. The internal materials at high temperatures will require special alloys to resist oxidation and corrosion. For high pressures and wide dimensions, higher voltage power supplies will be required. All of these factors must be considered in developing a cost effective design for HTHP precipitation.

CONCLUSIONS

The laboratory program for HTHP electrostatic precipitation has verified the following conclusions:

1. There are no temperature or pressure limitations to electrostatic precipitation over the range studied.
2. Precipitation becomes more efficient with increasing temperature and pressure. This is in direct contrast to the trend of other particulate collection devices.
3. Critical pressure increases with temperature.
4. Negative critical pressure is higher than positive.
5. Negative currents are higher than positive in most cases.

REFERENCES

1. J. R. Bush, P. L. Feldman, M. Robinson, "Development of a High Temperature, High Pressure Electrostatic Precipitator," EPA-600/7-77-132, November, 1977.
2. M. Robinson, "Electrostatic Precipitation" in Air Pollution Control, W. Strauss, ed., Vol. 1, Wiley Interscience, New York, 1971, pp 227-335.
3. R. F. Brown, "An Experimental High Temperature High Pressure Electrostatic Precipitator Module Design and Evaluation," Research-Cottrell, Inc., Bound Brook, NJ, 1969.
4. F. W. Schmitz, "Electrostatic Precipitation up to 1300°F & 100 PSIG Pilot Plant Tests on Fluidized Bed Combustor," Research-Cottrell, Inc., Bound Brook, NJ, May, 1963.

5. Cooperman, P. "Spontaneous Ionization of Gases at High Temperature," Paper ES-MON-6, Inst. Electron Engrs., 1971.

6. M. Robinson, "Critical Pressures of the Positive Corona Between Concentric Cylinders in Air," J. Appl. Phys. 40, 5107-5112 (1969).

7. P. L. Feldman, "Effects of Particle Size Distribution on the Performance of Electrostatic Precipitators", Research-Cottrell, Inc., Presented at APCA Meeting, Boston, 1975.

8. Hoke, et al., "Studies of the Pressurized Fluidized Bed Coal Combustion Process," EPA-600/7-77-107, September, 1977.

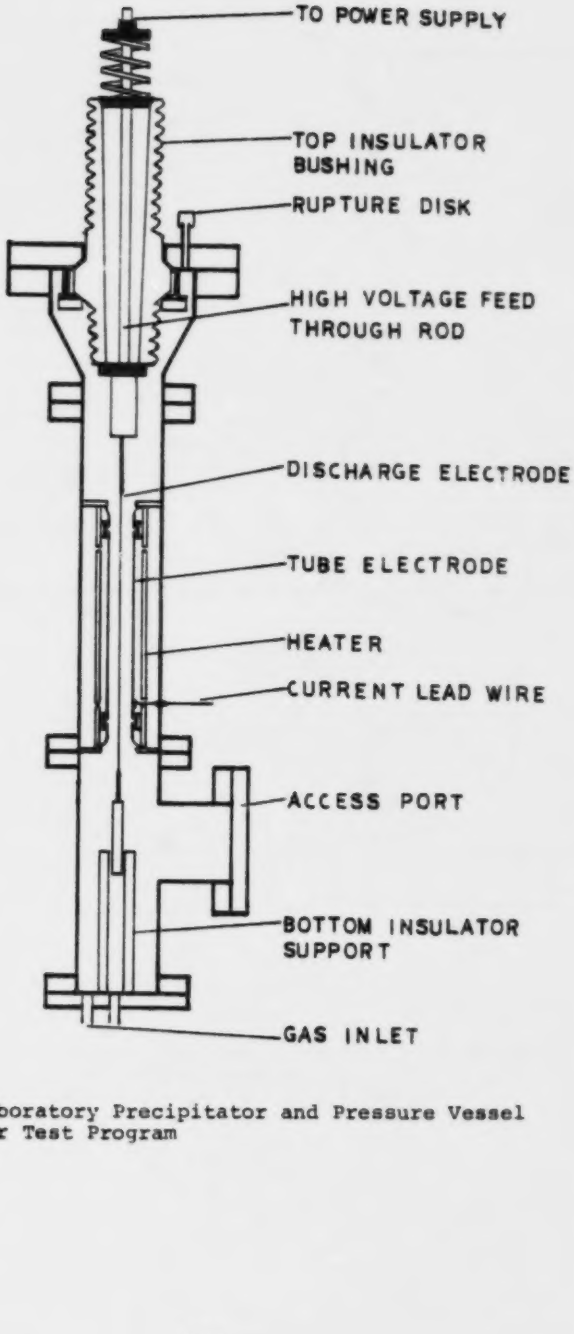
TO POWER SUPPLY
TOP INSULATOR BUSHING
RUPTURE DISK
HIGH VOLTAGE FEED THROUGH ROD
DISCHARGE ELECTRODE
TUBE ELECTRODE
HEATER
CURRENT LEAD WIRE
ACCESS PORT
BOTTOM INSULATOR SUPPORT
GAS INLET

Figure 1. Laboratory Precipitator and Pressure Vessel for Test Program

Reproduced from
best available copy.

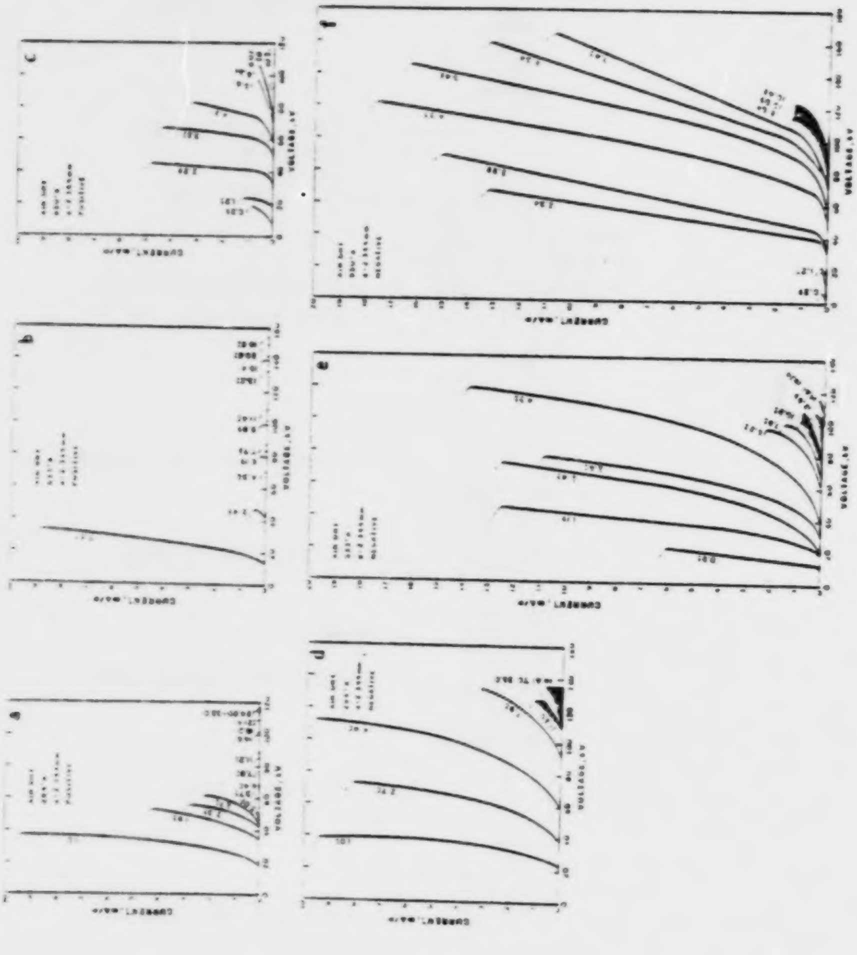

Figure 2. Current-Voltage and Density Curves Taken in Dry Air at Temperatures of 294 K, 533 K, and 950 K for a 2.344 mm Wire Electrode

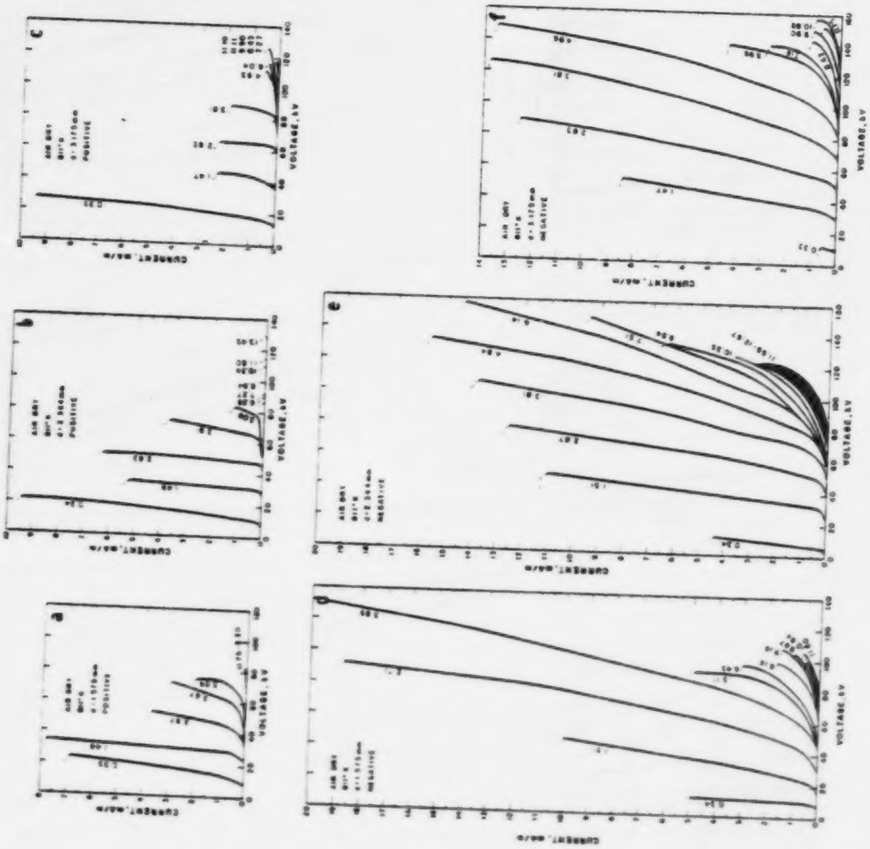

Figure 3. Current-Voltage and Density Curves Taken in Air at a Temperature of 811 K for Wire Electrodes of 1.575 mm, 2.344 mm, and 3.175 mm.

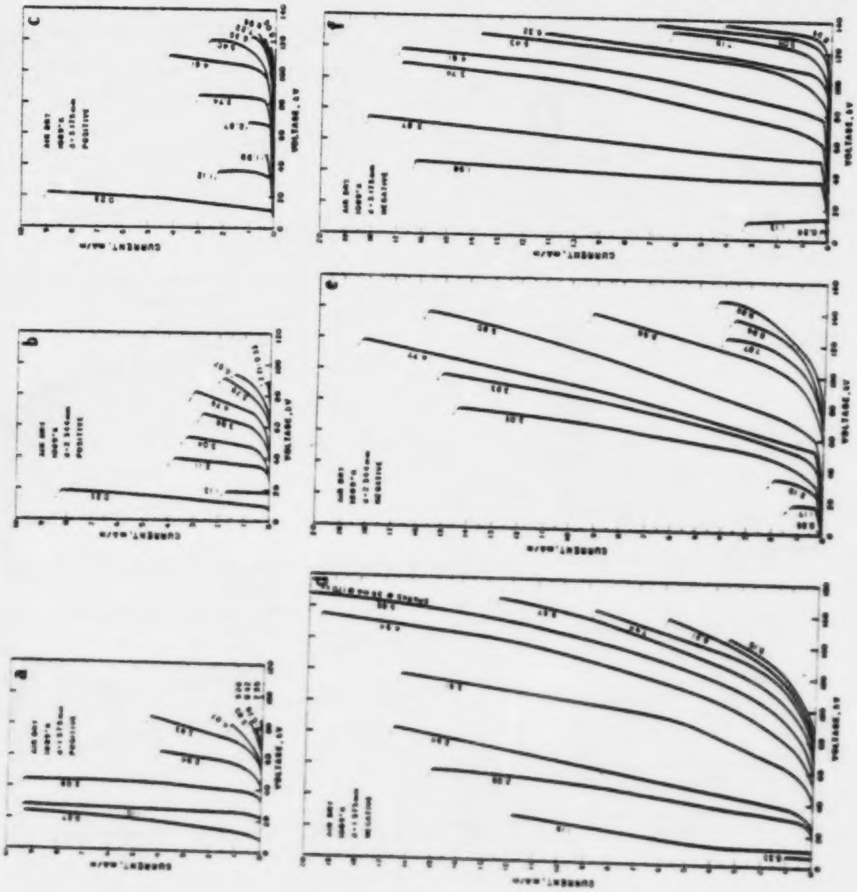

Figure 4. Current-Voltage and Density Curves taken in Air at a Temperature of 1089 K for Wire Electrodes of 1.575 mm, and 3.175 mm.

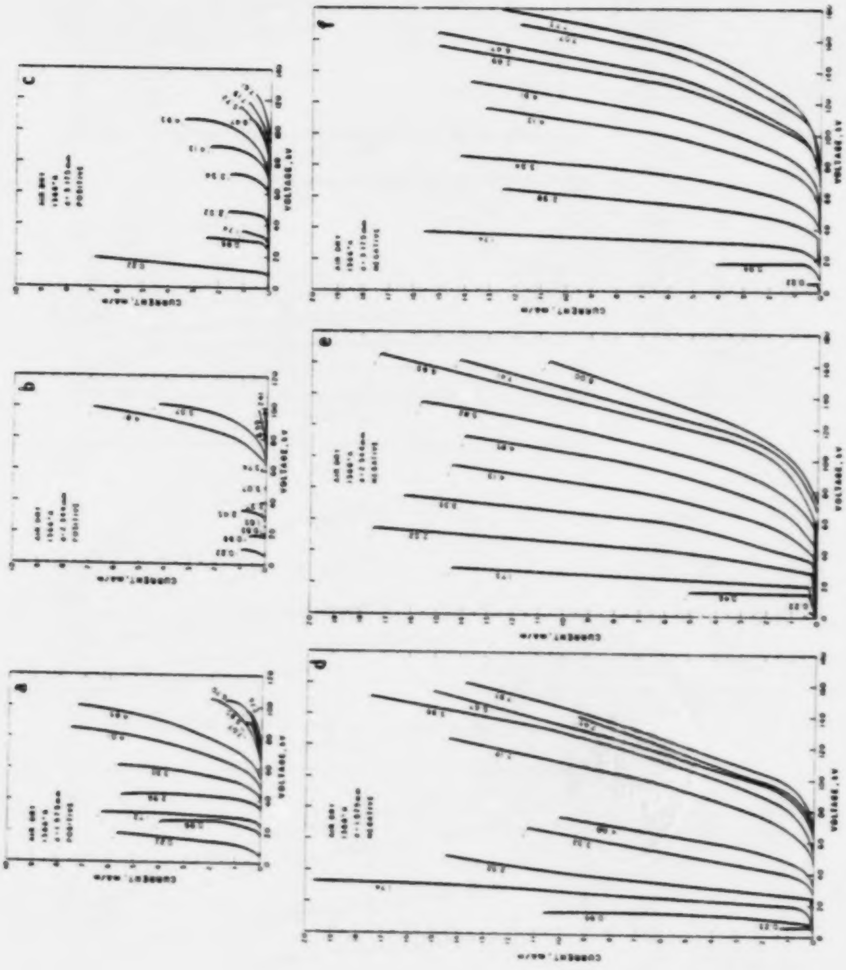

Figure 5. Current-Voltage and Density Curves Taken in Air at a Temperature of 1366 K for Wire Electrodes at 1.575 mm, 2.344 mm, and 3.175 mm.

Reproduced from best available copy.

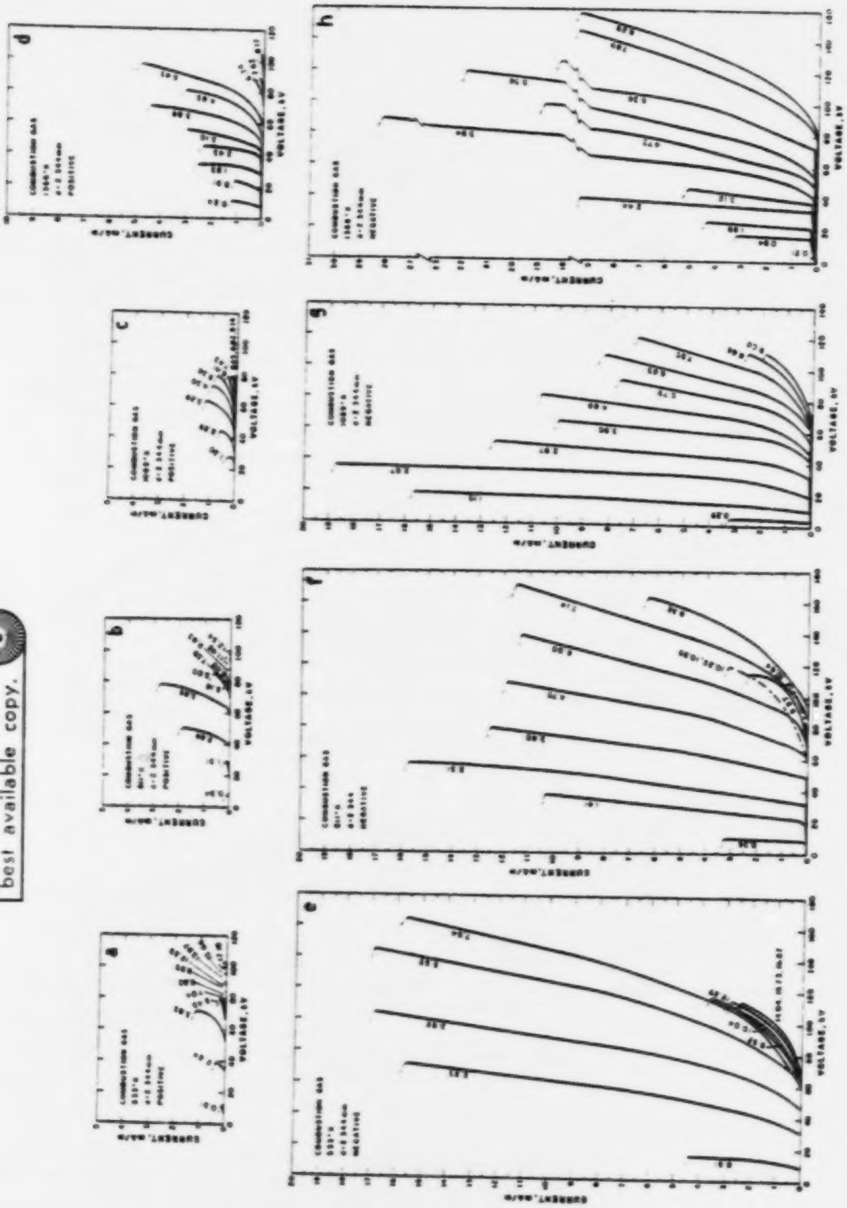

Figure 6. Current-Voltage and Density Curves Taken in a Simulated Combustion Gas Mixture for Temperatures of 533 K, 1089 K, and 1366 K using a 2.344 mm Wire Electrode

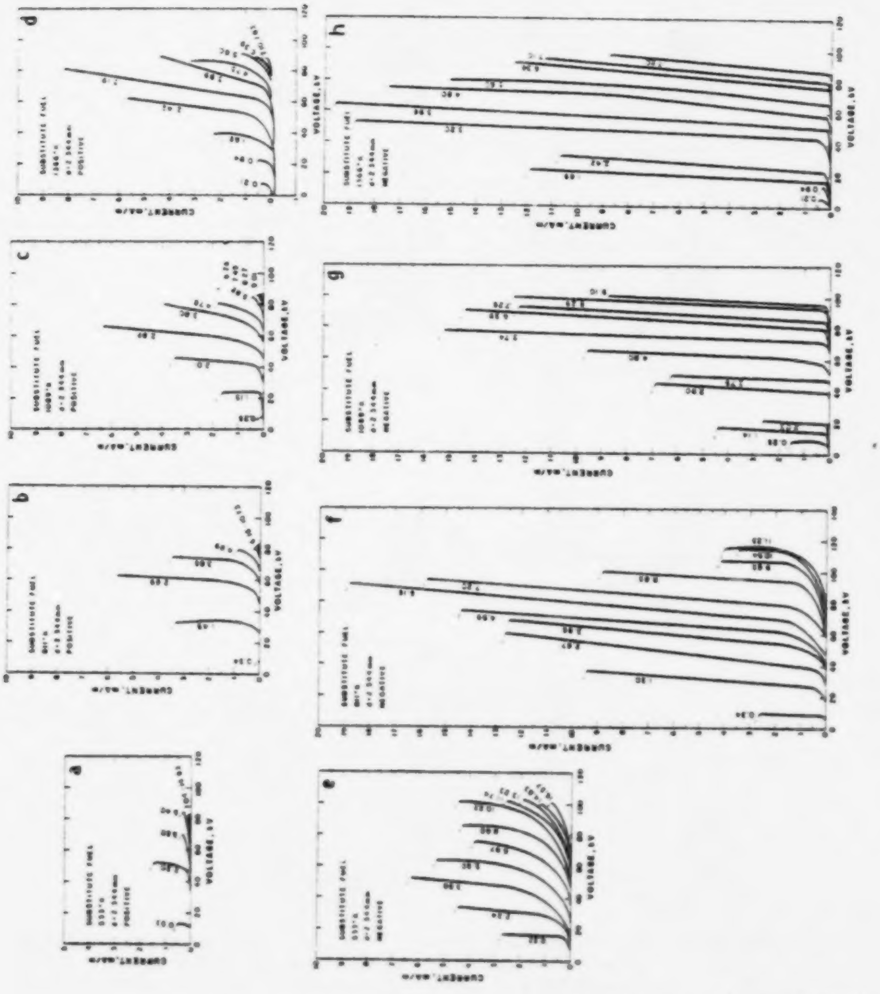

Figure 7. Current-Voltage and Density Curves Taken with a Substitute Fuel Gas Mixture at Temperature of 533 K and 1366 K for a 2.344 mm Wire Electrode

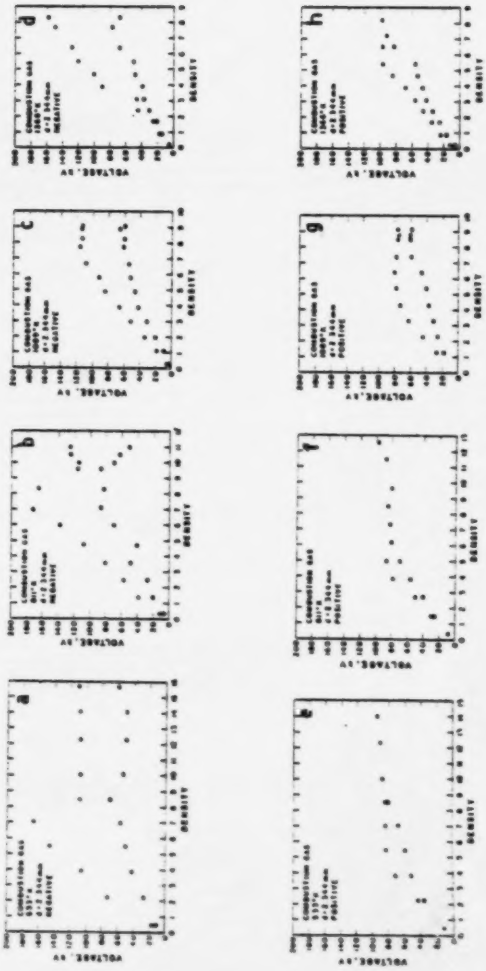

Figure 8. Sparking and Corona Starting Voltages for a Simulated Combustion Gas Mixture as a Function og Relative Gas Denisty at 533 K, 811 K, 1089 K, and 1366 K for a 2.344 mm Wire Electrode

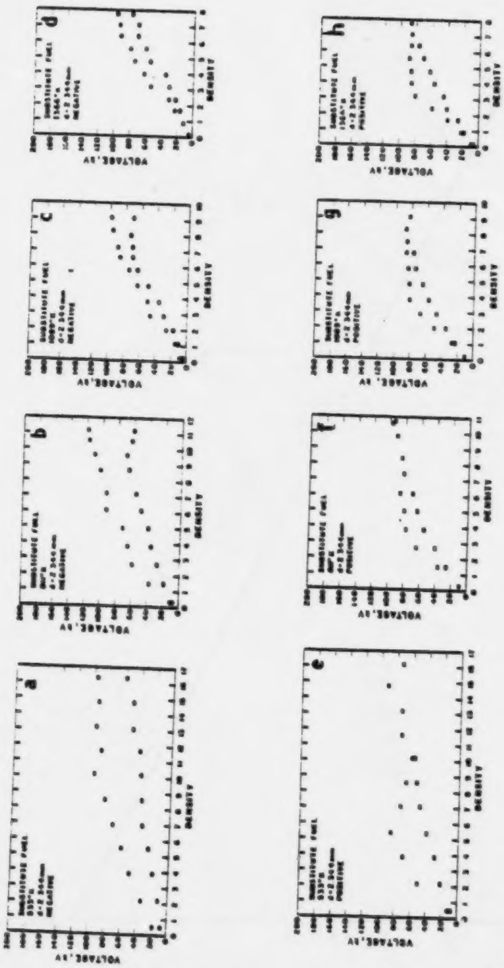

Figure 9. Sparking and Corona Starting Voltages in a Substitute Fuel Gas Mixture as a Function of Relative Gas Density at 533 K, 811 K, 1089 K, and 1366 K for a 2.344 mm Wire Electrode

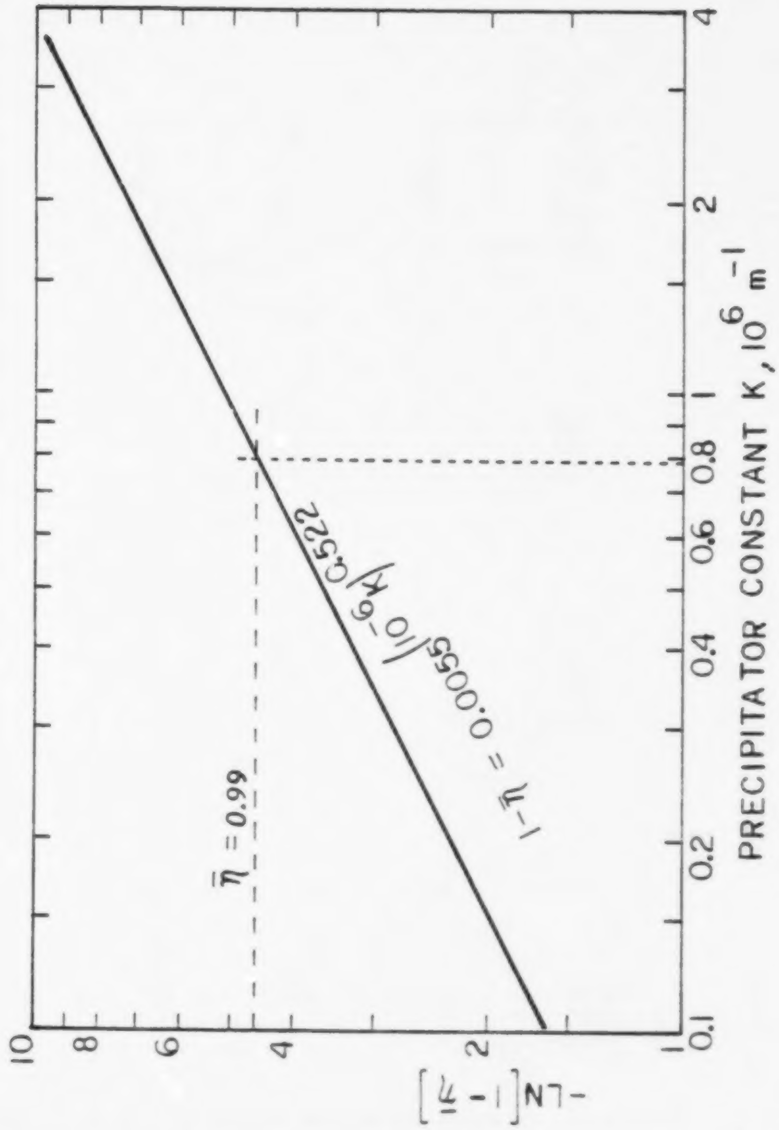

Figure 10. Precipitator Performance Design for Exxon Mini-plant Pressurized Fluidized Bed Combustion with Conditions of T = 1089 K, P = 910 kPa, $\bar{d}$ = 6 microns, σ = 2.72.

BARRIER FILTRATION FOR HTHP PARTICULATE CONTROL

Michael A. Shackleton
Acurex Corporation
485 Clyde Avenue
Mt. View, CA 94042

Dr. Dennis C. Drehmel
U.S. Environmental Protection Agency
Research Triangle Park, NC 27711

ABSTRACT

Research at bench scale has shown that fine particle control at high temperature and pressure can be achieved using barrier filtration by ceramic fiber filters. Evidence supporting this contention includes: (1)"blanket" ceramic fiber materials (felts) consisting of small diameter fibers (3.0 micrometers) appear to be the most promising materials for high temperature and high pressure applications because of their combination of good filtration performance and relatively high strength; (2) accelerated media cleaning tests at high temperatures and pressures show that several ceramic filter structures are capable of surviving in excess of 50,000 cleaning pulses while maintaining pressure drop at acceptable levels; (3) flyash dust feeding tests of 200 hours duration showed high collection efficiency (99.99 percent) and control of pressure drop even at high dust concentrations over a range of filter face velocity from 2.5 to 9 cm/sec.

INTRODUCTION

The need for hot gas cleanup associated with the development of advanced coal utilization technology such as pressurized fluidized bed combustion (PFBC) and gasification combined cycle plants has been apparent for several years. Unfortunately, current trends in the development of (PFBC) technology indicate there is a continuing hope that turbines can be adequately protected with particle removal from staged inertial separation devices. Military experience does not support this hope. Helicopter turbine engines have been fitted with small high efficiency 2.5 cm diameter cyclone tube banks to extend service life from unacceptable to moderately acceptable in this application, where dust loading is intermittent. The U.S. Army XM-1 Main Battle Tank is turbine powered. It employs a barrier filter system with a cyclone tube bank precleaner capable of providing engine intake air as clean as that required of heavy duty diesel engines. In the world's most severe dust conditions (Yuma Proving Ground, Yuma, Arizona), dust loadings at the rear deck of a tracked vehicle are about 17 g/Nm^3. Dust loadings in excess of this are encountered in the exhaust of the PFBC.

Predictions of the tolerance of large turbines to particulate loading have been made analytically by E. F. Sverdrup from the Westinghouse Research and Development Center and were published in March 1978.[1] Sverdrup's calculations indicate that cleaning of turbine expansion gas to a level of 4.6 mg/Nm^3 (0.002 grains/SCF) with all particles larger than 6 m removed is the current best estimate of the level of cleanliness needed for turbines. This analysis resulted in a maximum blade erosion of 0.10 inch in 10,000 hours of operation. This level of cleanliness is approximately 80 times less than the exit loading expected from three cyclones in series. Filtration tests at Acurex have shown removal efficiencies which resulted in a particulate exit loading considerably lower than that specified by Westinghouse.

Nearly every particulate removal device type has been proposed for HTHP application. These have included acoustic agglomerators, molten salt scrubbers, varieties of cyclones, granular beds, HTHP electrostatic precipitators and ceramic filters. Professor E. Weber from the University of Essen has published a review paper entitled "Problems of Gas Purification Occurring in the use of New Technologies for Power Generation."[2] In his paper, Professor Weber concludes that gravity and momentum force separators will not adequately remove particles from HTHP gas streams and will, therefore, be limited to use as precleaners. He also states that the required degree of cleaning can be achieved using fabric filters, and points out that fibrous materials are available which can withstand the temperatures expected in PFBC applications.

Granular bed filters have been considered the best available option for HTHP particulate control. Recent tests at the Exxon Miniplant[3] have shown that many problems remain to be solved to achieve high efficiency and long life in these devices.

Many of the particle removal devices which have been proposed for HTHP applications remove particles primarily through the mechanism of inertial impaction. These devices include all forms of cyclones, scrubbers and granular beds. Because gas viscosity increases with increasing temperature, performance of all inertial devices can be predicted to be worse at HTHP conditions than at room ambient conditions. Barrier filtration on the other hand is unique in that a theoretical basis exists to predict improved performance at high temperature and pressure conditions. This improvement results from the use of fine (3 μm) diameter ceramic fibers to construct the filter. Conventional filter media usually employ fibers of 10 to 20 μm in diameter. The fine diameter fibers increase the efficiency of the filter enough to overcome the adverse effects of increased temperature.

In August of 1976, Acurex began a program under EPA contract 68-02-2169 to demonstrate the feasibility of employing available ceramic fibers to the problem of high temperature and pressure filtration. Under the two year contract:

- The theory of barrier filtration was examined;
- A wide spectrum of ceramic papers, cloth and blanket felts were tested for filtration performance at room ambient conditions;
- Promising media from room ambient tests were subjected to accelerated cleaning tests at HTHP conditions for 50,000 cleaning pulses;
- The "best" media was tested under simulated PFBC conditions feeding flyash for 200 hours to determine filtration efficiency, pressure drop and cleanability as a function of air-to-cloth ratio.

Results of this program which demonstrated feasibility of HTHP filtration at air-to-cloth ratio up to 9 cm/sec are summarized below.

Filtration Theory Review

The theory of barrier filtration has been presented in many sources. The method used in this program was based on work by Torgeson, Whitby and Iinoya for single fibers and fiber beds. This method is described in the EPA Scrubber Handbook[4]. Key findings of the analysis were that low solidity ($\gamma = 0.02$) (the ratio of filter volume occupied by fiber) fine fiber beds could be expected to provide high filtration efficiency for fine particles; that is, even when loosely packed, fine (3 µm) diameter ceramic fibers should provide high efficiency filtration performance. Results of this analysis showing that low solidity fine fiber ceramic filters theoretically capture 0.5 µm particles at 90 percent efficiency were reported earlier[5]. The analysis also indicated that filters could be designed to operate at filter face velocity of up to perhaps 15 cm/sec and still maintain high efficiency.

Room Ambient Filter Media Tests

A large number of ceramic fiber filter media candidates were subjected to a series of filtration tests at room ambient conditions. These tests included some examples of conventional filter media for comparison. Included among the tests were:

- Dioctylphtalate (DOP) smoke penetration as a function of airflow velocity;
- Determination of maximum pore size (in micrometers);
- Measurement of permeability;
- Flat-sheet dust loading tests using A.C. fine test dust, (a standard 0 to 80 µm classified Arizona road dust). Overall collection efficiency and dust loading required to develop 3.7 kPa (15 inches H_2O) pressure drop are determined from this test which is operated at 10 cm/sec (20 ft/min) air-to-cloth ratio.

This data revealed which of the available ceramic media candidates would most likely provide good filtration performance. The data is provided in detail in EPA-600/7-78-194 and has also been reported previously.[6] A summary of findings from these tests is given below:

- Several of the ceramic paper and felt materials are capable of removing fine particles at high efficiency without excessive filter weights;
- The ceramic paper and felt materials have filtration characteristics and performed similarly to paper and felt commercial filter media in a series of filter media tests;
- The ceramic woven materials in general were characterized by large pores and poor collection efficiency in the dust loading tests. The range of parameters exhibited by the various materials, however, indicates that an acceptable woven ceramic filter media can probably be fabricated; but such filter media would have the same limitations as currently available woven filters. That is, acceptable performance would only occur at low air-to-cloth ratios.
- "Blanket" ceramic fiber materials (felts) consisting of small diameter fibers (3.0 μm) appear to be the most promising materials for high temperature and pressure tests because of their combination of good filtration performance and relatively high strength.

High Temperature/Pressure Mechanical Durability Tests

Two major questions concerning the suitability of ceramic fibers for HTHP filtration needed to be answered:

1. How durable are ceramic fiber structures when subjected to environmental conditions associated with filtration applications?
2. How well do ceramic fibers perform as filters in the HTHP environment?

Concerning the first of these questions, three ceramic filter media configurations survived a test during which the filter elements were subjected to 50,000 cleaning pulses. The objective of these tests was to simulate approximately 1 year of operation of mechanical cleaning loads on the media at high temperature and pressure. These tests showed that the low solidity fine fiber bed filters were undamaged by pulse cleaning loads. They also showed that the flyash dust cake was deposited essentially on the surface of the low solidity fiber bed media. Details of these tests were also reported earlier and in EPA-600/7-78-194.

High Temperature/Pressure Filtration Tests

Filter performance tests were intended to simulate actual filter operation at high temperatures and pressure for a period of 200 hours. The filter media configuration which we have selected as most promising consists of an approximately 1 cm thick layer of Saffil alumina blanket insulation material. This ceramic material was contained between two layers of knit 304 stainless steel screen. The stainless steel screen was suitable for these relatively short tests but will probably not survive long term exposure to the PFBC environment. However, we have fabricated similar filter elements substituting the stainless screen with a ceramic screen made using a leno weave. The ceramic screen and media filter elements have not as yet been tested but we are confident that they will be satisfactory.

Three 200 hour tests were attempted and completed. The tests were performed at a media face velocity of 2.5 (5 ft/min), 9 (18 ft/min) and 4.8 (9.5 ft/min) cm/sec and were performed in that order.

The first 200 hour test was performed at a nominal air-to-cloth ratio of 5 to 1 (2.54 cm/sec). Pulse duration was 150 msec. Pulse interval was one cleaning cycle every 10 minutes. Pulse pressure was 1100 kPa. Cleaning was performed "offline" with a 4 second bleed down followed by reverse flow for 2 seconds, the pulse superimposed followed by a 2 second settling period prior to continuing the filtration cycle. We now feel that the reverse flow portion of the cleaning cycle is unnecessary and offline pulse cleaning will be sufficient.

Exxon Miniplant flyash was used as the test dust. A fine dust D_{50} = 4 μM was used for the first 75 hours. When this dust was no longer available a coarse sample D_{50} = 19 μM was used for the remainder of the test.

Cumulative dust fed, total dust collected downstream and overall collection efficiency by mass are plotted as function of time on Figures 1, 2 and 3. For this test the inlet concentration was high (an overall average of 14.4 g/Nm^3). Shortly after the fine dust was substituted with the coarse, overall efficiency was reduced and the rate of penetration in weight per unit time was increased. Later in the test at about 120 hours and again at 150 hours the rate of dust feeding was reduced. The rate of penetration seemed to follow this. These occurrences are consistent with leakage through a defect mechanism in the media. Visual examination of the inside surface of media after the test revealed it to be substantially clean with some localized staining. Overall collection efficiency remained high throughout the test, never falling below 99.964 percent.

Outlet concentration as a function of time is shown on Figure 4. These results are lower on a mass basis than turbine requirements as reported by Sverdrup in EPA 600/9-78-004. The outlet concentrations for this first test were based on a flow of 0.566 Nm^3 per minute during the

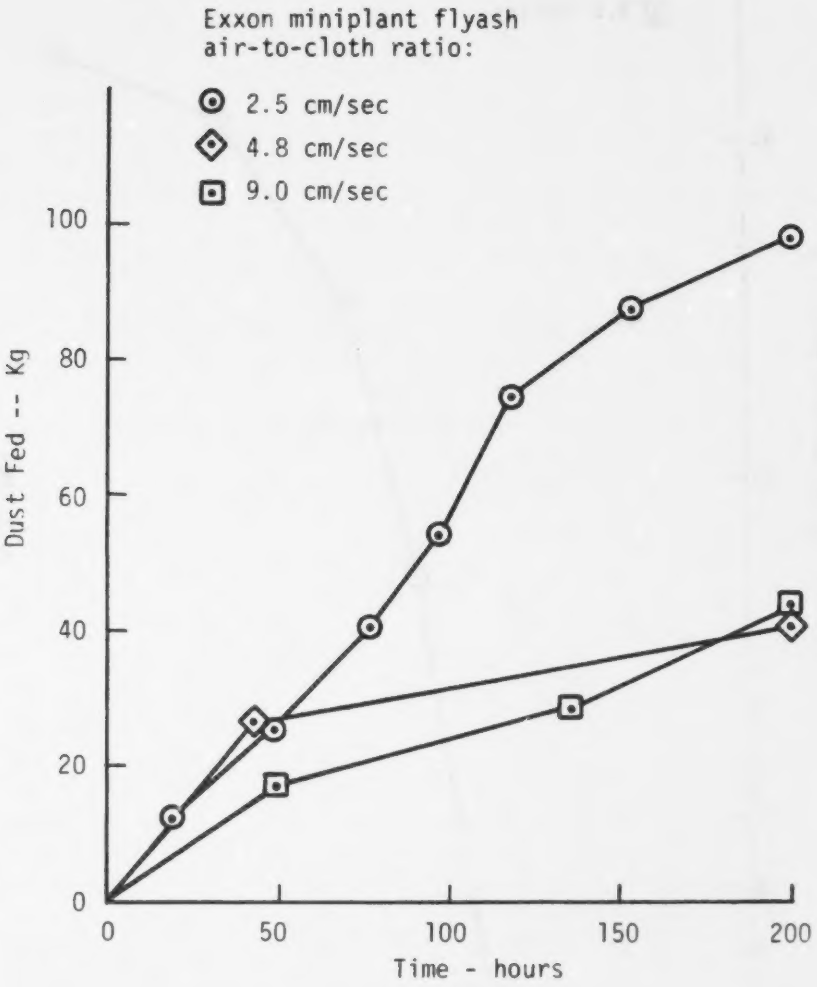

A-21850

Figure 1. Cumulative dust FED.

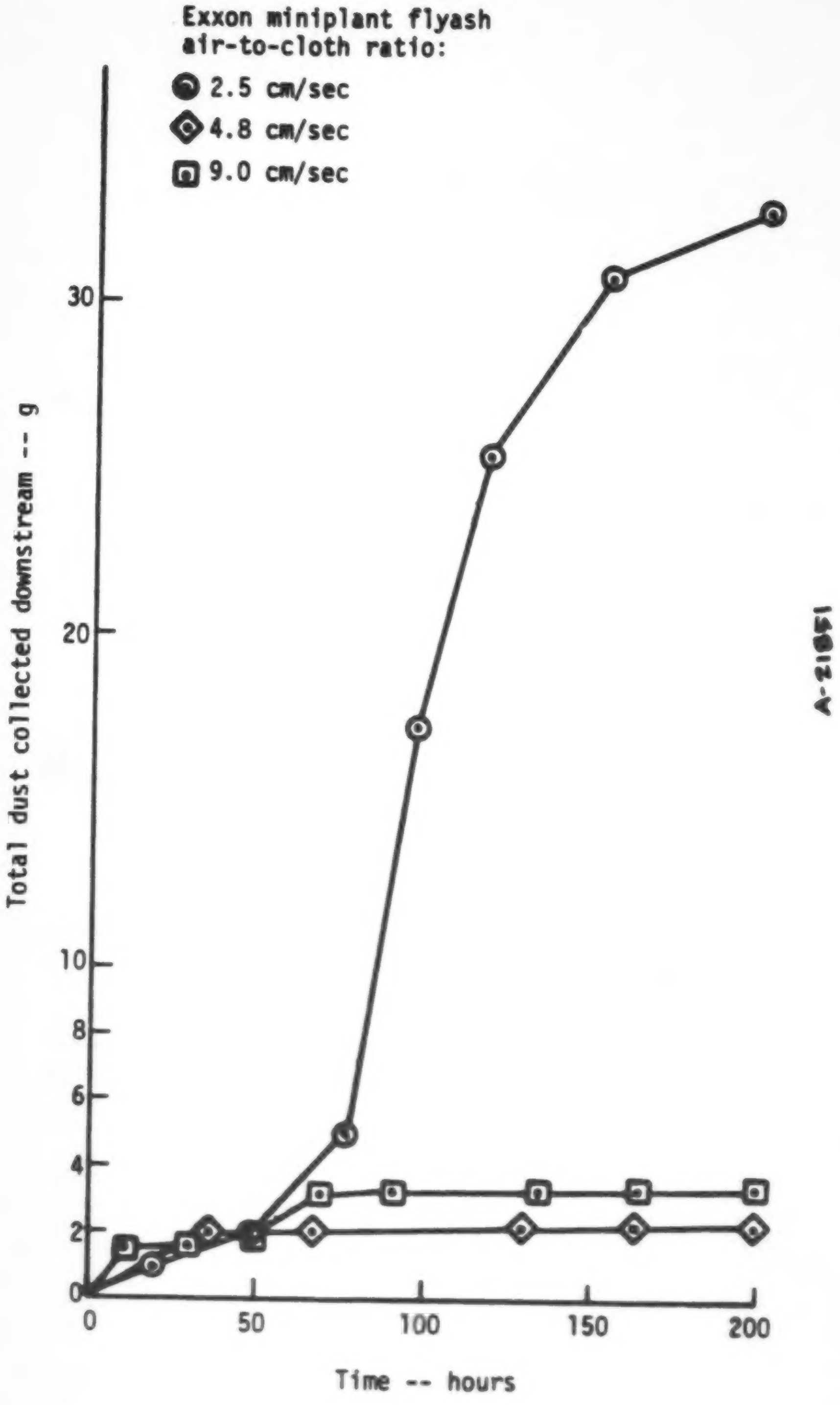

Figure 2. Total dust collected downstream.

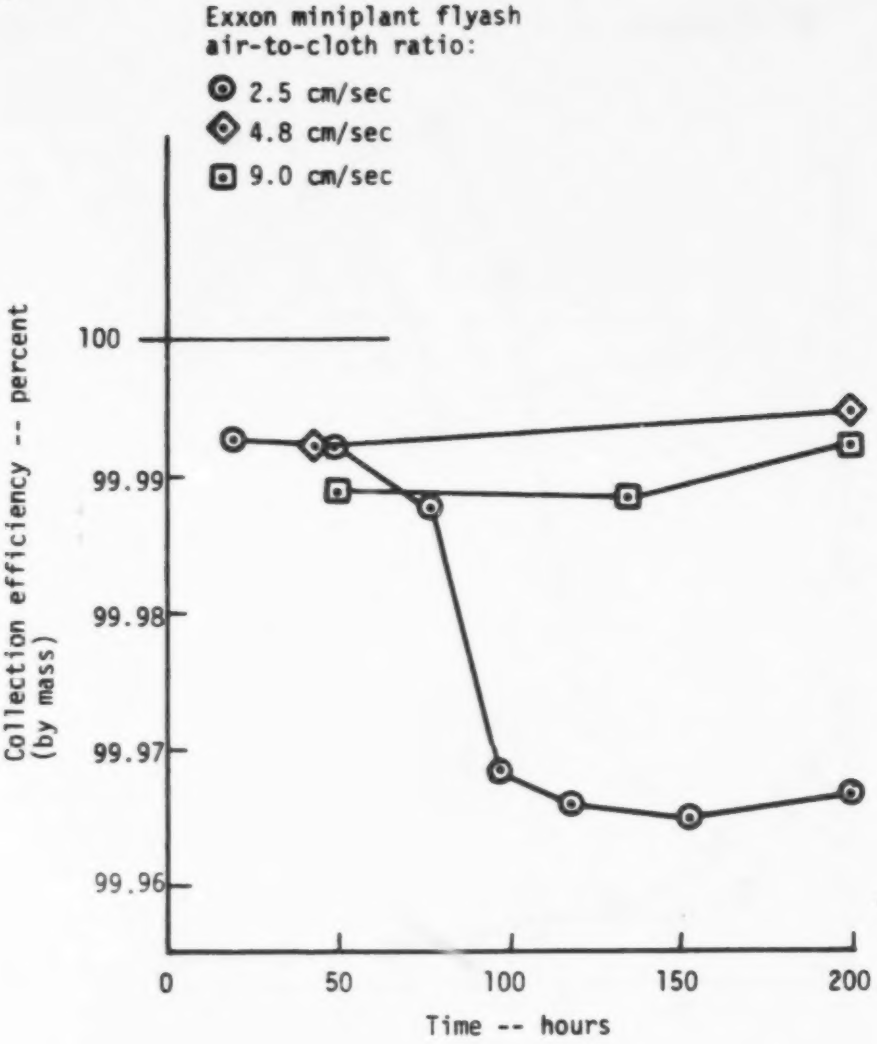

A-21892

Figure 3. Overall collection efficiency.

A-21853

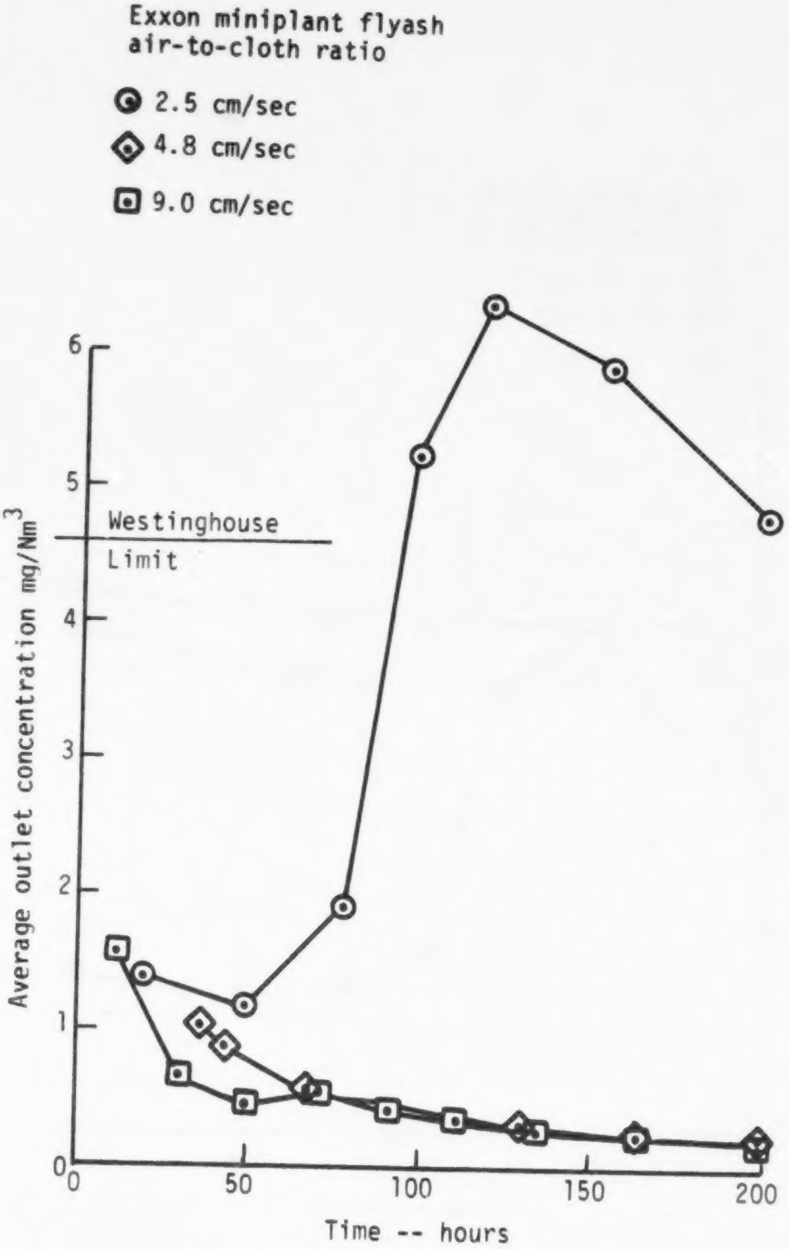

Figure 4. Average outlet concentration.

time that dust was being fed (200 hours). They do not include the additional flow which occurred during warmup and cooldown when the dust feeder was off. Because of various difficulties which occurred with the test rig, this first run was interrupted many times. Pressure drop was maintained at less than about 0.75 kPa (3 inches H_2O) over the entire test.

Results from subsequent tests showed lower outlet concentrations and led us to believe that the test filter used in the first test had a leak.

For the second 200 hour test we attempted to achieve the highest air-to-cloth ratio possible with the present test rig configuration. This test was performed at an air-to-cloth ratio of 9 cm/sec (18 ft/min). Because of compressor limitations it was only possible to maintain a system pressure of 500 kPa. Earlier tests were performed at system pressures of 930 kPa. Cleaning pulse pressure was set at 860 kPa to compensate for the reduced system pressure. Cleaning cycle pulse duration and pulse interval were the same as in the previous test at 2.5 cm/sec with both tests using offline cleaning.

As before, flyash from the Exxon Miniplant was used as the test dust. This dust had a $D_{50} = 19\ \mu m$. Cumulative dust fed, total dust collected downstream and overall collection efficiency are plotted as a function of time on Figures 1, 2 and 3. Outlet concentration as a function of time is shown in Figure 4. Overall collection efficiency for 200 hours was 99.992 percent. The filter, which has only $0.0929 m^2$ ($1\ ft^2$) of filter media area, removed 43,772 g (96.5 lb) of dust from 16,887 Nm^3 of air. Average inlet concentration was 2.59 g/Nm^3 and average outlet concentration for 200 hours was 0.2 mg/Nm^3. Thus, on a mass basis the outlet concentration is cleaner than projected turbine requirements. Pressure drop varied from about 0.5 kPa to 2.25 kPa (2 to 9 in H_2O) over the 10 minute cycle between cleaning events.

The third 200 hour test was performed at an intermediate air-to-cloth ratio of 4.8 cm/sec (9.5 ft/min). For this test, as for the higher velocity test, compressor limitations required that system pressure be set at 660 kPa. Cleaning pulse pressure was 1100 kPa. Other aspects of the cleaning cycle were the same as in the previous tests. The same dust was used (D_{50} = 19 μm). Cumulative dust fed, total dust collected downstream and overall collection efficiency by mass are plotted as a function of time on Figures 1, 2 and 3. Outlet concentration as a function of time is plotted on Figure 4. Cleaned down pressure drop was maintained at less than 1.25 kPa (5 in H_2O) throughout the test.

Outlet concentration as a function of face velocity (air-to-cloth-ratio) is plotted on Figure 5 for three time periods of 50, 100 and 200 hours. If we assume the filter used in the first test at 2.5 cm/sec developed a leak and extrapolate expected performance (dotted lines) it is apparent that outlet concentration is reduced as a function of time at all velocities. This result is similar to what one would expect from a test using conventional filter media in a room ambient dust feeding test.

Overall particle collection efficiency is plotted as a function of face velocity (air-to-cloth-ratio) on Figure 6 for three time periods of 50, 100 and 200 hours. Again, if the two discrepant data points are ignored, collection efficiency is substantially independent of face velocity in the range tested. This is consistent with a hypothesis which

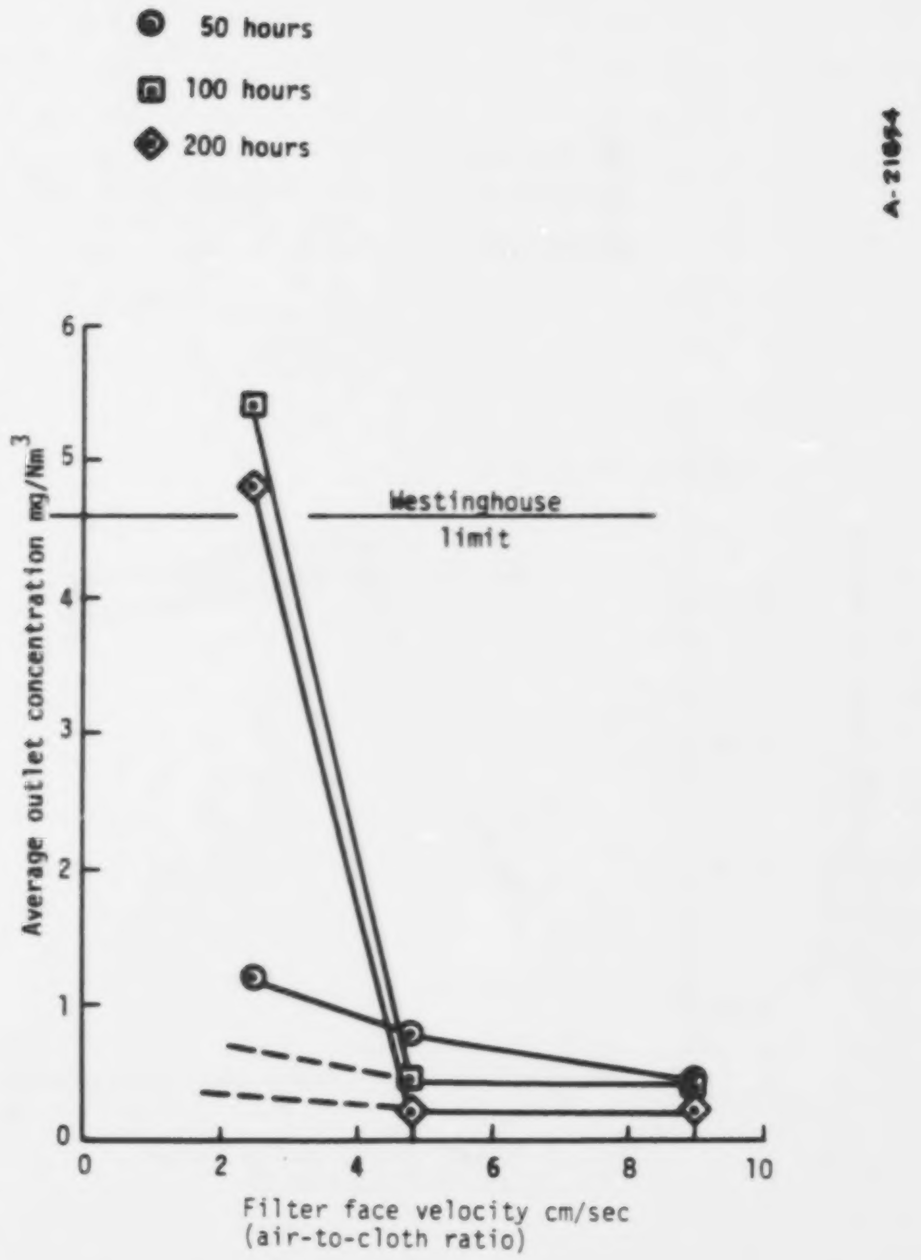

Figure 5. Outlet concentration as a function of face velocity.

A-21895

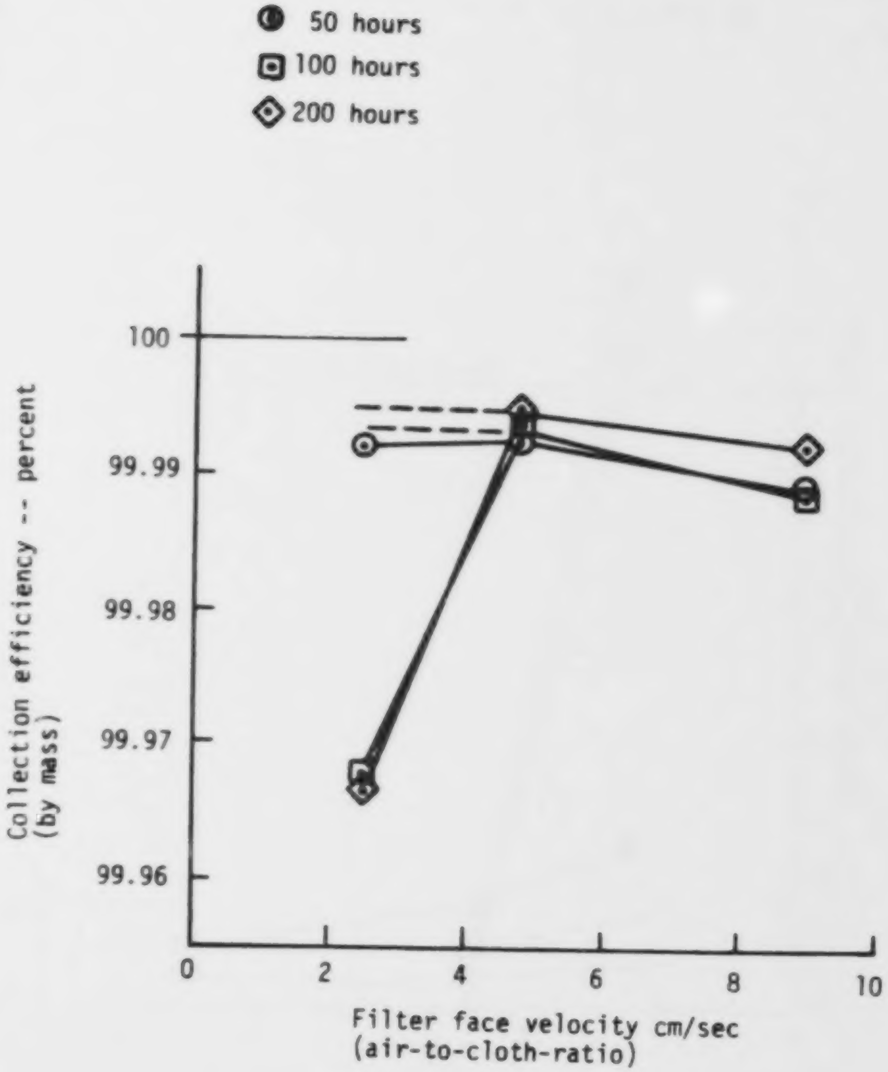

Figure 6. Collection efficiency as a function of face velocity.

holds that filter penetration occurs primarily during cleaning. The filter was cleaned at zero forward flow in all three tests (offline).

Conclusions

Developments in HTHP ceramic fiber filtration at Acurex have shown this technique is feasible. High efficiency fine particle collection results from the use of small fiber diameter (3 μm nominal) in the design of the filter media. The ability of the media to withstand cleaning stresses results from both fine fiber diameter and low solidity. The individual fibers are not held tightly together and because of their low mass do not exert large forces on each other. Filter cleaning is enhanced through the use of fine fibers and offline cleaning. The high collection efficiency of the fine fibers result in collection of particles near the surface of the media. Offline cleaning eliminates reintrainment of dust to the filter element being cleaned and to neighboring elements in the filter module taken offline. This feature also allows the filtration cycle to be accomplished at high velocity because it is reintrainment which limits air-to-cloth ratio in currently available pulse filter systems.

REFERENCES

1. Sverdrup, E. F., D. H. Archer, M. Menguturk, The Tolerance of Large Gas Turbines to "Rocks", "Dusts," and Chemical Corrodants, EPA-600/9-78-004, CONF-770970, p. 14-32, March 1978.

2. Weber, E., Problems of Gas Purification Occurring in the Use of New Technologies for Power Generation, EPA-600/9-78-004, CONF-770970, p. 249-277, March 1978.

3. Hoke, R. C., M. W. Gregory, Evaluation of a Granular Bed Filter for Particulate Control in Fluidized Bed Combustion, EPA-600/9-78-004, CONF-770970, p. 111-131, March 1978.

4. Calvert, S., Wet Scrubber Systems Study, Vol. I, EPA-R2-72-118a, NTIS No. PB213016.

5. Shackleton, M., J. Kennedy, Ceramic Fabric Filtration at High Temperatures and Pressures, EPA-600/9-78-004, CONF-770970, p. 193-234, March 1978.

6. Drehmel, D. C., M. Shackleton, High-Temperature Filtration, Proceedings of Third Symposium on Fabric Filters for Particle Collection, Tucson, Arizona, EPA sponsored, December 1977.

AEROSOL FILTRATION BY GRANULAR BEDS

Simon L. Goren*
Particulate and Multiphase Processes Program
National Science Foundation
Washington, D.C. 20550

ABSTRACT

Granular beds may find use in the filtration of large volumes of high temperature--high pressure gases. Review of the literature disclosed very little data for filter performance, even at ambient temperatures and pressures, for the flow conditions being proposed. Accordingly an experimental program was undertaken. The filter media used was 2mm diameter alumina spheres; the test aerosol was monodisperse potassium bipthalate particles of several sizes from 0.51μm to 3.91μm diameter; the gas was (dry) ambient air with superficial velocity ranging from 1 cm/sec to 100 cm/sec. Over this range of conditions the data indicates three capture mechanism are operative: impaction, gravitational sedimentation and Brownian diffusion. Empirical correlations are suggested for the three separate capture mechanisms for clean granular media. An important finding is that the individual grain efficiency due to impaction is much more sensitively dependent on the Stokes number than previously expected; at sufficiently high Stokes numbers, the measured efficiency decreases, presumably because of bounce or reentrainment of the potassium bipthalate particles.

INTRODUCTION

The moving granular bed filter developed by Combustion Power Company[1] operates with typical gas superficial velocities between 50 to 100 ft/min moving through a bed of spherical collectors or grains 0.2 cm in diameter.

---

*Current address: Department of Chemical Engineering, University of California, Berkeley, California 94720

Review[2] of the literature disclosed very little data for filtration efficiency under these conditions. Accordingly, a separate experimental program was undertaken to measure the filtration efficiency for a range of parameters relevent to the moving granular bed filter. A solid "non-sticky" aerosol was selected so that the present results would be directly comparable to Combustion Power Company's cold bed tests.[3] This report summarizes the experimental procedure, gives the data measured, and gives separate equations for the capture efficiency due to impaction, gravity settling and Brownian diffusion.

EXPERIMENTAL CONDITIONS

Solid, monodisperse, electrically neutral potassium bipthalate particles were used as the test aerosol. These were generated by subjecting a thin liquid jet of potassium bipthalate dissolved in clean filtered water to high frequency vibrations in a Berglund-Liu aerosol generator. The resulting droplets are mixed with a large volume of dry filtered air causing evaporation of the droplets to dryness and leaving solid spherical particles of potassium bipthalate. The particle size can be varied by using potassium bipthalate solutions of various concentrations. In the present studies five separate monodisperse sizes were used. The geometric diameters were 3.91μm, 2.78μm, 1.56μm, 0.93μm and 0.51μm. The density of solid potassium bipthalate is 1.636 gm/cm and the experiments were carried out at room temperature and atmospheric pressure. With adjustments for particle density, ρ_p, and mean free path corrections, C_s, the aerodynamic diameter D_{AERO} is readily related to the geometric diameter D_{GEO} by the formula

$$D_{AERO} = D_{GEO} \sqrt{\rho_p C_s}$$

The values of D_{GEO}, C_s and D_{AERO} of the particles used are listed below:

D_{GEO} μm	C_s	D_{AERO} μm
3.91	1.042	5.10
2.78	1.058	3.66
1.56	1.104	2.10
0.93	1.18	1.29
0.51	1.33	0.75

The Berglund-Liu generator is capable of generating about 9×10^6 particles/min in a total gas flow of about 90 ℓ/min giving a concentration of 10^5 particles/ℓ. The generated aerosols were electrically neutralized by exposure to a radioactive Krypton source and any remaining charged particles or gas ions were removed by passing the stream between oppositely charged metal plates.

The filter media used was 2 mm diameter alumina spheres provided by

Combustion Power Company. These were placed in a plexiglas tube of 4.39 cm internal diameter and supported by a coarse wire mesh screen which in turn was supported by a standard plastic support taken from a 47 mm Nuclepore filter. One may estimate that approximately 18% of the grains are within a "monolayer" of the tube wall. It would have been preferable to use beds of larger diameter to minimize possible wall effects, but this was not feasible owing to the limitations of the equipment if I was also to achieve the desired high superficial velocities. With suitable plumbing, I was able to draw between 1 and 90 ℓ/min of aerosol through the bed giving superficial velocities between 1.1 and 99 cm/sec. The flow through the bed was vertically downward.

Bed depth varied from 3 cm to 19.3 cm, The bed depth was adjusted to keep the measured penetration between 0.01 and 0.9 so that reliable values of the single grain efficiency could be calculated.

Penetration is defined as the number of particles leaving the bed to those entering. This was measured by consecutively withdrawing a sample (7 ℓ/min) from the outlet and the inlet of the granular bed through a Climet aerosol monitor.

The Climet monitor detects aerosol particles one by one by light scattering as they pass through an optically sensitive zone of the instrument. The optics of the Climet are such that each particle generates a separate electrical pulse largely proportional to the particle's surface area. With associated electronic equipment for manipulating and counting these pulses according to pulse height, we are able to obtain the particle size distribution. Observation of the size distribution verified that we were generating very monodisperse aerosols. This is important because we did not use isokinetic sampling; however, since the aerosol is monodisperse, the inlet and outlet samples are withdrawn through identical plumbing, and the penetration is the ratio of the two counts, particle losses due to non-isokinetic sampling or deposition on the tube walls cancel exactly and do not affect the calculations.

From the bed depth L, grain radius a_G, bed solids fraction α_G and penetration P, the individual grain efficiency η_G can be calculated according to the formula

$$\eta_G = -\frac{4a_G \ln P}{3\alpha_G L}$$

The bed solids fraction was not measured; for the purpose of reducing the data, a constant value 0.6 was assumed.

It must be emphasized that the penetration of aerosol through a granular bed filter depends on the loading of dust already captured within the bed. For the experiments reported here bed exposure to aerosol was of sufficiently short duration that all the data are appropriate to clean granular beds. It is important that data on the effect of dust loading be obtained, but this was beyond the scope of the present study.

RESULTS

The measured penetrations are listed in the Appendix for the various flow rates and particle sizes used. These also are shown graphically in Figure 1 where the single grain efficiency $\eta_G = -4a_G \ell nP/3\alpha_G L$ is plotted versus the volumetric flow rate. Starting with the lowest flow rate and the largest particle ($D_{GEO} = 3.91\mu m$), as the flow rate is increased the single grain efficiency at first decreases until a superficial velocity of about 9 cm/sec is reached; thereafter increasing the flow rate increases the efficiency until a superficial velocity of about 35 cm/sec is reached, after which further increases in flow rate result in a decreasing efficiency. These trends are explained qualitatively as follows: For the large particles and low flow rates, gravity settling appears to be the dominant capture mechanism. With increasing flow rate, less residence time is available for settling of the particles onto the surface of the grains so that the efficiency decreases with increasing velocity. For sufficiently large velocity, the particles attain sufficient inertia to bring the capture mechanism of impaction into play. Now increasing the flow rate gives the particles greater inertia and therefore, a larger capture efficiency. However, when hard-solid particles impinge with sufficient inertia on hard-solid surfaces, the particles may bounce and be reentrained in the flowing gas stream. For the particles with geometric diameter of $3.91\ell m$, it appears that above 35 cm/sec the probability of bouncing is increasing with increasing flow rate faster than the probability of collision is increasing. Consequently the efficiency of capture now decreases with increasing flow rate. "Sticky" particles such as hot fly ash will probably be less prone to bouncing than the solid potassium bipthalate used here. Reentrainment of previously deposited particles as opposed to bouncing may also be important here.

Similar trends are demonstrated by the data for the smaller particles. The transition velocities are shifted to higher velocities the smaller the particle. For the smallest particle used, $D_{GEO} = 0.51\mu m$, we were not able to achieve a sufficiently high gas velocity to cause impaction to become the dominant capture mechanism. As a result, the single grain efficiency decreases over the entire velocity range studied.

Another interesting observation is that at the lower velocities the single grain efficiency for the $0.51\mu m$ geometric diameter particles is larger than that for the $0.93\mu m$ particles at the same flow rate. This is explained by assuming Brownian diffusion has become an important capture mechanism for the small particles at low flow rates so that now the smaller the particle the more intense the Brownian diffusion and therefore the larger the efficiency. Further evidence suggesting Brownian diffusion is the gradual reduction of slope of the efficiency versus flow rate curves at low flow rates as we proceed to smaller particles.

To test the hypothesis that impaction is the dominant capture mechanism for the ascending portion of the curves, I have replotted the data in Figure 2 as efficiency η_G versus Stokes number Stk. Here Stk =

$2\rho_p a_p^2 C_s U/9\mu a_G$ where a_G is the grain radius, ρ_p the particle density, U the superficial velocity, μ the gas viscosity, C_s the Cunningham slip correction and a_p the particle radius. When impaction is the dominant capture mechanism η_G should depend solely on Stk and parameters that characterize the bed geometry; the bed geometry was not varied in the present study so that here η_G should depend only on Stk. For each particle size, the ascending part of the curve at high Stk superimposes on a single curve, at least until bouncing becomes prominent. This is very strong evidence of the dominance of impaction. A line fitted by eye gives the following formula for the single grain capture efficiency due to impaction:

$$\eta_I = 1270 \ \mathrm{Stk}^{9/4}$$

This is very different from a nearly first power dependence on Stk suggested previously[2] and based on the very limited data of Paretsky. Paretsky's data was limited to Stokes numbers between 10^{-3} and 3×10^{-3}; moreover, the present studies indicate that for these Stokes numbers and the 1.1μm diameter polystyrene latex particles used by Paretsky, the velocities used by Paretsky might not have been sufficiently large to make impaction the overwhelming capture mechanism.

As explained elsewhere[2], at present there is no quantitatively adequate theory for particle capture by impaction in packed beds because all such theories predict critical Stokes numbers below which zero collection occurs; no such sharp cutoff is evident even though the Stokes numbers for much of the ascending curve are below usually accepted critical values.

To test the hypothesis that gravity settling is the dominant capture mechanism for the descending portion of the curve for the larger particles, I have replotted in Figure 3 the data as efficiency η_G versus a gravity number Grv. Here $\mathrm{Grv} = 2\rho_p a_p^2 C_s g/9\mu U$ where g is the acceleration of gravity. The gravity number is the ratio of the particle's terminal velocity to the gas superficial velocity. When sedimentation is the dominant capture mechanism η_G should depend primarily on Grv and parameters that characterize the bed geometry. Again, bed geometry was not varied in the present study. Although not as evident as with the case for impaction, the data for all particles with the possible exception of the smallest particle appear to be approaching a single asymptotic curve as the gravity number increases and sedimentation therefore becomes more important. A tentative correlation for the single grain efficiency for gravity sedimentation based on these data is

$$\eta_G = 0.97 \ \mathrm{Grv}^{3/4}$$

This correlation is based on data for flow vertically downwards. Horizontal or vertical upwards flow might yield a somewhat different correlation.

Lastly, to test the hypothesis that Brownian diffusion is the dominant mechanism for the descending portion of the curve for the smaller particles, I have replotted in Figure 4 the data as efficiency versus the Peclet number Pe. Here $Pe = 2a_c U/D_p$ where $D_p = kTC_s/6\pi\mu a_p$ is the Brownian diffusion coefficient of the particle at temperature T. If Brownian diffusion is the dominant capture mechanism, then η_G should depend only on the Peclet number and bed geometry if the Reynolds number based on grain diameter is sufficiently small. The data for the two smallest particles superimpose at sufficiently small Peclet number which corresponds to sufficiently intense Brownian motion. That the data for the larger particles do not appear to approach this curve as Pe becomes small may be due to the moderate size of the grain Reynolds number or to the importance of sedimentation for these larger particles. A very tentative correlation based on these results for the single grain efficiency due to Brownian diffusion is

$$\eta_D = 232\ Pe^{-2/3}$$

The exponent on the Peclet number is in agreement with the theory for Brownian deposition from very low Reynolds number flows, but the coefficient is larger than that suggested by previous workers in beds of smaller grains at lower flow rates.

ACKNOWLEDGEMENTS

The work reported here was done for Combustion Power Company as part of CPC's contract No. EF-77-C-01-2579 with the Department of Energy. The author completed the work prior to commencing a one year appointment with the National Science Foundation.

REFERENCES

1. Geffken, J., J.L. Guillory and K.F. Phillips, "Performance Characteristics of Moving-Bed Granular Filters", Symposium on the Tranfer and Utilization of Particulate Control Tech., Denver, CO, July 24, 1978.
2. Goren, S. L., "A Mathematical Model for the Moving Granular Bed Filter", Report to Combustion Power Company, May, 1977.
3. Wade, G. L. "Performance and Modeling of Moving Granular-Bed Filter" EPA/DOE Symposium on High Temperature High Pressure Particulate Control, Washington, DC, September 21, 1977.

Although not explicitly referred to in the text, I include here for the convenience of readers a bibliography on granular bed filtration.

Balasubramanian, M. and A. Meisen, "A Note on the Diffusional Deposition of Aerosol Particles in Packed Beds." J. Aerosol Sci. 6, 461 (1975).

Bohm, L. and S. Jordan, "On Filtration of Sodium Oxide Aerosols by Multilayer Sand Bed Filters." J. Aerosol Sci., 7, 311 (1976).

Engelbrecht, H. I., "The Gravel Bed Filter--A New Approach to Gas Cleaning." J. Air Poll. Control Assoc., 15, 43 (1965).

Gebhart, J., C. Roth and W. Stahlofen, "Filtration Properties of Glass Bead Media for Aerosol Particles in the 0.1-0.2 μm Size Range." J. Aerosol Sci., 4, 355 (1973).

Goren, S. L. (University of California, Berkeley), "Modelling of a Moving Bed Granular Filter." Presented at: 9th Fine Particle Society Conference, Menlo Park, August 25-26, 1977.

Hoke, R. C. (Exxon Research & Development Company), "Evaluation of a Granular Bed Filter for Particulate Control in Fluidized Bed Combustion." Presented at: EPA/ERDA Symposium on High Temperature/Pressure Particulate Control, Washington, DC, Sept. 20-21, 1977.

Jackson, S. and S. Calvert, "Entrained Particle Collection in Packed Beds." A.I.Ch.E. Journal, 12, 1075 (1966).

Knettig, P. and J. M. Beeckmans, "Inertial Capture of Aerosol Particles by Swarms of Accelerating Spheres." J. Aerosol Sci., 5, 225 (1974).

Knettig, P. and J. M. Beeckmans, "Capture of Monodisperse Aerosol Particles in Fixed and in a Fluidized Bed." Canadian J. Chem. Eng., 52, 703 (1974).

Miyamoto, S. and H. L. Bohn, "Filtration of Airborne Particulates by Gravel Filters: I. Initial Collection Efficiency of a Gravel Layer." J. Air Poll. Control Assoc., 24, 1051 (1974).

Miyamoto, S. and H. L. Bohn, "Filtration of Airborne Particulates by Gravel Filters: II. Collection Efficiency and Pressure Drop in Filtering Fume." J. Air Poll. Control Assoc., 25, 40 (1975).

Paretsky, L., L. Theodore, R. Pfeffer and A. M. Squires, "Panel Bed Filters for Simultaneous Removal of Fly Ash and Sulfur Dioxide: II. Filtration of Dilute Aerosols by Sand Beds." J. Air Poll. Control Assoc., 21, 204 (1971).

Payatakes, A. C. and C. Tien, "Particle Deposition in Fibrous Media with Dendritic-like Pattern: A Preliminary Model." J. Aerosol Sci., 7, 85 (1976).

Schmidt, E. W. and J. A. Gieseke (Battelle Columbus Labs), "Filtration Theory for Granular Beds." Presented at: 10th Aerosol Technology Conference, Los Alamos and Albuquerque, September 26-28, 1977.

Squires, A. M. and R. Pfeffer, "Panel Bed Filters for Simultaneous Removal of Fly Ash and Sulfur Dioxide: I. Introduction." J. Air Poll. Control Assoc., 20, 534 (1970).

Thomas, J. W. and R. E. Yoder, "Aerosol Size for Maximum Penetration Through Fiberglass and Sand Filters." AMA Arch. Ind. Health, 13, 545 (1956).

Thomas, J. W. and R. E. Yoder, "Aerosol Penetration Through a Lead Shot Column: A Method of Particulate Size Estimation." AMA Arch. Ind. Health, 13, 550 (1956).

Yung, S-C, R. D. Parker, R. Patterson and S. Calvert (Air Pollution Technology, Inc.), "Granular Bed Filters for Particle Collection at High Temperature and Pressure." Presented at: EPA/ERDA Symposium on High Temperature/Pressure Particulate Control, Washington, DC, September 20,21, 1977.

APPENDIX DATA

Q ≡ flow rate in ℓ/min
P ≡ penetration

I. Data for
D_{GEO}=3.91μm
a_G =0.10cm
L^G =3.0 cm
α_G =0.6

Q	P
2	0.340
5	0.583
6.7	0.703
9.7	0.661
11.7	0.556
13.0	0.513
16.7	0.263
26.7	0.313
66.7	0.242
11.7	0.638
16.7	0.322
21.7	0.176
26.7	0.122
36.7	0.126
46.7	0.176
56.7	0.200

II. Data for
D_{GEO}=2.78μm
a_G =1.101cm
L^G =5.3 cm
α_G =0.6

Q	P
1	0.188
1.5	0.281
1.9	0.352
3.0	0.441
5.0	0.587
6.6	0.632
9.7	0.716
11.7	0.739
14.7	0.739
16.7	0.705
21.7	0.544
23.7	0.414
26.7	0.313
29.7	0.153
31.7	0.140
36.7	0.074
41.7	0.043
46.7	0.034
51.7	0.034
61.7	0.054
76.7	0.0889
86.7	0.129

III. Data for
D_{GEO}=1.56 μm
a_G =0.101cm
L^G =10.9 cm
α_G =0.6

Q	P
6.7	0.496
9.7	0.577
11.7	0.607
14.7	0.675
16.7	0.664
19.7	0.664
24.7	0.708
16.7	0.663
19.7	0.662
29.7	0.715
39.7	0.627
49.7	0.414
44.7	0.534
54.7	0.408
59.7	0.261
59.7	0.303
64.7	0.180
69.7	0.048
74.7	0.0323
69.7	0.0452
79.7	0.0194
84.7	0.0139
1	0.0956
3	0.332
5	0.466

IV. Data for
$D_{GEO}=0.93\mu m$
$a_G=0.101$ cm
$L=19.3$ cm
$\alpha_G=0.6$

Q	P
16.7	0.661
19.7	0.669
29.7	0.701
39.7	0.720
49.7	0.729
59.7	0.710
69.7	0.632
79.7	0.572
64.7	0.685
24.7	0.699
6.7	0.486
5	0.435
3	0.330
1	0.096
2	0.223

V. Data for
$D_{GEO}=0.51\mu m$
$a_G=0.101$ cm
$L=10.9$ cm
$\alpha_G=0.6$

Q	P
3	0.402
1	0.159
5	0.524
6.7	0.575
16.7	0.716
24.7	0.753
39.7	0.812
49.7	0.787

Data for
$D_{GEO}=0.51\mu m$
$a_G=0.101$ cm
$L=19.3$ cm
$\alpha_G=0.6$

Q	P
59.7	0.728
69.7	0.756
79.7	0.758
89.7	0.804
49.7	0.745

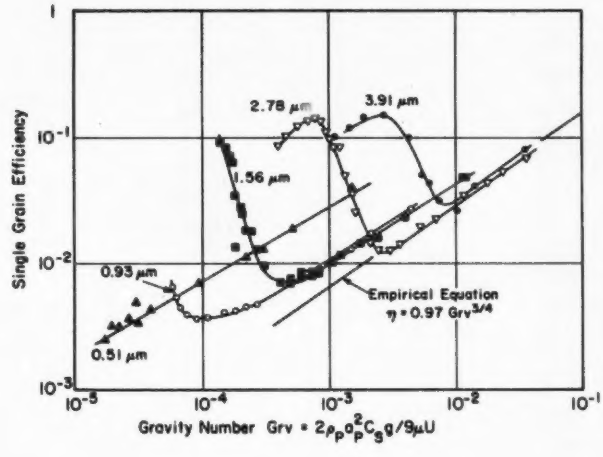

Figure 3

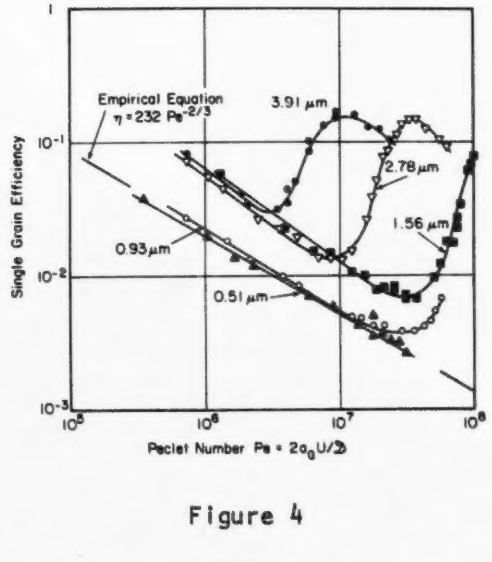

Figure 4

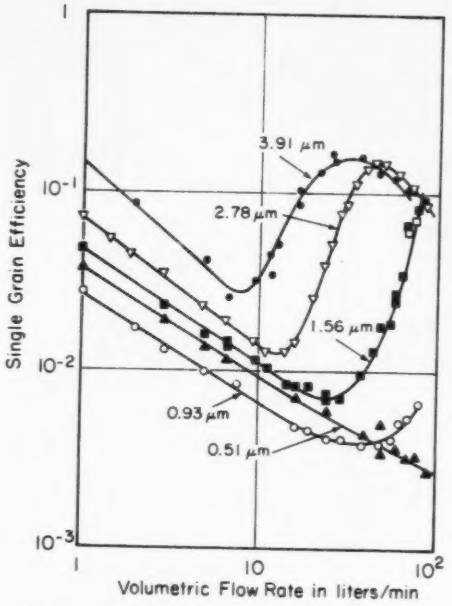

Note: 1 liter/min gives face velocity of 1.1 cm/sec.

Figure 1

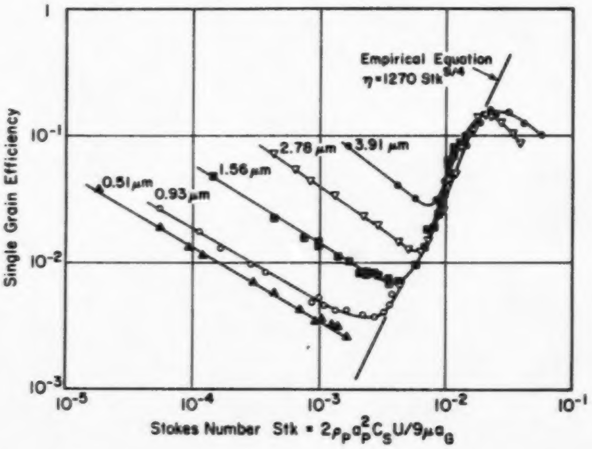

Figure 2

PERFORMANCE CHARACTERISTICS OF MOVING-BED GRANULAR FILTERS

John Geffken
Department of Energy
Washington, D.C.

J. L. Guillory
Combustion Power Company, Inc.
Menlo Park, California

K. E. Phillips
Combustion Power Company, Inc.
Menlo Park, California

ABSTRACT

The Department of Energy is sponsoring a multiphase program to investigate the filtration potential of the moving-bed granular filter (GBF) for application in pressurized high temperature energy conversion systems. Phase I which has been completed included the development of a mathematical model, a parametric test series in a 1800 acfm GBF, and investigations of potential dust plugging problems at the inlet screen. During the experimental program, collection efficiencies in excess of 99% and filter outlet loadings less than 0.005 gr/acf were demonstrated. Finally, it was shown that controlled media spillage from the inlet screen prevented dust deposits which might otherwise impare performance.

INTRODUCTION

The purpose of this paper is to summarize the activities and conclusions of a moving-bed granular filter (GBF) development program conducted by Combustion Power Company, Inc., for the U.S. Department of Energy. The objectives of this program were to (1) identify the mechanisms involved in moving-bed granular filtration, (2) quantify the performance of a practical GBF configuration analytically and experimentally and (3) address certain operational problems known to exist in devices of this type.

The modern GBF configuration which is the subject of this report is illustrated in Figure 1. Particle collection is accomplished by causing the particulate laden gas to move radially outward in crossflow through an annulus of granular collecting material (media). The downward flow rate of the granular bed is selected such that the deposition rate of particulate onto the media and its removal rate from the active filtration zone result in steady-state operation which is compatible with both filtration requirements and gas-side pressure drop limitations. The inner screen confining the annulus of media is perforated such that some controlled counter-current spillage is allowed thereby preventing excessive deposition of particulate in the gas passages. The outer screen is sized for complete retention of media.

In order to close the media loop, a pneumatic transport system conveys the "dirty" media to a small fluid bed located immediately above the GBF vessel. Turbulent action in the pneumatic transport system and the fluid bed removes particulate deposits from the media which, concentrated in the small (transport plus fluid bed) gas stream, are collected in a conventional bag filter. The cleaned media is distributed by over-flow legs from the fluid bed into the annulus above the active filtration zone and ultimately reenters the active zone in approximately plug flow.[1]

THEORETICAL ANALYSIS[2,3]

The purpose of theoretical investigations in this project was to identify and define key relationships to be incorporated in a computerized model of GBF performance.

Collection Model

Based on observations of the operation of similar commercial devices and a survey of published literature, it was concluded that GBF collection performance does not involve any unique mechanisms of filtration. However, it was found that few references addressed either the annular configuration or cross-flow bed motion. It was therefore necessary to collect approximate model information from a variety of sources and ultimately assess the effectiveness of the model on its ability to predict, after judicious selection of simple gain factors, GBF collection performance over a significant operating range. The collection efficiency model selected was

$$\eta = \underbrace{\frac{1}{\epsilon}\left[\overset{\text{STOKES NUMBER}}{\frac{C d_p^{\,2}\, U \rho_p}{9 d_c \mu}}\right]^3}_{\text{IMPACTION}} + \underbrace{\frac{3}{2}\left[\frac{d_p}{d_c}\right]}_{\text{INTERCEPTION}} + \underbrace{\frac{4.36}{\epsilon}\left[\overset{\text{PECLET NUMBER}}{\frac{d_c U}{D}}\right]^{-2/3}}_{\text{DIFFUSION}} + \underbrace{\frac{0.384}{\epsilon}\left[\overset{\text{GRAVITATION NUMBER}}{\frac{U_t}{U}}\right]^{3/4}}_{\text{SEDIMENTATION}}$$

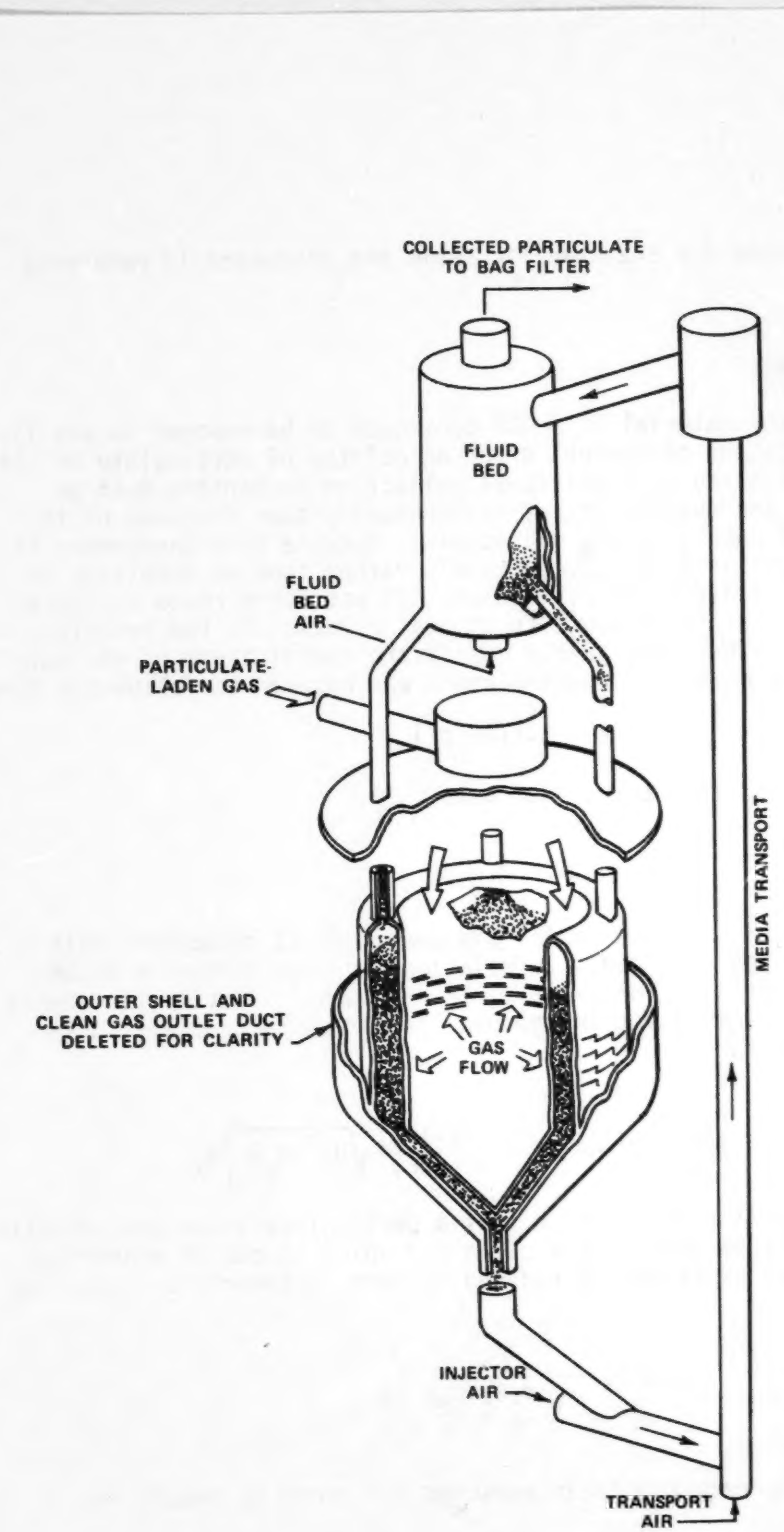
COLLECTED PARTICULATE
TO BAG FILTER
FLUID
BED
FLUID
BED
AIR
PARTICULATE-
LADEN GAS
MEDIA TRANSPORT
OUTER SHELL AND
CLEAN GAS OUTLET DUCT
DELETED FOR CLARITY
GAS
FLOW
INJECTOR
AIR
TRANSPORT
AIR

Figure 1. Moving-bed granular filter

Sources and rationale for the specific terms are discussed in reference (2).

Reentrainment Model

Since collector material in a GBF continues to be exposed to gas flow and shear from adjacent collectors after deposition of particulate on its surface, any model based on traditional collection mechanisms must be modified to allow the possibility of reintroducing some fraction of the collected material back into the gas stream. Because this phenomenon is thought to represent an inability to retain rather than an inability to collect some small fraction of particulate, it was appropriate to represent reentrainment with a separate functional relation to the principal process variables rather than merely modify the coefficients of the collection terms. The model for reentrainment was assumed to follow the form

$$\eta = 1-K\left[UU_m C_s\right]$$

where K was evaluated from actual GBF data.

Gas Flow Model

Pressure gradients in the radial and longitudinal directions within the bed were described by Ergun's correlation for flow through a packed bed of granular material. For example, if orthogonal velocity components U_x and U_y exist at some point in the bed, the pressure gradient in the x-direction has the form

$$\frac{dP}{dx} = \left[\frac{150(1-\varepsilon)^2\mu}{\varepsilon^3(\phi dc)^2} + \frac{1.75(1-\varepsilon)}{\varepsilon^3(\phi dc)}\sqrt{U_x{}^2+U_y{}^2}\right]U_x$$

In order to describe the observation that a particulate-laden bed exhibits an increase in pressure drop over a clean bed which is out of proportion to that which can be explained by reduced voidage, a sphericity reduction

$$\phi = \frac{\phi_o}{1 + \frac{d_c P_c}{4}\left(\sum_1^m \frac{Cs}{d_p \rho_p}\right)}$$

was postulated to correct the Ergun equation for particle deposition.

Computer Model

A two-dimensional axisymmetric finite-difference model was developed to represent the active filtration zone of the GBF. Each element in the model was forced to simultaneously obey continuity in media, gas and particulate flow consistent with input boundary conditions relating to gas and particulate flow as well as certain geometrical constraints. The integrated effects of all the elements resulted in a gas pressure drop, outlet particle loading and outlet particle size distribution.

Comparison With Experimental Data

Table I gives sample comparisons between analytical predictions and measured collection performance of a GBF. A discussion of aspects of GBF behavior which could not be measured directly (in-bed velocity distribution, captured particulate concentration profiles in the bed, etc.) is included in Reference (2).

Table 1.

COMPARISON OF ANALYTICAL

PREDICTIONS WITH EXPERIMENTAL DATA

	V, fpm	M lb/min	L gr/scf	L_{DIST} %	Efficiency			
					η_T	η_1	η_2	η_3
Test C1631 (t=7.6in, dm=1.9mm)	120	70.0	0.320	20/24/56	86.3	67.9	86.0	92.8
Run S1631-H					81.5	59.2	74.2	92.3
Test C16130 (t=7.6in, dm=0.8mm)	119	175.0	0.559	7/14/79	98.0	86.7	95.6	99.5
Run S16130-H					99.2	95.3	99.4	99.5

EXPERIMENTAL PROGRAM [4,5,6]

A GBF similar to that illustrated in Figure 1 was constructed for cold flow testing. It was designed so that the following dimensions could be changed without major structural modifications:

- Bed Thickness (3.8 in., 7.6 in., 15.3 in.)
- Active Screen Length (26.5 in., 53.0 in.)
- Media Diameter (0.8 mm, 1.9 mm, 3.5 mm)

The GBF test system is shown in Figure 2. Operating capacities for the DOE program were as follows:

- Air Flow Rate--400 to 4000 cfm
- Inlet Dust Loading*--0.2 to 2.0 grains/scf
- Median Dust Size*--1.5 to 15+μm
- Media Circulation--30 to 300 lb/min

Nine subexperiments, each representing a unique combination of bed thickness, screen length, media diameter and median dust size, were conducted.

Each subexperiment consisted of a series of tests in which the inlet particulate concentration (L_i), approach velocity (V), and media rate (M) were varied independently. Selection of independent variable combinations to be tested within a given subexperiment were based on a Latin Square experimental design. Major dependent variables measured during each test included outlet dust loading, outlet size distribution and filter pressure drop. A total of 121 tests of this type were conducted.

Data Reduction

It was shown from dimensional considerations that both the collection efficiency η and the dimensionless pressure drop (Newton number) $\Delta P/\rho V^2$ could be given as functions of the same six dimensionless numbers:

$$\eta = f\left(\frac{V\rho d_m}{\mu}, \frac{d_m}{d_p}, \frac{t}{d_m}, \frac{H}{t}, L_i, M\right)$$

and

$$\frac{\Delta P}{\rho V^2} = g\left(\frac{V\rho d_m}{\mu}, \frac{d_m}{d_p}, \frac{t}{d_m}, \frac{H}{t}, L_i, M\right)$$

---

* Alumina Hydrate ($Al_2O_3 \cdot 3H_2O$) was used to produce the dust loading in the cold flow GBF tests.

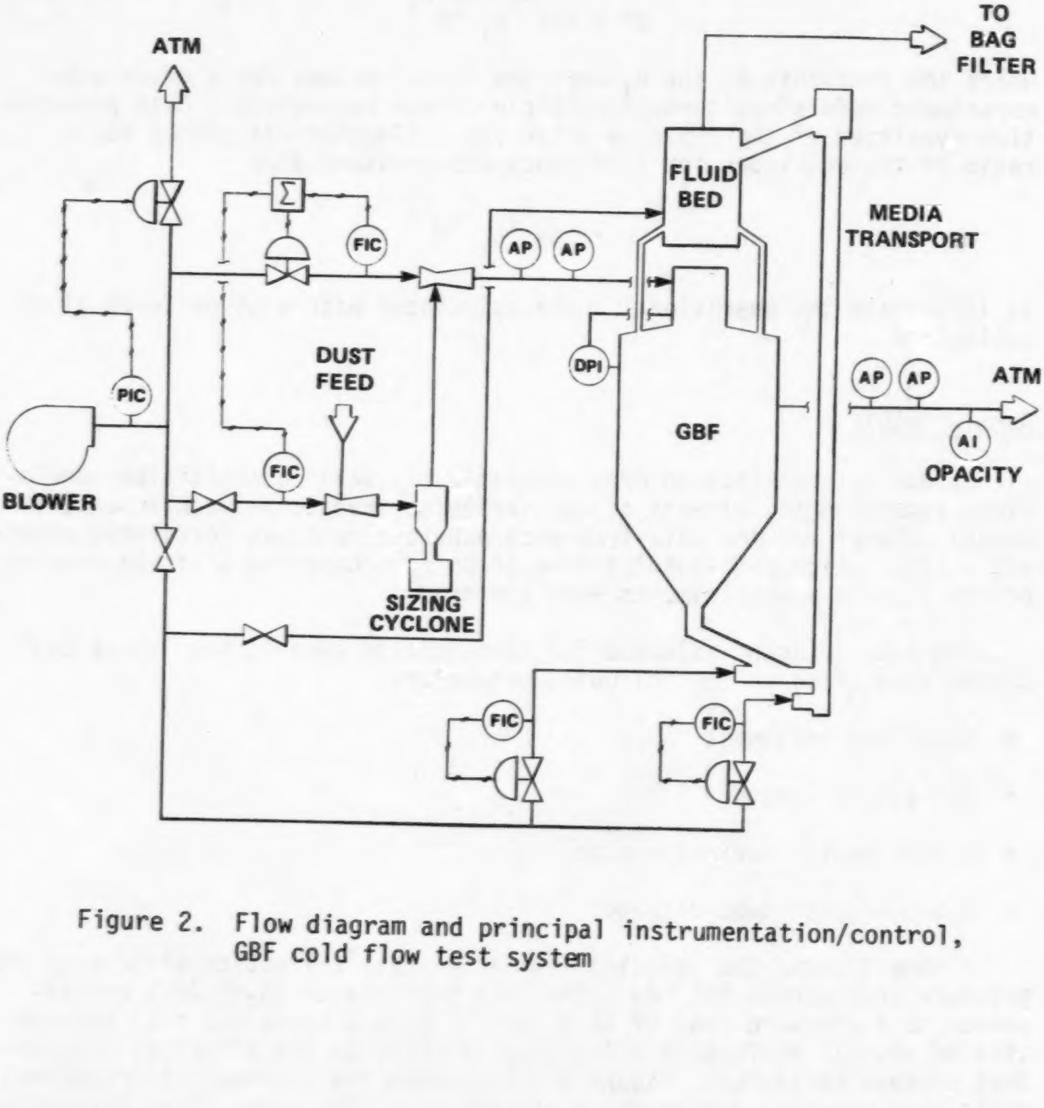
TO
BAG
FILTER
ATM
FLUID
BED
MEDIA
TRANSPORT
Σ
FIC
AP
AP
DPI
DUST
FEED
PIC
AP
AP
ATM
GBF
AI
OPACITY
FIC
BLOWER
SIZING
CYCLONE
FIC
FIC

Figure 2. Flow diagram and principal instrumentation/control, GBF cold flow test system

Since the test program was not large enough to evaluate complete functional dependencies with acceptable reliability, simpler equations were chosen for regression models:

$$\eta = A_0 V^{A_1} L_i^{A_2} M^{A_3}$$

and

$$\Delta P = B_0 V^{B_1} L_i^{B_2} M^{B_3}$$

where the constants A_i and B_i were the "best" values for a given subexperiment determined through multiple linear regression. Data presentation consisted of the above relation for collection efficiency and a ratio of the equations for efficiency and pressure drop

$$\frac{\eta}{\Delta P} = C_0 V^{C_1} L_i^{C_2} M^{C_3}$$

to illustrate the operational costs associated with a given level of collection.

Sample Results

It was not possible to draw statistically valid quantititive conclusions regarding the effects of the variables changed between subexperiments. Therefore, the data from each subexperiment was correlated separately after which semi-quantitative graphical comparisons of the results of the various subexperiments were prepared.

The subexperiment selected for presentation here is the "thick bed" series identified by the following parameters:

- 15.3" bed thickness
- 53" active length
- 1.9 mm median media diameter
- 2.6 μm median dust diameter

Figure 3 shows the relation between overall collection efficiency and pressure drop across the bed. The best performance (η_T=0.995) corresponded to a pressure drop of 14.8 IWd. Figure 4 shows the best correlation of overall collection efficiency directly to the principal independent process variables. Figure 5 illustrates the extremes of fractional efficiency observed during the subexperiment. The lower (less favorable) curve corresponds to low inlet dust loading, low approach velocity and high media rate. The effect of reentrainment is evident in the asymptotic approach to efficiencies less than 100% in the large size range.

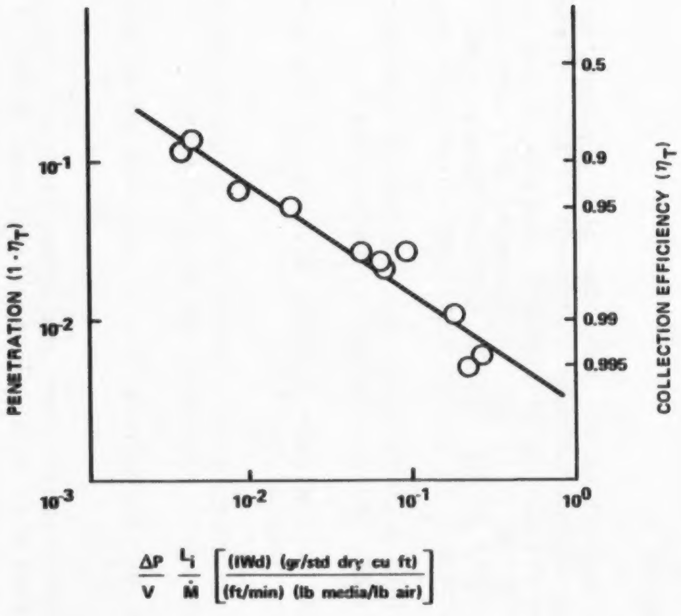

Figure 3. Influence of pressure drop function on overall collection efficiency, thick bed configuration

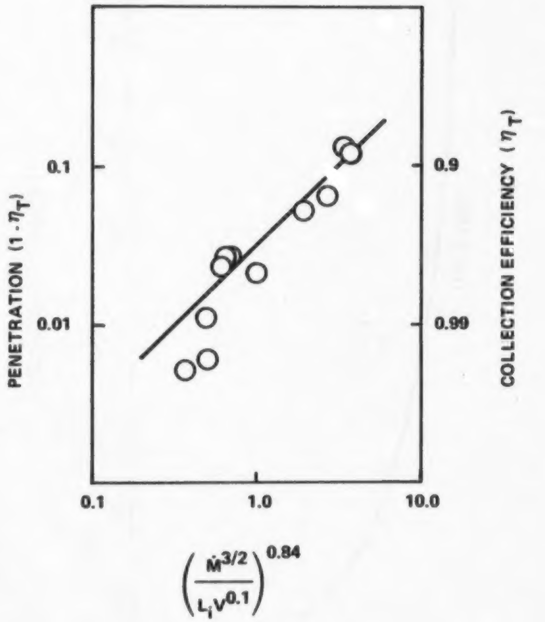

Figure 4. Direct correlation of principal independent variables to overall collection efficiency, thick bed configuration

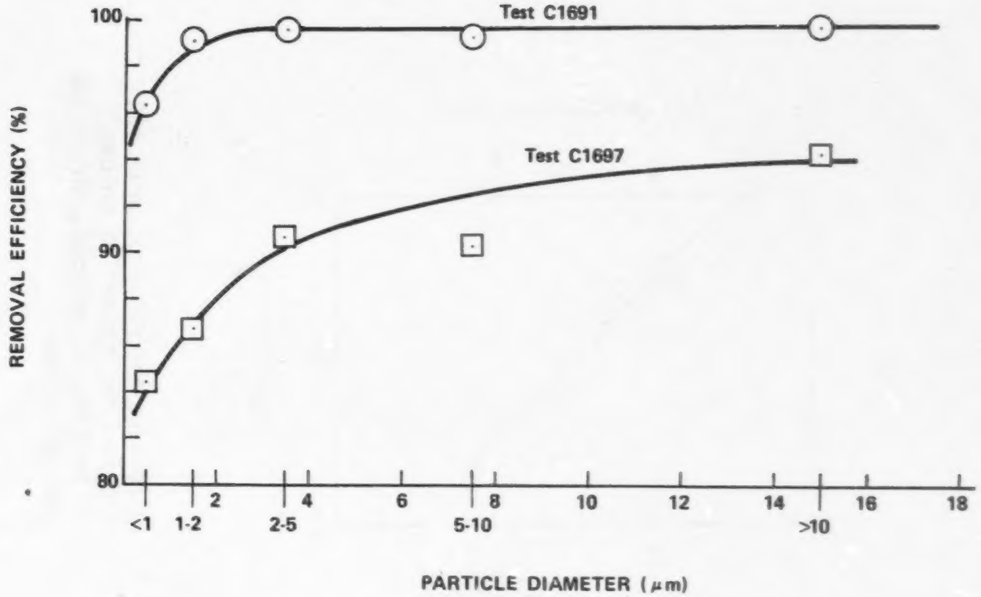

Figure 5. Influence of operational parameter combinations on fractional efficiency, thick bed configuration

FRONT FACE CLEANING[7]

It has been recognized for some time that a potential problem area in long-term operation of either continuous or intermittant media flow granular filters relates to particulate pluggage of the media retention screen exposed to the dirty gas. A separate test apparatus incorporating a pie-shaped section of the annular GBF configuration was constructed to study various concepts in continuous inlet screen cleaning.

Figure 6 illustrates five concepts considered for this program. Of these, (a), (b), and (c) were actually constructed.

Tests devised to evaluate the effectiveness of the various cleaning schemes were generally of two types:

- Measurement of dust layer build-up rate during operation at specified dust loading, media rate, and approach velocity.
- Observations of recovery ability after a period of operation with no media flow.

Since there were certain non-comparable aspects of each design (e.g., air flow associated with media blast), final evaluation also included qualitative and semi-quantitative observations by a committee of engineers assigned to the project.

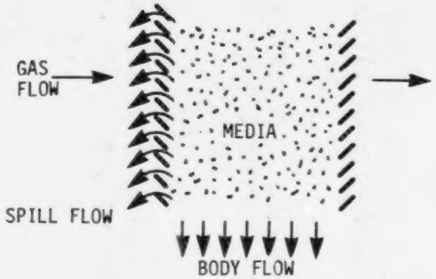
GAS FLOW
MEDIA
SPILL FLOW
BODY FLOW

a. CONTROLLED FRONT-FACE SPILLAGE

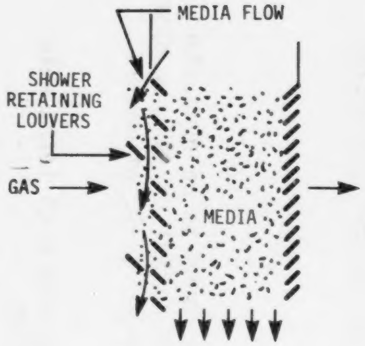
MEDIA FLOW
SHOWER RETAINING LOUVERS
GAS
MEDIA

b. FRONT-FACE SHOWER

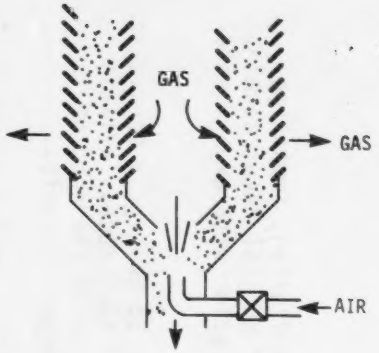

c. MEDIA BLAST

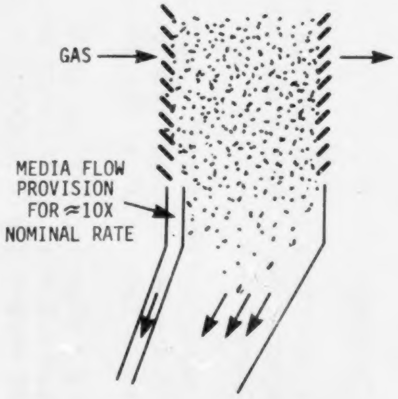
GAS
MEDIA FLOW PROVISION FOR ≈10X NOMINAL RATE

d. PREFERENTIAL MEDIA FLOW

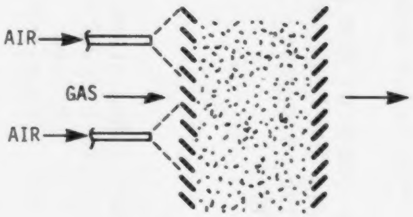

e. BLOW DOWN NOZZLES

Figure 6. Front-face deposit removal concepts

CONCLUSIONS[8]

Theoretical Analysis

- The four traditional collection mechanisms (diffusion, impaction, interception and sedimentation) combined with partial reentrainment of certain size ranges shows promising correlation with experimental data.
- The mathematical model showed GBF performance to be highly sensitive to incoming media cleanliness. The effect of such added resistance was shown to improve small particle collection at the cost of increased pressure drop and reentrainment of larger particles.
- The relative importance of the various mechanisms shifts dramatically between atmospheric and high temperatures (1600 F). Preliminary indications are that increased temperature will improve collection in most applications.

Experimental Program

- The continuous moving bed granular filter was found to be consistently capable of particulate removal efficiencies in excess of 98% for dust loadings (0.2-2.0 gr/sdcf) and size distributions (1-10 μm median) associated with many combustion operations.
- Submicron collection above 90% was associated with high inlet velocities, high inlet loadings, and low media rates.
- The beds with larger t/d_m and t/H ratios were most effective in retention of large particulates.

Front Face Cleaning

- The most favorable screen configuration tested was the slotted screen which retained media during shutdown but allowed natural spillage during operation.
- Loss of media spillage action at the inlet results in deposit building up on the gas approach side of the screen and reduced media activity along the inside of the screen.
- None of the cleaning devices tested were capable of rejuvenating front-face actions on line once media flow problems occurred behind the front screen due to excessive dust concentrations.

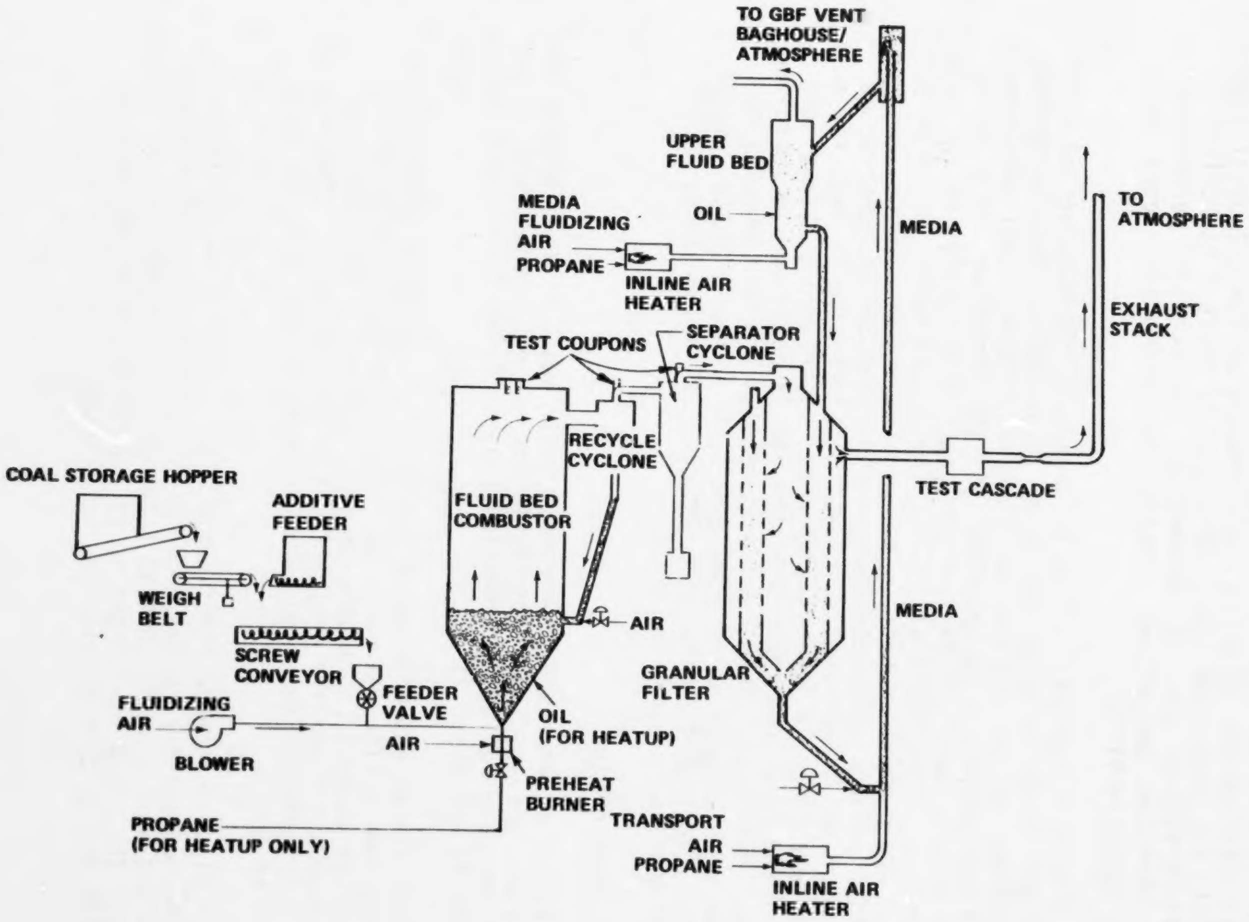
TO GBF VENT
BAGHOUSE/
ATMOSPHERE
UPPER
FLUID BED
MEDIA
FLUIDIZING
AIR
PROPANE
OIL
INLINE AIR
HEATER
MEDIA
TO
ATMOSPHERE
EXHAUST
STACK
TEST COUPONS
SEPARATOR
CYCLONE
RECYCLE
CYCLONE
TEST CASCADE
COAL STORAGE HOPPER
ADDITIVE
FEEDER
FLUID BED
COMBUSTOR
WEIGH
BELT
AIR
MEDIA
SCREW
CONVEYOR
GRANULAR
FILTER
FEEDER
VALVE
FLUIDIZING
AIR
BLOWER
AIR
OIL
(FOR HEATUP)
PREHEAT
BURNER
PROPANE
(FOR HEATUP ONLY)
TRANSPORT
AIR
PROPANE
INLINE AIR
HEATER

Figure 7. Phase II - hot flow GBF test system

PHASE II: HIGH TEMPERATURE GBF PERFORMANCE

The objectives of the current phase of the GBF development program are to (1) investigate the effects of elevated temperature and coal/sorbent particulate on GBF filtration performance at low (<4 psig) pressure, (2) update the analytical model developed in Phase I to reflect high-temperature effects and, (3) demonstrate long duration performance relative to corrosion, deposition, erosion, filtration efficiency, reliability, and controlability.

The hot flow test system is shown in Figure 7. It consists of a $4.9ft^2$ fluid bed combustor with conical air distributor, recycle cyclone, separator cyclone, GBF and 4-blade gas turbine cascade. Coal and sorbent are premixed and pneumatically injected into the combustor via a rotary feeder. The GBF is identical in size and basic construction to the cold flow model with a filter depth of 15.3". The filter media is 1.9 mm alumina beads. The combustor, recycle cyclone, separator cyclone, and interconnecting ductwork are refractory lined. The GBF is constructed of Incoloy 800 H and is externally insulated. Provision is made for test specimens to be exposed in low velocity areas upstream of, within, and downstream of the GBF. Ash removed by the GBF is collected in a cyclone and baghouse. Pressures, flows, and temperatures are continuously recorded by the data acquisition system used in the Phase I tests. Inlet and outlet ash concentration and size distribution are measured by EPA Method 5 and Andersen cascade impactor.

GBF Screens Configuration

The inlet GBF screen used for Phase I tests was a slotted screen that permitted front face spillage. No difficulty was experienced with either plugging or recovery following intentional overloading. This same design is being used in the Phase II tests.

The outlet screen was originally designed for complete retention of media. Since some difficulty was experienced in progressive plugging with media after several hours of cold flow testing, a new design is being evaluated which permits controlled spillage of media. The results to date in both cold and hot flow tests show no serious plugging with either media or ash.

The cold flow tests used inlet and outlet screens with identical heights. The mathematical model shows that more favorable performance can be attained with a taller outlet screen which will flatten the outlet velocity profile. This is thought to be especially important with an outlet screen design that permits media spillage.

Parametric Tests

A series of 36 steady state tests will be conducted in the $4.9ft^2$ FBC facility using Illinois #6 coal. The effects of the following GBF variables will be evaluated:

- Filter inlet combustion gas temperature (up to 1600 F).
- Filter inlet combustion gas superficial velocity (up to 150 fpm).
- Media circulation rate.
- Inlet loading (up to 2 gr/acf)

Data from these tests will be used to update the mathematical model and to determine the operational conditions under which the long duration performance tests will be run. The updated model will be used to predict GBF performance of commercial size units operating on coal at various temperatures, pressures, and inlet loadings.

Hot Flow Performance Tests

Following the parametric tests, a 1000 hour coal combustion test will be conducted in which sorbent will be added as required to meet SO_2 emission standards and a corrosion inhibitor added to control sulfidation. The test will be divided into 100,200, 300, and 400 hour segments to provide progressive data on erosion, corrosion, deposition, and GBF screen performance.

Summary

Although the tolerance of gas turbines to dust loading (defined by acceptable blade life) is affected by the size and nature of the particles, the consensus is that GBF performance must be targeted for 0.005 gr/acf with essentially complete removal of particulate larger than 5μm. The cold flow tests conducted during Phase I demonstrated that the GBF is capable of that level of collection although performance under hot flow conditions with coal ash has yet to be demonstrated. Successful results from low pressure hot flow tests during Phase II will provide the technical justification for proceeding with high pressure hot flow tests in the next phase of GBF development for gas turbine applications.

ACKNOWLEDGEMENTS

This work was funded by the U.S. Energy Research and Development Administration (Department of Energy) under Contract No. EF-77-C-01-2579.

REFERENCES

1. Guillory, J.L. Filtration Performance of a Moving Bed Granular Filter. (Presented at the Fifth International Conference on Fluidized Bed Combustion. Washington, D.C. December 12-14, 1977)

2. Wigton, H. and G. Wade. Theoretical Analysis of Granular Bed Filtration Principles and Performance Prediction. (DOE Report HCP/T-2579/18, January,1978).

3. Wigton, H.F. Mathematical Model of a Cross-Flow Moving Bed Granular Filter. (Presented at the Fifth International Conference on Fluidized Bed Combustion. Washington, D.C. December 12-14, 1977).

4. Phillips, K.E. Particle Sampling Facility Operation. (DOE Report HCP/T-2579/10, November, 1978).

5. Guillory, J.L. Cold Flow Test Program, Data Analysis and Observations. (DOE Report HCP/T-2579/15, January, 1978).

6. Wade, G.L. Performance and Modeling of Moving Granular-Bed Filters. (Presented at the EPA/ERDA Symposium on High Temperature/Pressure Particulate Control. Washington, D.C., September 20, 1977).

7. Phillips, K.E. Filter Front Face Cleaning Experiments. (DOE Report HCP/T-2579/9, October, 1977).

8. Wade, G., H. Wigton, J. Guillory, G. Goldbach, K. Phillips. Granular Bed Filter Development Program Final Report. (DOE Report HCP/T-2579/19, April, 1978).

SYMBOLS

Principal Arabic

C	Cunningham slip correction factor; concentration
d	Diameter
D	Mass diffusion coefficient
H	Active filter height
L	Dust loading
M	Media rate (media mass flow/air mass flow)
t	Filter thickness
U,V	Velocity

Principal Greek

ε	Void fraction
η	Collection efficiency
μ	Viscosity
ρ	Density
ϕ	Sphericity

Subscripts

c	Collector	p	Particulate
i	Inlet	s	Collected particulate in media
m	Media	t	Terminal
o	Original (clean)	T	Total